



THE UNIVERSITY OF  
**WAIKATO**  
*Te Whare Wānanga o Waikato*

Research Commons

<http://researchcommons.waikato.ac.nz/>

## Research Commons at the University of Waikato

### Copyright Statement:

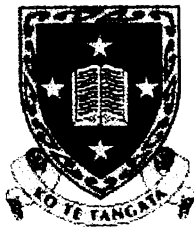
The digital copy of this thesis is protected by the Copyright Act 1994 (New Zealand).

The thesis may be consulted by you, provided you comply with the provisions of the Act and the following conditions of use:

- Any use you make of these documents or images must be for research or private study purposes only, and you may not make them available to any other person.
- Authors control the copyright of their thesis. You will recognise the author's right to be identified as the author of the thesis, and due acknowledgement will be made to the author where appropriate.
- You will obtain the author's permission before publishing any material from the thesis.

**STRATIGRAPHY, CHRONOLOGY,  
AND CORRELATION  
OF THE PLIO-PLEISTOCENE (c. 2.2–0.8 Ma)  
KAUROA ASH SEQUENCE,  
WESTERN CENTRAL NORTH ISLAND, NEW ZEALAND**

A thesis submitted in fulfilment of the requirements for the degree  
of Doctor of Philosophy in Earth Sciences at  
The University of Waikato



**The  
University  
of Waikato**

*Te Whare Wānanga  
o Waikato*

Joanna L. Horrocks

Department of Earth Sciences  
The University of Waikato

September 2000



## ABSTRACT

The Kauroa Ash beds (K-beds) comprise a 12–20 m-thick sequence of extremely weathered, clay-rich (40-95% <4  $\mu\text{m}$  clay) beds of tephra and loess, and associated paleosols. Found in isolated remnants throughout the western central North Island, the sequence comprises 15 defined members, with as many as 44 constituent macroscopic beds. The type site, 'Woodstock', near Raglan, is the most comprehensive sequence known, but other sites (e.g. Papakura Creek and Tiritirimatangi Peninsula) contain units not found or poorly defined at Woodstock.

Field properties as well as magnetic susceptibility measurements and particle-size analysis characterise the facies in the sequence. Field properties (in particular colour, consistence, macrofabric) describe the lithostratigraphy. The sequence contains five interpretive (i.e. genetic) 'facies': paleosols, primary tephra, very weathered tephra (possibly composite beds), loess and 'tephric loess' beds. At least seven loess beds are (newly) identified in the sequence: K4a, K5, K6ai, K8ai, K8bi, K10a and K14ai.

Mass-specific susceptibility and frequency-dependent susceptibility results partly conform to established models (developed mostly on Chinese loess-paleosol deposits) of susceptibility enhancement in paleosols and depletion in loess. Many parts of the sequence do not appear to conform to this model and the results more closely resemble the inverse relationship found on Alaskan loess-paleosol beds. Frequency-dependent susceptibility is reliable in delineating paleosols by their 'ultrafine' ferrimagnetic mineral content, and citrate-bicarbonate-dithionite treatments successfully remove all iron oxides so that remeasurement of susceptibility isolates a strictly 'pedogenic', rather than lithogenic, fraction.

Laser diffraction particle-size analysis shows that the Kauroa Ash beds are texturally reasonably homogenous. They have bimodal particle-size distributions with the most dominant mode at around 11.25  $\phi$  inferred to be the product of intense and prolonged weathering. Other modes are variously centred on 7–8.5  $\phi$  and, despite weathering and pedogenesis, have some relationship to the original depositional particle-size distributions because trends between facies (i.e. genetic units) are delineated. Principal components analysis objectively characterises these modes as (Wentworth size classes) 'very fine clay' and 'coarse silt', although there is no proportional relationship between them, supporting a post-depositional origin for the former mode.

The chronology of the sequence, previously poorly defined, is greatly improved by a combination of tephrochronologic correlations, fission-track dating, and paleomagnetism. Five zircon fission-track dates provide independent age 'spikes' and range from  $2.24 \pm 0.29$  Ma in the basal member, K1, to  $1.28 \pm 0.11$  Ma for the distal ignimbrite unit K12a. Paleomagnetism is invaluable in providing additional age information. The top of the sequence, member K15, is dated as  $>0.78$  Ma (Brunhes-Matuyama boundary) because of its reversed polarity; two episodes of normal polarity are found in beds K14b and K2b and are inferred to represent the Jaramillo (1.07-0.99 Ma) and Olduvai (1.95-1.79 Ma) subchrons, respectively. Beds underlying the Kauroa Ash sequence are also of normal polarity, indicating that they were deposited in the Gauss Chron ( $>2.6$  Ma).

Identification and correlation of tephtras by conventional means (fingerprinting by their lithological or geochemical properties) is impossible in the Kauroa Ash sequence because the beds have no remaining volcanic glass, which has instead been altered to an

assemblage of authigenic phases (clays) by weathering and pedogenesis. However, a new technique analysing fresh glass found as melt inclusions in quartz grains is successful in circumventing this problem. Inclusions represent samples of non-degassed magma that became entrapped during phenocryst growth prior to eruption. The glass has remained unaltered because it is hermetically sealed in a chemically resistant phenocryst, which has protected it from weathering processes. Electron microprobe analysis of the glass inclusions yield results which are wholly reasonable for glass (totals ranging from 93-97%; low standard deviations of <1%), and a number of provisional correlations are established by comparing the major element composition of Kauroa Ash tephra beds with those of proximal deposits. The Kauroa Ash sequence may contain deposits correlated with at least seven major TVZ eruptions, in many cases expanding the known extent of the (distal) deposit and, for the first time answering the question as to the origin of the Kauroa Ash beds.

These correlations, together with an improved chronology, enable the Kauroa Ash sequence to be placed in a regional stratigraphic framework alongside other New Zealand Plio-Pleistocene sequences such as those in the Wanganui Basin, Wairarapa, Cape Kidnappers and Port Waikato. Using paleosols as chrono- and climatostratigraphic entities (correlated to warm periods in global climate), the sequence can also be placed alongside a global reference, the marine oxygen isotope stratigraphy. A further correlation to the Chinese loess-paleosol record suggests that large parts of the Kauroa Ash sequence were deposited in an incremental manner akin to deposition of loess, so that the sequence is not only a record of TVZ volcanism, but also of Plio-Pleistocene paleoclimate.

## ACKNOWLEDGEMENTS

A huge thank you to my chief supervisor, David Lowe, without whose help, optimism and never-ending enthusiasm, I'm sure I never would have got through this! Also to Cam Nelson and Roger Briggs for their help, advice and guidance – thank you.

This study was made possible by the funding assistance of a Commonwealth Scholarship from New Zealand Vice Chancellors Committee. Also, I am indebted as always (literally) to my parents for their continued financial support.

For assistance with field work, thank you to David, Roger, Cam, Richard Smith, Laurie Gaylor, and Dave Campbell (for abseiling assistance). To various other unwitting assistants: thanks for sounding interested. A special thank you to Penny for enduring that cold, wet, miserable day on Tiritirimatangi Peninsula!

Thanks, also, to all the technicians who helped me with lab work, especially Renat Radosinsky, for advice on everything from thin sections to Freehand, and John Patterson, Victoria University of Wellington, for invaluable help with the microprobe.

A big thank you to Brent Alloway, Phil Shane, Paul Froggatt, and Peter Kamp for unpublished glass data, as well as other helpful comments and advice.

I am also grateful for other advice, comments and reviews from: Brad Pillans (paleomagnetism), Mike Singer (magnetic susceptibility), Phil Tonkin (soils, K-beds), Tasha Black (tephras), Stephen Stokes (paleoenvironments), and Richard Smith (volcanology).

To all the other long-suffering PhD students (at one time or other) at the University of Waikato, especially Jeanette Gillespie, Penny Cooke, Shaun Hayton, Stephen Krippner, Steve Hood, John Menneer, Haydon Jones, Barbara Hobden, Jayanthi Jayawardene, Deborah Bowyer, Avon McIntyre – thank you all for making my time here enjoyable.

And finally, to family, friends, flatmates: Linda, Peter, Leonie, Gini, Derek, June, Jo, Lesley, Liz, Jeanette, Boodle, Mike, Richard, Aaron, Julie, Shaun, Greg, Heidi, Sheryl, Olly, Mark Grace, DD, JMS. Thank you for support, friendship, food, amusement and entertainment!

*For my grandparents: Elizabeth, James, Marjorie, Geoffrey  
and  
Jeanette L. Gillespie (29.8.59-4.10.00)*

# TABLE OF CONTENTS

<b>1 INTRODUCTION</b>	<b>1</b>
<b>1.1 New Zealand Plio-Pleistocene Stratigraphy</b>	<b>1</b>
<b>1.2 Background: Previous Work on Kauroa Beds</b>	<b>4</b>
1.2.1 Early identification and definition	4
1.2.2 Development of ideas	5
1.2.3 Recent review and re-evaluation	7
1.2.4 Summary	8
<b>1.3 This Study</b>	<b>8</b>
1.3.1 Aims	8
1.3.2 Objectives	9
1.3.3 Methodology	9
1.3.4 Field sites	10
1.3.5 Definitions	11
1.3.5.1 Definition of the Kauroa Ash sequence	11
1.3.5.2 Nomenclature	12
<b>2 LITHOSTRATIGRAPHY</b>	<b>14</b>
<b>2.1 Introduction</b>	<b>14</b>
2.1.1 Lithostratigraphy	14
2.1.2 Paleosols	14
2.1.3 Tephra	16
2.1.4 Loess	16
2.1.5 ‘Tephric loess’	17
<b>2.2 Kauroa Ash Sequence in the Western Waikato</b>	<b>18</b>
2.2.1 Distribution	18
2.2.2 Main field sites	19
2.2.2.1 Woodstock	19
2.2.2.2 Papakura Creek	19
2.2.2.3 Tiritirimatangi Peninsula	19
2.2.2.4 Other sections	26
<b>2.3 Field Properties of Kauroa Ash Members</b>	<b>26</b>
2.3.1 Visual identification of beds	26
2.3.2 Identification of paleosols	33
2.3.3 Tephra (‘volcanigenic’) beds	34
2.3.4 Loess beds	35
2.3.5 Tephric-loess beds	35
<b>2.4 Facies Classification</b>	<b>35</b>
<b>2.5 Identification and Definition of Additional Units</b>	<b>38</b>
2.5.1 Oparau Tephra at Papakura Creek	38
2.5.1.1 Characteristics	38
2.5.1.2 Distribution	43
2.5.2 Other units of note at Papakura Creek	43
2.5.2.1 Unit PCM1	43
2.5.2.2 Unit PCM3	45

2.5.3 Tiritiri ignimbrite at Tiritirimatangi Peninsula	46
2.5.3.1 Characteristics	46
2.5.3.2 Distribution	48
<b>2.6 Summary</b>	<b>48</b>
<b>3 MAGNETIC SUSCEPTIBILITY</b>	<b>50</b>
<b>3.1 Introduction</b>	<b>50</b>
3.1.1 Magnetic susceptibility as a paleoenvironmental proxy	50
3.1.2 Origin of the susceptibility signal	50
3.1.3 Magnetic susceptibility studies in New Zealand	51
3.1.4 Magnetic susceptibility in the identification of paleosols	52
<b>3.2 Objectives</b>	<b>53</b>
<b>3.3 Sampling</b>	<b>53</b>
<b>3.4 Mass-specific Susceptibility</b>	<b>54</b>
3.4.1 Methodology	54
3.4.2 Results	55
3.4.3 Discussion	55
3.4.3.1 Mass-specific susceptibility as a stratigraphic correlation tool	55
3.4.3.2 Mass-specific susceptibility of paleosols	59
3.4.3.3 Mass-specific susceptibility of loess beds	61
3.4.3.4 Mass-specific susceptibility of tephra beds	62
3.4.4 Summary	63
3.4.5 Revised objectives	63
<b>3.5 Frequency-dependent Susceptibility</b>	<b>64</b>
3.5.1 Methodology	64
3.5.2 Results	65
3.5.3 Discussion	65
3.5.3.1 Frequency-dependent susceptibility of paleosols	65
3.5.3.2 Frequency-dependent susceptibility of loess beds	67
3.5.3.3 Frequency-dependent susceptibility of tephra beds	69
3.5.3.4 Summary	69
<b>3.6 Citrate-Bicarbonate-Dithionite Analysis</b>	<b>70</b>
3.6.1 Theory	70
3.6.2 Methodology	70
3.6.3 Results	71
3.6.4 Discussion	71
<b>3.7 Conclusions</b>	<b>74</b>
<b>4 PARTICLE-SIZE ANALYSIS</b>	<b>77</b>
<b>4.1 Introduction</b>	<b>77</b>
4.1.1 The study of particle size	77
4.1.2 Particle-size analysis of the Kauroa Ash sequence	78
4.1.3 Laser diffraction particle-size analysis	78
<b>4.2 Sample Preparation</b>	<b>79</b>

4.2.1 Sample size	79
4.2.2 Sample homogeneity	79
4.2.3 Sample pretreatment	80
<b>4.3 Results</b>	<b>80</b>
4.3.1 General particle-size characteristics of the Kauroa Ash sequence	80
<b>4.4 Analysis and Discussion</b>	<b>86</b>
4.4.1 Characterisation of sample types	86
4.4.2 Percentage of sand, silt and clay	87
4.4.3 Volume-weighted mean and standard deviation	90
4.4.4 Principal Component Analysis and U-ratio	92
4.4.4.1 Principal components of Kauroa Ash samples	92
4.4.4.2 Principal components of sample types	94
4.4.4.3 U-ratio in particle-size analysis of weathered deposits	96
<b>4.5 Conclusions</b>	<b>96</b>
<b>5 CHRONOLOGY</b>	<b>99</b>
<b>5.1 Introduction</b>	<b>99</b>
<b>5.2 Tephrochronology</b>	<b>99</b>
5.2.1 Introduction	99
5.2.2 Correlations	100
5.2.2.1 Upper limit	100
5.2.2.2 Lower limit	101
5.2.3 Discussion	104
<b>5.3 Zircon fission-track</b>	<b>104</b>
5.3.1 Introduction	104
5.3.2 Methodology	104
5.3.3 Results	105
5.3.4 Discussion	106
<b>5.4 Paleomagnetism</b>	<b>107</b>
5.4.1 Introduction	107
5.4.2 Methodology	109
5.4.2.1 Sample collection	109
5.4.2.2 Measurement of NRM	110
5.4.2.3 Components analysis	110
5.4.3 Results	111
5.4.3.1 Obtaining characteristic I and D from vector components diagrams	111
5.4.3.2 Construction of a paleomagnetic column	112
5.4.4 Discussion	113
<b>5.5 Conclusions</b>	<b>116</b>
<b>6 TEPHROCHRONOLOGY</b>	<b>114</b>
<b>6.1 Introduction</b>	<b>114</b>
6.1.1 Tephra studies in New Zealand	114
6.1.2 Plio-Pleistocene volcanism	121
6.1.3 Source areas and deposits	122

6.1.3.1 Basaltic sources	122
6.1.3.2 Coromandel Volcanic Zone	124
6.1.3.3 Taupo Volcanic Zone	124
6.1.3.4 Stratigraphy of major rhyolitic eruptions	125
6.1.4 Distal tephra deposits	126
6.1.4.1 The nature of distal tephra deposits	127
6.1.5 Methods of correlation	128
6.1.6 Glass inclusions in quartz	129
<b>6.2 Sample Preparation and Methodology</b>	<b>130</b>
6.2.1 Laboratory	130
6.2.2 EMP slide preparation	130
6.2.3 Microprobe methodology	131
<b>6.3 Results</b>	<b>133</b>
<b>6.4 Correlations</b>	<b>136</b>
6.4.1 Correlation of K12, Oparau Tephra and Ongatiti Ignimbrite	136
6.4.1.1 Results	136
6.4.1.2 Discussion	138
6.4.2 Correlation of PCM1 (Papakura Creek)	138
6.4.2.1 Results	141
6.4.2.2 Discussion	141
6.4.3 Correlation of PCM3 (Papakura Creek), WS2 (Woodstock) and TTM3 (Tiritirimatangi Peninsula)	142
6.4.3.1 Results	142
6.4.3.2 Discussion	142
6.4.4 Correlation of PCM2 (Papakura Creek) and TTM2 (Tiritirimatangi Pen.)	144
6.4.4.1 Results	146
6.4.4.2 Discussion	146
6.4.5 Correlation of K3	147
6.4.5.1 Results	147
6.4.5.2 Discussion	149
6.4.6 Correlation of WS3 (K13a, Woodstock)	149
6.4.6.1 Results	150
6.4.6.2 Discussion	150
6.4.7 Correlation of WS1 (K15c, Woodstock)	150
6.4.7.1 Results	152
6.4.7.2 Discussion	152
6.4.8 Correlation of Tiritiri ignimbrite	152
6.4.8.1 Results	154
6.4.8.2 Discussion	156
6.4.9 Correlation of TTM4 (Tiritirimatangi Peninsula)	157
6.4.9.1 Results	157
6.4.9.2 Discussion	157
<b>6.5 Conclusions</b>	<b>159</b>
6.5.1 Summary of correlations	159
6.5.2 Assessment of the glass inclusion technique	160
<b>7 PLIO-PLEISTOCENE STRATIGRAPHY:</b>	<b>163</b>
<b>7.1 Introduction</b>	<b>163</b>



7.1.1 New Zealand Plio-Pleistocene stratigraphy	163
7.1.2 An integrated approach	163
<b>7.2 Methodology</b>	<b>164</b>
<b>7.3 New Zealand Sequences</b>	<b>166</b>
7.3.1 Composite Kauroa Ash sequence column	166
7.3.2 Wanganui Basin	168
7.3.3 East Coast – Wairarapa	172
7.3.4 East Coast – Hawke’s Bay	172
7.3.5 Kaihu Group – Port Waikato – Auckland	175
<b>7.4 Correlation of North Island Plio-Pleistocene Deposits</b>	<b>177</b>
7.4.1 Magnetostratigraphy	177
7.4.2 Tephrochronology	180
7.4.2.1 Late Pliocene	180
7.4.2.2 Early Pleistocene	180
7.4.2.3 Mid Pleistocene	181
7.4.2.4 Areal extent of eruptions	181
7.4.3 Chronostratigraphy	182
7.4.4 Correlation of the Kauroa Ash sequence to the marine oxygen isotope record	183
<b>7.5 Conclusions</b>	<b>185</b>
<b>8 CONCLUSIONS:</b>	<b>190</b>
<b>8.1 Introduction</b>	<b>190</b>
<b>8.2 Paleovolcanology</b>	<b>190</b>
8.2.1 Techniques for the analysis of weathered tephra deposits	190
8.2.2 Correlations to dated deposits	191
8.2.3 Current known extent of the Ongatiti Ignimbrite	192
8.2.4 Volcanic hazards in the western central North Island	191
8.2.5 Onset of TVZ explosive volcanism	191
8.2.6 Conclusions	192
<b>8.3 Paleopedology</b>	<b>193</b>
8.3.1 Characterisation of Kauroa Ash sequence paleosols	193
8.3.2 Interpretation of paleosols	194
8.3.3 Correlation to the Chinese loess-paleosol record	196
8.3.4 Model of pedogenic upbuilding	196
8.3.5 Conclusions	199
<b>8.4 Paleoclimate</b>	<b>200</b>
8.4.1 Plio-Pleistocene chronology of the Kauroa Ash sequence	200
8.4.2 Loess deposits	201
8.4.3 Identification and characterisation of Kauroa Ash sequence loess	202
8.4.4 Oldest period of loess accumulation in New Zealand	203
8.4.5 Conclusions	203
<b>8.5 Stratigraphy, Chronology, and Correlation of the Kauroa Ash Sequence</b>	<b>204</b>

## LIST OF FIGURES

### CHAPTER 1: INTRODUCTION

<b>Figure 1.1</b> Location map, North Island, New Zealand.	3
<b>Figure 1.2</b> Generalised stratigraphic column, Woodstock section.	4
<b>Figure 1.3</b> Main field area, western Waikato.	6

### CHAPTER 2: LITHOSTRATIGRAPHY

<b>Figure 2.1</b> Stratigraphy of (upper) Woodstock section.	20
<b>Figure 2.2</b> Stratigraphy and field properties, Woodstock section.	21
<b>Figure 2.3</b> Stratigraphic relationships at Papakura Creek.	22
<b>Figure 2.4</b> Stratigraphy and field properties, Papakura Creek.	23
<b>Figure 2.5</b> Stratigraphic relationships at Tiritirimatangi Peninsula.	24
<b>Figure 2.6</b> Stratigraphy and field properties, Tiritirimatangi Peninsula.	25
<b>Figure 2.7</b> Stratigraphy of Ohiapopoko Cone section.	27
<b>Figure 2.8</b> Stratigraphy of Foxs Centre section.	27
<b>Figure 2.9</b> Stratigraphy of Bryant Home section.	28
<b>Figure 2.10</b> Stratigraphy of Waiterimu section.	28
<b>Figure 2.11</b> Stratigraphy of Aotea Harbour section.	29
<b>Figure 2.12</b> Stratigraphy of Taharoa Corner section.	29
<b>Figure 2.13</b> Stratigraphy of Wyllies Hill section.	30
<b>Figure 2.14</b> Stratigraphy of Hinuera Quarry.	30
<b>Figure 2.15</b> Facies of the Kauroa Ash sequence.	37
<b>Figure 2.16</b> Flattened pumices in the Oparau Tephra.	39
<b>Figure 2.17</b> Small lithics in the Oparau Tephra.	39
<b>Figure 2.18</b> Oparau Tephra – K11 contact.	40
<b>Figure 2.19</b> Oparau Tephra outcrops on Kawhia Harbour.	42
<b>Figure 2.20</b> Maximum observed thickness of the Oparau Tephra.	42
<b>Figure 2.21</b> Bed PCM1 at Papakura Creek.	44
<b>Figure 2.22</b> Stratigraphy of PCM1 at Papakura Creek.	44
<b>Figure 2.23</b> PCM3 at Papakura Creek.	45
<b>Figure 2.24</b> Tiritiri ignimbrite on Tiritirimatangi Peninsula.	46
<b>Figure 2.25</b> Base of the Tiritiri ignimbrite, and Kauroa Ash members.	47

<b>Figure 2.26</b> Cross-bedding features in the top of the Tiritiri ignimbrite.	47
--	----

### **CHAPTER 3: MAGNETIC SUSCEPTIBILITY**

<b>Figure 3.1</b> Magnetic susceptibility parameters for Woodstock.	56
<b>Figure 3.2</b> Magnetic susceptibility parameters for Papakura Creek.	57
<b>Figure 3.3</b> Magnetic susceptibility parameters for Tiritirimatangi Peninsula.	58
<b>Figure 3.4</b> Post CBD treatment change in mass-specific susceptibility.	72

### **CHAPTER 4: PARTICLE-SIZE ANALYSIS**

<b>Figure 4.1</b> Example particle-size distribution curves, by sample type.	81
<b>Figure 4.2</b> Percentage of sand, silt and clay, Woodstock section.	84
<b>Figure 4.3</b> Percentage of sand, silt and clay, Papakura Creek.	85
<b>Figure 4.4</b> Soil texture classification diagram.	83
<b>Figure 4.5</b> Mean particle-size distribution of sample types.	86
<b>Figure 4.6</b> Comparison of 'typical' loess and soil particle sizes.	87
<b>Figure 4.7</b> Soil texture classification diagram showing loess samples.	89
<b>Figure 4.8</b> Weighted mean and standard deviation of Woodstock samples.	91
<b>Figure 4.9</b> Regression plots of principal components and size classes.	93
<b>Figure 4.10</b> Matrix plot of principal components of Woodstock data.	94

### **CHAPTER 5: CHRONOLOGY**

<b>Figure 5.1</b> Map of Maungatawhiri Volcanic Centre.	102
<b>Figure 5.2 (a)</b> Stratigraphic relations, Ohiapopoko Cone.	103
<b>Figure 5.2 (b)</b> Interbedded Kauroa Ash beds and basaltic deposits.	103
<b>Figure 5.3</b> Field orientation of paleomagnetism samples.	109
<b>Figure 5.4</b> 'Z-plot' vector components diagram.	111
<b>Figure 5.5</b> Magnetostratigraphy of Woodstock section.	113
<b>Figure 5.6</b> Magnetostratigraphy of (lower) Papakura Creek section.	114
<b>Figure 5.7</b> Normal ignimbrite unit, PCM1, Papakura Creek.	114
<b>Figure 5.8</b> Geomagnetic polarity timescale of the last 3.5 Ma.	115
<b>Figure 5.9</b> Chronology of the Kauroa Ash sequence.	119

## CHAPTER 6: TEPHROCHRONOLOGY

<b>Figure 6.1</b> Location of main volcanic centres, North Island.	123
<b>Figure 6.2</b> Glass inclusions in quartz grains.	131
<b>Figure 6.3</b> Backscattered electron images of glass inclusions.	132
<b>Figure 6.4</b> Backscattered electron image (and negative) of an inclusion.	132
<b>Figure 6.5</b> Correlation of K12, Oparau Tephra and Ongatiti Ignimbrite.	137
<b>Figure 6.6</b> Comparison of PCM1 and possible correlatives.	140
<b>Figure 6.7</b> Comparison of PCM3, TTM3 and WS2.	143
<b>Figure 6.8</b> Comparison of PCM2, TTM2 and possible correlatives.	145
<b>Figure 6.9</b> Comparison of K3 and possible correlatives.	148
<b>Figure 6.10</b> Comparison of WS3 and possible correlatives.	151
<b>Figure 6.11</b> Comparison of WS1 and possible correlatives.	153
<b>Figure 6.12</b> Comparison of Tiritiri ignimbrite and possible correlatives.	155
<b>Figure 6.13</b> Comparison of TTM4 and Rangitawa Tephra.	158
<b>Figure 6.14</b> Correlation of main Kauroa Ash sequence beds.	161
<b>Figure 6.15</b> Reference sheet: stratigraphic columns and location map.	162

## CHAPTER 7: PLIO-PLEISTOCENE STRATIGRAPHY

<b>Figure 7.1</b> Location of regions and reference sites, North Island.	165
<b>Figure 7.2</b> Composite stratigraphic column, Kauroa Ash sequence.	167
<b>Figure 7.3</b> Lithostratigraphy of the Rangitikei River section.	170
<b>Figure 7.4</b> Lithostratigraphy of sections from East Coast basins.	171
<b>Figure 7.5</b> Lithostratigraphy of Cape Kidnappers, Hawke's Bay.	174
<b>Figure 7.6</b> Lithostratigraphy of Okariha and Oruarangi sections.	176
<b>Figure 7.7</b> Regional correlation of New Zealand Plio-Pleistocene sequences.	178
<b>Figure 7.8</b> Correlation of Kauroa Ash sequence to the MOI stratigraphy.	184

## CHAPTER 8: CONCLUSIONS – PALEOENVIRONMENTS

<b>Figure 8.1</b> Distribution of the Ongatiti Ignimbrite.	190
<b>Figure 8.2</b> Known extent of distal correlatives of the Ongatiti Ignimbrite.	190
<b>Figure 8.3</b> Correlation of Kauroa Ash sequence to the Xifeng section.	197

## LIST OF TABLES

<b>Table 2.1</b> Relationship between loess, tephra and soil formation.	15
<b>Table 2.2</b> Summary of field properties of the Kauroa Ash sequence.	31
<b>Table 2.3</b> Facies classification of K-beds at Woodstock.	36
<b>Table 3.1</b> Magnetic parameters for samples from Alaska and China.	60
<b>Table 3.2</b> Development of paleosols.	66
<b>Table 3.3</b> Contribution of ultrafine grains to MSS in loess beds.	68
<b>Table 3.4</b> Range of susceptibility values by sample type.	69
<b>Table 3.5</b> Summary of magnetic susceptibility values of K-beds.	75
<b>Table 4.1</b> Particle-size scales and size classes.	82
<b>Table 4.2</b> Mean sand, silt and clay content.	83
<b>Table 4.3</b> Average percentage of sand, silt and clay by bed type.	88
<b>Table 4.4</b> Principal components of particle-size data.	93
<b>Table 4.5</b> R-squared values of principal components and size classes.	95
<b>Table 5.1</b> Summary of previous radiometric ages on Rangitawa Tephra.	100
<b>Table 5.2</b> Zircon fission-track results for Kauroa Ash beds.	105
<b>Table 5.3</b> Ages and error-weighted mean of distal Ongatiti Ignimbrite.	107
<b>Table 5.4</b> Ages and error-weighted mean of Ongatiti Ignimbrite.	107
<b>Table 6.1</b> Some possible correlatives of Kauroa Ash beds.	126
<b>Table 6.2</b> Major element analyses of Kauroa Ash beds	134
<b>Table 6.3</b> Major element analyses of possible correlatives.	134
<b>Table 6.4</b> Summarised tephrochronological correlations.	159
<b>Table 7.1</b> Inferred ages and MOI stages of Kauroa Ash members.	185
<b>Table 8.1</b> Inferred ages of loess deposits in the Kauroa Ash sequence.	203

# 1 INTRODUCTION

---

## 1.1 NEW ZEALAND PLIO-PLEISTOCENE STRATIGRAPHY

Quaternary marine and terrestrial sequences around New Zealand contain numerous tephra horizons that are the product of voluminous eruptions (100-1000 km<sup>3</sup>) from the central North Island volcanic zone (e.g. Newnham et al., 1999a; Shane, 2000). These large rhyolitic eruptions typically consist of two main eruptive phases: a plinian fall phase, and a pyroclastic flow or 'ignimbrite-generating' phase. As well as having a catastrophic effect on proximal locations, the eruptions are of a magnitude that result in the deposition of material over a vast area of land and sea (e.g. Nelson et al., 1985; Shane, 1994; Wilson et al., 1995a; Carter et al., 1995; Wilson, in press). This is especially advantageous to Earth Sciences, because the eruptives are essentially geologically instantaneous, and, if they can persist through weathering and erosion, produce distinctive 'time plane' marker horizons (e.g. Pillans and Kohn, 1981, 1998; Kohn et al., 1992). The widespread nature of these deposits and extension into distal locations means they are more likely to be preserved than eruptives in proximal, near-vent locations. These are complex and typically incomplete (e.g. Krippner et al., 1998) whereas deposits in distal locations remain relatively unaffected and thus record a more complete eruptive history (e.g. Shane et al., 1996a, 1998). The disadvantage of deposits in distal locations is that they are generally thin (reduced thickness with increased distance from source) and are thus vulnerable to modification by soil-forming processes, weathering and erosion (Moore, 1991; Manning, 1996). However, if the volcanic system is a productive one, as in New Zealand (Houghton et al., 1995; Wilson et al., 1995b), subsequent eruptions reaching distal locations will bury the antecedent deposit, thereby usually aiding its preservation. Thousands of years of volcanic activity can result in a comprehensive suite of deposits and identification of these buried tephra layers would provide a strong stratigraphic and chronologic framework for Quaternary studies in New Zealand (Lowe and Newnham, 1999; Shane, 2000).

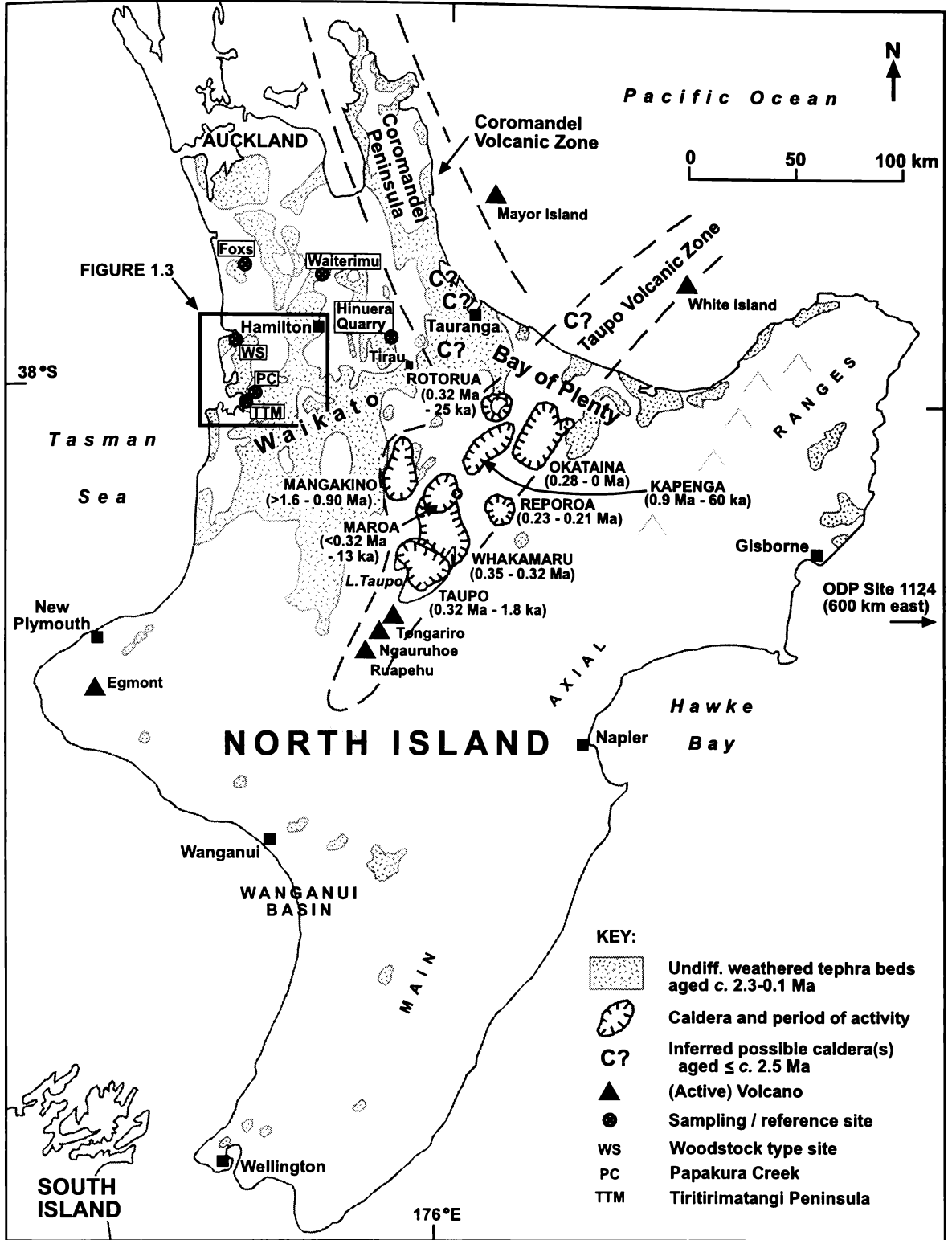
A terrestrial sequence of deposits has the potential to provide more than a region's volcanological history, however. It can also be a record of other environmental parameters operative at the time of deposition. Tephra deposits are subject to modification by influxes of other sediments through erosion and deposition. A common

addition is loess, a fine-grained aeolian deposit generally indicative of increased comminution and erosion of sediments under glacial climates (e.g. Derbyshire, 1995; Smalley, 1995). Both types of deposit are subject to weathering of existing minerals and soil-forming processes in general. Rates and degree of weathering reflect contemporary climatic conditions, specifically temperature and moisture availability. In due course, under warmer climates and stable site conditions, a soil will form on the deposit. After burial by a new tephra deposit, or large influx of other sediments, the soil becomes a buried soil or paleosol, a bed representative of the old land surface and environmental conditions present at the time of formation. Together, the various properties of tephra-loess-paleosol sequences can be very useful in the reconstruction of past climate changes, particularly in the Quaternary period (e.g. Palmer and Pillans, 1996).

Major advances in this field took place in the 1980s when work on the loess-paleosol sequences of China demonstrated that terrestrial records (as opposed to deep-marine and ice-core records) also have the ability to record high-resolution information about past climatic change (e.g. Heller and Liu, 1984; Liu, 1985; Kukla, 1987). Several parameters, such as magnetic susceptibility and particle size analysis, provide proxy records of paleoclimate and, when measured through a dated sequence, allow inferences to be made about environmental change in the Quaternary (e.g. An and Porter, 1997; Meng et al., 1997; Maher, 1998; Lu et al., 1999; Ding et al., 2000).

The Chinese loess record is unparalleled for its thickness and continuity, but New Zealand is well-suited for the occurrence of these deposits due to a history of periodic glaciation, active volcanism and tectonic activity, all of which have given rise to repeated periods of accumulation, weathering and erosion (Newnham et al., 1999a). Several New Zealand sequences have provided considerable information on Quaternary history (e.g. Pillans and Wright, 1990; Shane et al., 1996a; Black et al., 1996; Palmer and Pillans, 1996; Newnham et al., 1999a). The Wanganui Basin, southwest North Island (Figure 1.1) has, in particular, been a detailed source of information on Plio-Pleistocene stratigraphy and paleoenvironments (e.g. Alloway et al., 1993; Pillans et al., 1994; Naish et al., 1996, 1998; Carter and Naish, 1998a, 1999).

Distal tephra deposits in New Zealand are not usually of the extent and resolution of the thick successions of cyclic sedimentary deposits in the Wanganui Basin. However, they can provide some very useful paleoenvironmental information, and with reliable



**Figure 1.1** Location map (schematic), North Island, New Zealand (partly after Lowe et al., in press).



correlation (by tephrochronology) can be ‘linked in’ to other marine and terrestrial sequences to take advantage of their established chronologies (Pillans, 1994; Palmer and Pillans, 1996; Lowe and Newnham, 1999).

Western-central North Island is one such ‘distal location’ with a long history of deposition of pyroclastic flow and fall deposits originating predominantly from the adjacent Taupo Volcanic Zone (TVZ; Nelson et al., 1989), but also potentially from the Coromandel Volcanic Zone (CVZ; Figure 1.1; Lowe et al., in press). Deposition throughout the Quaternary in particular has resulted in a suite of tephra deposits, some with loessic material, most with paleosols developed on them, that have the potential to add to what we know of the region’s history. In the Waikato region one such succession of deposits is known as the Kauroa Ash Formation.

## 1.2 BACKGROUND: PREVIOUS WORK ON KAUROA BEDS

### 1.2.1 Early identification and definition

The name ‘Kauroa Ash Formation’ was first proposed by Ward (1967) to describe a sequence of seventeen tephra beds exposed in an outcrop at the entrance to ‘Woodstock Farm’ near Raglan (hereafter known as the ‘Kauroa Ash sequence’). They were defined as being those beds underlying a younger formation, defined as the ‘Hamilton Ash Formation’, and resting on weathered basalt (Figure 1.2). Ward described these beds as occurring “north of Otorohanga and west of Tirau in the central part of the North Island of New Zealand” (Figure 1.1). The age of the beds was thought to be late Pleistocene. It was additionally noted that in some locations the lower beds of the sequence were intercalated with basaltic deposits, suggesting that the emplacement of Kauroa beds was co-eval with local (Okete and Pirongia) volcanism. Subsequently, the New Zealand Soil Survey report 1 (Pullar et al., 1973) noted Ward’s findings, adding an assumed age range for the sequence of 125-150 ka. The sequence is broadly mapped on the New Zealand Soil Bureau Map 134/1

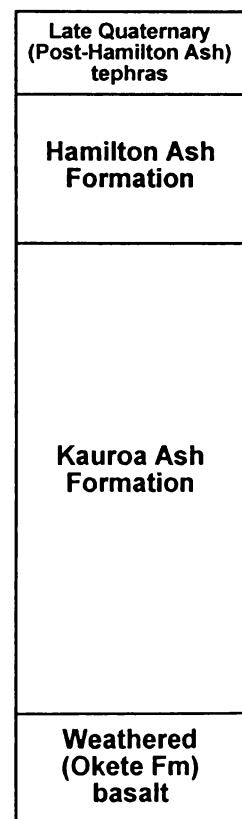


Figure 1.2 Generalised stratigraphic column, Woodstock section.

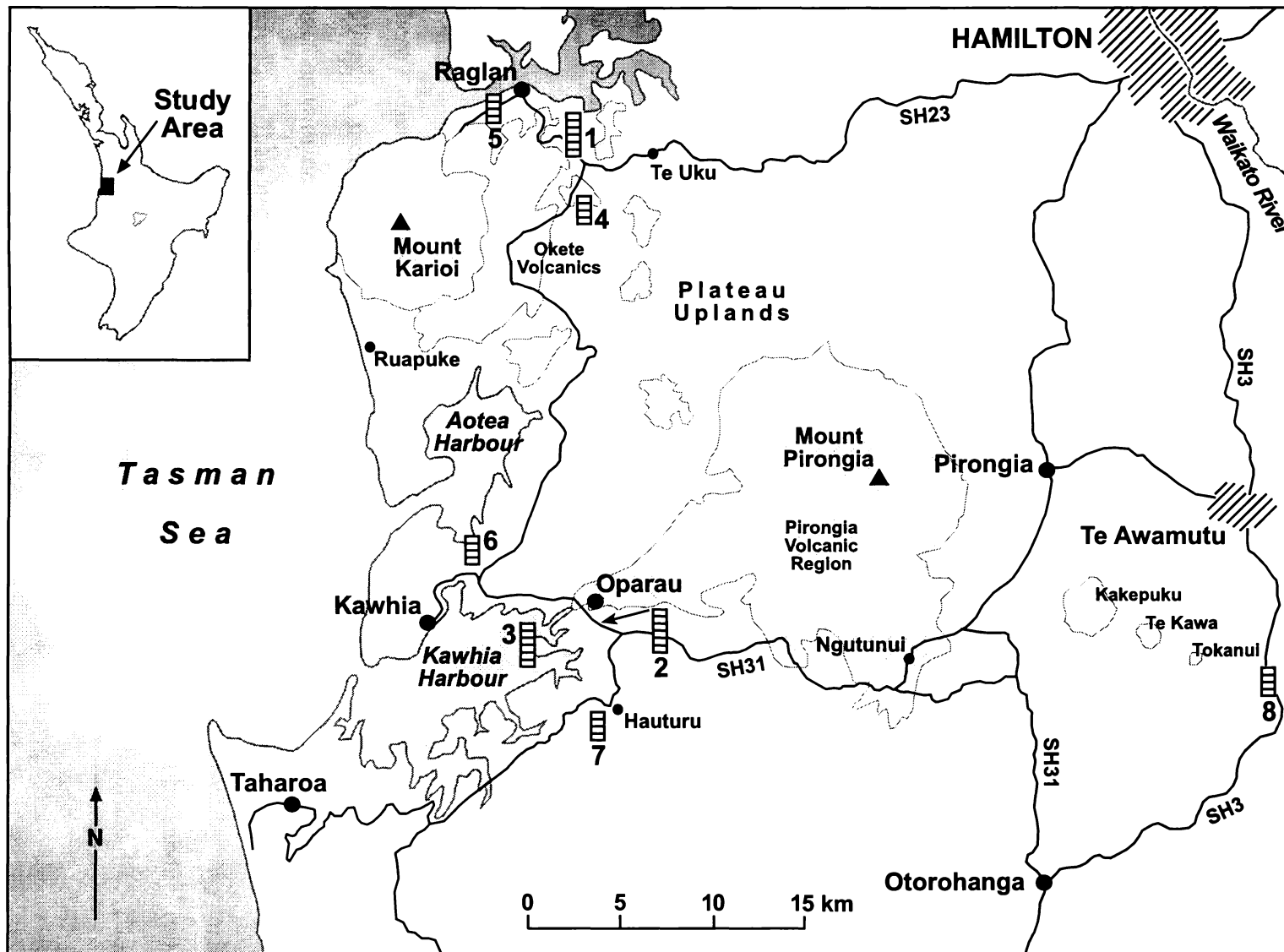
as part of 'undifferentiated brown tuffs' (with the Hamilton Ash Formation and other post-Kauroa beds).

Ward's (1967) work was modified by Pain (1975) who described and defined one Kauroa member, not previously differentiated by Ward, in greater detail. The member was named the Oparau Tephra and was said to occur consistently in sections southwest and southeast of Pirongia (Figure 1.3), but not in Ward's Woodstock section. The member was described as being a characteristically massive tephra, separated from the top of the sequence by at least eight tephra, including two other massive tephra-flow derived (i.e. ignimbrite) units. Pain expressed the view that this member was the distal end of an ignimbrite sheet that originated in the volcanic plateau of the central North Island. He further suggested that the well-defined Ongatiti Ignimbrite was a possible correlative, though was unable to provide any supporting evidence other than assumed stratigraphic juxtaposition. He was also unable to provide any examples of the stratigraphic relationships between the Ongatiti Ignimbrite and other Kauroa Ash members.

Davoren (1976) studied the Kauroa beds exposed in a building site on Waikato University campus. He identified five separate units, named them (bottom to top) KI, KII, KIII, KIV and KV, and analysed their physical, mineralogical and elemental properties. Four of the beds (KI, KIII, KIV and KV), dominated by halloysite with allophane, quartz, feldspar and cristobalite accessory minerals, were said to be of a rhyolitic origin. The other bed, KII, was said to be dominated by allophane (estimated by difference), with halloysite, quartz, and cristobalite accessories, and inferred to be of an andesitic source. The thesis produced no conclusive evidence as to the source or chronology of the beds, but suggested that they were of early Pleistocene to late Pliocene age.

### *1.2.2 Development of ideas*

The most recent detailed work on the stratigraphy and composition of the Kauroa Ash sequence is Salter's (1979) thesis study that described the physical, chemical and mineralogical properties of several beds at Ward's (1967) Woodstock type-site. Salter identified twenty-six beds, including ten paleosols, and classified the sequence into fifteen members, K1 (base) to K15 (top). Distinctive features, such as kaolinite books



**KEY:**

- Road
- Town
- ▲ Volcano
- ▤ ▥ Sections

- 1 Woodstock (type section)
- 2 Papakura Creek
- 3 Tiritirimatangi Peninsula
- 4 Ohiapopoko Cone
- 5 Bryant Home section
- 6 Aotea Harbour
- 7 Taharoa Corner
- 8 Wyllies Hill

Grid references in text

Not on map: Hinuera Quarry, Foxs Centre, Waiterimu (Figure 1.1)

**ALEXANDRA VOLCANIC GROUP**

- ▭ Convergent margin series
- ▭ Alkalic intraplate series (Okete Volcanics)

**Figure 1.3** Main field area, western Waikato

and stacks in beds K3 and K12, were noted. The study could not establish any definitive age or source area, but did suggest an age range of 0.7 to 1.1 Ma based on the estimated the time required for the weathering of the ten paleosols, and the Taupo Volcanic Zone as a source area due to the rhyolitic nature of the deposits.

Kirkman (1980) included some work on the Kauroa Ash sequence, comparing the mineralogy of some Kauroa beds with those of the so-called rhyolitic Pahoia Tuffs in the Bay of Plenty region. He concluded that intensive weathering had taken place in the tephras at both sections. Indeed, analyses showed that all weatherable minerals had been almost completely destroyed, particularly in the oldest tephras. The large amounts of the stable clay mineral halloysite in most of the tephras further emphasized the long weathering history of the beds.

A study of the Alexandra and Ngatutura Volcanics (Briggs et al., 1989) provided further insight into the age of the Kauroa Ash sequence. As previously reported by Keane (1985), the basal member, K1, was noted as occurring intercalated with co-eruptives of K/Ar-dated alkali basalts (basanite) of the Okete Volcanics at nearby Ohiapopoko ( $2.26 \pm 0.08$  Ma) and Cleaves cone ( $2.25 \pm 0.10$  Ma) of the Maungatawhiri centre. This suggested the base of the sequence was considerably older (2.25 Ma) than previously thought. An age of  $<1.81$  Ma was additionally assigned by Briggs et al. (1989) to members K12 (Oparau Tephra; Pain, 1975) and K15 (Waiterimu Ash; Ward, 1967) because these members unconformably overlie co-eruptives of K/Ar-dated alkali basalts (hawaiite) of the Ngatutura Volcanics at Foxs centre ( $1.81 \pm 0.07$  Ma).

### *1.2.3 Recent review and re-evaluation*

These earlier findings were summarised in a conference field-trip report (Briggs et al., 1994a). A modified version of Salter's (1979) Woodstock stratigraphy was reported together with new clay mineralogical data. These data were based on more reliable techniques than used previously to estimate short-range order clays (T.G. Shepherd, unpublished data; Shepherd, 1994). The Kauroa beds were characterised by very high clay ( $<2 \mu\text{m}$  fraction) contents, ranging from 69-92%, and dominated by kandite<sup>1</sup> (60-95%), with smaller amounts of goethite (2-15%), and minor allophane (0.5-2%),

---

<sup>1</sup> Includes both kaolinite and halloysite.

ferrihydrite (0.1-1%) and gibbsite (<0.1-2%). The small proportions of primary minerals present were dominated by quartz, cristobalite, (titano)magnetite, ilmenite and zircon. A further review of the nomenclature and stratigraphy of the Hamilton and Kauroa Ash sequences (Lowe et al., in press) additionally illustrated the wide range of possible correlatives of the Kauroa beds. Numerous widespread silicic pyroclastic deposits found in sequences across the North Island, and in deep-sea cores, may be co-eval with members of the Kauroa Ash sequence (on the basis of their inferred age). Possible source areas were noted to include younger volcanic centres in the southern CVZ or older volcanic centres in the TVZ, or both (Figure 1.1).

#### *1.2.4 Summary*

These previous studies have established that the Kauroa Ash Formation is a sequence of extremely weathered tephra deposits, predominantly rhyolitic but possibly with some andesitic content. The sequence spans some considerable duration as evidenced by a minimum of ten paleosols, as defined by Salter (1979), and the base may be of late Pliocene age. No detailed chronology has been established; however, some provisional ages have been reported (Briggs et al., 1989; Lowe et al., in press). Sources are suggested (from inferred age and silicic nature) to be either late CVZ or early TVZ centres, or both. The Kauroa beds are exposed at disparate locations around the Waikato region, but typically only poorly so and it is thought that the Woodstock type section is the most complete sequence available.

### 1.3 THIS STUDY

#### *1.3.1 Aims*

Fergusson's (1986) 'Geology of Inland Kawhia' thesis study revealed that several exposures of the Kauroa Ash sequence occur around Kawhia Harbour and noted that,

"The tephrostratigraphy of these ash beds is an exacting study in itself and beyond the scope of this thesis".

This study aims to build on previous work by providing such an analysis of the Kauroa Ash sequence in the western Waikato region. Specifically it aims to elucidate the distribution, characteristics, chronology, stratigraphic context and paleoenvironmental significance of the sequence.

This is a challenging endeavour because of the nature of these beds. Most members of the sequence are so highly weathered that they are comprised of little else other than clay. Identification of members and beds is not always clear, and various field characteristics usually used for correlation have been 'blurred' by weathering. Primary minerals are sparse, preventing mineralogical studies and most dating methods. Initial reports suggested that no volcanic glass remains, precluding conventional tephra fingerprinting. Another major aim of this thesis is thus to devise and utilise methods for circumventing these problems, and to find ways of accessing what information remains in old, highly weathered deposits such as these.

### *1.3.2 Objectives*

The major objectives of this study are as follows:

1. To provide higher resolution information on the character of Kauroa members than has been previously reported.
2. To attempt to gain that information using different analytical methods than those used in previous studies.
3. To identify useful field characteristics so that future workers can more easily identify major or significant units.
4. To gain a better understanding of the chronology of the sequence.
5. To attempt to identify and correlate some of the tephras.
6. To ascertain stratigraphic relationships to other sequences by placing the Kauroa Ash sequence into local, regional and global contexts.
7. To assess the paleoenvironmental significance of the Kauroa Ash sequence.

### *1.3.3 Methodology*

**Chapter 2** establishes the general stratigraphy of the sequence. It concentrates primarily on field observations with a view to attaining a lithostratigraphy and facies-like categorisation of Kauroa Ash members. In particular, it aims to provisionally identify beds that are primarily paleosol, tephra or loess units.

**Chapter 3** analyses the magnetic properties of the sequence. High-resolution magnetic susceptibility values are reported for two main sections. This work helps to refine the

stratigraphy of the sequence as well as providing some potentially useful paleoenvironmental information.

**Chapter 4** reports detailed particle-size data acquired on a lasersizer. Textual classification helps to characterise sample types (paleosol, tephra, loess) as well as acting as a potential paleoenvironmental proxy.

**Chapter 5** aims to improve on the chronology of the sequence, reporting known tephrochronological information and some new zircon fission-track dates. It also presents the paleomagnetism of the sequence, acquired on the two main sections. Key geomagnetic boundaries and reversals are identified.

**Chapter 6**, building on Chapter 5, attempts further tephrochronological correlations. Members of the Kauroa Ash sequence are used to test a new tool for the identification of tephras – the acquisition of major element composition from glass inclusions in quartz grains. The major element composition is presented for several beds and correlations to known and established tephra units are attempted.

**Chapter 7** attempts to take these correlations further, by placing the Kauroa Ash sequence within the New Zealand Plio-Pleistocene stratigraphic framework. Significant New Zealand sequences of similar age range are identified and their correlation to the Kauroa Ash sequence column illustrated. The sequence is placed in a global context, with a correlation to the marine oxygen isotope record.

**Chapter 8** aims to summarise findings of this work with an evaluation of the paleoenvironmental significance, illustrating what is learnt about the New Zealand Plio-Pleistocene climate and volcanic system from this sequence.

#### *1.3.4 Field sites*

Three main sites, together with reference to less complete sites, are used for analysis of the Kauroa Ash sequence in this study. The three main sites represent the only sections known that have over half the Kauroa members present. They are:

- Woodstock (WS) [S13/095096] – this is the type section of the Kauroa Ash Formation as proposed by Ward (1967).
- Papakura Creek (PC) [R15/788479] – this is the Oparau Tephra type section as proposed by Pain (1975).
- Tiritirimatangi Peninsula (TTMP) [R15/748458] – this comprises a thick exposure on the west coast of a Kawhia Harbour peninsula.

Detailed sampling and laboratory work was undertaken at these sites. Other sections are used to provide supplementary observations in the thesis:

- Ohiapopoko Cone (OC) [R14/787722] – lower members, includes some important stratigraphic relationships with other formations.
- Foxs Centre (FC) [R13/756076] – K12 and K15 with stratigraphic relations to local volcanism.
- Aotea Harbour Entrance (AH) [R15/718504] – upper members, particularly thick K14 and K15.
- Bryant Home (BH) [R14/705737] – several upper members, stratigraphic relationship to local laharic deposits.
- Hinuera Quarry (HQ) [T16/461614] – upper members, stratigraphic relationship to Ongatiti Ignimbrite.
- Taharoa Corner (TC) [R15/801437] – exposure of some upper members.
- Wyllies Hill (WH) [S15/155445] – upper members.
- Waiterimu (WAI) [S13/095096] – type location for Waiterimu Ash member (uppermost Kauroa Ash member, K15; Ward, 1967).

Most of the sites are shown in Figure 1.3. Further information (including stratigraphic columns for the main sites) is given in Chapter 2.

### *1.3.5 Definitions*

#### 1.3.5.1 Definition of the Kauroa Ash sequence

The limits of the Kauroa Ash sequence are defined as follows: the top of the sequence (top of K15) is distinguished by its sharp contact with the overlying Hamilton Ash



Formation, a 3 to 5 metre-thick sequence of strongly weathered, clay-textured tephra beds described in the Waikato region (Ward 1967; Pain, 1975). The oldest member of this formation, bed H1/2 (also known as the Ohinewai Ash or Tephra; Ward, 1967; Vucetich et al., 1978; and more recently, the Rangitawa Tephra; Kohn et al., 1992), is an extremely widespread, prominent marker bed, being distinguished by its typically pale yellowish brown colour and a yellow, quartz-rich coarse sandy layer forming the sharp boundary with the underlying Kauroa material. It is dated at c. 0.35 Ma (Lowe et al., in press). The uppermost Kauroa Ash member, K15, was individually defined by Ward (1967) as the 'Waiterimu Ash Member'. The type locality for this member is near Waiterimu, about 30 km north of Hamilton (Figures 1.1, 2.8; Lowe et al., in press). This member is exposed in numerous localities in the northern Waikato (Ward, 1967).

The base of the sequence, K1, rests on a variety of materials, the most common of which were found to be: weathered basaltic material derived from Okete and Karioi volcanoes (e.g. at Woodstock type-site); volcanic breccias of the Pirongia Formation (e.g. at Tiritirimatangi Peninsula); aeolian sands of the Kaihu Formation (e.g. east of Kawhia Harbour region); weathered Jurassic sediments (e.g. at Taharoa and south Kawhia Harbour region); and in most other localities weathered greywacke.

#### 1.3.5.2 Nomenclature

Tephra nomenclature follows that of Froggatt and Lowe (1990), Shane (2000), Lowe and Hunt (in press) and Hunt and Lowe (in press).

'Tephra' is defined as the collective term for all unconsolidated, primary pyroclastic products of a volcanic eruption (Froggatt and Lowe, 1990; Lowe and Hunt, in press). Since this definition no longer specifies origin or emplacement method (as per earlier definitions e.g. Thorarinsson, 1974) it is a useful general term for the description of the volcanic material in the Kauroa Ash sequence. Genetic terms are avoided because, except in a few circumstances, parent material, origin and mode of emplacement are usually impossible to discern.

There are a few variants to this definition. A stratigraphic entity composed of tephra may also be referred to as a 'tephra layer', 'tephra bed' or 'tephra horizon' (Hunt and Lowe, in press). 'Tephric' is used to denote reworked deposits or that weathered from

antecedent primary tephra deposits (Lowe and Hunt, in press). 'Pyroclastic' is a broader term than tephra as it includes both unconsolidated and consolidated (welded or hardened) clastic material (Hunt and Lowe, in press). 'Ignimbrite' denotes what is inferred to be the primary deposit of a pyroclastic flow or flows (Froggatt and Lowe, 1990). 'Ash' is a grain-size term (Hunt and Lowe, in press) but is retained in the title of the sequence because (a) its size connotation is still accurate in terms of the Kauroa members (grain size of deposits are all <2 mm), and (b) the sequence is formally defined as the Kauroa Ash Formation.

Other derivative terms used include: 'tephrochronology' (*sensu stricto*) is defined as the use of tephra deposits as time-stratigraphic marker beds to establish numerical or relative ages (Shane, 2000; Lowe and Hunt, in press); 'tephrostratigraphy' is the study of sequences of tephra layers and associated deposits, including their age relationships and distinctive properties (physical, mineralogical, geochemical or isotopic composition; Hunt and Lowe, in press); and 'tephrofacies' describes different facies of unconsolidated pyroclastic deposits pertaining to a single eruptive episode (Lowe and Hunt, in press).

Other terms are defined where appropriate.

## 2 LITHOSTRATIGRAPHY

---

### 2.1 INTRODUCTION

#### 2.1.1 Lithostratigraphy

Lithostratigraphy is the fundamental building block of stratigraphy, the organisation of the geological record into stratigraphic units on the basis of observed changes in the character of the deposits (Boggs, 1995). In this chapter, field descriptions and observations are presented with the aim of organising the Kauroa Ash sequence into a lithostratigraphic framework.

Conventional lithostratigraphic units are employed. The Kauroa beds have previously been termed a 'formation', the definition of which is well-defined upper, lower and lateral boundaries that can be traced and mapped over considerable distances. Field evidence presented below will show that this is indeed the case for the Kauroa beds, though the beds are now collectively termed a 'sequence'. As established in previous work (e.g. Salter, 1979), the sequence is divided into fifteen members, each of which consists of one or more beds. Members K1-K15 are thought to be somewhat arbitrarily defined in places, but the framework is well established and will not be changed. However, additional constituent units and subunits (volcanigenic) are recognised as a result of this study and are outlined below.

The intention is to go a step further and organise observed lithostratigraphic members and beds into a 'facies-like' categorisation. A semi-interpretative approach is adopted, with an inferred method of genesis stated where possible. 'Facies', in this case, fall into three main categories: paleosols, tephra and loess. For the purposes of this study, they are defined below.

#### 2.1.2 Paleosols

Paleosols are soils of an environment or landscape of the past (Lowe, 1996). They are important features of New Zealand Quaternary deposits especially, and some can be correlated over wide areas (Campbell, 1986). Few have been formalised as stratigraphic

entities, yet identification of paleosols can provide extensive information on buried geomorphic surfaces, paleolandforms, unconformities and paleoenvironments (Eden and Furkert, 1988; Palmer, 1994; Lowe, 1996). As such, they are invaluable to Quaternary studies (Newnham et al., 1999a).

Reliable, unequivocal criteria for recognising paleosols have yet to be developed, but in the case of paleosols on tephra and loess they are usually distinguished by their darker colours and finer textures compared with underlying beds (Kennedy, 1994). Paleosols can also be differentiated by their macromorphology: well-developed blocky, polyhedral and/or prismatic structures, increased organic matter accumulation or abundance of root channels (e.g. Campbell, 1986; Rankey and Farr, 1997). Other studies have used parameters such as amino acid levels, K and P content and bulk density to identify and characterise paleosols in sequences (e.g. Kimber et al., 1994; Almond, 1996; Palmer and Pillans, 1996).

A genetic linkage between climate and paleosol development (especially on loess) is well established (e.g. Derbyshire et al., 1995; Rankey and Farr, 1997; Maher, 1998). Paleosols developed on tephra sequences also provide potential for paleoclimatic interpretations even though the rate of accumulation of tephra deposits is not directly related to climate change and paleosols may be aggradational (Newnham et al., 1999a). Studies have shown that environmental factors, together with tephra composition, determine the rate and type of weathering, and resultant clay minerals (e.g. Lowe, 1986, 1995; Hodder et al., 1990; Alloway et al., 1992; Lowe and Percival, 1993; Cronin et al., 1996). The relationship between accumulation of tephra and loess, and soil formation under different climates is summarised in Table 2.1.

**Table 2.1** Model of the relationship between the accumulation of loess or tephra and the formation of soil during periods of different climates, Wanganui region.

Climate	Accumulation of loess/tephra vs. soil formation
Warm (interglacial)	Soil formation > tephra >> AV loess >> QF loess
Mild (interstadial)	Soil formation $\geq$ tephra $\geq$ AV loess > QF loess
Cool (glacial-stadial)	QF loess $\geq$ or $\leq$ AV loess $\geq$ tephra > soil formation
Cold (glacial)	QF loess >> AV loess >> tephra >> soil formation

Notes:

AV, andesitic-volcanic; QF, quartzo-feldspathic

Source: After Palmer and Pillans (1996) and Newnham et al. (1999a)

Whereas the chronology of the last 50 ka is reasonably well known, the stratigraphy and chronology prior to this is still being developed, and any information that can be added will be of benefit. Some of the oldest paleosols recognised in New Zealand are on tephras of the Kauroa Ash sequence (Ward, 1967; Campbell, 1986), and this study has the potential to add resolution to the existing information available.

### 2.1.3 Tephra

The definition of 'tephra' in this study is outlined in Section 1.3.5.2.

The main value of tephra layers is their geologically instantaneous, widespread nature, meaning they are extremely useful as stratigraphic time-planes and/or marker horizons. As such, silicic tephras have been studied in New Zealand for over 60 years leading to a detailed understanding of their stratigraphy, distribution, and processes of eruption (Lowe, 1990; Froggatt and Lowe, 1990; Lowe and Newnham, 1999; Shane, 2000).

In the central North Island, eruptions from multiple volcanic centres (Figure 1.1) have resulted in extensive volcanic deposits, in places tens of metres thick (Lowe and Newnham, 1999; Shane, 2000). One difficulty near source, however, is that subsequent eruptions have tended to obliterate earlier deposits, and the stratigraphic record is incomplete (Krippner et al., 1998). It is possible that the accessible deposits in this proximal zone represent only a fraction of the eruptive history of the North Island (Shane et al., 1995, 1996a, 1996b; Shane, 2000). Tephra sequences in distal areas may be more complete in favourable circumstances, with many eruptions represented by (albeit) thinner deposits. Distal tephras are also often chemically and mineralogically more homogenous, and can have consistently distinctive physical characteristics (Moore, 1991; Manning, 1996; Black, 1992; Shane et al., 1996a).

### 2.1.4 Loess

Loess has been widely defined by many different authors. Many definitions are unnecessarily descriptive or prescriptive, when the reality is that, like many deposits, loess has significant natural variation in terms of thickness, grain size, colour, mineralogy, geochemical composition, geotechnical characteristics and morphology. Pye (1995) therefore advocated a relatively simple definition, describing loess as "a

terrestrial clastic sediment, composed predominantly of silt-sized particles, which is formed essentially by the accumulation of wind-blown dust". Lowe (1980) made a distinction between the descriptive definition of loess, that it is essentially unbedded and well-sorted silt, and the genetic definition of loess, that it is an aeolian deposit, ultimately of glacial origin.

Loessic beds have not previously been identified in the Kauroa Ash sequence. However, in recent years, visitors to the Woodstock section have remarked on the likelihood of there being some present. Though not comparable to the thick deposits found on the Chinese Plateau, there are considerable loess deposits in New Zealand (Cowie, 1964; Collen and Vella, 1984; Campbell, 1986; Kennedy, 1988, 1994). Most recently, Pillans and Wright (1990) and Palmer and Pillans (1996) described a 17-m-thick, 500 ka continuous sequence from the Wanganui Basin that contains 11 distinct loess beds. It seems entirely possible, therefore, that there could be at least some loess in a Waikato-based Quaternary sequence.

Loess is reported to have several distinguishing features. Colour is dominantly yellowish brown (Munsell colours 10YR 5/4-5/6); it is of friable to firm consistence (moderately weak to moderately firm soil strength); and it is usually permeable with weakly developed blocky or massive structures. Textures may range from clay in the oldest loesses, to clay loams in the younger loesses, to silt loams and fine sandy loams in the youngest loess (< 25 ka) (Kennedy, 1988). Pesci (1990) listed additional features, noting loess is "a loose deposit with coarse silt predominant in grain size, unstratified, porous, permeable... pale yellow colour".

### 2.1.5 'Tephric loess'

Pye (1995) recognised that the mineralogical variation between loess in different parts of the world reflects the nature of the surficial geology. The loess found in North Island, New Zealand, is likely to be different to a degree from that found elsewhere, in that a large proportion of it is comprised of reworked rhyolitic (and andesitic) tephra eroded from the central volcanic region (Vucetich, 1982; Kennedy, 1988, 1994). The term 'tephric loess' is suggested to describe such deposits (Pullar and Pollok, 1973; Milne and Smalley, 1979; Kennedy, 1994; Smalley, 1995; Newnham et al., 1999a).

There are some difficulties with 'tephric loess' as a term, however, such as the amount of tephra material required to justify using the adjective 'tephric'. Identification can also be problematic, especially where post-depositional pedogenic processes have taken place; any such deposit thus becomes largely indistinguishable from either 'reworked tephra' or 'loess' in the classical sense (Lowe, 1980). Therefore, for the purposes of this study an arbitrary distinction has been made: in the case of loess beds, where little or no evidence of a volcanic provenance can be discerned, the term 'loess' is used; where the bed is 'loess-like' but with evidence of appreciable tephric material (barring pumice lapilli, as per Kennedy, 1994), the term 'tephric loess' is used.

## 2.2 KAUROA ASH SEQUENCE IN THE WESTERN WAIKATO

### 2.2.1 Distribution

Reconnaissance fieldwork revealed patchy exposures of Kauroa Ash beds (K-beds) at a wide range of locations across the western central North Island. The sequence is incomplete (does not contain all of members K1-K15) in most places, however, and apart from the two sections already known, Woodstock (Ward, 1967; Salter, 1979) and Papakura Creek (Pain, 1975), only one other thick (>10 m) section, on the Tiritirimatangi Peninsula, was found.

The K-beds are particularly well preserved in the Raglan and Kawhia districts on the west coast (Figure 1.3). In the Raglan district, moderately thick sequences (>2 m) are found on flat lying and gently sloping surfaces on the tops of ridges composed of basaltic lava or Tertiary mudstone, and on mounds of scoria and tuff. At Kawhia, K-beds are especially well exposed in cliffs around the harbour, and in road-cuttings through the relatively low-lying undulating hill country surrounding it. K-beds are not found on the ranges between the west coast and SH31, presumably removed by erosion, though occasional sections are found in the plateau uplands between Raglan and Kawhia. These latter sections are usually shallow, consisting of just one or two members or beds, making identification and definition near impossible if a 'marker bed' is not present. It is clear that the long comprehensive sequences found are the exception rather than the norm, and that the majority of the Kauroa Ash sequence has been eroded away.

### 2.2.2 Main field sites

Throughout the thesis, grid references for all sites are based on the 1:50,000 metric map series NZMS 260, and comprise sheet number and coordinates.

#### 2.2.2.1 Woodstock

‘Woodstock’<sup>1</sup>, near Raglan (Figure 1.3), is the type locality as proposed by Ward (1967). The 15 m-thick section contains the 15 members of the sequence, and may contain as many as 44 constituent beds. It is underlain by basaltic deposits of the Okete Volcanic Formation, and overlain by the Hamilton Ash Formation with a marked unconformity.

Figure 2.1 illustrates the section, noting some of the key members. The stratigraphy is detailed in the Figure 2.2 (key for Figures 2.1-2.14 on page 26).

#### 2.2.2.2 Papakura Creek

‘Papakura Creek’, near Oparau (Figure 1.3), is the type locality of the Oparau Tephra, as proposed by Pain (1975). The 20 m-thick section contains members K6 to K15 (base obscured) and is overlain by the Hamilton Ash Formation. Dominating the sequence is the c. 3.5 m-thick ignimbrite, the Oparau Tephra. The section also contains two other distal ignimbrites, here informally named PCM1 and PCM3. PCM2 was also assigned a separate name because of noteworthy field characteristics<sup>2</sup>.

Figure 2.3 illustrates the section, noting boundaries between members. The stratigraphy is detailed in Figure 2.4.

#### 2.2.2.3 Tiritirimatangi Peninsula

The ‘Tiritirimatangi Peninsula’ section is a c. 28 m-thick exposure on the western end of the peninsula. It contains most of units K3 to K15 (K6 to K8 are evidently missing) and is dominated by the c. 6 m-thick Tiritiri ignimbrite that forms the current shoreline.

---

<sup>1</sup> The name derives from the original name of the adjacent farm.

<sup>2</sup> Extremely high quartz crystal content of the bed.



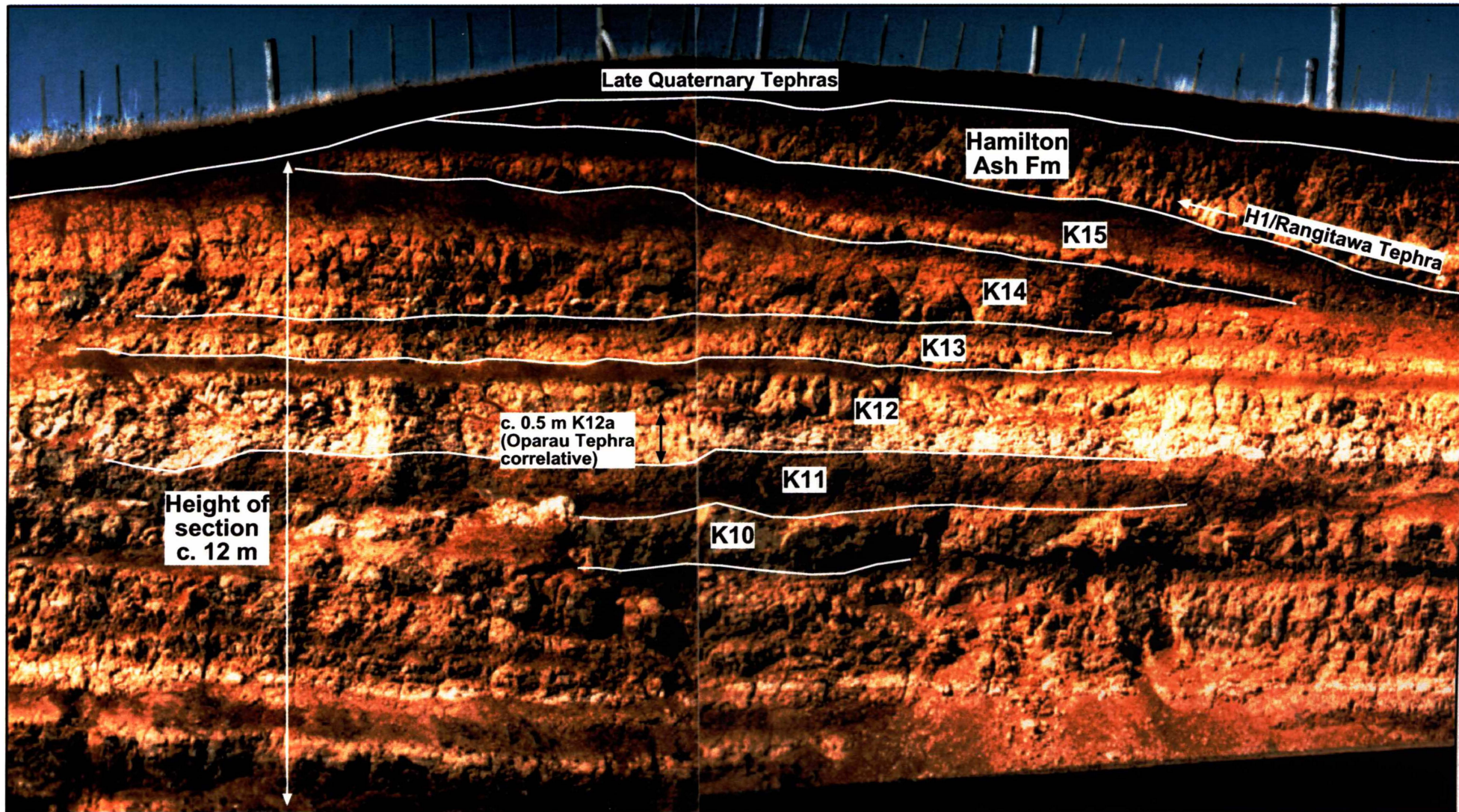


Figure 2.1 Stratigraphy of (upper) Woodstock section, Kauroa Ash sequence type site (Photo H.S. Gibbs). Lowermost beds are out of view (left).

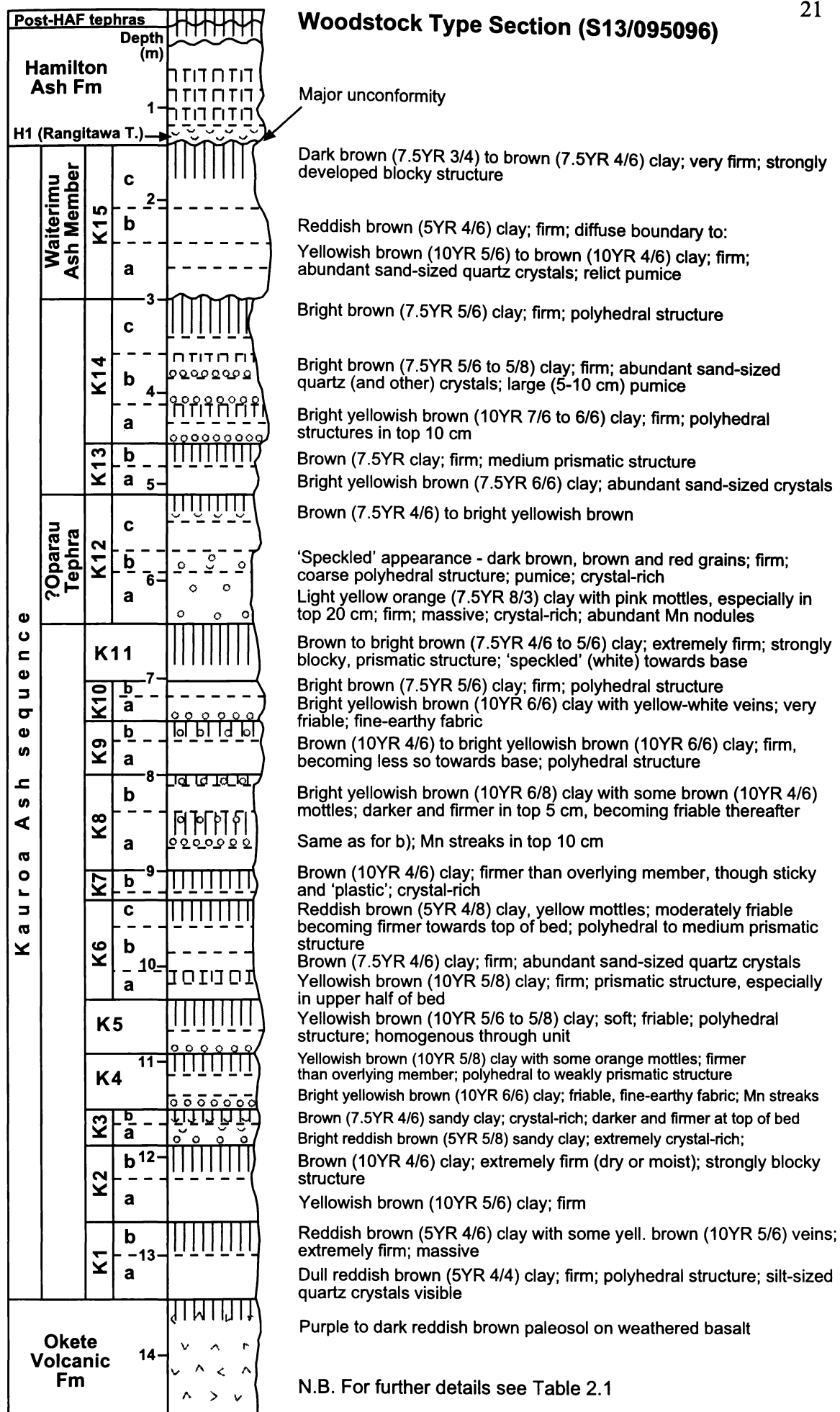


Figure 2.2 Stratigraphy and field properties of Woodstock type site (key on page 26).



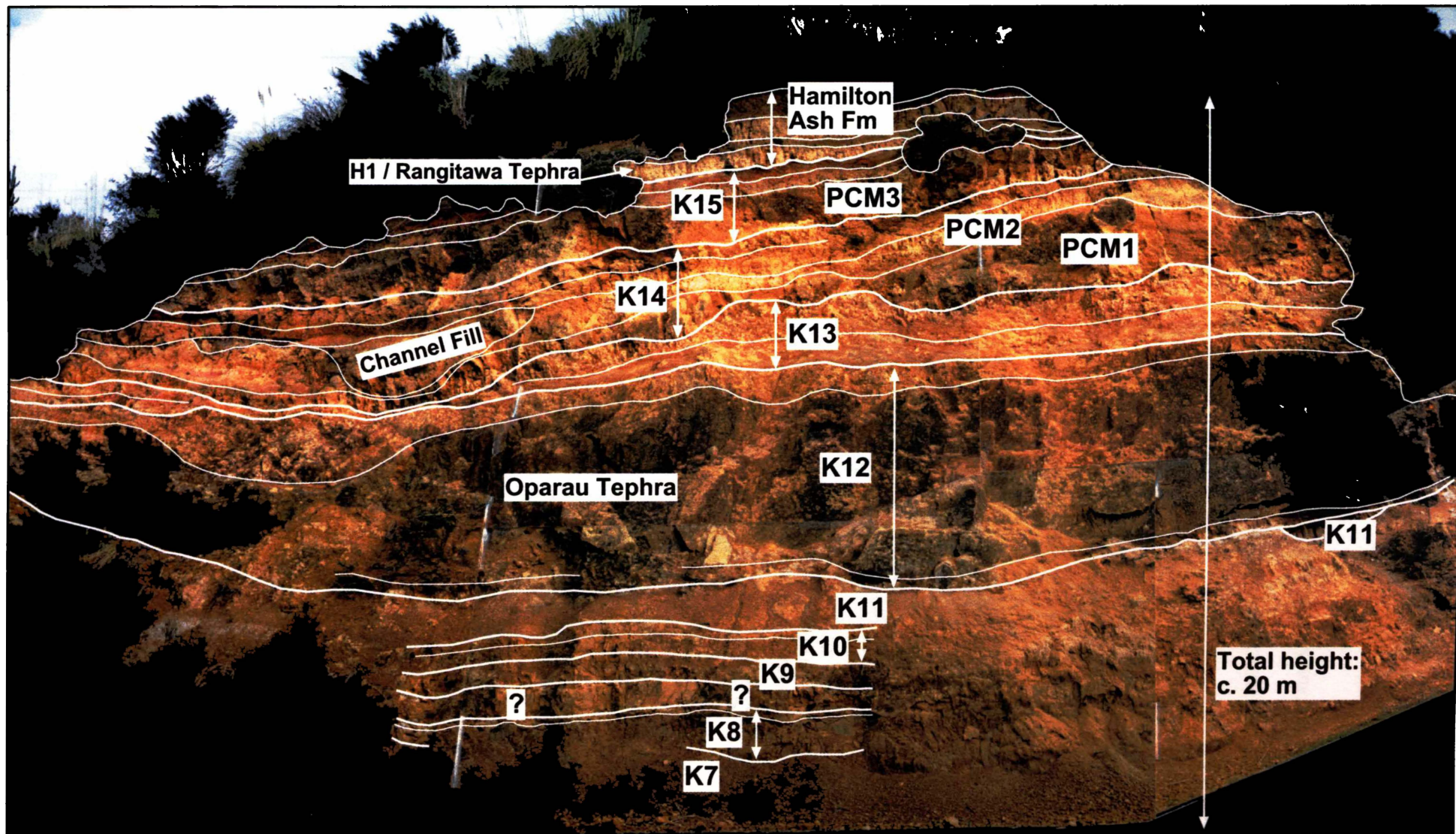


Figure 2.3 Annotated photograph of the stratigraphic relationships at the Papakura Creek site (type site of the Oparau Tephra).

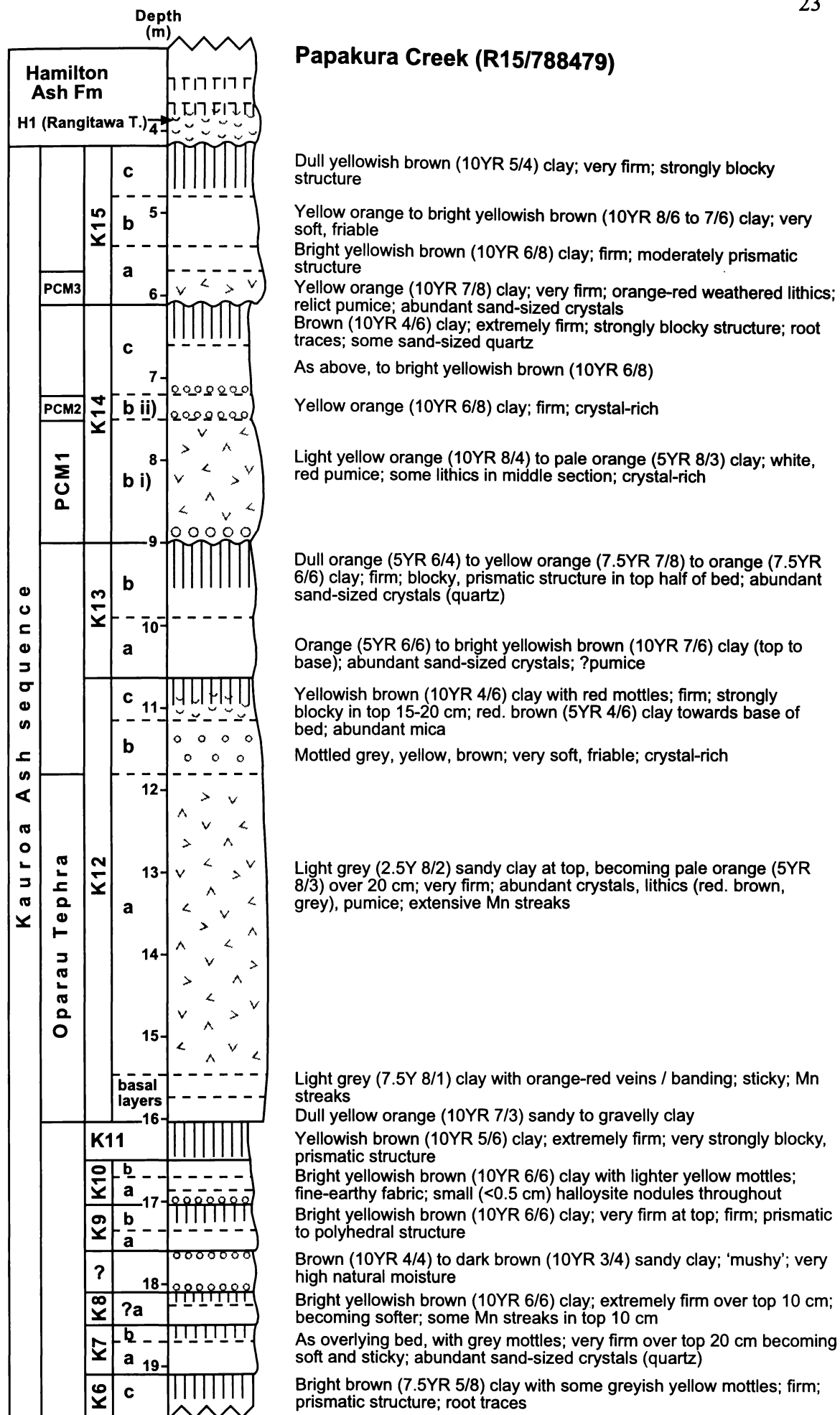


Figure 2.4 Stratigraphy and field properties of Papakura Creek section (key on page 26).



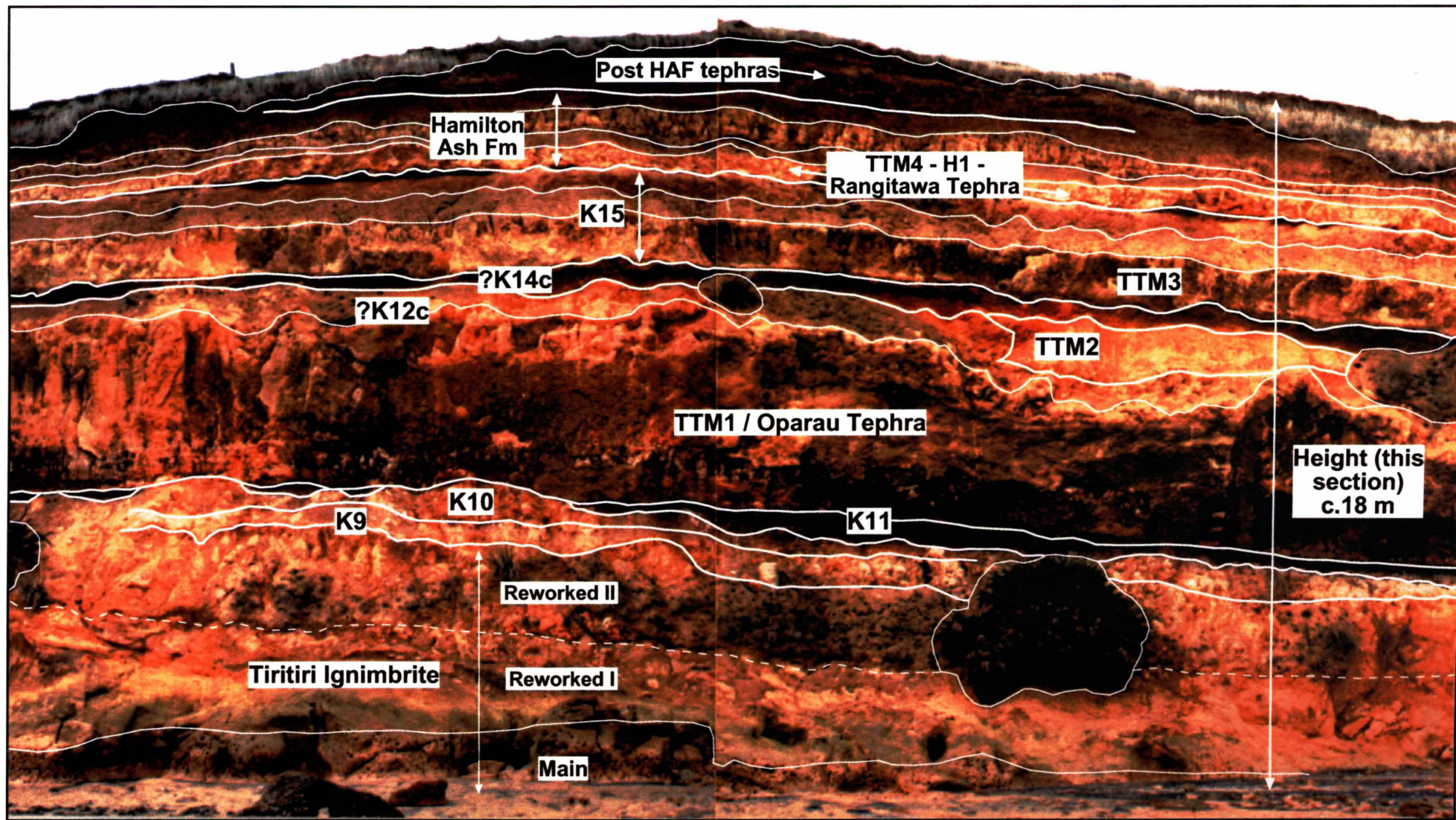


Figure 2.5 Annotated photograph of the stratigraphic relationships at the Tiritirimatangi Peninsula site

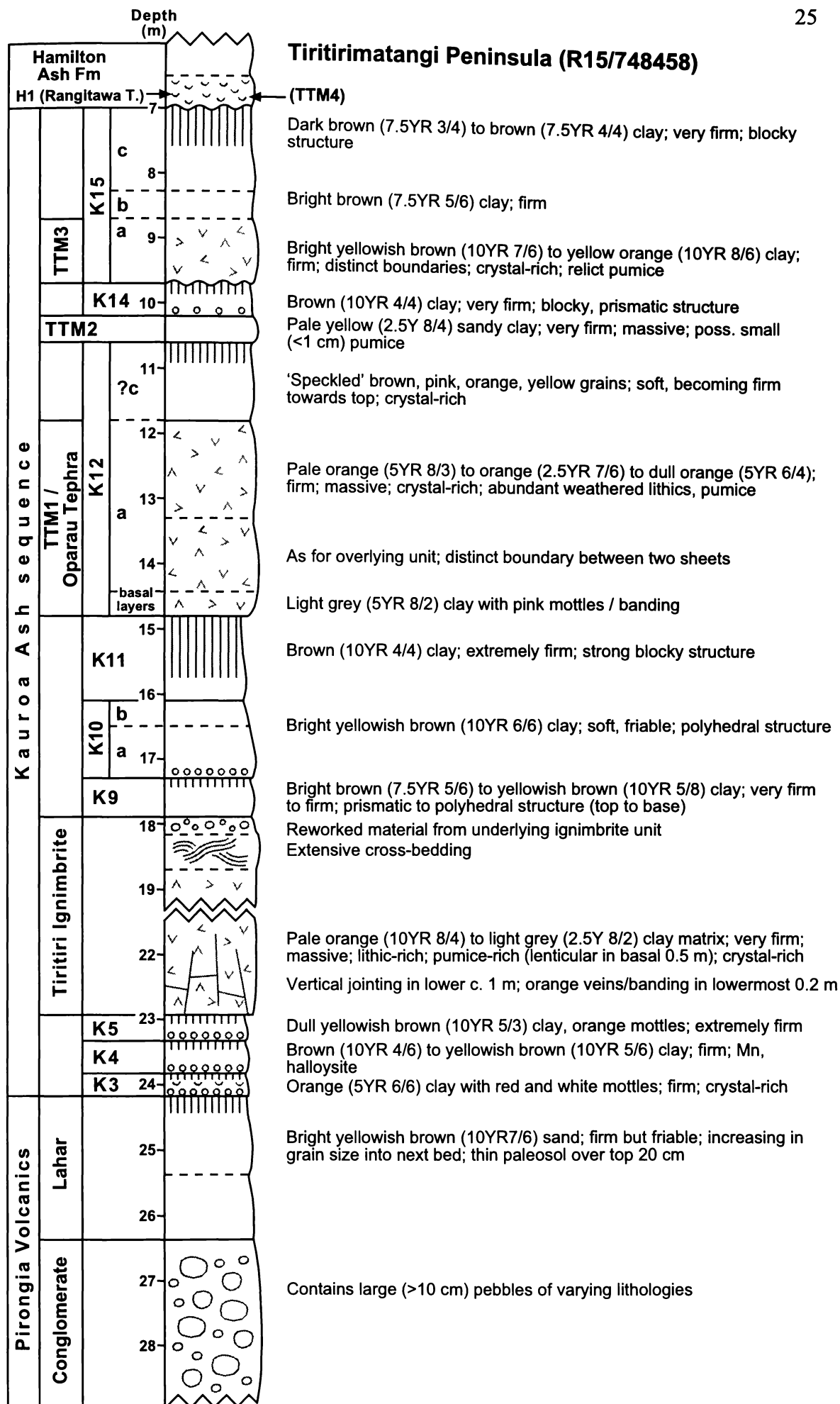


Figure 2.6 Stratigraphy and field properties of Tiritirimatangi Peninsula section (key on page 26).

This unit was defined by Fergusson (1986). Further south along the peninsula, the Tiritiri ignimbrite rests on three Kauroa members (K3-K5) that are in turn underlain by a lahar deposit of the Pirongia Volcanics. At least three other major tephra deposits (possibly ignimbrites) are seen in the exposure; they are informally named TTM1 – TTM3. TTM1 is provisionally correlated (stratigraphic evidence and field observations) with the Oparau Tephra, though it is considerably more weathered than that seen at the type section nearby.

Figure 2.5 illustrates the section, noting some of the key members. The stratigraphy is detailed in Figure 2.6.

#### 2.2.2.4 Other sections




Other, shallow, sections examined in this study are illustrated in Figures 2.7 – 2.14.

### 2.3 FIELD PROPERTIES OF KAUROA ASH MEMBERS

This section is largely a compilation of observations from all sections examined. A summary of field properties is outlined in Table 2.2. Descriptions are after Milne et al. (1995).

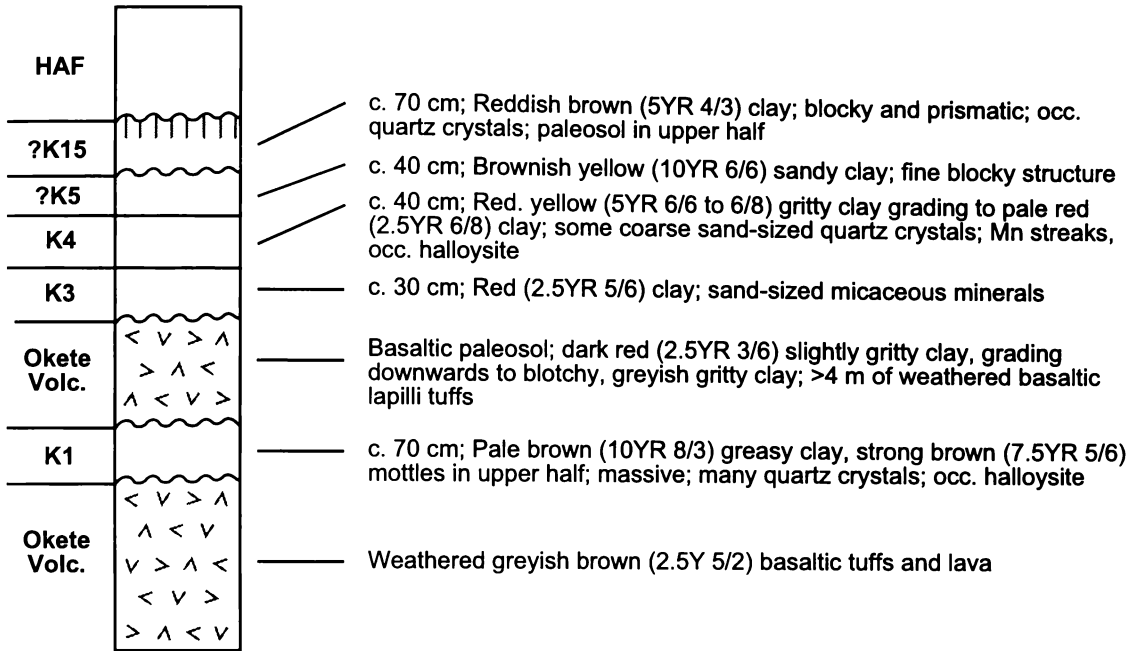
#### 2.3.1 *Visual identification of beds*

Individual beds in any single section are usually easily definable in the field due to their differing characteristics, most notably colour and consistence. Colours vary from dark to bright browns, to yellowish browns and occasional red, orange, yellow and white-toned beds. Consistences under moist conditions range from friable to extremely firm. Where only a few beds are present in shallower sections, identification is somewhat more difficult and other characteristics, in addition to stratigraphic position, are usually required for correlation and assignment of member names.

<u>KEY TO FIGURES 2.1-2.14:</u>	
	Paleosol
oooooo	Halloysite nodules
~ ~ ~ ~	Micaceous flakes
∨ ^ < ^	Primary volcanic unit
	Cross-bedding
	Gravel to pebble-sized material
	Vertical jointing
<b>HAF</b>	Hamilton Ash Formation
<b>Rang T.</b>	Rangitawa Tephra

**Maungatawhiri  
Ohiapopoko Cone\***

(R14/787722)

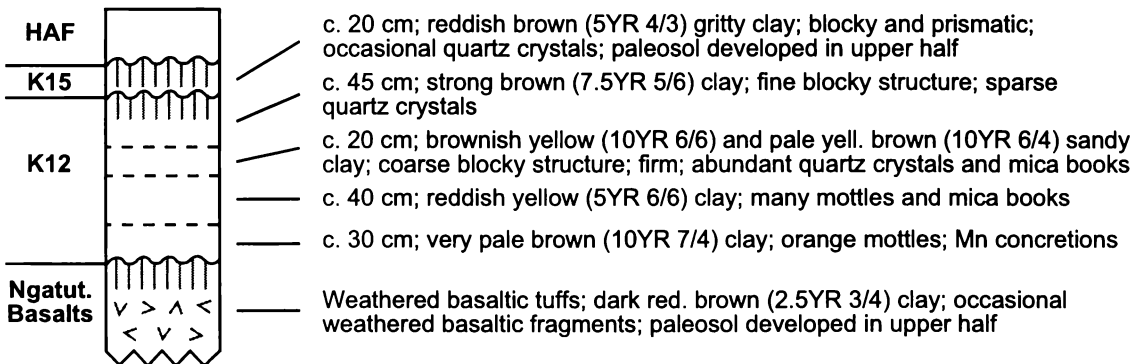


**Figure 2.7** Stratigraphy of section at Ohiapopoko Cone, east side of Kauroa-Te Mata Road (after Briggs et al., 1989)

\* Section '4' on Figure 1.3; key on page 26

**Foxs Centre\***

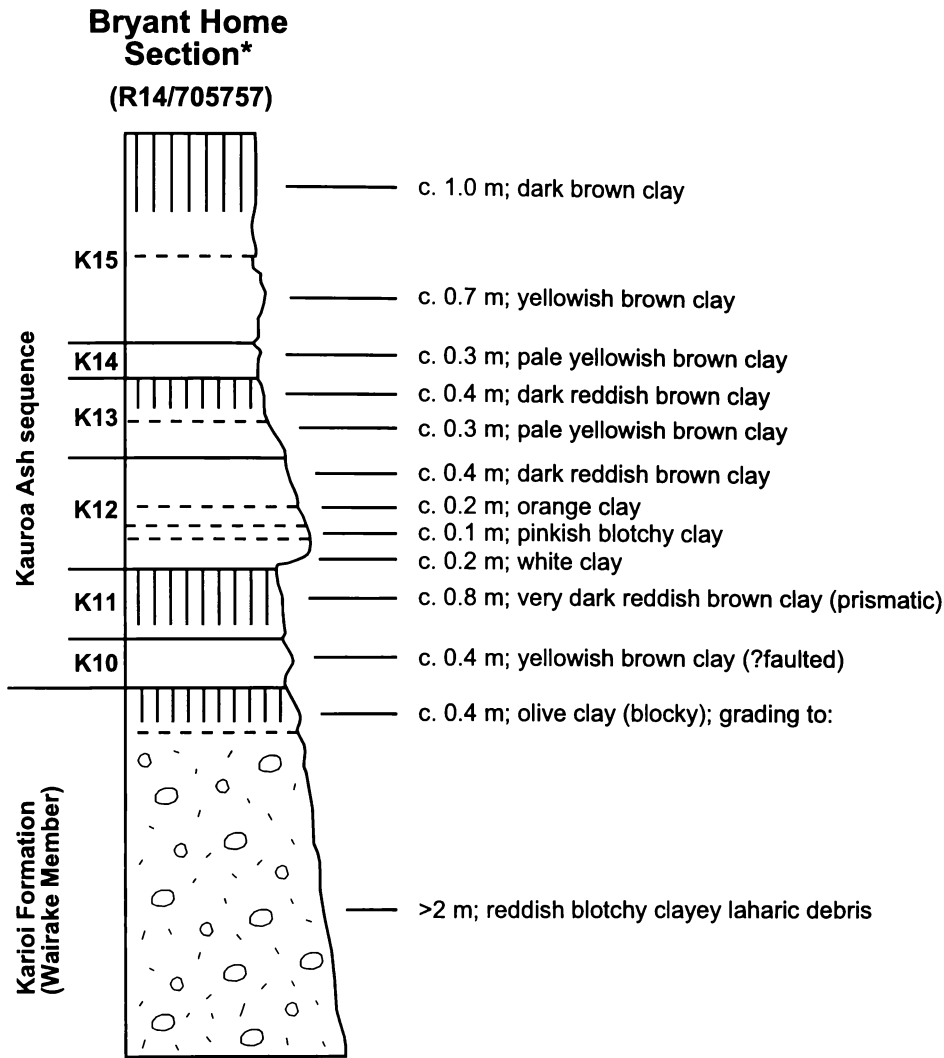
(R13/756076)



**Figure 2.8** Stratigraphy of section at Foxs Centre, south side of Waikaretu Road (after Briggs et al., 1989)

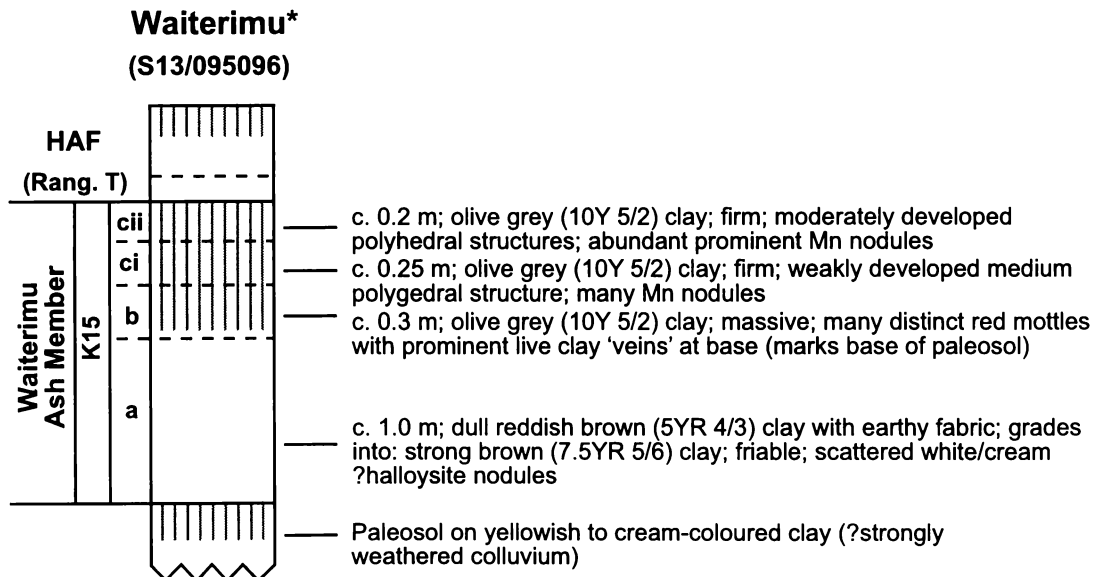
\* Location on Figure 1.1; key on page 26





**Figure 2.9** Stratigraphy of the Bryant Home section, east side of Whanga Road (after Lowe et al., in press)

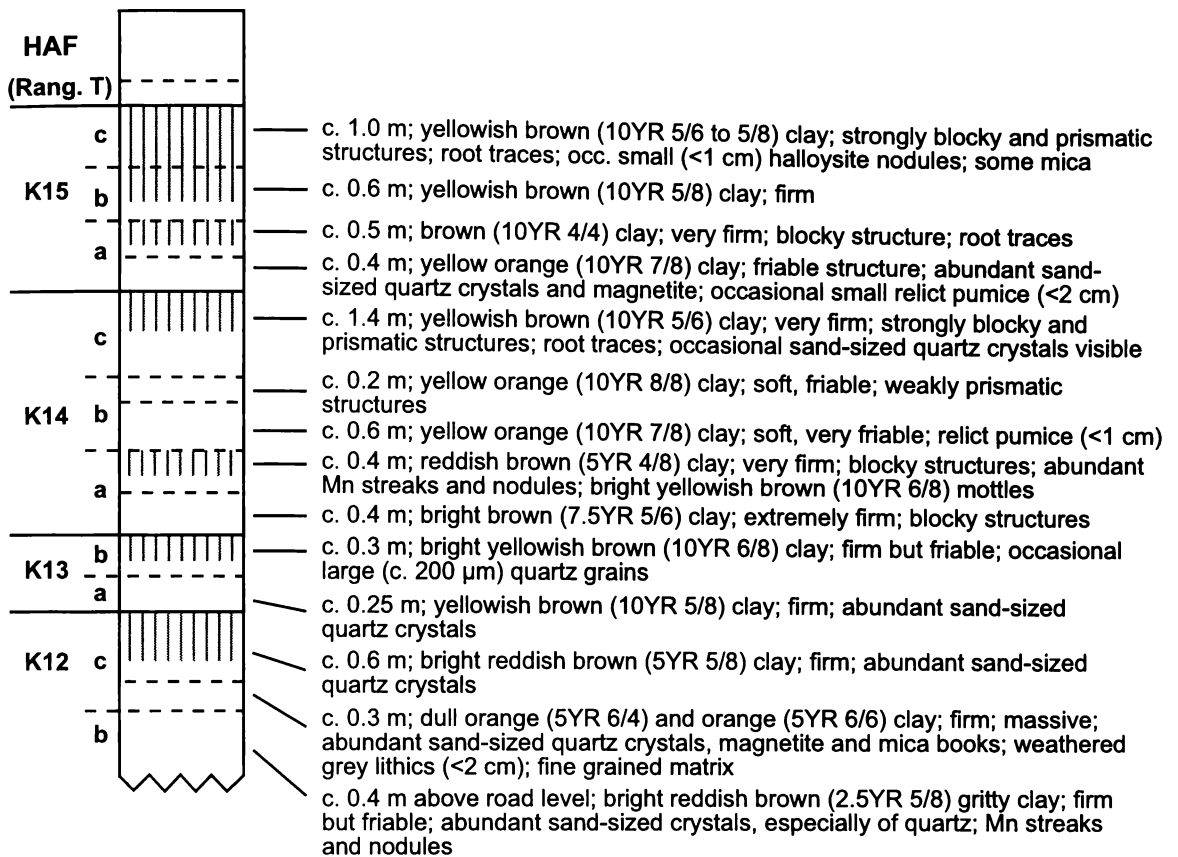
\* Section '5' on Figure 1.3; key on page 26



**Figure 2.10** Stratigraphy of Waiterimu section, Tahuna Road (type locality for Waiterimu Ash Member [K15] of Ward, 1967)

\* Location on Figure 1.1; key on page 26

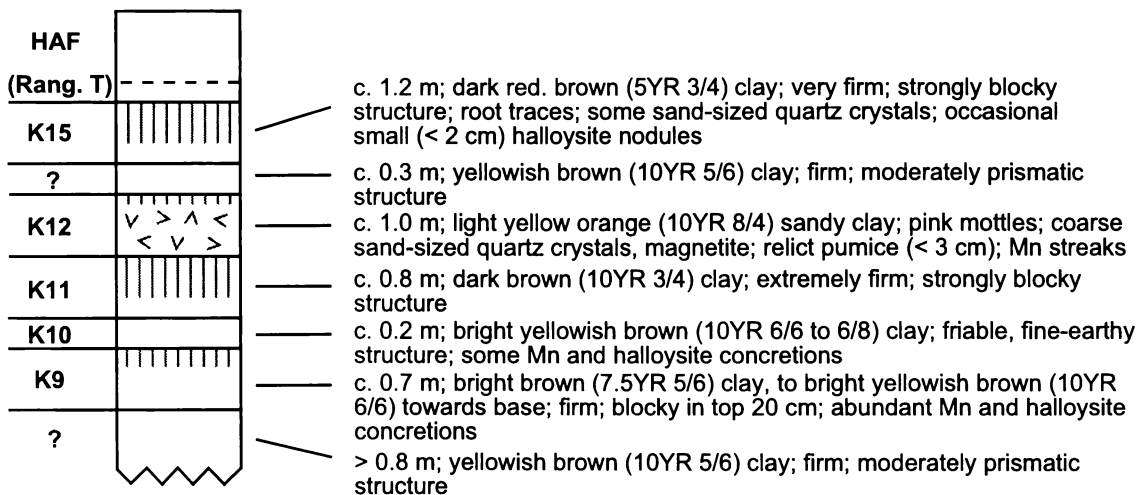
**Aotea Harbour\***  
(R15/718504)



**Figure 2.11** Stratigraphy of Aotea Harbour section, east side of Aotea Road

\* Section '6' on Figure 1.3; key on page 26

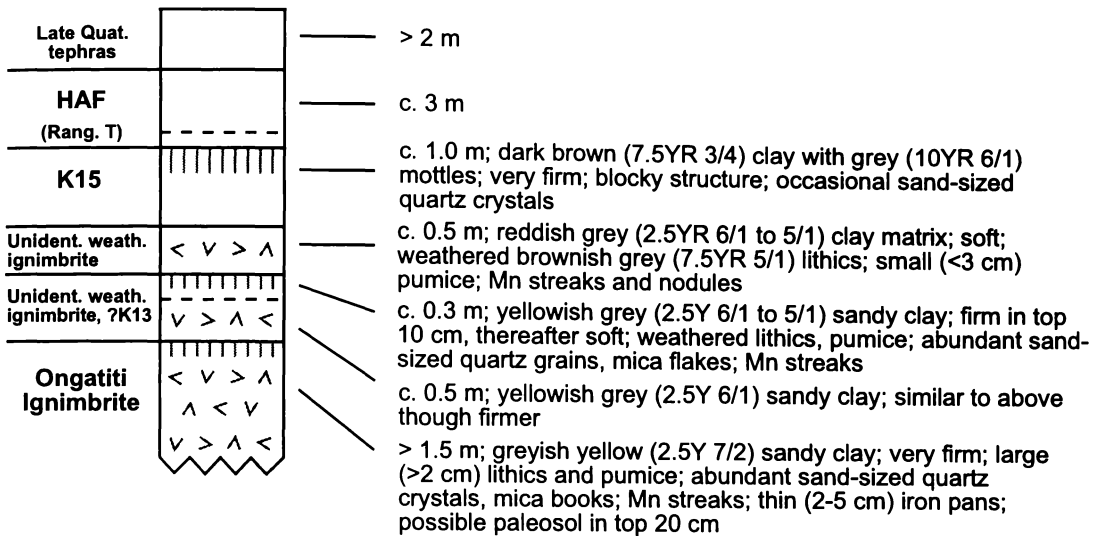
**Taharoa Corner\***  
(R15/801437)



**Figure 2.12** Stratigraphy of Taharoa Corner section, Kawhia Harbour Road

\* Section '7' on Figure 1.3; key on page 26

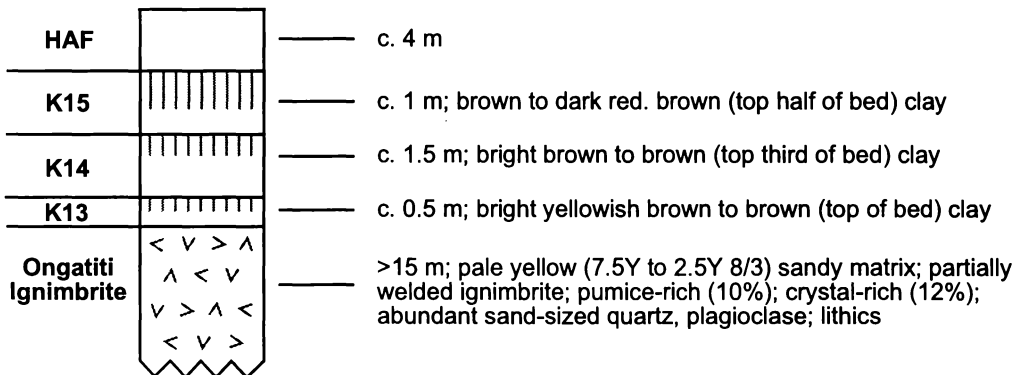
**Wyllies Hill\***  
(S15/155445)



**Figure 2.13** Stratigraphy of Wyllies Hill section, east side of SH3

\* Section '8' on Figure 1.3; key on page 26

**Hinuera Quarry\***  
(T16/461614)



**Figure 2.14** Stratigraphy of Hinuera Quarry section, off SH27

\* Location on Figure 1.1; key on page 26

**Table 2.2** Summary of field properties of the Kauroa Ash sequence.

MEMBER	BED	DESCRIPTION/LITHOLOGY
K15	c	Distinct but irregular upper boundary with Hamilton Ash. Dark brown (7.5YR 3/4) clay grading into brown (7.5YR 4/6) clay over 20 cm. Very firm at top, becoming gradually less so. Well-developed blocky structure. Abundant sand-sized crystals visible (quartz).
	b	Reddish brown (5YR 4/6) clay. Firm. Diffuse boundary marking structural change to:
	a ii	Bright brown (7.5YR 5/6) clay grading into orange (7.5YR 6/6) clay over 10 cm. Firm. Massive. Abundant (tiny) crystals; possible small pumice fragments.
	a i	Brown (10YR 4/6) clay. Very firm. Very fine-grained. Some small pumices (1-6 cm); sand -sized crystals visible.
K14	c	Bright brown (7.5YR 5/6-5/8) clay homogenous through unit. Some sand-sized crystals visible, in places, abundant crystals forming discrete layers (<1 cm thickness). Firm. Polyhedral structure. Halloysite nodules mark base.
	b ii	Bright brown (7.5YR 5/6-5/8) clay. Firm. Abundant sand-sized crystals.
	b i	Bright brown (7.5YR 5/6-5/8) clay. Firm. Large pumice fragments (5-10 cm), red staining. Siliceous concretions. Abundant sand-sized crystals (mostly quartz). Large halloysite nodules / bed at base.
	a	Distinct colour change to a very much lighter 'bright yellowish brown' (10YR 7/6-6/6). Firm. Polyhedral structure. Halloysite nodules forming a distinct layer at the base of the unit.
K13	b	Significant colour change from unit above to brown (7.5YR 4/6) clay. Firm. Medium prismatic structure.
	a	Increasing in value to bright yellowish brown (7.5YR 6/6). Diffuse, indistinct boundary to:
K12	c	Brown (7.5YR 4/6) clay gradually increasing in value to bright yellowish brown (7.5YR 6/6) clay. Firm. Coarse polyhedral structure. Indistinct boundary to:
	b	Matrix same in colour, but increasing in 'speckled' nature, some dark brown, brown and red grains – coarse polyhedral structure, crystal / mineral rich. Occasional relict pumice fragments. Suggests is partly or wholly reworked material from underlying bed. Diffuse boundary but distinct change into:
	a	Light yellow orange (7.5YR 8/3) clay, with pink mottles, especially towards the top. Firm, massive. Crystal rich. Extensive small halloysite (white / pink) and manganese (brown / black) nodules throughout. Mass-emplaced unit, weathered distal ignimbrite.
K11		Straight, distinct boundary. Brown to bright brown (7.5YR 4/6-5/6) clay. Extremely hard when dry or moist, large strongly developed prismatic structure. Towards the base of the unit becomes 'speckled' (white, brown, dark brown).
K10	b	Bright brown (7.5YR 5/6) clay. Firm, abundant (quartz) crystals visible. Polyhedral structure.
	a	Bright yellowish brown (10YR 6/6-6/8) clay, with yellow-white veins. Very friable, fine-earthly fabric. Halloysite nodules mark a distinct boundary at base.

K9	b	Brown (10YR 4/6) clay, extensive manganese nodules, and some small halloysite nodules. Firm, becoming slightly less so towards the base. Diffuse boundary to:
	a	Colour increasing in value towards the base – brown to yellowish brown to bright yellowish brown (10YR 5/6-6/6). Polyhedral structure.
K8	b	Bright yellowish brown (10YR 6/8) clay, with some brown (10YR 4/6) mottles. Darker and firmer in the top 5-10 cm. Friable thereafter. Blocky structure. Halloysite nodules mark a distinct boundary to:
	a	Similar in colour and mottling. Extensive manganese nodules towards the top of the bed. Becoming more friable down the unit. Diffuse lower boundary.
K7		Brown (10YR 4/6) clay. Distinct textural change. Firmer than overlying unit, more 'plastic'. Abundant sand-sized crystals visible; probable tephra unit.
K6	c	Reddish brown (5YR 4/6-4/8) clay. Moderately friable, becoming firmer towards the top of the bed. Polyhedral structure.
	b	Brown (7.5YR 4/6) clay. Firm. Abundant sand-sized crystals visible, probable tephra unit.
	a	Yellowish brown (10YR 5/8) clay. Firm. Some weak prismatic structures.
K5		Yellowish brown (10YR 5/6-5/8) to bright brown (7.5YR 5/6-5/8) clay. Soft, friable. Polyhedral structure. Homogenous throughout the unit.
K4	c	Yellowish brown (10YR 5/8) clay with some yellow orange (10YR 7/8) mottles. Firmer than overlying unit. Abundant silt-sized quartz visible. Polyhedral to weakly prismatic structure.
	b	Bright yellowish brown (10YR 7/6) clay. Moderately firm. Occasional crystals visible.
	a	Bright yellowish brown (10YR 6/6) clay. Friable, fine-earthly fabric. Polyhedral structure. Mn staining and nodules. Distinct boundary marked by halloysite nodules.
K3	b	Brown (7.5YR 4/6) sandy clay. Abundant sand-sized crystals throughout. Darker and firmer at the top of the bed.
	a	Bright reddish brown (5YR 5/8) clay. Distinct (primary) tephra bed. Extremely crystal rich – coarse sand-sized crystals easily visible (primarily quartz, mica and magnetite). Prismatic structures towards the top of the unit. Occasional small halloysite nodules. Sharp distinct boundary marked by halloysite nodules.
K2	b	Brown (10YR 4/6) clay. Extremely hard when dry or moist. Well-developed blocky structure. Some small manganese nodules near top of unit.
	a	Yellowish brown (10YR 5/6) clay. Firm.
K1	b	Reddish brown (5YR 4/6) clay. Extremely firm. Massive. Some yellowish brown (10YR 5/6) veins visible.
	a	Dull reddish brown (5YR 4/4) clay. Firm. Polyhedral structure. Possible relict pumice. Tiny (?silt-sized) quartz grains visible.

### 2.3.2 Identification of paleosols

As defined by Ward (1967) and subsequently Pain (1975), the Kauroa Ash sequence is separated from the overlying Hamilton Ash Formation by a well-defined erosional disconformity. Below this, the uppermost member, K15, is separated from underlying members by a minor unconformity. Thereafter, no major discontinuities are discernible, and deposition appears to have been fairly 'continuous'.

The presence of some strongly developed<sup>3</sup> paleosols indicates, however, that certain land surfaces persisted (hence soils developed or evolved) for some considerable amount of time before another significant eruption occurred, or that tephra accumulated in thin increments via pedogenic 'upbuilding' (Almond and Tonkin, 1999). The term 'paleosol' is used here in the sense of one or more buried soil horizons, typically B horizons (e.g. Bt, Btg, Bw), that represent part of the solum of a soil profile once at or near the land surface.

Very strongly developed paleosols are found at the top of members K1, K5, K6, K11, K13 and K15. All are a dark brown colour sometimes with a reddish hue, extremely firm consistence, and often with blocky or prismatic structures. Many also exhibit clay veins and manganese nodules that appear similar to those found in the modern soil (e.g. Hamilton or Naike soils) where tephra is exposed at the surface. Furthermore, in many cases, it is possible to see soil plant and organism impressions (root traces or rootlet pseudomorphs), all indicative that the material was once part of the solum of a modern soil profile. As a result, these beds are very distinctive and provide excellent marker horizons.

Moderately developed<sup>4</sup> paleosols are also formed on members K8, K9, K12 and K14. In addition to these ten paleosols previously identified by Salter (1979), this study recognises four additional moderately developed paleosols. These occur at the top of beds K2b, K3b, K4c, and K14a (e.g. Figure 2.2). There is also the possibility that weak paleosols have been formed on K6a, K7, K8a and K14b. Thus there is a total of at least 14 and possibly 18 paleosols in the sequence.

---

<sup>3</sup> Dark brown colour, very firm consistence, strongly developed pedality with blocky or prismatic structures.

<sup>4</sup> Dark brown colour, firm consistence, blocky or prismatic structures.

As noted by previous workers (Ward, 1967; Salter, 1979; Kirkman, 1980), all beds have very high clay contents. Halloysite is by far the major component (T.G. Shepherd, unpublished data; Briggs et al., 1994a; Shepherd, 1994). It is found throughout the sequence, sometimes forming a discrete but distinct white bed between adjoining units, or as layer of nodules<sup>5</sup>, for example between K14 and K13, K10 and K9, K4 and K3, etc. It is often found in association with extensive Mn nodules. This would suggest that silicon enrichment through wetting-drying and perching (slow drainage) has occurred (Stevens and Vucetich, 1985; Lowe, 1986).

### 2.3.3 Tephra ('volcanigenic') beds

Very few of the Kauroa Ash members could unequivocally be called 'primary tephra', such is the extent of their weathering. However, various features are indicative of a volcanigenic origin (i.e. ultimately tephra deposits). These include the presence of: pumice fragments (usually small, < 1 cm), abundant silt to sand-sized crystals, siliceous concretions, streaks of manganese oxides, occasional (weathered-out) lithic pseudomorphs, and a generally paler colour than the paleosols developed on them. A sharp contact with underlying members is also suggestive, though not necessarily definitive, of a rapid emplacement.

Some beds are particularly easy to recognise in the field, forming distinct marker beds: K3, bright pinkish-orange in colour, has abundant coarse sand and micaceous crystals and a sharp contact with the underlying K2 paleosol marked with small halloysite concretions; K12a is a pale pink-white bed with darker pink mottles, abundant sand-sized crystals visible throughout (especially quartz), extensive Mn staining, massive, firm and with sharp boundaries.

Other members with characteristics suggestive of a volcanigenic origin are: the lower portions of K1, K4c, K7, K10b, K12b, K14bi, K15a, b and c. Some units, especially K12b and K14bii, are thought to represent reworking of the underlying unit or a subsequent phase of the same eruption. No bedding features are evident, such

---

<sup>5</sup> Vary in diameter from 1 to 10 cm. Nodules are extremely hard but can be broken with a hammer to reveal a greyish white material with streaks and blotches of pinkish red material, probably an iron oxide. X-ray diffraction analysis of the white material showed it to be composed of well-ordered halloysite (Kirkman, 1980).

characteristics being unlikely to have survived the weathering and pedogenesis that has taken place.

#### 2.3.4 Loess beds

Some beds appear to have no particularly diagnostic features (K4a-b, K5, K6a, K8ai, K8bi, K10a and K14a). These beds are typically a yellow-brown to bright-yellowish brown clay, sometimes with faint bright brown to orange mottles. In consistence, they range predominantly from moderately firm to friable, have a fine-earthy fabric, and in structure range from spheroidal to structureless (massive). No sand-sized crystals are visible to the naked eye. All these features contrast with those of tephra (volcanogenic) beds. The working hypothesis from these observations is that these beds represent 'loess' deposits, and are designated as such hereafter.

#### 2.3.5 Tephric-loess beds

A final type of deposit is recognised and is thought to be a combination of tephra and loess and is here designated 'tephric loess'. These are beds that have characteristics of both tephra and loess (yellow-brown colour, brown mottles, varying in consistency from firm to friable, visible silt-sized crystals, etc.), and are inferred to be loess formed through erosion and deposition of tephric material. An alternative origin is that they are the result of frequent but thin accessions of tephra (and possibly other wind-blown material) to form a composite bed that is difficult or impossible to definitively categorise as either 'tephra' or 'loess'. As discussed earlier, a genetic origin is difficult to prove where the deposits are as strongly weathered as the Kauroa Ash sequence. However, from field observations, these beds, K2a, K4b, K9a, and K14c, have sufficiently different characteristics from both those described as 'tephras' and those described as 'loess' to warrant a separate category. It is appreciated that these beds may well be extremely weathered tephra, but they are here provisionally separated on the basis of additional 'loess-like' properties.

### 2.4 FACIES CLASSIFICATION

Based on its field properties alone, the Kauroa Ash sequence has been divided into facies, loosely based on concepts common in sedimentology. Wilson and Walker (1982) defined facies as "rock units that can be defined by their morphology, relative



superposition, composition and grain-size characteristics". The Kauroa Ash sequence has been divided as such, though in this case 'facies' are also interpretive (i.e. genetic): paleosols, tephra ('primary' and 'very weathered'), loess and 'tephric-loess'. Facies units are defined on a 'bed-by-bed' basis (listed in Table 2.3; illustrated in Figure 2.15).

**Table 2.3** Facies classification of K-beds at Woodstock.

MEMBER	BED	PALEOSOL	DOMINANT FACIES
K15	c	Paleosol (vs) <sup>a</sup>	(Tephra, vw)
	b		Tephra, vw
	a ii		Tephra, vw
	a i		Tephra
K14	c ii	Paleosol (m) <sup>a</sup>	(Tephric-Loess) <sup>c</sup>
	c i		Tephric-loess
	b ii	Paleosol (w) <sup>b</sup>	Tephra, vw
	b i		Tephra
	a ii		Loess
a i	Loess		
K13	b	Paleosol (vs) <sup>a</sup>	---
	a		Tephra
K12	c ii	Paleosol (m) <sup>a</sup>	(Tephra)
	c i		Tephra, vw
	b		Tephra
	a		Tephra
K11		Paleosol (vs) <sup>a</sup>	---
K10	b		Tephra
	a		Loess
K9	b	Paleosol (m) <sup>a</sup>	---
	a		Tephric-loess
K8	b ii	Paleosol (m) <sup>a</sup>	(Loess) <sup>c</sup>
	b i		Loess
	a ii	Paleosol (w) <sup>b</sup>	(Loess)
	a i		Loess
K7	b	Paleosol (w) <sup>b</sup>	(Tephra, vw)
	a		Tephra, vw
K6	c	Paleosol (vs) <sup>a</sup>	---
	b ii		Tephra, vw
	b i		Tephra, vw
	a ii	Paleosol (w) <sup>b</sup>	(Loess) <sup>c</sup>
	a i		Loess
K5	b	Paleosol (s) <sup>a</sup>	(Loess)
	a		Loess
K4	c	Paleosol (m) <sup>b</sup>	(Tephra) <sup>c</sup>
	b		Tephric-loess
	a		Loess
K3	b	Paleosol (m) <sup>b</sup>	(Tephra)
	a		Tephra
K2	b	Paleosol (m) <sup>b</sup>	(Tephric-loess) <sup>c</sup>
	a		Tephric-loess
K1	b	Paleosol (vs) <sup>a</sup>	---
	a		Tephra, vw

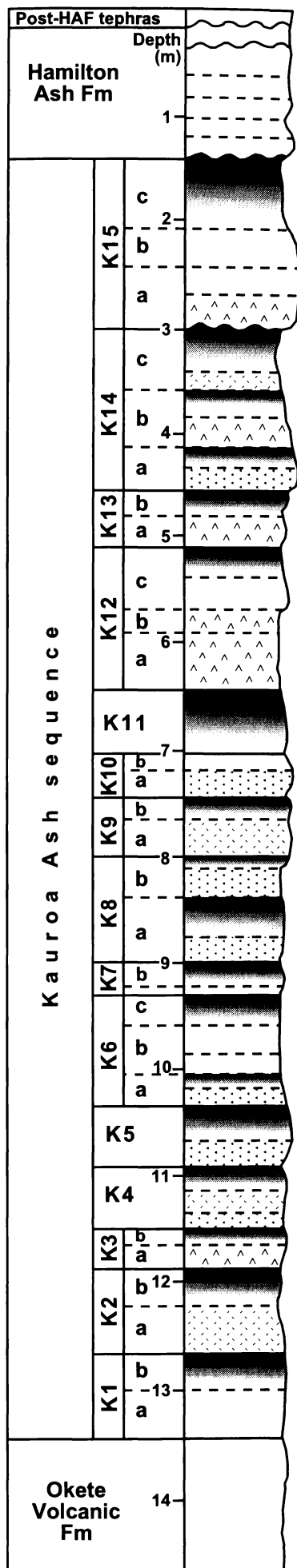
**PALEOSOLS:**

(vs) very strongly, (s) strongly, (m) moderately, (w) weakly developed paleosol  
<sup>a</sup> as defined by Salter (1979); <sup>b</sup> as defined by this study.


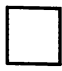



**FACIES:**

<sup>c</sup> best estimation of parent material; 'vw' very weathered

--- paleosol is dominant facies / parent material not determinable



KEY:

-  Paleosol<sup>‡</sup>
-  Very weathered tephra / soil
-  (Primary) tephra fall / ignimbrite
-  Tephric-loess
-  Loess

**Figure 2.15** Facies of the Kauroa Ash sequence.  
 (based on the Woodstock type section)  
<sup>‡</sup> Paleosol is the dominating facies

## 2.5 IDENTIFICATION AND DEFINITION OF ADDITIONAL UNITS

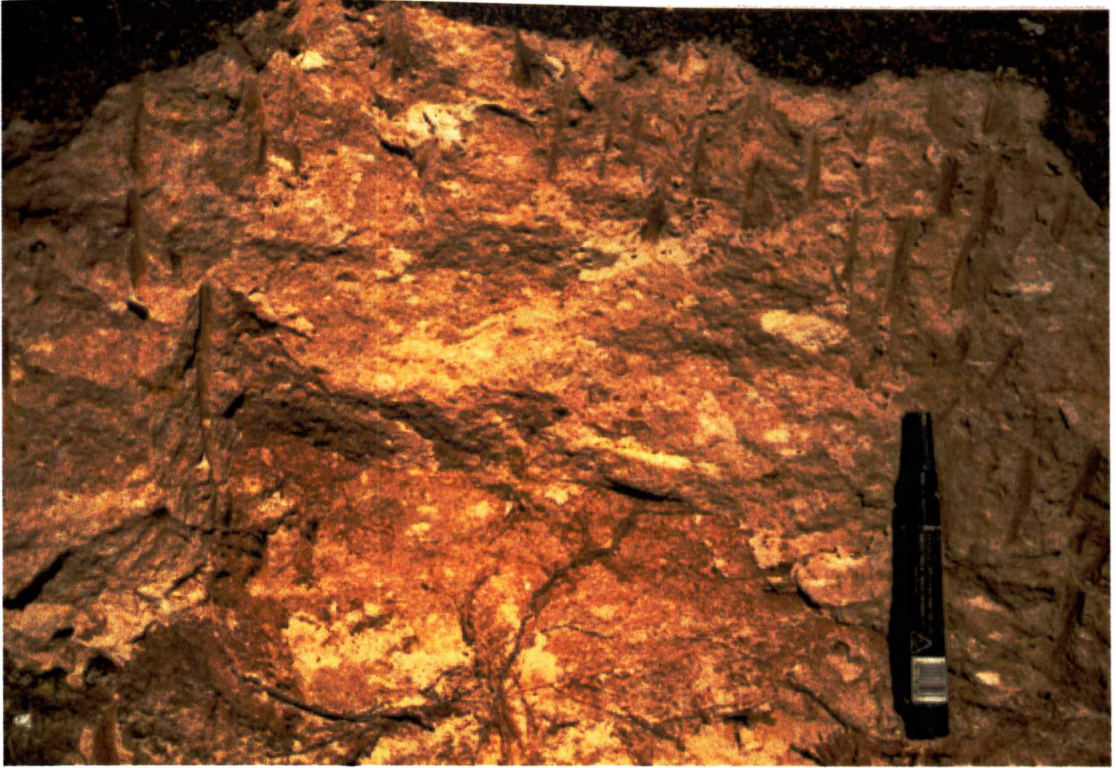
The Woodstock type section is the most comprehensive known and is, by definition, representative of the Kauroa Ash sequence depositional history. However, some members or beds are poorly defined at Woodstock and these are better represented at other reference sites (e.g. Waiterimu Ash, K15; Figure 2.10). Moreover, some reference sites contain beds that do not appear to be present at Woodstock. Such beds will therefore be described here, and their stratigraphic relationship to the Woodstock type-site will be assessed in later chapters.

### 2.5.1 Oparau Tephra at Papakura Creek

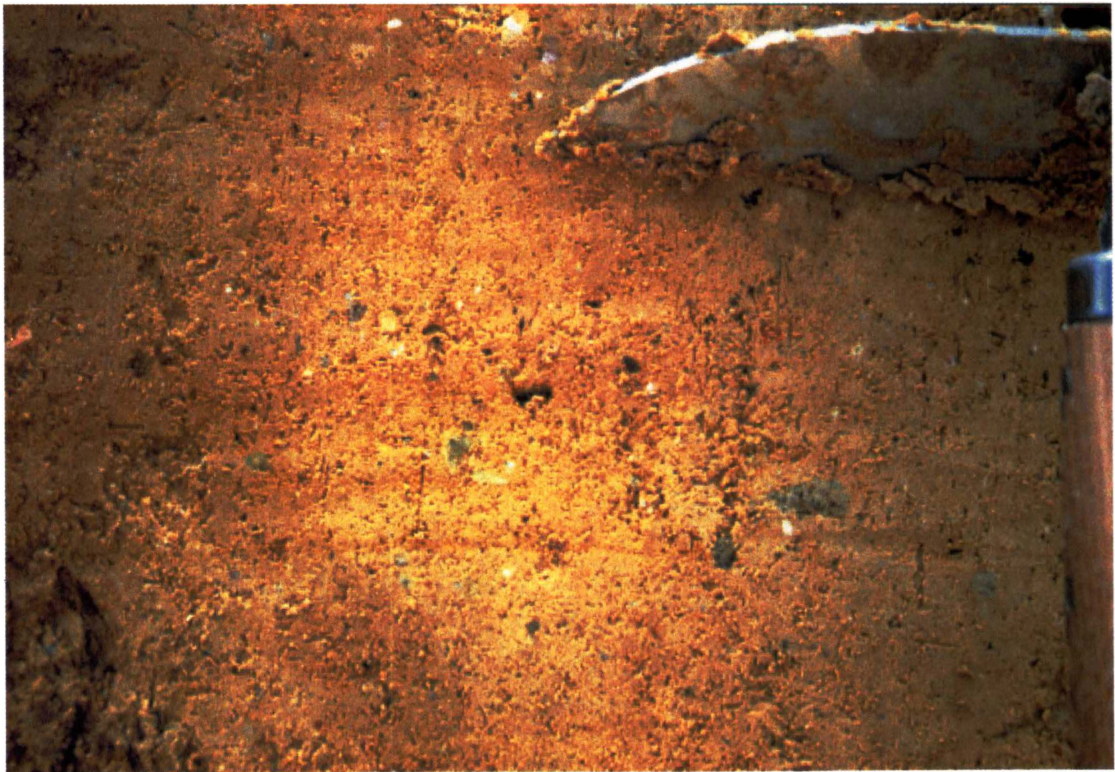
#### 2.5.1.1 Characteristics

At the type-site (R15/788479), the Oparau Tephra (equivalent to K12a, Figure 2.3) is a massive pyroclastic flow unit, approximately 3-4 m in thickness (Figures 2.3 and 2.4). Where freshly exposed, the Oparau has a white sandy clay matrix (2.5Y 8/1-8/2), although weathered surfaces can range from yellowish-browns (e.g. 10YR 6/2-6/6) to pinks (e.g. 5YR 8/3-8/4) to oranges (e.g. 5YR 7/6-7/8). In most cases, the Oparau Tephra is still reasonably firm (although attempts at drilling for paleomagnetic samples were unsuccessful due to the high clay content which produced collapse fairly quickly), but where significantly degraded it can be quite crumbly and friable. It contains weathered angular to subangular clasts of lapilli-sized pumice, lenticular in lower parts of the deposit (7.5YR 8/1; 5YR 8/3; Figure 2.16), and variably argillised lithics (e.g. 2.5YR 5/1; 2.5YR 4/6; Figure 2.17). It is crystal-rich throughout, with large and abundant quartz crystals as well as grains of magnetite, glass and zircon immediately obvious in the field.

In most cases, the base of the unit is easily definable by a sharp wavy contact with an underlying strongly weathered paleosol developed on an older Kauroa member (as seen in Figure 2.18 (a) and (b)). The paleosol is extremely firm, with a strongly developed prismatic structure and a dark yellow brown (10YR 3/4) colour. At other localities (not underlain by Kauroa members), the contact with aeolian sands of the Kaihu Formation is sharp and distinct, but is typically more graded and irregular on volcanic breccias of



**Figure 2.16** Flattened pumices in lower parts of the Oparau Tephra (pen is 15 cm tall), Papakura Creek (R15/788479).



**Figure 2.17** Small (<1 cm) lithics in the Oparau Tephra (blade is 10 cm long), Wyllies Hill (S15/155445).





**Figure 2.18 (a)** Oparau Tephra – K11 contact (basal layer is c. 10 cm thick), Papakura Creek (R15/788479).



**Figure 2.18 (b)** Oparau Tephra – K11 contact (hammer is c. 30 cm tall), near Hauturu (R15/801437).

the Pirongia Volcanics. The basal contact surface probably represents a significant disconformity, as attested by the strong paleosol on the underlying Kauroa bed.

The lowermost part of the Oparau Tephra is typically layered in several distinct bands, inferred to be 'flow banding' typical of some pyroclastic flow units (evident in Figure 2.18 a). At Papakura Creek the base of the unit comprises three main parts. The lowermost unit resting on the K11 paleosol is dull yellow orange (10YR 7/3-7/4), soft and gritty in consistence because of the presence of predominantly sand- to gravel-sized grains. It is very crystal rich, with abundant visible quartz grains, some small (<1 cm) grey lithics (banded rhyolite) and some large (2-6 cm) rip-up clasts derived from the underlying paleosol (Figure 2.16 (b)). Above this there is a gradual fining upwards of grain size, before a distinct change to a very much harder, clay-rich consistence, decreasing in chroma to a greyer shade of dull yellow orange (10YR 7/2). The aforementioned flow-banding is evident in this 30 cm section, marked by distinct orange veins. The third section is the base of the main ignimbrite unit, characterized by a well-defined straight boundary and by a change to hard, virtually lithified clay, and the typical white/grey/yellow/orange/pink variegated colour scheme.

The top of the Oparau Tephra is less distinct than the base because it grades into the overlying Kauroa bed (K12b) over several centimetres. K12b, is a yellow brown blocky clay, crystal rich and of varying thicknesses (0.5-1 m; at the Tiritirimatangi Peninsula site this bed has cross-bedding structures, very likely indicative of reworking there). There are considerable differences in texture and colour between the Oparau Tephra and the overlying beds (including the reworked bed at Tiritirimatangi Peninsula) to make the unit reasonably easy to recognise in most sections and thus a useful 'marker bed'. Particular diagnostic field characteristics are:

1. A (mostly) firm, massive pyroclastic flow unit;
2. Stratigraphic position within the Kauroa Ash sequence;
3. Base resting on extremely firm, strongly developed paleosol;
4. Colour - matrix ranging from white (2.5Y 8/1) to pink (5YR 8/3) and clasts of (2.5YR 5/1) to (2.5YR 4/6);
5. Presence of gravel-sized clasts in a massive sandy-clay matrix;
6. Extensive flattening of pumiceous clasts in lower parts of the unit.





**Figure 2.19** Oparau Tephra outcrops (c. 5 m thick) on Kawhia Harbour cliffs (R15/753484).



**Figure 2.20** Maximum observed thickness (c. 8.5 m) of Oparau Tephra, Kawhia Harbour Road, near Hauturu (R15/801437).

### 2.5.1.2 Distribution

The Oparau Tephra is well exposed in road cuttings between Oparau and Otorohanga, in many of the outcrops along the south-east shoreline of Kawhia Harbour (Figure 2.19), and in many locations in the inland area bounded by Kawhia, Raglan, Hamilton and Otorohanga. Indeed, this unit together with assorted other Kauroa beds appears to provide the main component of the Early to Mid Quaternary cover deposits in this area (Late Quaternary provided by Hamilton Ash and Post-Hamilton Ash tephtras).

Thicknesses appear to vary between 2 and 4 m, with a maximum thickness of c. 8.5 m being recorded on the Kawhia Harbour Road, 1.5 km north of Hauturu (Figure 2.20). A distinctive geomorphological feature of this unit was found to be its sudden lateral 'pinching-out' and local variability, the most changeable of the unit's distinctive field characteristics.

### 2.5.2 *Other units of note at Papakura Creek*

#### 2.5.2.1 Unit PCM1

Unit PCM1 appears to be the highly weathered, distal portion of an ignimbrite sheet. At the Papakura Creek site, it is present as a 'wedge-shaped' deposit to the far right (western end) of the section (Figures 2.3, 2.4 and 2.21), pinching out to a thin 'composite' bed in the main part of the section. From the contour of the beds to the left of the unit, it appears likely that some minor erosional event (possibly marked by a stream channel) removed a large part of the original PCM1, along with parts of other underlying units. Subsequent deposits have infilled this depression, in particular unit PCM3, thereby smoothing over the feature.

PCM1 has a maximum thickness of 1.5 m, and can be divided into three subunits, each inferred to represent different phases of the eruption (Figure 2.22). The upper 35 cm, PCM1 c), is a pumice concentration zone, devoid of lithics, with evidence of a paleosol developed on the top 15 cm. The lower boundary is gradual, but there is a distinct change to the underlying bed, PCM1 b)ii), which has rare lithics and rare pumice. PCM1 b)i) has abundant lithics and crystals, and is lithified (indurated). The boundary with PCM1 a) is sharp, distinct and almost straight. The lowermost 50 cm of the unit



consists of a further pumice concentration zone. Pumices are well sorted and have an average size of 3-4 cm in diameter. Occasional siliceous concretions (<2 cm in diameter) are evident throughout the unit.

The base is marked by an 8-10 cm bed of extremely large halloysite nodules, some reaching a diameter of 15 cm. Below this is the strongly-developed paleosol of K13b (K14a thought to be missing).

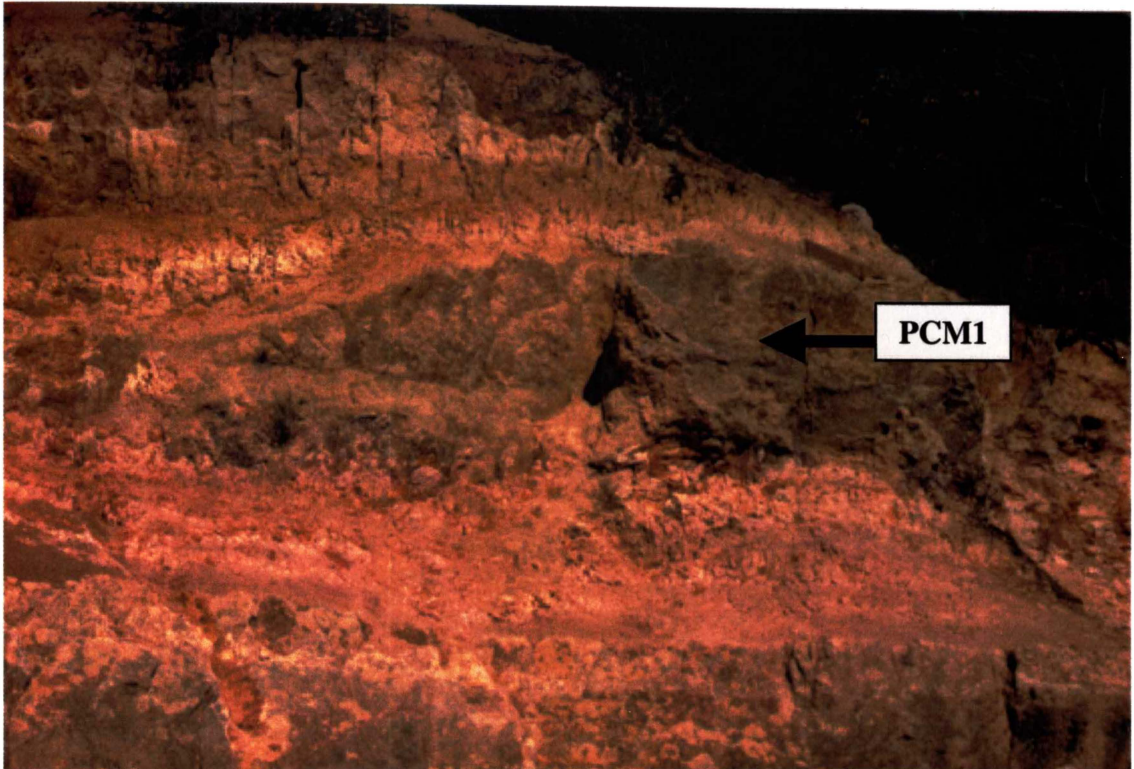


Figure 2.21 Bed PCM1 at Papakura Creek (R15/788479)

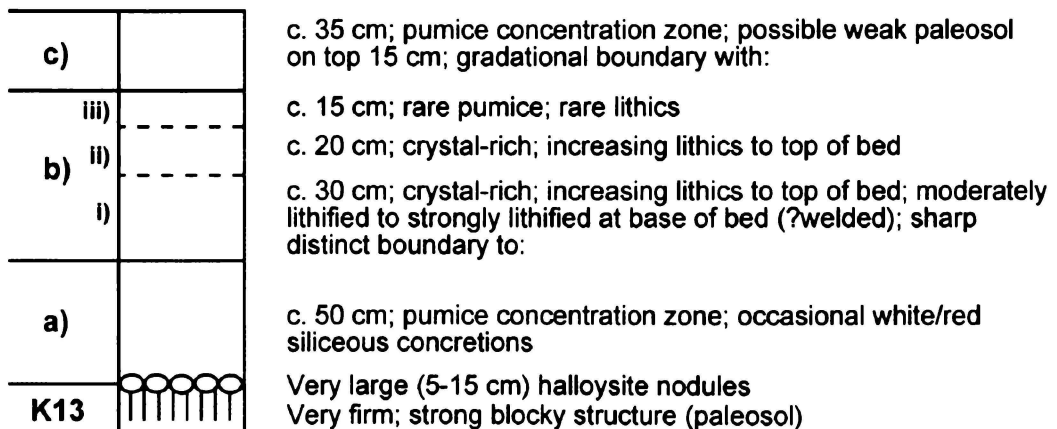
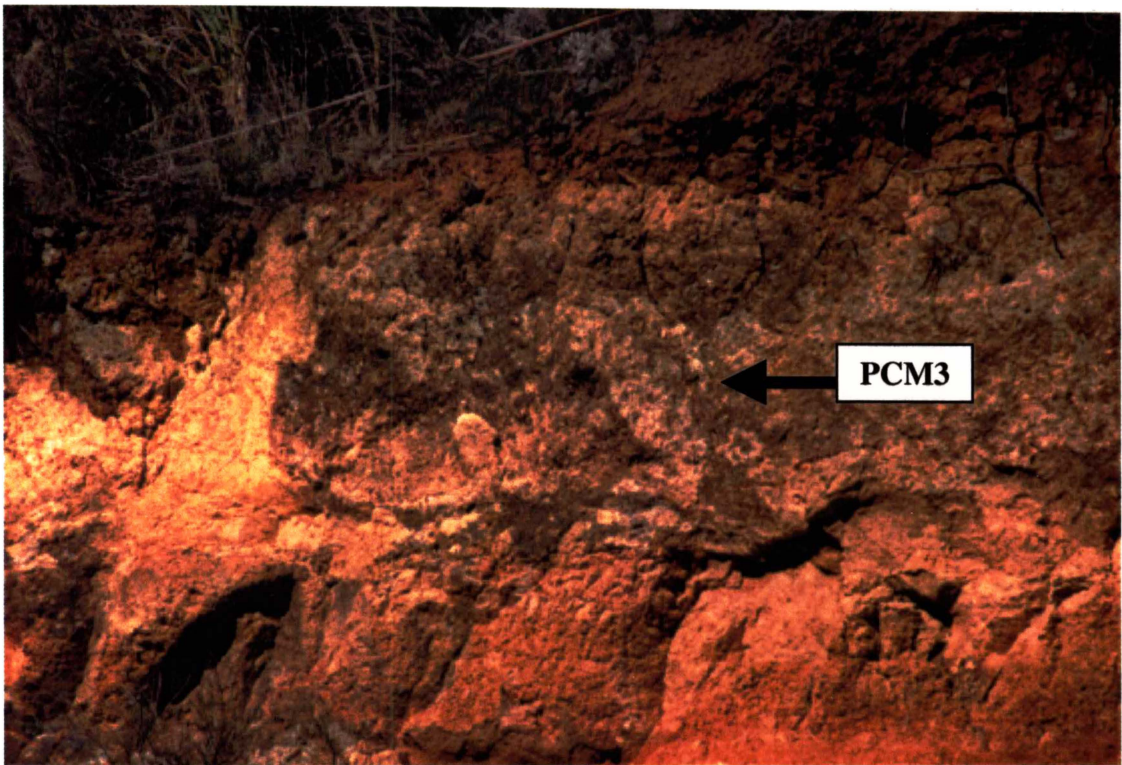


Figure 2.22 Stratigraphy of PCM1 at Papakura Creek.

### 2.5.2.2 Unit PCM3

PCM3 appears to be an ignimbrite deposit, though is less definitive than PCM1 (Figure 2.23). It has a maximum thickness of 0.8 m (minimum 0.3 m), is poorly sorted and has no internal bedforms. Possible small (<1 cm) orange-red lithics are observable, together with abundant sand-sized quartz grains. Relict pumice clasts (1-3 cm in diameter) are evident throughout the otherwise fine-grained matrix, and it is this characteristic that most readily distinguishes it from other tephra deposits. The unit is lithified in places.



**Figure 2.23** PCM3 at Papakura Creek (R15/788479).

Though based on a limited set of features, a likely interpretation of the bed's origin is that it is the distant 'vener facies' of an ignimbrite sheet, derived from the depositional phase where air-ingestion fluidisation affects the entire flow, spreading a thin, fluidised layer across the whole landscape (Wilson and Walker, 1982). This type of deposit is commonly found on the outer fringes of rapidly-emplaced ignimbrites where the flow volume has been significantly reduced.

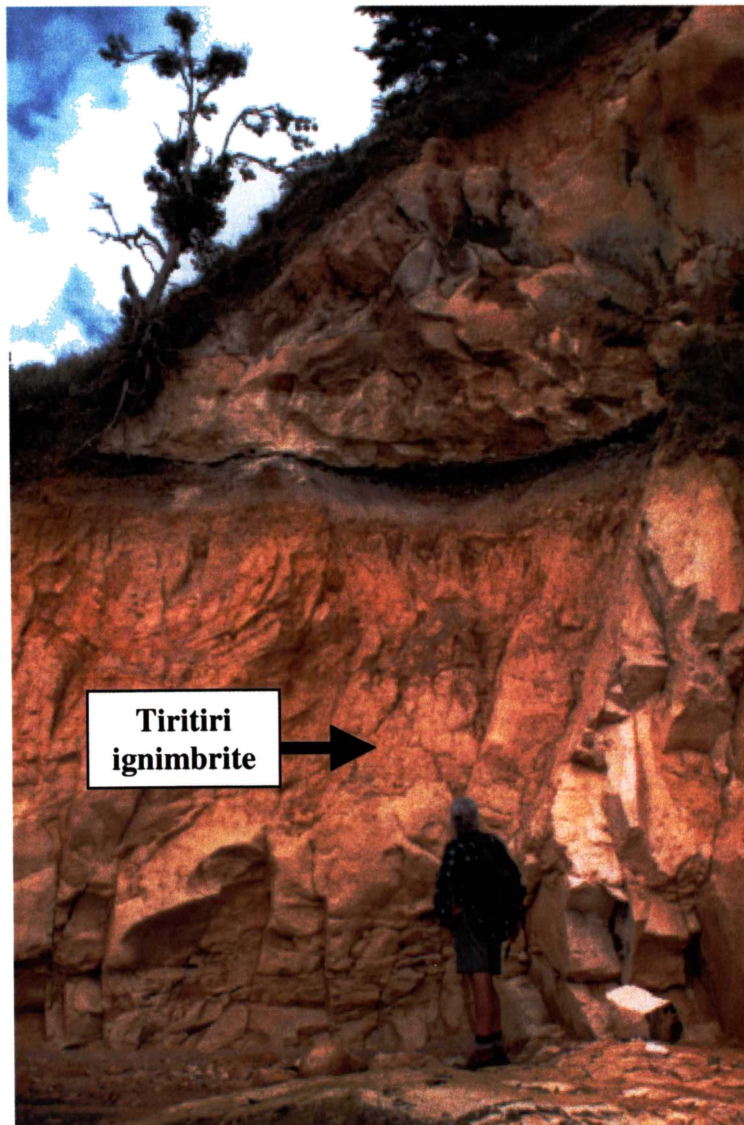
PCM3 comprises Unit K15a at the Papakura Creek site. It is also present at Woodstock as K15a, but it is a much thinner layer there.



### 2.5.3 Tiritiri ignimbrite at Tiritirimatangi Peninsula

#### 2.5.3.1 Characteristics

First identified and named by Fergusson (1986), the Tiritiri ignimbrite is a distal pyroclastic flow deposit. It is between 6 and 8 m thick on the Tiritirimatangi Peninsula (Figure 2.24), displays incipient vertical jointing, and has sharp, well defined boundaries – at the top, it has a low relief contact with some of the overlying Kauroa members, and at the base a well-defined lateral contact with breccias of the Pirongia Volcanic Formation (Figure 2.25). The upper 0.5-2.0 m appears to be reworked, showing extensive cross-bedding features (seen in Figure 2.26).

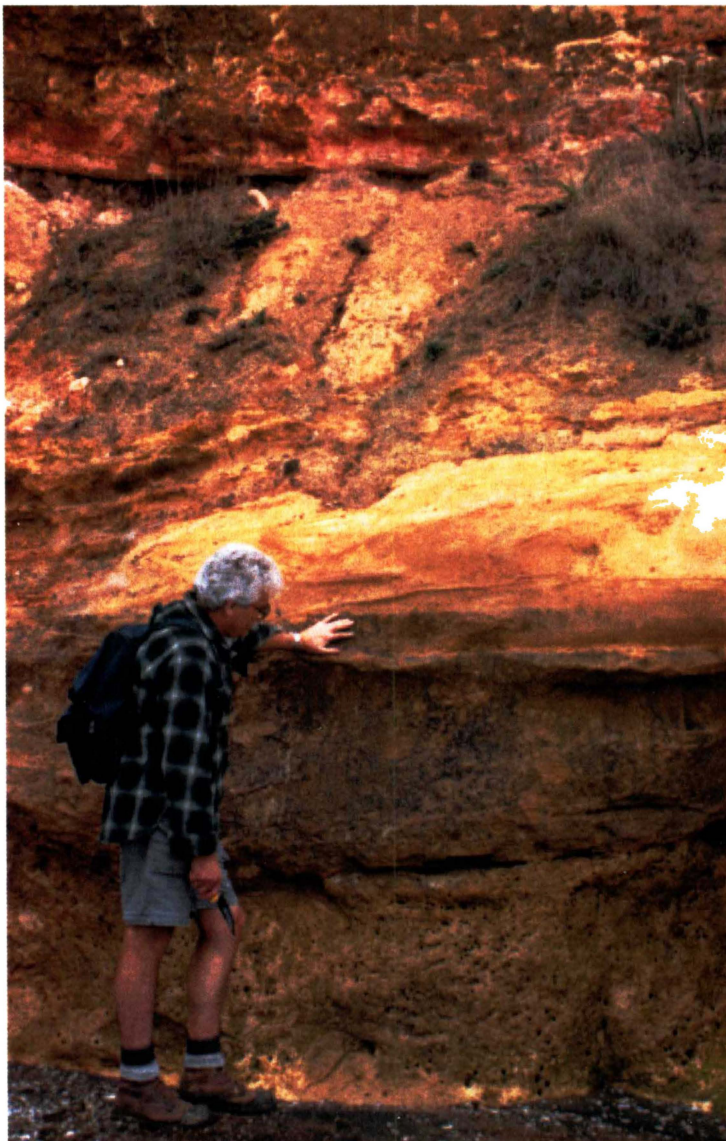


**Figure 2.24** The c. 7 m Tiritiri ignimbrite on Tiritirimatangi Peninsula (R15/747456; man is c. 1.8 m tall).





**Figure 2.25** (above) Base of the Tiritiri ignimbrite (just above grassy material), Kauroa Ash members and Pirongia Volcanics (below trowel; trowel is c. 20 cm tall). South-west end of Tiritirimatangi Peninsula (R15/748455).



**Figure 2.26** (left) Cross-bedding features in the top of the Tiritiri ignimbrite, Tiritirimatangi Peninsula (R15/748459).

For the most part the Tiritiri ignimbrite is highly weathered, though there are some patches that are considerably less so. The weathered parts exhibit pale to orange brown colors (e.g. 10YR 8/4-7/6), while relatively unweathered sections are a paler creamy brown (e.g. 2.5Y 8/2-8/4). A definitive characteristic of the Tiritiri ignimbrite is the occurrence of flattened pumices, particularly abundant in the lower 2-3 m of the deposit. Thus the term 'lenticulite' was proposed by Fergusson (1986) and seems appropriate given the extent of the feature. Also evident in the field are weathered lithic fragments, usually dark brown, some Mn-staining (matrix), together with abundant sand-sized quartz and plagioclase crystals.

### 2.5.3.2 Distribution

Tiritiri ignimbrite has been found only in one location, namely on the west, harbour-facing, shoreline of Tiritirimatangi Peninsula (R15/748458). Here it is a maximum of 8 m thick and it is somewhat surprising that a pyroclastic flow deposit of some considerable thickness (presumably resulting from an eruption of a significant magnitude) is not preserved elsewhere in the region. This produces several hypotheses as to its existence here: the deposit was valley-ponded in the antecedent Pirongia Volcanics topography and is thus misleadingly over-thickened in this locality; the ignimbrite was 'channeled' to this area on the west coast while the majority of the eruption went elsewhere, or; an extremely large erosional event occurred shortly after its deposition to all-but eliminate the deposit. Alternatively it may only be recorded at depth (obscured), or it could have significantly different characteristics at other locations, resulting in the lack of correlation.

## 2.6 SUMMARY

The Kauroa Ash sequence is found in scattered locations in the western and northern Waikato, predominantly mantling low-lying hill country. Thick (>10 m) sections are the exception and have been observed only in three locations. Other, shallower, less comprehensive sections are observed around the region, but identification of members is near impossible if a marker bed is not present. This is because several members (as well as members of the Hamilton Ash Formation) have very similar physical characteristics.

Field observations confirm the strongly weathered nature of all members of the Kauroa Ash sequence. This pervasive feature creates ambiguity in characterisation of the beds,

all beds being significantly altered from their primary depositional state. However, field properties suggest broad facies types are distinguishable for the Kauroa Ash beds.

Multiple paleosols have been identified in the sequence. Indeed, it seems likely that most of the sequence has undergone pedogenesis to a greater or lesser degree. Where strongly developed there is almost no indication of parent material and paleosols have been classified as a separate facies type.

All tephra in the sequence are strongly weathered with only a few retaining enough characteristics to be called a 'primary' (i.e. non-reworked) tephra. The majority of the tephra are presumed to be fallout deposits, though the presence of pumice in some beds suggests a pyroclastic flow origin, or that they have been reworked.

Some beds have certain field properties that readily distinguish them from other beds. Namely, they are considerably softer and friable than most, have a fine-earth fabric, and are generally bright yellowish-brown in colour. These beds are inferred to be loess.

Further beds have a similar appearance to those designated loess, but retain characteristics of weathered tephra beds, such as abundant sand-sized crystals. These have been provisionally defined as 'tephric-loess'.

The Woodstock type section may be the most complete section available. However, certain members (e.g. K13 to K15) are better represented (are thicker) elsewhere. Other members still may be absent from this site. Some thick tephra units have been observed in locations other than at Woodstock (e.g. Oparau Tephra, Tiritiri ignimbrite, PCM1, PCM3). These may or may not correlate to thinner members or beds at Woodstock.

## 3 MAGNETIC SUSCEPTIBILITY

---

### 3.1 INTRODUCTION

#### *3.1.1 Magnetic susceptibility as a paleoenvironmental proxy*

The magnetic properties of certain deposits are known to carry high-resolution information about their geomagnetic and climatic histories and as a result have become increasingly important to a wide range of researchers (e.g. Butler, 1992). Of most interest are the properties of remanence and susceptibility. Remanence is the 'permanent' magnetisation acquired at or shortly after deposition; it is this that is responsible for recording geomagnetic polarity changes and, as such, has been used for many years in establishing a base chronology on which other chronologies can be superimposed. This aspect will be discussed in a later chapter on chronology. Susceptibility is a more recent discovery and can be described as the 'magnetisability' of a material, or the degree to which a material reacts when subjected to a known external magnetic field. Essentially, it measures the type and amount of magnetic material present, from which inferences can be made about the deposit's paleoenvironmental history.

Magnetic susceptibility was first widely used during the 1980s in the study of the Chinese loess-paleosol sequences. Many studies (e.g. Heller and Liu, 1982, 1984, 1986; Liu, 1985, 1988; Kukla, 1987; Kukla et al., 1988) illustrated how magnetic susceptibility profiles readily differentiated paleosol and loess units, and noted that paleosols had susceptibility values over twice those of unmodified loess. Because paleosols are known to form under conditions that can generally be characterised as 'warm and wet', whereas unmodified loess represents a dry, cold environment, the concept of susceptibility as a climate proxy was initiated (Heller and Liu, 1982) and has since been utilised in many studies of paleoclimate (e.g. An et al., 1991; Maher and Thompson, 1992, 1995; An and Porter, 1997; Xiao et al., 1999; An, 2000).

#### *3.1.2 Origin of the susceptibility signal*

The specific origin of the susceptibility signal lead to some early controversy, still not

yet fully resolved (Meng et al., 1997; Han and Jiang, 1999). Heller and Liu (1982, 1984, 1986) suggested that there was a relative enrichment of detrital magnetite in soils during interglacial periods as a result of concentration by decalcification and soil compaction processes. Kukla et al. (1988) and Kukla and An (1989), however, proposed that high-level subaerial transport and deposition of ultrafine magnetite from distant sources contributed the majority of the susceptibility signal. They assumed that this influx was constant through time, forming the dominant component during warm interglacials where sedimentation was low, but was diluted during glacials when large amounts of low-susceptibility silt were deposited, lowering the overall susceptibility. Both of these models are plausible, but they also neglect other important aspects of deposition and pedogenesis, in particular the possibility of authigenesis of magnetite (and other ferrimagnetic minerals) during soil formation. With further work and revisions to these models, a clear link has been established between climate and susceptibility. It has been demonstrated and is now generally accepted that the presence of higher concentrations of single domain and superparamagnetic (up to c. 0.05  $\mu\text{m}$ ) magnetite in paleosol units is due predominantly to its *in situ* formation during soil forming periods (e.g. Heller et al., 1991; Liu et al., 1990, 1991; Maher and Thompson, 1991, 1995; Verosub et al., 1993; Singer et al., 1996). Ultrafine-grained magnetite is the characteristic product of inorganic precipitation (Maher and Taylor, 1988) and bacterial magnetosome formation (Fassbinder et al., 1990). Both of these processes are sensitive to the temperature and wetness (drainage) of the soil and hence reflect the climatic regime at the time of soil formation, production being high during warm interglacial periods. Meng et al. (1997) further concluded a significant component of the magnetic susceptibility signal derives from the decomposition of plants<sup>1</sup> (thereby reflecting density of the paleo-vegetation cover), adding a further dimension to the pedogenic hypothesis of magnetic susceptibility enhancement. It is for these reasons that, where resolution and rates of deposition are high enough, this pedogenically-derived signal can be correlated so well with the climatically-derived oxygen isotope signal (e.g. Ding et al., 1994; Bloemendal et al., 1995; Lu et al., 1999; Liu et al., 1999).

### 3.1.3 Magnetic susceptibility studies in New Zealand

Froggatt (1988) found that for two late Quaternary sequences in New Zealand, magnetic

---

<sup>1</sup> Decomposing plant material releases iron oxides; grains are 0.1 – 1.0  $\mu\text{m}$  in diameter, falling within the single domain or 'pseudo-single domain' category (Meng et al., 1997). Secondary ferrimagnetic minerals have been shown to be present in organically-rich topsoils (Maher and Taylor, 1988).



properties fitted the established model of susceptibility-enhancement in interglacial periods. Peaks in susceptibility ( $\chi$ ) corresponded to weathered horizons recognised as paleosols, whereas lower  $\chi$  corresponded to relatively less-weathered loess or tephra deposits. In most cases, peaks in  $\chi$  were approximately twice the value of  $\chi$ -lows in the loess. Although these sequences are considerably younger than the Kauroa sequence, Froggatt found that the  $\chi$ -curve could easily be related to the marine oxygen isotope stratigraphy, illustrating the utility of the magnetic susceptibility method in New Zealand. Palmer and Pillans (1996) attained a similar outcome with their study of 500 ka loess-paleosol sequences in the Wanganui area.

Apart from the ultimate aim of providing a magnetic chronology that facilitates correlation to established Quaternary chronologies, measurements of magnetic properties of the depositional record in New Zealand have considerable potential to aid in more fundamental objectives: the recognition of paleosols, loess and degraded tephra horizons, as well as breaks in deposition, and potentially, the correlation of such units from section to section. In highly weathered deposits such as the Kauroa Ash sequence, therefore, magnetic properties can be of use in establishing or refining the stratigraphy where other methods are inconclusive, and for correlating between Kauroa Ash sections.

#### *3.1.4 Magnetic susceptibility in the identification of paleosols*

Reliable identification of paleosols can be particularly useful for establishing sequences of Quaternary events. There are, however, a number of problems and potential pitfalls associated with paleosol recognition and stratigraphy. Lateral changes in paleosols occur over short distances due to weathering differences in response to parent material, climate, soil moisture or drainage, and time (Martini and Chesworth, 1992). The extent of diagenetic alteration after burial also creates doubt in many instances as to the value of some paleosols as stratigraphic entities, and where tephra deposits are thinly bedded and the paleosol is not within a distinctive 'lithological' unit, superficial features are not suitable for positive paleosol identification and correlation as they are likely to be time transgressive (Campbell, 1986). The problem of paleosol identification in thinly bedded deposits was reported by Birrell and Pullar (1973) where individual paleosols were not recognised on all of the tephra as the accessions of (distal) ash had been frequent and thin. As a result composite, rather than discrete, soils and paleosols had been formed

(e.g. Lowe, 1986). A similar finding was shown by Alloway et al. (1995) for distal, composite tephra-derived soils in northern Taranaki. All of these phenomena are likely to be present in the Kauroa Ash sequence and magnetic susceptibility represents a new and real possibility of paleosol identification in the case of degraded and composite-tephra units.

### 3.2 OBJECTIVES

The objectives of using magnetic susceptibility measurements in this study are as follows:

1. To provide a means to support or modify the stratigraphy established by field techniques.
2. To determine whether magnetic susceptibility can be used to show differences between tephra, loess and paleosol units, and to correlate these from section to section.
3. To evaluate the overall usefulness of magnetic susceptibility as a paleoenvironmental tool in tephra-loess-paleosol deposits (in New Zealand).

### 3.3 SAMPLING

Sampling for laboratory magnetic susceptibility measurements took place as part of the main sampling programme. To first establish a broad idea of magnetic susceptibility stratigraphy, a hand-held field susceptibility meter (a Gisco *Kappameter*) was used. This involved digging the section back as far as possible, typically c. 0.5 m, and taking an average from five or more readings of the *Kappameter*, used by applying the end of the meter flat to the section and pressing a key for the measurement. The instrument proved remarkably consistent and reproducible, and allowed a useful sampling strategy to be constructed. It furthermore proved invaluable in getting quick measurements on some sites where detailed sampling was not undertaken. Samples were thus taken at intervals with due consideration to the member stratigraphy and suggested by the *Kappameter*, distances between samples ranging from 2 to 10 cm in most cases. This was found to be an appropriate frequency to achieve a good resolution without generating unnecessarily repetitious data.

As with all techniques, there are some limitations involved with the use of magnetic susceptibility and these needed to be considered at the outset:

1. Disturbance of deposits and/or obliteration of stratigraphy by bioturbation or other pedogenic mixing processes, or by geological processes (e.g. redeposition or erosion).
2. Migration of clays, chemical compounds or elements (e.g. ferrous iron) in sequences through leaching or other pedogenic processes.

These processes are prevalent in some soils, and it was decided that the best course of action was to look for indications of such activity and avoid them when sampling or otherwise note their existence.

### 3.4 MASS-SPECIFIC SUSCEPTIBILITY

#### 3.4.1 Methodology

In the laboratory, a small amount of sample was first dried and then crushed in a pestle and mortar and packed into 10 cm<sup>3</sup> plastic pots. The pots were then inserted in turn into a Bartington MS2B dual frequency sensor and their response to high and low frequency fields measured on a Bartington MS2 magnetic susceptibility meter. This does three things: it creates a magnetic field, detects the magnetisation in the sample, and calculates the ratio or magnetic susceptibility between the two. The resulting data are the volume susceptibility, or 'κ', and represent the ratio of the field to magnetisation in dimensionless SI units. Single sample susceptibility is not normally expressed on a volumetric basis, however, but on a dry mass basis, and so the κ value is divided by the bulk density of the sample. The new adjusted value, the mass-specific susceptibility, is given the symbol  $\chi$  and has units of m<sup>3</sup> kg<sup>-1</sup>. In formula terms:

$$\chi_{lf} = \kappa / \rho$$

where ' $\chi_{lf}$ ' is the low frequency mass-specific susceptibility (in m<sup>3</sup> kg<sup>-1</sup>), κ is the volume susceptibility and ρ is the bulk density of the sample (kg m<sup>-3</sup>). Conventionally,  $\chi_{lf}$  values are expressed on a scale of 10<sup>-6</sup> so that the units become μm<sup>3</sup> kg<sup>-1</sup>.

### 3.4.2 Results

Calculated magnetic susceptibility values are shown in Appendix A.

This method proved highly reproducible. Repeated measurements of the same sample produced identical results virtually every time. Remarkably, there is also a strong correlation between the (high-tech) Bartington laboratory results and the initial (low-tech) Kappameter field results with, in most cases, good agreement between the two sets of data<sup>2</sup>. The Kappameter is therefore highly recommended for providing reliable data (albeit low resolution) in a quick and easy manner as compared to the laboratory method, which, although uncomplicated, takes far more time.

Figures 3.1, 3.2 and 3.3 show mass-specific susceptibility curves (bold line; frequency-dependent susceptibility discussed in section 3.5) for the three main sections, Woodstock, Papakura Creek and Tiritirimatangi Peninsula. Overall, the data are pleasing for their coherence, with very few chaotic or anomalous points. Subtle changes are likely to be real because of their consistence through two or more samples, and it is suggested that given the right deposits there may be a high limit to the resolution this method can provide with only the difficulties of sampling thin layers hindering what is attainable.

### 3.4.3 Discussion

#### 3.4.3.1 Mass-specific susceptibility as a stratigraphic correlation tool

The susceptibility curve was invaluable in providing an alternative magnetostratigraphy to the lithostratigraphy devised previously as a result of field descriptions. Members and beds are easily definable by breaks and changes in the curve; most units were found to be distinctive by their magnetic mineralogy alone. The data were also particularly helpful in the early stages of fieldwork when trying to verify correlation between the main sections. In places the field observations were not sufficient to confidently establish a correlation between sequences/members, yet the shapes and magnitudes of the susceptibility curve proved they were more than likely the same. The opposite can also be true, however, with the susceptibility data being somewhat misleading in the

---

<sup>2</sup> On a volume susceptibility basis.

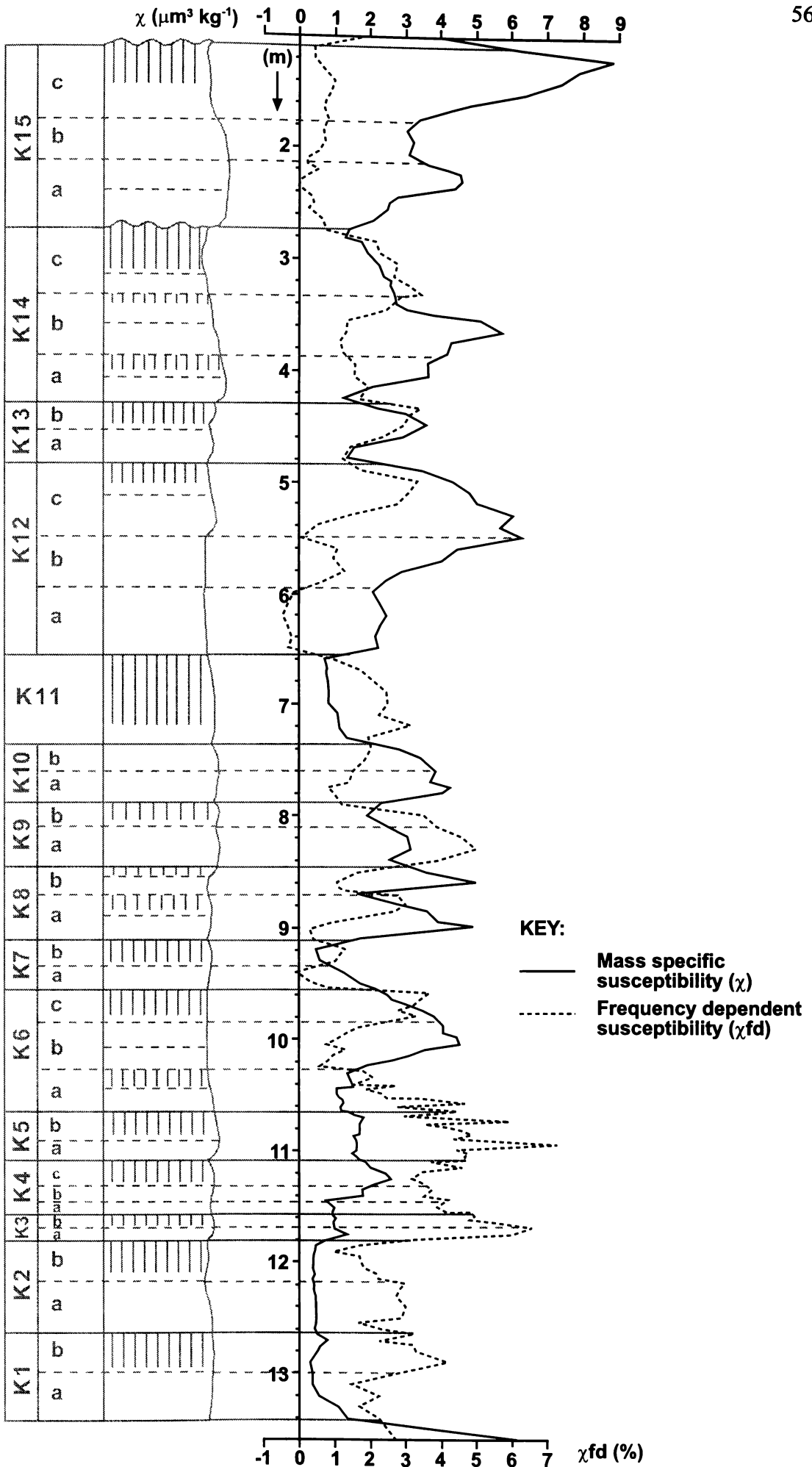


Figure 3.1 Magnetic susceptibility parameters for the Woodstock section.

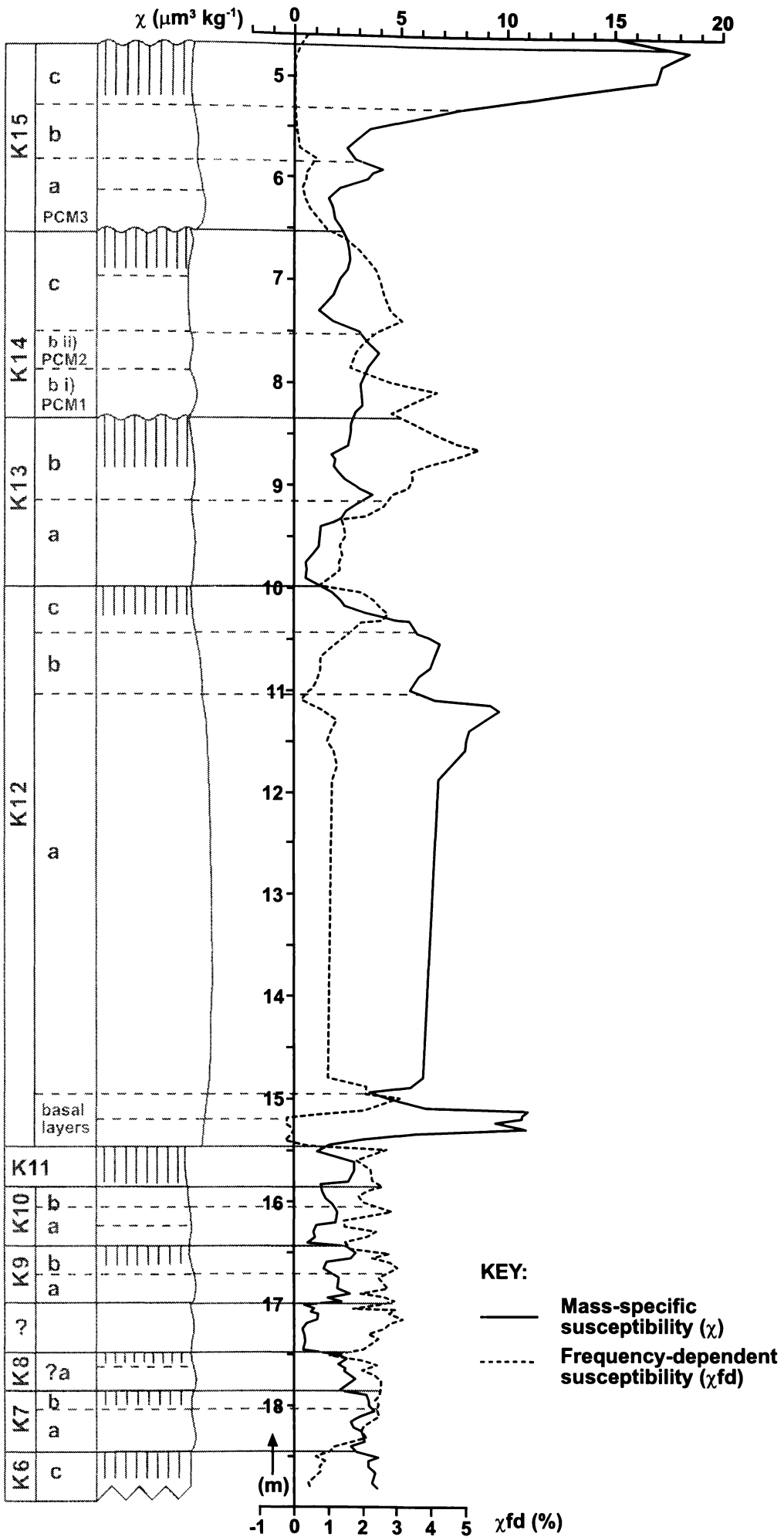


Figure 3.2 Magnetic susceptibility parameters for the Papakura Creek section.

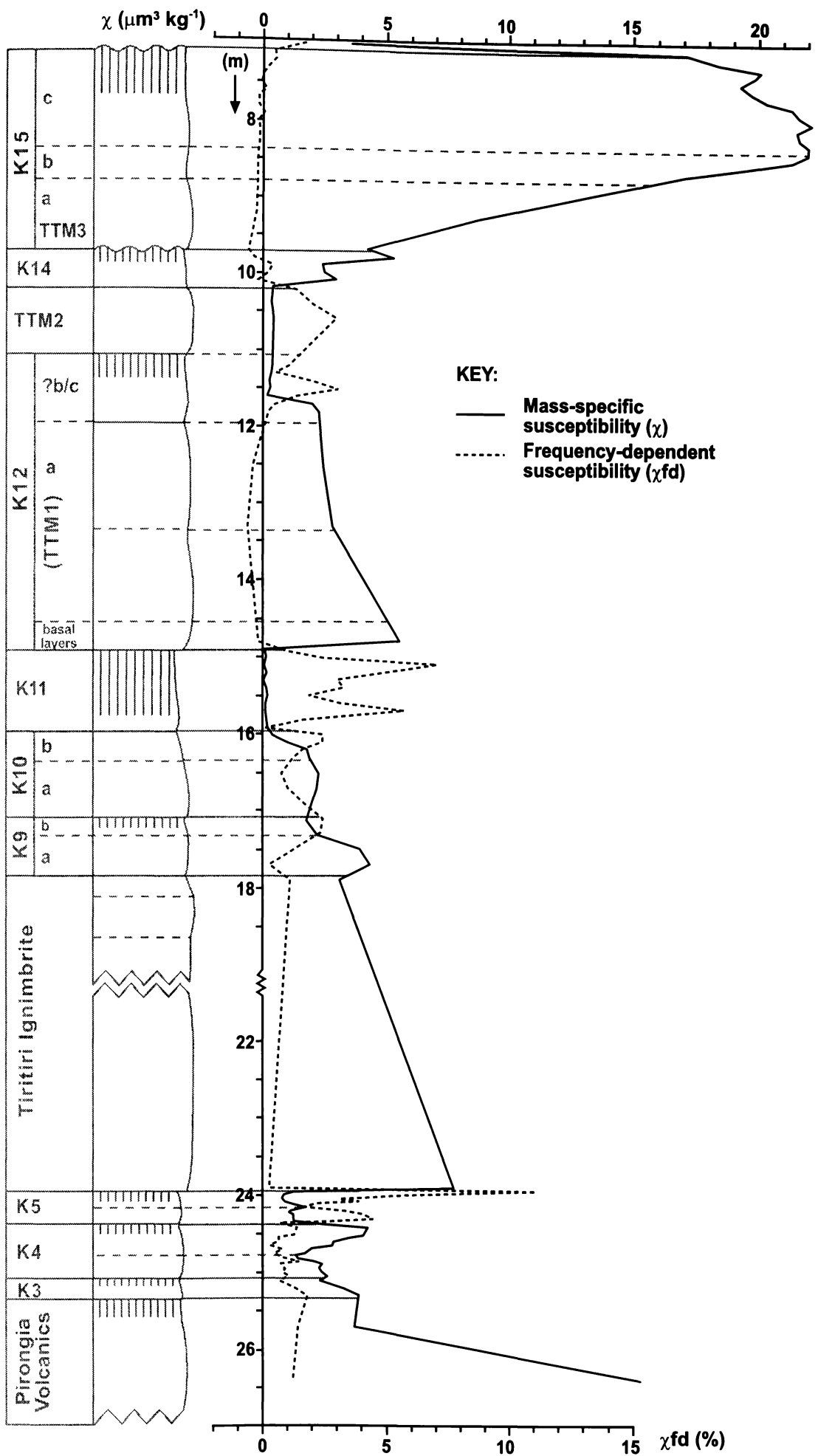


Figure 3.3 Magnetic susceptibility parameters for the Tiritirimatangi Peninsula section.

middle-lower portion of the sequence (K11-K6). Here the data do not correlate so well, but in this case field descriptions proved more conclusive (distinctive field properties of those beds) and the correlation is confident nonetheless. It should be remembered that although the primary material may have been the same, and the sites will have had broadly similar environmental and climatic histories, these locations have different geomorphology, aspect and drainage, the deposits differ in thickness, and so have had different weathering and pedogenic histories for at least part of the time the sequences accumulated. Over 1-2 Ma, this can result in dissimilar end products.

For the most part though, and especially in the upper parts of the sequence, the agreement is good, and in places it is definitive. K15, for example, shows excellent agreement between the sites with clear definition of the subunits, especially K15b. It also highlights that subtle changes such as the slight indentation at the top of the K15c curve are consistently represented in the results. Although the shapes of the  $\chi$  curves are more or less the same for the reference sections, the actual  $\chi$  values can vary considerably among correlative beds. For example, the peak value at the top of K15c has a  $\chi$  of  $8.8 \mu\text{m}^3 \text{kg}^{-1}$  at Woodstock,  $18.4 \mu\text{m}^3 \text{kg}^{-1}$  at Papakura Creek and  $22.1 \mu\text{m}^3 \text{kg}^{-1}$  at Tiritirimatangi Peninsula, yet there seems little doubt, as outlined above and from field evidence, that K15 is the same unit at all sites. Because this value is consistently reproducible, there is no reason to believe it is false. Rather, there is some reason for susceptibility-enhancement in K15 at Papakura Creek and Tiritirimatangi Peninsula sections though it is at a relative rate (the curve shape is the same). Such enhancement could be the result of minor geomorphological or paleodrainage differences (i.e. different weathering pathways and/or amount and type vegetation cover; Lowe, 1986) between the sites that have resulted in different degrees of fine-grained magnetite production (i.e. governing the strength of the susceptibility signal). Another possible explanation is that these sites have received additional thin accessions of loess or tephric material (e.g. andesitic tephra) as compared to the more-distal Woodstock site. Some members (e.g. K12 to K15) are certainly thicker at Papakura Creek than at Woodstock, though this is not the case at Tiritirimatangi Peninsula.

#### 3.4.3.2 Mass-specific susceptibility of paleosols

In the case of paleosols, absolute  $\chi$  values were sometimes conflicting. Initially, the established model of susceptibility-enhancement in paleosols was adhered to, with  $\chi$ -



high values assumed to represent paleosols. However, further work revealed that this model is not necessarily valid for this sequence because of the variation in  $\chi$  seen in the paleosol horizons. For example, some of the strongly developed paleosols identified in the previous chapter (e.g. K6, K13 and K15) showed moderately high to high  $\chi$ , while others (e.g. K1, K5 and K11) showed low to very low  $\chi$ . The results for these latter beds are therefore not reconcilable with the model of susceptibility enhancement in paleosols.

There are two questions to consider here. Firstly, why do certain paleosols have such low susceptibility when pedogenesis is said to normally enhance susceptibility? And secondly, why do some paleosols have high susceptibility and some have low susceptibility (i.e. no trend for the sequence)?

There is precedence for an inverse relationship between magnetic susceptibility and soil formation, having been reported for Alaskan loess (shown in Table 3.1; Begét and Hawkins, 1989; Begét et al., 1990; Begét, 1996; Liu et al., 1999), and for Siberian loess (Chlachula et al., 1997, 1998). The hypothesis in most of these cases was that the susceptibility-climate signal reflects the influence of wind intensity, strong winds occur in glacial periods, weaker winds occur in interglacials<sup>3</sup> (Begét et al., 1990; Begét, 1996). Liu et al. (1999) inferred a different and/or complementary mechanism, suggesting that  $\chi$ -depletion occurred through waterlogging of soils during interglacial periods, with reducing conditions tending to gradually transform part of the magnetite and maghemite content into iron hydroxides (more suited to these soil conditions but their weakly 'paramagnetic' properties make only a small contribution to  $\chi$ ).

**Table 3.1** Magnetic parameters for two sets of samples from Alaska (AK) and Luochuan (LC), China<sup>a</sup>.

Sample	Type	$\chi$ ( $\mu\text{m}^3 \text{kg}^{-1}$ )	$\chi_{\text{fd}}$ (%) <sup>b</sup>
AK1	Paleosol	3.63	3.40
AK2	Loess	11.56	0.83
AK3	Loess	17.75	0.30
LC1	Paleosol	14.69	10.02
LC2	Loess	7.55	8.03
LC3	Loess	5.27	6.15

<sup>a</sup> Data from Liu et al. (1999)

<sup>b</sup> Frequency-dependent susceptibility, discussed in section 3.5

<sup>3</sup> Reflecting density sorting during aeolian transport – dense magnetic minerals are recorded only in distal locations during strong winds (Begét et al., 1990; Begét, 1996).

There is evidence of considerable wetting-drying cycles (i.e. short-lived reducing conditions) in Kauroa Ash beds (abundant Mn nodules) but only limited evidence of longer periods of waterlogging (gleying; grey veins). However gleyisation cannot be ruled out as a contributing factor, and typical reductimorphic features of gleying may have been obscured or destroyed as a result of further weathering or diagenesis. Similarly, variation in wind intensity is a plausible hypothesis for this locality, being a distal location with an analogous source of primary ferrimagnetic grains (TVZ) as for the Alaskan localities. It seems clear that the different magnetic behaviour of these paleosols (K1, K5, K11) indicates that some aspect of climate (humidity, precipitation, wind intensity, vegetation?) during these interglacials resulted in the conversion of ferrimagnetic minerals into hard and/or paramagnetic minerals (resulting in low  $\chi$ ).

The puzzling disparity between paleosol beds (some have high- $\chi$ , some have low- $\chi$ ) is also seen in Alaska. A recent study (Vlag, 1998) demonstrated high- $\chi$  paleosols at two sites, suggesting at least some interglacials experienced conditions similar to those on the Chinese Plateau (conditions favouring susceptibility enhancement in paleosols) rather than that inferred for other Alaskan paleosols (gleyisation and/or low wind intensity). The Kauroa Ash sequence seems to suggest a similar (variable) pattern of interglacial highs and lows in  $\chi$ . Since these variations must relate to the production (and possible destruction) of fine-grained ferrimagnetic minerals (the susceptibility signal), it must be concluded that the interglacials that these paleosols originate from were of different intensities or types (i.e. variations in temperature, precipitation, etc.), thereby invoking different weathering regimes and/or pathways. Paleosols with high- $\chi$  are, in this scenario, inferred to have been formed under lower precipitation and/or warmer conditions (better soil drainage), while those with low- $\chi$  are inferred to have been formed under higher precipitation / slower drainage.

These hypotheses are expanded in subsequent sections.

#### 3.4.3.3 Mass-specific susceptibility of loess beds

The loess beds (K4a, K5, K6a, K8ai, K8bi, K10a and K14a) also show significant variation. Four of them (K4a, K5, K6a and K14a) have low- $\chi$ , following the established model of susceptibility-depletion in loess. However, K8ai, K8bi, and K10a instead have

a relatively high- $\chi$  of 3.0-4.0  $\mu\text{m}^3 \text{kg}^{-1}$ , values that are higher than for many of the Kauroa paleosols.

Following the theories of Begét et al. (1990) and Begét (1996), this could indicate cold periods of exceptionally high wind intensities, resulting in a greater proportion of dense, coarse-grained magnetite. Alternatively, since the majority of loess in the central North Island is specifically tephric-loess, these beds may have received a significant proportion of (high-ferrimagnet) tephra (e.g. andesite tephra), resulting in the high  $\chi$  values. A final possible explanation is that these units accumulated as thin increments, with pedogenic processes (production of superparamagnetic grains) acting on each increment in an 'upbuilding' manner (Almond and Tonkin, 1999; Lowe, in press; Chapter 8). The paleosols in the upper parts of these units would hence represent either a prolonged hiatus and/or a transition to a warmer climate.

#### 3.4.3.4 Mass-specific susceptibility of tephra beds

Tephra and other volcanigenic beds (indurated ignimbrite units e.g. Oparau Tephra, Tiritiri ignimbrite) seem to vary quite substantially in  $\chi$ , being neither high nor low on a regular basis. K3 has a very low  $\chi$  of 1.4  $\mu\text{m}^3 \text{kg}^{-1}$ ; K6 has a moderately high  $\chi$  of 4.4  $\mu\text{m}^3 \text{kg}^{-1}$ ; K12 = 2.2  $\mu\text{m}^3 \text{kg}^{-1}$ , K14b = 4.2  $\mu\text{m}^3 \text{kg}^{-1}$  and K15a = 2.6  $\mu\text{m}^3 \text{kg}^{-1}$ . This is not entirely surprising as any individual volcanic eruption has its own primary mineralogical signature that will have a direct effect on susceptibility (authigenesis of magnetic minerals). Pillans and Wright (1990), for example, concluded that the majority of variation in susceptibility seen in the Rangitatau East core (Wanganui Basin) was controlled largely by volcanism rather than by climate. Tephra flux is likely to be a dominant factor in the susceptibility signal of the Kauroa Ash sequence as well.

There is another consideration, however. Where tephra beds are undifferentiated and are possibly composite or multisequal soils (i.e. comprising thin accessions of tephra), differences in  $\chi$  will also result from climate (and pedogenesis) at the time of deposition. In this case, climate would become the dominant force, presumably bringing the sequence 'in line' with the established model of susceptibility enhancement rather than the 'chaotic' effect that sporadic tephra input has (random input of lithogenic magnetic minerals). Incremental tephra accumulation and its susceptibility signal

would, in this manner, closely resemble that of loess in that it is essentially mimicking a loess-like 'upbuilding' system.

#### 3.4.4 Summary

The mass-specific susceptibility measurements have in this study given rather mixed results. On one hand, the measurements, all reproducible, were invaluable in elucidating thin, previously unidentified beds/subunits and providing an alternative stratigraphy to the subjective, broad-scale field observations (a supporting stratigraphy was particularly important in the case of the Kauroa Ash sequence because intense weathering has, in many cases, 'blurred' the boundaries between beds). Susceptibility values also aided correlation in a consistent manner.

With respect to facies, however, the values were sometimes inconsistent, with lows or highs in  $\chi$  failing to regularly identify paleosol, loess or tephra units and therefore provide use as a reliable characterisation tool in this study. Absolute values were not always consistent for the same member or bed in two locations, though relative magnitudes (shape of  $\chi$  curves) were, and can still be effectively used in this manner.

Provisionally, it would seem that in the Kauroa Ash sequence, the magnetic mineralogy of beds has been influenced by a great many environmental and climatic factors, as well as by the irregular influx of tephric material. While this method lived up to expectation in some areas (stratigraphy), it provided little help in others (characterisation).

#### 3.4.5 Revised objectives

Magnetic susceptibility has thus far been of limited use in one objective of this study, characterisation. However, there is still the question of paleoenvironmental significance. Namely, is it possible to isolate a climate-controlled aspect of the susceptibility signal for the Kauroa Ash sequence?

Mass-specific susceptibility is only one part of mineral magnetism and there are additional measurements that can be used to complement and refine these data.

The aim is to ascertain what paleoclimate signal remains and whether it can be accessed. The objective is to demonstrate the presence of specifically pedogenically-derived, ultrafine, magnetite grains.

According to Maher and Thompson (1991), this can be accomplished by three main methods:

1. the size of the 'frequency-dependent' component;
2. citrate-bicarbonate-dithionite treatments to isolate ultrafine (inferred pedogenic-origin) magnetite (e.g. Verosub et al., 1993; Hunt et al., 1995);
3. particle-size analysis.

### 3.5 FREQUENCY-DEPENDENT SUSCEPTIBILITY

#### 3.5.1 Methodology

Measurements made at two frequencies are referred to as frequency-dependent susceptibility. The procedure is to acquire  $\kappa$  readings in magnetic fields of low (0.46 kHz; ' $\kappa_{lf}$ ') and high (4.6 kHz; ' $\kappa_{hf}$ ') frequency. The percentage difference between  $\kappa_{lf}$  and  $\kappa_{hf}$  reflects variations in the ferrimagnetic grain size from superparamagnetic (SP) to single domain (SD) state. SP grains become 'blocked' at higher frequencies and act as SD grains, thus contributing less to the overall susceptibility signal than when measured at lower frequency (Maher and Thompson, 1991; Heller et al., 1991; Liu et al., 1992). Samples without these grains will show identical  $\kappa$  values at the two frequencies. Thus a high susceptibility paleosol horizon should theoretically have a large frequency-dependent component, whereas loess or tephra beds contain little, if any, SP ferrimagnetic grains and should have a small to non-existent frequency-dependent component.

Frequency-dependent susceptibility is expressed as a percentage of the original  $\chi_{lf}$  value:

$$\chi_{fd}\% = (\chi_{lf} - \chi_{hf} / \chi_{lf}) \times 100$$

Significant differences are usually in the order of 1-10%.

### 3.5.2 Results

Figures 3.1, 3.2 and 3.3 also show the frequency-dependent susceptibility for Woodstock, Papakura Creek and Tiritirimatangi Peninsula sections (dotted line).

As with mass-specific susceptibility, these data are consistent and reproducible. They are similarly useful in picking out boundaries between members and beds, with (for the most part) each bed having its own distinctive frequency-dependent susceptibility signature. This provides further confirmation of the stratigraphy thus far established, and of the frequency susceptibility method and theory in general.

The data do not, however, vary in accordance with the mass-specific susceptibility data which, given the inability of the latter to provide use as a characterisation tool, is an advantageous feature.

### 3.5.3 Discussion

#### 3.5.3.1 Frequency-dependent susceptibility of paleosols

The frequency-dependent susceptibility ( $\chi_{fd}$ ) of beds identified as paleosols in the previous chapter (tops of K1, K5, K6, K8, K9, K11, K12, K13, K14 and K15) shows excellent agreement with the model of superparamagnetic susceptibility enhancement. With the exception of one bed, K15c, all have a moderately high frequency-dependent component of a significant 2-4%; K15c is slightly lower at 1%. In each case, the top of the unit is clearly marked by a peak or increase in  $\chi_{fd}$ , perfectly picking out the inferred paleosols. It is even able to distinguish between 'strengths' of paleosols (development of pedality), a provisional classification based on arbitrary percentage boundaries is suggested in Table 3.2 below. These are based on the average  $\chi_{fd}$  of those beds identified as 'weakly', 'moderately' or 'strongly developed' paleosols in the previous chapter. This would not necessarily apply to other sequences. Liu et al. (1999) showed that  $\chi_{fd}$  is a relative measure, with  $\chi_{fd}$  of c. 3% being considered 'significant' and indicative of paleosols in Alaskan loess (see Table 3.1); Chlachula et al. (1998) considered anything >1% to be a paleosol in Siberian loess. On the Chinese Plateau, the  $\chi_{fd}$  for paleosols is generally 7-10%, and for loess, 2-7% (Xifeng, Luochuan sections; Liu et al., 1992).



**Table 3.2** Development of paleosols as suggested by frequency dependent susceptibility.

$\chi_{fd}\%$	Development
1-2	weakly developed paleosol
2-3	moderately developed paleosol
3-4	strongly developed paleosol
>4	very strongly developed paleosol

The additional beds identified as paleosols as a result of this study (K2, K3, K4, K14a, K14b) also have significant  $\chi_{fd}\%$ , with K3 and K4 suggesting ‘strongly developed’ paleosols, and K2, K14a and b suggesting ‘weakly developed’ paleosols. The  $\chi_{fd}\%$  for the further two beds (top of K7 and K8a) tentatively described as being ‘possible weak paleosols’ in Chapter 2 is also revealing, with the top of K7 showing a weak though distinct peak, and K8a showing a very clear peak of ‘moderately developed’ significance, lending weight to their characterisation.

An interesting feature of the paleosol  $\chi_{fd}$  is that it tends to reach a peak at approximately 10-30 cm from the top of a unit. This is inferred to be the result either of mixing with lower  $\chi_{fd}\%$  material from above the bed, or that some of the ultrafine material has been translocated and concentrated down the profile as a result of lessivage or leaching processes. Additionally, paleosols (as determined purely by  $\chi_{fd}$ ) seem to extend deeper into the underlying bed or beds than determined by field observations alone. This suggests field identification may be somewhat conservative and/or field properties alone do not show the full extent of the paleosol. It is also likely that the majority of Kauroa Ash beds have experienced considerable weathering and pedogenesis.

Thus, in the case of paleosols,  $\chi_{fd}$  conforms well to the established model, with significant ‘highs’ in  $\chi_{fd}\%$  providing evidence of increased concentrations of ultrafine magnetic material produced as a result of intensive pedogenesis and/or bacterial magnetosome formation (e.g. through decomposition of vegetation). It seems that in this study  $\chi_{fd}$  is of ultimate use in elucidating the position and strength of paleosols, where  $\chi$  did not appear to conform to standard models and field identification was sometimes only tentative.

There is still the question of why, if ultrafine material (i.e. derived through pedogenesis)

is high (high  $\chi_{fd}\%$ ), mass-specific susceptibility is still (relatively) low, when ultrafine material is supposed to markedly boost the  $\chi$  signal. The answer may be in the type of ultrafine material present. The ideal conditions for the formation of ultrafine magnetite are in soils that are well drained but alternately wetted ( $\text{Fe}^{2+}$  produced) and dried ( $\text{Fe}^{2+}/\text{Fe}^{3+}$  oxide precipitated), with a supply of organic matter and Fe, and near-neutral pH conditions (Maher and Thompson, 1995; Singer et al., 1996; Maher, 1998). Rainfall is likely the key here, and given a well-drained soil with sufficient iron and organic matter, higher concentrations of ultrafine magnetite and maghemite will form where rainfall is high than where rainfall is low, resulting in higher susceptibility<sup>4</sup> (Maher and Thompson, 1995; Maher, 1998). Absence or loss of magnetic iron oxides (low susceptibility) is apparent in very acid, podsol-type profiles and waterlogged (modern) soils (Maher, 1998). Alternatively, where the climate is drier, and the more oxic forms of iron are dominant, susceptibility is also lower (M.J. Singer, pers. comm., 1999).

Therefore where Kauroa beds have high  $\chi_{fd}\%$  but low or moderate  $\chi$ , it is fair to assume there is ultrafine material present, but that the more oxic iron oxides (e.g. hematite) are prevalent. If that frequency-dependent component were magnetite or maghemite,  $\chi$  would be significantly higher and vary in accordance with  $\chi_{fd}\%$ .

### 3.5.3.2 Frequency-dependent susceptibility of loess beds

Trends in  $\chi_{fd}$  in the beds designated as possible loess units are not as clear-cut as for paleosols. The upper four loess beds, K14a, K10, K8bi and K8ai (moderately high to high- $\chi$ ), have a relatively low  $\chi_{fd}$  of 0-1%, certainly not a 'significant' frequency-dependent component and therefore are inferred not to have much, if any, ultrafine magnetic grains. This would conform to the previously established model where a low  $\chi_{fd}\%$  is typically associated with loess units. However, the lower three loess beds, K4a, K5, K6a (low- $\chi$ ), also have a moderate to high  $\chi_{fd}$  of 2-4%, a finding inconsistent with the established model.

It should be remembered, however, that  $\chi_{fd}$  is a ratio of  $\chi_{hf}/\chi_{lf}$ , so that a  $\chi_{fd}$  of 1%,  $\chi$  of  $5 \mu\text{m}^3 \text{ kg}^{-1}$  is the same as a  $\chi_{fd}$  of 5%,  $\chi$  of  $1 \mu\text{m}^3 \text{ kg}^{-1}$ , i.e.  $0.05 \mu\text{m}^3 \text{ kg}^{-1}$  of

---

<sup>4</sup> This is because ferrimagnetic iron oxides like magnetite and maghemite have greater susceptibilities than the weakly magnetic oxides, e.g. hematite and goethite (Singer et al., 1996; Maher, 1998; Fontes et al., 2000).

susceptibility from ultrafine grains. Table 3.3 illustrates  $\chi$ -parameters for each loess bed, demonstrating that all beds actually have approximately similar amounts of ultrafine grains. The exception is K5, which is not surprising as this bed is considered to be a paleosol throughout as well. The average contribution of ultrafine material to the loess beds (excluding K5) is  $0.04 \mu\text{m}^3 \text{kg}^{-1}$ ; the average contribution for the paleosols is  $0.07 \mu\text{m}^3 \text{kg}^{-1}$ ; and for the tephras  $0.03 \mu\text{m}^3 \text{kg}^{-1}$ .

**Table 3.3** Contribution of ultrafine grains to mass-specific susceptibility in loess beds.

Loess bed	Mean $\chi_{fd}$ (%)	Mean $\chi$ ( $\mu\text{m}^3 \text{kg}^{-1}$ )	Ultrafine grains ( $\mu\text{m}^3 \text{kg}^{-1}$ )
K14a	1.83	1.69	0.03
K10a	1.17	3.97	0.05
K8bi	1.04	5.00	0.05
K8ai	0.54	3.52	0.02
K6a	2.96	1.15	0.03
K5	4.48	1.60	0.07
K4a	4.09	0.90	0.04

These results (that loess beds have a similar contribution of ultrafine grains to  $\chi$ ) do not totally explain the difference between the two groups of loess beds however. They may have similar contribution from ultrafine grains, but overall susceptibility still varies – some beds have more magnetic material than others. One answer to this disparity is that the latter group of beds (K4-K6) is not, in fact, loessic in origin. This explanation is not favoured, however, because the field properties (colour, consistence etc.) of this latter group are, if anything, more convincing of a loessic origin than the former group. Alternatively, a range of climatic and environmental factors could account for these differences. Singer et al. (1996) listed up to seven different pedogenic processes<sup>5</sup> that determine the magnetic properties of deposits; further climatic<sup>6</sup> and geomorphic factors<sup>7</sup> could apply.

Of relevance may be the coarse-grained magnetite theory (high wind intensity) of Begét et al. (1990) and Begét (1996). The fact that ultrafine grains are only a small percentage of the total  $\chi$  of these beds, illustrates that a greater proportion of the signal has been acquired through coarser-grained magnetic minerals.

<sup>5</sup> Preferential accumulation, transformation, leaching, neoformation, biosynthesis, leaching, solubilisation (Singer et al., 1996).

<sup>6</sup> Temperature, precipitation, wind intensity, organic matter content etc. (e.g. Maher and Thompson, 1995; Meng et al., 1997).

<sup>7</sup> Slope, drainage, depth of burial, thickness of deposit etc. (e.g. Lowe, 1986)

### 3.5.3.3 Frequency-dependent susceptibility of tephra beds

Tephra beds were found to have reasonable consistency (between beds) in  $\chi_{fd}\%$ . Most had low to no frequency-dependent component indicating a relative dearth of ultrafine pedogenic grains. Where  $\chi$  was also moderate to high, this would indicate that the magnetic material present is comprised primarily of inherited lithogenic magnetic minerals. The clearest example of this is the weathered distal ignimbrite unit K12a that has an average  $\chi$  of  $2.2 \mu\text{m}^3 \text{kg}^{-1}$  and a  $\chi_{fd}\%$  that is slightly negative (i.e., in reality, 0%). This shows that the magnetisability of this sample was actually higher (only marginally so) at the higher frequency magnetic field, indicating a complete lack of ultrafine magnetic material, so that any remaining susceptibility signal may be attributed to primary, lithogenic, minerals. Other tephra units have similarly non-existent  $\chi_{fd}\%$ , for example K15a, K7a, and K6b; some have a low  $\chi_{fd}$  of around 1%, namely K15b, K14b, and K13a. These are inferred to be beds of a volcanic origin but which have had some considerable pedogenic processes acting on them<sup>8</sup>.

### 3.5.3.4 Summary

In general this method, which has sometimes been ineffective in other studies, appears to have worked well here.  $\chi_{fd}\%$  has routinely picked out paleosol beds, and lows in  $\chi_{fd}\%$  seem to represent tephra horizons quite well. The beds designated as loess are somewhat ambiguous, but probably have a relatively small frequency-dependent component in conjunction with a reasonably high mass-specific susceptibility. This, in broad terms, would at least set them apart from paleosols that appear to have a high  $\chi_{fd}\%$  and a strangely low  $\chi$ , while tephra units are the opposite, with low  $\chi_{fd}\%$  and intermediate  $\chi$  (summarised in Table 3.4).

**Table 3.4** Range of susceptibility values by sample type.

Sample type	$\chi$ ( $\mu\text{m}^3 \text{kg}^{-1}$ )	$\chi_{fd}$ (%)
Paleosol	0.5 - 2.0 (max. range: 0.5-9.0)	High: 2.0 - 5.0
Tephra	2.0 - 4.0 (max. range: 0.5-9.0)	Low: -0.5 - 1.5
Loess	1.0 - 5.0	Intermediate: 0.5 - 4.0

<sup>8</sup> Field properties do not suggest they are 'paleosols'. The  $\chi_{fd}\%$  in this case merely indicates some contribution of pedogenic iron oxides.

The entire Kauroa sequence is so highly weathered that it is likely all beds have been affected by ultrafine material production (or comminution to) to some degree. In this study (and others) it is probably more effective to look at relative values, how the  $\chi$  or  $\chi_{fd}\%$  of any particular bed compares to those above and below it. Absolute  $\chi$  and  $\chi_{fd}\%$  values are unlikely to be reliably definitive, though can provide many clues to their origin.

### 3.6 CITRATE-BICARBONATE-DITHIONITE ANALYSIS

#### 3.6.1 Theory

Frequency-dependent susceptibility is one method of determining the percentage of ultrafine ferrimagnetic grains in a sample. Fine and Singer (1989) reported that an alternative method, the citrate-bicarbonate-dithionite (CBD) treatment and extraction (first developed by Mehra and Jackson, 1960), could more accurately distinguish between pedogenic and lithogenic (inherited) magnetic grains in soils. Sodium dithionite is a strong reducing agent that reduces and solubilises secondary iron oxides (goethite, hematite and maghemite); once reduced, the  $\text{Fe}^{2+}$  is chelated by the citrate (Hunt et al., 1995). After centrifugation the supernatant is extracted and the susceptibility of the residue re-measured.

Studies have subsequently shown (Fine and Singer, 1989; Fine et al., 1989; Singer et al., 1992, 1996; Hunt et al., 1995; Sun et al., 1995; van Oorschot and Dekkers, 1999) that CBD extraction is particularly effective in the dissolution and removal of strictly pedogenic ferrimagnetic grains (superparamagnetic and single domain grains, less than 0.5  $\mu\text{m}$ ), while leaving the primary magnetic grains inherited from the soil parent material essentially untouched. Evidence presented in those studies and in Verosub et al. (1993) and Singer et al. (1996) supports the use of the term “pedogenic” to describe whatever the CBD process removes from samples, and is thus a useful tool in the identification of paleosols where the distinction between beds is difficult to determine.

#### 3.6.2 Methodology

1. Place 4 g of ground sample into a 50 ml centrifuge tube
2. Add 4 g of sodium dithionite powder and 20 ml of 22% citrate solution

3. Mix by shaking vigorously by hand, sitting 10 minutes in an ultrasonic bath, and leaving for 16 hours on an end-over-end shaker
4. Centrifuge tubes at 1500 rpm for 15 minutes
5. Carefully pipette off solution
6. Add 20 ml more citrate solution, repeat steps 3 – 5.
7. Put tube and residual contents into an oven to dry
8. Gently grind the residual and put into a 10 cm<sup>3</sup> susceptibility pot, weigh contents and pack with foam to prevent movement of grains
9. Re-measure / re-calculate mass-specific susceptibility.

### 3.6.3 Results

Figure 3.4 shows the difference between pre- and post-CBD mass-specific susceptibility for the Woodstock section. For ease of comparison, post-CBD  $\chi$  is expressed here as a percentage difference from the original  $\chi$  value so that if a sample has a  $\chi^{\text{CBD}}\%$  of 10, 10% of the susceptibility signal has been lost and is inferred to be the result of the loss of ultrafine magnetic grains.

### 3.6.4 Discussion

The most noticeable feature of the  $\chi^{\text{CBD}}\%$  is its relative similarity to the frequency-dependent curve. This is entirely expected as the two methods essentially measure the same thing in two different ways – this method by extraction of the relevant fraction and remeasurement at the same field, the latter by measurement at two different magnetic fields taking advantage of grain size differences in ‘magnetisability’. It is pleasing, therefore, that the two data sets are so similar for it confirms that both methodologies are working correctly and that the variation between beds is real.

There are slight differences between some beds and in general this can be described as the  $\chi^{\text{CBD}}\%$  being somewhat more ‘exaggerated’ as compared to the  $\chi_{\text{fd}}\%$ : highs in  $\chi^{\text{CBD}}\%$  are proportionally greater than lows in  $\chi^{\text{CBD}}\%$ ; the range between ‘high’ and ‘low’ is greater than in  $\chi_{\text{fd}}\%$ . This is likely because  $\chi^{\text{CBD}}$  measures (the removal of) superparamagnetic grains and single domain grains, while  $\chi_{\text{fd}}$  measures (the effect of) only superparamagnetic grains. Theoretically, the difference between the two parameters would measure the contribution of single domain grains. The result is that the paleosols become even more noticeable as evidenced by peaks in  $\chi^{\text{CBD}}\%$  at e.g. K14c, K13b, K12c, K11 etc., reinforcing the interpretation established in the previous



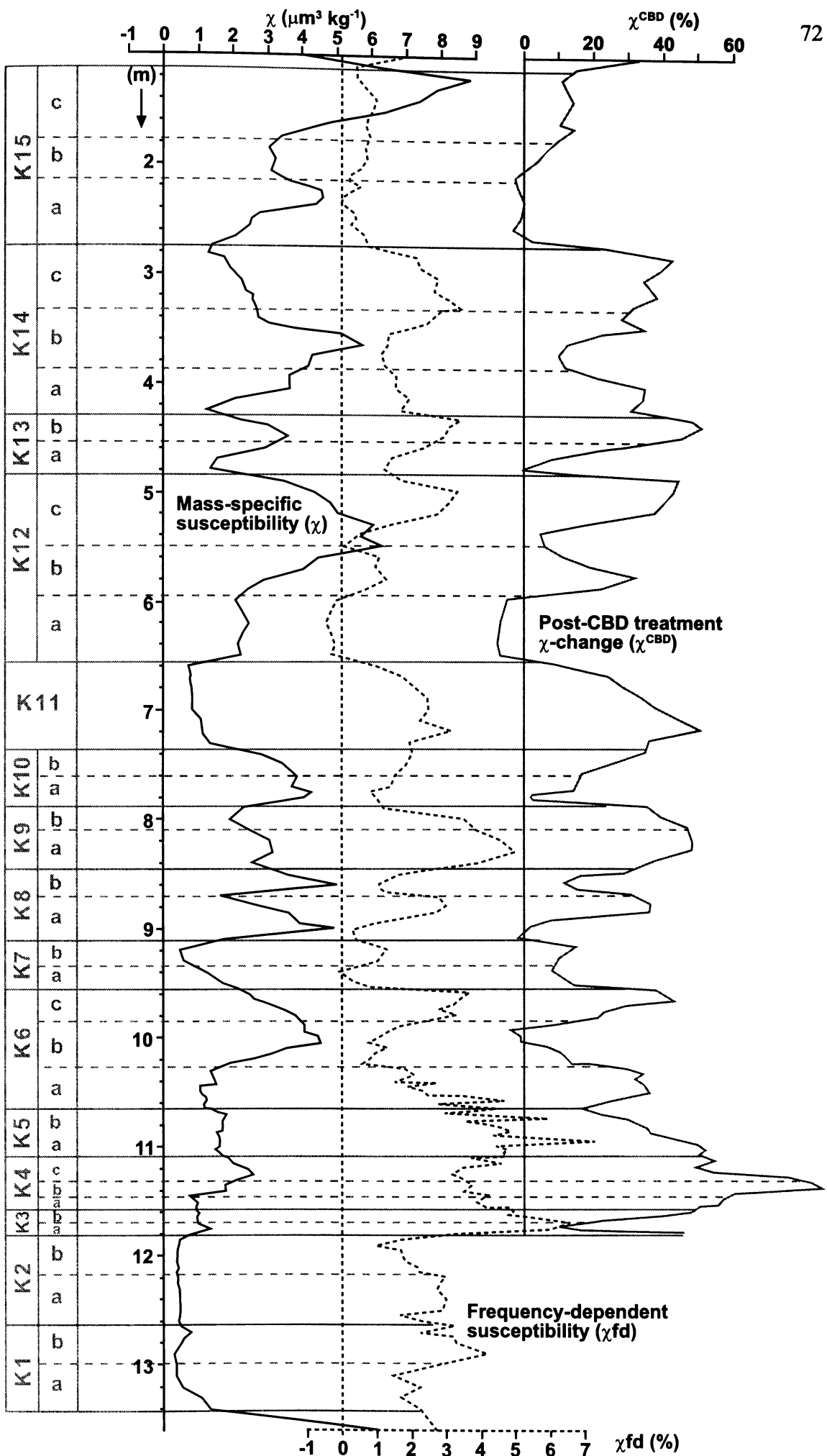


Figure 3.4 Post CBD-treatment change in mass-specific susceptibility (Woodstock).

section. Sometimes the  $\chi^{\text{CBD}}\%$  can prove helpful in deciding characterisation where  $\chi_{\text{fd}}$  was ambiguous. For example, weak paleosols were suggested for the units K14a and b and in both cases the  $\chi^{\text{CBD}}\%$  is more pronounced, lending weight to their previously tentative characterisation.

Lows in  $\chi^{\text{CBD}}\%$  are similarly marked, with a relative dearth of ultrafine material (SP+SD grains) suggested for beds K15, K13a, K12a, K10a, K8ai, K6bii, etc. Once again, as seen with  $\chi_{\text{fd}}$ , these units are those that are high in primary volcanic material. Following the pedogenic vs. lithogenic magnetic material theory, this is as expected, with relatively<sup>9</sup> less pedogenic processes having acted on these probably mass-emplaced units.

The post-CBD susceptibility varies significantly from the  $\chi_{\text{fd}}$  in only a few places. Aside from the usual exaggeration described earlier, there are two beds where  $\chi^{\text{CBD}}\%$  is completely divergent from  $\chi_{\text{fd}}\%$ . K4b shows a particularly marked peak as compared to the underlying and overlying beds, a feature that is absent in the bed's  $\chi_{\text{fd}}\%$ . In addition, the  $\chi^{\text{CBD}}\%$  of K3a is extremely low where its  $\chi_{\text{fd}}\%$  was particularly high, the former making more sense because of its marked primary volcanic nature; soil formation processes are evident in unit K3b (where reworking of the underlying bed has resulted in a paleosol) but not K3a, and it would therefore be hypothesised that this unit should not have any ultrafine magnetic material as is the case with other tephra units. These are the only two cases of serious disagreement and it seems there must have been some unusual processes at work here.

In general it can be seen that CBD treatments have produced similar results to  $\chi_{\text{fd}}$  in that it accurately picks out paleosol units as having a high percentage of ultrafine material, and tephra beds as having a low percentage of ultrafine material. It provided no further help in the case of loess units, having much the same proportion that  $\chi_{\text{fd}}$  suggested.

---

<sup>9</sup> The keyword is 'relatively', since all the Kauroa Ash sequence is extremely weathered and has probably experienced some degree of pedogenesis.

### 3.7 CONCLUSIONS

Magnetostratigraphy forms a fundamental part of this study for its role in establishing an alternative stratigraphy for the Kauroa Ash sequence. Each susceptibility parameter, and especially all three taken together, is able to distinguish between beds in a clear and definitive manner. Furthermore it is consistent and reproducible making it a reliable stratigraphic tool. Table 3.5 summarises the magnetic susceptibility properties of each of the K-beds.

While individual beds may be characterised by their magnetic susceptibility signature, facies (e.g. paleosol, loess, tephra) are not so easily distinguished. Some resemble the model established for Chinese loess-paleosol samples while others more closely resemble that noted for Alaskan samples, making the Kauroa beds particularly difficult to decipher:

- Paleosols were seen to display predominantly high  $\chi_{fd}\%$  and  $\chi^{CBD}\%$ , so much so that this may be considered a diagnostic characteristic. Conversely,  $\chi$  was seen to vary to a considerable degree and no clear pattern could be established. The former parameters suggest paleosols contain a greater proportion of ultrafine magnetic grains compared to other beds. However, this does not appear to have a significant effect on the overall  $\chi$ , the latter being neither consistently high nor low. This suggests differences in either quantity and type of primary magnetic minerals (inherited from parent material), or that differing amounts and types of secondary iron oxides have been formed and/or lost as a result of varying climatic, and weathering or pedogenic regimes.
- Loess beds showed some variation in magnetic parameters, ranging from low to moderately high  $\chi$ ,  $\chi_{fd}\%$  and  $\chi^{CBD}\%$ . There is an inverse relationship between  $\chi$  and  $\chi_{fd}\%$ , with some beds having high  $\chi$  and low  $\chi_{fd}\%$ , and other having low  $\chi$  and high  $\chi_{fd}\%$ . Despite the apparent differences, this actually points to approximately similar contributions from ultrafine grains, being less overall than paleosols. There is evidence, however, that some or all of the loess beds have experienced considerable pedogenesis, presumably upbuilding in an incremental manner. The differences in  $\chi$  point again to the numerous climatic and/or environmental factors that could have influenced the evolution of these deposits.

**Table 3.5** Simplified summary of magnetic susceptibility values of K-beds.

Member	Bed	Mass-specific susceptibility ( $\chi$ ) <sup>1</sup>	Frequency-dependent susceptibility ( $\chi_{fd}$ ) <sup>2</sup>	Post-CBD treatment susceptibility ( $\chi^{CBD}$ ) <sup>3</sup>
K15	c	high <sup>4</sup>	low <sup>5</sup>	moderate <sup>6</sup>
	b	moderate	low	low
	a ii	high	low	low
	a i	moderate to low	low	low
K14	c ii	moderate	moderate	high
	c i	moderate	high	high
	b ii	high	moderate	high
	b i	high	moderate	moderate
	a ii	moderate	moderate	moderate
	a i	low	moderate	high
K13	b	high	high	high
	a	moderate	moderate	low
K12	c ii	high	high	high
	c i	high	moderate to low	low
	b	moderate	moderate	high
	a	moderate	low	low
K11		low	moderate	high
K10	b	high	moderate	moderate
	a	high	low	low
K9	b	moderate	moderate	high
	a	moderate	high	high
K8	b ii	moderate	high	moderate
	b i	high	moderate	low
	a ii	moderate	high	high
	a i	high	moderate	low
K7	b	low	moderate	moderate
	a	moderate	low	moderate
K6	c	moderate	high	high
	b ii	high	moderate	low
	b i	high to moderate	low	moderate
	a ii	moderate	moderate	high
	a i	moderate	high	moderate
K5	b	moderate	high	moderate
	a	moderate	high	high
K4	c	moderate	high	high
	b	moderate	high	high
	a	low	high	high
K3	b	low	high	high
	a	low	high	moderate
K2	b	low	moderate	---
	a	low	moderate	---
K1	b	low	moderate	---
	a	low	moderate	---

KEY*	<sup>4</sup> 'high'	<sup>6</sup> 'moderate'	<sup>5</sup> 'low'
<sup>1</sup> $\chi$ ( $\mu\text{m}^3 \text{kg}^{-1}$ )	>4	1-4	<1
<sup>2</sup> $\chi_{fd}$ (%)	>3	1-3	<1
<sup>3</sup> $\chi^{CBD}$ (%)	>30	10-30	<10

\*These values are arbitrary, and are designed to show relative differences between K-beds. They will not (necessarily) apply to other sequences. Refer to Figure 3.4 for precise values.

- Tephra beds show the variation in magnetic properties that was expected of an independent, allochthonous source of magnetic minerals.  $\chi$  shows considerable variation, though  $\chi_{fd}\%$  and  $\chi^{CBD}\%$  are usually low, indicating the small contribution (less than for loess beds) of ultrafine grains to the susceptibility signal. There is no doubt the tephra beds are strongly weathered, but they have experienced proportionally less pedogenesis than other beds (probably less contribution from organic matter). That being said, it is possible some of the tephra beds have accumulated as thin deposits in an incremental manner to form composite beds. In this case, they may have experienced upbuilding pedogenesis in effectively the same manner as for loess beds. For the most part, however, the magnetic properties illustrate the dominant effect of volcanism on the susceptibility signal, being overridden by climatic (pedogenic) factors in a few instances only.

Since the susceptibility signal is likely dependent on so many climatic, environmental and geomorphic factors (which govern the type and amount of secondary minerals formed), it is difficult or impossible to isolate the cause of any differences in susceptibility parameters. There is no simple explanation, for example, why the sequence does not consistently follow either the Chinese or Alaskan models. There are two main possible factors at work: either there has been great variation in climate – ‘glacial’ and ‘interglacial’ are insufficient to describe the variation in conditions, in particular, there may be great variation between interglacials, or, significantly different weathering or pedogenic regimes have been in operation at various times in the development of the sequence.

The magnetic properties of modern soils (e.g. Maher, 1998) indicate that interpretation of paleosol-loess-tephra magnetic properties must be done on a site-specific basis; disparity in results from studies in China, Alaska and Siberia further confirm this assertion. Kauroa Ash sequence magnetic properties also support a sequence-by-sequence analysis (or at least region-by-region), following none of these previous studies to a complete degree.

## 4 PARTICLE-SIZE ANALYSIS

---

### 4.1 INTRODUCTION

#### 4.1.1 *The study of particle size*

The proportion of particles in different size fractions can be an important parameter in the study of soils and associated parent materials including tephra. Textural classification may allow inferences to be made about provenance, as well as being an indicator of the degree of weathering. In a study undertaking a characterisation and paleoenvironmental analysis of paleosol, loess and tephra beds, these parameters are clearly important.

A study by Vandenberghe et al. (1997) demonstrated the usefulness of particle-size analysis in paleoclimatic reconstruction. Measurements on a Chinese loess column provided clear differences between (buried) soil and loess units, with loess samples shown to have a more positively (larger size) skewed particle-size distribution than soil samples. This study also utilised the 'U-ratio', the ratio of 44-16  $\mu\text{m}$  and 16-5  $\mu\text{m}$  size material, to illustrate the paleoclimatic uses of particle-size analysis: the 44-16  $\mu\text{m}$  fraction is inferred to represent the dust-bearing monsoons typical of glacials, while the 16-5  $\mu\text{m}$  is inferred to represent the finer dust of interglacials. The ratio between these fractions was used to illustrate inferred paleoclimatic differences over time and was able to be compared with an oxygen isotope curve.

Particle-size analyses have also been employed in the study of loess (e.g. Benney et al., 1988) and tephric-loess (e.g. Lowe, 1981) in New Zealand. 'Typical' loess is usually characterised in the literature as ranging from 20-50  $\mu\text{m}$  with a modal particle size of about 30  $\mu\text{m}$  (Kennedy, 1982; Pye, 1987). However, Pye (1995) reported that in practice the modal size could show considerable variability depending on location. It is generally accepted, though, that the great majority of primary loess deposits contain more than 50% silt-sized particles (Winspear and Pye, 1995). Weathered loess is primary loess whose aeolian sedimentary characteristics have been markedly modified by weathering, soil formation or diagenesis. The deposit usually contains more clay (up



to 60%) than unweathered loess (Pye, 1987).

Various parameters of particle-size analysis were measured on the Kauroa samples with the aim of identifying trends in particle-size characteristics for each sample type. Positive identification would provide an additional means of characterising these deposits, as well as provide a potential proxy for paleoenvironmental interpretation. The study of loess plays a large part in this chapter because this unit type, more than the others, is most often defined by its particle-size characteristics.

#### *4.1.2 Particle-size analysis of the Kauroa Ash sequence*

Salter (1979) analysed 26 samples for particle size in his study of the Kauroa Ash sequence. Methodologies used in that study were hydrometer, centrifuge and hydrophotometer. This study aims to provide a higher resolution study, in terms of both quantity and accuracy, of the particle-size characteristics of the Kauroa Ash sequence. With this in mind, half of the samples from the Woodstock type-site (a total of 90) were analysed, with selected samples (representative of each unit, totaling 34) chosen from the Papakura Creek site. Analysis of further samples was deemed unnecessary due to the repetitious nature of the results (samples proving quite similar) and the cost-constraint on large numbers of samples.

#### *4.1.3 Laser diffraction particle-size analysis*

Samples were analysed on a Malvern Mastersizer-S, a fully automatic particle sizer, based on the laser diffraction principle. This states that particles of a given size diffract light through a given angle, the angle increasing with decreasing particle size. In the case of the Mastersizer, a laser is passed through the suspension, and the diffracted light focused on a multi-element ring detector, which senses the angular distribution of scattered light intensity. The distribution is expressed in terms of equivalent spheres, and is volume-based; output is in a set of size classes that have been optimised to the detector geometry and optical configuration to give the best resolution. All parameters are derived from this fundamental distribution (Rawle, 1993).

According to Buurman et al. (1997), particle-size analysis by laser diffraction has great potential for use in soil science, especially for detailed comparison of samples from the

same sequence to establish homogeneity of parent materials, for textural changes caused by weathering, and for changes in aggregation. The laser sizer, in particular, gives easily accessed, detailed and accurate information relating to fine fractions (clays) (Muggler et al., 1997). This is in contrast to traditional methods (e.g. hydrometer or pipette analysis) that are time-consuming and can be inaccurate in these smaller fractions (Konert and Vandenberghe, 1997; Beuselinck et al., 1998).

## 4.2 SAMPLE PREPARATION

There are several considerations in the preparation of samples for laser diffraction particle-size analysis.

### 4.2.1 *Sample size*

Determining a suitable sample size for laser diffraction is an important issue because the clay content of a sample contributes strongly to ‘obscuration’<sup>1</sup> which, if too high or low (>30%, <10%), can render the measurement inaccurate. Coarse sands would require several grams of sample, but in this study where clays dominate, only very small samples in the order of 100s of milligrams are required. Several pilot samples were analysed to determine the optimum sample weight, and it was demonstrated that 0.5 g was an appropriate amount that produced satisfactory obscuration values for most samples. Some samples required re-sampling and remeasurement at 0.3 g, and it is suggested that future workers of similar sorts of samples (depending on estimated clay fraction) consider a range of 0.2-1.0 g. It is useful to get this right at the outset as the extensive pretreatments required of these samples means that multiple replicates of samples are impractical, and time-consuming.

### 4.2.2 *Sample homogeneity*

Soil samples can be notoriously inhomogenous, and it is obvious that the representativeness of samples of a few hundred milligrams may be questionable (Buurman et al., 1997). Efforts must therefore be made to ensure the best selection of

---

<sup>1</sup> The measure of the amount of sample added to the tank. Unscattered light is focused on the obscuration detector. If there is no sample present then the obscuration is zero. When the sample is introduced some of the light is absorbed, reflected, diffracted and scattered (Rawle, 1993).

subsample. In this study, subsamples were taken from air-dried samples, and care was taken to first homogenise the material in an attempt to eliminate any sorting that may have taken place in the storage container.

#### 4.2.3 Sample pretreatment

Samples for laser diffraction have to be pretreated to remove aggregation and dispersed to prevent flocculation, the latter being particularly important where allophane (which has a variable charge and a high propensity for flocculation) may be present. Consideration was given to pretreatment and dispersion techniques suggested by Wada and Harward (1974), Whitton and Churchman (1987), Alloway et al. (1992) and Buurman et al. (1997), and the following procedure was devised and tested. It was successful in disaggregating and dispersing floccs.

1. Measure 0.5 g of air-dried sample into a glass vial
2. Add 10 ml of 10% hydrogen peroxide
3. 5 minutes in ultrasonic bath
4. 1 hour on shaker table
5. Leave overnight
6. 5 minutes in ultrasonic bath
7. Heat gently on a hot plate - allow moisture to evaporate but do not allow samples to become dry
8. Add 10 ml sodium hexametaphosphate ('calgon')
9. 5 minutes in ultrasonic bath
10. 1 hour on shaker table
11. If not all completely disaggregated, leave overnight and repeat 8-9 as required.

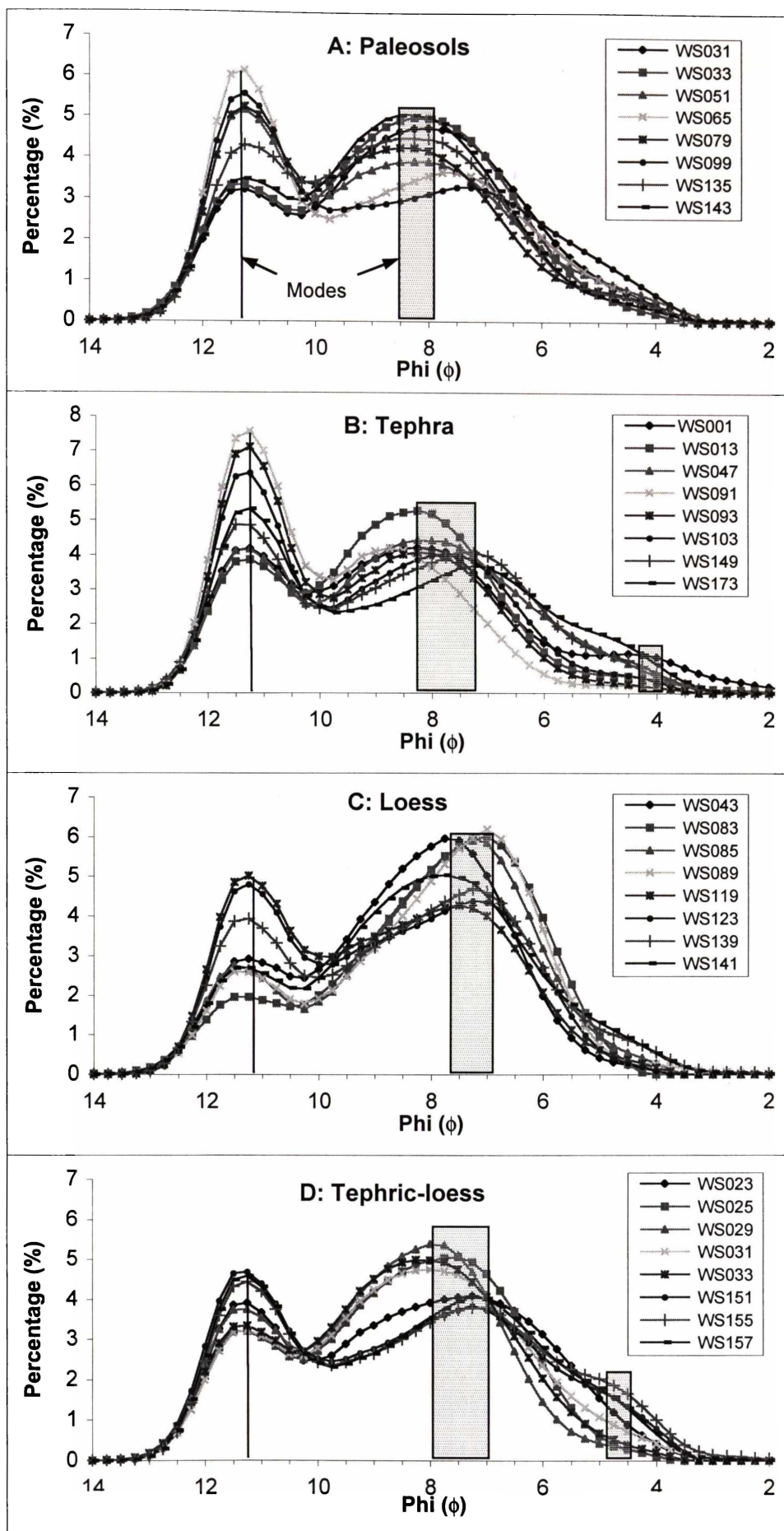
### 4.3 RESULTS

#### 4.3.1 General particle-size characteristics of the Kauroa Ash sequence

Figure 4.1 shows some typical raw distribution curves<sup>2</sup> of samples from the Woodstock type section, categorised by sample type. Visual analysis of these curves gives an immediate indication of general characteristics of the Kauroa Ash beds. The majority of samples are typically bimodal, some polymodal, and a large proportion of the volume concentration is clay-sized (i.e. smaller than  $8 \phi / 4 \mu\text{m}$ ), with a significant proportion being centred on a peak at  $11.25 \phi$  ( $0.5 \mu\text{m}$ ). These latter features largely reflect the major characteristic of these beds, their intensely weathered and altered state.

---

<sup>2</sup> See Table 4.1 for phi-micron comparisons.



**Figure 4.1** Example particle-size distribution curves by sample type. (WS-numbers are sample numbers)

**Table 4.1** Particle-size scales<sup>1</sup> and size classes.

Wentworth Size Class <sup>2</sup>	Microns ( $\mu\text{m}$ )	Phi ( $\phi$ )
Coarse sand	>500	1
	420	1.25
Medium sand <sup>3</sup>	350	1.5
	300	1.75
	250	2
	210	2.25
	177	2.5
Fine sand	149	2.75
	125	3
	105	3.25
Very fine sand	88	3.5
	74	3.75
	63	4
	53	4.25
Coarse silt	44	4.5
	37	4.75
	31	5
	26	5.25
Medium silt	22	5.5
	18.6	5.75
	15.6	6
	13.1	6.25
Fine silt	11.0	6.5
	9.3	6.75
	7.8	7
	6.6	7.25
Very fine silt	5.5	7.5
	4.6	7.75
	3.9	8
	3.3	8.25
Coarse clay	2.8	8.5
	2.3	8.75
	2.0	9
	1.64	9.25
Medium clay	1.38	9.5
	1.16	9.75
	0.98	10
	0.82	10.25
Fine clay	0.69	10.5
	0.58	10.75
	0.49	11
	0.41	11.25
Very fine clay	0.35	11.5
	0.29	11.75
	0.24	12
	0.21	12.25
'Ultrafine' clay	0.17	12.5
	0.15	12.75
	0.12	13
	<0.06	14

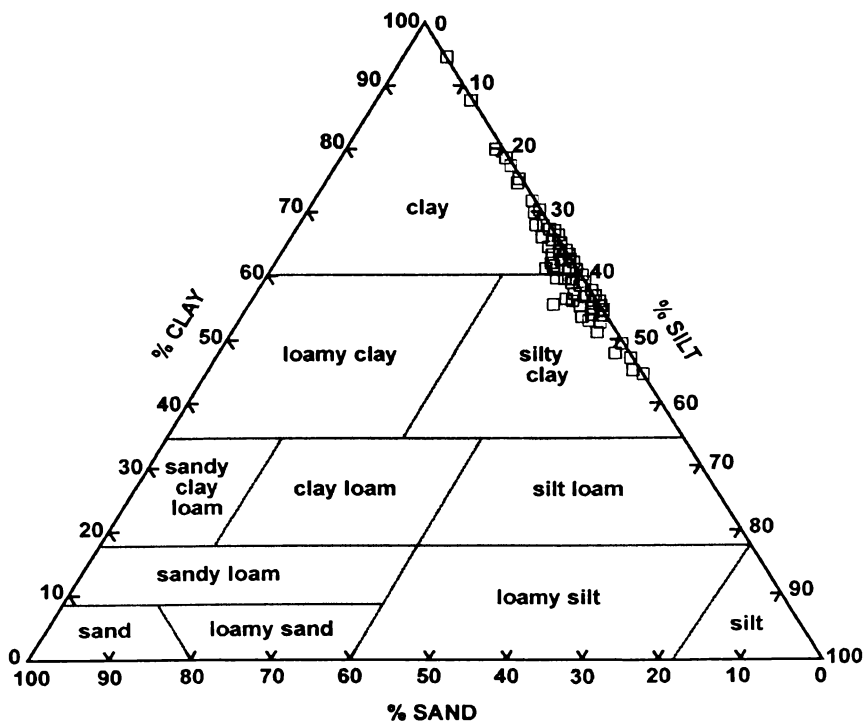
<sup>1</sup> Particle-size range covered by Malvern Mastersizer-S.<sup>2</sup> After Folk (1968)<sup>3</sup> Particle sizes given imply 'greater than' e.g. medium sand comprises those particles >250  $\mu\text{m}$  - <500  $\mu\text{m}$ .

Some summary statistics give a more complete picture. Figures 4.2 and 4.3 show the sand (63-500  $\mu\text{m}$ ), silt (4-63  $\mu\text{m}$ ) and clay (<4  $\mu\text{m}$ ) percentages for Woodstock (WS) and Papakura Creek (PC) samples. It can be seen that in most cases, clays form the dominant portion of the particle-size range, with a maximum of 96% and a minimum of 43% at WS; maximum 80% and minimum 41% at PC. Silt is second-most dominant, WS with a maximum of 57% and a minimum of 4% silt, PC having a maximum 59% and a minimum 17% silt-sized particles. Sand content is, in most cases, minor to negligible, reaching a maximum of 5.4% at WS and 7.6% at PC and a minimum of 0% at both locations. Means for all Kauroa beds at the two sites are shown in Table 4.2.

**Table 4.2** Mean sand, silt and clay content at Woodstock and Papakura Creek.

SITE	<i>n</i>	SAND % (63-500 $\mu\text{m}$ )	SILT % (63-4 $\mu\text{m}$ )	CLAY % (< 4 $\mu\text{m}$ )
Woodstock	101	1.0	39.4	59.6
Papakura Creek	38	2.2	35.3	62.5

Plotting sand, silt and clay percentages on a ternary diagram for soil texture analysis (Figure 4.4), confirms what was suspected in the field, that all Kauroa beds are 'Clay' to 'Silty clay' using Milne et al. (1995).



**Figure 4.4** Soil texture classification diagram showing the textural classification of Woodstock samples (soil texture classes after Milne et al., 1995).

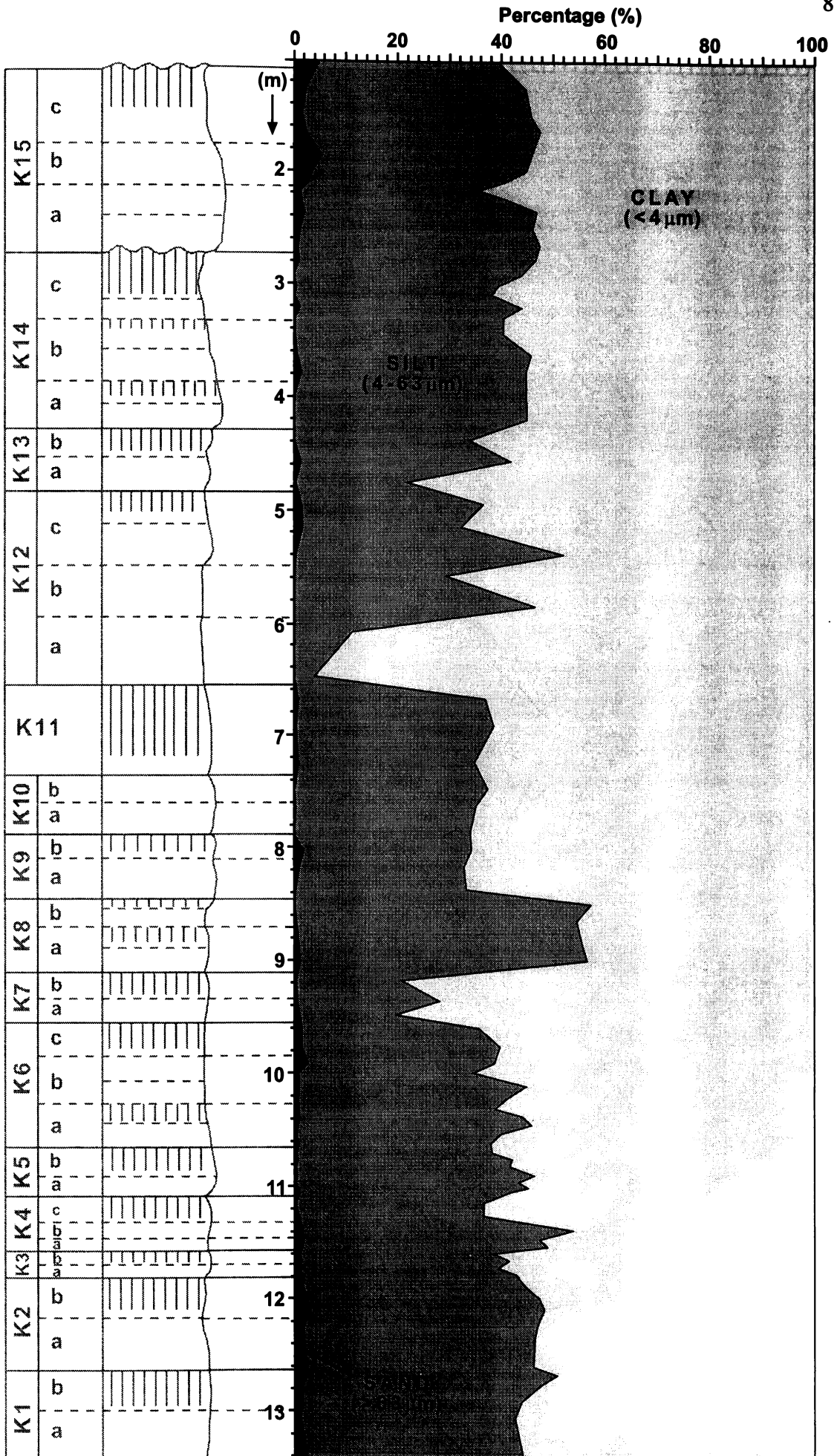


Figure 4.2 Percentage of sand, silt and clay at the Woodstock type section.



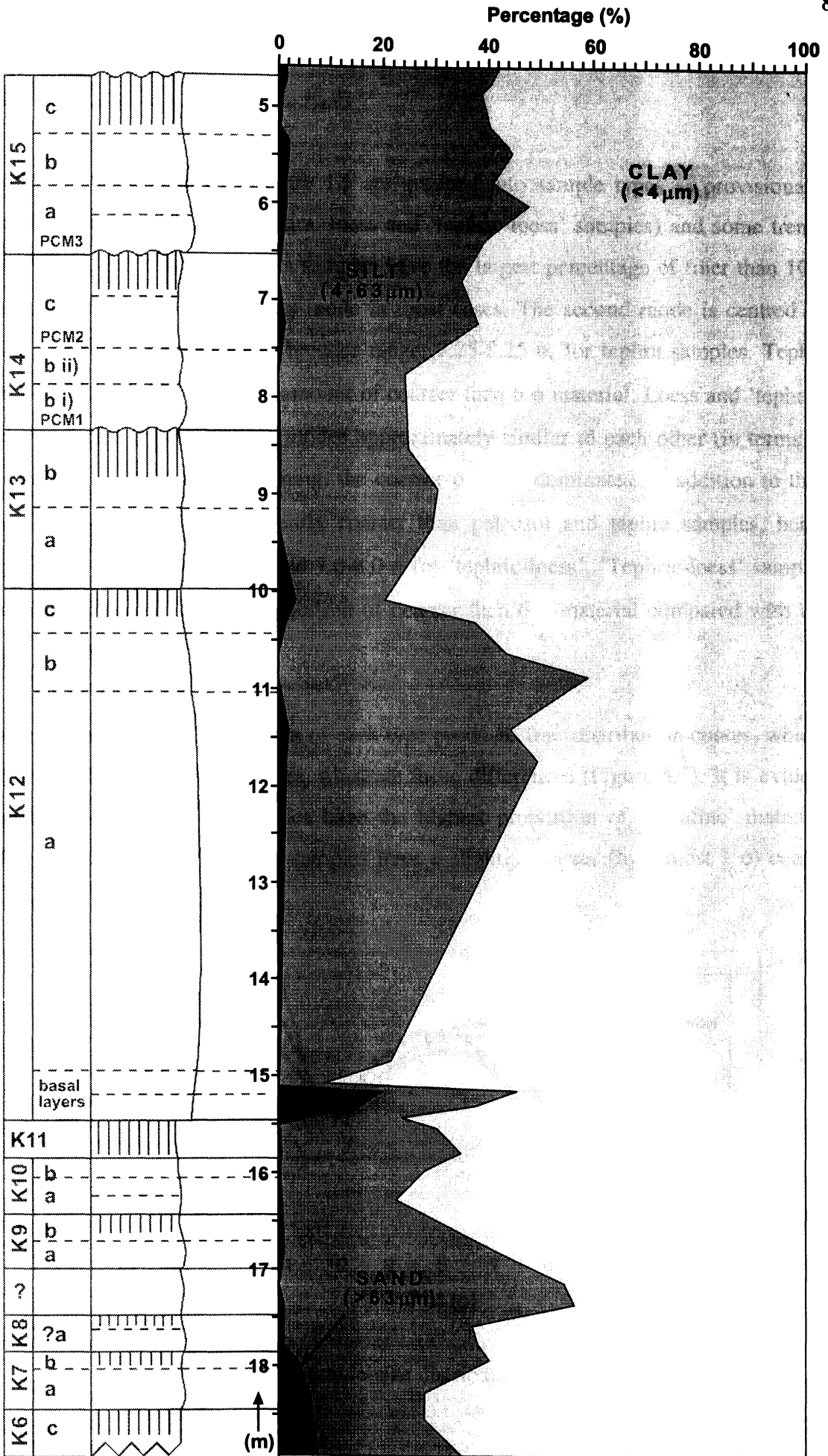


Figure 4.3 Percentage of sand, silt and clay at the Papakura Creek section.

## 4.4 ANALYSIS AND DISCUSSION

## 4.4.1 Characterisation of sample types

The distribution curves in Figure 4.1 are grouped into sample types as provisionally identified earlier (paleosol, tephra, loess and 'tephric-loess' samples) and some trends are evident. Paleosol and tephra samples have the largest percentage of finer than 10  $\phi$  particles, this being the primary mode in most cases. The second mode is centred on 8.0-8.5  $\phi$  for paleosols, and a broader range, 7.25-8.25  $\phi$ , for tephra samples. Tephra samples also display a greater amount of coarser than 6  $\phi$  material. Loess and 'tephric-loess' samples appear to have modes approximately similar to each other (in terms of percentage of each) or, if anything, the coarser- $\phi$  mode dominates. In addition to this, the coarse- $\phi$  mode is consistently coarser than paleosol and tephra samples, being typically 7.0-7.75  $\phi$  for loess and 7.0-8.0  $\phi$  for 'tephric-loess'. 'Tephric-loess' samples additionally have a greater proportion of coarser than 6  $\phi$  material compared with the loess samples.

Taking an average of all samples of each type produces four distribution curves, which, while similar in overall structure, illustrate these differences (Figure 4.5). It is evident that tephra and paleosol samples have the highest proportion of 'ultrafine' material, while loess and 'tephric-loess' samples have a slightly coarser (by almost 1  $\phi$ ) coarse mode.

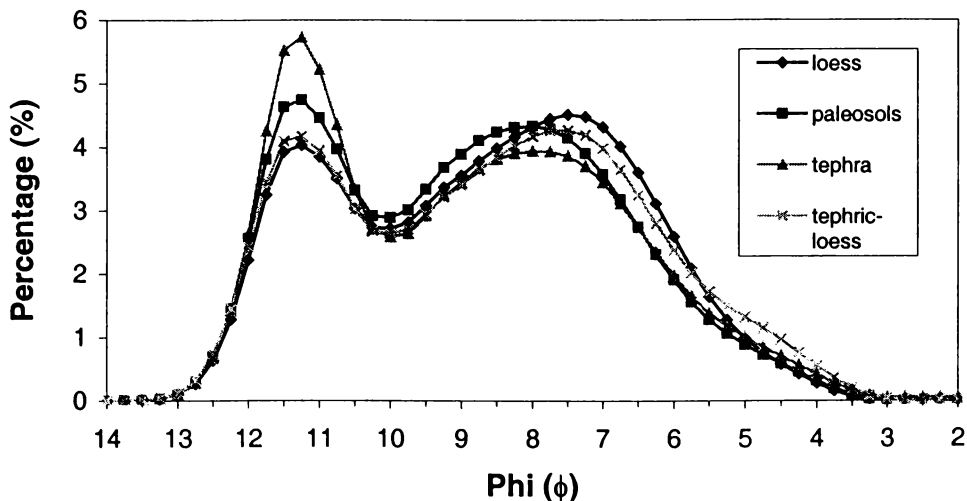
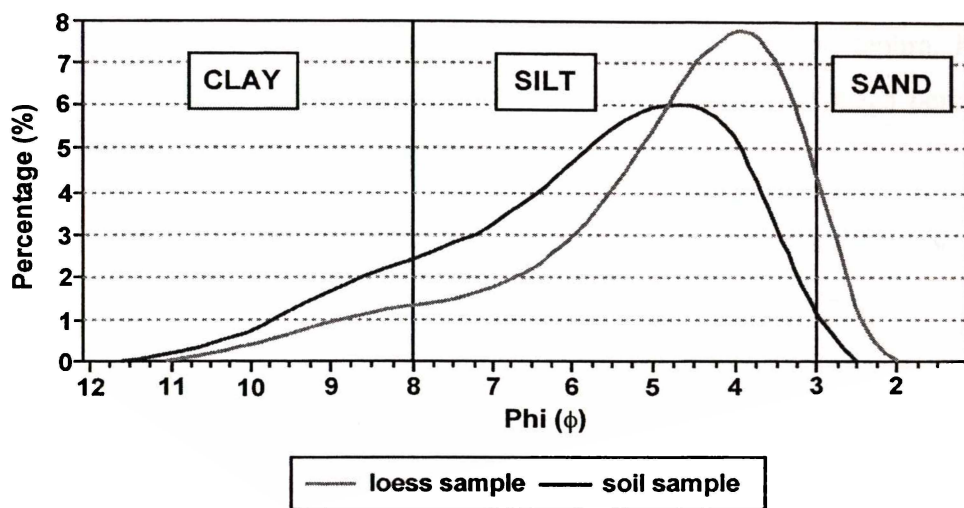


Figure 4.5 Mean particle-size distribution of sample types.

Vandenberghe et al. (1997) compared distribution curves of a ‘typical loess’ sample and a ‘typical soil’ sample (Figure 4.6). While the particle sizes of those samples are much larger and do not match directly with loess and paleosol samples in this study<sup>3</sup>, one feature is relevant – the loess sample has a mode that is typically 1  $\phi$  larger than the soil sample. It is remarkable that despite the extreme age and extensive weathering the Kauroa samples have undergone, they still appear to have retained this characteristic.

The trends observed here will be discussed further with the use of some summary statistics.



**Figure 4.6** Comparison of particle-size distributions of a typical loess and a typical soil sample (after Vandenberghe et al., 1997).

#### 4.4.2 Percentage of sand, silt and clay

Figures 4.2 and 4.3 show that some units have a characteristic particle size (in terms of sand-silt-clay contents) while others do not. K8 at Woodstock, for example, clearly stands out as having a relatively low (45%) clay content and a relatively high (55%) silt content compared with other beds; K12a has an extremely high clay (95%) and very low (>5%) silt content; K15b at Woodstock is distinguished by its relatively high (3-5%) sand content. However, many consecutive units also have very uniform particle-size characteristics with no feature of their sand, silt or clay contents to distinguish between them (e.g. K9-K11).

<sup>3</sup> Samples in Vandenberghe et al. (1997) were <50 ka and much less weathered than (most) samples in this study.

In terms of characterising unit types, therefore, sand-silt-clay ratios would seem to be of limited help. Paleosol beds (e.g. tops of K1, K5, K6, K11, K13 and K15) have little distinguishing particle size, conforming, for the most part, to the sand-silt-clay average. As expected, tephra beds (K1, K3, K4c, K7, K10b, K12a and b, K14bi and ii, K15a, b and c) have the most variation, but in general have slightly higher-than-average clay content (60-75%) and higher-than-average sand content (>1%). Loess and 'loess-like' beds (e.g. K4a-b, K5, K6a, K8, K10a and K14a) have a slightly higher-than-average silt content (40-50%).

Thus on closer inspection slight trends can be discerned, and these are quantifiable when the samples were divided into the genetic groups – paleosol, tephra, loess or 'tephric-loess' – and averages calculated. Table 4.3 summarises the mean percentages of sand, silt and clay for each sample type.

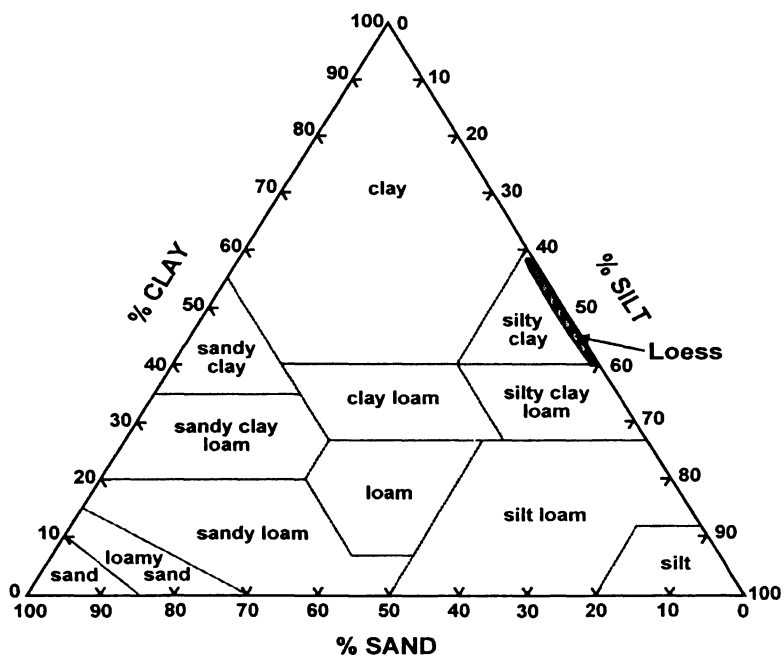
**Table 4.3** Average percentage of sand, silt and clay by (genetic) bed type.

SAMPLE TYPE	<i>n</i>	SAND % (63-500 µm)	SILT % (63-4 µm)	CLAY % (< 4 µm)
Paleosol	27	0.7	38.8	60.5
Tephra	37	1.3	36.3	62.4
Loess	24	0.6	43.6	55.8
'Tephric-Loess'	13	1.3	42.3	56.4

The differences are not large, but as with the analysis in Section 4.4.1., suggest some logical distribution characteristics for each unit type. Tephra-derived samples have the highest clay content, illustrating, perhaps, the fine-grained nature of the original deposits (given that these are distal deposits and particle size usually decreases with distance from source). It also represents their age and the low resistance of most volcanic minerals (especially pyroclastic, i.e. fragmental, material) to weathering, with many of the tephra units in the Kauroa Ash sequence having been intensely altered since deposition. This too is illustrated in the mean percentage of clay-sized particles in the paleosols, the 60.5% figure pointing to a fine-grained deposit that has undergone intensive pedogenic processes. Tephra and paleosols are seemingly differentiated by a slight difference in percentage of sand-sized particles, and perhaps in silt percentage where tephra samples seem to have the least of all the four sample-types. Loess samples have, on average, 5% less clay-sized particles and 5% more silt-sized particles than in the paleosol and tephra samples. Loess is in part defined by its dominant silt fraction, though samples of this age would not, necessarily, be expected to have retained that characteristic. This statistic shows that these samples do still have a greater proportion

of silt-sized particles than other samples, and it may be assumed that this feature was more pronounced at the time of deposition. The last group of samples, 'tephric-loess', has silt and clay proportions similar to those in the loess samples, but more sand and clay-sized particles. This pattern is suggestive of a combination of loess and tephra particle-size characteristics.

As a further note on loess samples, a large proportion of them plotted in the 'silty clay' section of the soil texture classification diagram in Figure 4.4, the exception being K10a which has slightly less silt, and the addition being K1, K2 and K14b and c. This is interesting when compared with the example textures given by Pye (1995) (Figure 4.7). There, too, loess plots neatly into the 'silty clay' section of the diagram and this accords with the trends suggested above.



**Figure 4.7** Soil texture classification diagram (of Great Britain) showing the textural composition of loess (after Hodgson, 1974, and Pye, 1995; note texture classes are slightly different from those in Figure 4.4).

It should be noted that the observed trends in sand, silt and clay percentages could not be described as 'consistent' through all samples and certainly could not be used for anything other than tentative characterisation purposes. What is also evident is the distinct lack of good correlation between the two sites, in terms of absolute values or even relative differences. Average sand, silt and clay percentages for all samples at the two sites (Figures 4.2 and 4.3) are not contradictory, but on a bed-by-bed basis little similarity is evident. Even the aforementioned 'stand-out' beds (e.g. K8, K12a and

K15b) fail to distinguish themselves as such at the PC site, and this really undermines the use of texture as a correlation tool. However, as suggested by Buurman et al. (1997), it has been useful as a general characterisation tool on a site-specific basis.

Overall, in the case of these two sites, it would be difficult to determine stratigraphy 'blindly' by sand-silt-clay proportions. Some beds do differentiate themselves by virtue of their distinctive particle-size characteristics, and with knowledge of unit types, minor trends can be observed. However, it would seem that without prior knowledge of unit types or boundaries, it would be very difficult to distinguish between them based on textural evidence alone in these sorts of weathered deposits.

#### *4.4.3 Volume-weighted mean and standard deviation*

Volume-weighted mean and standard deviation have been employed in stratigraphic studies to provide a quick estimation of average particle size and sorting. They are presented here (Figure 4.8) for evidential purposes but with the understanding that 'mean', in particular, has limited value when particle-size populations are bimodal as is the case here.

The standard deviation curve, for the most part, varies in accordance with the mean particle-size curve, which in turn shows significant similarity to the sand percentage curve (when viewed on an expanded x-axis – not so evident in Figures 4.2 and 4.3). This is not entirely surprising and can be explained as follows. Nearly all samples have a major particle-size mode at 11  $\phi$  (0.5  $\mu\text{m}$ ), presumably representing the weathered (mostly pedogenic) fraction present in all beds. This acts as a common lower boundary, so that any (albeit small) increase in sand percentage has a significant effect on the mean value, which in turn affects the range and sorting represented by the standard deviation. Thus, a slightly increased sand percentage has no concomitant decrease in clay content, reflecting the independent, post-depositional (in situ) origin of the latter. This therefore has the effect of 'stretching' the particle-size range and generating a standard deviation curve that closely matches both the mean particle size and sand percentage.

As such, there is little characterisation value to these parameters in this study, even though it is commonly used in other studies. Only where a bed is extremely dominant in

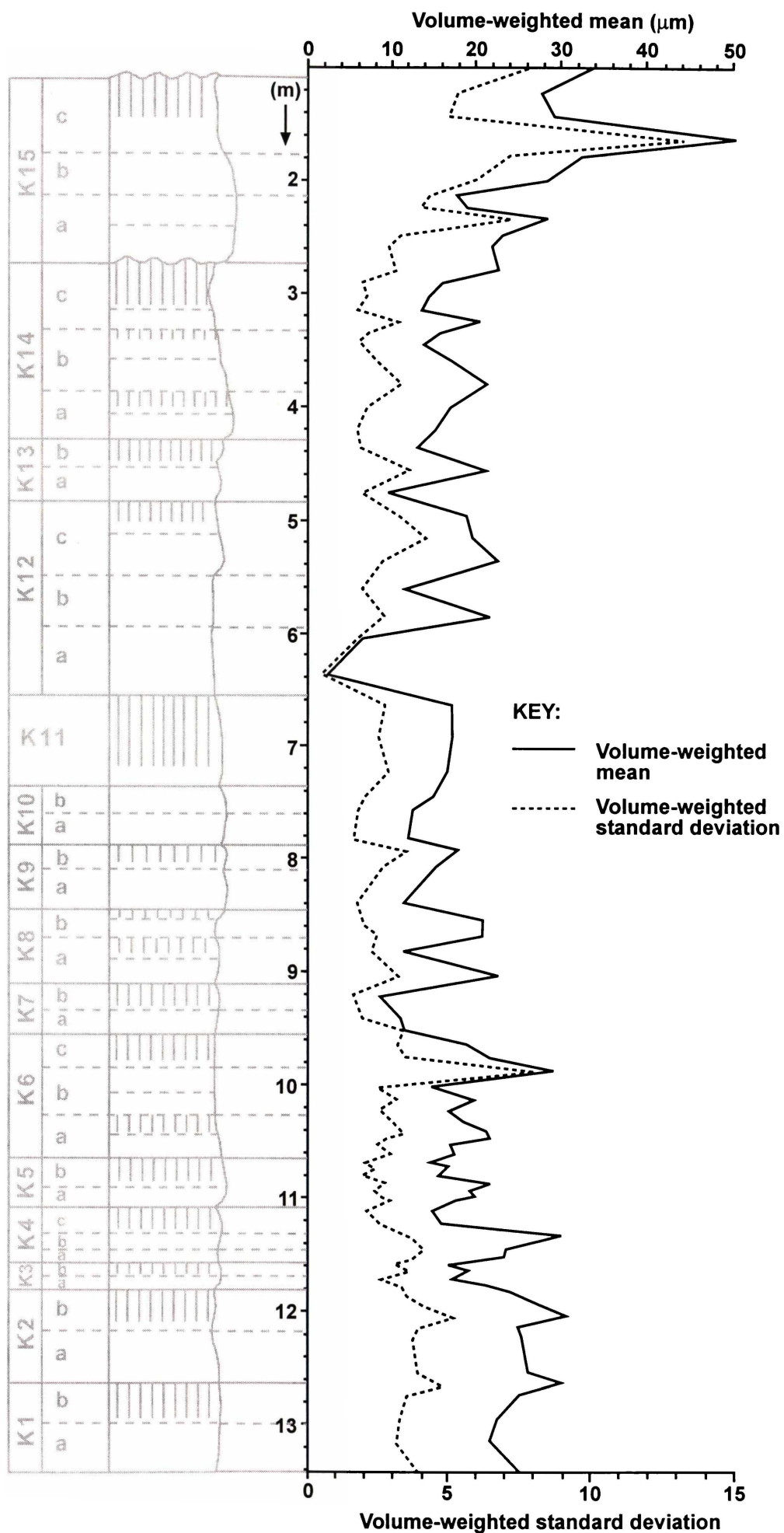


Figure 4.8 Weighted mean and standard deviation of Woodstock samples.



clay (as in K12a) is it well sorted (low standard deviation). Loess beds (>40% silt) should be well sorted according to standard definitions, but because of the lower  $11 \phi$  peak, appear to have a high standard deviation. This reflects the higher quantity of silt in the deposits, having the same effect as a small quantity of sand. If the pedogenic phases could have been eliminated, they would have had a lower standard deviation, reflecting the (slight) dominance of silt.

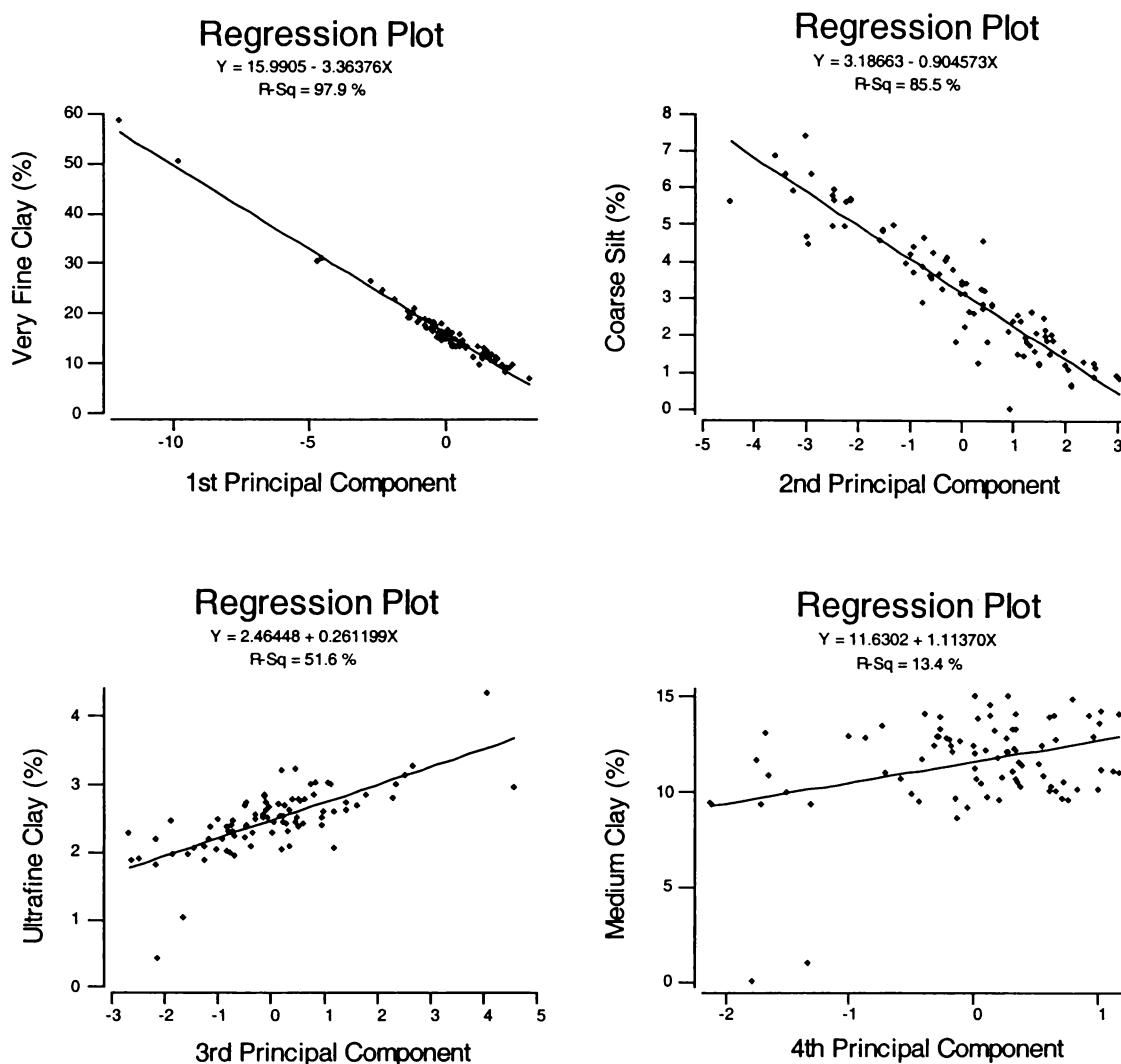
#### 4.4.4 Principal Component Analysis and U-ratio

Principal Component Analysis (PCA) is a standard mathematical tool used to provide insight into the structure of a variance-covariance matrix (Davis, 1986). The principal components of a population of observations are the characteristic vectors of the covariance matrix constructed from the population. Projecting the data into their principal components generally results in a compact and meaningful representation in which the first few characteristic vectors describe the major modes of data variation. In other words, PCA performs feature extraction from a large data matrix and hence lends itself to the description of the large data sets generated by particle-size analysis of several samples. Apart from a general analysis of covariance, the first principal component is additionally said to be an indication of the energy levels in the depositional environment (Davis, 1986).

PCA was used by Vandenberghe et al. (1997) to validate the use of the U-ratio, the ratio of the 44-16  $\mu\text{m}$  : 16-5  $\mu\text{m}$  size fractions. The first principal component of their grain-size data (accounting for 87% of the variance) had strong positive loadings for the fine-silt fractions, and negative loadings for the coarse-silt fraction, supporting the use of the U-ratio as a paleoenvironmental proxy.

##### 4.4.4.1 Principal components of Kauroa Ash samples

Principal components (four) were calculated for Kauroa Ash samples (Woodstock site). To establish the size range to which they were related, each component was plotted against each size class and R-square values calculated. The highest R-square value available for each component represents the 'best-fit' size class (i.e. the size class that accounts for the majority of the first, second, third and fourth characteristic vectors of the data set). These are shown in Figure 4.9 and Table 4.4.



**Figure 4.9** Regression plots of principal components and size classes

**Table 4.4** Principal components of particle-size data from the Woodstock section.

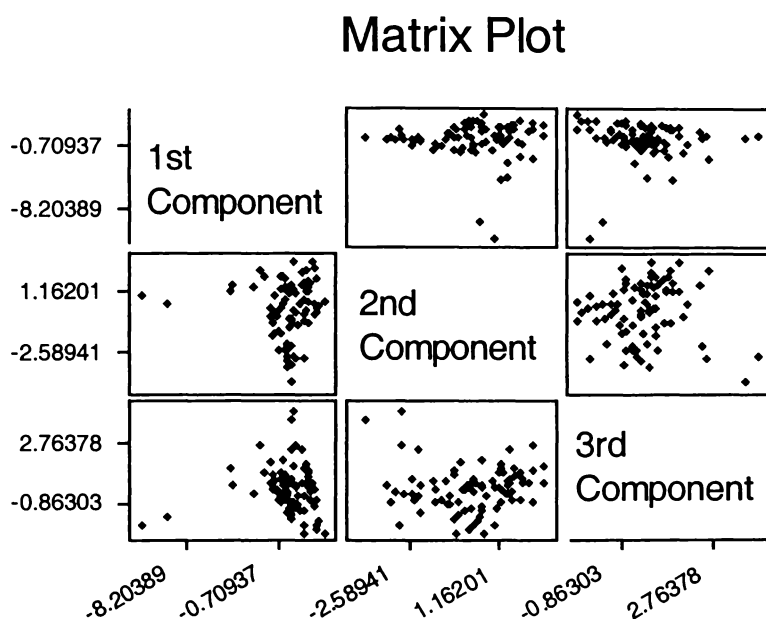
Principal Component	Best R-squared value	Size Class <sup>1</sup>	Size Range
First	97.9%	Very Fine Clay	0.24-0.5 $\mu\text{m}$
Second	85.5%	Coarse Silt	16-63 $\mu\text{m}$
Third	51.6%	Ultrafine Clay	< 0.24 $\mu\text{m}$
Fourth	13.4%	Medium Clay	1-2 $\mu\text{m}$

<sup>1</sup> Wentworth size classes as shown in Table 4.1

The first principal component of the data has a very strong correlation to 'very fine clay' and likely represents the pedogenic component of the particle-size distribution (represented by the marked 11.25  $\phi$  mode seen in the distribution curves). This supports the assertion that the primary process evident in these deposits is in situ weathering. The second principal component correlates well to the 'coarse silt' fraction, accounting for (the majority of the volume of) the second mode seen in the distribution curves. The

relative strength of this component (high R-squared value) relates to the strong bimodality of these samples. The third and fourth principal components have considerably less directionality than the first two, indicating these are only small vectors – the first two are the dominant components present.

Plots of each principal component to the others (first to third components) resulted in little directionality and only limited clustering (Figure 4.10). This indicates there is no real relationship between each characteristic vector. Processes responsible for the production of these dominant size fractions are not acting in tandem or in a proportional manner.



**Figure 4.10** Matrix plot of first, second and third principal components of the Woodstock section particle-size data set.

#### 4.4.4.2 Principal components of sample types

The first and second principal components were calculated for each sample type and their relationships to each size class examined with the use of R-squared values (Table 4.5). The results serve as a statistical confirmation of the earlier visual analysis of the distribution curves (and sand, silt and clay averages) for each sample type. There are small differences between sample types, mostly in terms of emphasis of mode (size class with the highest R-squared value). In all cases except tephric-loess samples, the first component is extremely dominant. The second components show more variation in

**Table 4.5** R-squared values (%) of the relationship between principal components and size classes, by sample type, Woodstock section.

Size Class <sup>1</sup>	All samples		Paleosol		Loess		Tephra		Tephric-loess	
	1 <sup>st</sup> Comp	2 <sup>nd</sup> Comp	1 <sup>st</sup> Comp	2 <sup>nd</sup> Comp	1 <sup>st</sup> Comp	2 <sup>nd</sup> Comp	1 <sup>st</sup> Comp	2 <sup>nd</sup> Comp	1 <sup>st</sup> Comp	2 <sup>nd</sup> Comp
Coarse sand	-	-	-	-	-	-	-	-	-	-
Medium sand	-	-	-	-	-	-	-	-	-	-
Fine sand	0.9	27.2	6.9	0.1	0.0	29.9	5.1	46.6	17.2	38.0
Very fine sand	0.6	69.3	6.8	43.6	0.2	54.2	12.4	71.3	71.0	89.1
Coarse silt	2.9	35.5	0.4	38.1	0.0	80.0	20.1	79.2	67.0	99.0
Medium silt	21.3	51.4	21.7	53.3	19.1	36.1	38.8	48.5	33.0	85.4
Fine silt	62.4	1.3	64.3	3.4	62.9	0.2	76.9	9.1	0.1	23.0
Very fine silt	80.5	11.7	82.9	19.1	74.2	11.8	86.4	2.2	73.5	95.4
Coarse clay	55.5	32.7	54.1	42.8	26.0	22.0	69.8	11.5	73.4	96.3
Medium clay	47.2	16.3	15.9	25.0	14.5	12.8	76.5	2.4	73.1	92.8
Fine clay	95.4	1.1	96.6	0.0	96.5	3.9	97.2	5.5	86.8	29.2
Very fine clay	97.9	0.6	96.5	0.0	92.3	4.5	99.0	3.7	85.6	29.9
Ultrafine clay	14.3	3.2	0.0	8.1	19.5	1.5	37.6	2.4	5.6	7.6

1. Wentworth size classes (Table 4.1).

2. Bold shading represents the main contribution to each principal component; lighter shading shows secondary contribution. Since the limits of each size classes are somewhat arbitrarily defined, the main contribution to each principal component will not necessarily fall in one class. Some samples or sample types will have a broader range of contribution than others (relating to kurtosis of mode).

strength. Tephric-loess samples stand apart from others for their unusually strong, broad range second component, indicating a large volume contribution from medium clay through to very fine sand. This is interpreted to reflect the range of particle-size contribution from mixed (tephra plus loess) parent material.

Differences between principal components of each sample type and the average of all samples are thus relatively minimal, reflecting those variations already discussed. In this sense, the Kauroa Ash sequence is demonstrated to be texturally reasonably homogenous.

#### 4.4.4.3 U-ratio in particle-size analysis of weathered deposits

Because of these findings, the application of the U-ratio would have little meaning for these samples: the principal components of these data do not match the sediment-size fractions involved in the calculation (16-5  $\mu\text{m}$ ; 44-16  $\mu\text{m}$ ). Indeed, for this reason, the U-ratio is unlikely to be appropriate for any samples as weathered as those in this study. The ratio was devised for loess deposits that are substantially less weathered and does not account for the fining of particle size that comes with weathering. If a similar diagnostic ratio is desired it should be constructed with respect to the principal components of the particular data set.

## 4.5 CONCLUSIONS

Particle-size analysis produced some mixed results for the Kauroa samples. Some trends in 'genetic' sample type have been observed (particle-size distributions of paleosol, tephra, loess and 'tephric-loess' samples) and a tentative 'particle-size' stratigraphy established. However, many of the samples displayed very similar particle-size characteristics, in particular, a dominance of the very fine clay to fine clay fractions.

These limitations noted, the technique can still provide some useful information on the character of weathered deposits, and some points of significance are documented:

- Kauroa Ash samples (Woodstock type site) have a mean clay (<4  $\mu\text{m}$ ) content of c. 60%, a mean silt (4-63  $\mu\text{m}$ ) of c. 39%, and a mean sand (>63  $\mu\text{m}$ ) content of c. 1% ( $n=101$ ). Papakura Creek samples showed similar mean values.

- The majority of Kauroa Ash samples have bimodal particle-size distributions.
- The 'fine' mode is, in every case, centred on 11.25  $\phi$  ('very fine clay') and is inferred to be the product of weathering and/or pedogenesis.
- The size and exact position of the 'coarse' mode varies with sample type, but is generally between 7 and 8  $\phi$ .
- Loess samples had, on average, a 'coarse' mode that was 1  $\phi$  coarser than paleosol or tephra samples. This is the same difference seen in unweathered loess and paleosol samples.
- 'Tephric-loess' samples were demonstrated to have particle-size characteristics of both tephra and loess samples.
- Volume-weighted mean has no significance for bimodal particle-size populations; its meaningful application is additionally hampered by a large clay-sized peak representing extreme weathering.
- Principal components analysis is a useful objective way of describing correlations in particle-size data.
- The U-ratio is unsuitable for weathered deposits. Alternative ratios can be devised from principal components.

The general similarity in results, from top to bottom of the sequence, irrespective of bed type, demonstrates that this sequence as a whole is extremely weathered (minimum 43% <4  $\mu\text{m}$  clay). Weathering has had a 'smoothing' effect on the particle-size data, with the original (antecedent) particle-size distributions long having been erased by disaggregation and decomposition to clay-sized particles. This smoothing effect is even more marked for particle-size analysis than it is for magnetic susceptibility (previous chapter). This is because weathering has a direct effect on particle size (disaggregation and decomposition of particles) as opposed to the more indirect effect it has on magnetic mineralogy (the translocation of ultrafine particles and production of pedogenic ferrimagnetic grains).

Particle-size analysis is not a useful correlation tool for the Kauroa Ash sequence. While averages of all samples at each site are approximately the same (e.g. sand, silt, clay content; Table 4.2), individual beds or units often show little resemblance to others and texture alone would not be able to establish correlation. This undoubtedly reflects the varying weathering regimes arising from geomorphological and micro-environmental differences between sites, as well as from differing thicknesses of original deposits due

to location (distance from sources). Particle-size distributions are very sensitive to types and quantity of weathering, illustrated in these data sets where although the parent material, climate and time<sup>4</sup> for weathering is the same for each bed, the resulting distributions are quite different.

---

<sup>4</sup> Three of the five factors determining weathering (with topography and vegetation) (e.g. Lowe, 1986).

## 5 CHRONOLOGY

---

### 5.1 INTRODUCTION

Establishing a chronology is an important part of the analysis of any sequence of deposits. A broad stratigraphic context has been established for the Kauroa Ash sequence in the preceding chapters, but this is of limited value if it cannot be placed within the wider New Zealand geological chronostratigraphic framework. Stratigraphy alone offers relative age information relating to superposition of beds (e.g. K1 is older than K2), but provides little in the way of potential chronologic resolution of the sequence. It is clear that 'absolute' or numerical ages are required to further the worth of this sequence. These are acquired through direct radiometric dating (Colman et al., 1987), or by use of age-equivalent stratigraphic markers (Lowe and Walker, 1997) via the correlation of synchronous signals that have been radiometrically dated elsewhere.

Ages are often acquired in stages. This sequential process will be demonstrated in this chapter and the next, where various lines of evidence are examined to add to the known chronology. The upper and lower age limits of the Kauroa sequence are first established by tephrochronology, giving minimum and maximum age constraints of the tephra deposits lying immediately above and below the uppermost and lowermost Kauroa Ash members. Six fission-track dates then provide additional information about selected points in the sequence. Finally, paleomagnetic directions on several beds form a magnetostratigraphy, which imparts further chronologic information by means of correlation with the global record of paleomagnetic reversals.

### 5.2 TEPHROCHRONOLOGY

#### *5.2.1 Introduction*

The use of tephra deposits as stratigraphic markers that can be used for correlation and chronologic purposes is well documented (e.g. Froggatt and Lowe, 1990; Lowe and Newnham, 1999; Shane, 2000; Hunt and Lowe, in press). This is discussed in greater detail in the next chapter in which selected tephra beds of the Kauroa sequence are characterised using electron microprobe analysis of glass melt inclusions. In terms of establishing a chronology for the Kauroa Ash sequence, tephrochronology provides a



starting point from which other methods can be added: the sequence is enclosed within known and dated volcanic deposits, the ages of which provide minimum and maximum ages for the K-beds.

## 5.2.2 Correlations

### 5.2.2.1 Upper limit

The youngest unit of the Kauroa Ash sequence, K15, is overlain by members of the Hamilton Ash Formation, the oldest unit of which is H1. The boundary is marked by a well-defined erosional unconformity, potentially representing considerable time between deposition of the Kauroa and Hamilton beds. Nevertheless, H1 provides a minimum age for the Kauroa Ash sequence.

H1, also known as the 'Ohinewai Ash' (Ward, 1967) or 'Ohinewai Tephra' (Vucetich et al., 1978), has been identified as the Rangitawa Tephra based on correlations with other tephra deposits in the central and southern North Island (e.g. Pillans and Kohn, 1981), and in deep-sea cores (e.g. Nelson et al., 1985; Froggatt et al., 1986; Pillans et al., 1996). Correlation was based on similarities of stratigraphic position and mineralogy, and on major element compositions of glass obtained by electron microprobe analysis. The Rangitawa Tephra is thought to be a distal correlative of the biotite and quartz-bearing Whakamaru group of ignimbrites erupted from Whakamaru or Taupo volcanoes (Kohn et al., 1992). It has been the subject of numerous dating efforts due to its usefulness as an easily recognisable, widespread marker horizon. These are summarised in Table 5.1.

**Table 5.1** Summary of previous radiometric ages on Rangitawa Tephra and correlatives<sup>1</sup>.

Method	Age (Ma $\pm$ 1 $\sigma$ )	<i>n</i>	Reference <sup>2</sup>
Fission track (isothermal plateau, glass)	0.35 $\pm$ 0.02	4	1, 2, 3
Fission track (external detector, zircon)	0.35 $\pm$ 0.04	5	2, 3
Mean fission track age	0.345 $\pm$ 0.012	9	3
Marine oxygen isotope stratigraphy <sup>3</sup>	0.340 $\pm$ 0.007	2	3, 4
<sup>40</sup> Ar/ <sup>39</sup> Ar (single crystal laser fusion)	0.302 $\pm$ 0.008	4	3

<sup>1</sup>Modified from Lowe et al. (in press)

<sup>2</sup>1, Alloway et al. (1993); 2, Kohn et al. (1992); 3, Pillans et al. (1996); 4, Nelson (1988)

<sup>3</sup>Weighted mean ages for *n* determinations that are considered reliable by Kohn et al. (1992) and Pillans et al. (1996).

In addition to the dates obtained on the Rangitawa Tephra, Lowe et al. (in press) reported the first radiometric age obtained directly on any member of the Hamilton Ash Formation. A zircon fission track age of  $0.38 \pm 0.04$  Ma was calculated for H1, a date that is statistically indistinguishable from the fission track and astronomical ages obtained for its proposed correlative, the Rangitawa Tephra.

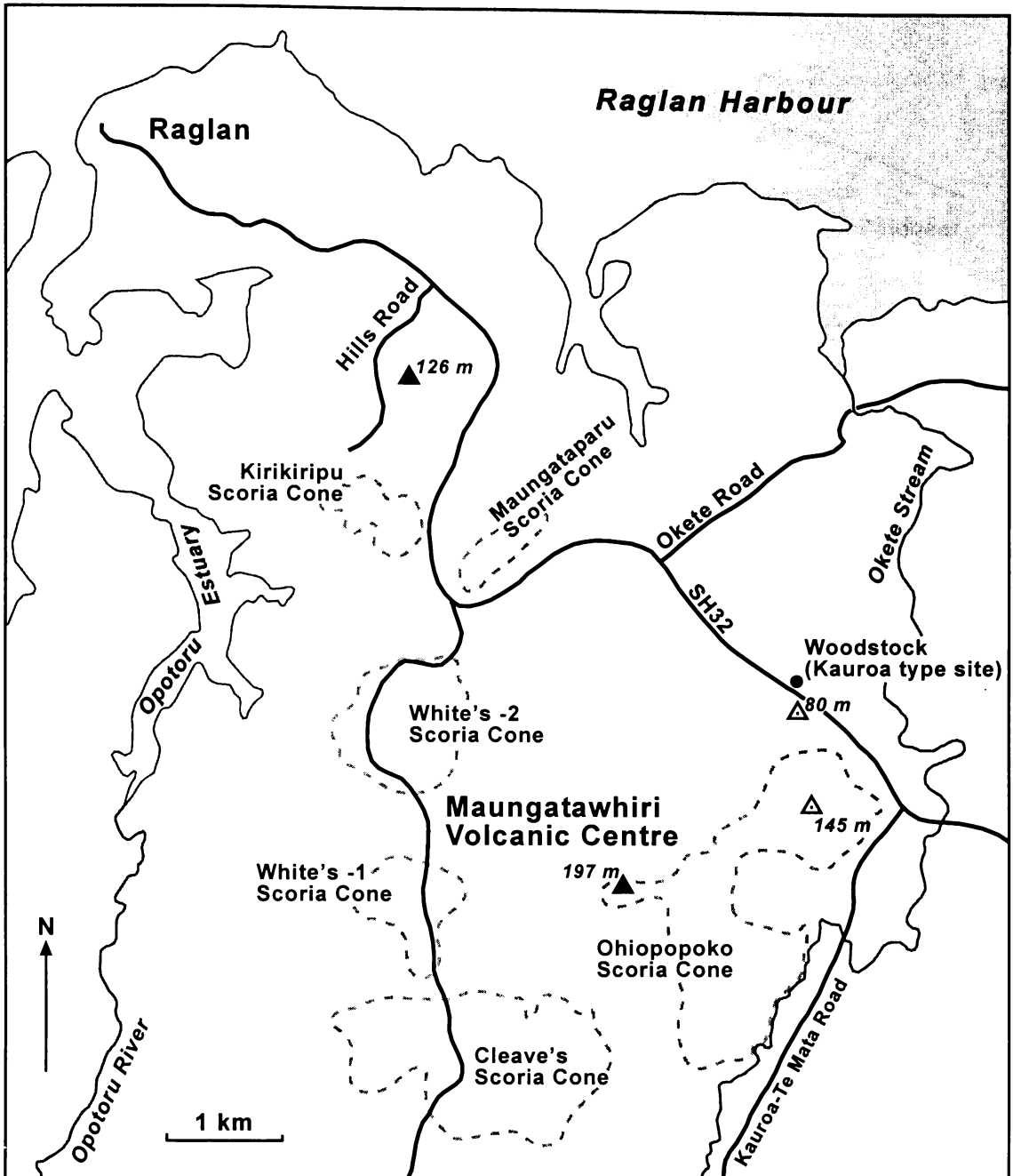
The minimum age for the Kauroa Ash sequence is thus set at  $0.38 \pm 0.04$  Ma (H1; Lowe et al., in press) or  $0.345 \pm 0.012$  Ma (mean fission-track age, Rangitawa Tephra; Pillans et al., 1996).

A maximum age for upper half of the sequence has also been defined. An incomplete sequence of Kauroa beds (K12 and K15) unconformably overlies the Ngatutura Volcanics at Foxs centre, northern Waikato (stratigraphy shown in Figure 2.9). Basaltic tuff (hawaiite) taken from this centre was K/Ar dated at  $1.81 \pm 0.07$  Ma (Briggs et al., 1989), meaning K12 (and K15) cannot be older than 1.81 Ma.

#### 5.2.2.2 Lower limit

Keane (1985) observed that the earliest Kauroa members (K1 and 2) were intercalated with basaltic tephtras erupted from the Maungatawhiri centre. This is evident at two different sites, the flank of Ohiapopoko cone and near the summit of Cleaves cone (map, Figure 5.1). At both cones, K1 is under and overlain by weathered basaltic scoria and tuff; at Cleaves cone there is a suggestion that K2 may also be overlain by a Maungatawhiri lapilli tuff. Stratigraphic relations are shown in Figure 5.2.

Briggs et al. (1989) obtained K/Ar dates for lavas (basanite) associated with the Maungatawhiri centre of  $2.26 \pm 0.08$  Ma (Ohiapopoko cone) and  $2.25 \pm 0.10$  Ma (Cleaves cone). Maungatawhiri is a monogenetic volcano, postulated to have a short eruptive cycle of no more than tens of years (Briggs et al., 1989). For this reason it is fair to assume that scoria and tuffs from the centre have essentially the same age as the dated lavas, thus assigning an age of 2.25-2.26 Ma to both the basaltic lapilli tuffs and K1 enclosed within them. On this basis, K1 is inferred to have been deposited rapidly and between intermittent volcanism on Maungatawhiri.



**Figure 5.1** Map showing the proximity of the Woodstock type section to the Maungatawhiri Volcanic Centre (partly after Keane, 1985).

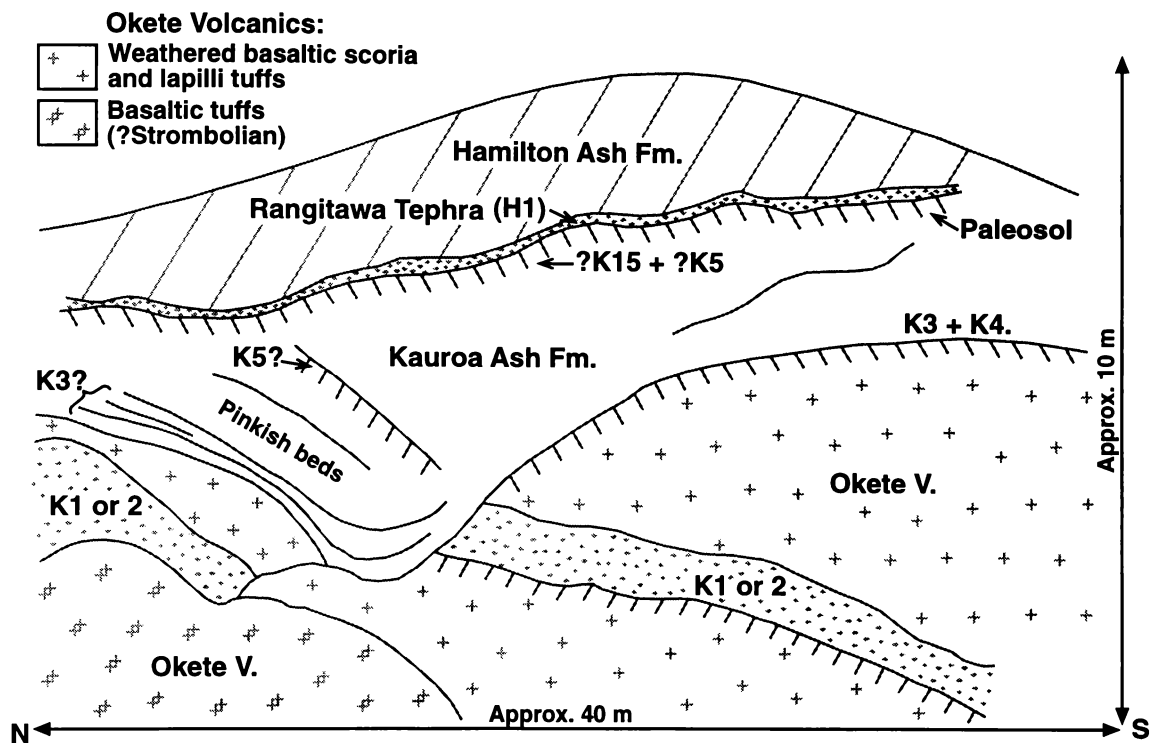


Figure 5.2 a) Stratigraphic relations, Ohiapopoko Cone (after Briggs et al., 1994).

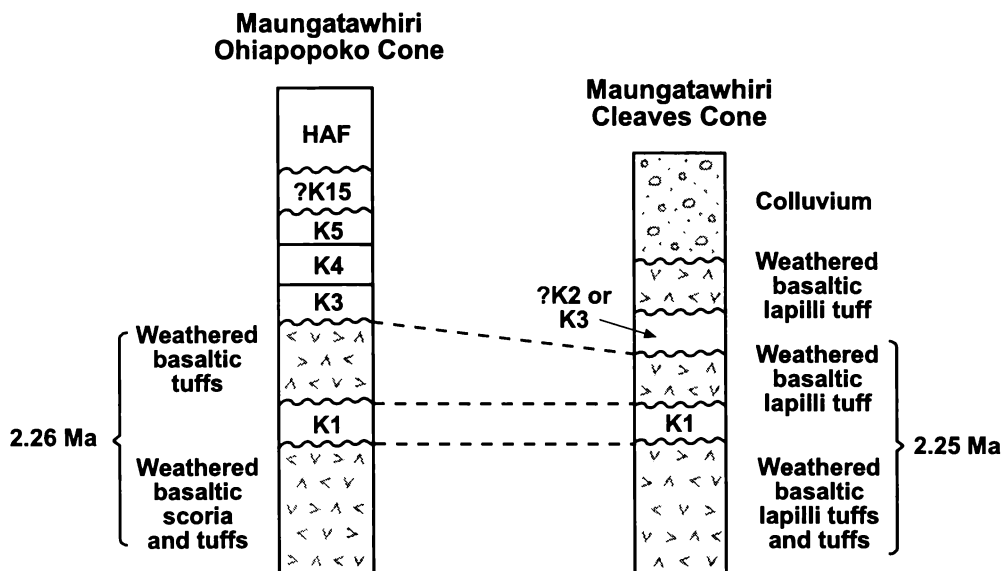


Figure 5.2 b) Interbedded Kauroa Ash beds and (dated) basaltic deposits, Maungatawhiri cones. HAF, Hamilton Ash Formation (adapted from Briggs et al., 1989).

### 5.2.3 Discussion

On the basis of tephrochronology, minimum and maximum ages can be assigned to the oldest and youngest Kauroa units. K1 has been demonstrated to have an age of c. 2.25 Ma, while K15 is inferred to be >0.38 Ma and <1.81 Ma. This suggests eruption and deposition of the Kauroa beds commenced in the late Pliocene, co-eval with activity at local basaltic centres, and continued through to the Mid to Late Pleistocene.

## 5.3 ZIRCON FISSION-TRACK

### 5.3.1 Introduction

Fission Track (FT) is a well-established radiometric dating method based on radiation damage due to spontaneous fission of  $^{238}\text{U}$ . In minerals containing uranium, fission fragments cause damage trails or 'tracks' in the wake of their movement through the host crystal lattice. Tracks can be counted under an optical microscope after polishing the sample and etching the surface with a suitable chemical solvent. After counting, the sample is heated to remove 'fossil' fission tracks and then irradiated by a slow neutron beam, which produces a new set of fission tracks as a result of the fission of  $^{235}\text{U}$ . The number of induced fission tracks is proportional to the uranium content and this enables the  $^{238}\text{U}$  content of the sample to be calculated. Sample age is then obtained from knowledge of the spontaneous fission rate of  $^{238}\text{U}$  (Hurford and Green, 1983).

Fission-track analysis may be undertaken on a wide variety of minerals in different rock types, though it has been most commonly carried out on zircon, apatite and glass in tephra (Hurford and Carter, 1991). Zircon is a common accessory mineral in igneous deposits and as such was deemed the most expedient mineral to use in this study.

### 5.3.2 Methodology

Several large samples of tephra were taken from the Woodstock type section, as well as one from the Oparau Tephra at the Papakura site. Analytical techniques followed those reported by Green (1985) and Kamp et al. (1989). Zircon concentrates were obtained by repeated wet sieving, ultrasonic cleaning and electromagnetic separation techniques (as described in section 6.2.1.), followed by heavy liquid separation. A sodium polytungstate (SPT) solution with a density of 3.0 was used to effectively separate

'light' and 'heavy' mineralogies, the zircon separate being retained in the nonmagnetic, heavy fraction. Some 'handpicked' separation was required, but otherwise the near-pure separate was embedded in FEP Teflon™ at c. 300 °C, ground and polished to reveal internal surfaces.

Etching took place in molten KOH-NaOH eutectic solution at c. 205 °C for about 50 hours until all spontaneous tracks were revealed. Mica external detectors were then sealed in contiguous contact with the polished mounts using heat-shrink plastic. Irradiation of the mounts took place in the X-7 facility of the HIFAR reactor, New South Wales. After irradiation the mica detectors were etched in 40% HF for 24 minutes at 24 °C. FT density determinations were undertaken using a Zeiss Axioplan™ optical microscope. Tracks were counted by two operators (JMT, IJL) and the zeta calibration method applied (Hurford and Green, 1983; Green, 1985; Hurford and Watkins, 1987; Lowe et al., in press).

### 5.3.3 Results

FT ages were calculated using the standard FT-age equation (Hurford and Green, 1983) with conventional errors (Green, 1981) quoted at  $\pm 1\sigma$ , as used by Kohn et al. (1992). Results are shown in Table 5.2.

**Table 5.2** Zircon fission-track (ZFT) results for selected beds of the Kauroa Ash sequence<sup>1</sup>.

Member	Operator	Age (Ma)	Weighted Mean
K12	JMT	1.41 ± 0.13	<b>1.28 ± 0.11</b>
	IJL	0.99 ± 0.20	
K12_2 <sup>2</sup>	IJL	<b>0.71 ± 0.10</b>	<b>1.68 ± 0.12</b>
OPARAU	IJL	<b>1.41 ± 0.20</b>	
K3	JMT	1.70 ± 0.16	
	IJL	1.65 ± 0.22	<b>1.43 ± 0.17</b>
K2	JMT	1.50 ± 0.22	
	IJL	1.33 ± 0.29	
K1	JMT	<b>2.24 ± 0.29</b>	

<sup>1</sup>Data in Lowe et al., in press

<sup>2</sup>Grains thought to be under-etched and so almost certainly too young.

The probability of grains counted in a sample belonging to a single population of ages is assessed by a chi-square statistic (Galbraith, 1981). A probability of less than 5% may indicate that the grains represent a mixed population. Two samples, K1 and K12\_2,

'failed' the chi-square test, suggesting multiple populations of grains. Single grain ages ranged from  $0.6 \pm 0.5$  to  $4.9 \pm 1.4$  Ma for K1 and  $0.0 \pm 0.0$  and  $2.5 \pm 1.5$  Ma for K12\_2. There is no legitimate reason to exclude either the low- or high-age crystals, and therefore the mean age is shown. Inclusion of the apparently 'too old' or 'too young' grains does not significantly affect the sample mean anyway, and is within the error estimates quoted. However, in the case of K12\_2, IJL reported that the grains had likely been under-etched and so the age estimation would almost certainly be too young. This age is discarded in favour of the alternate date on K12.

Comparisons using the test statistic  $T'$  on the ZFT ages show that they are consistent with the stratigraphy: K12 ( $1.28 \pm 0.11$  Ma) is significantly younger than K3 ( $1.68 \pm 0.12$  Ma) but not K2 ( $1.43 \pm 0.17$  Ma) (though K3 and K2 themselves are statistically indistinguishable); and K1 is significantly older than all ages on the overlying Kauroa Ash members. K12 and OPARAU, inferred by magnetic susceptibility and other data to be the same unit, also have statistically indistinguishable ages.

#### 5.3.4 Discussion

The ZFT age obtained on the basal member of the Kauroa Ash sequence, K1, is identical to the K-Ar-based age obtained by Briggs et al. (1989) on the equivalent unit using tephrochronology, thus supporting its validity. The error-weighted mean of this date together with those from Ohiapopoko and Cleaves cones is  $2.255 \pm 0.061$  Ma ( $n=3$ ).

Members K2 and K3 are not separable by ZFT alone. However, K3 stratigraphically overlies K2 with an intervening paleosol and therefore must be younger by possibly some tens of thousands of years.

K12 is considered equivalent to the Oparau Tephra (Pain, 1975; Salter, 1979; cf. Chapter 3). There is a suggestion that these deposits in turn are a distal correlative of the Ongatiti Ignimbrite (Pain, 1975), a well-dated unit (1.21-1.25 Ma) from the Mangakino Volcanic Centre. Shane et al. (1996a) also suggested another distal correlative for the Ongatiti Ignimbrite, the Mangatewaiiti tephra (dated at  $1.23 \pm 0.09$  and  $1.24 \pm 0.07$  Ma). A distal ignimbrite, 'Or-6', at Port Waikato is also thought to be a correlative of the Ongatiti Ignimbrite, and is ITPFT dated at  $1.14 \pm 0.06$  Ma (B.V. Alloway, pers. comm.,

2000). ZFT ages for K12 ( $1.28 \pm 0.11$  Ma) and Oparau ( $1.41 \pm 0.20$  Ma) are consistent with each other (they are statistically indistinguishable), as well as with their proposed correlatives, the Ongatiti Ignimbrite, Mangatewaiiti tephra and Or-6. The error weighted mean of the distal units (counts on K12, Oparau, Mangatewhaiiti, Or-6) is  $1.211 \pm 0.037$  Ma ( $n = 6$ ; Table 5.3). This illustrates a close similarity with the Ongatiti ages, the error weighted mean of which is  $1.230 \pm 0.016$  Ma ( $n = 7$ ; Table 5.4).

**Table 5.3** Ages and error-weighted mean of inferred distal correlatives of the Ongatiti Ignimbrite.

Unit	Age (Ma)
K12	$1.41 \pm 0.13$
	$0.99 \pm 0.20$
Oparau	$1.41 \pm 0.20$
<b>Error-weighted mean</b>	<b><math>1.31 \pm 0.10</math> (<math>n = 3</math>)</b>
Mangatewhaiiti tephra <sup>1</sup>	$1.23 \pm 0.09$
	$1.24 \pm 0.07$
Or-6, Port Waikato <sup>2</sup>	$1.14 \pm 0.07$
<b>Error-weighted mean</b>	<b><math>1.211 \pm 0.037</math> (<math>n = 6</math>)</b>

<sup>1</sup> Shane et al. (1996a); <sup>2</sup> B.V. Alloway (pers. comm., 2000)

**Table 5.4** Ages and error-weighted mean of the Ongatiti Ignimbrite.

Method / Material	Age (Ma)	Reference <sup>1</sup>
ITPFT – glass	$1.25 \pm 0.12$	1
	$1.23 \pm 0.09$	2
K/Ar – hornblende separate	$1.25 \pm 0.09$	3
<sup>40</sup> Ar/ <sup>39</sup> Ar – feldspar separate	$1.25 \pm 0.06$	4
	$1.23 \pm 0.02$	5
	$1.21 \pm 0.04$	6
	$1.24 \pm 0.07$	2
<b>Error-weighted mean</b>	<b><math>1.230 \pm 0.016</math> (<math>n = 7</math>)</b>	

<sup>1</sup>1 Black et al. (1996); 2 Shane et al. (1996a); 3 Soengkono et al. (1992); 4 Pringle et al. (1992); 5 Briggs et al. (1993); 6 Houghton et al. (1995).

## 5.4 PALEOMAGNETISM

### 5.4.1 Introduction

The primary objective of paleomagnetic research is to obtain a record of past configurations of the geomagnetic field. Recognisable patterns of alternating polarity ('normal' and 'reversed' magnetisation) in stratigraphic units can be used for chronological and correlation purposes, providing unique, globally significant, stratigraphic markers (Hailwood, 1989).



Ferromagnetic grains in rocks or sediments acquire magnetisation, or remanence, at the time of formation and during their history. This remanence is known as natural remanent magnetisation (NRM) and is typically composed of more than one component. Primary NRM is that acquired in the direction of the geomagnetic field at the time of rock formation and is the part sought most often in paleomagnetic investigations. However, secondary NRM components can be acquired subsequent to rock deposition and can alter or obscure primary NRM (Butler, 1992).

There are three main forms of primary NRM: thermoremanent magnetisation (TRM) acquired through cooling from high temperatures; chemical remanent magnetisation (CRM), resulting from the growth of ferromagnetic grains below the Curie temperature during diagenesis and metamorphism; and detrital remanent magnetisation (DRM), the physical alignment of detrital ferromagnetic grains acquired during the deposition and formation of sedimentary rocks (Butler, 1992; Dunlop, 1995). TRM is the form of remanent magnetisation acquired by most igneous rocks, though tephra-fall deposits (as well as paleosols etc.) may be affected by CRM and DRM to some extent.

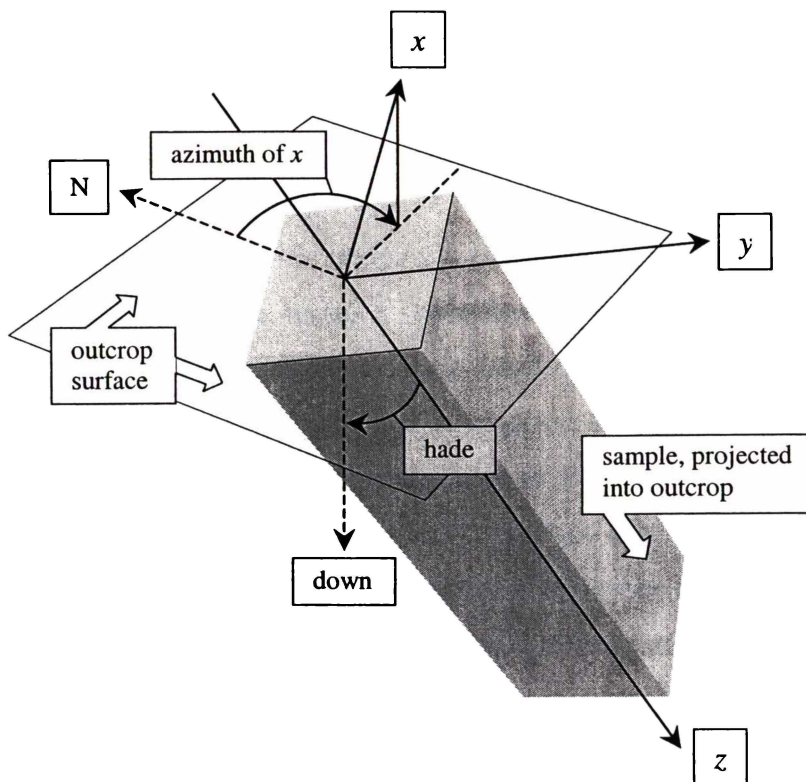
Secondary NRM is acquired through viscous remanent magnetisation (VRM). VRM is a remanent magnetisation that is gradually acquired during exposure to weak magnetic fields: in terms of paleomagnetism, it is that resulting from the action of the geomagnetic field long after formation of the rock. This feature is sometimes known as 'overprinting' for its tendency to obscure the original paleomagnetic direction of the rock. From this viewpoint, VRM is undesirable 'noise' that has to be removed in order to access the primary NRM.

Demagnetisation procedures remove components of NRM. Some are easily removed and are referred to as 'low-stability components'; this allows isolation of the more resistant 'high stability components', logically inferred to be primary NRM. This is not always the case, however, and convention dictates the highest stability component of NRM that is isolated by partial demagnetisation is referred to as 'characteristic component' of NRM (ChRM). This avoids the assumption of origin time associated with 'primary NRM' (Butler, 1992).

### 5.4.2 Methodology

#### 5.4.2.1 Sample collection

Samples for paleomagnetism were taken at each of the two main sites at Woodstock and Papakura Creek. In all cases (ignimbrites included), units were too soft to obtain the preferred sample type of drill cores. Instead, small oriented block samples were collected by pressing 2-cm<sup>3</sup> plastic cubes into a fresh outcrop, or carving a block and placing it in the cube to maintain physical integrity. In each case, the samples orientation ( $z$ , and  $y$  of the  $x$ - $z$  plane as in Figure 5.3) was measured while still 'attached' to the outcrop. If strata have been tilted by tectonic disturbance, the dip angle and azimuth of bedding strike are additionally required to calculate a 'bedding-tilt correction'. A small bedding correction was required at Woodstock, but not at Papakura Creek. After orientation measurements, samples were marked for orientation (arrow drawn on front and back) and identification and returned to the laboratory.



**Figure 5.3** Field orientation of samples (modified from Butler, 1992). The  $z$ -axis points into the outcrop; the  $x$ -axis is in the vertical plane (orthogonal to  $z$ ); the  $y$ -axis is horizontal. Angles measured in the field are: the 'hade' of the  $z$ -axis (angle of  $z$  from vertical) and geographic azimuth of the horizontal projection of the  $+x$  axis measured clockwise from geographic north.

#### 5.4.2.2 Measurement of NRM

In the laboratory samples were alternately demagnetised on an alternating field (AF) demagnetiser, and measured for remanence on a Molspin spinner magnetometer (housed in the Department of Earth Sciences, University of Waikato). Full stepwise demagnetisation was performed at 0, 5, 10, 15, 20, 25, 30, 40, 50 and 60 milliTeslas (mT) with the aim of removing any VRM from the relatively weakly magnetised samples; remanence was measured at each stage. Data from the magnetometer were fed into a computer and, together with field data (orientation and bedding-tilt correction), calculations of NRM directions were performed. Vector directions are described in terms of inclination,  $I$ , with respect to horizontal at the collecting location and declination,  $D$ , with respect to geographic north. They were plotted on 'vector component diagrams', 2-dimensional diagrams that are able to display 3-dimensional information by projecting the vector onto two orthogonal planes (Zijderveld, 1967). Characteristic  $I$  and  $D$  for the sample could then be calculated by application of 'best-fit' lines. Points were selected by eye; best-fit lines were applied statistically by computer.

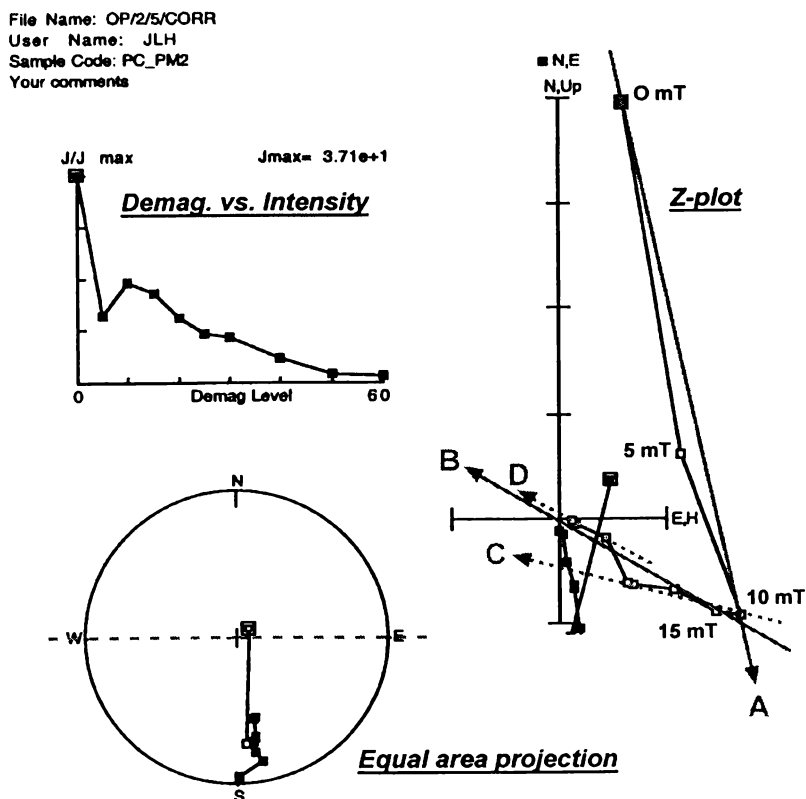
#### 5.4.2.3 Components analysis

Progressive demagnetisation, while necessary, can often result in significant scatter in otherwise linear trajectories of vector components. In particular, where samples are weakly magnetised or where ChRM is only a small percentage of total NRM, scatter can be high, and a quantitative technique is required to obtain the best-fit line and characteristic  $I$  and  $D$ . Principal components analysis (PCA) can be calculated in Z-plot by picking the demagnetisation levels which constrain a straight line to the origin, thereby isolating a trajectory of vector points that characterise the ChRM. Selection of these points is the critical observation, and it should reflect the removal (by progressive demagnetisation) of a single vector of constant direction. Breaks in a straight line indicate the removal of secondary overprints; these have to be avoided in order to obtain an accurate ChRM. Output from PCA is in terms of characteristic  $I$  and  $D$ , as well as a maximum angle of deviation (MAD), calculated to provide a quantitative measure of the precision with which the best-fit line is determined. MAD should not be more than  $15^\circ$ . Finally,  $I$  and  $D$  were plotted against sample depth to produce a paleomagnetic column.

### 5.4.3 Results

#### 5.4.3.1 Obtaining characteristic I and D from vector components diagrams

An example of a vector components diagram is shown in Figure 5.4. It is clear that points 0, 5 and 10 mT comprise a vector component (A) that, while co-linear, does not intersect the origin of the diagram and therefore cannot be primary NRM. This is inferred to be a low stability, secondary component (VRM). From 10 mT onwards, however, the points form a trajectory (B) that trends toward the origin. It is possible to further split this trajectory into two vectors (C and D), which would suggest that C is another secondary component (co-linear points that do not intersect the origin), while D is the highest-stability (ChRM) component (intersects the origin). However, neither component has exactly constant directionality (e.g. points 15 and 20 mT of vector C would intersect the origin taken on their own), and it could be that C and D may just be a factor of normal scatter. Vector B is thus more representative of the points as a whole.



**Figure 5.4** ‘Z-plot’ vector components diagram of a reversed polarity Kauroa Ash sequence sample, PC\_PM2, showing characteristic vectors A-D.

Components analysis of a best-fit line on points 10-60 mT (vector B) produces a characteristic D of 170.7, I of 32.5 and MAD of 5.4, the latter well within requirements,

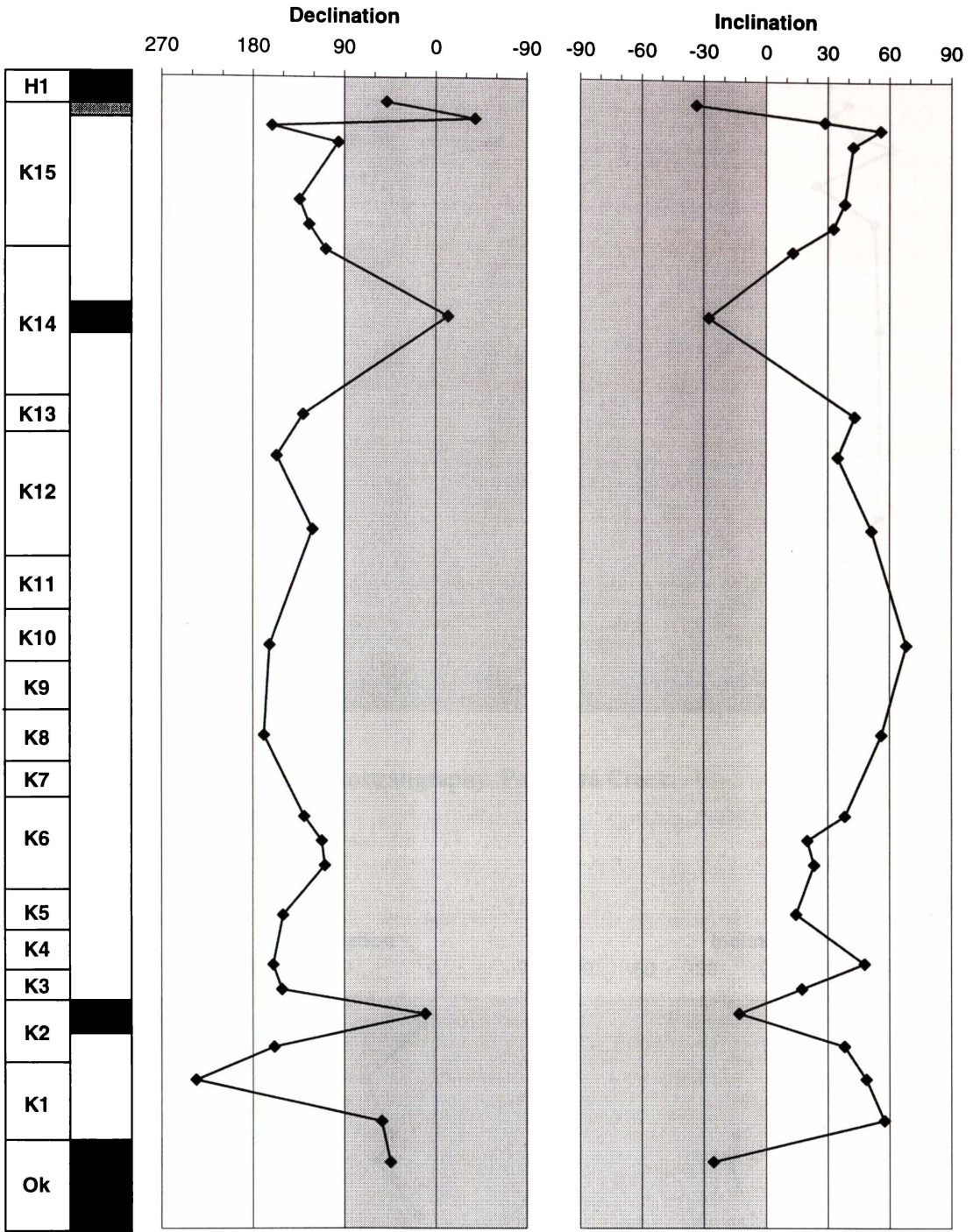
confirming this trajectory has sufficiently constant directionality. Also shown in Figure 5.4 is a plot illustrating progress of demagnetisation vs. intensity of signal, and an equal area projection – a 3-dimensional ‘stereographic’ plot of the data. In the latter diagram, open boxes plotted in the northern hemisphere half of the diagram are ‘normal’ polarity, closed boxes in the southern half of the diagram are ‘reversed’ polarity. This sample, PC\_PM2 (base of the Oparau Tephra) is clearly reversed polarity.

Components diagrams for all samples are compiled in Appendix C. It can be seen that some samples are significantly more scattered than the example shown above. However, it is usually possible to find at least two points that constrain a best-fit line to the origin. In other cases, samples are less scattered, showing straight lines to the origin with relatively few anomalous points, and a small low-stability VRM component. All samples have at least some secondary component.

#### 5.4.3.2 Construction of a paleomagnetic column

Z-plot was mainly used to obtain characteristic inclination and declination for each sample. These were then plotted by sample depth to construct a paleomagnetic column. In the Southern Hemisphere reversed polarity samples plot between +90 and +270 degrees declination and 0 and +90 degrees inclination. ‘Normal’ polarity samples plot between +90 and –90 degrees declination and –90 and 0 degrees inclination. If a sample plots ‘normal’ in D and reversed in I (or vice versa) it is interpreted as ‘intermediate’ polarity – essentially, it is of ambiguous or indeterminate polarity (B.J. Pillans, pers. comm., 1998). This usually means either the VRM component was not removed, or the sample was too weakly magnetised, producing extremely scattered data and components of NRM could not be determined (Butler, 1992). Deposits that acquire remanence in transitional periods of the geomagnetic field (i.e. at reversal boundaries) also display ‘intermediate’ polarity. Transitions between the two polarity states require at least 4-5 ka for the full directional change (Bogue and Merrill, 1992; Merrill and McFadden, 1994) so anything deposited in that time would have strong influences in both directions. Despite the scatter in some samples, primary paleomagnetic polarity (N or R) was usually clear even though the precise primary direction varied depending on the points selected for analysis.

Figures 5.5 and 5.6 show paleomagnetic columns for Woodstock and the lower part of



**KEY:**

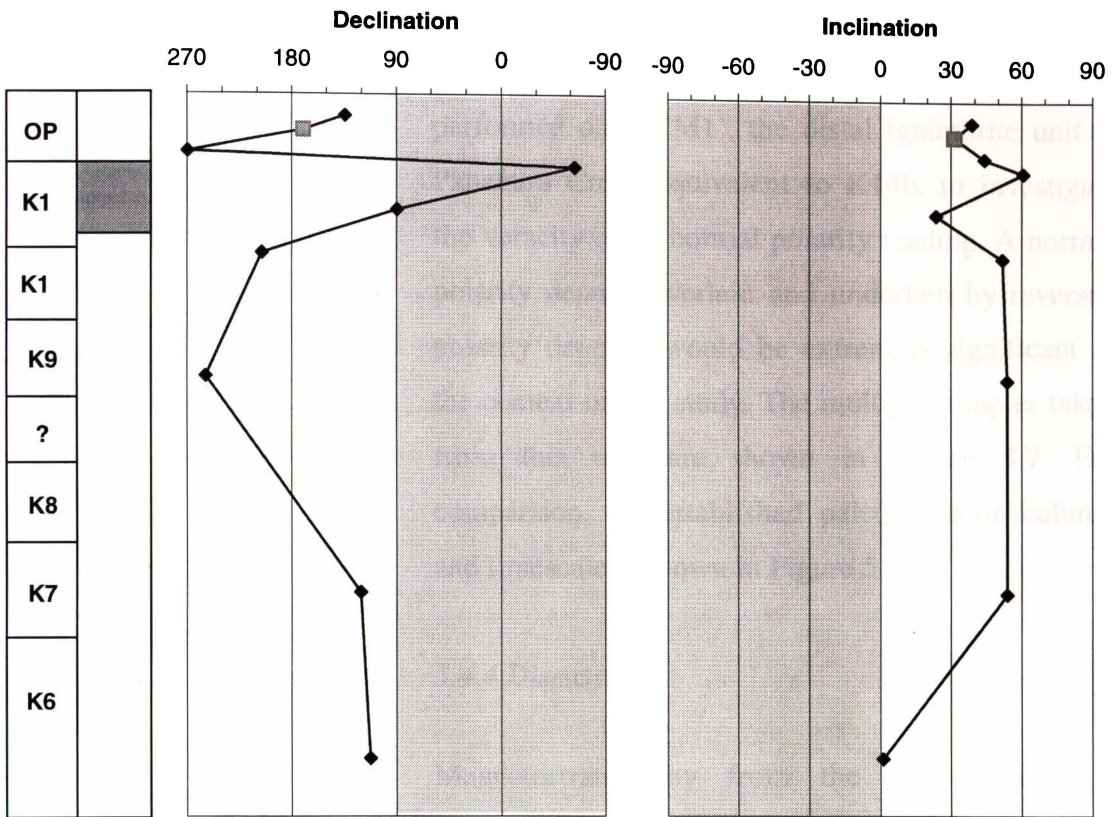
- Reversed polarity
- Intermediate polarity
- Normal polarity

**H1** = Lowermost Hamilton Ash bed

**Ok** = Okete Volcanic Fm.

**Figure 5.5** Magnetostatigraphy of the Kauroa Ash sequence, Woodstock section.

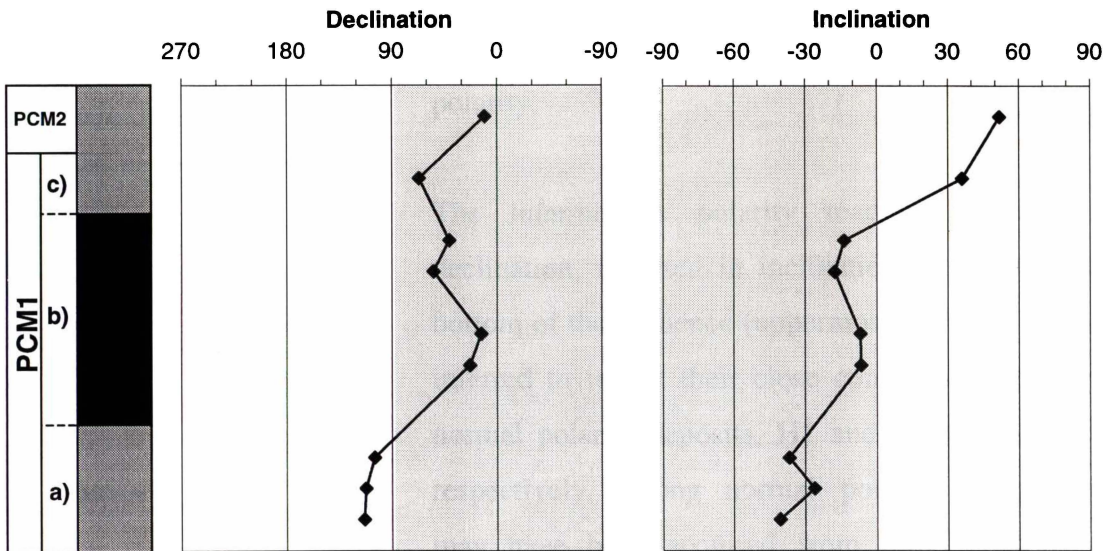




**Figure 5.6** Lower section magnetostratigraphy, Papakura Creek.

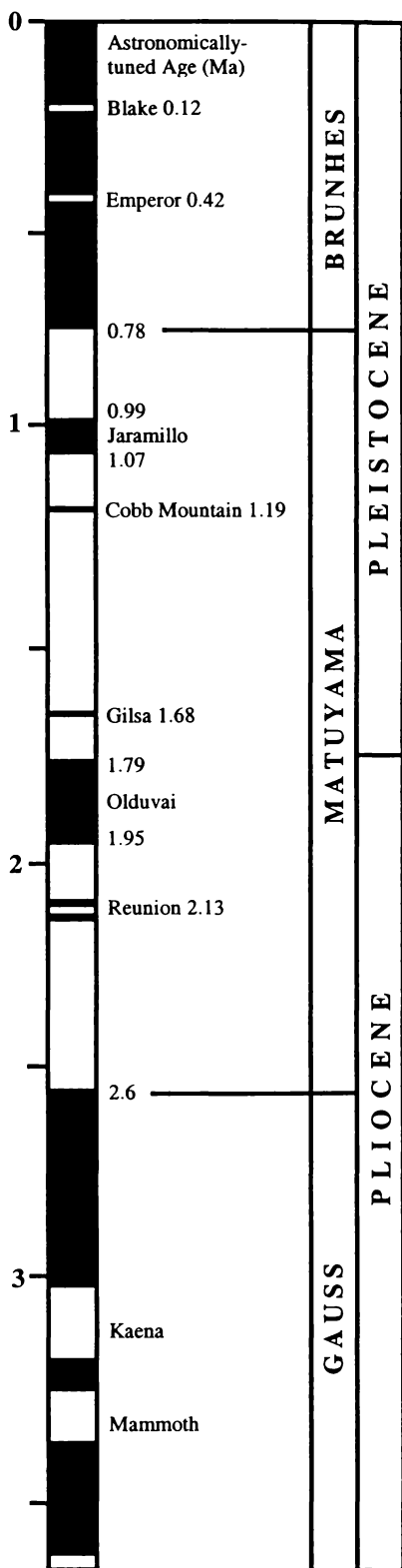
■ Sample shown in Figure 5.4

**OP** = Oparau Tephra



**Figure 5.7** Normal ignimbrite unit PCM1, Papakura Creek.

the section at Papakura Creek, respectively; the sample in the example above, PC\_PM2 (the base of the Oparau Tephra), is highlighted in Figure 5.6. A more detailed study was



**Figure 5.8** Geomagnetic polarity timescale of the last 3.5 Ma, after Shackleton et al. (1990) and Funnell (1995). Black areas indicate normal polarity; unshaded areas indicate reversed polarity.

performed on 'PCM1', the distal ignimbrite unit at Papakura Creek equivalent to K14b, to investigate the veracity of its normal polarity reading. A normal polarity deposit overlain and underlain by reversed polarity deposits would be extremely significant in the context of this study. The multiple samples taken from this unit are shown in Figure 5.7. For comparison, the established paleomagnetic column and timescale is shown in Figure 5.8

#### 5.4.4 Discussion

Magnetostratigraphy from the Woodstock type section (Figure 5.5) shows that the majority of the sequence is reversed polarity with just a few exceptions: H1 is normal polarity; the uppermost K15 sample is intermediate polarity; K14b and K2b are normal polarity; K1a is intermediate polarity; and Okete basalt underlying the sequence is normal polarity.

The intermediate polarity readings (normal in declination, reversed in inclination) at the top and bottom of the sequence (uppermost K15 and K1) are inferred to reflect their close contact with adjacent normal polarity deposits, H1 and Okete Volcanics, respectively. Strong normal polarity components may have been acquired from these deposits as VRM. Subsequently, incomplete removal of the VRM component in the demagnetisation process would result in an intermediate polarity. Alternatively, a particularly strong VRM component could have completely overwritten the original



ChRM. The intermediate polarity of K15c (though only one of three samples taken from that bed) could additionally result from physical translocation of ferromagnetic grains (e.g. illimerisation into paleosol), or derive from its deposition (or persistence of the landsurface) close to the Brunhes-Matuyama boundary. Reversed polarity readings seem to stabilise thereafter, even within the same unit, and it seems very likely, given the chronological information already available (fission-track dates), that the entire Kauroa sequence is encapsulated within the Matuyama Chron (0.78-2.6 Ma; Fig 5.8).

Results from the lower part of the Papakura Creek section (Figure 5.6) are consistent with this conclusion. Samples represent units from Oparau Tephra (K12a) to K6. They are predominantly of reversed polarity, with two samples showing intermediate polarity (normal polarity in declination, reversed in inclination). These anomalous samples display a reasonable amount of scatter though, and are inferred to be very weakly magnetized deposits where the polarity is ambiguous or indeterminate. Their position in the sequence (K11), however, would suggest a reversed polarity, as they are older than the Jaramillo Subchron<sup>1</sup> (Jaramillo is younger than K12) and unlikely to be as old as the Olduvai Subchron<sup>2</sup> (cf. dates on K2 and K3).

There remain two critical points of interest in the Kauroa sequence. K2b displays a stable and consistent normal polarity (three samples; MAD = <3°). The position of this unit in the sequence suggests the normal polarity signal results from its deposition (or the paleosol developed) in or close to the Olduvai Subchron<sup>3</sup>, since it lies between K1 (2.25 Ma) and K12 (1.31 Ma) and has reversed polarity deposits under- and overlying it. This conclusion makes the bed an extremely useful marker horizon.

The fission-track date on this unit,  $1.43 \pm 0.17$  Ma, is not consistent with the age range of the Olduvai Subchron, however. Evidence now suggests this fission track date is too young – the normal polarity of K2b means it is older than 1.79 Ma (end of Olduvai). In addition, the overlying bed, K3, is dated at  $1.68 \pm 0.12$  Ma and this date seems consistent with its position stratigraphically overlying the Olduvai Subchron. It is likely that, as for sample K12\_2, the K2 grains were under-etched in the preparation phase, thus giving it an anomalously young age.

---

<sup>1</sup> Normal polarity event in the Matuyama Chron dated at 0.99 – 1.07 Ma (Figure 5.8)

<sup>2</sup> Normal polarity event in the Matuyama Chron dated at 1.79 – 1.95 Ma (Figure 5.8)

<sup>3</sup> Gilsa and Reunion excursions are also theoretical possibilities, though are much shorter episodes.

The final point of importance in the Kauroa magnetostratigraphic sequence relates to bed K14b. The normal polarity of this bed may have been ascribed to VRM were it not for its position in the Kauroa sequence – somewhat younger than K12/Oparau Tephra (the error-weighted mean age for these deposits in the Kauroa sequence is  $1.31 \pm 0.10$  Ma; Table 5.3), and somewhat older than the Brunhes-Matuyama boundary<sup>4</sup> (0.78 Ma), making it a feasible position for the Jaramillo Subchron<sup>5</sup>. Though the bed at Woodstock (K14b) is thin and extremely weathered, at Papakura Creek the unit is present as a 2-m-thick weathered distal ignimbrite, named PCM1 in this study. More extensive paleomagnetic investigations were completed on this deposit (Figure 5.7) and the results are consistent with those from Woodstock (K14b). A strong normal polarity signal prevails in four of the eight samples, with the remaining four showing intermediate to normal polarity. These intermediate samples are at the base and top of the deposit and are consistent with a VRM acquired through being under- and overlain by reversed polarity beds. MADs on all these samples were less than  $7^\circ$ , making it very likely that this is a ‘real’ signal. It is thus concluded that PCM1 was deposited in the Jaramillo Subchron, constraining its age to between 0.99 and 1.07 Ma.

## 5.5 CONCLUSIONS

Relative and numerical dates obtained are summarised on the stratigraphic/paleomagnetic column in Figure 5.9. The three dating methods used in this chapter have combined to provide a new chronological framework for the Kauroa Ash sequence that includes several dates at key intervals in the sequence. The results show strong consistencies between the dating methods and most ages are supported by more than one line of evidence:

- K15, known to be (considerably) older than  $0.345 \pm 0.012$  Ma from tephrochronology and stratigraphy, has a magnetostratigraphic age  $>0.78$  Ma.
- A normal polarity for K14b is consistent with its stratigraphic position between K15 and K12, and a strong contender is the Jaramillo Subchron; both sections show evidence of normal polarity at this point. Thus K14b (PCM1) is likely to

---

<sup>4</sup> K15 and K14c are reversed

<sup>5</sup> The Cobb Mountain excursion is also theoretically possible, though is a very short-lived ‘target’ compared with the Jaramillo. Excursions of this duration ( $<100$  ka; see also Gilsa and Reunion) have been termed ‘cryptochrons’ for their short time-span (Cande and Kent, 1992); are often only ‘localised’ phenomena and are likely found only in the most detailed, high resolution, continuous records (Merrill and McFadden, 1994).

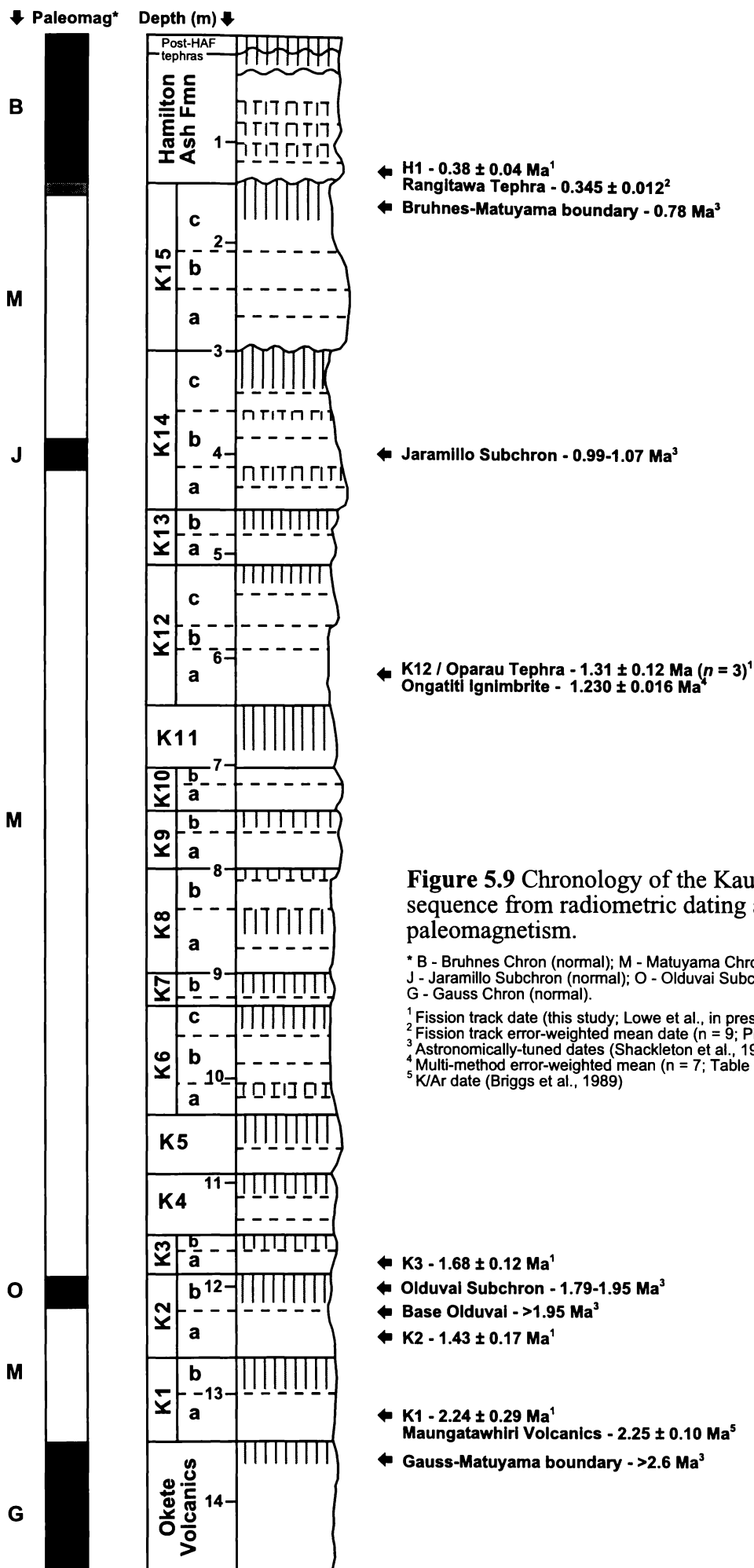
be aged 0.99-1.07 Ma.

- Fission-track ages on K12 ( $1.28 \pm 0.11$  Ma) and Oparau Tephra ( $1.41 \pm 0.20$  Ma) are statistically similar in age, lending weight to the stratigraphic evidence that they are correlatives.
- A fission-track age of  $1.68 \pm 0.12$  Ma on K3 is consistent with the normal polarity (Olduvai Subchron; 1.79-1.95 Ma) of the underlying bed, K2b.
- Tephrochronology suggests K1 is aged 2.25 Ma (K-Ar date on intercalated basalts), accordant with its fission-track age of  $2.24 \pm 0.29$  Ma. Its reversed polarity also supports an age  $<2.6$  Ma (Gauss-Matuyama boundary).

These ages enable some factual statements to be made about the deposition of the Kauroa Ash sequence:

- Onset of deposition (K1) was in the late Pliocene, after the Gauss-Matuyama transition and co-eval with the eruption of local volcanics (Pirongia, Okete).
- K3 was deposited close to the Plio-Pleistocene boundary (1.81 Ma) as defined by its fission-track age ( $1.68 \pm 0.12$  Ma) and normal polarity (possible late-Olduvai origin).
- Deposition through the early Pleistocene (1.8-1.3) must have been reasonably 'uniform' with 20 macroscopic beds (multiple microscopic beds may also be present) and up to 18 paleosols being recognised. The chronology through this period is examined by further tephrochronological work in Chapter 6 and correlation to other New Zealand sequences in Chapter 7.
- The lower half of the sequence (in terms of thickness; K1-K12) was deposited in two-thirds of the total time span of the sequence (2.25-1.31 Ma). The upper half of the sequence was deposited in one-third of the total time (1.31->0.78 Ma). Therefore, deposition rates (from continuing eruptions), or preservation thereof, appear to have increased in the middle Pleistocene.
- The unconformity between K15 and H1 represents approximately 0.5 Ma (>0.78-0.345 Ma). There may have been eruptions during this interval but significant erosion must have occurred because there are no deposits evident.

The ages presented here are tested and supported by the electron microprobe-based tephrochronological work in the next chapter.



**Figure 5.9** Chronology of the Kauroa Ash sequence from radiometric dating and paleomagnetism.

\* B - Bruhnes Chron (normal); M - Matuyama Chron (reversed);  
J - Jaramillo Subchron (normal); O - Olduvai Subchron (normal);  
G - Gauss Chron (normal).

<sup>1</sup> Fission track date (this study; Lowe et al., in press)

<sup>2</sup> Fission track error-weighted mean date ( $n = 9$ ; Pillans et al., 1996)

<sup>3</sup> Astronomically-tuned dates (Shackleton et al., 1990; Funnell, 1995)

<sup>4</sup> Multi-method error-weighted mean ( $n = 7$ ; Table 5.4)

<sup>5</sup> K/Ar date (Briggs et al., 1989)

## 6 TEPHROCHRONOLOGY

---

### 6.1 INTRODUCTION

Tephrochronology, defined by Thorarinsson (1974) as the “stratigraphic and chronologic study of tephra layers”, has come to be used as the stand-alone term for the study of all chronological aspects of tephra beds, their characterisation and identification, for the purposes of correlation and dating (Shane, 2000; Hunt and Lowe, in press). Strictly speaking ‘tephrochronology’ relates to the use of tephra as time-stratigraphic marker beds to establish numerical or relative ages (Lowe and Hunt, in press). The geologically instantaneous nature of tephra fall and pyroclastic flow deposits make them essentially isochronous marker horizons. In addition, their wide dispersal, resulting from high plinian eruption columns or from elevated tephra material associated with ignimbrite emplacement (co-ignimbrite ash) dispersed by prevailing winds, means they can be used and correlated over a vast area (Walker, 1981). Thus, there are two important aspects in the use of tephra in stratigraphic studies: the ability to directly date the tephra by various radiometric means, and the ability to correlate tephra beds by a variety of lithologic, mineralogic and geochemical methods (Shane, 2000). As such, tephra have been used in numerous studies in New Zealand (Lowe and Newnham, 1999) and elsewhere (e.g. Sarna-Wojcicki and Davis, 1991; Westgate et al., 1992; Dugmore et al., 1996; Machida, 1999; Narcisi and Vezzoli, 1999).

This chapter summarises the efforts to correlate members of the Kauroa Ash sequence to units that have an established name and age. Possible correlatives are identified and results are presented from a novel electron microprobe study.

#### *6.1.1 Tephra studies in New Zealand*

Silicic tephra beds erupted from the Coromandel Volcanic Zone (CVZ) and Taupo Volcanic Zone (TVZ) in the North Island are found in many New Zealand Quaternary sequences. The central TVZ, in particular, is one of the most frequently active, large rhyolitic centres on Earth (Wilson et al., 1995b). During the Quaternary it is known to have been the location of numerous caldera-forming plinian eruptions that have resulted in large (>100 km<sup>3</sup>) ignimbrite and fall deposits. Explosive activity commenced at

around 1.6 Ma (Houghton et al., 1995) or earlier (Shane et al., 1996a; Krippner et al., 1998); prior to this large-scale rhyolitic volcanism was located mainly in the Coromandel Volcanic Zone (Adams et al., 1994).

New Zealand tephrochronology, the correlation and chronology of these deposits, has been an important discipline since the early 20<sup>th</sup> century (Lowe, 1990). With the long volcanic history of the North Island, tephra studies are an important area of research and work has increased in volume with recent improvements to correlation and dating techniques. Through this work, there is now a good understanding of the physical volcanology of pyroclastic deposits, together with their stratigraphic and chronologic inter-relationships (Lowe and Newnham, 1999). Shane (2000) divided the current stratigraphic framework of tephra deposits in New Zealand into three uneven time intervals:

1. Post-64 ka – well constrained in terms of age, distribution and correlation.
2. Pre-64 ka (>1.6-0.06 Ma) – some tephra constrained in age by ITPFT, Ar-Ar and paleomagnetism; most cannot be assigned to a particular vent with certainty, but can be used for correlation purposes.
3. Miocene and Pliocene – poorly constrained, few horizons used in stratigraphic studies.

This study is concerned both with the second and third of these intervals, the Kauroa Ash sequence being of Plio-Pleistocene age.

### *6.1.2 Plio-Pleistocene volcanism*

In comparison with many later records, Plio-Pleistocene tephrochronology often suffers from incomplete and discontinuous sequences, together with generally poor age control. However, several studies have reported on the numerous and extensive distal deposits dating from this time, and with better age control on near-source deposits, and improvements in dating techniques in general (Lowe and Newnham, 1999), there is great potential for improving the stratigraphy of Plio-Pleistocene volcanism.

At least 13 major ignimbrite-forming eruptions are known for the interval 0.06-1.6 Ma (Wilson, 1986; Houghton et al., 1995), with numerous smaller eruptions likely. Shane et

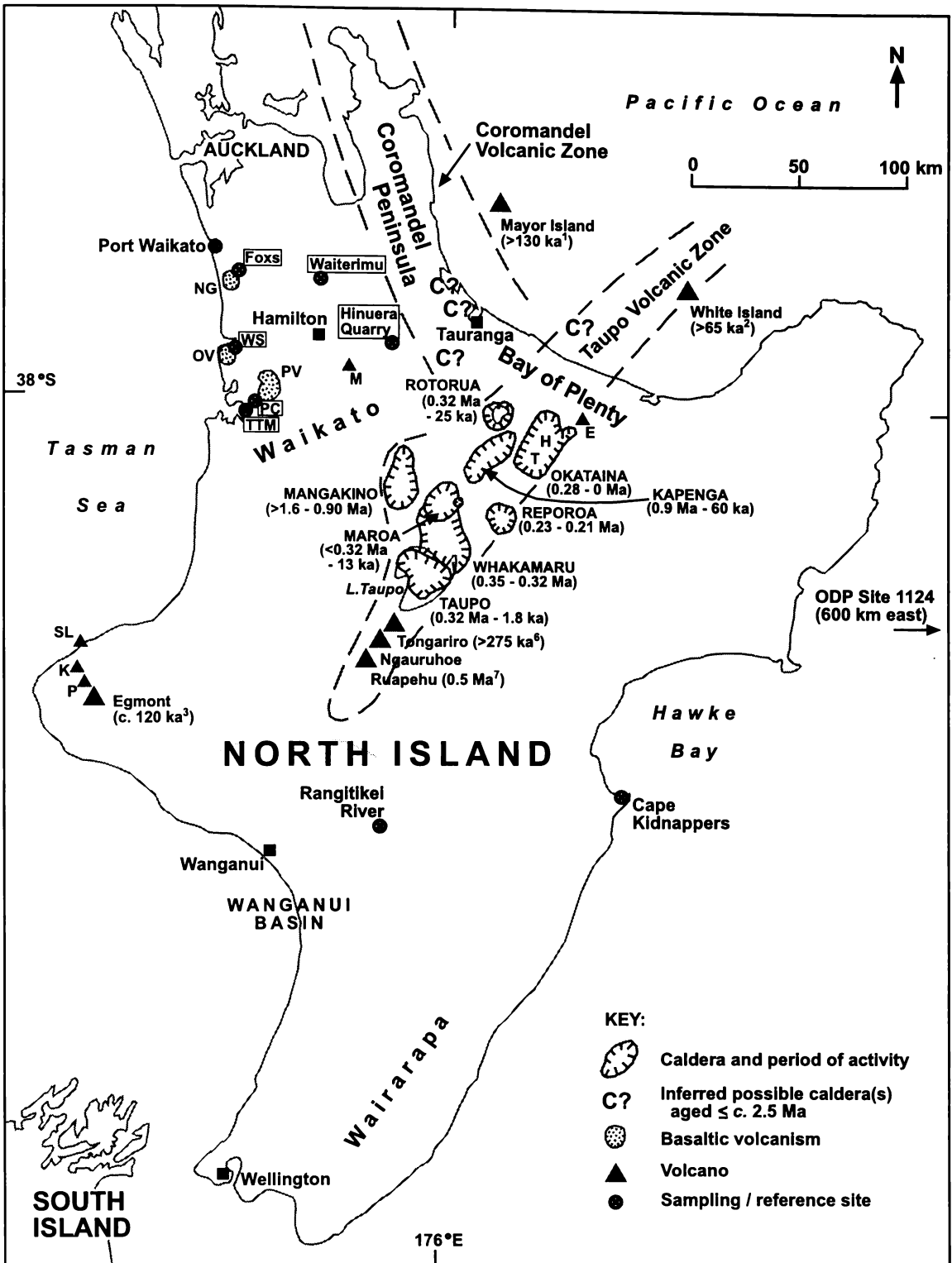
al. (1996a) reported at least 54 different pyroclastic eruptive events during the period c. 2.0-0.6 Ma recorded in distal sedimentary basins (Wanganui and Wairarapa) in southern North Island. Other studies describe one or more distal tephra beds of Quaternary age that could be correlatives of Kauroa beds (e.g. Moore, 1991; Pillans et al., 1994; Wilson et al., 1995a; Black et al., 1996). A particularly important recent advance has been the acquisition of deep-sea cores from New Zealand's continental shelf (e.g. ODP Leg 181 Site 1124) where an extremely detailed record of Quaternary (and older) volcanism has been recorded and is currently undergoing analysis (Carter et al., 1999). Units from the Kauroa Ash sequence have the potential to correlate with many of these previously identified and described tephra beds, thus placing them into a New Zealand Quaternary framework.

### 6.1.3 Source areas and deposits

The source area(s) of the Kauroa Ash sequence have yet to be determined, but with an emerging chronology several options become available (Figure 6.1). The sequence is predominantly rhyolitic in nature, meaning the major source areas will be the TVZ and, to a lesser extent, the CVZ. However, the K-beds close proximity to basaltic centres, namely the Alexandra Volcanic Group thought to be active at the time of the earliest Kauroa units (Briggs et al., 1989; Goles et al., 1996), means the Kauroa sequence was possibly subject to influx of some basaltic material.

#### 6.1.3.1 Basaltic sources

The Alexandra Volcanics are the most voluminous of the Waikato basalt fields and consist of two main series: one alkalic (Okete Volcanics) and one calcalkalic (Karioi, Pirongia, Kakepuku, Te Kawa; Figure 1.3; Briggs and McDonough, 1990; Briggs et al., 1994b). They are thought to have erupted over a fairly limited time span from 3.8-1.8 Ma (Briggs et al., 1989), the latter part of which is co-eval with the earliest Kauroa units (Figure 5.2). In places, the Kauroa Ash sequence is underlain with Pirongia Volcanics (e.g. Kawhia Harbour; Figures 1.3, 2.6), while in others, Kauroa units are intercalated with Okete Volcanics (e.g. Ohiapopoko Cone, Briggs et al., 1989, 1994a). No definable basaltic horizons have been discerned within the sequence, though basaltic sources are represented: Ward (1967) noted that the second bed at Te Uku (site close to Woodstock type section) contains a volcanic bomb, 30 cm in diameter and composed of basalt, that



**Figure 6.1** Location of the main volcanic centres active during the Plio-Pleistocene in the North Island, New Zealand, and sites referred to in text (mainly after Houghton et al., 1995; Wilson et al., 1995b; Lowe and Newnham, 1999). Many smaller non-rhyolitic volcanoes have been omitted.

WS, Woodstock type site; PC, Papakura Creek; TTM, Tiritirimatangi Peninsula; PV, Pirongia Volcanics; OV, Okete Volcanics (2.74-1.6 Ma<sup>4</sup>); NG, Ngatutura (1.83-1.54 Ma<sup>4</sup>); M, Maungatautari (c. 1.8 Ma<sup>2</sup>); E, Edgecumbe, T, Tarawera volcano, H, Haroharo volcano (<0.28 Ma<sup>2</sup>); P, Pouakai volcano (c. 0.25 Ma<sup>5</sup>); K, Kaitake volcano (c. 0.6 Ma<sup>5</sup>); SL, Sugar Loaf Islands (c. 1.7 Ma<sup>5</sup>).

<sup>1</sup> Wilson et al. (1995c); <sup>2</sup> Wilson et al. (1995b); <sup>3</sup> Alloway et al. (1995); <sup>4</sup> Briggs et al. (1989);

<sup>5</sup> Price et al. (1999); <sup>6</sup> Hobden et al. (1996); <sup>7</sup> Hackett and Houghton (1989).



has crumpled the bedding of the deposit. The bomb must have originated from a nearby source because of its mass, and was likely derived from one of the scoria cones in Okete Valley. In addition, occasional weathered fragments of Tertiary mudstone and siltstone (10-15 mm in size) are found in the lower Kauroa beds (K1-3) in the Raglan region. These are inferred to have been erupted from nearby Okete phreatomagmatic vents and suggest the beds in which they are found were emplaced during periods of basaltic activity. However, overall, the widespread distribution of the Kauroa beds indicates the beds were not derived from these local eruptive centres but from much larger, more explosive sources.

#### 6.1.3.2 Coromandel Volcanic Zone

The Coromandel Volcanic Zone (CVZ) is thought to have evolved more or less continuously through the early Miocene to early Pliocene, c. 18-4 Ma (Adams et al., 1994; Shane, 2000). During this time the locus of volcanism moved irregularly east and southwards, so that minimum ages of calderas are younger progressively southwards. Following this trend, younger centres still are found in the southern CVZ region. They are not well defined and are poorly dated, but possible calderas thought to be < 2.5 Ma have been inferred at Katikati (Brathwaite and Christie, 1996), Te Puna (Briggs et al., 1996), and Kaimai summit (Wilson et al., 1995b). Eruptives from these possible calderas are thought to have been considerably more rhyolitic than those from older centres of the CVZ, and this is evidenced by voluminous ignimbrites mapped in the Tauranga region. The youngest of these ignimbrites are of a similar age to early Kauroa units and may represent proximal correlatives of one or more K-beds. For example, of particular interest is the Waiteariki Ignimbrite, an extensive large-volume welded ignimbrite that forms the Whakamarama Plateau and underlies the Tauranga Basin (Briggs et al., 1996). It was emplaced prior to the uplift of the Kaimai Range and has a K-Ar age of  $2.18 \pm 0.15$  Ma (Takagi, 1995), theoretically overlapping in age with the older Kauroa beds.

#### 6.1.3.3 Taupo Volcanic Zone

The TVZ (onland) is a 100 km-long and 60 km-wide volcano-tectonic complex, the result of northwest-dipping subduction of the Pacific plate beneath the North Island. It has been the dominant locus of Quaternary volcanic activity in New Zealand, and is

notable on a global scale for its numerous caldera-forming, ignimbrite-producing, large-scale explosive eruptions – in area and volume, at least comparable to the Yellowstone system (Houghton et al., 1995).

As with the CVZ, the TVZ has experienced migrating centres of activity (generally west to east across the central North Island) over the last c. 1.6 Ma or more (Wilson et al., 1995b). The oldest centre is the Mangakino caldera, a rhyolite volcano, believed to be comparable in size to the currently ‘active’ centres of Okataina and Taupo. Mangakino was generally thought to have been active in two periods of caldera-forming eruptions, from 1.62 to 1.51 Ma and 1.23 to 0.91 Ma (Briggs et al., 1993), though there is now mounting evidence that it may have been active long before this time (Shane et al., 1996a; Krippner et al., 1998). During this period (>1.62 to 0.91 Ma) Mangakino is known to have been the source of many large-volume (>100 km<sup>3</sup>) ignimbrite eruptions, three of which (Ongatiti, Rocky Hill and Unit E/Kidnappers) are among the most voluminous units known in New Zealand (Briggs et al., 1993; Wilson et al., 1995a). Other eruptions have spread pyroclastic material (flow and fall) over an extensive area and Mangakino eruptives can be found from Wairarapa to Auckland and from Wanganui to Hawke’s Bay.

#### 6.1.3.4 Stratigraphy of major rhyolitic eruptions

Major rhyolitic eruptions of Plio-Pleistocene age are listed in Table 6.1. Some are known to have extended far into distal regions (e.g. Ongatiti, Rocky Hill and Unit E/Kidnappers), while others are thought to be more localised (e.g. Ngaroma). It is probable, however, because of limited outcrop availability, that the volumes and distribution of most are minima, and all are potentially more widespread and voluminous than currently known. As a result, no known large ignimbrite-forming eruption should be ruled out as a possible correlative of distal deposits in the Kauroa sequence.

The major source is likely to be the Mangakino centre, dominantly active for most of the period of interest. This centre is known to be the location of all the eruptions from Ngaroma to Marshall. Source vents of the preceding and succeeding eruptions are less certain.

**Table 6.1** Some possible correlatives of Kauroa Ash beds – Plio-Pleistocene rhyolitic eruptions.

NAME	AGE (Ma)		AGE (Ma)	POLARITY ‡ (Where known)
	Briggs et al. (1993) <sup>40</sup> Ar/ <sup>39</sup> Ar	Houghton et al. (1995) <sup>40</sup> Ar/ <sup>39</sup> Ar	Other <sup>1-8</sup> ITPFT	
Kupe			0.64 ± 0.08 <sup>4</sup>	N
Kidnappers 'F'			0.79 ± 0.06 <sup>8</sup>	
Kidnappers 'E'			0.86 ± 0.05 <sup>8</sup>	
Kidnappers 'D'			0.88 ± 0.04 <sup>8</sup>	
Kaukatea			0.87 ± 0.05 <sup>4</sup>	R
Marshall	0.91 ± 0.02	0.95 ± 0.03		R
Kaahu	0.92 ± 0.07			R
Rocky Hill	0.97 ± 0.02	1.00 ± 0.05		N (Jaramillo)
Kidnappers 'B'			1.00 ± 0.10 <sup>4</sup>	N
Potaka			0.99 ± 0.09 <sup>4</sup>	
Potaka			1.00 ± 0.03 <sup>3</sup>	N
Potaka			1.05 ± 0.05 <sup>1,2</sup>	
Unit E / Kidnappers	1.01 ± 0.06	0.97 ± 0.04		N
Ahuroa	1.19 ± 0.03	1.18 ± 0.02		I
Unit D	1.18 ± 0.02	1.20 ± 0.04		
Ongatiti	1.23 ± 0.02	1.21 ± 0.04	1.25 ± 0.12 <sup>5</sup>	R
Rewa			1.20 ± 0.18 <sup>2</sup>	
Rewa			1.29 ± 0.12 <sup>4</sup>	
Tephra 166			1.42 ± 0.14 <sup>4</sup>	
Ignimbrite C	1.62 ± 0.11	1.68 ± 0.07		
Ignimbrite B	1.51 ± 0.02	1.53 ± 0.04		
Ngaroma	1.60 ± 0.03	1.55 ± 0.05		R
Mangapipi			1.60 ± 0.18 <sup>4</sup>	
Pakihikura			1.63 ± 0.17 <sup>1</sup>	R
Pakihikura			1.63 ± 0.15 <sup>2</sup>	R
Akupe			1.64 ± 0.16 <sup>4</sup>	
Tephra 288			1.64 ± 0.13 <sup>4</sup>	
Tephra 108			1.68 ± 0.14 <sup>4</sup>	
Tephra 131			1.71 ± 0.12 <sup>4</sup>	
Vinegar Hill			1.75 ± 0.13 <sup>7</sup>	
Tephra 158			1.79 ± 0.17 <sup>4</sup>	R?
Waipuru			1.87 ± 0.15 <sup>1</sup>	N (Olduvai)
Waiteariki			2.18 ± 0.15 <sup>6</sup>	R

<sup>1</sup> Alloway et al. (1993); <sup>2</sup> Pillans et al. (1994); <sup>3</sup> Shane et al. (1995); <sup>4</sup> Shane et al. (1996a);<sup>5</sup> Black et al. (1996); <sup>6</sup> Takagi (1995); <sup>7</sup> Naish et al. (1996); <sup>8</sup> Shane et al. (1996b).

‡ N – normal; R – reversed; I - intermediate

#### 6.1.4 Distal tephra deposits

The distal environment represents great potential for the preservation of tephra layers that have been obliterated by subsequent explosive eruptions in the 'near-vent' proximal zone. Shane et al. (1996a), for example, described tephra beds in southern North Island that are suggestive of a major period of rhyolitic volcanism at c. 1.79-1.60 Ma, activity that is not represented in proximal regions, or which may be inaccessible as evidenced by Krippner et al. (1998). Proximal records also tend to be dominated by ignimbrite

sheets and fallout units are poorly preserved (Wilson, 1986), resulting in incomplete and discontinuous sequences. Distal locations, on the other hand, are less directly affected by major explosive activity and thus potentially record a more comprehensive eruptive history of the region. The widespread nature of these deposits means they can also be used as stratigraphic marker horizons on a regional scale (100-1000 km), thereby facilitating correlation between the fore-arc (eastern) and the back-arc (western) regions of the North Island, and, when records become available, the ocean basin (ODP Site 1124; Carter et al., 1999).

Distal records also have their limitations, however, and difficulties arise from sections that are not completely exposed, are reworked, mixed, weathered or altered as a result of the thinness of the beds or their proximity to soil-forming environments (shallowness). All these features inhibit the potential for correlation with proximal as well as other distal deposits. Despite these difficulties, progress in the study of distal tephra has been made, especially in the dating of deposits (Alloway et al., 1993). Other technological advances make the study of extremely weathered deposits, such as the Kauroa Ash sequence, possible.

#### 6.1.4.1 The nature of distal tephra deposits

Distal units in the Waikato region (predominantly K-beds) are so weathered that specific emplacement mechanisms are generally not discernable. However, it is probable that they were similar to those listed by Moore (1991), who concluded that distal pyroclastic deposits in the Auckland region were introduced by five possible mechanisms:

1. Direct plinian fall forming a mantling layer.
2. Direct distal pyroclastic flow, usually valley-filling and not retaining characteristics of proximal deposits.
3. Co-ignimbrite tephra fall associated with distal pyroclastic flows.
4. A buoyant ash cloud (surge deposit) at the distal margins of a pyroclastic flow, forming a mantling layer.
5. Co-ignimbrite ash cloud generated by pyroclastic flows interacting with seawater, forming localised mantling layers.

### 6.1.5 Methods of correlation

In early tephrochronological studies, tephra correlation was based on the stratigraphy, distribution pattern and physical properties of deposits, with petrographical analysis being applied in later studies. However, it is now clear that tephra deposits can have considerable three-dimensional complexities that often result in deposits from the same eruption having vastly different characteristics (facies; Hildreth and Mahood, 1985; Wilson, 1991). Some common limitations on correlation are the result of:

1. Discontinuous primary distribution resulting from eruption mechanics or topographic controls, or both.
2. Fragmentary preservation reflecting erosional susceptibility.
3. Post-depositional alteration and re-working.
4. Lithological sorting – the character of eruptive units can change rapidly over short distances.
5. Thickness – deposits become thinner and lack distinguishing bedding with increasing distance from the vent.

A considerable effort has been made to develop those methods of tephra identification that are least affected by depositional and diagenetic processes. The problems confronted and methods most appropriate for identification and correlation will vary from sequence to sequence, notably as functions of age, alteration and preservation. With the above limitations in mind, methods of correlation fall into six main categories:

1. Stratigraphic – physical continuity, stratigraphy, facies models.
2. Magnetic – thermal remanent magnetisation (TRM) directions.
3. Petrographic – distinctive lithic fragments, concentration zones of lithics/pumice, petrographic singularities e.g. shard shapes, types of phenocrysts or phenocryst assemblages (especially ferromagnesian minerals).
4. Chemical – microprobe analyses of glass, ferromagnesian minerals and Fe-Ti oxides.
5. Isotopic – light stable-isotope ratios.
6. Radiometric – various dating methods.

Kauroa beds present a particular challenge to correlation. As described earlier, they have few distinguishing field characteristics as a result of their age and intense alteration (as well as for the reasons given above). Primary minerals are extremely sparse and so very large samples are required to obtain even the tiniest amount of sand-sized grains, disabling most petrographic studies. Volcanic glass shards are non-existent and so glass-based elemental analyses are out of the question. However, some recent studies in the U.S.A. have provided a potential way of circumventing these problems.

#### *6.1.6 Glass inclusions in quartz*

The chemical composition of volcanic glass provides a well-established means for the stratigraphic correlation of tephra, and numerous studies have provided evidence of the application of electron microprobe (EMP) analysis to enable geochemical fingerprinting of tephra by their major element abundances (e.g. Westgate and Gorton, 1981; Froggatt, 1983, 1992; Lowe, 1988a, 1988b; Stokes et al., 1992; Hunt and Hill, 1993, 1996, Shane et al., 1996a). Fingerprints of distal tephra facilitate correlation to known source deposits. In this way, EMP analysis of volcanic glass is invaluable for identifying distal tephra where direct correlation would not otherwise be possible.

With increasing age, however, major changes in the composition of the deposit can occur, and the pristine volcanic glass required of EMP analysis may become altered to an assemblage of authigenic phases (clays). Volcanic glass shards have been weathered from all Kauroa beds; where glass remains it is too altered for EMP work. The prospect of correlation using this technique would seem improbable were it not for a new stratigraphic tool pioneered by Delano et al. (1994). They reported that fresh rhyolitic glass can be found in (weathered) Middle Ordovician K-bentonites as melt inclusions in phenocrysts of quartz, zircon and apatite. The melt inclusions represent quenched samples of non-degassed magma that became entrapped during phenocryst growth prior to eruption (Roedder, 1984). The glass inclusions have remained unaltered since eruption because they are hermetically sealed in chemically resistant phenocrysts, which have protected them from chemical alteration by diagenetic fluids. Thus for the elements of interest, these glass inclusions have remained chemically-closed systems since their entrapment. Careful EMP analysis of such glass results in a geochemical fingerprint that can be used for correlation purposes (Webster and Duffield, 1991;

Delano et al., 1994; Webster et al., 1995; Hanson et al., 1996), thereby circumventing the problem posed by degraded samples.

## 6.2 SAMPLE PREPARATION AND METHODOLOGY

Sample preparation procedures followed the suggestions of Froggatt and Gosson (1982), Lewis and McConchie (1994), and Froggatt (1983, 1992). These are summarised below.

### 6.2.1 Laboratory

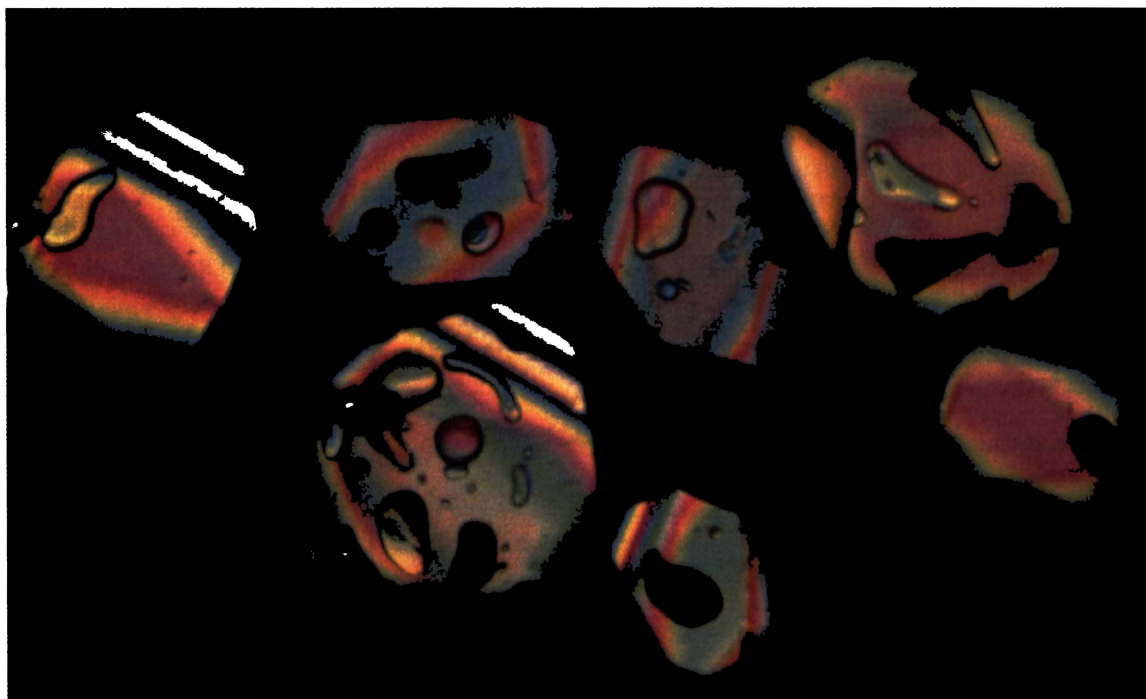
1. Repeated dispersal and disaggregation.
2. Repeated 'decanting' of fine clays using Stokes Law settling charts.
3. Wet sieve to obtain the  $>63 \mu\text{m}$  size fraction (several repeat-sievings, disaggregation with a sonic probe). Air-dry.
4. Removal of ferrimagnetic material (magnetite and titanomagnetite) with a vertically-oriented Franz separator on full power.
5. Heavy liquid separation (SPT) to give 'light' and 'heavy' subsamples.
6. Sonic probe cleaning of subsamples. Air-dry.
7. Repeated small incremental electromagnetic separation using a Franz Isodynamic Separator to obtain a pure quartz fraction.
8. Largest possible quartz grains chosen.

### 6.2.2 EMP slide preparation

Epoxy resin blocks drilled with seven holes were first used to make thin sections of several samples on individual slides (Froggatt and Gosson, 1982). However, with the first use of the microprobe this was found to be highly impractical for this kind of work, the samples being much too small to supply enough grains with glass inclusions in them. At first, suitable quartz grains were hand picked under an optical microscope, but this was extremely time consuming and required a great deal of precision. Instead it was found easier to produce one full slide (i.e. thin section) per sample. This required substantially more time polishing slides and slightly more time on the microprobe itself, but was the preferred choice overall.

### 6.2.3 Microprobe methodology

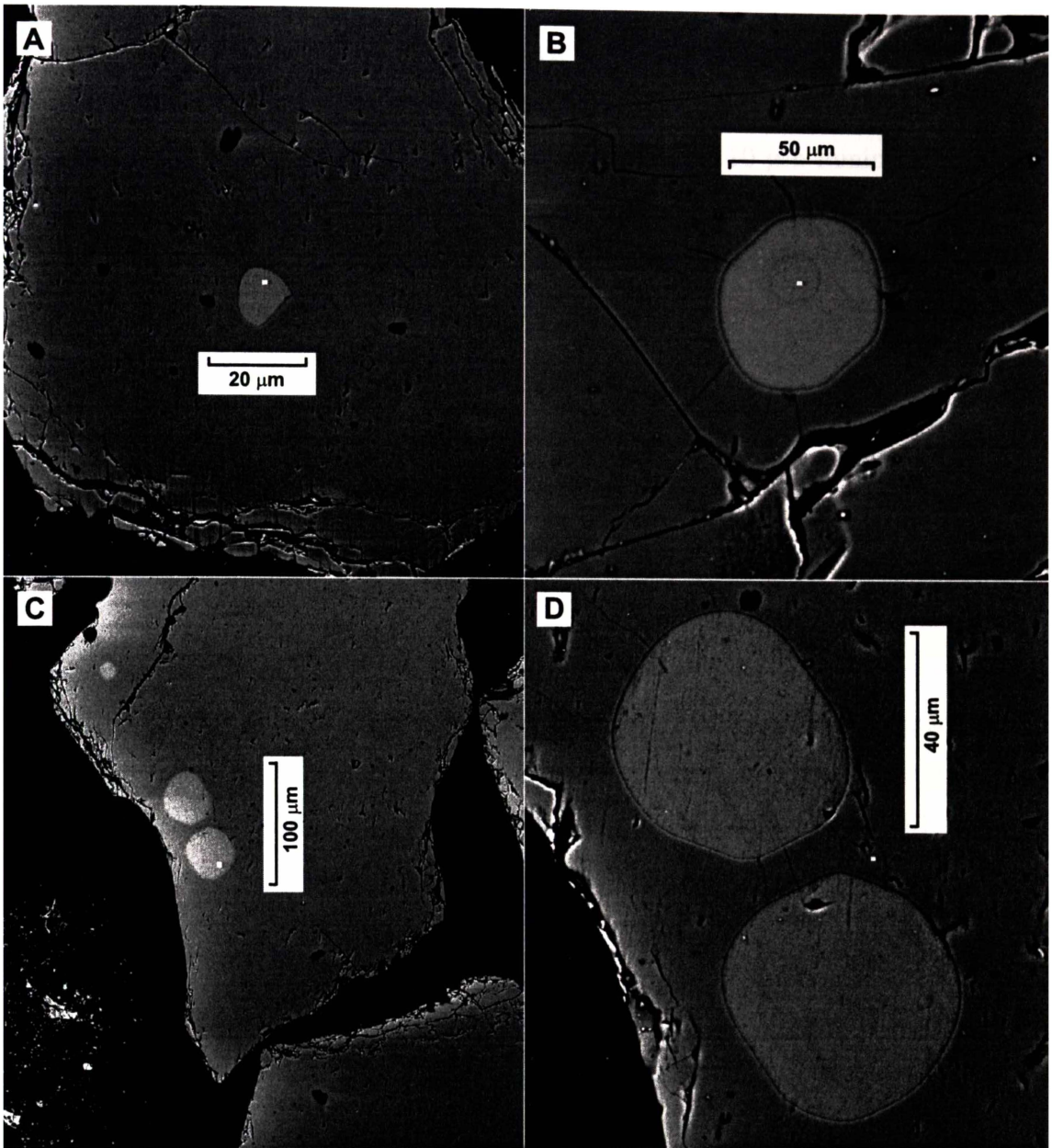
The glass inclusions are easily visible under the petrographic microscope (Figure 6.2) and under the backscattered electrons of the scanning electron microscope (SEM) (Figure 6.3 a-d). Under cross-polarised light on the former, they are visible as circular or elliptical forms, usually brownish-purple in colour, distinct from the grey-white interference colours of the background quartz grains. Under the SEM, inclusions show up as 'bright spots' on the quartz grains, which, on higher magnification, appear to have a 'rim'<sup>1</sup> around them (see Figure 6.4). Operating these microscopes in tandem (attached to the EMP) facilitates reliable and easy identification of glass inclusions in quartz. With quick and easy identification possible, the easiest method was found to be systematic 'patrolling' of the X and Y axes, stopping to probe each inclusion encountered. Inclusion abundances varied, with some samples having so many inclusions that only a small part of the slide needed to be covered. Some samples had very few inclusions (<7), and others none. Analyses were acquired for a total of 14 samples.



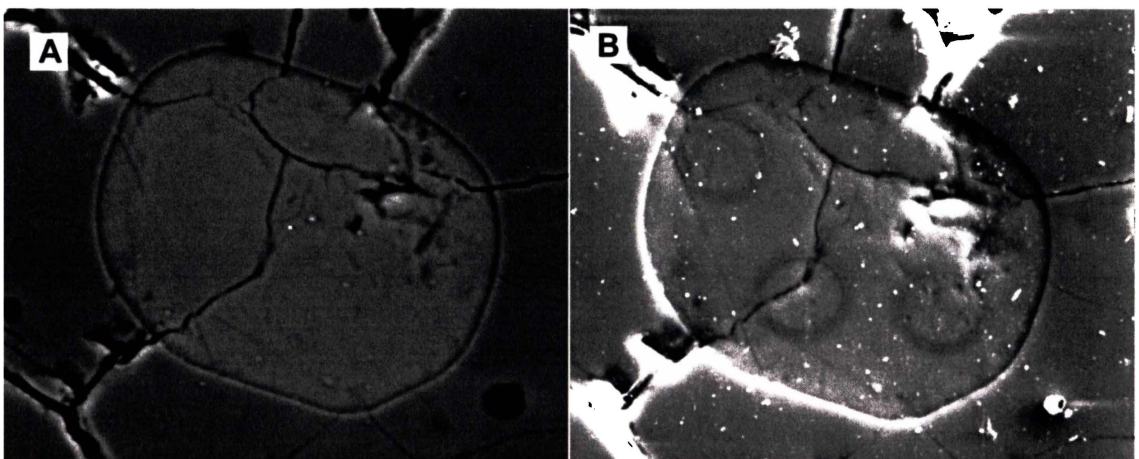
**Figure 6.2** Glass inclusions in quartz grains under a petrographic microscope (source: Delano et al., 1994).

<sup>1</sup> Pin-point probing of this 'rim' showed it was not different from the inclusion in terms of major elements. Subsequently, a negative SEM image showed it was merely a relief feature (see Figure 6.4b) – where the glass had been more highly eroded by the polishing process than the surrounding glass.





**Figure 6.3** Backscattered electron images of glass inclusions in quartz grains.



**Figure 6.4** Backscattered electron images of a glass inclusion: A - 'rim' seen on some inclusions; B - negative image showing relief features ('spots' are from a 10 μm beam).

Most inclusions were large enough (the largest inclusions were  $>80\ \mu\text{m}$  in diameter) that one or more standard  $20\ \mu\text{m}$  beam(s) (with an 8 nA current at 15 kV, following Froggatt, 1983, 1992) could be comfortably placed on them. Where inclusions were significantly smaller, the beam was reduced accordingly (to  $10\ \mu\text{m}$  minimum), though these EMP conditions were used only in samples with relatively sparse inclusions. Homogeneity was tested on several scales: intra-inclusion, intra-grain and intra-sample.

The microprobe used in this study was a JEOL 733 Superprobe housed at the Analytical Facility, Research School of Earth Sciences, Victoria University of Wellington. Nine elements were selected (Table 6.2) and analyses are presented as oxides except Cl.

### 6.3 RESULTS

Major element compositions (individual inclusion analyses) are recorded in Appendix D, while mean values and errors are shown in Table 6.2. These are compared with published and unpublished geochemical analyses on glass (Table 6.3; Appendix E) for previously described Plio-Pleistocene eruptives. Ages are given in Table 6.1 (above). This established stratigraphy is the basis for assigning names, sources and ages to the unnamed Kauroa units in this study.

One way of comparing analyses is to plot various elements against one another in bivariate or trivariate plots (e.g. FeO [total], CaO Na<sub>2</sub>O, K<sub>2</sub>O and MgO). Such plots have been employed as diagnostic tools in many studies, and were used to highlight similarities and differences in samples in this study. For each Kauroa unit of interest, FeO (total) vs CaO, Na<sub>2</sub>O vs K<sub>2</sub>O and FeO (total) vs MgO for Kauroa samples were plotted alongside possible correlatives (determined by established chronology or stratigraphy). Plots are shown in Figures 6.5 through 6.13.

Correlation of each sample (or group of samples) will be discussed in turn: background and possible correlatives are outlined for each sample; and major element composition, in conjunction with other stratigraphic and chronologic information, is assessed.

A fold-out information sheet with map and simplified stratigraphic columns is provided for readers convenience (Figure 6.15; end of chapter, page 163).

**Table 6.2** Major element analyses\* of Kauroa Ash beds (EMP analyses of *n* glass inclusions in quartz grains)\*\*.

NAME	SiO <sub>2</sub>	Al <sub>2</sub> O <sub>3</sub>	TiO <sub>2</sub>	FeO <sup>†</sup>	MgO	CaO	Na <sub>2</sub> O	K <sub>2</sub> O	Cl	Water	<i>n</i>
WS1 (K15c)	77.56 (0.50)	12.65 (0.21)	0.21 (0.11)	1.04 (0.23)	0.15 (0.05)	0.75 (0.10)	2.93 (0.37)	4.57 (0.18)	0.00 (0.00)	5.14 (0.87)	24
WS2 (K15a)	77.72 (0.54)	12.60 (0.28)	0.15 (0.07)	1.05 (0.16)	0.14 (0.05)	0.87 (0.18)	3.07 (0.31)	4.00 (0.32)	0.23 (0.06)	5.89 (1.03)	21
WS3 (K13)	77.71 (0.36)	12.51 (0.20)	0.12 (0.04)	0.96 (0.14)	0.08 (0.04)	0.65 (0.12)	3.19 (0.16)	4.44 (0.26)	0.24 (0.07)	6.05 (0.60)	21
K12	77.91 (0.80)	12.54 (0.42)	0.13 (0.06)	1.07 (0.17)	0.10 (0.03)	0.76 (0.16)	3.06 (0.43)	4.02 (0.25)	0.26 (0.05)	5.16 (1.00)	28
K3	77.85 (0.64)	12.93 (0.40)	0.14 (0.05)	1.17 (0.17)	0.15 (0.04)	1.05 (0.15)	2.86 (0.24)	3.79 (0.19)	0.27 (0.07)	6.41 (0.73)	15
PCM3	77.65 (0.36)	12.67 (0.16)	0.16 (0.05)	1.05 (0.11)	0.12 (0.02)	0.80 (0.11)	3.11 (0.20)	4.14 (0.20)	0.23 (0.12)	5.84 (0.83)	24
PCM2	77.44 (0.30)	12.48 (0.20)	0.15 (0.05)	0.87 (0.13)	0.09 (0.03)	0.73 (0.10)	3.67 (0.15)	4.13 (0.20)	0.22 (0.05)	5.08 (0.62)	15
PCM1	77.08 (0.44)	12.44 (0.19)	0.15 (0.02)	1.35 (0.15)	0.13 (0.02)	0.79 (0.05)	3.64 (0.12)	4.00 (0.21)	0.28 (0.05)	5.50 (0.53)	7
OPARAU T.	76.40 (0.40)	12.79 (0.25)	0.21 (0.09)	1.21 (0.17)	0.13 (0.04)	0.85 (0.10)	3.80 (0.20)	4.18 (0.14)	0.29 (0.08)	5.41 (0.88)	23
TTM4	77.18 (0.35)	12.58 (0.19)	0.21 (0.08)	1.07 (0.21)	0.13 (0.06)	0.75 (0.12)	3.11 (0.28)	4.60 (0.17)	0.23 (0.07)	4.04 (1.09)	16
TTM3	77.92 (0.36)	12.69 (0.20)	0.16 (0.06)	1.04 (0.13)	0.13 (0.06)	0.79 (0.14)	2.97 (0.28)	4.11 (0.27)	0.23 (0.09)	4.28 (0.90)	18
TTM2	77.71 (0.28)	12.73 (0.30)	0.16 (0.07)	1.04 (0.16)	0.12 (0.05)	0.73 (0.09)	3.72 (0.15)	3.93 (0.18)	0.31 (0.07)	6.05 (0.99)	11
TTM1	77.39 (0.81)	12.86 (0.30)	0.14 (0.06)	0.86 (0.20)	0.11 (0.04)	0.61 (0.09)	3.71 (0.20)	4.22 (0.28)	0.21 (0.08)	5.88 (0.79)	15
TIRITIRI IG.	77.96 (0.28)	12.39 (0.11)	0.10 (0.04)	1.17 (0.07)	0.08 (0.02)	0.77 (0.10)	3.54 (0.11)	3.71 (0.12)	0.21 (0.02)	5.21 (0.56)	7

\*Normalised to 100% volatile-free basis; standard deviations in parantheses. \*\* Full analyses in Appendix D

<sup>†</sup>Total iron expressed as FeO

**Table 6.3** Major element analyses\* of possible correlatives (EMP analyses of *n* glass shards, except where shown)\*\*.

NAME	SiO <sub>2</sub>	Al <sub>2</sub> O <sub>3</sub>	TiO <sub>2</sub>	FeO <sup>†</sup>	MgO	CaO	Na <sub>2</sub> O	K <sub>2</sub> O	Cl	Water	<i>n</i>
Rangitawa <sup>1</sup>	77.34 (0.28)	12.21 (0.09)	0.14 (0.04)	1.04 (0.05)	0.12 (0.12)	0.82 (0.03)	3.59 (0.17)	4.52 (0.16)	0.22 (0.02)	5.92 (0.61)	10
Rangitawa <sup>2</sup>	77.55 (0.27)	12.59 (0.16)	0.14 (0.03)	1.14 (0.06)	0.12 (0.07)	0.79 (0.03)	3.55 (0.18)	4.14 (0.16)	-	4.95 (0.92)	10
Kupe <sup>3</sup>	77.58 (0.37)	12.10 (0.17)	0.14 (0.03)	1.29 (0.12)	0.10 (0.04)	0.91 (0.09)	3.80 (0.16)	3.84 (0.13)	0.24 (0.05)	3.88 (0.71)	11
Kidnappers 'F' <sup>4</sup>	78.02 (0.46)	12.20 (0.27)	0.15 (0.04)	1.25 (0.15)	0.11 (0.02)	0.78 (0.06)	3.88 (0.19)	3.45 (0.18)	0.16 (0.02)	5.96 (1.17)	10
Kidnappers 'E' <sup>4</sup>	77.63 (0.38)	11.97 (0.12)	0.21 (0.04)	1.39 (0.10)	0.13 (0.03)	0.91 (0.04)	3.85 (0.11)	3.78 (0.17)	0.24 (0.01)	6.54 (1.12)	11
Kidnappers 'D' <sup>5</sup>	77.73 (0.37)	12.15 (0.18)	0.15 (0.03)	1.04 (0.07)	0.14 (0.03)	0.99 (0.07)	3.69 (0.13)	3.87 (0.18)	0.23 (0.04)	6.66 (1.71)	25
Kidnappers 'C' <sup>5</sup>	77.98 (0.18)	12.18 (0.12)	0.13 (0.02)	0.89 (0.07)	0.11 (0.02)	0.82 (0.07)	3.49 (0.13)	4.25 (0.27)	0.16 (0.03)	6.06 (1.27)	11
Kaukatea <sup>6</sup>	76.69 (0.21)	12.60 (0.07)	0.15 (0.04)	1.53 (0.09)	0.13 (0.04)	1.00 (0.06)	4.08 (0.20)	3.66 (0.18)	0.19 (0.02)	6.02 (0.61)	10
Kaukatea <sup>3</sup>	76.27 (0.39)	12.77 (0.16)	0.22 (0.03)	1.63 (0.15)	0.16 (0.03)	1.07 (0.06)	4.27 (0.06)	3.40 (0.25)	0.21 (0.03)	6.25 (1.21)	11
Marshall IG <sup>7</sup>	77.78 (0.26)	12.56 (0.19)	0.14 (0.03)	1.39 (0.08)	0.11 (0.03)	0.93 (0.08)	3.61 (0.14)	3.49 (0.13)	-	-	17
Marshall N <sup>7</sup>	77.49 (0.39)	12.53 (0.13)	0.16 (0.03)	1.30 (0.08)	0.12 (0.03)	1.00 (0.07)	3.54 (0.24)	3.71 (0.12)	-	-	17

Kaahu <sup>†8</sup>	74.20	13.73	0.20	2.96	0.47	1.87	1.89	4.44	0.00	-	?
Rocky Hill <sup>9</sup>	77.70 (0.46)	12.18 (0.19)	0.20 (0.10)	1.19 (0.18)	0.01 (0.02)	0.79 (0.12)	3.47 (0.26)	4.10 (0.21)	0.26 (0.03)	-	11
Waiuku ignimbrite <sup>10</sup>	77.46 (0.31)	12.58 (0.12)	0.12 (0.05)	1.07 (0.13)	0.09 (0.03)	0.91 (0.13)	3.70 (0.10)	3.92 (0.15)	0.18 (0.02)	5.28 (0.39)	11
Kidnappers B <sup>4</sup>	76.24 (0.26)	12.84 (0.12)	0.17 (1.55)	1.55 (0.07)	0.13 (0.03)	1.08 (0.03)	4.22 (0.13)	3.62 (0.10)	0.16 (0.02)	7.48 (1.56)	10
Potaka <sup>1</sup>	78.07 (0.22)	11.87 (0.16)	0.14 (0.02)	1.19 (0.08)	0.10 (0.05)	0.99 (0.06)	3.72 (0.19)	3.68 (0.15)	0.22 (0.02)	6.01 (0.52)	11
Potaka <sup>3</sup>	77.80 (0.28)	12.12 (0.15)	0.10 (0.04)	1.08 (0.14)	0.09 (0.03)	0.88 (0.09)	3.59 (0.18)	4.12 (0.24)	0.22 (0.03)	3.56 (1.18)	13
Potaka <sup>6</sup>	77.43 (0.37)	12.31 (0.15)	0.13 (0.02)	1.13 (0.07)	0.11 (0.01)	0.90 (0.07)	3.75 (0.13)	4.03 (0.19)	0.23 (0.01)	5.63 (1.04)	18
Unit E / Kidnappers <sup>11</sup>	78.82 (0.45)	12.32 (0.20)	0.12 (0.05)	1.00 (0.13)	0.12 (0.03)	0.90 (0.10)	3.72 (0.21)	3.69 (0.21)	0.18 (0.02)	5.36 (1.43)	10
Ahuroa <sup>12</sup>	77.44 (0.32)	12.13 (0.15)	0.09 (0.08)	1.51 (0.12)	0.06 (0.03)	0.60 (0.21)	4.37 (0.13)	3.61 (0.22)	0.21 (0.13)	7.65 (2.17)	6
Unit D (flow) <sup>12</sup>	77.67 (0.24)	11.94 (0.11)	0.11 (0.03)	1.43 (0.06)	0.07 (0.01)	0.62 (0.04)	4.24 (0.07)	3.71 (0.13)	0.22 (0.02)	4.63 (1.44)	8
Unit D (fall) <sup>12</sup>	77.68 (0.19)	11.91 (0.11)	0.09 (0.02)	1.39 (0.06)	0.06 (0.01)	0.64 (0.04)	4.23 (0.05)	3.76 (0.11)	0.24 (0.03)	4.97 (0.74)	7
Ongatiti <sup>8</sup>	77.35 (0.31)	12.41 (0.18)	0.13 (0.03)	1.27 (0.13)	0.10 (0.02)	0.74 (0.11)	3.35 (0.11)	4.33 (0.18)	0.27 (0.05)	-	10
Ongatiti <sup>12</sup>	77.38 (0.19)	12.13 (0.08)	0.15 (0.04)	1.30 (0.07)	0.11 (0.03)	0.94 (0.06)	3.64 (0.10)	4.05 (0.11)	0.30 (0.03)	4.27 (0.54)	10
Rewa <sup>3</sup>	75.63 (0.59)	12.99 (0.34)	0.18 (0.05)	1.99 (0.23)	0.16 (0.04)	1.28 (0.15)	4.25 (0.19)	3.37 (0.21)	0.17 (0.03)	5.40 (1.31)	13
Rewa <sup>6</sup>	76.21 (0.82)	13.08 (0.28)	0.16 (0.03)	2.02 (0.20)	0.14 (0.04)	1.05 (0.16)	3.98 (0.27)	3.24 (0.47)	0.19 (0.02)	5.93 (1.94)	24
Tephra 166 <sup>13</sup>	75.78 (0.55)	13.09 (0.23)	0.18 (0.03)	1.82 (0.10)	0.11 (0.05)	0.97 (0.16)	4.28 (0.16)	3.69 (0.12)	0.21 (0.04)	5.17 (0.69)	9
Ngaroma <sup>†8</sup>	71.28	15.35	0.33	3.59	0.32	1.14	3.71	4.20	0.00	-	?
Mangapipi <sup>3</sup>	74.95 (0.27)	13.17 (0.17)	0.18 (0.03)	2.29 (0.12)	0.13 (0.02)	1.17 (0.06)	4.38 (0.14)	3.56 (0.18)	0.18 (0.02)	6.21 (1.36)	13
Mangapipi <sup>6</sup>	75.70 (1.40)	13.11 (0.37)	0.14 (0.04)	2.10 (0.14)	0.11 (0.03)	0.98 (0.13)	4.29 (0.27)	3.16 (0.36)	0.21 (0.03)	5.74 (0.64)	78
Mangapipi <sup>7</sup>	76.09 (0.55)	13.15 (0.35)	0.14 (0.04)	2.08 (0.15)	0.10 (0.03)	0.95 (0.15)	4.22 (0.52)	3.26 (0.39)	-	-	89
Pakihikura <sup>1</sup>	78.14 (0.26)	12.33 (0.15)	0.10 (0.05)	1.30 (0.09)	0.10 (0.04)	1.14 (0.08)	3.40 (0.16)	3.32 (0.15)	0.16 (0.02)	5.96 (1.56)	14
Pakihikura <sup>6</sup>	77.59 (0.28)	12.41 (0.17)	0.11 (0.03)	1.27 (0.13)	0.10 (0.02)	1.20 (0.06)	3.77 (0.11)	3.43 (0.13)	0.15 (0.04)	6.20 (1.08)	60
Akupe <sup>7</sup>	75.74 (0.57)	13.59 (0.13)	0.14 (0.03)	2.03 (0.09)	0.12 (0.02)	1.05 (0.06)	3.94 (0.55)	3.39 (0.21)	-	-	10
Tephra 288 <sup>13</sup>	77.73 (0.37)	12.50 (0.16)	0.10 (0.02)	1.10 (0.09)	0.10 (0.02)	1.02 (0.07)	3.46 (0.10)	3.85 (0.23)	0.14 (0.02)	4.39 (0.82)	10
Mangahou <sup>3</sup>	75.61 (0.42)	13.11 (0.14)	0.21 (0.03)	1.72 (0.15)	0.22 (0.04)	1.52 (0.11)	3.66 (0.14)	3.75 (0.15)	0.20 (0.02)	7.06 (0.72)	13
Mangahou <sup>7</sup>	75.36 (0.31)	13.64 (0.13)	0.16 (0.03)	2.18 (0.08)	0.14 (0.02)	1.20 (0.13)	3.86 (0.37)	3.46 (0.38)	-	-	24
Tephra 108 <sup>13</sup>	73.78 (0.53)	13.88 (0.24)	0.20 (0.03)	2.14 (0.37)	0.16 (0.02)	1.26 (0.08)	4.57 (0.35)	3.83 (0.47)	0.20 (0.03)	7.55 (1.17)	16
Tephra 131 <sup>13</sup>	75.53 (0.18)	12.76 (0.11)	0.16 (0.03)	1.80 (0.08)	0.10 (0.02)	0.85 (0.05)	3.80 (0.17)	4.88 (0.08)	0.14 (0.03)	7.17 (0.58)	9
Vinegar Hill <sup>6</sup>	76.62 (0.17)	12.51 (0.11)	0.23 (0.03)	1.39 (0.05)	0.17 (0.03)	1.16 (0.04)	3.13 (0.09)	4.59 (0.12)	0.20 (0.03)	5.15 (0.68)	10
Vinegar Hill <sup>14</sup>	75.89 (0.29)	12.97 (0.22)	0.24 (0.06)	1.44 (0.13)	0.24 (0.09)	1.17 (0.07)	3.13 (0.20)	4.63 (0.17)	0.29 (0.04)	6.87 (0.51)	21
Tephra 158 <sup>13</sup>	75.25 (0.28)	13.14 (0.16)	0.12 (0.04)	1.73 (0.10)	0.07 (0.01)	0.94 (0.05)	4.20 (0.10)	4.32 (0.16)	0.25 (0.03)	5.02 (1.00)	13
Waipuru <sup>6</sup>	75.61 (0.20)	13.61 (0.16)	0.14 (0.02)	1.49 (0.10)	0.13 (0.04)	0.93 (0.05)	3.56 (0.17)	4.38 (0.20)	0.18 (0.02)	6.54 (0.85)	10
Waipuru <sup>14</sup>	75.72 (0.32)	13.68 (0.15)	0.14 (0.04)	1.44 (0.13)	0.14 (0.03)	0.89 (0.05)	3.48 (0.19)	4.31 (0.18)	0.21 (0.04)	7.69 (0.88)	23

\*Normalised to 100% volatile-free basis; standard deviations in parantheses. \*\*Full analyses in Appendix E

<sup>†</sup>Total iron expressed as FeO. <sup>‡</sup>Major-element (wt.%) XRF composition of pumice.

<sup>1</sup>Allaway et al. (1993); <sup>2</sup>Shane et al. (1995); <sup>3</sup>Pillans (1994); <sup>4</sup>Shane et al. (1996b); <sup>5</sup>Black (1992); <sup>6</sup>Shane et al. (1996a); <sup>7</sup>P.C. Froggatt (pers comm, 2000); <sup>8</sup>Briggs et al. (1993);

<sup>9</sup>Moyle, (1989); <sup>10</sup>B.V. Allaway (pers comm, 2000); <sup>11</sup>P.J.J. Kamp (pers comm, 2000); <sup>12</sup>Black et al. (1996); <sup>13</sup>P.A.R. Shane (pers comm, 2000); <sup>14</sup>Naish et al. (1996).

## 6.4 CORRELATIONS

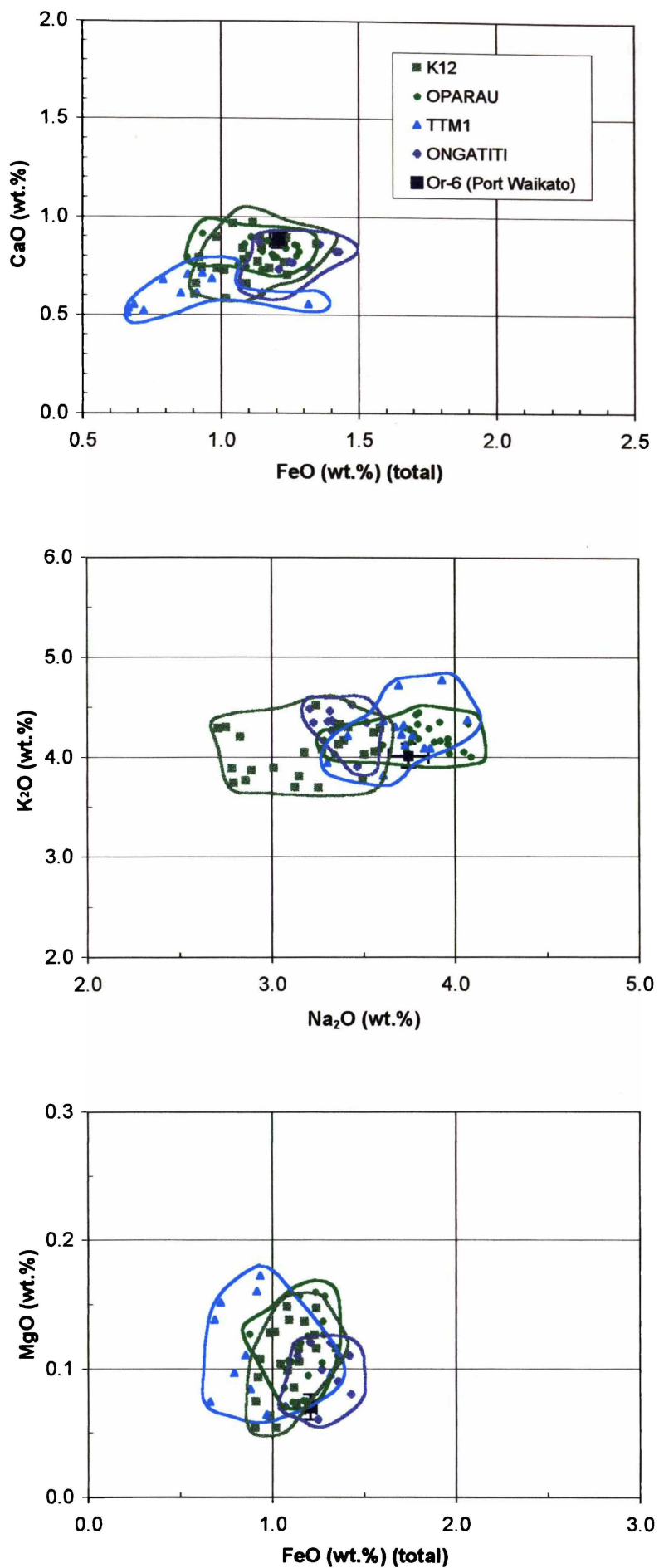
### 6.4.1 Correlation of K12, Oparau Tephra and Ongatiti Ignimbrite

As far back as 1975, C.F. Pain surmised that the Oparau Tephra might be a distal correlative of the Ongatiti Ignimbrite. This assertion was based on the proximity of an exposure of Ongatiti Ignimbrite to one of his Oparau sites north of Otorohanga. He could find no exposures showing the transition between the two, however, and thus could offer no firm evidence for the correlation. Salter (1979), too, supported the idea of an Oparau-Ongatiti correlation and indeed went on to suggest K12 was also a correlative. His evidence was also circumstantial, and it is clear that more definitive proof is needed to fully demonstrate this correlation.

#### 6.4.1.1 Results

Chapter 3 showed the correlation between the two main sites (Woodstock and Papakura Creek) based on magnetic susceptibility stratigraphy. Chapter 5 also presented similar fission track dates for the two Kauroa units (K12, Oparau Tephra) and illustrated their similarity to the Ongatiti Ignimbrite. This stratigraphic and chronologic evidence supports the contention that K12 correlates with the Oparau Tephra and that the Ongatiti Ignimbrite is a possible proximal correlative. Geochemical results presented here further corroborate this correlation.

Figure 6.5 shows plots of the three main units in question, together with the unit from Tiritirimatangi Peninsula inferred to be the Oparau Tephra (TTM1) and 'Or-6', a distal ignimbrite at Port Waikato, also inferred to be a correlative of Ongatiti Ignimbrite (B.V. Alloway, pers. comm., 2000). The plots show that K12, Oparau Tephra and TTM1 are compositionally identical with one another and with the Ongatiti Ignimbrite, showing very similar ranges and values for the elements selected; Or-6 (mean value and errors only) also plots within the data spread of the other units. The greatest variation amongst samples is in Na<sub>2</sub>O. This oxide is the most difficult to assay in glass using the EMP (Froggatt, 1983; Stokes and Lowe, 1988). Some of the inclusions in K12 were quite small and on several occasions the smaller beam size had to be employed. Commonly, EMP may underestimate Na<sub>2</sub>O, especially with narrower beam sizes, and this would explain the nearly 1 % spread in K12 data. The  $3.06 \pm 0.30$  wt. % Na<sub>2</sub>O average of K12,



**Figure 6.5** Correlation of K12, Oparau Tephra and Ongatiti Ignimbrite.



lower than that of Oparau Tephra, TTM1, Or-6 and Ongatiti Ignimbrite ( $3.80 \pm 0.20$ ,  $3.71 \pm 0.20$ ,  $3.70 \pm 0.10$ , and  $3.64 \pm 0.10$  wt. %, respectively) is thus likely to be of no real significance. These results, together with the other evidence, imply that K12, Oparau Tephra, TTM1, and Or-6 are correlatives of Ongatiti Ignimbrite.

#### 6.4.1.2 Discussion

These data go a long way towards confirming the correlation of K12 and Oparau Tephra with the Ongatiti Ignimbrite, a long-since held belief that could not be verified until now. The composition of the newly described TTM1 is also consistent with K12, Oparau Tephra and Ongatiti Ignimbrite.

The correlation is particularly useful in providing another valuable 'age-spike' in the Kauroa sequence. The  $^{40}\text{Ar}/^{39}\text{Ar}$  age of  $1.23 \pm 0.02$  Ma obtained by Briggs et al. (1993) on the Ongatiti Ignimbrite is consistent with the error weighted mean fission-track age of Oparau Tephra and K12 ( $1.31 \pm 0.10$  Ma) presented in the previous chapter. The assignment of the Ongatiti age to K12 is thus a firm 'tie-point' in the middle of Kauroa sequence, a point from which other correlations can be made.

The lack of glass shards in the three distal units meant a firm correlation could not previously be established. However, the inclusion method was able to get around this, giving good support for the correlation and perhaps even more importantly, proving the geochemistry of glass inclusions can be profitably employed to test such hypotheses. The success of this pilot study meant other Kauroa units could be correlated in this manner.

#### 6.4.2 Correlation of PCM1 (Papakura Creek)

The 3-m-thick distal ignimbrite PCM1 (correlating to K14bi; see Figures 2.3 and 2.4) stratigraphically overlies the Oparau Tephra and thus has an age of  $<1.23 \pm 0.02$  Ma. It has at least one major unit (K13) separating it from the Oparau. Polarity measurements (Chapter 5) showed PCM1/K14b to be 'normal' with 'reversed' beds under- and overlying it, suggesting it falls within the Jaramillo Subchron. This is PCM1's most diagnostic feature, reducing the possible correlatives to three major ignimbrite eruptions: Unit E/Kidnappers Ignimbrite, Potaka Tephra and Rocky Hill Ignimbrite.

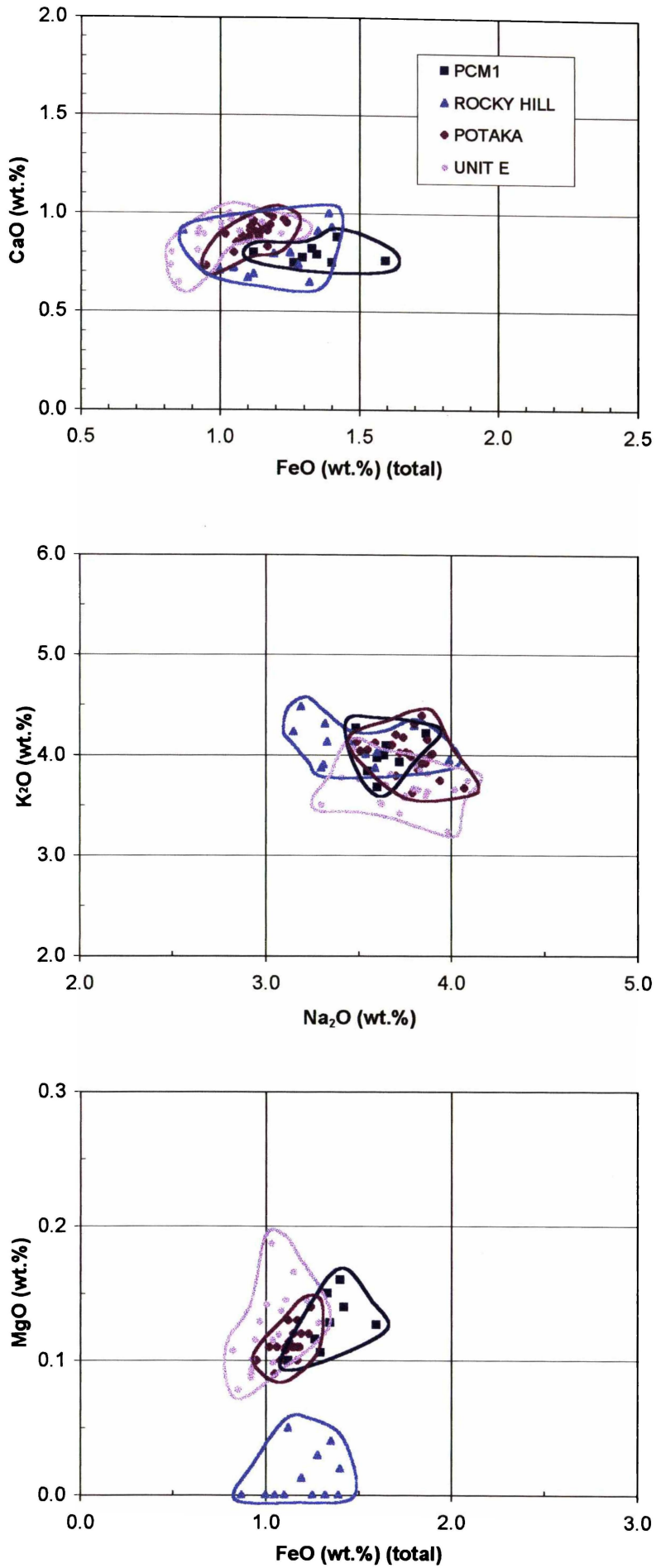
These are considered briefly below before an examination of their major element compositions.

The Unit E/Kidnappers Ignimbrite has been correlated for >385 km and has been described as probably the most widespread ignimbrite yet recorded (Wilson et al., 1995a). The deposit has been reported at multiple locations across the central North Island under a variety of names (Wilson et al., 1995a). In the majority of locations the ignimbrite comprises two flow units separated, in the northern distal area at least, by a few centimetres of fall deposit. The age is constrained by its normal polarity: given the Jaramillo Subchron occurs in isotope stages 27-29, the Kidnappers is thought to have erupted in early stage 28 (between 1.005 and 1.02 Ma using the astronomical timescale; Wilson et al., 1995a). The eruptive source is not well established, but is likely to be Mangakino Volcano, the predominantly active caldera of that time.

The Potaka Tephra is widespread in the southern North Island (Shane, 1994) though is thought to have reached as far north as Auckland (P.A.R. Shane, pers. comm., 2000) and is certainly a feasible correlative for any Waikato deposit. There is some confusion as to its relation to the Kidnappers Ignimbrite, whether the Potaka is indeed the same eruptive, a phase of the same eruption, a volcanoclastic reworking of the Kidnappers (Shane, 1991), or some entirely separate unit. Shane (1994) believed in some close association of the two, while P.J.J. Kamp (pers. comm., 1999) described a section in the Wanganui where the two are stratigraphically separated by marine sediment (Potaka stratigraphically overlies Kidnappers); Wilson et al. (1995a) suggest the Potaka Tephra is a composite deposit that includes both distal Kidnappers and Rocky Hill ignimbrites. They are certainly similar in age, the Potaka ranging from  $1.05 \pm 0.05$  Ma (Alloway et al., 1993) to  $0.99 \pm 0.09$  Ma (Shane et al., 1996a). Shane (1994) placed the Potaka early in isotope stage 27, giving it an astronomically-determined age of 1.00-0.99 Ma.

The Rocky Hill Ignimbrite was described in detail by Moyle (1989). It is a voluminous and widespread eruptive, and welded portions occur as isolated remnants scattered throughout the western central North Island, at least 85 km from source (Briggs et al., 1993). It may be present as far north as the south Auckland region (B.V. Alloway, pers. comm., 2000). In the proximal region (around Mangakino), Rocky Hill Ignimbrite stratigraphically overlies Unit E. It has been  $^{40}\text{Ar}/^{39}\text{Ar}$  dated at  $0.97 \pm 0.02$  (Briggs et al., 1993) and  $1.00 \pm 0.05$  (Houghton et al., 1995).





**Figure 6.6** Comparison of PCM1 and possible correlatives.

The major element compositions of Unit E/Kidnappers, Potaka and Rocky Hill are compared with unit PCM1 in Figure 6.6.

#### 6.4.2.1 Results

The plots in Figure 6.6 show there is little difference between the Kidnappers, Potaka and PCM1 for the elements selected. PCM1 shows at face value slightly higher FeO (tot) but this is within error limits. Rocky Hill has low MgO but this feature is not seen in all Rocky Hill samples and does not necessarily preclude a correlation.

#### 6.4.2.2 Discussion

Given the similarity of the three possible correlatives in terms of age, polarity and major element composition there is little that can be done in this study to definitively determine which is the true correlative of PCM1 (given the weathered state of this distal deposit). The low MgO of Rocky Hill Ignimbrite may preclude it as a correlative. A further factor that may suggest a distinction is the description of the Kidnappers Ignimbrite as comprising “two flow-units”, a feature that is definitely evident in PCM1. It should also be remembered that some workers (e.g. Shane, 1994; Wilson et al., 1995a) consider Unit E, Kidnappers Ignimbrite and Potaka Tephra to be essentially the same deposit. Results presented here certainly support this suggestion: namely, Potaka Tephra is compositionally identical to Unit E/Kidnappers Ignimbrite, and both are similar to PCM1. Perhaps trace element or REE analyses (e.g. using LA-ICPMS, if feasible using melt inclusions within quartz) may eventually further clarify the situation.

Names aside, there is still much gained from this near-correlation. It can be said that almost certainly PCM1 is one of the three – the polarity alone is a definitive feature, and the major element geochemistry is clearly quite similar. Either way it is evident that PCM1 has an age of 1.02-0.99 Ma (ages of Unit E/Kidnappers Ignimbrite, Potaka Tephra and Rocky Hill Ignimbrite; I will use ‘c. 1.0 Ma’) and falls somewhere in isotope stages 28 or 27, another excellent tie-point in the Kauroa sequence.

### 6.4.3 Correlation of PCM3 (Papakura Creek), WS2 (Woodstock) and TTM3 (Tiritirimatangi Peninsula)

PCM3 appears to be another (extremely weathered) ignimbrite unit, most readily visible at the Papakura Creek site (Figures 2.3 and 2.4), stratigraphically overlying member K14, and underlying beds K15 b and c. According to the previous correlation (above) this imparts a maximum age of 1.0 Ma to the unit; minimum age is provided by the Brunhes-Matuyama boundary (0.78 Ma) because K15 b and c are of reversed (Matuyama) polarity.

There are four major eruptions known to date from this time, Rocky Hill through to Kaukatea (Table 6.1). These are plotted with PCM3 in Figure 6.7. Also shown are the beds thought to be correlatives of PCM3 at Woodstock (sample WS2) and at Tiritirimatangi Peninsula sites (sample TTM3).

#### 6.4.3.1 Results

The major element compositions shown in Figure 6.7 confirm that PCM3 correlates with WS2 (K15a at Woodstock) and TTM3 at Tiritirimatangi Peninsula. Despite having quite widely dispersed data, they plot on top of each other, supporting the correlation first suggested by magnetic susceptibility stratigraphy in Chapter 3.

The plots also show that none of the known (named) proximal units is a convincing correlative for PCM3. Rocky Hill Ignimbrite is the closest match in FeO (tot), CaO, Na<sub>2</sub>O and K<sub>2</sub>O, but is distinctly dissimilar in MgO. Kaukatea and the Marshall units have generally higher FeO (tot), CaO, Na<sub>2</sub>O and lower K<sub>2</sub>O. Statistically, however, the Marshall ignimbrites cannot be excluded from contention (most elements within one standard deviation).

#### 6.4.3.2 Discussion

The age of the Rocky Hill Ignimbrite ( $0.97 \pm 0.02$  Ma, Briggs et al., 1993; or  $1.00 \pm 0.05$  Ma, Houghton et al., 1995) would seem to be too old for PCM3. The unit is separated from PCM1 (c.1.0 Ma) by K14 b and c, a well-developed paleosol, and a minor disconformity, likely to represent more than c. 30 ka. An age closer to 0.90 Ma

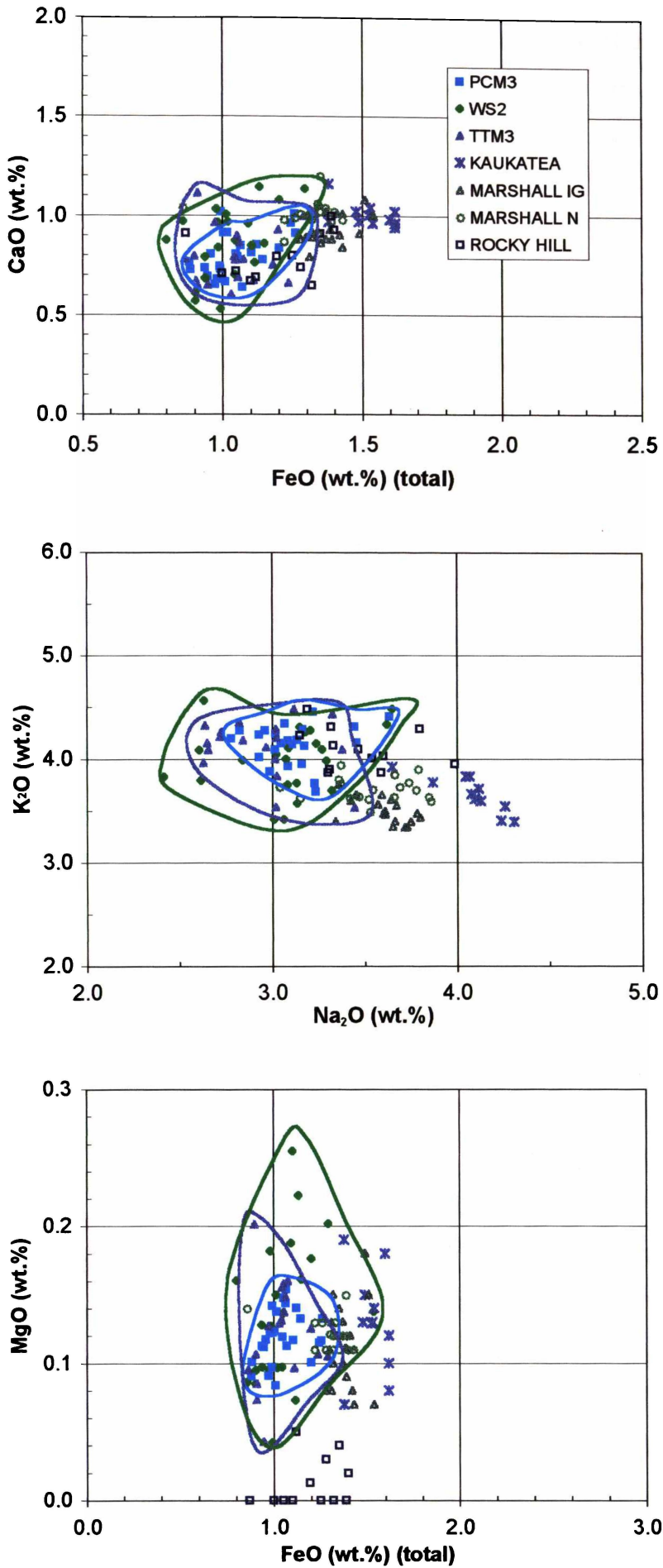


Figure 6.7 Comparison of PCM3, TTM3, WS2 and possible correlatives.

would seem more realistic but compositionally neither the Marshall ( $0.91 \pm 0.02$  Ma, Briggs et al., 1993) nor Kaukatea ( $0.87 \pm 0.05$  Ma, Shane et al., 1996a) are convincing matches based on major element analyses. Stratigraphically, the Kaukatea Tephra remains a strong possibility (cf. Chapter 7).

PCM3 (and Kauroa Ash bed correlatives) may not, of course, be correlated with any of these established units. It is entirely possible that alternative eruptions occurred and were not preserved in the stratigraphic record, or that they lie as yet undiscovered, undescribed or unpublished. It is established in this study that PCM3 represents a considerable distal ignimbrite unit present in the western Waikato region, sometimes as much as half a metre in thickness, recorded at several locations, with a probable age of  $\sim 0.85$ - $0.95$  Ma.

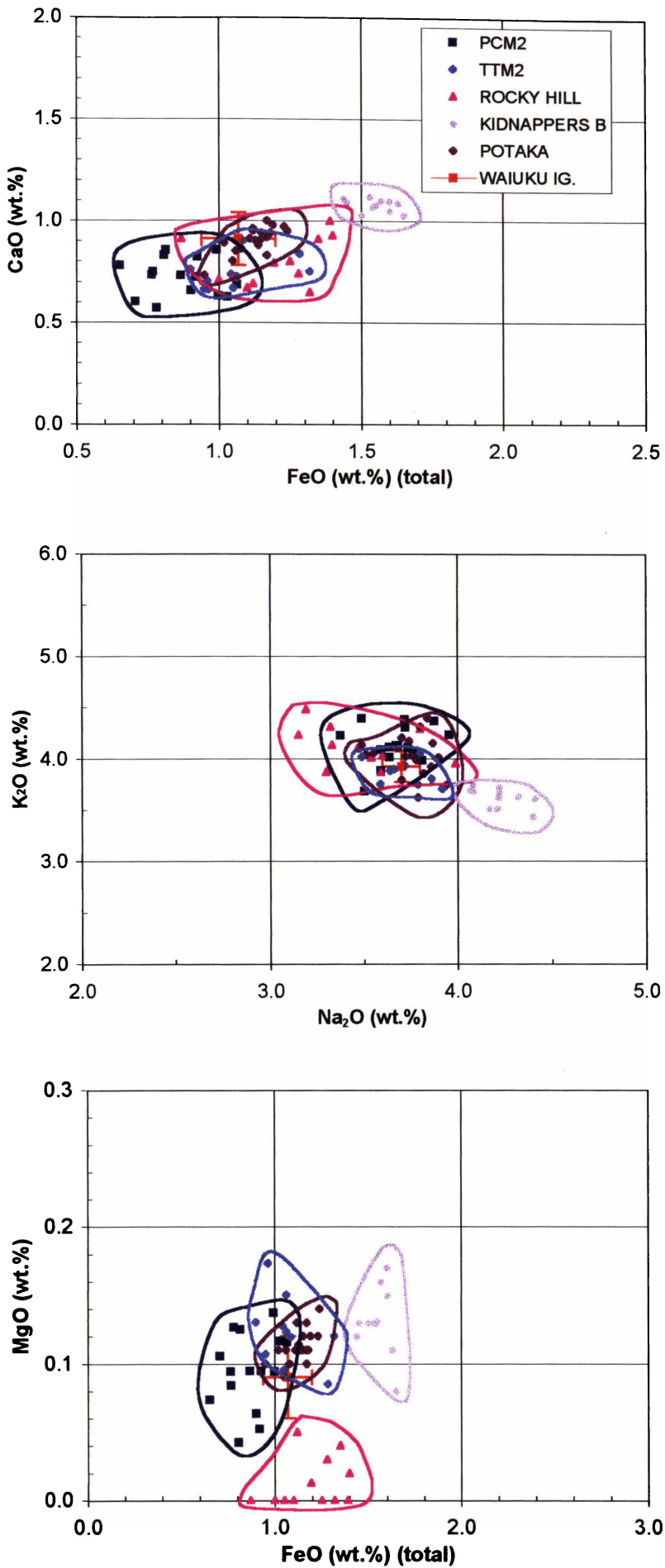
#### 6.4.4 Correlation of PCM2 (Papakura Creek) and TTM2 (Tiritirimatangi Pen.)

PCM2 (correlating to K14bii) is a coarse pumiceous ash bed of note for its extremely high crystal content. It has poorly-defined, gradational boundaries, but its pumice content suggests it was a pyroclastic flow unit of some kind, perhaps the extreme distal and/or surge deposit facies of an ignimbrite eruption. PCM2 is thought to correlate to the bed TTM2 at the Tiritirimatangi Peninsula site. TTM2 lies within approximately 2 m of undifferentiated K-bed-type material, between TTM1 (Oparau Tephra) and TTM3 (PCM3, K15a). It is pale beige coloured, moderately crystal-rich, contains small (2 mm) pumice lapilli, with a fine-grained matrix. It is laterally discontinuous, but where present has well-defined boundaries and seems to be mass-emplaced. Overlying this is an unconsolidated crystal-rich layer that grades into a hard, blocky paleosol, these properties together similar to those of K14c at Papakura Creek.

The age of PCM2 and TTM2 is constrained by PCM1 (c. 1.00 Ma) and  $0.78 \text{ Ma}^2$  (the beds above PCM2 are reversed polarity), but it directly overlies PCM1 and is thus thought to be (much) closer in age to the former. Possible correlatives are thus the Potaka Tephra<sup>3</sup>, Kidnappers B and Rocky Hill Ignimbrite<sup>3</sup>, and the major element compositions of these deposits are plotted in Figure 6.8. Mean values are plotted also for Waiuku ignimbrite, a distal ignimbrite at Port Waikato (Oruarangi section) that may

<sup>2</sup> In the absence of a strong correlation for PCM3 (which would otherwise constrain the minimum age).

<sup>3</sup> Since Potaka and Rocky Hill stratigraphically overlie Unit E/Kidnappers Ignimbrite and none has been definitely assigned to PCM1, Potaka and Rocky Hill are possible correlatives for PCM2 also.



**Figure 6.8** Comparison of PCM2, TTM2 and possible correlatives.

be a correlative of Rocky Hill Ignimbrite (B.V. Alloway, pers. comm., 2000). This deposit has been ITPFT dated at  $1.04 \pm 0.08$  Ma (B.V. Alloway, unpublished data).

#### 6.4.4.1 Results

PCM2 has a relatively low FeO (tot) of  $<1.1$  wt. % (mean =  $0.87 \pm 0.13$  wt.%), making it quite distinctive. This feature precludes correlation to Kidnappers B that has much higher FeO (tot) of  $>1.4$  wt.% (mean =  $1.55 \pm 0.07$  wt.%). This latter unit also has higher Na<sub>2</sub>O and lower K<sub>2</sub>O than PCM2.

Figure 6.8 (and raw data, Table 6.2) shows TTM2 has a close association with PCM2, having a similar spread of data for all elements. Waiuku, Potaka and Rocky Hill all have a similar major element geochemistry to PCM2 and TTM2, except for the low MgO of Rocky Hill (mean MgO of PCM2 is  $0.09 \pm 0.03$  wt.% compared with that of Rocky Hill,  $0.01 \pm 0.02$  wt.%). As outlined earlier this does not necessarily preclude correlation, however.

#### 6.4.4.2 Discussion

PCM2 and TTM2 seem to be correlatives, and both correlate well to the other distal unit, Waiuku ignimbrite. Potaka Tephra and Rocky Hill Ignimbrite are both possible proximal correlatives of PCM2/TTM2: their major element compositions are quite similar and stratigraphically, the proposed correlations are both feasible. The supporting magnetostratigraphic evidence is inconclusive: the polarity of a sample taken for paleomagnetism in K14bii was of 'intermediate' polarity, meaning it may have been 'reversed' with a 'normal' overprint, 'normal' with a 'reversed' overprint, or transitional between the two. The last two possibilities would suggest a 'normal' polarity for PCM2, and would be consistent with either a Potaka or Rocky Hill correlation. A 'reversed' polarity for PCM2 would mean it correlates to a currently unknown eruptive.

Potaka and Rocky Hill are well-dated units, close in age. As for PCM1, a tentative correlation to both produces an age of between  $1.05 \pm 0.05$  (Potaka; Alloway et al., 1993) and  $0.97 \pm 0.02$  (Rocky Hill; Briggs et al., 1993). Clearly, PCM2 is likely to have been erupted soon after (within c. 50 ka) of PCM1.

### 6.4.5 Correlation of K3

At Woodstock a lithologically distinctive member is K3, the bright orange-pink coloured, pumice and crystal-rich bed 11-12 m below the current land surface. Salter (1979) inferred K3 to be the product of a pyroclastic flow rather than tephra-fall unit, and possibly a correlative of the Waiteariki Ignimbrite. We can say now that this proposed correlation is unlikely because the Waiteariki, dated at  $2.18 \pm 0.15$  Ma, is almost certainly too old for K3. The emplacement process of this member is also ambiguous. The ~5 mm pumice lapilli found in K3a do not automatically indicate an ignimbrite origin for K3: a typical plinian fall deposit is capable of containing 5-10 mm lapilli 60-80 km downwind of source, an eruption approaching “ultraplinian” proportions can spread lapilli >10 mm in diameter distances of >200 km<sup>4</sup>. Thus for K3 to be derived from primary fall, c. 100 km from source presuming a Mangakino origin, the eruption would have to have been fairly energetic (plume height 30-50 km) with the dispersal axis to the north-northwest. This would represent one of the larger (in terms of energy and volume) Mangakino plinian eruptions. An ignimbrite origin is somewhat easier to accept, especially given other factors such as its crystal-rich nature and probable lithic-content (most have been weathered to clays).

Evidence to the question of age is available in the fission-track date of  $1.68 \pm 0.12$  Ma and the normal polarity of the underlying bed, K2b (see Chapter 5). This places K3 after the end of the Olduvai Subchron (1.79–1.95 Ma; Shackleton et al., 1990). Possible correlatives in this age range include Vinegar Hill Tephra, and three unnamed but quite ‘substantial’ tephtras found in the Wanganui Basin, 158, 131 and 108; also shown is Waipuru Tephra, within age range of K3 though normal polarity (Shane et al., 1996a; P.A.R. Shane, pers. comm., 1999). The major element compositions of these units are plotted in Figure 6.9.

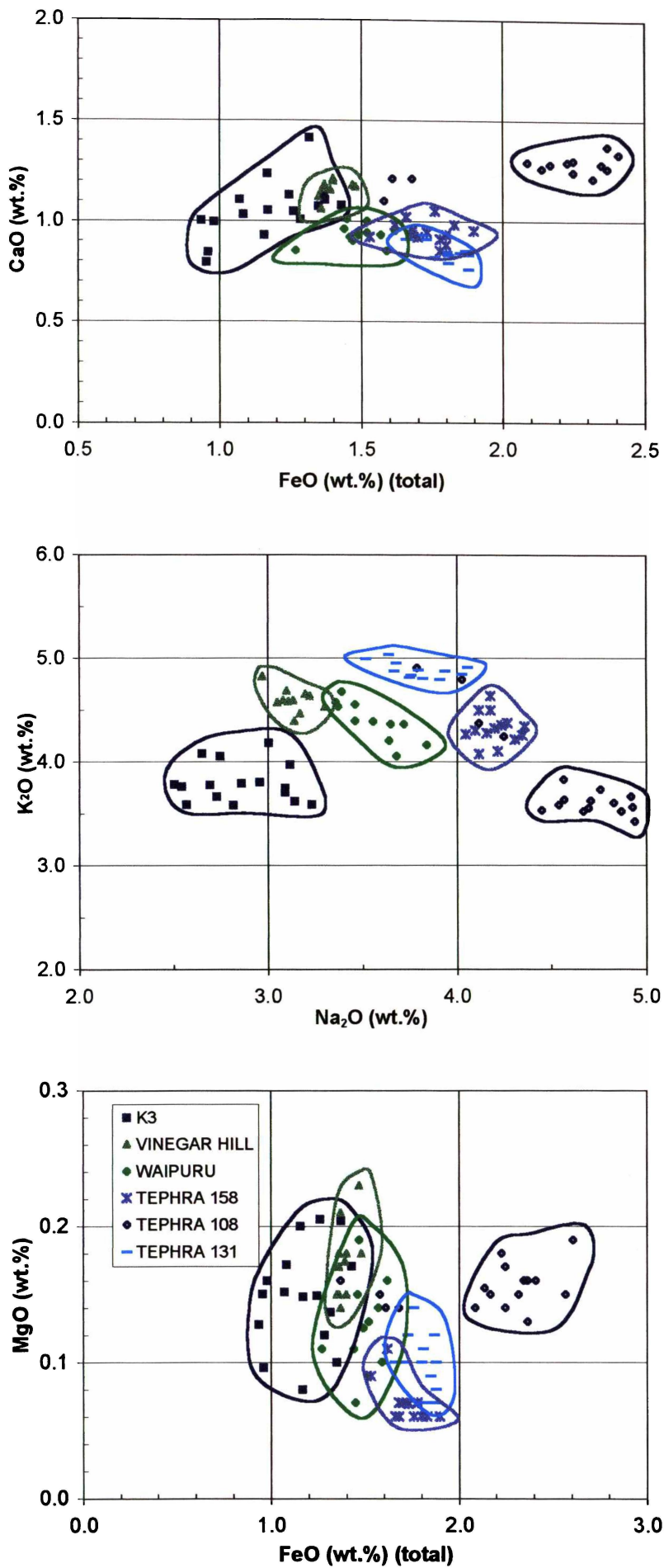
#### 6.4.5.1 Results

The data points in Figure 6.9 are considerably less clustered (have wider ranges) than in previous plots making it easier to dismiss units with obviously dissimilar composition to K3. It is clear, for example, that tephtras 158, 131 and 108 have significantly higher

---

<sup>4</sup> Pumice lapilli, 10 mm in diameter, are found in the plinian Hatepe Ash (Phase Y2 of c. 200 AD Taupo eruption) up to 80 km from source. Pumice lapilli, >10 mm in diameter, in the “ultraplinian” Taupo eruption (Phase Y5) are found 210 km from source (R.T. Smith, pers. comm., 2000).





**Figure 6.9** Comparison of K3 and possible correlatives.

Na<sub>2</sub>O, FeO (tot) and, to a lesser extent, K<sub>2</sub>O. All plot in confined clusters, visually and statistically distinct from K3.

Waipuru Tephra plots closer to K3 in some elements than others. Four elements, SiO<sub>2</sub>, Al<sub>2</sub>O<sub>3</sub>, Na<sub>2</sub>O and K<sub>2</sub>O, are statistically irreconcilable with those of K3; other elements are within error limits. Figure 6.9 shows Waipuru Tephra data points are mostly distinct from those of K3.

Vinegar Hill data plots closest to K3 of the known 'possible correlatives'. All elements except SiO<sub>2</sub> and K<sub>2</sub>O are within error limits.

#### 6.4.5.2 Discussion

Tephtras 158, 131 and 108 are unlikely to be correlatives of K3 because of their significantly different major element composition. Waipuru Tephra is an improbable match because of its higher Na<sub>2</sub>O and K<sub>2</sub>O (and other elements), and normal polarity. The closest correlation based on these compositional data, is the Vinegar Hill Tephra. This tephra has been described previously in the Wanganui Basin. It is a 0.2 m-thick, pink-grey, normally graded, laterally continuous vitric ash bed, the lower 0.1 m of which is a coarse pumiceous ash (up to 1 mm) which grades into 0.1 m of fine ash (Naish et al., 1996). This description is not inconsistent with that of K3, although it is clearly significantly less weathered and so physical properties cannot be compared. The age for Vinegar Hill Tephra,  $1.75 \pm 0.13$  Ma (Naish et al., 1996), is also consistent with that of K3, and it is reversed polarity.

It is also possible that K3 could correlate to a different, possibly undescribed, eruptive. However, on available evidence K3 is provisionally correlated to Vinegar Hill tephra.

#### 6.4.6 Correlation of WS3 (K13a, Woodstock)

K13a has an age that is constrained by K12a (Ongatiti Ignimbrite; c. 1.23 Ma) and K14b (c. 1.0 Ma). Both K12 and K13 have paleosols developed on them suggesting a considerable hiatus preceding and succeeding the emplacement of K13a. Two major eruptions occurred in this time period, producing eruptives known as Unit D (ignimbrite and fall) and Ahuroa Ignimbrite. Nelson et al. (1989) described a sequence at Port

Waikato (Oruarangi section) that has three pyroclastic deposits between an inferred Ongatiti Ignimbrite correlative (Or-6) and Waiuku ignimbrite dated at  $1.04 \pm 0.08$  Ma (B.V. Alloway, pers. comm., 2000). From oldest to youngest they are: Or-8, Or-10, Or-11. All units are shown plotted in Figure 6.10.

#### 6.4.6.1 Results

WS3 has low FeO (tot) and relatively high K<sub>2</sub>O and low Na<sub>2</sub>O giving it a distinctive major element composition. None of the possible correlatives has a similar composition, however, all having higher FeO (tot) and low K<sub>2</sub>O and high Na<sub>2</sub>O.

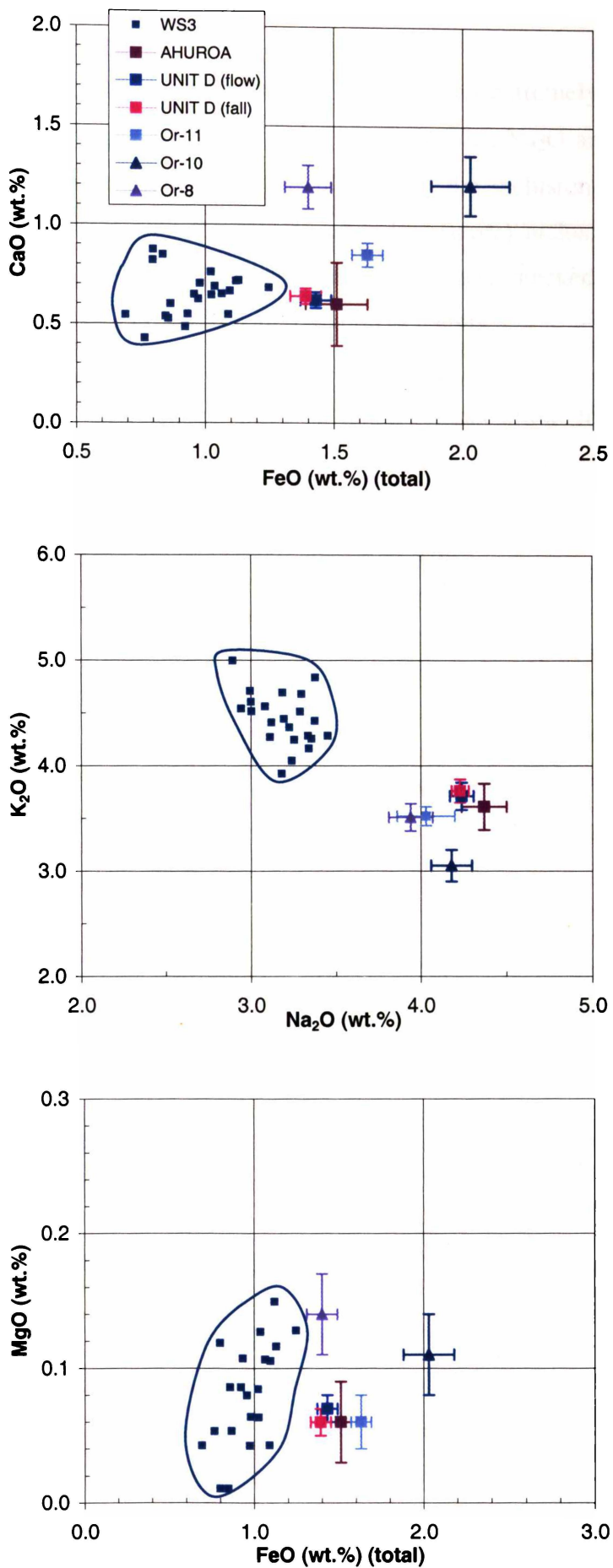
#### 6.4.6.2 Discussion

Neither the two voluminous ignimbrite eruptions (Unit D and Ahuroa) nor the unnamed eruptives at Port Waikato seem to be a good match for K13. There is thus no known correlative for this unit, even though it is widespread in the Waikato and west coast regions of the North Island.

#### 6.4.7 Correlation of WS1 (K15c, Woodstock)

K15, the youngest member of the Kauroa Ash sequence, was named the 'Waiterimu Ash Member' by Ward (1967). In this study I recognise three beds making up the member: K15a, a distal ignimbrite at the Papakura Creek site, K15b a weathered tephra and K15c, a weathered tephra with a firm, blocky paleosol developed on the top 40-50 cm (at least). K15b and c are too weathered to determine genetic origin, but may be composite beds formed through incremental accumulation of tephra (no visible horizonation).

The age of K15c is constrained by the Brunhes-Matuyama boundary (K15c has reversed polarity), 0.78 Ma, and by the age of K14bii, c. 1.0 Ma. Several large eruptions are known for this time, and are shown with WS1 (K15c) in Figure 6.11. Also plotted are four tephra beds from the Cape Kidnappers section, Kidnappers 'C' to 'F', that are thought to be of similar age (correlation to this site is discussed further in Chapter 7).



**Figure 6.10** Comparison of WS3 and possible correlatives.

#### 6.4.7.1 Results

Plots of major element composition show that WS1 has an extremely broad range of chemistry (large standard deviations), especially in FeO (tot), Na<sub>2</sub>O and MgO. This is not thought to result from operational difficulties with the inclusion technique – no problems were encountered with the sample, abundant (large) inclusions were found and there was no need to reduce the beam size. Standards were checked before and after analysis of WS1 and showed no significant variation in results.

Most of the possible correlatives have different composition to WS1, having consistently higher CaO and lower K<sub>2</sub>O in particular. One sample, Kidnappers 'C', stands out as the closest match. This has lower FeO (tot), CaO and higher K<sub>2</sub>O than the rest of the deposits and generally plots on or near WS1 data.

#### 6.4.7.2 Discussion

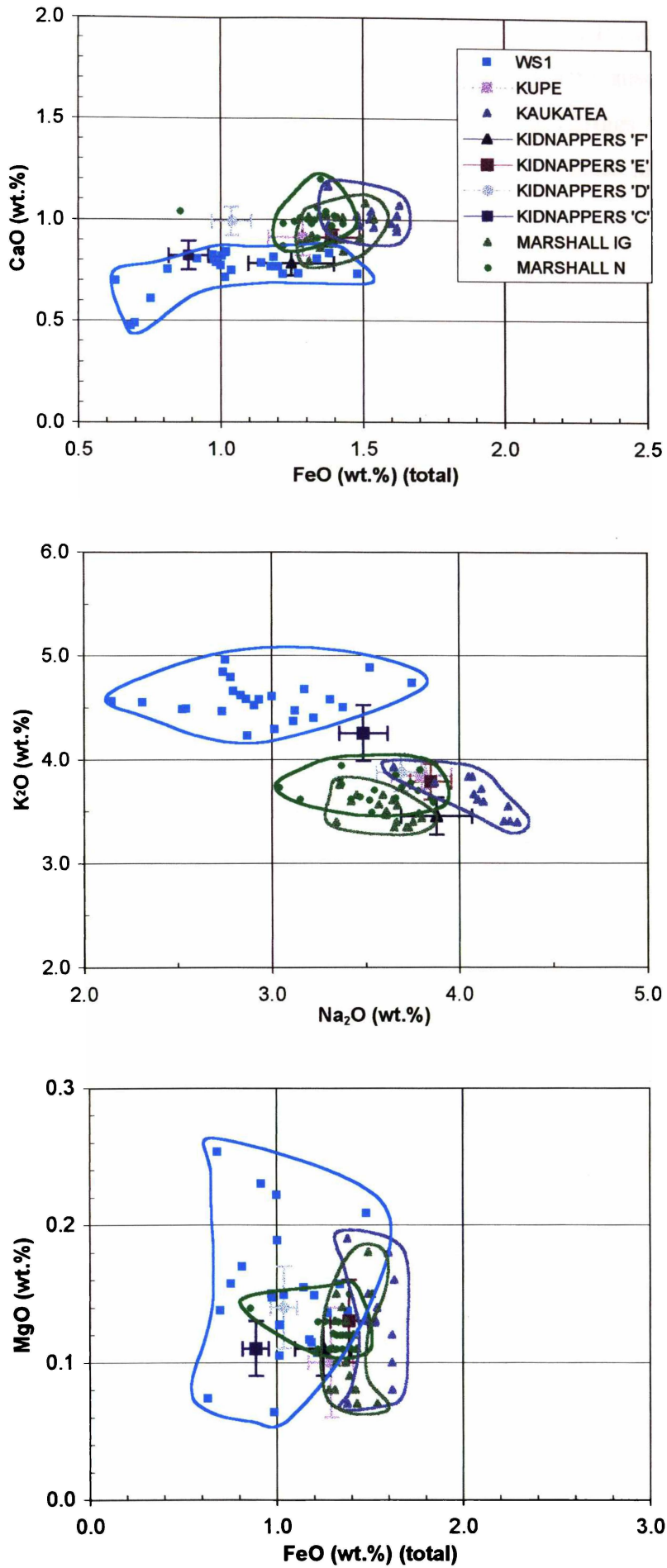
Figure 6.11 highlights one distal deposit, Kidnappers 'C' as a possible correlative of K15c. However, none of the known proximal deposits originating from this time period seems to be a good fit. Kidnappers 'C' is undated, but has a relative age of  $>0.88 \pm 0.04$  Ma (i.e. older than Kidnappers 'D').

The large spread in K15c data may indicate that it is a composite tephra bed, composed of two or more minor eruptions from the same vent (with similar geochemistry). The sample size required for Kauroa beds is so large (typically several kilograms) because of the high clay content, and so more than one eruption could be represented in one sample.

#### 6.4.8 Correlation of Tiritiri ignimbrite

The Tiritiri ignimbrite is a 6-8 m-thick weathered ignimbrite on Tiritirimatangi Peninsula in Kawhia Harbour. There is no evidence of a correlative elsewhere in the region, yet the eruption that produced it was clearly of a significant magnitude, this locality being over >100 km from known rhyolitic sources.

Numerical dating has been unsuccessful, though some idea of age is possible from



**Figure 6.11** Comparison of WS1 and possible correlatives.

relative dates. At the base, Tiritiri ignimbrite is separated from a Pirongia Volcanics lahar deposit by Kauroa Ash members K3-K5 (inferred by magnetic susceptibility; see Figure 2.21). Pirongia Volcanics range from 2.74-1.60 Ma (Briggs et al., 1993). However, some of these dates are thought to be too young and a more likely minimum age has been suggested to be c. 1.80-2.00 Ma (R.M. Briggs, pers. comm., 2000). Lahar deposits often relate to later stages of volcanism (after major cone construction is completed), so it could be assumed that the lahar deposit at Tiritirimatangi Peninsula originates from this time. This would be consistent with the established stratigraphy, K3 having an age of  $1.68 \pm 0.12$  Ma. K4 and 5, though insubstantial here, are more significant at Woodstock and may also represent a considerable duration of time (accumulated loess and/or tephra, and with paleosols developed on them). A maximum age for the Tiritiri ignimbrite under this scenario is thus inferred to be c. 1.70 Ma.

As for minimum age, the Tiritiri ignimbrite is separated from TTM1 (weathered Oparau Tephra) by K9-K11. Ages and origins of these beds are uncertain, but they are likely to represent landscapes that persisted for some considerable time, K11 alone being a very substantial paleosol in terms of both thickness and degree of pedogenic development. With Oparau Tephra,  $1.23 \pm 0.03$  Ma, providing a minimum age, a more realistic minimum for Tiritiri ignimbrite is suggested to be c. 1.35 Ma based on the presence of the K9 and K11 paleosols.

The age of Tiritiri ignimbrite is thus inferred to fall in the range 1.70-1.35 Ma, meaning that numerous possible correlatives of this deposit are likely. Known eruptives dating from this time (that have major element glass data available) are shown in comparison to glass inclusion data for Tiritiri ignimbrite in Figure 6.12.

#### 6.4.8.1 Results

It is immediately obvious that many of the eruptive units are quite different from Tiritiri ignimbrite. In particular, Tephra 166, Mangapipi, Akupe, Mangahou, Tephra 108 and Tephra 131 all have significantly higher FeO (tot) than Tiritiri ignimbrite. Only Pakihikura Pumice and Tephra 288 have major element compositions that are statistically reconcilable. These two units, in fact, have very similar compositions to those of the Tiritiri ignimbrite, the data points overlapping in all elements.

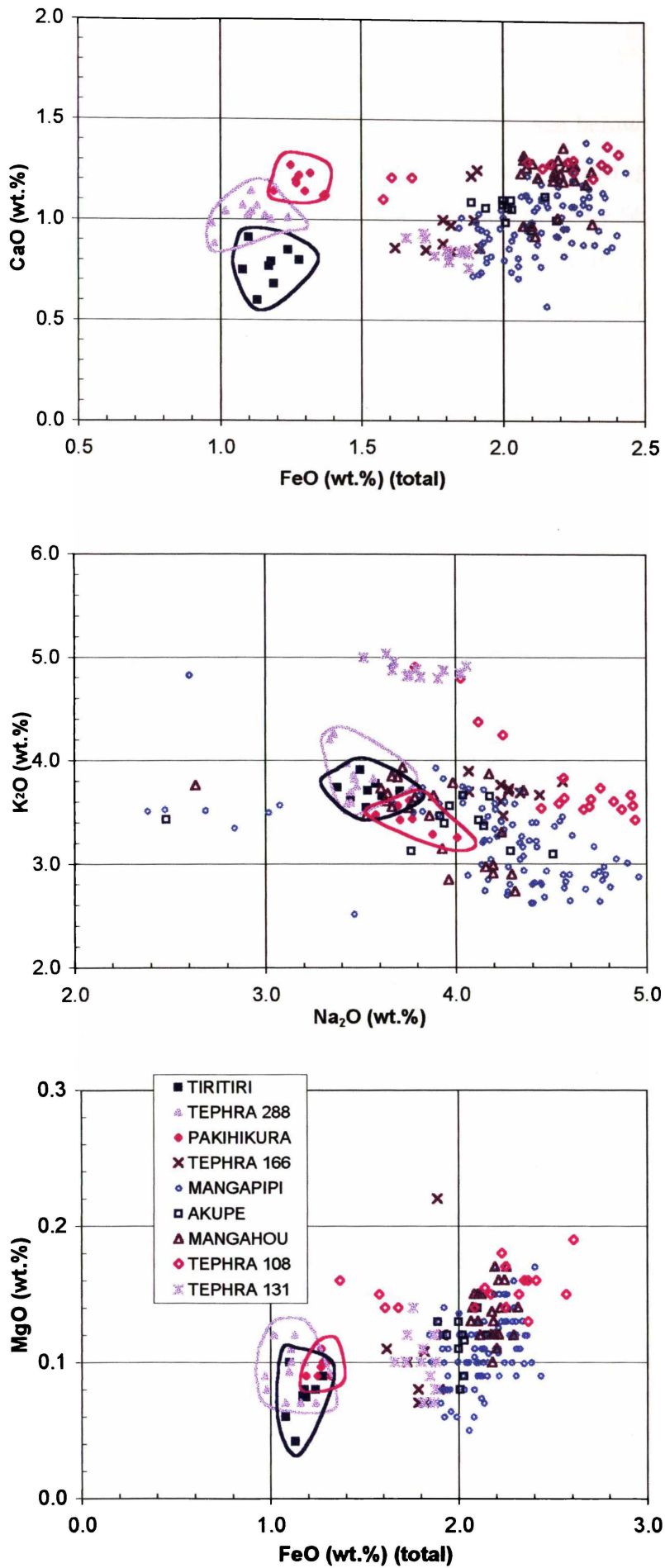


Figure 6.12 Comparison of Tiritiri ignimbrite and possible correlatives.



#### 6.4.8.2 Discussion

Based on the close match of major element data, either (or both – see below) of these two units, Tephra 288 and Pakihikura Pumice, may be correlatives of Tiritiri ignimbrite. Their physical properties provide further clues. Tephra 288 is described by Shane et al. (1996a) as a c. 3 m-thick ignimbrite at the base of the Makaroro River section (Ruahine-Wakarara Ranges). It is massive, non-welded, mainly ash and fine lapilli, and is inferred by P.A.R. Shane (pers. comm., 2000) to be a phreatomagmatic low-aspect-ratio flow deposit, violently emplaced because it is also found at several localities in Hawke's Bay. Pakihikura Pumice, in contrast, is a fall deposit: massive, pinkish-white ash, usually thin (<40 cm). It is found in a variety of sediments in many sections throughout the Wanganui Basin, sometimes as primary fall material, sometimes in reworked form (P.A.R. Shane, pers. comm., 2000). The genetic (fallout or reworked) origin of Pakihikura Pumice would thus seem unsuitable as a correlative for Tiritiri Ignimbrite, though its similar composition could indicate it is a different phase of the same eruptive episode. The same could be said for the relationship of Tephra 288 to Pakihikura Pumice, because the latter is found immediately overlying Tephra 288 in the Makaroro River section.

A further alternative is the Ngaroma Ignimbrite. No glass data are available for this and no inclusions could be found in quartz grains from it (at the type locality). However it has some physical characteristics that are identical to those of the Tiritiri ignimbrite: a eutaxitic texture oriented parallel to the underlying contact (both are 'lenticulites'), a chalky texture attributed to pervasive recrystallisation and vapour-phase alteration, the presence of a ground layer (suggesting that the ignimbrite was energetically emplaced), and extensive columnar jointing in the lower half of the deposit. Moreover, in the neighbouring King Country, the Ngaroma Ignimbrite is overlain by the Ongatiti Ignimbrite or separated only by a minor erosional contact, or both – a similar stratigraphy to that of the Tiritirimatangi Peninsula site. What is not consistent is that the Ngaroma is not thought to be one of the larger Mangakino eruptions. In the King Country, 35–40 km from source, the Ngaroma is c. 3–4 m in thickness. On the west coast, towards 80 km from its inferred source, Tiritiri ignimbrite is 6–8 m thick. Thickening of ignimbrite sheets away from source is not unprecedented, however. Bailey and Carr (1994) reported that the Matahina Ignimbrite thickens away from source, attaining a maximum thickness of 140 m in a fault-angle trough c. 30 km from

source (Haroharo Caldera, Okataina Volcanic Zone). The emplacement of the Tiritiri ignimbrite could have been similarly determined by topography, perhaps ponding in a paleovalley formed by the underlying Pirongia Volcanics.

Tephra 288 would thus appear to be the best match for Tiritiri Ignimbrite, though the other two possibilities, Pakihikura Pumice and Ngaroma (or an undescribed alternative), should not be discounted. All three of these possible correlatives are well dated and together constrain the age of the Tiritiri to between  $1.60 \pm 0.03$  Ma (Ngaroma Ignimbrite; Briggs et al., 1993) and  $1.64 \pm 0.13$  Ma (Tephra 288; Shane et al., 1996a), i.e., somewhere in marine oxygen isotope (MOI) stages 58-55.

The assignment of this age to Tiritiri ignimbrite also forms the maximum and minimum ages of K5 and K9, respectively. It does not have direct implications for K6-K8, however, as their stratigraphy relative to the Tiritiri ignimbrite is unknown.

#### 6.4.9 Correlation of TTM4 (Tiritirimatangi Peninsula)

TTM4 overlies the K15c paleosol at Tiritirimatangi Peninsula and is thought to be H1 of the Hamilton Ash Formation. It has lobe-like 'flame' structures at the base and large quartz grains in the lowermost 15 cm, characteristic features of H1 (Ward, 1967; Tonkin, 1970). The major element composition of this bed is compared here with that of the widespread Rangitawa Tephra ( $0.35 \pm 0.04$ ; Kohn et al., 1992; Lowe et al., in press) to confirm the correlation (Figure 6.13).

##### 6.4.9.1 Results

Figure 6.13 shows that the major element composition of TTM4 has a close association to that of Rangitawa Tephra, with data points overlapping in every case. Mean values for each element (Tables 6.2 and 6.3) correlate to within one standard deviation.

##### 6.4.9.2 Discussion

These data confirm TTM4 at Tiritirimatangi Peninsula (H1) almost certainly correlates to the widespread Rangitawa Tephra.

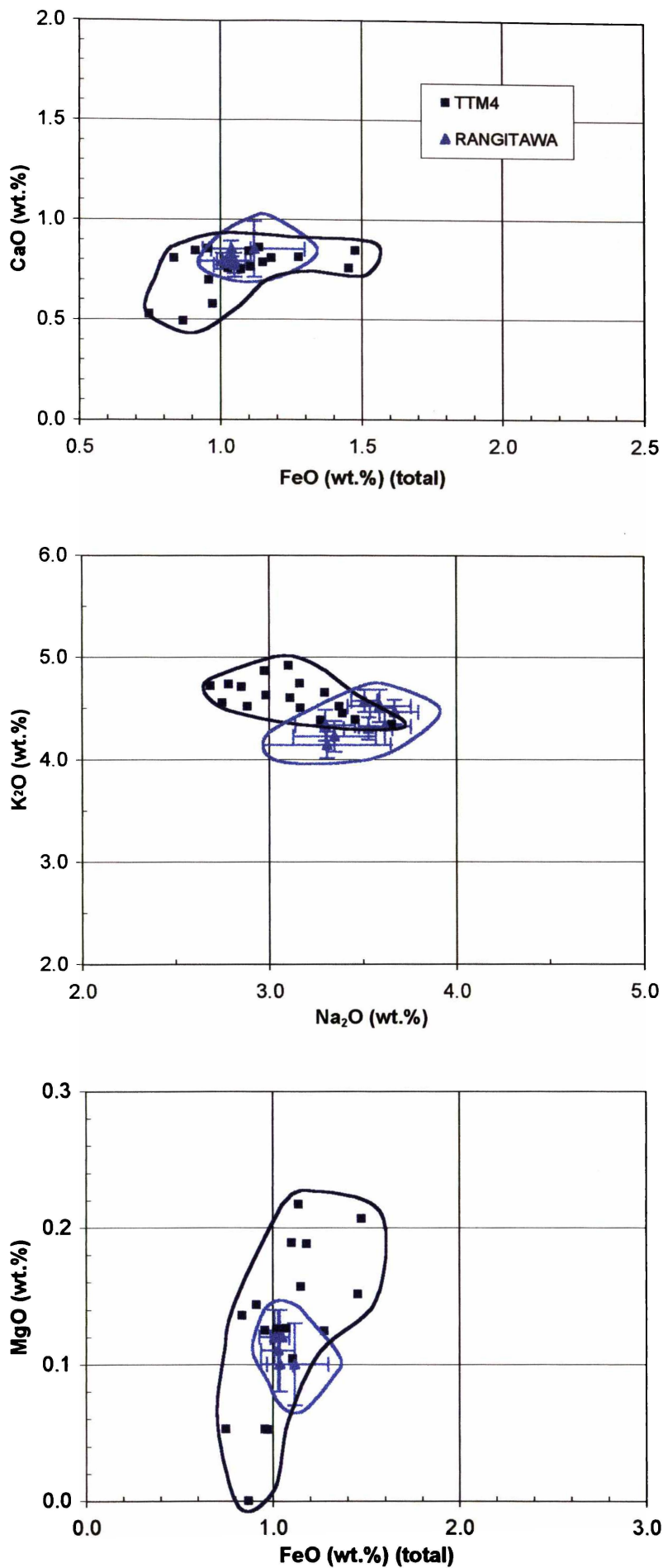


Figure 6.13 Comparison of TTM4 and Rangitawa Tephra.

## 6.5 CONCLUSIONS

The identification and correlation of tephra beds using geochemical fingerprinting of glass inclusions in quartz grains, the first such application in New Zealand, has enabled a stratigraphic framework for the Kauroa Ash sequence to be produced. This would otherwise have been impossible because of the extremely weathered state and lack of volcanic glass shards characteristic of all Kauroa beds.

### 6.5.1 Summary of correlations

Table 6.4 shows the summarised results of the microprobe study, the possible correlatives of each of the major Kauroa Ash beds, together with their inferred age or age range.

**Table 6.4** Summarised tephrochronological correlations of Kauroa Ash sequence samples resulting from electron microprobe analysis of glass inclusions in quartz grains.

Sample	Kauroa correlative	Possible proximal correlatives	Confidence of correlation*	Inferred age or range (Ma)
WS1 (K15c)		Kidnappers 'C'	4	>0.78-0.95
WS2 (K15a)	PCM3/TTM3	---	2	0.85-0.95
WS3 (K13)		---		1.23-1.00
K12	Oparau, TTM1	Ongatiti Ignimbrite	1	1.23 ± 0.03
K3		Vinegar Hill	2	1.68 ± 0.12 <sup>†</sup> (1.75 ± 0.13 <sup>‡</sup> )
PCM3	TTM3/WS2	---	2	0.85-0.95
PCM2		TTM2	4	1.00-0.85
PCM1	TTM2	Unit E/Kidnappers (Potaka)	2	1.01 ± 0.06
OPARAU	K12, TTM1	Ongatiti Ignimbrite	1	1.23 ± 0.03
TTM4	(H1)	Rangitawa Tephra	1	0.35 ± 0.04
TTM3	PCM3/WS2	---	2	0.85-0.95
TTM2	PCM1	Unit E/Kidnappers (Potaka)	4	1.00-0.85
TTM1	K12, Oparau	Ongatiti Ignimbrite	1	1.23 ± 0.03
TIRITIRI IG.	---	Tephra 288 (Ngaroma; Pakihikura)	2-3	1.60-1.64

\* On a scale of 1-4, where 1 is high and 4 is low.

<sup>†</sup> Direct date on K3

<sup>‡</sup> Age of Vinegar Hill Tephra

--- No correlative assigned

Some correlations are provisional only, but they represent the best match based on available evidence. Even a choice of two or three correlatives offers some reasonably precise age control, and provides a good starting point from which to continue. Other correlations are more certain, with several lines of evidence pointing to one likely

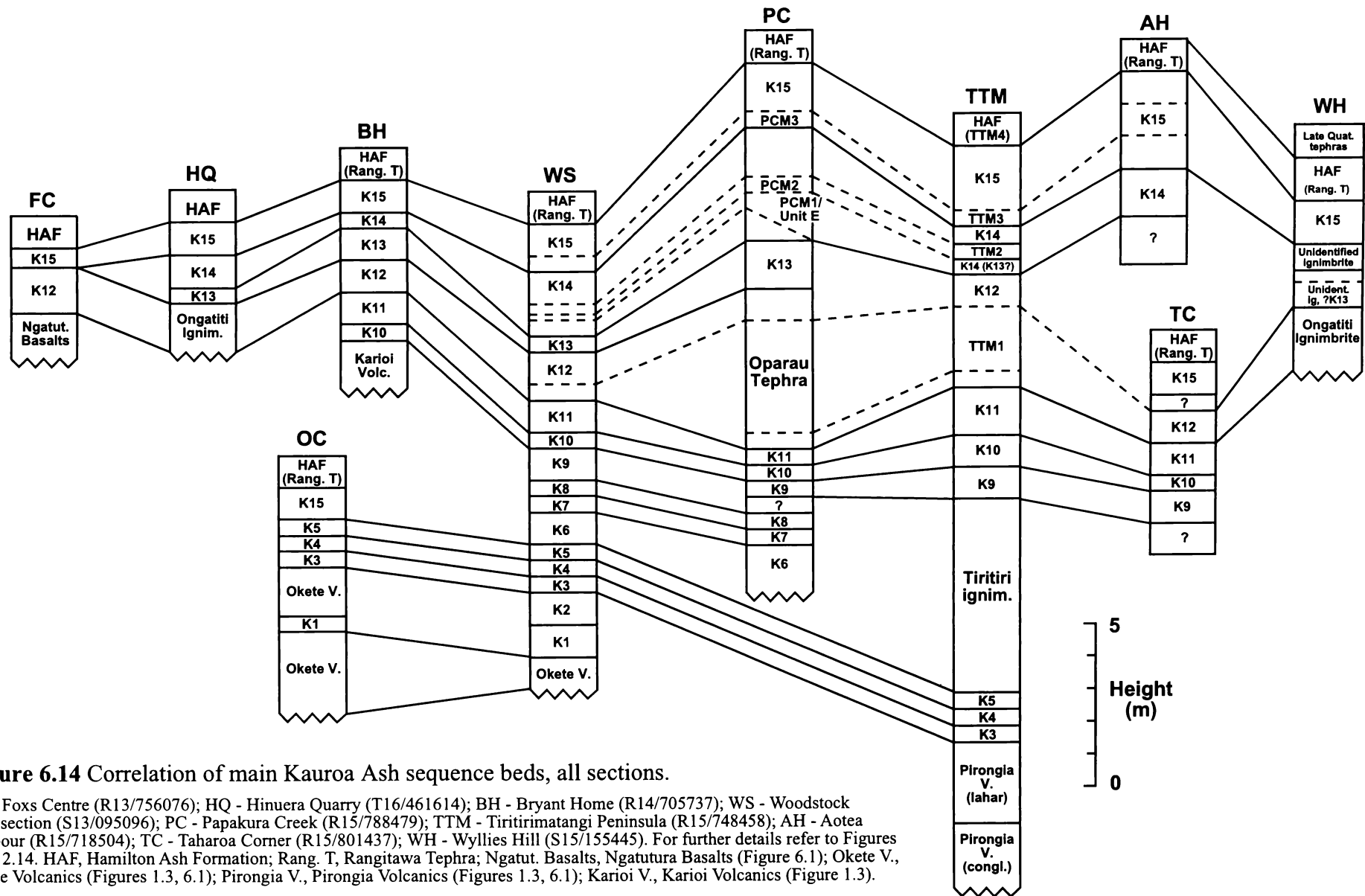
(proximal) eruptive. The most advantageous outcome of these correlation efforts is that most beds in the Kauroa sequence can at least now be assigned an age range to within about 200-300 ka. This could be considered imprecise in some fields of work, but for these beds it is a major step forward.

Correlations between sections were previously established using magnetic susceptibility stratigraphy, but are now confirmed by glass inclusion major element compositions (correlations shown in Figure 6.14). In addition, a new 'composite' Kauroa Ash sequence stratigraphic column can now be drawn (Figure 7.2), with units from all sites included. This stratigraphy allows correlation to other New Zealand Plio-Pleistocene sequences, putting the Kauroa Ash sequence in a regional stratigraphic framework for the first time (Chapter 7).

#### *6.5.2 Assessment of the glass inclusion technique*

This pilot study has proved the microprobe analysis of glass inclusions in quartz grains to be an entirely feasible, even simple, undertaking. Methodologically, it is straightforward, if only a little 'fiddly' in preparation. Microprobe analysis itself requires a little more time and care than that of traditional glass shard studies, but is also basically uncomplicated. Results typically show good totals and low standard deviations, and all in all have been shown to be an entirely acceptable alternative to glass shard-derived data.

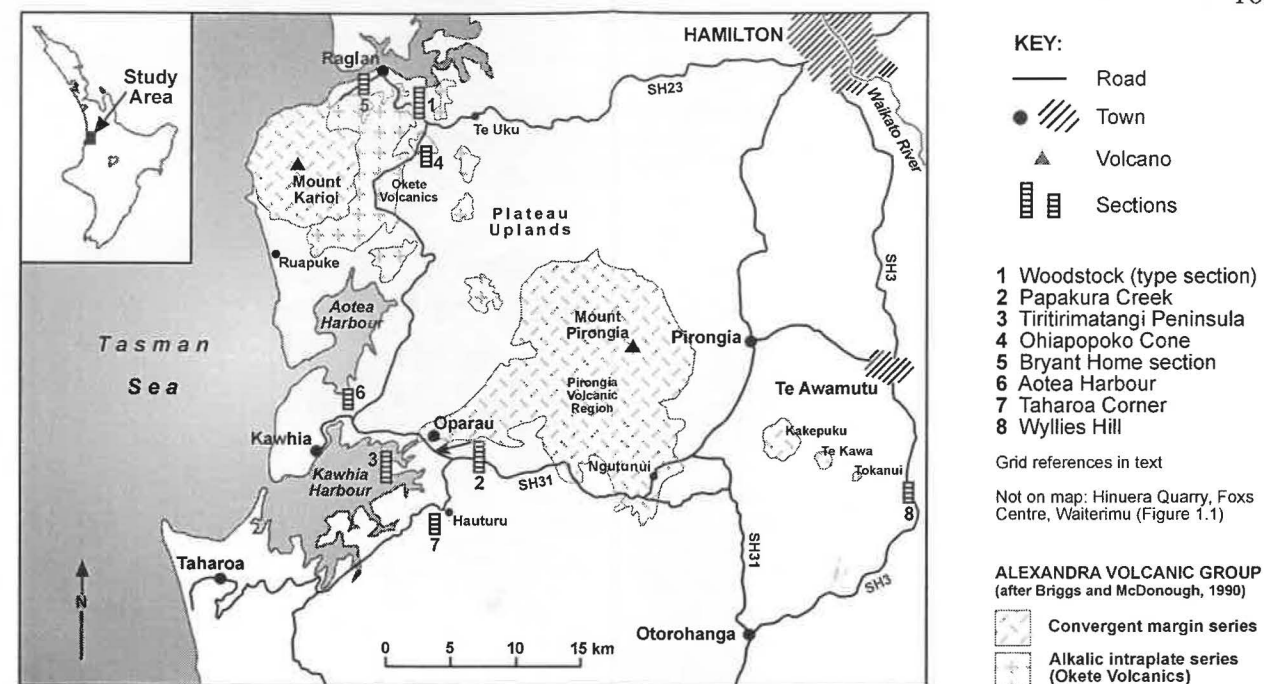
Limitations of the technique are few. Most difficulties experienced in this study relate only to standard limitations of microprobe work: many examples given above illustrate the difficulty of correlating eruptions from the presumed-same volcanic centre, major element compositions often being too similar to determine between them. It is not a major limitation, however, most compositions enabling determination of what a deposit is not, even if it cannot prove for certain what it is. EMP is still of utmost value for facilitating informed speculation which, in conjunction with other age and stratigraphic data, can often lead to more confident conclusions.



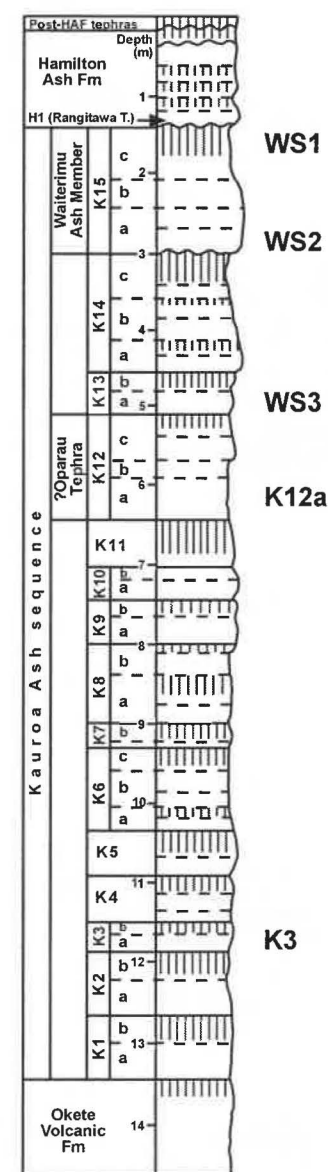
**Figure 6.14** Correlation of main Kauroa Ash sequence beds, all sections.

FC - Foxx Centre (R13/756076); HQ - Hinuera Quarry (T16/461614); BH - Bryant Home (R14/705737); WS - Woodstock type section (S13/095096); PC - Papakura Creek (R15/788479); TTM - Tiritirimatangi Peninsula (R15/748458); AH - Aotea Harbour (R15/718504); TC - Taharoa Corner (R15/801437); WH - Wyllies Hill (S15/155445). For further details refer to Figures 2.1 - 2.14. HAF, Hamilton Ash Formation; Rang. T, Rangitawa Tephra; Ngatut. Basalts, Ngatutura Basalts (Figure 6.1); Okete V., Okete Volcanics (Figures 1.3, 6.1); Pirongia V., Pirongia Volcanics (Figures 1.3, 6.1); Karioi V., Karioi Volcanics (Figure 1.3).

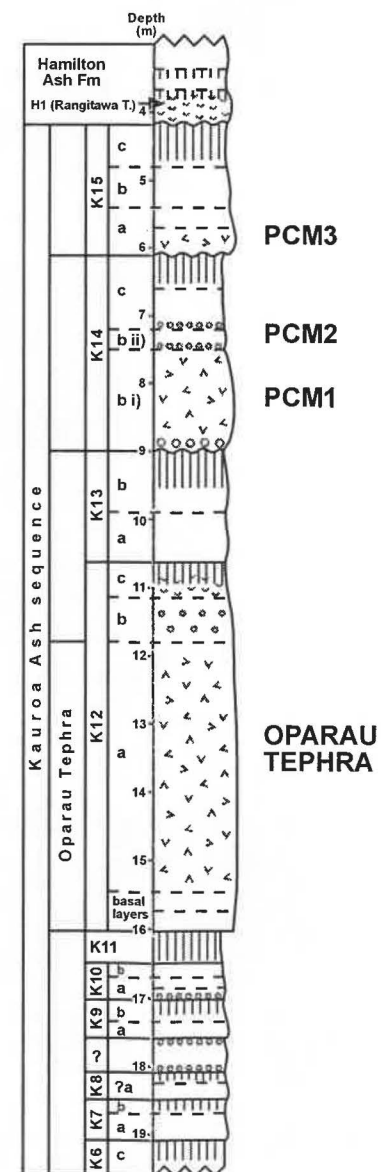
**Figure 6.15** Reference sheet: stratigraphic columns for Woodstock, Papakura Creek and Tiritirimatangi Peninsula, showing samples used for correlations; map of main field area. For further details refer to maps, Figures 1.1, 1.3, 6.1; and stratigraphic relations, Figures 2.1-2.6.



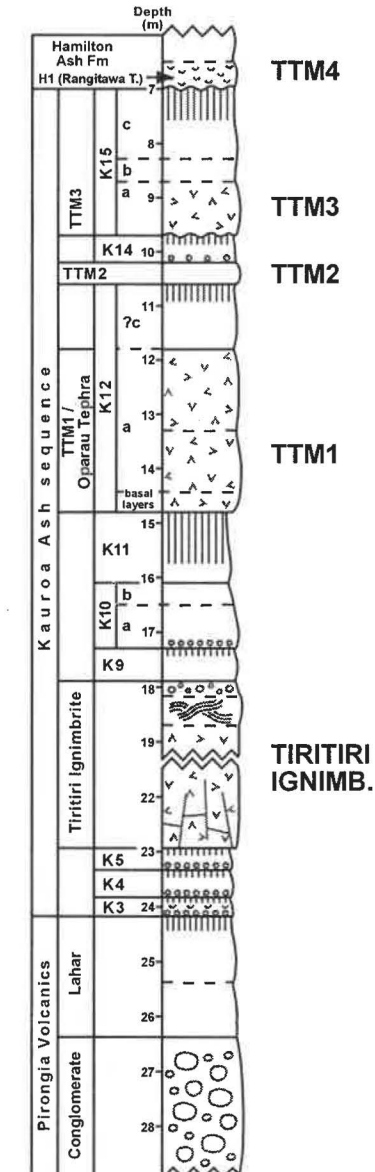
**WOODSTOCK**



**PAPAKURA CREEK**



**TIRITIRIMATANGI PENINSULA**



## 7 PLIO-PLEISTOCENE STRATIGRAPHY:

### *Kauroa Ash sequence in a New Zealand context*

---

#### 7.1 INTRODUCTION

##### *7.1.1 New Zealand Plio-Pleistocene stratigraphy*

New Zealand has an abundance of Plio-Pleistocene strata that have resulted from its unique geography and geology (Pillans, 1991; Newnham et al., 1999a). The islands remote oceanic, mid-latitude location (34-47°S) in the South Pacific means that the landmass is sensitive to environmental changes (modern climates extend from sub-tropical to sub-alpine). Geological characteristics of New Zealand such as its active tectonism and volcanism, elevation supporting glaciers, extensive coastline and productive soil formation, ensure that these changes are recorded in a variety of deposits. As a result, comprehensive Quaternary (and older) sequences are found throughout the country containing volcanic deposits, marine sediments, alluvial and glacial deposits, paleosols and loess. Together these deposits provide excellent opportunities for correlation and dating and, as such, New Zealand sequences offer great potential for paleoenvironmental reconstructions.

##### *7.1.2 An integrated approach*

The current interest in (Quaternary) climate changes, their mechanisms and environmental responses has resulted in extensive research across many disciplines. Marine cores, with their long, continuous records of deposition, led the way in the 1970s, and continue to provide the global framework. However, on-land strata at key sites have become increasingly recognised for their ability to add to the paleo-environmental record. The future of this research seems certain to be in the successful multidisciplinary integration of ideas and approaches (Lowe, 1996; Newnham et al., 1999a). In particular, Pillans (1991) recommended full attention should be paid to attaining correlations of marine and terrestrial sequences, as well as direct correlations of diverse on-land sequences. In the vast and varied depositional environments of New Zealand, this is a particularly relevant endeavour.



Concomitant to the need for a multidisciplinary approach to Quaternary stratigraphy is the need to examine that stratigraphy on a variety of scales, from local to regional to global. Local correlation, such as has been demonstrated for the Kauroa Ash sequence, is the essential starting point. For the potential of that research to be fully realised it should be placed alongside sequences of similar age in a regional context (the New Zealand stratigraphic framework) and, finally, that regional correlation should ideally be placed in a global context.

## 7.2 METHODOLOGY

Correlation of terrestrial sequences can be a particular interpretive challenge. Terrestrial sequences are generally fragmentary and discontinuous, except in rare examples such as the Chinese loess sequences (e.g. Heller and Liu, 1982, 1984; Kukla, 1987; Lu et al., 1999), and hence correlations can be difficult. New Zealand has a significant advantage over many other locations, however, having widespread rhyolitic tephra layers that facilitate local, regional and New Zealand-wide correlations. Additionally, paleomagnetic data represent a globally synchronous signal and are increasingly available for stratigraphic sequences. Magnetostratigraphy is critical to any correlation effort and establishing the key paleomagnetic tie-points<sup>1</sup> is usually a good basis from which to start. From this basic framework further correlations can be established in the present and future to continually expand what is known of the regional stratigraphic record.

To this end, a composite Kauroa column has been constructed using elements from the three main sampling sites, Woodstock, Papakura Creek and Tiritirimatangi Peninsula. The main useful points of correlation are established and illustrated. Similarly, schematic columns are reproduced from other research, and the correlation between them is shown (locations of sections are shown in Figure 7.1).

In order to facilitate useful correlation between the sequences, a semi-chronostratigraphic ('time-plane') approach has been adopted (definitions as for Boggs, 1995). This aims to correlate isochronous units (units formed during the same span of

---

<sup>1</sup> In this case, the Gauss-Matuyama boundary (2.58 Ma), the Olduvai Subchron (1.94-1.76 Ma), the Jaramillo Subchron (1.07-0.99 Ma), and the Brunhes-Matuyama boundary (0.78 Ma) (Carter and Naish, 1998a).

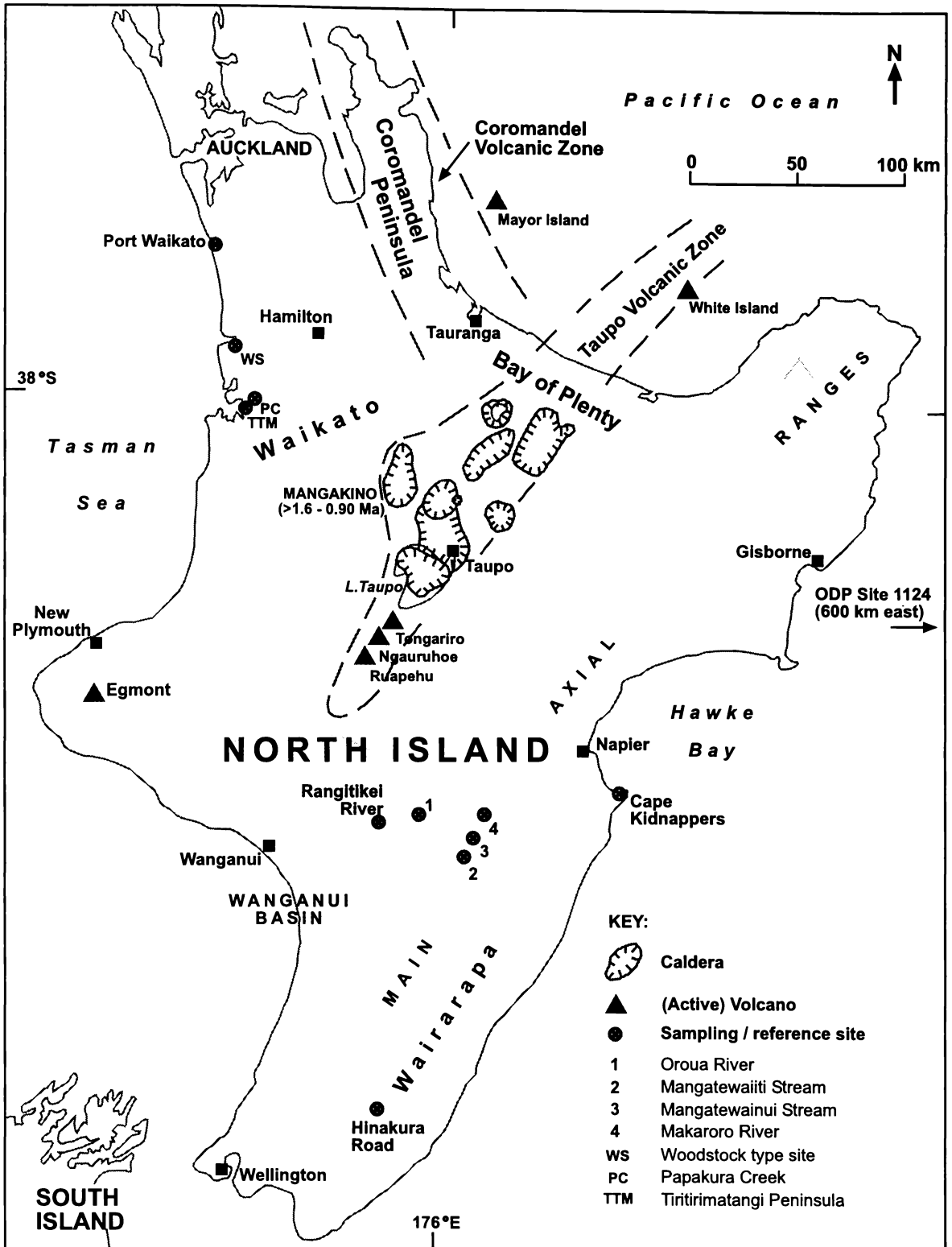


Figure 7.1 Location of regions and reference sites, North Island, New Zealand.

time) rather than attempt a purely litho- or tephrostratigraphic correlation of units/beds. This latter approach would yield relatively few correlations (especially where the depositional environment is distal and identifications are somewhat tentative) and thus add relatively little information to the New Zealand framework. Establishing 'planes' of similar age (towards a geochronologic classification) can be more useful in multidisciplinary studies where sequences may be of the same age but of a different stratotype. It is also potentially more relevant to paleoenvironmental reconstructions, where a chronostratigraphic correlation would allow examination of several diverse but contemporaneous units for maximum possible (paleoenvironmental) information input (Aubrey et al., 1999).

### 7.3 NEW ZEALAND SEQUENCES

#### 7.3.1 Composite Kauroa Ash sequence column

Figure 7.2 shows the composite column constructed for the Kauroa Ash sequence in this study. Comprised predominantly of the stratigraphy found at the type section at Woodstock, it also includes 'missing' units that are represented in other sections. Note that the major unknown in this sequence is the placement of the Tiritiri Ignimbrite – since there is only one exposure of the deposit it is impossible to be sure of its stratigraphic position between units K5 and K9. Indeed, a correlation to one of the units (K6-K8) cannot be ruled out. The composite column illustrates the main points of interest to a regional correlation: primary – paleomagnetism and tephrochronology; secondary – paleosols.

Previous chapters have established the probable inclusion of four significant paleomagnetic features in the Kauroa Ash sequence: the transition from Gauss Normal to Matuyama Reversed polarities (e.g. Okete Volcanics to K1), the Olduvai Subchron (K2b), the Jaramillo Subchron (K14b) and the transition from Matuyama Reversed to Brunhes Normal polarities (K15-H1). These are key reference points on which to make broad-scale correlations.

Some tephrochronological information is known:

- The source of K1 is unknown (though presumed to be TVZ rhyolitic volcanism), but has been dated at c. 2.25 Ma.

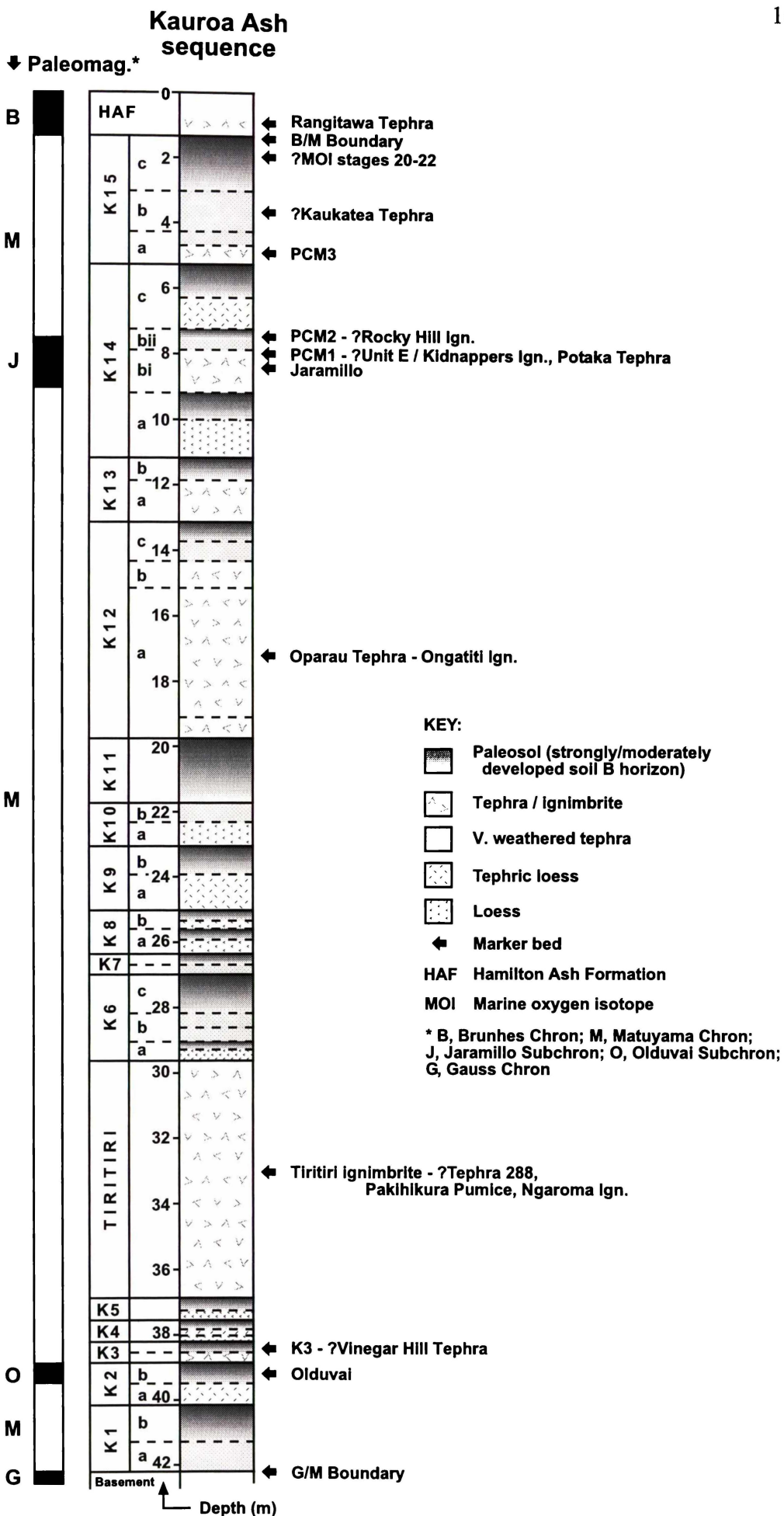


Figure 7.2 Composite stratigraphic column, Kauroa Ash sequence.

- K3 has been provisionally correlated with Vinegar Hill Tephra ( $1.75 \pm 0.13$  Ma).
- Tiritiri ignimbrite is a possible correlative of Tephra 288 of Shane et al. (1996a) or the Pakihikura Pumice (age range 1.60-1.64 Ma).
- K12a / Oparau Tephra has been correlated to the Ongatiti Ignimbrite ( $1.23 \pm 0.02$  Ma).
- K14bi (PCM1) is provisionally correlated with Unit E / Kidnappers Ignimbrite ( $1.01 \pm 0.06$  Ma; alternative correlatives, Potaka Tephra and Rocky Hill Ignimbrite, have identical ages).
- K15a is an unidentified distal ignimbrite (possible correlative of the Kaukatea Tephra,  $0.87 \pm 0.05$  Ma) with an inferred age range (c. 0.85-0.95 Ma).
- The top of the sequence is constrained by H1, the Rangitawa Tephra ( $0.35 \pm 0.02$  Ma).

Secondary lines of (proxy) evidence may also have use. The Kauroa sequence has several well-developed paleosols as well as at least four units of notable loessic material. Both of these facies types have considerable paleoenvironmental and paleoclimatic significance and may be useful in a correlation effort.

### 7.3.2 Wanganui Basin

The Wanganui Basin is a 200 x 200 km sedimentary basin in southwest North Island, situated in a back-arc position relative to the Australian-Pacific plate boundary. Plio-Pleistocene subsidence of the basin was broadly matched by sedimentation, and its subsequent smooth and rapid uplift during the late Quaternary has resulted in what is regarded as one of the most complete, undeformed shallow marine records in the world (Carter and Naish, 1998a). The basin contains up to 4000 m of Plio-Pleistocene sediments, with shallow marine strata dominating the sequence. Cyclical packages of unconformity-bound sequences of sediment form 47 superposed cyclothem representing glacio-eustatic sea-level fluctuations on the New Zealand continental shelf since oxygen isotope stage 100, c. 2.5 Ma<sup>2</sup> (e.g. Pillans, 1994; Pillans et al., 1994; Naish et al., 1997; Carter and Naish, 1998a, Abbott and Carter, 1999). As such, Wanganui strata are contemporaneous with the Kauroa Ash sequence and correlation could be possible.

---

<sup>2</sup> Or 58 cycles since oxygen isotope stage MG6 / 3.6 Ma (Naish et al., 1998)

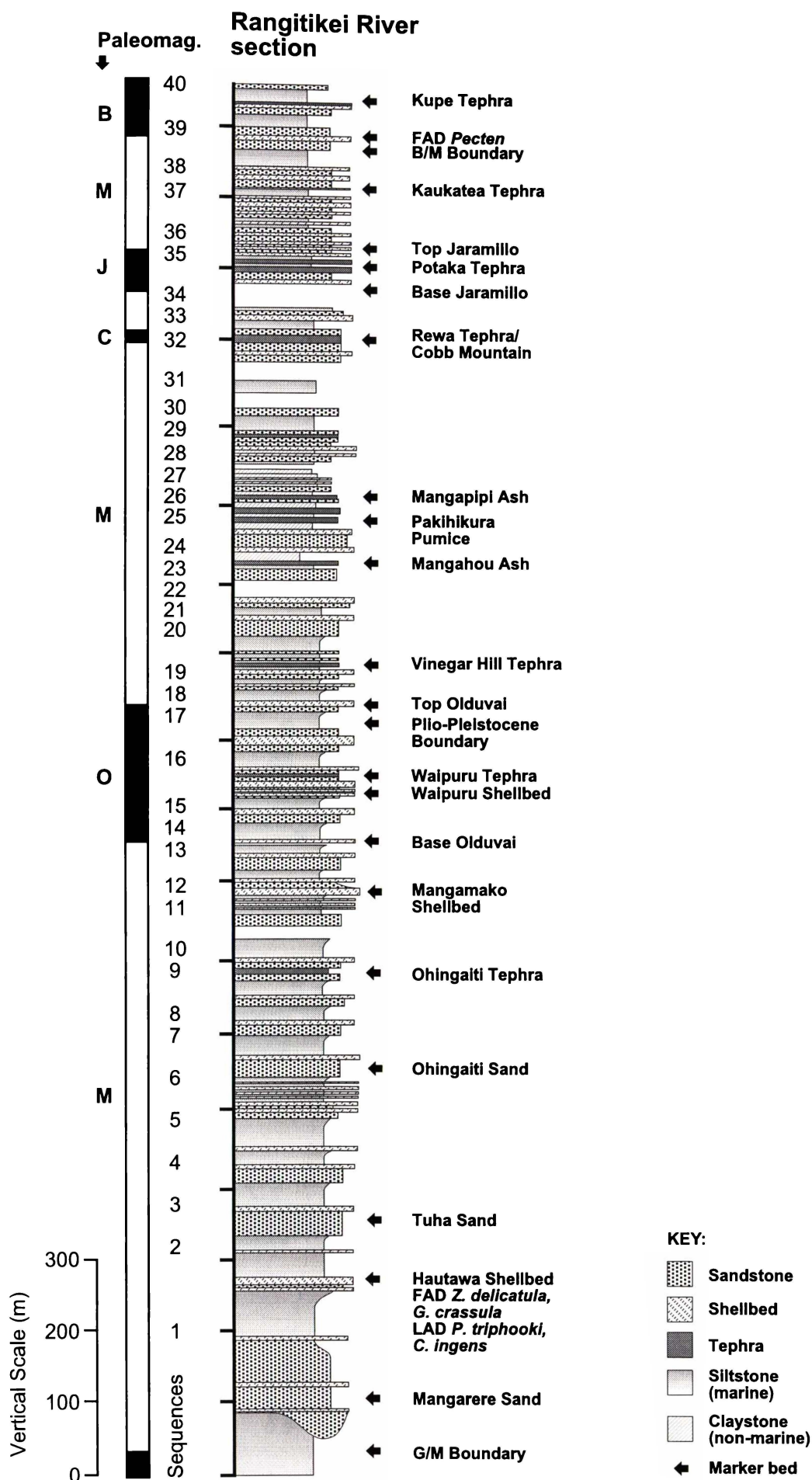
Wanganui sediments have been extensively dated by many different methods including biostratigraphy (Abbott, 1997; Carter and Naish, 1998b), tephrostratigraphy (Shane et al., 1995, 1996a,b; Naish et al., 1996, 1998), fission-track (Alloway et al., 1993), oxygen isotopes (Carter et al., 1996; Naish et al., 1996; Naish, 1998), magnetostratigraphy (Turner and Kamp, 1990; Pillans et al., 1994), and amino acid racemisation (Pillans, 1990; Bowen et al., 1998). Successful correlation to this reference section could thus potentially yield supplementary ages on Kauroa units (or any other bed or section). In addition, Wanganui sections have been astronomically calibrated providing a valuable link to marine records (Pillans, 1994; Naish et al., 1998).

Subduction along the Hikurangi margin during the Plio-Pleistocene has meant back-arc silicic volcanism has contributed substantial volumes of volcanogenic sediment to the Wanganui Basin (Naish et al., 1996). Discrete tephra horizons and volcanoclastic units are found throughout the basin, although the majority of silicic beds are of Pleistocene age (Alloway et al., 1993; Pillans et al., 1994; Naish et al., 1996; Shane et al., 1996a). Volcanoclastic sediment containing rhyolitic pumice, gravel and sand are derived mostly by fluvial transport from the central North Island volcanic plateau, although some beds are probably primary tephra-fall deposits resulting from the larger TVZ explosive eruptions. Fingerprinting of glass shards has revealed heterogenous and homogenous populations of glass shards indicative of this distinction (Pillans et al., 1994; Naish et al., 1996). Several major units have been described in detail and glass geochemistry and age data are available for numerous beds (e.g. Pillans et al., 1994; Shane, 1994; Naish et al., 1996; Shane et al., 1996a).

Figure 7.3 shows a redrawn version of the Rangitikei River section, one of the longest composite sections in the Wanganui<sup>3</sup> (after Naish et al., 1996; Carter and Naish, 1998a, 1999), while Figure 7.4 shows sections from the easternmost side of the Wanganui Basin / east coast region (after Shane et al., 1996a). Paleomagnetic reversals are clearly illustrated. In addition, the sections have many major tephra units including the Waipuru Tephra (1.87 Ma), Vinegar Hill Tephra (1.75 Ma), Mangahou Ash, Pakihikura Pumice (1.63 Ma), Mangapipi Ash (1.60 Ma), Rewa Tephra (1.29 Ma), Potaka Tephra (1.05 Ma) and Kaukatea Tephra (0.87 Ma), as well as several unnamed (numbered) tephra deposits. Many of these eruptive units have, in this study, been discussed as possible correlatives of Kauroa units.

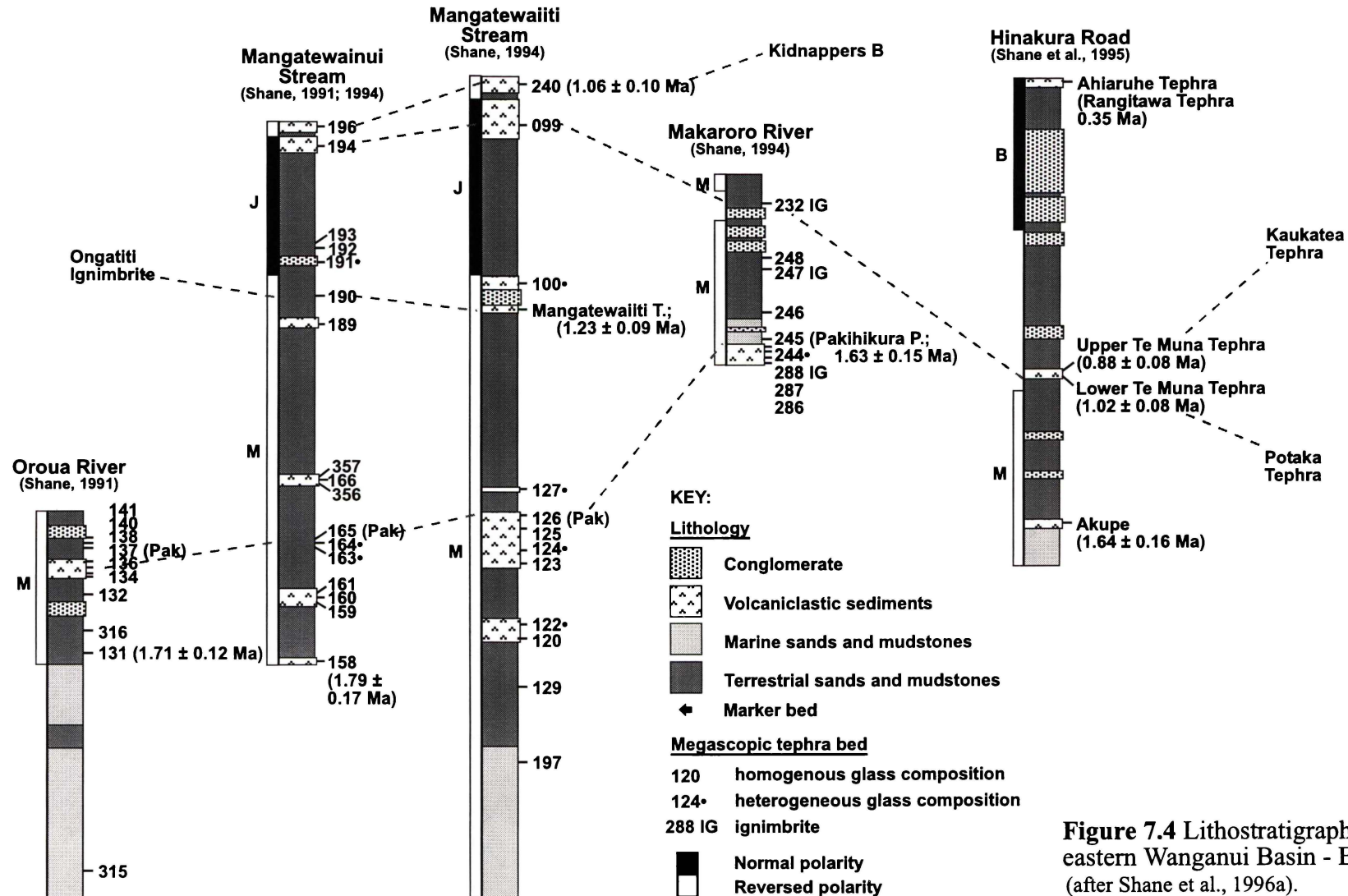
---

<sup>3</sup> Note: work is still ongoing on this section and certain beds are subject to revision.



**Figure 7.3** Lithostratigraphy of the Rangitikei River section, Wanganui Basin (after Naish et al., 1996; Carter and Naish, 1998a, 1999).

EASTERN WANGANUI - EAST COAST | WAIRARAPA



**Figure 7.4** Lithostratigraphy of sections from eastern Wanganui Basin - East Coast (after Shane et al., 1996a).



### 7.3.3 East Coast – Wairarapa

The east coast of the North Island, New Zealand (defined as that area east of the main axial ranges, Figure 7.1), occupies a fore-arc setting relative to the Australian-Pacific plate margin. The region is characterised by mountain belts and sedimentary basins of Miocene to Recent age, several of which are now exposed on land. One such basin in the southern part of this region, the Wairarapa, records a marine regression sequence spanning >4.9 Ma – 22 ka. The sequence is exposed mainly in two areas, the Mangaopari Stream area, and the Hinakura Road area (Figure 7.4; Shane et al., 1995). Both have been the subject of extensive work including the investigation of cyclothems (Beu and Edwards, 1984), sedimentary facies models (Woolfe, 1993) and tephrostratigraphy (Seward, 1979; Shane, 1990; Shane and Froggatt, 1991; Shane et al., 1995).

The Pliocene to Recent sequence found in the Wairarapa commonly contains at least 13 macroscopic tephra beds with homogenous glass populations (Shane et al., 1995, 1996a). At least two of these beds (Lower Te Muna Tephra,  $1.02 \pm 0.08$  Ma, and Upper Te Muna Tephra,  $0.88 \pm 0.08$  Ma) are contemporaneous with the Kauroa Ash sequence. The Lower Te Muna Tephra has been correlated to the Potaka Tephra (1.0 Ma; Shane, 1994), having identical mineralogy, major element and REE glass chemistry. The Upper Te Muna Tephra is correlated by the same means to the widespread Kaukatea Tephra found in the Wanganui and East Coast regions ( $0.87 \pm 0.05$  Ma; Shane et al., 1996a). The Upper and Lower Te Muna tephrae are separated by c. 1 m of loess. The beds together form part of the Pleistocene Te Muna Formation, thought to have been emplaced in fully terrestrial conditions during a depositional phase of basin infilling (Shane et al., 1995). Cyclic facies representing glacio-eustatic sea-level changes are superposed. A change in tectonic regime to one of mainly uplift occurred in the Late Pleistocene (Ahiaruhe Formation; Collen and Vella, 1984).

The upper, Late Pleistocene, part of the Wairarapa sequence also contains the 0.35 Ma Rangitawa Tephra.

### 7.3.4 East Coast – Hawke's Bay

Further north in the east coast region a thick sedimentary sequence of Middle

Pleistocene age is exposed on the cliffs between Black Reef and Clifton near Cape Kidnappers, Hawke's Bay. The sequence, known as the Kidnappers Group, comprises alternating fluvial and shallow-marine sediments with several interbedded tephra layers; it is interpreted as a record of Middle Pleistocene glacio-eustatic sea-level change (Kamp, 1990; Black, 1992; Shane et al., 1996b). No significant unconformities have been found in the Group<sup>4</sup> and as such the sequence is considered to be more or less complete (Black, 1992).

The Cape Kidnappers section (Figure 7.5; after Black, 1992; Shane, 1994; Shane et al., 1996b) contains at least 18 megascopic tephra beds, some are primary (pyroclastic fall or flow deposits) whereas some have been emplaced by fluvial processes. All are calc-alkaline rhyolitic tephtras with mineral assemblages similar to those of TVZ eruptives (Black, 1992). Shane et al. (1996b) grouped the tephra beds into nine eruptive events, named A-I. The oldest event, A, is a 0.5-1.5 m massive, nonwelded ignimbrite. It has an ITPFT age of  $0.99 \pm 0.09$  Ma and is correlated with the Potaka Tephra (Shane, 1994). Immediately overlying this unit is c. 6 m of cross-stratified, fluvial, volcaniclastic sediments, deposited in at least four phases. Each is separated by a paleosol and their episodic nature suggests that they are flood deposits (Shane, 1994). This four-phase unit is dated  $1.00 \pm 0.10$  Ma and has been correlated with similar units<sup>5</sup> in other east coast sections (Shane et al., 1996a). Two other Kidnappers units (E, F) have ITPFT dates, a third (D) has been Ar/Ar dated (Figure 7.5; Shane et al., 1996b). They are possible correlatives of the Kaukatea Tephra ( $0.87 \pm 0.05$  Ma). The youngest of the nine eruptive beds (I) is thought to occur at the onset of marine oxygen isotope (MOI) Stage 16, c. 0.65 Ma.

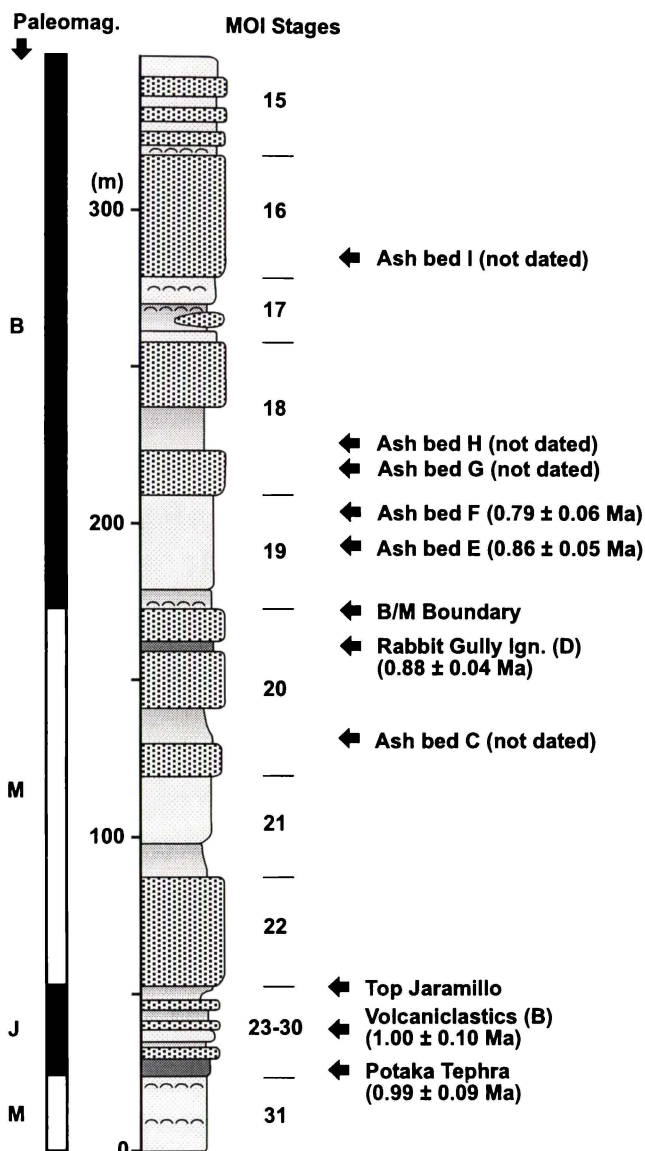
The normal polarity Jaramillo Subchron interpretation of Kidnappers A and B is consistent with their ages (0.99-1.00 Ma). However, the ages of E and F are at odds with the Brunhes Chron (<0.78 Ma) interpretation of the magnetostratigraphy (Black, 1992). It is possible, though, that the normal polarity sites have been affected by overprinting that has masked the original remanence (Shane et al., 1996b). Alternatively, if the paleomagnetism is correct (primary remanence is normal with

---

<sup>4</sup> Minor unconformities produced during subsequent transgressions are found. They are inferred to represent the absence of glacial sediments (Black, 1992).

<sup>5</sup> Bed 196 in the Mangatewainui Stream section and bed 240 in the Mangatewhaiiti Stream section (Shane et al., 1996b). The ITPFT date of  $1.06 \pm 0.10$  Ma of the latter is consistent with a date calculated for Unit B at Cape Kidnappers.

## Cape Kidnappers



**KEY:**

 Conglomerate

 Sandstone

 Mudstone

 Ignimbrite

 Shellbed

 Marker bed

**MOI** Marine oxygen isotope

**Figure 7.5** Lithostratigraphy of Cape Kidnappers, Hawke's Bay (after Black, 1992; Shane, 1994; Shane et al., 1996b).

no overprinting), the errors on the dates mean they are statistically reconcilable with a Brunhes age, but this would then preclude correlation with the Kaukatea Tephra that has a reversed polarity.

The dates and magnetostratigraphy acquired for this section suggest that it is contemporaneous with the upper parts of both the Rangitikei River sequence (Castlecliff section) and the Kauroa Ash sequence.

### 7.3.5 Kaihu Group – Port Waikato – Auckland

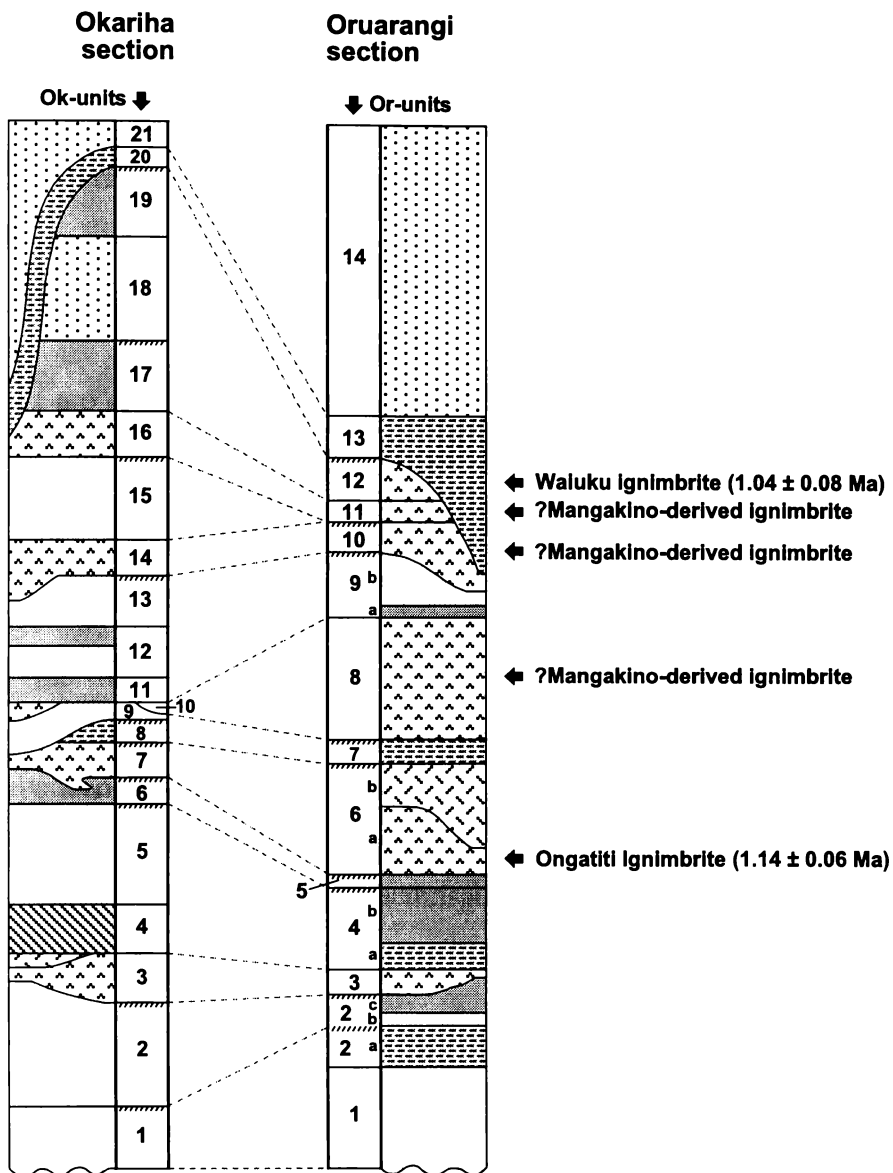
The Kaihu Group comprises all coastal and incidental volcanigenic facies of late Neogene age found along the western coastline of North and South Auckland regions<sup>6</sup> (Stokes and Nelson, 1991). The sequence generally consists of coastal sand deposits of shallow marine, beach and dune origin, with volcanigenic sediment interspersed throughout; several distal silicic ignimbrites are evident (Nelson et al., 1989; Stokes and Nelson, 1991). The area forms a modern back-arc basin that has been evolving from a previous, Miocene, back-arc system (Ballance, 1976). Varying sediment provenances (based on sand mineralogy) found in Kaihu Group members are likely to be the result of the active tectonism associated with this evolution (Stokes and Nelson, 1991).

Two correlated sections 5 km south of Port Waikato (Okariha and Oruarangi sections) contain at least five units that are inferred to have a primary volcanic rather than sedimentary origin (Nelson et al., 1989). The units, 0.1 to 3.0 m thick, enclosed within coastal alluvial plain sediments, are interpreted as distal ignimbrites because of their whitish colour, pumiceous nature and ash texture (Nelson et al., 1989). Major element glass chemistry shows homogenous populations of grains suggesting single-event, mass-emplaced, pyroclastic deposits (B.V. Alloway, unpublished data).

Figure 7.6 illustrates the main lithostratigraphy and inferred paleoenvironments of the Okariha and Oruarangi sections. Or-12 (Waiuku ignimbrite) has been ITPFT dated at  $1.04 \pm 0.08$  Ma (B.V. Alloway, unpublished data) and is a possible correlative of the Rocky Hill Ignimbrite<sup>7</sup> (B.V. Alloway, pers. comm., 2000), although this has yet to be unequivocally demonstrated. Or-6 is a primary ignimbrite unit that has been dated at

<sup>6</sup> As far south as Taharoa (Stokes et al., 1989).

<sup>7</sup> There is now evidence to suggest Or-12 correlates with the Kidnappers Ignimbrite rather than the Rocky Hill Ignimbrite (B.V. Alloway, pers comm., 2001).



**Figure 7.6** Lithostratigraphy of Okariha and Oruarangi sections, Port Waikato (after Nelson et al., 1989; B.V. Alloway, pers.comm., 2000).

$1.14 \pm 0.06$  Ma and correlates (on the basis of major element composition) with the Ongatiti Ignimbrite (B.V. Alloway, pers. comm., 2000). At least three eruptive events occur between the two identified units. Likely correlatives of these units include the widespread TVZ eruptions (probably from Mangakino volcano) outlined in Table 6.1 – Unit D, Ahuroa, Kidnappers Ignimbrite, Potaka Tephra and Kidnappers B. Four more Okariha – Oruarangi units have dates pending that may enable further correlation.

These sections are of Middle Pleistocene age and are thus contemporaneous with late members of the Kauroa Ash sequence, as well as with the deposits at Cape Kidnappers and upper Rangitikei River sections.

Future interest may lie in sections recently exposed by road excavations at numerous localities in the Auckland region. Preliminary work on two sections, Northwest Motorway and Mangere Motorway, has revealed an extensive sequence of rhyolitic tephra interbedded with organic carbonaceous sediments, possibly of Early to Mid-Quaternary age (Alloway and Newnham, 1995; Newnham et al., 1999b). Work in progress, including geochemical characterisation and ITPFT dating, will enable correlation to other sections, including possibly to some of the sites outlined in this chapter.

#### 7.4 CORRELATION OF NORTH ISLAND PLIO-PLEISTOCENE DEPOSITS

Figure 7.7 illustrates a preliminary correlation of the benchmark Plio-Pleistocene sequences identified above.

##### 7.4.1 *Magnetostratigraphy*

The key Plio-Pleistocene paleomagnetic intervals and boundaries seem to be well represented in North Island deposits. On the largest scale, the Gauss-Matuyama and Matuyama-Brunhes boundaries are readily identified and are critical ‘age-spikes’ where they occur. Only the Rangitikei River section and Kauroa Ash sections have lower contacts with Gauss-age deposits, but nearly all sections have clear contacts between Matuyama and Brunhes-age deposits.

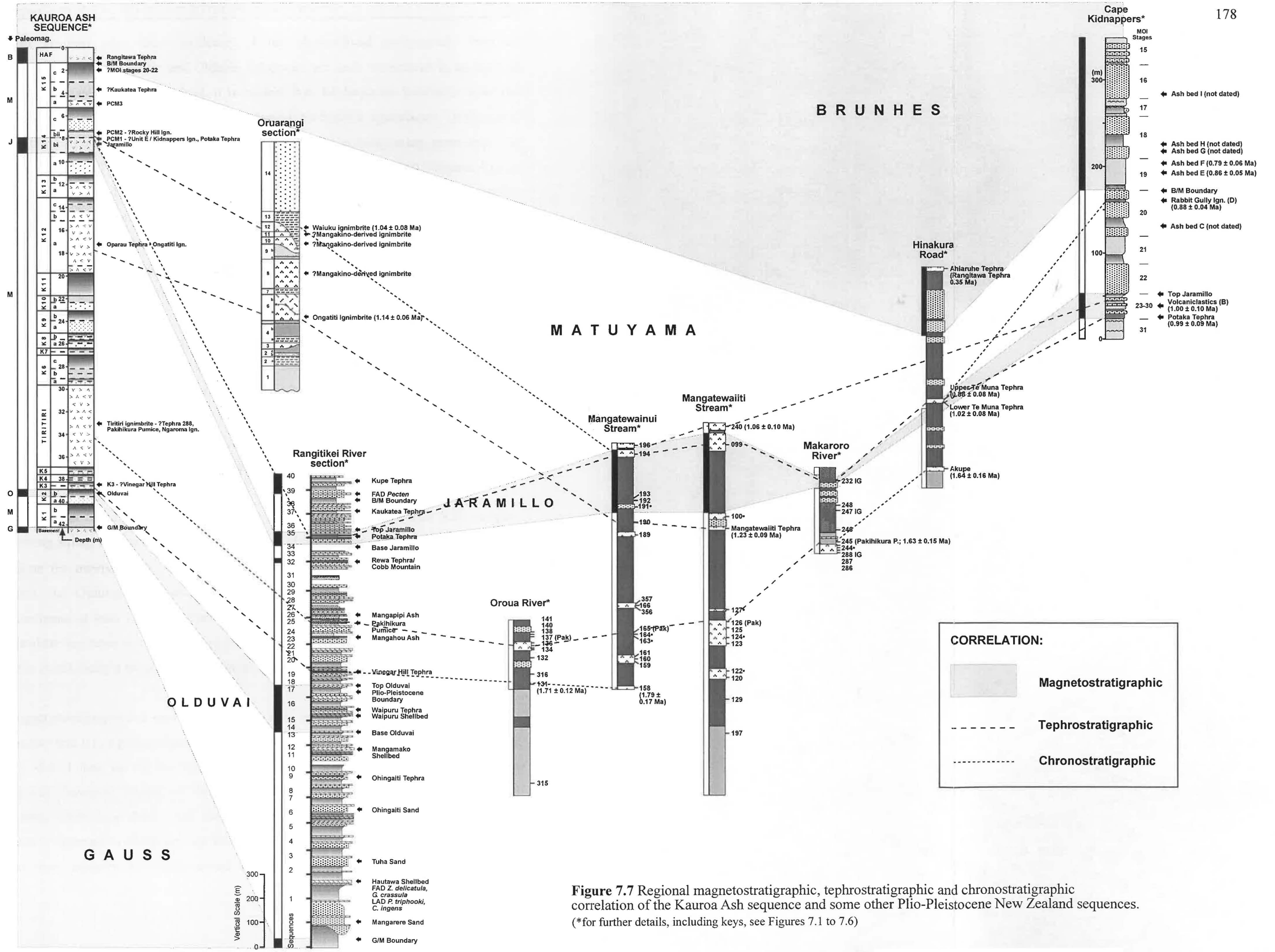


Figure 7.7 Regional magnetostratigraphic, tephrostratigraphic and chronostratigraphic correlation of the Kaurua Ash sequence and some other Plio-Pleistocene New Zealand sequences. (\*for further details, including keys, see Figures 7.1 to 7.6)

Most sections also show evidence of the shorter-lived geomagnetic intervals (subchrons). The Jaramillo and Olduvai Subchrons are well represented in sections of the appropriate age range. Indeed, it is evident that the Jaramillo Subchron 'saw' the eruption of at least three large-scale Mangakino-derived ignimbrites (Kidnappers Ignimbrite, Potaka Tephra, Rocky Hill Ignimbrite), and possibly many more since the reversal occurred during a period of intense activity in the Mangakino Volcanic Centre (e.g. Briggs et al., 1993; Houghton et al., 1995). The Kauroa Ash sequence contains the 1.5 m-thick ignimbrite, PCM1 (K14bi; probably Kidnappers Ignimbrite or Potaka Tephra), which marks the position of the Jaramillo Subchron. K14bii may also have been deposited in the Jaramillo Subchron because it has intermediate polarity. In the Wanganui region, the Jaramillo is represented by up to 50 m of sediment including shell beds, mudstone, sandstone and the Potaka Tephra. In the East Coast basins it is represented by the Potaka Tephra and approximately 20 m of volcanoclastic material (Ash bed B). The reversal would likely be found in the Port Waikato sections if magnetostratigraphy measurements were undertaken. The Oruarangi section has several members and beds between  $1.14 \pm 0.06$  and  $1.04 \pm 0.08$  Ma that could represent the Subchron; Waiuku ignimbrite has been provisionally correlated to Rocky Hill Ignimbrite, which has normal (Jaramillo) polarity.

The Olduvai Subchron is identified in the Kauroa Ash sequence, with K2b samples showing strong normal polarity components. A zircon fission-track date of  $1.68 \pm 0.12$  Ma on the overlying bed, K3a, is consistent with this conclusion. In the Wanganui Basin, the Olduvai is represented by up to 200 m of sediment, including four cyclothem, at least 18 sedimentary beds and the Waipuru Tephra. It is not recognised elsewhere (sections shown in Figure 7.7) due to a lack of appropriately aged sections, but it seems likely it would be represented if accessible sections were available.

Magnetostratigraphy has served as the main tool in the correlation of these sequences. The fact that it is a global signal means it potentially can be represented in most sections and should thus be the basis on which to begin any correlation. Some caution is required, however. Studies of New Zealand Pleistocene sediments (e.g. Roberts and Pillans, 1993) have shown that their paleomagnetic remanences are often weak and multi-component in character, and thus difficult to resolve. This study, too, illustrated that many samples have pronounced secondary components. However, this can be



resolved with careful sampling and stepwise demagnetisation, and with multiple samples where necessary.

#### 7.4.2 *Tephrochronology*

The sequences correlated in Figure 7.7 illustrate that there has been a several-million-year-long history of North Island rhyolitic volcanism, that it has a high-event frequency, and that many of its eruptions have been widely dispersed. The sequences also reassert the importance of the distal zone as a recorder of volcanism – they show evidence of many more eruptions than are recorded in the proximal (central North Island) zone.

##### 7.4.2.1 Late Pliocene

The Kauroa Ash sequence contains deposits from at least two major eruptions of late Pliocene age, K1 and K2. Their weathered state has precluded definitive identification, but, it is known that K1 was deposited c. 2.25 Ma (and <2.6 Ma, >1.95 Ma on the basis of tephrochronology, reversed polarity), and that K2b was deposited or modified (pedogenesis) during the Olduvai, 1.95-1.79 Ma. The Wanganui Basin appears to record only two significant eruptions during this time, the Ohingaiti Tephra and the Waipuru Tephra. A third, the Mangamako Tephra, is reworked and dispersed within metres of marine sediment and is andesitic in composition. Eastern Wanganui and East Coast sections do not record any eruptives (or do not go back this far). These two sequences (Kauroa Ash, Wanganui Basin) thus suggest there were at least two Late Pliocene eruptions of significant enough magnitude to be preserved in distal locations. Their source is probably a centre in the Coromandel Volcanic Zone (later period of activity) or in the TVZ (early period of activity, possibly Mangakino Volcano)<sup>8</sup>.

##### 7.4.2.2 Early Pleistocene

In contrast to the late Pliocene, the Early Pleistocene, seems to have been a period of particularly intense volcanism. Vinegar Hill Tephra (in both the Kauroa Ash and Wanganui sequences) represents the onset of this period, and there is evidence of numerous eruptions between the Olduvai and Jaramillo subchrons, a period of c. 0.7 Ma

---

<sup>8</sup> Tephrae in the Wanganui Basin have broadly similar rhyolitic compositions, comparable to later TVZ eruptives (Naish et al., 1996).

duration. The Kauroa Ash sequence may contain more than ten tephras (beds K3a – K14a) during this time, though most beds are too weathered to be certain that there are ten or that all are primary tephras – many beds may be composite (multisequal). The Rangitikei River section records at least seven tephras, while other eastern Wanganui / East Coast sections (Mangatewainui Stream, Mangatewaiiti Stream) record up to twelve tephras in any one sequence. All these beds have the potential to correlate to each other though no definitive correlations have been established and there is a possibility they represent numerous different eruptions. Tephras erupted during this time are likely to be the product of early TVZ volcanism, probably from the Mangakino Volcanic Centre. A late Coromandel Volcanic Zone source is also a possibility (Lowe et al., in press).

#### 7.4.2.3 Mid Pleistocene

Three eruptions have already been documented within the Jaramillo Subchron. In addition, several eruptions (thought to be Mangakino sourced) also occurred immediately after the Jaramillo. Proximal evidence (e.g. Briggs et al., 1993) suggests that Kaahu, Marshall and Kaukatea eruptions occurred within c. 0.2 Ma of the end of the Jaramillo (the deposits are of reversed polarity). Wanganui and East Coast sections record more eruptions in and around this time, including Kidnappers B to ?H. Two of the thicker Kauroa Ash members, K14 and K15, were deposited during this time (1.0 Ma and <0.78 Ma) and may represent multiple eruptions themselves. Two of three beds for which major element chemistry was attainable (K14ci, K15a) had homogenous glass populations, and it is possible that they are correlatives of the aforementioned eruptives<sup>9</sup>.

#### 7.4.2.4 Areal extent of eruptions

Any direct tephrostratigraphic correlation made between these sequences, in many cases separated by several hundred kilometres<sup>10</sup>, is immediately indicative of how widespread the unit is. Potaka Tephra, in particular, may be represented in all sequences, suggesting this represents a deposit from an extremely large magnitude eruption that covered essentially the entire North Island and beyond. Other eruptions may have been of a

---

<sup>9</sup> They may also represent deposits from other Plinian eruptions that are unrecorded or poorly exposed near-source.

<sup>10</sup> Oruarangi to: Kawhia – 80 km, Rangitikei River – c. 280 km, Mangatewaiiti – c. 300 km, Cape Kidnappers – c. 330 km, Hinakura Road – c. 420 km. Rangitikei to Cape Kidnappers – c. 120 km.

similar scale: the Pakihikura Pumice appears to have extended over much of the southern North Island – if a correlation to the Tiritiri ignimbrite is established it would have been even more extensive; the Vinegar Hill Tephra seems to be present at least from Wanganui to the Waikato; and distal correlatives of the Ongatiti Ignimbrite are found at far greater distances from source (Kawhia Harbour and Port Waikato on the West Coast, Mangatewainui and Mangatewaiiti Streams east of the axial ranges) than previously known.

Given the revised extent of these deposits, it would not be surprising for them to be found at even greater distances from source in the future. The best chance for this will be the analysis of deep marine cores from around New Zealand. In particular, the recently-acquired ODP (Leg 181) Site 1124 core, 600 km to the east of the North Island, contains at least 140 tephra layers, up to 0.9 m in thickness, that date back to c. 11 Ma (Carter et al., 1999). The identification and dating of these layers will no doubt have far-reaching implications for redefining the history of North Island rhyolitic volcanism and the distribution of the products (Newnham et al., 1999a).

#### 7.4.3 Chronostratigraphy

Chronological information (numerical and relative dates) has enabled the correlation of several more co-eval deposits in these sequences. These correlations do not quite mark 'isochronous' strata so much as 'near-isochronous' strata, arbitrarily defined as within c. 0.05 Ma of each other to maintain some degree of contemporaneity. This has the useful effect of further packaging beds into chronostratigraphic units.

A notable example of this is the connection between the Kauroa ignimbrite unit PCM2/K14bi and the Potaka Tephra in the Wanganui Basin and elsewhere. Magnetostratigraphy, tephrostratigraphy and the major element composition of this unit suggest it to be one of Kidnappers Ignimbrite, Potaka Tephra or Rocky Hill Ignimbrite (Chapter 6). This lack of definitive identification would preclude any tephrostratigraphic correlation. However, since these three deposits are known to have been emplaced in relatively quick succession, a chronostratigraphic correlation to the Potaka Tephra is legitimate. This enables another correlation to the upper Rangitikei River section. Furthermore, the chronostratigraphic unit 'Potaka-B/M boundary' formed by it

provides a possible correlative for the tephras K15c and K15b – the Kaukatea Tephra ( $0.87 \pm 0.05$  Ma).

K14bii is similarly correlated to the Waiuku ignimbrite in the Oruarangi section. This unit has an identical age to the Kidnappers Ignimbrite and Potaka Tephra and is thought to be the Rocky Hill Ignimbrite, deposited shortly after the Potaka Tephra. A chronostratigraphic correlation here in no way precludes a future tephrostratigraphic correlation (between these two or other alternatives). Indeed, it highlights the correlation possibilities of the three unidentified distal ignimbrites in this sequence (Or-8, 10 and 11): essentially contemporaneous units include Potaka Tephra, Kidnappers Ignimbrite, Kidnappers B and Rewa Tephra.

Tiritiri ignimbrite also had a tentative identification, to either the identically-aged Pakihikura Pumice or Tephra 288 IG (Makaroro River section). A chronostratigraphic correlation to the Pakihikura Pumice here determines the age range ( $1.75 \pm 0.15$  to  $1.63 \pm 0.18$  Ma) and marine oxygen isotope (Stages 61-50<sup>11</sup>) setting for the loessic Kauroa Ash beds K4 and K5<sup>12</sup> – being bounded by the K3-Vinegar Hill Tephra correlation.

#### *7.4.4 Correlation of the Kauroa Ash sequence to the marine oxygen isotope record*

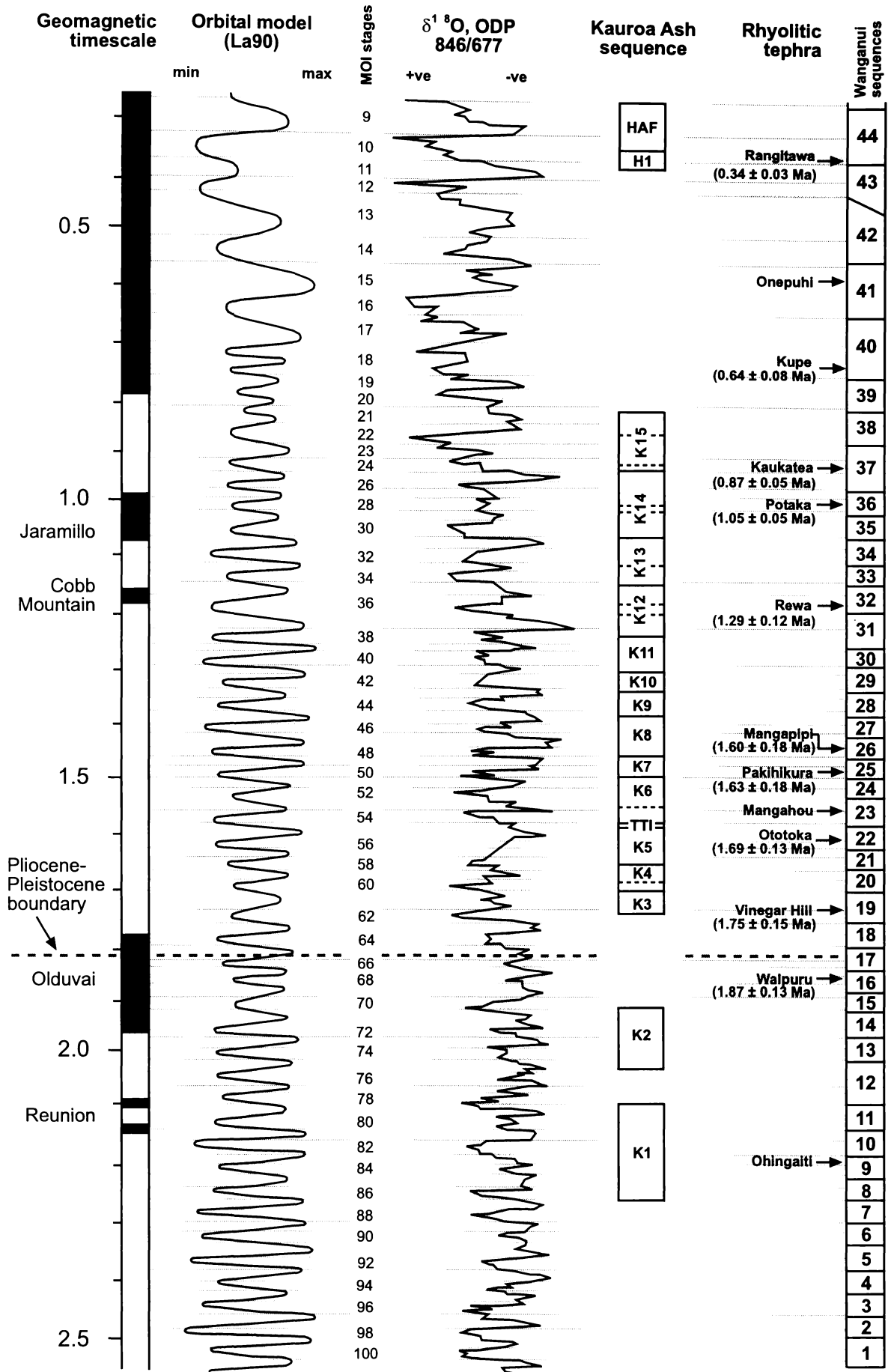
With the aid of information acquired in this study, it is possible to attempt a correlation between members of the Kauroa Ash sequence and the marine oxygen isotope record (Figure 7.8; after Lourens et al., 1996; Naish et al., 1998). Utilised heavily in this endeavour is the assumption that strongly developed paleosols in the Kauroa Ash sequence correlate to interglacials, and that loessic units correlate to glacials.

It is unlikely the Kauroa Ash sequence is the result of continuous deposition. Some major hiatuses in deposition are shown (e.g. between K1 and K2, K2 and K3, K3 and K4); others are likely but it is impossible to know where, and the result is the boundaries between members are arbitrary. If chronology is improved at some time in the future, specific location of boundaries will be revisable.

---

<sup>11</sup> There is some disparity in the age of the Pakihikura Pumice. It is dated at  $1.63 \pm 0.18$  Ma; however, it is found in Wanganui cyclothem 25/S5 – MOI Stage 50 – which is c. 1.50 Ma (Carter and Naish, 1998a).

<sup>12</sup> Possibly also K6, K7 and K8 since the exact stratigraphic position of the Tiritiri ignimbrite in this sequence is indefinite.



**Figure 7.8** Correlation of Kauroa Ash sequence to marine oxygen isotope stratigraphy (after Lourens et al., 1996; Naish et al., 1998).

From these correlations it is suggested the base of the Kauroa sequence falls in MOI stage 86, the top somewhere in stages 21-20. Oxygen isotope stages are very well dated (astronomically tuned) so that approximate ages now become available for each of the Kauroa beds (Table 7.1). It is emphasised that these correlations are provisional only.

**Table 7.1** Inferred ages and MOI stages of Kauroa Ash members.

Member	Inferred Age (Ma)	MOI Stage
K15	c. 0.94-0.80 Ma	24-21
K14	c. 1.07-0.94 Ma	30-25
K13	c. 1.15-1.07 Ma	35-31
K12	c. 1.23-1.15 Ma	38-35
K11	c. 1.30-1.23 Ma	41-38
K10	c. 1.34-1.30 Ma	42-41
K9	c. 1.38-1.34 Ma	44-43
K8	c. 1.45-1.38 Ma	48-45
K7	c. 1.50-1.45 Ma	50-49
K6	c. 1.60-1.50 Ma	54-51
K5	c. 1.65-1.60 Ma	58-55
K4	c. 1.70-1.65 Ma	60-58
K3	c. 1.75-1.70 Ma	61
K2	c. 2.05-1.90 Ma	75-71
K1	c. 2.25-2.10 Ma	86-79

## 7.5 CONCLUSIONS

It was important to place the Kauroa Ash sequence alongside sequences of similar age in order to put the Kauroa Ash sequence in its proper context, the New Zealand Plio-Pleistocene stratigraphic framework. The results have shown that the sequence can be successfully correlated to several other North Island sequences by means of magnetostratigraphy, tephrostratigraphy and chronostratigraphy, and that additional information can be gained from doing so. Conclusions from this exercise include:

- It is clear that magnetostratigraphy is a very useful way of ‘packaging’ deposits. The global polarity signature is a signal impressed on all sediments, transcendent of type and source, forming a skeletal framework from which to begin.
- All sequences illustrated in this study have significant volcanigenic content throughout their profiles; emplacement has been at relatively regular intervals throughout the Plio-Pleistocene.

- Despite the difficulty of attaining (and resulting lack of) direct correlations between distal and proximal eruptives, it seems evident that many events recorded in distal locations are not represented in the proximal zone.
- With the size and frequency of these deposits (eruptions), it is likely TVZ volcanism was even more prolific than previously thought.
- With the aid of paleosols and loess units, the Kauroa Ash sequence can be provisionally correlated to the marine oxygen isotope stratigraphy. This is particularly significant as it adds a considerable amount of (albeit tentative) 'new' age data. Furthermore, it places the Kauroa Ash sequence in a global framework.

## 8 CONCLUSIONS:

### *Paleoenvironments of the Kauroa Ash sequence*

---

#### 8.1 INTRODUCTION

This study of the Kauroa Ash sequence has attempted to attain four major goals: a multidisciplinary approach, the application of new analytical techniques, an improvement of chronological control, and the placement of the sequence in the New Zealand stratigraphic framework. Conclusions of this work are summarised here under three broad themes: paleovolcanology, paleopedology and paleoclimate.

#### 8.2 PALEOVOLCANOLOGY

The Kauroa Ash sequence encapsulates many of the difficulties associated with the identification, characterisation and correlation of distal tephra and ignimbrite deposits. Most deposits have suffered extensive erosion due in part to their thinness, in part because they are fragmental and non-welded, and because of other factors. Distribution is patchy and isolated as a result and long sequences of deposits are uncommon or rare. Similarly, these distal facies have been subject to intense weathering and alteration (and consequently have few primary minerals and high clay contents), and possibly reworking (some 'tephras' may be present as 'tephric-loess'). However, careful analysis of such weathered, distal deposits can produce some positive results, as demonstrated here. Methodologies employed in the analysis of tephra beds in this study are reviewed, followed by some of the main findings and the implications of these.

##### *8.2.1 Techniques for the analysis of weathered tephra deposits*

Field properties and observations are needed to establish the general stratigraphy of weathered deposits. Certain characteristics (crystal content, presence of pumice, lithics etc.) establish possible genetic origins in the less weathered beds, though these can often be absent or inconclusive in thinner and/or more intensely altered beds. Many of the Kauroa Ash sequence beds cannot be distinguished from one another solely on the basis of field properties. Colour is often the property that, with stratigraphic position, defines beds, and this is not a particularly reliable or persistent parameter. A facies-like



interpretation is possible, however.

Magnetic susceptibility parameters demonstrated that most primary tephra beds have low to no frequency-dependent components indicating a relative dearth of ultrafine pedogenic grains. Mass-specific susceptibility results were random as expected, reflecting the allochthonous input of lithogenic magnetic minerals.

Particle-size analysis showed tephra samples averaged the greatest proportion of clay-sized material, illustrating the low resistance of many volcanic minerals to weathering. This also suggests that many of the undifferentiated tephra beds have experienced considerable pedogenesis and that whereas some beds are paleosols (*sensu stricto*), most beds in the Kauroa Ash sequence have been subject to considerable chemical weathering or soil-forming processes.

Greatest success was gained with the use of a new electron microprobe-based method. Because the Kauroa Ash sequence is so extensively weathered, resistant minerals, including quartz, represent the largest part of the silt- and sand-sized mineralogy of the beds. Careful electron microprobe analyses of volcanic glass (melt) inclusions trapped within quartz grains demonstrated a critically important way of circumventing the problems of correlating weathered tephra beds: geochemical fingerprints can be obtained on such inclusions in the same manner as those obtained from glass shards. This facilitated the comparison of major element compositions of many Kauroa Ash tephra deposits to those of known and dated proximal deposits, as well as with compositions of distal correlatives.

The measurement of paleomagnetism to derive ages from the geomagnetic polarity timescale was also a successful method, even on such strongly weathered deposits (see below). Zircon-fission track dating, undertaken on relatively few beds, also provided new chronological data on the Kauroa Ash sequence.

### *8.2.2 Correlations to dated deposits*

A much-improved chronology for the Kauroa Ash sequence was established in this study through a combination of fission-track dates, tephrochronologic correlations and, perhaps most importantly, paleomagnetism. This last technique added four crucial ages

to the sequence, equivalent to the Matuyama-Brunhes boundary (0.78 Ma; K15-H1 boundary), the Jaramillo Subchron (1.07-0.99 Ma; K14b), the Olduvai Subchron (1.95-1.79 Ma; K2b), and the Gauss-Matuyama boundary (2.6 Ma; Okete Volcanics-K1 boundary). Together, these age 'spikes' enabled further tephrochronologic correlations to be made.

A number of correlations of Kauroa Ash members to dated eruptives have been established. It is evident the Kauroa Ash sequence contains deposits correlated provisionally with at least seven major TVZ eruptions, including: (1) K3a, Vinegar Hill Tephra (c. 1.75 Ma); (2) Tiritiri ignimbrite, Tephra 288 (or Pakihikura Pumice, Ngaroma Ignimbrite; c. 1.6 Ma); (3) Oparau Tephra/K12a, Ongatiti Ignimbrite (1.23 Ma); (4) K14bi/PCM1, Kidnappers Ignimbrite (or Potaka Tephra; c. 1.0 Ma); (5) K14bii/PCM2, Rocky Hill Ignimbrite (c. 1.0 Ma); (6) K15a/PCM3, the deposit from an unidentified ignimbrite-producing eruption (c. 0.92 Ma); and (7) K15b, ?Kaukatea Tephra (c. 0.87 Ma). The identification of Kauroa Ash members as distal correlatives of these established units in many cases expands the known extent of the deposit and, for the first time, answers in part the question as to the origin of the Kauroa Ash sequence beds.

### *8.2.3 Current known extent of the Ongatiti Ignimbrite*

This study has established two distal facies of the c. 1.23 Ma Ongatiti Ignimbrite: a 2-5 m-thick weathered ignimbrite, known as the Oparau Tephra, and found primarily in the Kawhia Harbour region; and the more common <1.0 m-thick, extremely weathered (>90% clay) K12a unit, possibly a veneer facies, found extensively in western central North Island, but especially in the Raglan district. Two other distal correlatives are noted: Or-6, an ignimbrite at Port Waikato, South Auckland region (B.V. Alloway, pers. comm., 2000); and Mangatewhaiti Tephra, a 4-m-thick tephra in the eastern Wanganui Basin-east coast region (Shane et al., 1996a). The locations of these correlatives are some tens of kilometres or more beyond the known extent, according to Briggs et al. (1993) maps of the Ongatiti Ignimbrite (Figure 8.1). The correlations in this study greatly expand the known areal extent of the distal portions of the Ongatiti Ignimbrite, and a new estimate of distribution is shown in Figure 8.2. The boundary in Figure 8.2 represents a minimum extent, encompassing only known pyroclastic flow deposits; possible co-eval fall deposits (or 'syn-ignimbrite' fall deposits) are currently unknown.

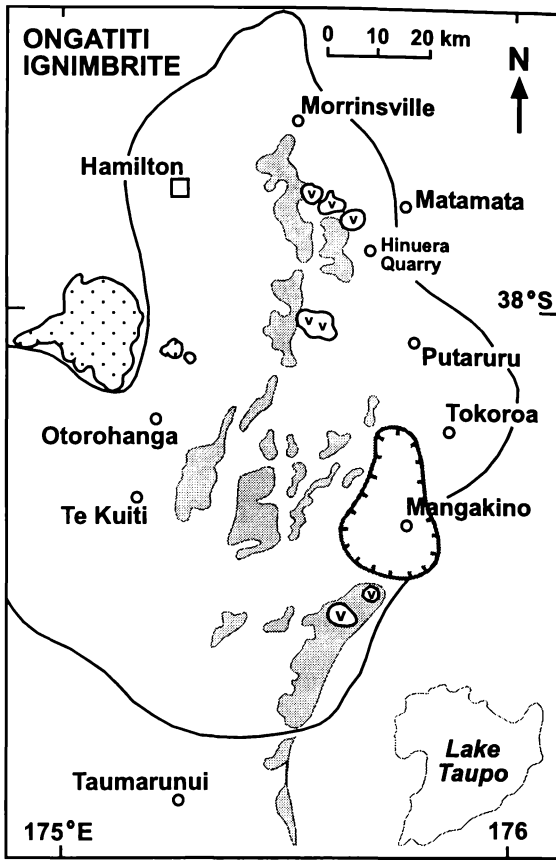


Figure 8.1 (left) Distribution of the Ongatiti Ignimbrite (after Briggs et al., 1993).

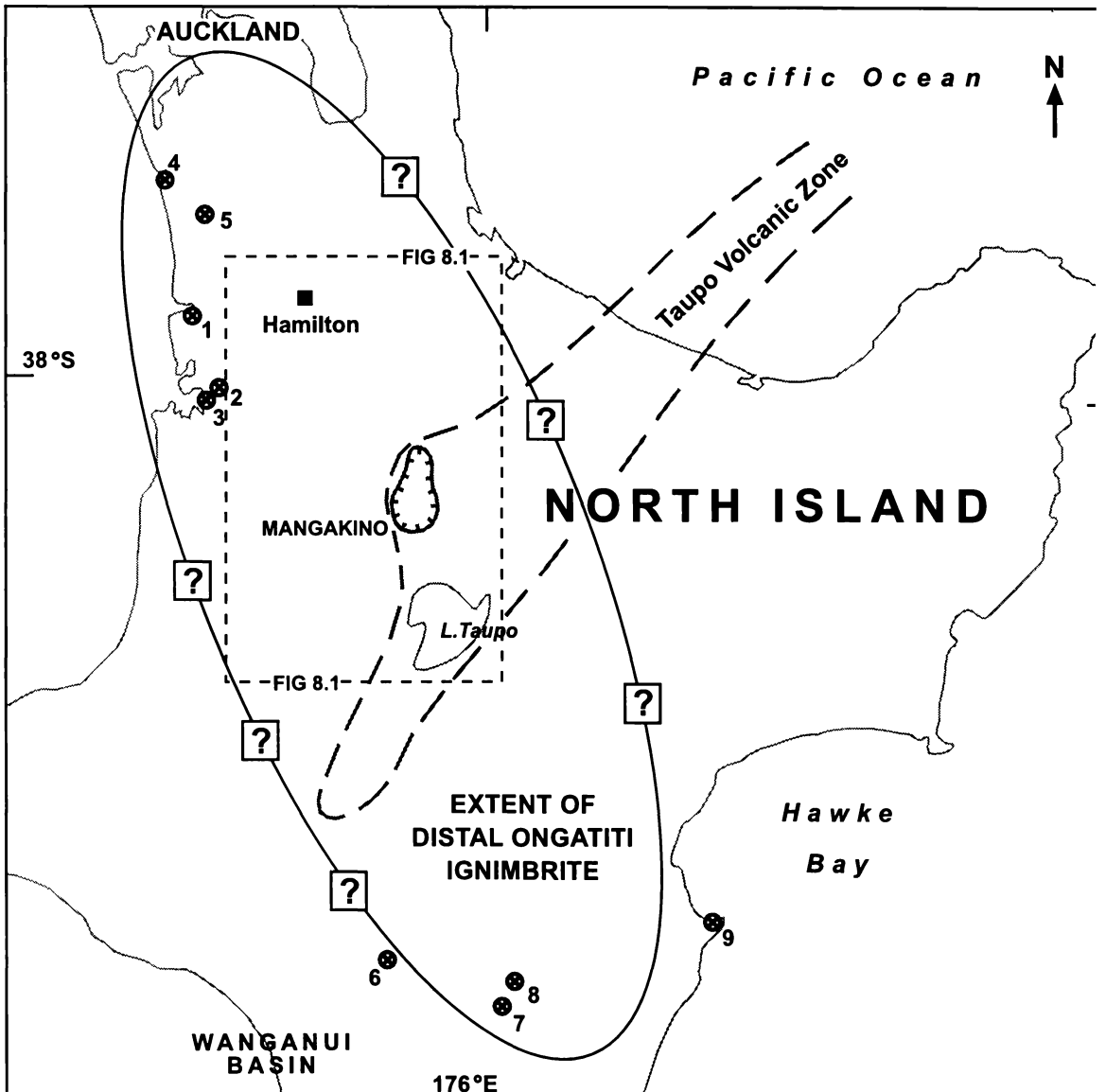
KEY:

- Basaltic volcanics
- Andesitic volcanics
- Greywacke basement

Figure 8.2 (below) Known extent of distal correlatives of the Ongatiti Ignimbrite.

KEY:

- Sampling / reference site
- 1 Woodstock
- 2 Papakura Creek
- 3 Tiritirimatangi Peninsula
- 4 Port Walkato
- 5 Foxs Centre
- 6 Rangitikei River
- 7 Mangatewai Stream
- 8 Mangatewai Stream
- 9 Cape Kidnappers



It should be noted that deposits on the margin of this extent (especially on the west coast) are sometimes up to 5 m in thickness, implying that the distal portion of the ignimbrite sheet may have extended much further.

The volume and distribution of this deposit suggests that the eruption that generated it was a particularly violent event, perhaps analogous in scale to the eruptions that produced, for example, the well-documented Kidnappers Ignimbrite (Wilson et al., 1995a), Potaka Tephra (Shane, 1994) or Kawakawa Tephra (Wilson, 1991, in press; Carter et al., 1995). These studies reported estimated volumes for these eruptives in the range of 400-1000 km<sup>3</sup>. It is feasible the Ongatiti Ignimbrite had a similar volume. It is a low aspect ratio<sup>1</sup> ignimbrite suggesting high initial velocity, continued high mobility (maintained fluidity) and substantial bulk volume to keep travelling and depositing material for >150 km.

#### *8.2.4 Volcanic hazards in the western central North Island*

The extent of the Ongatiti Ignimbrite and other widely dispersed tephra deposits (Kauroa Ash members) in the western central North Island regions should serve as a reminder of the potential magnitude of the volcanic hazard there. As outlined for the Auckland region (Alloway and Newnham, 1995; Newnham et al., 1999b), a substantial volcanic threat to west coast regions of the North Island lies with the more distant silicic centres of the TVZ, in particular, the currently 'active' centres of Okataina and Taupo. It is clear that a deposit such as the 7-m-thick Tiritiri ignimbrite, the 3-m thick Oparau Tephra, or even the 0.5-m-thick PCM3 (K15a) would cause enormous loss of life, devastation of property and vegetation, as well as a total collapse of infrastructure and services. The tephrostratigraphical record suggests that while eruptions of this magnitude may be a 'regular' occurrence on a geological timescale, they are extremely rare on an anthropogenic timescale. Nevertheless, every part of New Zealand is under the threat from TVZ volcanism.

#### *8.2.5 Onset of TVZ explosive volcanism*

The onset of explosive volcanism in the TVZ is generally thought to coincide with activity beginning in the Mangakino caldera at c. 1.6 Ma (Briggs et al., 1993; Houghton

---

<sup>1</sup> The ratio of average thickness of a deposit to the diameter of a circle that covers the same area.

et al., 1995; Wilson et al., 1995b). Recently, however, there is evidence that TVZ rhyolitic volcanism began earlier than this, possibly at c. 1.8 Ma (see below).

Krippner et al. (1998) reported there was likely to be a significant quantity of buried rhyolite lava in the volcanic pile of the Mangakino Volcanic Centre. They concluded that the presence of rhyolitic lava lithics in the earliest known Mangakino-derived ignimbrite, Ngaroma, suggested a period of rhyolitic precursory activity before explosive volcanism (i.e., >c. 1.6 Ma; Krippner et al., 1998).

Shane et al. (1996a) described several stratigraphic sequences in the eastern Wanganui Basin and noted a concentration of tephras (in terms of volume and frequency) in the interval from the Olduvai Subchron, 1.79 Ma, to 1.6 Ma. It was inferred from this that the initiation of the TVZ at around 1.8 Ma was associated with a major period of explosive rhyolitic volcanism.

The Kauroa Ash sequence supports these hypotheses with a minimum of three silicic eruptives known for the period >c. 1.6 Ma. Tiritiri ignimbrite is correlated to deposits aged c. 1.6 Ma, and stratigraphically underlying this unit are at least five Kauroa Ash members, K1-K5, three of which may contain primary pyroclastic material: K3 is provisionally correlated with the Vinegar Hill Tephra, aged at  $1.75 \pm 0.13$  Ma, and with major element composition consistent with a TVZ source (Naish et al., 1996); K2a is older than the Olduvai Subchron (i.e. aged >1.95 Ma); and K1a is co-eval with local Maungatawhiri basaltic eruptives (Okete Volcanics) and is aged at c. 2.25 Ma. K4 and K5 are composed of significant quantities of loess, but may also contain some tephric material. In particular, bed K4b is moderately crystal-rich, a characteristic that is not seen in loess beds. These members are thus considerably older than the 1.6 Ma age ascribed to the onset of TVZ volcanism. K1, in particular, potentially represents the oldest TVZ eruption known (c. 2.25 Ma), if it could be positively assigned a Mangakino (or other TVZ centre) source.

### 8.2.6 Conclusions

1. Most of the thicker primary tephra beds in the Kauroa Ash sequence (and other distal sequences) represent large-magnitude eruptive events on the basis of their thickness, distribution and distance from source (>100 km). It is likely,

therefore, that a considerably greater cumulative eruptive volume has been produced by the TVZ than previous estimates, based on proximal eruptives, have suggested (e.g. Briggs et al., 1993; Houghton et al., 1995).

2. The extent of TVZ eruptives, in particular the distal facies, suggests that the majority of the North Island is at risk from the hazard they present.
3. The preservation of these eruptives in distal locations has enabled a revision of the volcanic history of the TVZ, in particular the onset of explosive activity there. The numbers of Kauroa Ash members support the findings of Shane et al. (1996a) and Krippner et al. (1998), which suggested that TVZ explosive volcanism began considerably earlier than previously demonstrated. Evidence presented here suggests onset of activity may have been as early as c. 2.25 Ma.

### 8.3 PALEOPEDOLOGY

The stratigraphic and paleoenvironmental significance of paleosols has long been recognised because of the genetic linkage between their formation and evolution, and climate (Tonkin et al., 1974; Campbell, 1986; Eden and Furkert, 1988; Newnham et al., 1999a). Reliable identification of paleosols was thus an important objective in this study. The aim was to be able to use paleosol units as 'climatostratigraphic' entities, facilitating correlations to other sequences and possibly the marine oxygen isotope record.

Numerous (up to 18) paleosols, effectively strongly developed B horizons of various sorts, have been identified in the Kauroa Ash sequence. They are formed on tephra or loess beds; some are sufficiently developed that the parent material is indiscernible. All are inferred, by definition, to represent a persistent landsurface of the past, and possibly warm interglacial or interstadial conditions.

#### *8.3.1 Characterisation of Kauroa Ash sequence paleosols*

Paleosols have been characterised in this study by a combination of field properties, magnetic susceptibility measurements, and particle-size analysis. Observation of physical characteristics is still, perhaps, the strongest evidence of buried paleosols.

Kauroa Ash sequence paleosols are typically dark brown to dark reddish brown, very firm in consistence, have strong blocky or prismatic structures, show evidence of root traces or organism impressions, and some gleyisation (reductimorphic) features, including 'rusty' mottles and manganese concretions or nodules (redox segregations). As such, most paleosols are interpreted to be Bt or Bg horizons using Clayden and Hewitt (1994) nomenclature. All features are seen in the modern soil, though some (e.g. K1 or K11) have a more strongly developed pedality; others (e.g. K9b or K12c) are less developed.

Magnetic susceptibility measurements provided a valuable addition to the field observations. One parameter, mass-specific susceptibility, did not always conform to the established model of susceptibility enhancement in paleosols. However, frequency-dependent susceptibility and CBD-modified susceptibility were found to be reliable diagnostic features, exactly picking out field-defined paleosols by means of their enhanced ultrafine iron oxide content, a pedogenic rather than lithogenic feature.

Particle-size analysis showed paleosols to have a higher percentage of clay sized particles than loess samples, though (weathered) tephra samples had a similarly high proportion. Parameters such as sand, silt and clay content or weighted mean particle size, because of the high degree of weathering for the entire sequence, were not good methods of correlation for this sequence, though they did illustrate some relative differences between facies.

### *8.3.2 Interpretation of paleosols*

Interpretation of paleoenvironmental significance of paleosols typically rests on the principle of inferring past conditions from the observed relationships between present-day soils and environments. However, a difficulty in this study (and others) has been that it is rarely possible to separate the influences of numerous environment-related variables (e.g. climate, vegetation, drainage) from those of other soil-forming factors (e.g. parent material, time) where soil units are so weathered (perhaps even if they were not). This illustrates the problem of equifinality, namely that many different processes can lead to the production of similar forms. The physical characteristics of the paleosols of the Kauroa Ash sequence are generally similar (and resemble modern soils on weathered tephra beds such as Hamilton Ash). However, magnetic susceptibility

measurements suggest that many of them are in some way different (high-frequency-dependent susceptibility but very high or very low mass-specific susceptibility), implying that they have evolved through a variety of genetic pathways.

Having determined the dominant influence that volcanism, through tephra deposition, has had on this sequence, it would seem unlikely that the succession of paleosols of the Kauroa Ash sequence would correlate to the Chinese loess-paleosol record which has developed under the dominant influence of climate change through glacial-interglacial cycles. However, studies on the weathering of tephra sequences in different settings in New Zealand have shown that environmental factors, especially temperature and rainfall, together with tephra composition, may govern the types and rates of clay formation in some circumstances (e.g. Stevens and Vucetich, 1985; Hodder et al., 1990; Lowe and Percival, 1993; Lowe, 1986, 1995).

Shepherd (1994) analysed the clay mineralogy of the Kauroa Ash beds and found that halloysite dominated the beds, with a lesser proportion, on average, in paleosols (c. 70%) than in other beds (c. 80%). Remaining allophane in the beds was primarily the Al-rich type, though a remnant amount of Si-rich allophane was found in beds K4a and K8bi (Briggs et al., 1994a), in this study designated loess beds. These results suggest that, in accordance with the Si-leaching model, formation of halloysite and Si-rich allophane dominated in glacials (cold/dry conditions) when less leaching resulted in more silica in solution (Singleton et al., 1989; Parfitt, 1990); a greater proportion of Al-rich allophane was formed in interglacials via strong leaching (loss) of silica (Parfitt and Kimble, 1989). A complication to this model occurs if drainage were restricted (e.g. because of an impeded layer, or the presence of a very firm paleosol, etc.; Lowe, 1986). More halloysite (or Si-rich allophane) would tend to form because of the reduced leaching of silica in such a situation (Lowe and Percival, 1993). Beds of halloysite nodules (some >10 cm in diameter) found at intervals in the Kauroa Ash sequence demonstrate this accumulation of 'silica' has occurred, and the clay mineralogy of these deposits may therefore be largely unrelated to climatic controls. Such a situation was described by Stevens and Vucetich (1985) for some weathered tephra beds in the Te Kuiti area.

Kauroa Ash beds have relatively uniform and minor amounts of ferrihydrite (0.1-1%; there is no trend for paleosols/non-paleosols; Briggs et al., 1994a). Crystalline Fe oxides



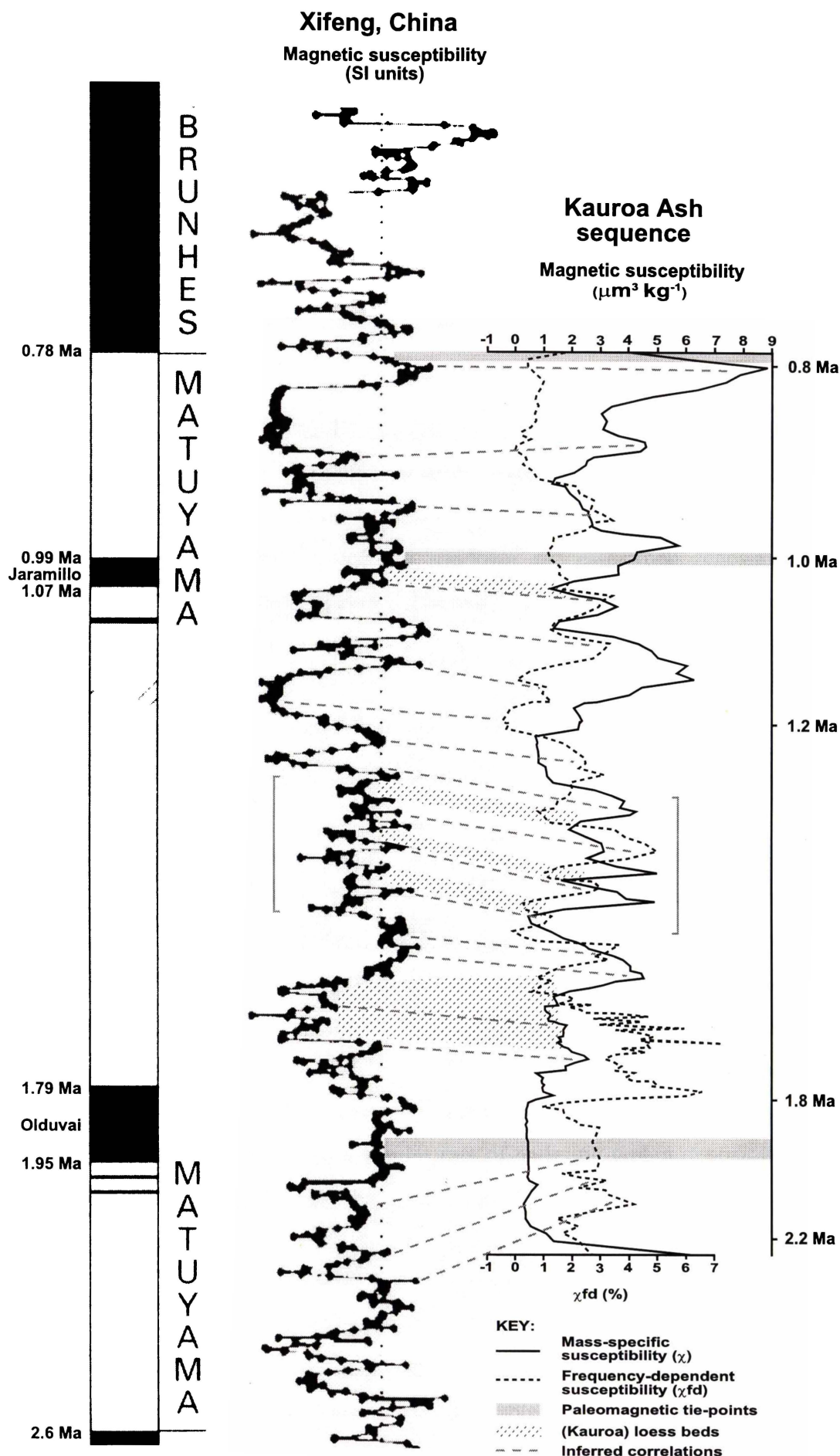
(e.g. goethite, hematite) have slightly higher proportions in paleosols than other beds, suggesting increased production by pedogenesis in interglacials. This finding is supported by post-CBD-treatment magnetic susceptibility measurements (cf. Chapter 3) that showed a significantly greater proportion of iron oxides had been removed from paleosol beds than from other beds.

### *8.3.3 Correlation to the Chinese loess-paleosol record*

The clay mineralogy of the Kauroa beds suggests to a large extent that the sequence has a paleoclimatic signature, even though the rate of tephra accumulation is not directly related to climate change (Newnham et al., 1999a). As a result, the Kauroa Ash sequence and the Chinese loess-paleosol records (Xifeng section) were compared using magnetic susceptibility parameters (Figure 8.3). The Kauroa Ash sequence susceptibility curve is slightly modified in that the thickest (>0.3 m) tephra beds, presumably emplaced instantaneously, have been reduced in thickness so that they represent a 'single' point in time. This modification was minimal, though, since most beds and members at this site (Woodstock type section) are typically thin and so the depth-time relationship is little affected.

The correlation between the sequences is facilitated by the presence of common magnetostratigraphic tie-points and tephrochronological ages in the Kauroa Ash sequence. The pattern of magnetic susceptibility for the Chinese deposits, taken to represent a glacial (low susceptibility) to interglacial (high susceptibility) paleoclimate signal, can be matched to a considerable extent to the pattern of mass-specific and frequency-dependent magnetic susceptibility for the Kauroa Ash deposits. Frequency-dependent susceptibility was used for many parts of the sequence because it was established in Chapter 3 that it was a more reliable indicator of paleosols than mass-specific susceptibility.

The apparent near synchrony in susceptibility for much of the sequence has implications for the history of deposition of the Kauroa Ash sequence. The question that arises is: why do the Kauroa susceptibility signals seemingly coincide with those of the Xifeng loess sequence when deposition in the former is largely tephric (i.e. tephra deposition is unrelated to climate) as opposed to loess (i.e. loess deposition is related to climate)?



**Figure 8.3** Correlation of magnetic susceptibility curves for the Xifeng loess-paleosol record, northern China (after Kukla, 1987; Lowe and Walker, 1997) and the Kauroa Ash sequence.

### 8.3.4 Model of pedogenic upbuilding

One possible explanation for this match is that part of the Kauroa Ash sequence (undifferentiated 'weathered tephra' beds and paleosol facies) may comprise in part tephric material that has accumulated in an incremental fashion at, for the timescales operative, a relatively 'uniform' rate. In this manner, the tephra flux would effectively behave in the same way as loess, and the landscape represents a continuously aggrading surface.

Almond and Tonkin (1999) and Lowe (in press) described a process of 'upbuilding pedogenesis' whereby the accumulation of material such as loess or tephra, and soil formation, occur contemporaneously, and soils are formed by a balance of upbuilding processes in addition to the conventional 'topdown' processes (pedogenesis acting on a preexisting body of sediment or rock). The distinguishing characteristic of upbuilding pedogenesis is that each increment of soil or other material below the A horizon has experienced processes characteristic of all horizons above it: the whole sequence essentially becomes a giant upbuilding pedon (Tonkin et al., 1998; Almond and Tonkin, 1999; Lowe, in press).

Modern-day analogues tend to support the application of this hypothesis to the Kauroa Ash sequence. It is evident that many of the tephra-derived soils in the western central North Island (e.g. Kainui and Tirau soils) are composite (multisequal) soils (Lowe, in press). Only at more proximal sites do thick tephra layers, emplaced instantaneously, give rise to new soils (e.g. Taupo soil). Waikato lake core records show that for the last 15 ka, tephtras (dominantly rhyolitic but with significant andesitic components) fell on the landscape once every 340 years on average (Lowe, 1988a, 1988b). In Taranaki, Alloway et al. (1995) calculated a similar rate of andesitic tephra deposition with one event per 330 years, based on at least 76 eruptive events from Taranaki in the last 28 ka. Thus, by extrapolation to a longer time interval, a distal (Kauroa Ash) sequence spanning c. 1.4 Ma (2.2 Ma minus 0.8 Ma) potentially represents as many as c. 4000 eruptive events from North Island volcanoes active in this period. If so, even halving the rate to take into account wind dispersal effects, fewer active volcanoes in the early Pleistocene, and so on, this amounts to a considerable (incremental) tephra flux.

Such upbuilding would be subject to three modifications in the case of the Kauroa Ash sequence:

1. The rate and intensity of pedogenesis would be dependent on climate: there would be increased pedogenesis in warmer (interglacial or interstadial) periods.
2. Colder (glacial or stadial) periods may see an increased (additional) influx of loess, resulting in faster upbuilding through a dilution effect, and less effective topdown pedogenesis.
3. Occasional deposition of thicker tephra material (e.g. K12a) would slow or stop upbuilding pedogenesis (retardant upbuilding) and topdown pedogenesis would temporarily take over within the thick deposit until incremental accumulation recommenced.

Pedogenesis (climate-related factors) would thus potentially have more of an impact on magnetic susceptibility than tephra input (parent material) for much of the time. The upbuilding-topdown switch may account for some of the variation seen in mass-specific susceptibility (type of magnetic mineral), while frequency-dependent susceptibility remains constant (size of magnetic minerals; concentration of ultrafine material in any period where rates of pedogenesis exceeded accumulation).

The extent of weathering in the Kauroa Ash sequence may also result in part from this process of incremental tephra accumulation and upbuilding pedogenesis. Particle-size analysis showed that most samples had an 11.25  $\phi$  peak as a common feature, suggesting most beds had undergone a common, probably pedogenic, process. Only the loess beds showed a reduction in this feature, which is consistent with less effective (though still active) pedogenesis acting through cold and cool climate periods.

Those beds identified as 'tephric-loess' beds would, in the sense of incremental tephra accumulation, represent some intermediate stage between 'mostly tephra' and 'mostly loess'. In reality, most of the sequence is probably a continuum of modified tephra, tephric-loess or loess, which ranges from weakly to moderately modified layers to intensely weathered paleosols and pedocomplexes, with occasional interspersed thicker, primary tephra deposits.

### 8.3.5 Conclusions

Paleosols are, in appropriate circumstances, of considerable value in Plio-Pleistocene research. In this study they have been shown to:

1. Represent important stratigraphic markers – the strongly developed, reddish-brown hues of, for example, K15, K14 or K11 paleosols helps to identify overlying units (H1/Rangitawa Tephra, PCM3 and K12/Oparau Tephra, respectively).
2. Provide a basis for correlation – some paleosols, or sequences of contiguous paleosols, have sufficiently diagnostic properties that enables their correlation on a local scale.
3. Have use as a relative dating tool – soil formation requires time for development; the direct link between soil formation and climate provided a means for tying many Kauroa Ash beds to marine oxygen isotope stratigraphy (Figure 7.8).
4. Provide paleoenvironmental information – strongly developed paleosols suggest interglacials of at least the magnitude and length of the Holocene; incremental accumulation of tephra may have resulted in effectively a continuous process of upbuilding pedogenesis interacting with ‘topdown’ pedogenesis.

## 8.4 PALEOCLIMATE

The Plio-Pleistocene period is characterised by extraordinary climate instability. Paleoclimatic records from the deep sea floor show that in the last 3 Ma more than 100 oscillations of warm and cold climate took place with a larger amplitude than any experienced during the Holocene (Kukla and Cílek, 1996). The Southern Alps, South Island, were a locus of Southern Hemisphere glaciation (Gage, 1985; Newnham et al., 1999a), though the highest points of the North Island may also have had minor glaciation (McArthur and Shepherd, 1990) and certainly central and southern North Island experienced severe climatic conditions (Pillans et al., 1993). The effects of some of these climate changes are now thought to be evident in the Kauroa Ash sequence.

#### 8.4.1 Plio-Pleistocene chronology of the Kauroa Ash sequence

The Kauroa Ash sequence ranges in age from c. 2.25 Ma to c. 0.8 Ma and is thus of Late Pliocene to Mid-Pleistocene age. Many of the members, K3-K11 especially, appear to have approximate durations of 30-50 ka<sup>2</sup> (correlation to marine oxygen isotope stratigraphy), suggesting that much of this sequence may conform to the regular c. 40 ka Milankovitch cyclicity. From K12 to K15, members span a greater duration and may reflect the dominance of the 100 ka Milankovitch cycle. This 'switch' in cycles at c. 1.2 Ma is evident in the oxygen isotope stratigraphy of ODP 846/677 in Figure 7.8. The pattern is similar to that described by Pisias and Moore (1981), and others (e.g. Kukla and Cílek, 1996; Williams et al., 1998), who subdivided the Quaternary as follows:

- Early Quaternary: 2.0-1.45 Ma (generally lower amplitudes of climate variability, with low amplitude at 41 ka).
- Middle Quaternary: 1.45-1.0 Ma (increasing amplitude of the 21 ka and 41 ka periods)
- Late Quaternary: 1.0-0 Ma (major increase in amplitude of climate variability near 100 ka and a lesser increase in variability at 41 ka)

The Kauroa Ash sequence is similarly divided:

- Late Pliocene: c. 2.25-1.7 Ma (K1 and K2 of uncertain duration)
- Early Pleistocene: c. 1.7-1.2 Ma (c. 40 ka cycles)
- Middle Pleistocene: c. 1.2-0.8 Ma (c. 100 ka cycles)

The correlation of Kauroa Ash members to Milankovitch cycles supports the hypothesis that (possible) incremental tephra accumulation has behaved like loess, and that this sequence effectively reflects large-scale climate changes (of interglacial-glacial proportions).

#### 8.4.2 Loess deposits

In many environments, a common manifestation of cold climate conditions is the production and deposition of loess, resulting (in the main) from increased aeolian and/or glacial erosion under reduced/less effective vegetative cover. Sequences with

---

<sup>2</sup> Longer members have at least two paleosols signifying two or more cycles.

intercalated loess have been described for Wanganui (Palmer and Pillans, 1996) and Mamaku Plateau (Kennedy, 1994; Newnham et al., 1999a), and elsewhere in the North Island, and loess is now recognised in the Kauroa Ash sequence. Up to seven periods of loess deposition may be present in the sequence. They are inferred to represent cold climate conditions when largely deforested environments prevailed over the North Island, lower sea levels meant increased exposure of the continental shelf, increased wind velocities maximised erosion, and enhanced freeze-thaw processes in the mountains resulted in the increased comminution of particles. In the context of the deposition of the Kauroa Ash sequence, the tephra flux was diluted with other material (and/or volcanic activity was at a minimum allowing loess rather than 'tephric-loess' to accumulate), and pedogenesis was at a greatly reduced rate.

#### *8.4.3 Identification and characterisation of Kauroa Ash sequence loess*

Loess deposits are identified in this study on the basis of field properties, magnetic susceptibility and particle-size analysis. They were seen to have field properties noticeably different from those of other beds, in particular colour (yellowish brown), consistence (softer and more friable than other beds), and structure (apedal fine-earthly to structureless). They generally lack most characteristics associated with paleosols (e.g. prismatic or blocky structures, root traces etc.) and with weathered tephras (e.g. visible silt- and sand-sized crystals, pumice clasts, etc.), typically having only some bright brown or orange mottles as notable features.

Magnetic susceptibility parameters for loess samples showed contradictory relationships: some loess beds (K14a, K10, K8bi and K8ai) had a moderately high mass-specific susceptibility combined with a low frequency-dependent susceptibility, while others (K4a, K5, K6a) had a low mass-specific susceptibility and a high frequency-dependent susceptibility. This apparent disparity evened out to a similar contribution of ultrafine pedogenic grains to the overall susceptibility signal, being only half as much as in paleosols. Pedogenesis may have occurred but at a much reduced rate compared with that of other beds/periods.

Particle-size analysis, obtained using high-resolution laser diffraction, illustrated some distinction between facies. Loess beds were demonstrated to have relatively less clay-sized ( $< 4 \mu\text{m}$ ) material (smaller 11.25  $\phi$  peak), and a broader 'coarse mode' centred on

7  $\phi$  (modes for samples of paleosols and tephra beds were centred on 6  $\phi$ ). Loess samples plotted in the 'silty clay' section of a soil texture classification diagram, whereas most other samples plotted as 'clay'.

#### 8.4.4 Oldest period of loess accumulation in New Zealand

Shane et al. (1995) described a loess deposit in the Wairarapa aged between 1.00 and 0.87 Ma (constrained by Lower and Upper Te Muna tephtras). It was suggested that the deposit represented the earliest period of loess deposition in New Zealand, with an antiquity nearly twice that of the previously 'oldest loess' in the Wanganui basin (c. 0.5 Ma; Pillans and Wright, 1990; Palmer and Pillans, 1996).

Loess deposits in the Kauroa Ash sequence are older than those in both of these locations. The youngest period of loess deposition at Woodstock is likely to be older than that in the Wairarapa, and the oldest is inferred to be as much as 1.70 Ma (Table 8.1). This means that the Kauroa Ash sequence, for now, has the oldest loess known in New Zealand (terrestrial realm).

**Table 8.1** Inferred ages of loess deposits in the Kauroa Ash sequence.

Loess bed	Inferred age	MOI stage
K14ai	c. 1.06 Ma	30
K10a	c. 1.32 Ma	42
K8bi	c. 1.40 Ma	46
K8ai	c. 1.44 Ma	48
K6ai	c. 1.57 Ma	54
K5a	c. 1.64-1.60 Ma	58-56
K4a	c. 1.70 Ma	60

Because loess accumulation is likely to have occurred in most cold periods, it seems possible that even older loess – up to c. 2.6 Ma when glacial ('Ice Age') conditions are thought to have begun – could be discovered, needing only a suitable environment for preservation.

#### 8.4.5 Conclusions

1. Cyclical changes in global climate are, to a large extent, evident in the Kauroa Ash sequence. Moderate to strongly developed paleosols are suggestive of a warm, wet climate, with extensive forest vegetation cover (interglacial



environment), whereas the presence of several units of loess point to deposition in a colder, drier climate with reduced vegetation cover (glacial or possibly periglacial environment).

2. Extrapolation of tie-points in the sequence to marine oxygen isotope stages has allowed approximate ages of members to be estimated. The period of time represented by members, in many cases, corresponds well to dominant Milankovitch periodicities.
3. The loess deposits in the Kauroa Ash sequence represent the oldest deposits known in New Zealand (terrestrial realm); the earliest period of deposition at the Woodstock site is inferred to be c. 1.7 Ma.

#### 8.5 STRATIGRAPHY, CHRONOLOGY, AND CORRELATION OF THE KAUROA ASH SEQUENCE

This study has made a number of stratigraphic and chronologic advances in what is known about the previously largely undifferentiated Plio-Pleistocene cover deposits of western central North Island, the Kauroa Ash sequence:

1. It has characterised the prevalent facies in the sequence;
2. It has established the occurrence of a number of widespread distal tephras, some of which have been identified and correlated to known and dated eruptives;
3. Other beds have been identified as composite, and are inferred to represent a record of paleoclimate;
4. Each member of the sequence has an inferred age that has been extrapolated from several magnetostratigraphic, tephrochronologic and radiometric tie-points;
5. In an analysis of its wider context, the sequence has been placed in regional and global stratigraphic frameworks with correlations to contemporaneous sequences in the North Island, and the marine oxygen isotope stratigraphy, respectively.

Traditional and novel methodologies have been employed to decipher these extremely weathered clay-rich deposits:

1. Field properties, magnetic susceptibility and laser-diffraction based particle-size analysis characterised the lithostratigraphy;
2. Tephrochronology, fission-track dating and paleomagnetism established a detailed chronology;
3. A new electron microprobe technique analysing glass inclusions in quartz grains was successful in providing major element compositions for geochemical fingerprinting and tephra correlation.

As a result, we now have a better idea of what exactly the Kauroa Ash sequence represents, its depositional history and paleoenvironments. The K-beds were previously termed the 'Kauroa Ash Formation', but use of the term 'formation' was essentially as a geographical 'hold-all' name, not strictly based on a geological formation. That term and level of ranking is now found to be inappropriate and should be abandoned. 'Formation' is defined by Boggs (1995) as a lithologically distinct stratigraphic unit; Froggatt and Lowe (1990) further defined a 'tephra formation' as that containing all the primary pyroclastic products of one eruptive episode. The K-beds clearly encompass numerous eruptive episodes, including defined formations, as well as other additions (loess) and variations (paleosols), and, within a paleoenvironmental context especially, the term 'sequence', denoting packages of strata, is now considered more appropriate.

## REFERENCES

- Abbott, S.T. (1997) Foraminiferal paleobathymetry and mid-cycle architecture of mid-Pleistocene depositional sequences, Wanganui Basin, New Zealand. *Palaios* 12, 267-281.
- Abbott, S.T. and Carter, R.M. (1999) Stratigraphy of the Castlecliffian type section: 10 mid-Pleistocene sequences from the Wanganui coast, New Zealand. *New Zealand Journal of Geology and Geophysics* 42, 911-111.
- Adams, C.J., Graham, I.J., Seward, D. and Skinner, D.N.B. (1994) Geochronological and geochemical evolution of late Cenozoic volcanism in the Coromandel Peninsula, New Zealand. *New Zealand Journal of Geology and Geophysics* 37, 359-379.
- Alloway, B.V. and Newnham, R. (1995) A preliminary assessment of the threat posed by distal silicic volcanism based on the Middle-Late Quaternary tephrostratigraphic record. *Geological Society of New Zealand Miscellaneous Publication* 81B, 73-83.
- Alloway, B.V., McGlone, M.S., Neall, V.E. and Vucetich, C.G. (1992) The role of Egmont-sourced tephra in evaluating the paleoclimatic correspondance between the bio- and soil-stratigraphic records of central Taranaki, New Zealand. *Quaternary International* 13/14, 187-194.
- Alloway, B.V., Pillans, B.J., Sandhu, A.S., and Westgate, J.A. (1993) Revision of the marine chronology in the Wanganui Basin, New Zealand, based on the isothermal plateau fission-track dating of tephra horizons. *Sedimentary Geology* 82, 299-310.
- Alloway, B.V., Neall, V.E. and Vucetich, C.G. (1995) Late Quaternary (post 28,000 year B.P.) tephrostratigraphy of northeast and central Taranaki, New Zealand. *Journal of the Royal Society of New Zealand* 25, 385-458.
- Almond, P.C. (1996) Loess, soil stratigraphy and Aokautere Ash on Late Pleistocene surfaces in south Westland, New Zealand: interpretation and correlation with the glacial stratigraphy. *Quaternary International* 34-36, 163-176.
- Almond, P.C. and Tonkin, P.J. (1999) Pedogenesis by upbuilding in an extreme leaching and weathering environment, and slow loess accretion, south Westland, New Zealand. *Geoderma* 92, 1-36.
- An, Z. (2000) The history and variability of the East Asian paleomonsoon climate. *Quaternary Science Reviews* 19, 171-187.
- An, Z. and Porter, S.C. (1997) Millennial-scale climatic oscillations during the last interglaciation in central China. *Geology* 25, 603-606.
- An, Z., Kukla, G.J., Porter, S.C. and Xiao, J. (1991) Magnetic susceptibility evidence of monsoon variation on the Loess Plateau of central China during the last 130,000 years. *Quaternary Research* 36, 29-36.
- Aubrey, M., Berggren, W.A., Van Couvering, J.A. and Steininger, R. (1999) Problems in chronostratigraphy: stages, series, unit and boundary stratotypes, global stratotype section and point and tarnished golden spikes. *Earth-Science Reviews* 46, 99-148.

- Bailey, R.A. and Carr, R.G. (1994) Physical geology and eruptive history of the Matahina Ignimbrite, Taupo Volcanic Zone, North Island, New Zealand. *New Zealand Journal of Geology and Geophysics* 37, 319-344.
- Ballance, P.F. (1976) Evolution of the Upper Cenozoic magmatic arc and plate boundary in northern New Zealand. *Earth and Planetary Science Letters* 28, 356-370.
- Begét, J.E. (1996) Tephrochronology and paleoclimatology of the last interglacial-glacial cycle recorded in Alaskan loess deposits. *Quaternary International* 34-36, 121-126.
- Begét, J.E. and Hawkins, D. (1989) Influence of orbital parameters on Pleistocene loess deposition in central Alaska. *Nature* 337, 151-153.
- Begét, J.E., Stone, D.B. Hawkins, D.B. (1990) Paleoclimatic forcing of magnetic susceptibility variations in Alaskan loess during the late Quaternary. *Geology* 18, 40-43.
- Benney, L.A., Kennedy, N.M., Kirkman, J.H. and Stewart, R.B. (1988) Mineralogical and textural discrimination of loess derived from a tephra near Rotorua, New Zealand. *Australian Journal of Soil Research* 26, 301-12.
- Beu, A.G. and Edwards, A.R. (1984) New Zealand Pleistocene and late Pliocene glacio-eustatic cycles. *Palaeogeography, Palaeoclimatology, Palaeoecology* 46, 119-142.
- Beuselinck, L., Govers, G., Poesen, J., Degraer, G. and Froyen, L. (1998) Grain-size analysis by laser diffractometry: comparison with the sieve-pipette method. *Catena* 32, 193-208.
- Birrell, K.S. and Pullar, W.A. (1973) Weathering of paleosols in Holocene and late Pleistocene tephtras in central North Island, New Zealand. *New Zealand Journal of Geology and Geophysics* 16, 687-702.
- Black, T. M. (1992) Chronology of the Middle Pleistocene Kidnappers Group, New Zealand and correlation to global oxygen isotope stratigraphy. *Earth and Planetary Science Letters* 109, 573-584.
- Black, T.M., Shane, P.A.R., Westgate, J.A. and Froggatt, P.C. (1996) Chronological and paleomagnetic constraints on widespread welded ignimbrites of the Taupo volcanic zone. *Bulletin of Volcanology* 58, 226-238.
- Bloemendal, J., Liu, X.M. and Rolph, T.C. (1995) Correlation of the magnetic susceptibility stratigraphy of Chinese loess and the marine oxygen isotope record: chronological and palaeoclimatic implications. *Earth and Planetary Science Letters* 131, 371-380.
- Boggs, S. (1995) *Principles of Sedimentology and Stratigraphy*. 2<sup>nd</sup> Edition. Prentice Hall, 774pp.
- Bogue, S. and Merrill, R.T. (1992): The character of the field during geomagnetic reversals. *Annual Review of Earth and Planetary Sciences* 20, 181-219.
- Bowen, D.Q., Pillans, B.J., Sykes, G.A., Beu, A.G., Edwards, A.R., Kamp, P.J.J. and Hull, A.G. (1998) Amino acid geochronology of Pleistocene marine sediments in the

Wanganui Basin: a New Zealand framework for correlation and dating. *Journal of the Geological Society* 155, 439-46.

Brathwaite, R.L. and Christie, A.B. (1996) Geology of the Waihi area, part sheets T13 and U13, scale 1:50,000. *Institute of Geological and Nuclear Sciences Geological Map* 21.

Briggs, R.M. and McDonough, W.F. (1990) Contemporaneous convergent margin and intraplate magmatism, North Island, New Zealand. *Contributions to Mineralogy and Petrology* 86, 77-88.

Briggs, R.M., Itaya, T., Lowe, D.J. and Keane, A.J. (1989) Ages of the Pliocene-Pleistocene Alexandra and Ngatutura Volcanics, western North Island, New Zealand, and some geological implications. *New Zealand Journal of Geology and Geophysics* 32, 417-427.

Briggs, R.M., Gifford, M.G., Moyle, A.R., Taylor, S.R., Norman, M.D., Houghton, B.F. and Wilson, C.J.N. (1993) Geochemical zoning and eruptive mixing in ignimbrites from Mangakino volcano, Taupo Volcanic Zone, New Zealand. *Journal of Volcanology and Geothermal Research* 56, 175-203.

Briggs, R.M., Lowe, D.J., Goles, G.G. and Shepherd, T.G. (1994a) Intra-conference tour day 1: Hamilton – Raglan – Hamilton. In: Lowe, D.J. (ed.) *Conference Tour Guides*, Inter-INQUA Field Conference on Tephrochronology, Loess and Paleopedology, University of Waikato, Hamilton. pp24-44.

Briggs, R.M., Okada, T., Itaya, T., Shibuya, H. and Smith, I.E.M. (1994b) K-Ar ages, paleomagnetism, and geochemistry of the South Auckland volcanic field, North Island, New Zealand. *New Zealand Journal of Geology and Geophysics* 37, 143-153.

Briggs, R.M., Hall, G.J., Harmsworth, G.R., Hollis, A.G., Houghton, B.F., Hughes, G.R., Morgan, M.D. and Whitbread-Edwards, A.R. (1996) Geology of the Tauranga area, sheet U14, scale 1:50,000. *Department of Earth Sciences, University of Waikato, Occasional Report* 22.

Butler, R.F. (1992): *Paleomagnetism: magnetic domains to geologic terrains*. Blackwell, Boston. 319pp.

Buurman, P., Pape, Th. and Muggler, C.C. (1997) Laser grain-size determination in soil genetic studies 1. Practical problems. *Soil Science* 162, 211-218.

Campbell, I.B. (1986) Recognition of paleosols in Quaternary periglacial and volcanic environments in New Zealand. In: Wright, V.P. (ed.) *Paleosols – their recognition and interpretation*. London, Blackwell, 208-41.

Cande, S.C. and Kent, D.V. (1992): A new geomagnetic polarity time-scale for the Late Cretaceous and Cenozoic. *Journal of Geophysical Research* 97, 13,917-13,951.

Carter, L., Nelson, C.S., Neil, H.L., and Froggatt, P.C. (1995) Correlation, dispersal, and preservation of the Kawakawa Tephra and other late Quaternary tephra layers in the Southwest Pacific Ocean. *New Zealand Journal of Geology and Geophysics* 38, 29-46.

- Carter, L., Carter, R.M., McCave, N. and Shipboard Scientific Party (1999) You don't know where it is until you drill: initial results from Leg 181 – SW Pacific gateway. *NIWA Water and Atmosphere* 7, 14-16.
- Carter, R.M. and Naish, T.R. (1998a) A review of Wanganui Basin, New Zealand: global reference section for shallow marine, Plio-Pleistocene (2.5-0 Ma) cyclostratigraphy. *Sedimentary Geology* 122, 37-52.
- Carter, R.M. and Naish, T.R. (1998b) Have local stages outlived their usefulness for the New Zealand Plio-Pleistocene? *New Zealand Journal of Geology and Geophysics* 41, 271-279.
- Carter, R.M. and Naish, T.R. (eds.) (1999) The highest resolution, chronostratigraphic and sequence stratigraphic record of the Plio-Pleistocene, Wanganui Basin, New Zealand. *Institute of Geological and Nuclear Sciences folio series 2, version 1999, 1*. Folder with 2 enclosures. Lower Hutt, New Zealand: Institute of Geological & Nuclear Sciences Limited.
- Carter, R.M., Abbott, S.T., Naish, T., and Saul, G. (1996) Basin analysis of the cyclothem record of oxygen-isotope stages 5-100, Wanganui Basin, western North Island. *N.Z. Eos* 77 (46), F328 (Abstract).
- Chlachula, J., Rutter N.W. and Evans, M.E. (1997) A late Quaternary loess-palaeosol record at Kurtakm southern Siberia. *Canadian Journal of Earth Science* 34, 679-686.
- Chlachula, J., Evans, M. and Rutter N.W. (1998) A magnetic investigation of a late Quaternary loess/palaeosol record in Siberia. *Geophysical Journal International* 132, 128-132.
- Clayden and Hewitt (1994) *Horizon notation for New Zealand soils*. Manaaki Whenua-Landcare Research, Lincoln, New Zealand. 30pp.
- Collen, J.D. and Vella, P. (1984) Hautotara, Te Muna and Ahiaruhe Formations, middle to late Pleistocene, Wairarapa, New Zealand. *Journal of the Royal Society of New Zealand* 14, 297-317.
- Colman, S.M., Pierce, K.L. and Birkeland, P.W. (1987) Suggested terminology for Quaternary dating methods. *Quaternary Research* 28, 314-319.
- Cowie, J.D. (1964) Aokautere Ash in the Manawatu District, New Zealand. *New Zealand Journal of Geology and Geophysics* 7, 67-77.
- Cronin, S.J., Neall, V.E. and Palmer, A.S. (1996) Investigation of an aggrading paleosol developed into andesitic ring-plain deposits, Ruapehu volcano, New Zealand. *Geoderma* 69, 119-135.
- Davis, J.C. (1986) *Statistics and data analysis in Geology*. John Wiley & Sons, New York. 646pp.
- Davoren, A. (1976) A pedological study of the Kauroa Ash Formation at the University of Waikato. Unpublished M.Sc. thesis, University of Waikato, Hamilton.

- Delano, J.W., Tice, S.J., Mitchell, C.E., and Goldman, D. (1994) Rhyolitic glass in Ordovician K-bentonites: A new stratigraphic tool. *Geology* 22, 115-118.
- Derbyshire, E. (1995) Aeolian sediments in the Quaternary record: an introduction. *Quaternary Science Reviews* 14, 641-643.
- Derbyshire, E., Kemp, R. and Meng, X. (1995) Variations in loess and palaeosol properties as indicators of palaeoclimatic gradients across the Loess Plateau, North China. *Quaternary Science Reviews* 14, 681-697.
- Ding, Z., Yu, Z., Rutter, N., and Liu, T.S. (1994) Towards an orbital time scale for Chinese loess deposits. *Quaternary Science Reviews* 13, 39-70.
- Ding, Z.L., Rutter, N.W., Sun, J.M., Yang, S.L. and Liu, T.S. (2000) Re-arrangement of atmospheric circulation at about 2.6 Ma over northern China: evidence from grain size records of loess-paleosol and red clay sequences. *Quaternary Science Reviews* 19, 547-558.
- Dugmore, A.J., Newton, A.J., Edwards, K.J., Larsen, G., Blackford, J.J. and Cook, G.T. (1996) Long-distance marker horizons from small-scale eruptions: British tephra deposits from the AD 1510 eruption of Hekla, Iceland. *Journal of Quaternary Science* 11, 511-516.
- Dunlop, D.J. (1995) Magnetism in rocks. *Journal of Geophysical Research* 100, 2161-74.
- Eden, D.N. and Furkert, R.J., (eds.) (1988) *Loess: its distribution, geology and soils*. A.A. Balkema, Rotterdam.
- Fassbinder, J.W.E., Stanjek, H. and Vali, H. (1990) Occurrence of magnetic bacteria in soil. *Nature* 343, 161-163.
- Fergusson, D.A. (1986) Geology of inland Kawhia: emphasis on Te Kuiti Group stratigraphy and sedimentation. Unpublished M.Sc. thesis, University of Waikato, Hamilton.
- Fine, P. and Singer, M.J. (1989) Pedogenic factors affecting magnetic susceptibility of northern California soils. *Soil Science Society of American Journal* 53, 1119-1127.
- Fine, P., Singer, M.J., La Ven, R., Verosub, K.L. and Southard, R.J. (1989) Role of pedogenesis in distribution of magnetic susceptibility in two California chronosequences. *Geoderma* 44, 287-306.
- Folk, R.L. (1968) *Petrology of Sedimentary Rocks*. Hemphill's, Austin, Texas. 170pp.
- Fontes, M.P.F., de Oliveira, T.S., da Costa, L.M. and Campos, A.A.G. (2000) Magnetic separation and evaluation of magnetization of Brazilian soils from different parent materials. *Geoderma* 96, 81-99.
- Froggatt, P.C. (1983) Toward a comprehensive Upper Quaternary tephra and ignimbrite stratigraphy in New Zealand using electron microprobe analysis of glass shards. *Quaternary Research* 19, 188-200.

- Froggatt, P.C. (1988) Paleomagnetism of the Last Glacial loess from two sections in New Zealand. In: Eden, D.N. and Furkert, R.J. (eds.) *Loess: its distribution, geology and soils*. A.A. Balkema, Rotterdam. pp59-68.
- Froggatt, P.C. (1992) Standardisation of the chemical analysis of tephra deposits. Report of the ICCT Working Group. *Quaternary International* 13-14, 93-96.
- Froggatt, P.C. and Gosson, G.J. (1982) Techniques for the preparation of tephra studies for mineral and chemical analysis and radiometric dating. *Publication of Geology Department, Victoria University of Wellington* 23, 12pp.
- Froggatt, P.C. and Lowe, D.J. (1990) A review of late Quaternary silicic and some other tephra formations from New Zealand: their stratigraphy, nomenclature, distribution, volume, and age. *N.Z. Journal of Geology and Geophysics* 33, 89-109.
- Froggatt, P.C., Nelson, C.S., Carter, L., Griggs, G. and Black, K.P. (1986) An exceptionally large late Quaternary eruption from New Zealand. *Nature* 319, 578-582.
- Funnell, B.M. (1995) Global sea-level and the (pen-) insularity of late Cenozoic Britain. In: Preece, R.C. (ed.) *Island Britain; a Quaternary Perspective*. The Geological Society, Bath, 3-14.
- Gage, M. (1985) Glaciation in New Zealand – the first century of research. *Quaternary Science Reviews* 4, 189-214.
- Galbraith, R.F. (1981) On statistical models for fission-track counts. *Mathematical Geology* 13, 471-478.
- Goles, G.G., Briggs, R.M. and Rosenberg, M.D. (1996) Late Pliocene stratigraphic succession and volcanic evolution of Karioi volcano, western North Island, New Zealand. *New Zealand Journal of Geology and Geophysics* 39, 283-294.
- Green, P.F. (1981) A new look at statistics in fission track dating. *Nuclear Tracks* 5, 77-86.
- Green, P.F. (1985) Comparison of zeta calibration baselines for fission track dating of apatite, zircon and sphene. *Chemical Geology* 58, 1-22.
- Hackett, W.R. and Houghton, B.F. (1989) A facies model for a Quaternary andesitic composite volcano: Ruapehu, New Zealand. *Bulletin of Volcanology* 51, 51-68.
- Hailwood, E.A. (1989) *Magnetostratigraphy*. Blackwell Scientific Publications, Oxford. 84pp.
- Han, J. and Jiang, W. (1999) Particle size contributions to bulk magnetic susceptibility in Chinese loess and paleosol. *Quaternary International* 62, 103-110.
- Hanson, B., Delano, J.W. and Lindstrom, D.J. (1996) High-precision analysis of hydrous rhyolitic glass inclusions in quartz phenocrysts using the electron microprobe and INAA. *American Mineralogist* 81, 1249-1262.
- Heller, F. and Liu, T.S. (1982) Magnetostratigraphic dating of loess deposits in China. *Nature* 300, 431-433.



- Heller, F. and Liu, T.S. (1984) Magnetism of Chinese loess deposits. *Journal of the Royal Astronomical Society* 77, 125-14.
- Heller, F. and Liu, T.S. (1986) Palaeoclimatic and sedimentary history from magnetic susceptibility of loess in China. *Geophysical Research Letters* 13, 1169-1172.
- Heller, F., Liu, X., Liu, T. and Xu, T. (1991) Magnetic susceptibility of loess in China. *Earth and Planetary Science Letters* 103, 301-310.
- Hildreth, W. and Mahood, G. (1985) Correlation of ash-flow tuffs. *Geological Society of America Bulletin* 96, 968-974.
- Hobden, B.J., Houghton, B.F., Lanphere, M.A. and Nairn, I.A. (1996) Growth of the Tongariro volcanic complex: new evidence from K-Ar age determinations. *New Zealand Journal of Geology and Geophysics* 39, 151-154.
- Hodder, A.P.W., Green, B.E. and Lowe, D.J. (1990) A two-stage model for the formation of clay. *Clay Minerals* 25, 313-27.
- Hodgson, J.M. (1974) (Ed.) *Soil survey field handbook*. Soil Survey of England and Wales, Technical Monograph No. 5, Harpendon.
- Houghton, B.F., Wilson, C.J.N., McWilliams, M.O., Lanphere, M.A., Weaver, S.D., Briggs, R.M. and Pringle, M.S. (1995) Chronology and dynamics of a large silicic magmatic system: Central Taupo Volcanic Zone, New Zealand. *Geology* 23, 13-16.
- Hunt, C.P., Singer, M.J., Kletetschka, G., TenPas, J. and Verosub, K.L. (1995) Effect of citrate-bicarbonate-dithionite treatment on fine-grained magnetite and maghemite. *Earth and Planetary Science Letters* 130, 87-94.
- Hunt, J.B. and Hill, P.G. (1993) Tephra geochemistry: a discussion of some persistent analytical problems. *The Holocene* 3, 271-278.
- Hunt, J.B. and Hill, P.G. (1996) An inter-laboratory comparison of the electron microprobe microanalysis of glass geochemistry. *Quaternary International* 34-36, 229-241.
- Hunt, J.B. and Lowe, D.J. (in press) Tephra nomenclature. *Journal of Archaeological Science*.
- Hurford, A.J. and Carter, A. (1991) The role of fission track dating in discrimination of provenance. In: Morton, A.C., Todd, S.P. and Houghton, P.D.W. (eds.) *Developments in Sedimentary Provenance Studies*. *Geological Society Special Publication* 57, 67-78.
- Hurford, A.J. and Green, P.F. (1983) The zeta age calibration of fission-track dating. *Isotope Geoscience* 1, 285-317.
- Hurford, A.J. and Watkins, R.T. (1987) Fission track age of the tuffs of the Bulnk Member, Bakate Formation, northern Kenya: a suitable fission track age standard. *Chemical Geology* 66, 209-216.

- Kamp, P.J.J. (1990) Kidnappers Group (Middle Pleistocene), Hawke's Bay. *Geological Society of New Zealand Miscellaneous Publication* 50B, 105-118.
- Kamp, P.J.J., Green, P.F. and White, S.H. (1989) Fission track analysis reveals character of collisional tectonics in New Zealand. *Tectonics* 8, 169-195.
- Keane, A.J. (1985) The age, form and volcanic mechanisms of the Okete Volcanics near Raglan. Unpublished M.Sc. thesis, University of Waikato, Hamilton.
- Kennedy, N.M. (1982) Tephric loess in Rotorua – Bay of Plenty Region. In: Wasson, R.J. (ed.) *Quaternary Dust Mantles of China, New Zealand and Australia*. pp119-22.
- Kennedy, N.M. (1988) Late Quaternary loess associated with the Mamaku Plateau, North Island, New Zealand. In: Eden, D.N. and Furkert, R.J. (eds.) *Loess: its distribution, geology and soils*. A.A. Balkema, Rotterdam. pp71-80.
- Kennedy, N.M. (1994) New Zealand tephrochronology as a tool in geomorphic history of the c. 140 ka Mamaku Ignimbrite and in relating oxygen isotope stages. *Geomorphology* 9, 97-115.
- Kimber, R.W.L., Kennedy, N.M. and Milnes, A.R. (1994) Amino acid racemisation dating of a 140,000 year old tephra-loess-paleosol sequence on the Mamaku Plateau near Rotorua, New Zealand. *Australian Journal of Earth Sciences* 41, 19-26.
- Kirkman, J.H. (1980) Mineralogy of the Kauroa Ash Formation of south-west and west Waikato, North Island, New Zealand. *New Zealand Journal of Geology and Geophysics* 23, 113-120.
- Kohn, B.P., Pillans, B. and McGlone, M.S. (1992) Zircon fission track age for middle Pleistocene Rangitawa Tephra, New Zealand: stratigraphic and paleoclimatic significance. *Palaeogeography, Palaeoclimatology, Palaeoecology* 95, 73-94.
- Konert, M. and Vandenberghe, J. (1997) Comparison of laser grain size analysis with pipette and sieve analysis: a solution for the underestimation of the clay fraction. *Sedimentology* 44, 523-535.
- Krippner, S.J.P., Briggs, R.M., Wilson, C.J.N. and Cole, J.W. (1998) Petrography and geochemistry of lithic fragments in ignimbrites from Mangakino Volcanic Centre: implications for the composition of the subvolcanic crust in western Taupo Volcanic Zone, New Zealand. *New Zealand Journal of Geology and Geophysics* 41, 187-199.
- Kukla, G. (1987) Loess stratigraphy in central China. *Quaternary Science Reviews* 6, 191-219.
- Kukla, G. and An, Z.S. (1989) Loess stratigraphy in central China. *Palaeogeography, Palaeoclimatology, Palaeoecology* 72, 203-225.
- Kukla, G. and Cílek, V. (1996) Plio-Pleistocene megacycles: record of climate and tectonics. *Palaeogeography, Palaeoclimatology, Palaeoecology* 102, 171-194.
- Kukla, G., Heller, F., Liu, X.M., Xu, T.M., Liu, T.S. and An, Z.S. (1988) Pleistocene climates in China dated by magnetic susceptibility. *Geology* 16, 811-814.

- Lewis, D.W. and McConchie, D. (1994) *Analytical Sedimentology*. Chapman & Hall, New York. 197pp.
- Liu, T.S. (ed.) (1985) *Loess and the Environment*. China Ocean Press, Beijing. 215pp.
- Liu, T.S. (1988) *Loess in China*. Springer-Verlag, Berlin.
- Liu, T.S., Ding, Z. and Rutter, N. (1999) Comparison of Milankovitch periods between continental loess and deep-sea records over the last 2.5 Ma. *Quaternary Science Reviews* 18, 1205-1212.
- Liu, X.M., Liu, T.S., Heller, F. and Xu, T.C. (1990) Frequency dependent susceptibility of loess and Quaternary paleoclimate. *Quaternary Sciences* 2, 41-50.
- Liu, X.M., Liu, T.S., Heller, F., Xu, T.C. and Yuan, B.Y. (1991) Paleomagnetic and paleoclimatic studies of Chinese loess. In: Liu, T.S. (ed.) *Loess, Environment and Global Change*. Science Press, Beijing. pp61-81.
- Liu, X.M., Shaw, J., Liu, T., Heller, F. and Yuan, B. (1992) Magnetic mineralogy of Chinese loess and its significance. *Geophysical Journal International* 108, 301-308.
- Lourens, L.J., Antonarakou, A., Hilgen, F.J., Van Hoof, A.A.M., Vergaud-Grazzini, C. and Zachariasse, W.J. (1996) Evaluation of the Plio-Pleistocene astronomical timescale. *Paleoceanography* 11, 391-413.
- Lowe, D.J. (1980) Tephric loess. *N.Z. Soil News* 28, 217-219.
- Lowe, D.J. (1981) Origin and composite nature of Late Quaternary airfall deposits, Hamilton Basin, New Zealand. Unpublished M.Sc. thesis, University of Waikato, Hamilton.
- Lowe, D.J. (1986) Controls on the rates of weathering and clay mineral genesis in airfall tephros: a review and New Zealand case study. In: Colman, S.M. and Dethier, D.P. (eds.) *Rates of Chemical Weathering of Rocks and Minerals*. Academic Press, Orlando. pp265-330.
- Lowe, D.J. (1988a) Late Quaternary volcanism in New Zealand: towards an integrated record using distal airfall tephros in lakes and bogs. *Journal of Quaternary Science* 3, 111-120.
- Lowe, D.J. (1988b) Stratigraphy, age, composition, and correlation of late Quaternary tephros interbedded with organic sediments in Waikato Lakes, North Island, New Zealand. *New Zealand Journal of Geology and Geophysics* 31, 125-165.
- Lowe, D.J. (1990) Tephra studies in New Zealand: an historical review. *Journal of the Royal Society of New Zealand* 20, 119-150.
- Lowe, D.J. (1995) Teaching clays: from ashes to allophane. In: Churchman, G.J., Fitzpatrick, R.W. and Eggleton, R.A. (eds.) *Proceedings of the 10<sup>th</sup> International Clay Conference, Adelaide, Australia*. CSIRO Publishing, Melbourne. pp19-23.
- Lowe, D.J. (ed.) (1996) Tephra, loess and paleosols – an integration. *Quaternary International* 34-36, 261pp.

- Lowe, D.J. (in press) Upbuilding pedogenesis in multisequal tephra-derived soils in the Waikato Region.
- Lowe, D.J. and Hunt, J.B. (in press) A summary of terminology used in tephra-related studies. *Quaternaire*.
- Lowe, D.J. and Newnham, R.M. (1999) Advances in Quaternary tephrostratigraphy and tephrochronology in New Zealand. *Quaternary Australasia* 17, 12-19
- Lowe, D.J. and Percival, H.J. (1993) Clay mineralogy of tephras and associated paleosols and soils, and hydrothermal deposits, North Island. *Guide Book for New Zealand Pre-Conference Field Trip F1, 10<sup>th</sup> International Clay Conference, Adelaide, Australia*. 110pp.
- Lowe, D.J., Tippett, J.M., Kamp, P.J.J., Liddell, I.J., Briggs, R.M. and Horrocks, J.L. (in press) Ages on weathered Plio-Pleistocene sequences, western North Island, New Zealand. *Quaternaire*.
- Lowe, J.J. and Walker, M.J.C. (1997) *Reconstructing Quaternary Environments*. Addison Wesley Longman, Harlow, Essex. 446pp.
- Lu, H., Liu, X., Zhang, F., An, Z. and Dodson, J. (1999) Astronomical calibration of loess-paleosol deposits at Luochuan, central Chinese Loess Plateau. *Palaeogeography, Palaeoclimatology, Palaeoecology* 154, 237-246.
- McArthur, J.L. and Shepherd, M.J. (1990) Late Quaternary glaciation of Mt Ruapehu, North Island, New Zealand. *Journal of the Royal Society of New Zealand* 20, 287-96.
- Machida, H. (1999) The stratigraphy, chronology and distribution of distal marker-tephras in and around Japan. *Global and Planetary Change* 21, 71-94.
- Maher, B.A. (1998) Magnetic properties of modern soils and Quaternary loessic paleosols: paleoclimate implications. *Palaeogeography, Palaeoclimatology, Palaeoecology* 137, 25-44.
- Maher, B.A. and Taylor, R.M. (1988) Formation of ultrafine-grained magnetite in soils. *Nature* 336, 368-370.
- Maher, B.A. and Thompson, R. (1991) Mineral magnetic record of the Chinese loess and paleosols. *Geology* 19, 3-6.
- Maher, B.A. and Thompson, R. (1992) Paleoclimatic significance of the mineral magnetic record of the Chinese loess and paleosols. *Quaternary Research* 37, 155-170.
- Maher, B.A. and Thompson, R. (1995) Paleorainfall reconstructions from pedogenic magnetic susceptibility variations in the Chinese loess and paleosols. *Quaternary Research* 44, 383-391.
- Manning, D.A. (1996) Middle-late Pleistocene tephrostratigraphy of the eastern Bay of Plenty, New Zealand. *Quaternary International* 34-36, 3-12.

- Martini, I.P. and Chesworth, W. (eds.) (1992) *Weathering, soils and paleosols*. Elsevier, New York. 618pp.
- Mehra, O.P. and Jackson, M.L. (1960) Iron oxide removal from soils and clays by a dithionite-citrate system buffered with sodium bicarbonate. *Clays and Clay Mineralogy* 7, 317-327.
- Meng, X., Derbyshire, E. and Kemp, R.A. (1997) Origin of the magnetic susceptibility signal in Chinese loess. *Quaternary Science Reviews* 16, 833-839.
- Merrill, R.T. and McFadden, P.L. (1994): Geomagnetic field stability: Reversal events and excursions. *Earth and Planetary Science Letters* 121, 57-69.
- Milne, J.D.G. and Smalley, I.J. (1979) Loess deposits in the southern part of the North Island of New Zealand. *Acta Geologica Academiae Scientiarum Hungaricae* 22, 197-204.
- Milne, J.D.G., Clayden, B., Singleton, P.L. and Wilson, A.D. (1995) *Soil description handbook*. Manaaki Whenua Press, Lincoln, Canterbury, New Zealand. 157pp.
- Moore, C.L. (1991) The distal terrestrial record of explosive rhyolitic volcanism: an example from Auckland, New Zealand. *Sedimentary Geology* 74,25-38.
- Moyle, A.R. (1989) Volcanic geology and geochemistry of the Rocky Hill Ignimbrite, Upper Waipa Valley. Unpublished M.Sc. thesis, University of Waikato, Hamilton.
- Muggler, C.C., Pape, Th. and Buurman, P. (1997) Laser grain-size determination in soil genetic studies 2. Clay content, clay formation, and aggregation in some Brazilian oxisols. *Soil Science* 162, pp219.
- Naish, T.R. (1998) Constraints on the amplitude of late Pliocene eustatic sea-level fluctuations: new evidence from the New Zealand shallow marine record. *Geology* 25, 1139-1142.
- Naish, T.R., Kamp, P.J.J., Alloway, B.V., Pillans, B., Wilson, G.S. and Westgate, J.A. (1996) Integrated tephrochronology and magnetostratigraphy for cyclothem marine strata, Wanganui Basin: implications for the Pliocene-Pleistocene boundary in New Zealand. *Quaternary International* 34-36, 29-48.
- Naish, T.R., Kamp, P.J.J. and Pillans, B. (1997) Recurring global sea-level changes recorded in shelf deposits near the G/M polarity transition, Wanganui Basin, New Zealand: Implications for redefining the Pliocene-Pleistocene boundary. *Quaternary International* 40, 61-77.
- Naish, T.R., Abbott, S.T., Alloway, B.V., Beu, A.G., Carter, R.M., Edwards, A.R., Journeaux, T.D., Kamp, P.J.J., Pillans, B.J., Saul, G., and Woolfe, K.J. (1998) Astronomical calibration of a southern hemisphere Plio-Pleistocene reference section, Wanganui Basin, New Zealand. *Quaternary Science Reviews* 17, 695-710.
- Narcisi, B. and Vezzoli, L. (1999) Quaternary stratigraphy of distal tephra layers in the Mediterranean – an overview. *Global and Planetary Change* 21, 31-50.

- Nelson, C.S. (1988) Revised age of a late Quaternary tephra at DSDP site 594 off eastern South Island, and some implications for correlation. *Geological Society of New Zealand Newsletter* 82, 35-40.
- Nelson, C.S., Froggatt, P.C. and Gosson, G.J. (1985) Nature, chemistry, and origin of late Cenozoic megascopic tephtras in Leg 90 cores from southwest Pacific. In Kennett, J.P. et al. (eds.) *Initial Reports of the Deep Sea Drilling Project 90*, 1161-1173.
- Nelson, C.S., Kamp, P.J.J. and Mildenhall, D.C. (1989) Late Pliocene distal silicic ignimbrites, Port Waikato, New Zealand: implications for volcanism, tectonics, and sea-level changes in South Auckland. *New Zealand Journal of Geology and Geophysics* 32, 357-370.
- Newnham, R.M., Lowe, D.J. and Williams, P.W. (1999a) Quaternary environmental change in New Zealand: a review. *Progress in Physical Geography* 23, 567-610.
- Newnham, R.M., Lowe, D.J. and Alloway, B.V. (1999b) Volcanic hazards in Auckland, New Zealand: a preliminary assessment of the threat posed by central North Island silicic volcanism based on the Quaternary tephrostratigraphical record. In: Firth, C.R. and McGuire, W.J. (eds.) *Volcanoes in the Quaternary. Geological Society, London, Special Publications* 161, 27-45.
- van Oorschot, I.H.M., and Dekkers, M.J. (1999) Dissolution behaviour of fine-grained magnetite and maghemite in the citrate-bicarbonate-dithionite extraction method. *Earth and Planetary Science Letters* 167, 282-295.
- Pain, C.F. (1975) Some tephra deposits in the south-west Waikato area, North Island, New Zealand. *New Zealand Journal of Geology and Geophysics* 18, 541-550.
- Palmer, A.S. (1994) Paleosols: their importance for stratigraphic, paleopedological and paleoenvironmental studies of Quaternary sequences in New Zealand. *Programme and Abstracts, International Inter-INQUA Field Conference and Workshop on Tephrochronology, Loess and Paleopedology, University of Waikato, Hamilton.*
- Palmer, A.S. and Pillans, B.J. (1996) Record of climatic fluctuations from ca. 500 ka loess deposits and paleosols near Wanganui, New Zealand. *Quaternary International* 34-36, 155-162.
- Parfitt, R.L. (1990) Allophane in New Zealand – a review. *Australian Journal of Soil Research* 28, 343-60.
- Parfitt, R.L. and Kimble, J.M. (1989) Conditions for formation of allophane in soils. *Soil Science Society of America Journal* 53, 971-7.
- Pesci, M. (1990) Loess is not just accumulation of airborne dust. *Quaternary International* 7/8, 1-21.
- Pillans, B.J. (1990) Pleistocene terraces in New Zealand: a review. *New Zealand Journal of Geology and Geophysics* 33, 219-31.
- Pillans, B.J. (1991) New Zealand Quaternary stratigraphy: an overview. *Quaternary Science Reviews* 10, 405-418.

- Pillans, B.J. (1994) Direct marine-terrestrial correlations, Wanganui Basin, New Zealand: the last million years. *Quaternary Science Reviews* 13, 189-200.
- Pillans, B.J. and Kohn, B.P. (1981) Rangitawa Pumice: a widespread(?) Quaternary marker bed in Taranaki-Wanganui. *Geology Department, Victoria University of Wellington Publication* 20, 94-104.
- Pillans, B.J. and Kohn, B.P. (1998) The age of the Rangitawa Tephra. *Geological Society of New Zealand Newsletter* 115, 45-52.
- Pillans, B.J. and Wright, I. (1990) 500,000 year paleomagnetic record from New Zealand loess. *Quaternary Research* 33, 178-87.
- Pillans, B.J., McGlone, M.S., Palmer, A.S., Mildenhall, D., Alloway, B.V. and Berger, G.W. (1993) The Last Glacial Maximum in central and southern North Island, New Zealand: a paleoenvironmental reconstruction using Kawakawa Tephra Formation as a chronostratigraphic marker. *Palaeogeography, Palaeoclimatology, Palaeoecology* 101, 283-304.
- Pillans, B.J., Roberts, A.P., Wilson, G.S., Abbott, S.T., and Alloway, B.V. (1994) Magnetostratigraphic, lithostratigraphic and tephrostratigraphic constraints on Lower and Middle Pleistocene sea-level changes, Wanganui Basin, New Zealand. *Earth and Planetary Science Letters* 121, 81-98.
- Pillans, B.J., Kohn, B.P., Berger, G.W., Froggatt, P.C., Duller, G., Alloway, B.V. and Hesse, P.P. (1996) Multi-method dating comparison from Mid-Pleistocene Rangitawa Tephra, New Zealand. *Quaternary Science Reviews* 15, 1-14.
- Pisias, N.G. and Moore, T.C. (1981) The evolution of Pleistocene climate: a time series approach. *Earth and Planetary Science Letters* 52, 450-458.
- Price, R.C., Stewart, R.B., Woodhead, J.D. and Smith, I.E.M. (1999) Petrogenesis of high-K arc magmas: evidence from Egmont Volcano, North Island, New Zealand. *Journal of Petrology* 40, 167-197.
- Pringle, M.S., McWilliams, M.O., Houghton, B.F., Lanphere, M.A. and Wilson, C.J.N. (1992)  $^{40}\text{Ar}/^{39}\text{Ar}$  dating of Quaternary feldspar: examples from the Taupo Volcanic Zone, New Zealand. *Geology* 20, 531-534.
- Pullar, W.A. and Pollok, J.A. (1973) Paleosols and tephric loess associated with Okareka and Te Rere Tephra formations. *N.Z. Soil News* 21, 186-7.
- Pullar, W.A., Birrell, K.S. and Heine, J.C. (1973) Age and distribution of late Quaternary pyroclastic and associated cover deposits of central North Island, New Zealand [with accompanying explanatory notes]. *New Zealand Soil Survey Report* 2, 4 sheets, 32pp.
- Pye, K. (1987) *Aeolian Dust and Dust Deposits*. Academic Press, London.
- Pye, K. (1995) The nature, origin and accumulation of loess. *Quaternary Science Reviews* 14, 653-667.

- Rankey, E.C. and Farr, M.R. (1997) Preserved pedogenic mineral magnetic signature, pedogenesis, and paleoclimate change: Pennsylvanian Roca Shale (Virgilian, Asselian), central Kansas, USA. *Sedimentary Geology* 114, 11-32.
- Rawle, A. F. (1993) *The Basic Principles of Particle Size Analysis*. Application Note MRK034/02, Malvern Instruments Ltd, UK.
- Roberts, A.P. and Pillans, B.J. (1993) Rock magnetism of Lower/Middle Pleistocene marine sediments, Wanganui Basin. *Geophysical Research Letters* 20, 839-842.
- Roedder, E. (1984) Fluid inclusions. Mineralogical Society of America, *Reviews in Mineralogy* 12, 644pp.
- Salter, R.T. (1979) A pedological study of the Kauroa Ash Formation at Woodstock. Unpublished M.Sc. thesis, University of Waikato, Hamilton.
- Sarna-Wojcicki, A.M. and Davis, J.O. (1991) Quaternary tephrochronology. In: Morrison, R.B. (ed.), *Quaternary Nonglacial Geology, Conterminous U.S.; Geology of North America*, Geological Society of America K2, 93-116.
- Seward, D. (1979) Comparison of zircon and glass fission track ages from tephra horizons. *Geology* 7, 470-482.
- Shackleton, N.J., Berger, A. and Peltier, W.R. (1990): An alternative astronomical calibration of the lower Pleistocene time scale based on ODP site 677. *Transactions of the Royal Society of Edinburgh, Earth Sciences* 81, 256-261.
- Shane, P.A.R. (1990) Correlation of some Pliocene tuffs in southern Wairarapa, New Zealand, and comparison with biostratigraphic and Magnetostratigraphic data. *N.Z. Journal of Geology and Geophysics* 33, 349-354.
- Shane, P.A.R. (1991) Remobilised silicic tuffs in middle Pleistocene fluvial sediments, southern North Island, New Zealand. *New Zealand Journal of Geology and Geophysics* 34, 489-499.
- Shane, P.A.R. (1994) A widespread, early Pleistocene tephra (Potaka tephra, 1 Ma) in New Zealand: character, distribution and implications. *New Zealand Journal of Geology and Geophysics* 37, 25-35.
- Shane, P.A.R. (2000) Tephrochronology: a New Zealand case study. *Earth-Science Reviews* 49, 223-259.
- Shane, P.A.R. and Froggatt, P. (1991) Glass chemistry, paleomagnetism and correlation of middle Pleistocene tuffs in southern North Island, New Zealand and Western Pacific. *New Zealand Journal of Geology and Geophysics* 34, 203-211.
- Shane, P.A.R., Froggatt, P., Black, T., Westgate, J.A. (1995) Chronology of Pliocene and Quaternary bioevents and climatic events from fission-track ages on tephra beds, Wairarapa, New Zealand. *Earth and Planetary Science Letters* 130, 141-154.
- Shane, P.A.R., Black, T.M., Alloway, B.V. and Westgate, J.A. (1996a) Early to middle Pleistocene tephrochronology of North Island, New Zealand: implications for



volcanism, tectonism, and paleoenvironments. *Geological Society of America Bulletin* 108, 915-925.

Shane, P.A.R., Alloway, B.V., Black, T. and Westgate, J.A. (1996b) Isothermal plateau fission-track ages of tephra beds in an Early-Middle Pleistocene marine and terrestrial sequence, Cape Kidnappers, New Zealand. *Quaternary International* 34-36, 49-53.

Shane, P.A.R., Black, T.M., Eggins, S. and Westgate, J.A. (1998) Late Miocene marine tephra beds: recorders of rhyolitic volcanism in North Island, New Zealand. *New Zealand Journal of Geology and Geophysics* 41, 165-178.

Shepherd, T.G. (1994) Paleoclimatic implications of clay minerals and paleosols within strongly weathered Plio-Pleistocene tephra in the Waikato region, central North Island, New Zealand. *Programme and Abstracts, International Inter-INQUA Field Conference and Workshop on Tephrochronology, Loess and Paleopedology, Hamilton, New Zealand.*

Singer, M.J., Fine, P., Verosub, K.L. and Chadwick, O.A. (1992) Time dependence of magnetic susceptibility record of Chinese loess-paleosol sequences. *Geology* 21, 1011-1014.

Singer, M.J., Verosub, K.L., Fine, P. and TenPas, J. (1996) A conceptual model for the enhancement of magnetic susceptibility in soils. *Quaternary International* 34-36, 243-248.

Singleton, P.L., McLeod, M. and Percival, H.J. (1989) Allophane and halloysite content and soil solution silicon in soils from rhyolitic volcanic material, New Zealand. *Australian Journal of Soil Research* 27, 67-77.

Smalley, I. (1995) Making the material: the formation of silt-sized primary mineral particles for loess deposits. *Quaternary Science Reviews* 14, 645-651.

Soengkono, S., Hochstein, M.P., Smith, I.E.M. and Itaya, T. (1992) Geophysical evidence for widespread reversely magnetised pyroclastics in the western Taupo Volcanic Zone (New Zealand). *New Zealand Journal of Geology and Geophysics* 35, 47-55.

Stevens, K.F. and Vucetich, C.G. (1985) Weathering of Upper Quaternary tephra in New Zealand, 2. Clay minerals and their climatic interpretation. *Chemical Geology* 53, 237-247.

Stokes, S. and Lowe, D.J. (1988) Discriminant function analysis of late Quaternary tephra from five volcanoes in New Zealand using glass shard major element chemistry. *Quaternary Research* 30, 270-283.

Stokes, S. and Nelson, C.S. (1991) Tectono-volcanic implications of provenance changes in the late Neogene coastal sand deposits of Kaihu Group, South Auckland, New Zealand. *New Zealand Journal of Geology and Geophysics* 34, 51-59.

Stokes, S., Nelson, C., Healy, T.R. and MacArthur, N.A. (1989) The Taharoa ironsand deposit. In: Kear, D. (ed.) Mineral Deposits of New Zealand. *The Australian Institute of Mining and Metallurgy monograph* 13, 105-109.

Stokes, S., Lowe, D.J. and Froggatt, P.C. (1992) Discriminant function analysis and correlation of late Quaternary rhyolitic tephra deposits from Taupo and Okataina volcanoes, New Zealand, using glass shard major element composition. *Quaternary International* 13/14, 102-117.

Sun, W., Banerjee, K. and Hunt, C.P. (1995) The role of maghemite in the enhancement of magnetic signal in the Chinese loess-paleosol sequence: An extensive rock magnetic study combined with citrate-bicarbonate-dithionite treatment. *Earth and Planetary Science Letters* 133, 493-505.

Takagi, M. (1995) Miocene-Pliocene arc volcanism of the Hauraki region in North Island, New Zealand. Unpublished M.Sc. thesis, lodged in the Library, Hiruzen Research Institute, Okayama, Japan.

Thorarinsson, S. (1974) The terms tephra and tephrochronology. In: Westgate, J.A., Gold, C.M. (Eds.) *World Bibliography and Index of Quaternary Tephrochronology*. University of Alberta, Alberta, pp. xvii-xviii.

Tonkin, P.J. (1970) Contorted stratification with clay lobes in volcanic ash beds, Raglan-Hamilton region, New Zealand. *Earth Science Journal* 4, 129-140.

Tonkin, P.J., Runge, E.C.A. and Ives, D. (1974) A study of late Pleistocene loess deposits, south Canterbury, New Zealand. II. Paleosols and their stratigraphic implications. *Quaternary Research* 4, 217-31.

Tonkin, P.J., Almond, P.S., Alloway, B.V., Trangmar, B.B. and Palmer, A.S. (1998) The recognition and interpretation of aggradational and multisequal soils from different depositional environments: some New Zealand examples. *Quaternary International* 51-52, pp47.

Turner, G.M. and Kamp, P.J.J. (1990) Palaeomagnetic location of the Jaramillo Subchron and the Matuyama-Brunhes transition in the Castlecliffian stratotype section, Wanganui Basin, New Zealand. *Earth and Planetary Science Letters* 100, 42-50.

Vandenbergh, J., An, Z., Nugteren, G., Lu, H. and Van Huissteden, K. (1997) New absolute time scale for the Quaternary climate in the Chinese loess region by grain-size analysis. *Geology* 25, 35-38.

Verosub, K.L., Fine, P., Singer, M.J. and TenPas, J. (1993) Pedogenesis and paleoclimate: interpretation of the magnetic susceptibility record of Chinese loess-paleosol sequences. *Geology* 21, 1011-1014.

Vlag, P. (1998) The magnetic signal in loess-sequences in Alaska. *The Institute for Rock Magnetism Quarterly* 8, 1-7.

Vucetich, C.G. (1982) New Zealand tephra: as fine dust mantle, marker bed and as sediment source for loess. In: Wasson, R.J. (ed.) *Quaternary Dust Mantles of China, New Zealand and Australia*. pp111-118

Vucetich, C.G., Birrell, K.S., Pullar, W.A. (1978) Ohinewai Tephra Formation; a c. 150,000-year-old tephra marker in New Zealand. *New Zealand Journal of Geology and Geophysics* 21, 71-73.

- Wada, K. and Harwood, M.E. (1974) Amorphous clay constituents of soils. *Adv. Agron.* 26, 211-260.
- Walker, G.P.L. (1981) Generation and dispersal of fine ash and dust by volcanic eruptions. *Journal of Volcanology and Geothermal Research* 11, 81-92.
- Ward, W.T. (1967) Volcanic ash beds of the lower Waikato Basin, North Island, New Zealand. *New Zealand Journal of Geology and Geophysics* 10, 1109-1135.
- Webster, J.D. and Duffield, W.A. (1991) Volatiles and lithophile elements in Taylor Creek Rhyolite: Constraints from glass inclusion analysis. *American Mineralogist* 76, 1628-1645.
- Webster, J.D., Congdon, R.D. and Lyons, P.C. (1995) Determining pre-eruptive compositions of late Paleozoic magma from kaolinized volcanic ashes: Analysis of glass inclusions in quartz microphenocrysts from tonsteins. *Geochimica et Cosmochimica Acta* 59, 711-720.
- Westgate, J.A. and Gorton, M.P. (1981) Correlation techniques in tephra studies. In: Self, S. and Sparks, R.S.J. (eds.) *Tephra Studies*. Reidel, Dordrecht, pp73-94.
- Westgate, J.A., Walter, R.C. and Naeser, N. (eds.) (1992) Tephrochronology: stratigraphic applications of tephra. *Quaternary International* 13/14, 203pp
- Whitton, J.S. and Churchman, G.J. (1987) Standard methods for mineral analysis of soil survey samples for characterisation and classification in NZ Soil Bureau. *New Zealand Soil Bureau Scientific Report* 79, 27pp.
- Williams, M., Dunkerley, D., De Dekker, P., Kershaw, P. and Chappell, J. (1998) *Quaternary Environments*. 2<sup>nd</sup> Edition. Arnold, London. 329pp.
- Wilson, C.J.N. (1986) Reconnaissance stratigraphy and volcanology of ignimbrites from Mangakino Volcano. In: Smith, I.E.M. (ed.) *Late Cenozoic Volcanism in New Zealand*. *Royal Society of New Zealand Bulletin* 23, 179-193.
- Wilson, C.J.N. (1991) Ignimbrite morphology and the effects of erosion: a New Zealand case study. *Bulletin of Volcanology* 53, 635-644.
- Wilson, C.J.N. (in press) The 26.5 ka Oruanui eruption, New Zealand: an introduction and overview. *Journal of Volcanology and Geothermal Research*.
- Wilson, C.J.N. and Walker, G.P.L. (1982) Ignimbrite depositional facies: the anatomy of a pyroclastic flow. *Journal of the Royal Society of London* 139, 581-592.
- Wilson, C.J.N., Houghton, B.F., Kamp, P.J.J. and McWilliams, M.O. (1995a) An exceptionally widespread ignimbrite with implications for pyroclastic flow emplacement. *Nature* 378, 605-607.
- Wilson, C.J.N., Houghton, B.F., McWilliams, M.O., Lanphere, M.A., Weaver, S.D. and Briggs, R.M. (1995b) Volcanic and structural evolution of Taupo Volcanic Zone, New Zealand: a review. *Journal of Volcanology and Geothermal Research* 68, 1-28.

Wilson, C.J.N., Houghton, B.F., Pillans, B.J., Weaver, S.D. (1995c) Taupo Volcanic Zone calc-alkaline tephras on the peralkaline Mayor Island volcano, New Zealand: identification and uses as marker horizons. *Journal of Volcanology and Geothermal Research* 69, 303-311.

Winspear, N.R. and Pye, K. (1995) Textural, geochemical and mineralogical evidence for the origin of Peoria Loess in central and southern Nebraska, USA. *Earth Surface Processes and Landforms*.

Woolfe, K.J. (1993) Lakes Onoke and Wairarapa as modern analogues for the Hautotara and Te Muna formations (Mid-Pleistocene), southern Wairarapa, New Zealand. *Sedimentary Geology* 84, 123-137.

Xiao, J.L., An, Z.S., Liu, T.S., Inouchi, Y., Kumai, H., Yoshikawa, S. and Kondo, Y. (1999) East Asian monsoon variation during the last 130,000 Years: evidence from the Loess Plateau of central China and Lake Biwa of Japan. *Quaternary Science Reviews* 18, 147-157.

Zijderveld, J.D.A. (1967): A.C. demagnetisation of rocks: analysis of results. In: Collinson, D.W., Creer, K.M. and Runcorn, S. K. (eds.) *Methods in Paleomagnetism*. Elsevier, Amsterdam, pp254-286.

**APPENDIX A:  
MAGNETIC SUSCEPTIBILITY**

# MAGNETIC SUSCEPTIBILITY

## WOODSTOCK (PRE-CBD TREATMENT)

Sample	Depth	Sample	Low Frequency			High Frequency			MSS	Xfd%
		Weight	Av A	Av M	Corr K	Av A	Av M	Corr K		
WS001	1.30	11.34	-1.1	454.0	455.0	0.3	447.5	447.2	4.0	1.7
WS002	1.40	11.85	-1.9	742.2	744.0	1.0	741.7	740.8	6.3	0.4
WS003	1.50	12.09	-2.1	1060.5	1062.6	1.6	1059.2	1057.6	8.8	0.5
WS004	1.60	13.01	-2.6	1017.9	1020.4	2.2	1015.5	1013.3	7.8	0.7
WS005	1.70	12.61	-3.2	934.2	937.4	3.0	931.1	928.2	7.4	1.0
WS006	1.80	11.80	-3.7	751.2	754.9	3.8	751.8	748.0	6.4	0.9
WS007	1.90	11.98	-3.9	576.7	580.6	4.5	580.6	576.1	4.8	0.8
WS008	1.95	12.25	-4.1	531.5	535.6	5.4	537.1	531.7	4.4	0.7
WS009	2.05	11.69	-4.7	389.5	394.2	6.3	397.2	391.0	3.4	0.8
WS010	2.15	11.49	-5.3	346.9	352.2	7.2	356.9	349.7	3.1	0.7
WS011	2.25	11.08	-5.3	349.3	354.6	8.0	360.0	352.1	3.2	0.7
WS012	2.35	10.54	-5.6	323.0	328.6	8.5	335.3	326.9	3.1	0.5
WS013	2.40	10.54	-5.6	345.5	351.0	9.3	359.3	350.1	3.3	0.3
WS014	2.45	10.33	-5.7	369.4	375.0	0.4	374.5	374.1	3.6	0.3
WS015	2.50	10.37	-6.5	428.0	434.5	1.2	433.3	432.1	4.2	0.6
WS016	2.55	10.45	-6.9	467.8	474.7	1.4	474.8	473.4	4.5	0.3
WS017	2.60	10.49	-7.2	470.2	477.4	1.9	479.0	477.2	4.6	0.0
WS018	2.65	10.74	-7.6	461.9	469.4	2.5	471.9	469.4	4.4	0.0
WS019	2.75	10.88	-8.2	289.0	297.2	3.3	299.4	296.1	2.7	0.4
WS020	2.80	10.50	-8.8	261.9	270.7	4.1	273.7	269.6	2.6	0.4
WS021	2.85	10.97	-8.9	264.8	273.6	0.2	273.0	272.8	2.5	0.3
WS022	2.95	10.40	-8.6	203.3	211.9	0.6	211.0	210.5	2.0	0.7
WS023	3.05	10.88	-8.4	144.6	153.0	1.0	152.8	151.8	1.4	0.8
WS024	3.10	11.26	-8.6	143.6	152.2	1.4	151.4	150.0	1.4	1.4
WS025	3.15	10.66	-8.9	178.0	186.9	1.7	184.6	182.9	1.8	2.1
WS026	3.25	10.68	-9.3	196.8	206.1	1.9	203.3	201.4	1.9	2.3
WS027	3.35	11.41	-10.0	247.2	257.1	2.5	252.6	250.1	2.3	2.7
WS028	3.45	10.88	-0.1	258.7	258.8	3.2	255.0	251.8	2.4	2.7
WS029	3.50	10.91	-0.3	280.4	280.7	3.8	276.3	272.6	2.6	2.9
WS030	3.55	10.46	-0.3	269.5	269.8	4.3	265.8	261.5	2.6	3.1
WS031	3.60	10.80	-0.5	285.3	285.8	4.6	280.7	276.1	2.6	3.4
WS032	3.65	10.43	-0.8	279.6	280.4	5.1	277.4	272.3	2.7	2.9
WS033	3.70	9.83	-0.9	266.6	267.5	5.7	265.7	260.0	2.7	2.8
WS034	3.75	10.23	-1.3	306.9	308.1	6.5	306.9	300.4	3.0	2.5
WS035	3.80	9.58	-1.4	363.6	364.9	7.2	364.8	357.7	3.8	2.0
WS036	3.85	9.77	-1.1	498.0	499.1	7.8	500.0	492.2	5.1	1.4
WS037	3.95	9.53	-1.6	544.0	545.6	8.4	546.9	538.5	5.7	1.3
WS038	4.05	9.63	-2.2	410.0	412.1	8.6	415.9	407.4	4.3	1.2
WS039	4.15	9.34	-2.3	389.1	391.4	8.9	395.5	386.6	4.2	1.2
WS040	4.25	9.33	-2.5	338.0	340.4	9.7	344.8	335.1	3.6	1.6
WS041	4.35	9.68	-2.9	349.1	352.0	0.2	346.7	346.5	3.6	1.6
WS042	4.45	9.80	-3.1	203.2	206.2	0.7	202.9	202.2	2.1	1.9
WS043	4.55	9.16	-3.2	114.1	117.3	1.2	116.5	115.3	1.3	1.7
WS044	4.65	9.69	-3.2	213.7	216.9	1.8	211.3	209.5	2.2	3.4
WS045	4.70	10.29	-3.1	305.8	308.8	2.0	301.3	299.3	3.0	3.1
WS046	4.80	9.91	-2.9	353.2	356.1	2.2	347.8	345.6	3.6	2.9
WS047	4.90	9.62	-3.4	280.1	283.5	2.6	279.3	276.7	2.9	2.4
WS048	5.00	9.09	-4.1	141.0	145.1	2.9	145.8	142.9	1.6	1.5
WS049	5.10	9.18	-3.8	124.5	128.3	3.2	129.9	126.7	1.4	1.2
WS050	5.20	9.44	-3.7	325.5	329.2	3.6	327.1	323.5	3.5	1.7
WS051	5.30	10.28	-4.2	441.7	445.9	4.0	435.1	431.1	4.3	3.3
WS052	5.40	9.53	-4.8	451.6	456.4	4.4	446.5	442.1	4.8	3.1
WS053	5.50	9.78	-5.1	489.1	494.2	4.5	485.1	480.6	5.1	2.7
WS054	5.60	9.19	-5.2	547.8	552.9	4.7	549.4	544.8	6.0	1.5
WS055	5.70	9.36	-5.2	528.8	534.0	5.0	536.2	531.2	5.7	0.5
WS056	5.80	9.40	-5.6	587.6	593.2	5.4	598.1	592.7	6.3	0.1
WS057	5.90	9.96	-6.4	438.5	444.8	5.8	445.9	440.1	4.5	1.1
WS058	6.00	9.37	-6.1	370.7	376.7	6.2	379.2	373.1	4.0	1.0
WS059	6.10	8.74	-5.6	248.0	253.6	6.5	256.8	250.3	2.9	1.3

WS060	6.20	9.19	-6.1	218.1	224.2	6.7	229.6	222.9	2.4	0.6
WS061	6.30	9.30	-6.8	188.3	195.1	7.1	202.4	195.3	2.1	-0.1
WS062	6.40	9.84	-6.9	217.3	224.1	7.2	232.0	224.8	2.3	-0.3
WS063	6.50	10.37	-6.9	246.3	253.2	7.4	261.6	254.2	2.4	-0.4
WS064	6.60	10.79	-6.9	240.5	247.3	7.5	255.6	248.1	2.3	-0.3
WS065	6.70	11.20	-6.9	234.7	241.5	7.6	249.6	242.1	2.2	-0.2
WS066	6.80	10.99	-6.9	237.6	244.4	7.5	252.6	245.1	2.2	-0.3
WS067	6.90	9.33	-6.7	63.3	69.9	7.9	77.1	69.2	0.7	1.0
WS068	7.00	9.44	-6.7	67.0	73.7	4.2	77.2	73.0	0.8	1.7
WS069	7.10	9.54	-6.7	70.8	77.5	0.6	77.4	76.8	0.8	2.1
WS070	7.20	9.71	-7.3	74.0	81.3	1.2	80.5	79.3	0.8	2.5
WS071	7.30	10.12	-7.6	77.3	84.9	1.3	84.1	82.8	0.8	2.5
WS072	7.40	10.57	-8.0	105.0	113.0	1.5	111.9	110.4	1.1	2.3
WS073	7.50	9.96	-8.1	104.7	112.8	1.6	110.8	109.2	1.1	3.1
WS074	7.60	10.48	-7.6	135.3	142.8	2.1	142.1	140.0	1.4	2.0
WS075	7.70	9.60	-7.4	260.9	268.3	2.5	265.3	262.9	2.8	2.0
WS076	7.80	9.02	-8.1	301.6	309.6	2.6	306.5	303.9	3.4	1.9
WS077	7.90	7.04	-8.8	260.7	269.5	3.2	268.6	265.5	3.8	1.5
WS078	8.00	8.18	-8.4	296.6	304.9	4.1	304.7	300.6	3.7	1.4
WS079	8.05	7.41	-8.0	309.0	317.0	4.5	318.8	314.4	4.3	0.8
WS080	8.10	8.57	-8.2	338.6	346.8	4.4	347.9	343.5	4.0	1.0
WS081	8.20	8.65	-8.5	193.0	201.5	4.4	203.5	199.1	2.3	1.2
WS082	8.30	8.00	-9.0	145.9	154.9	4.8	154.3	149.5	1.9	3.5
WS083	8.40	9.07	-9.1	216.4	225.5	5.3	222.1	216.8	2.5	3.9
WS084	8.50	9.46	-8.9	278.1	287.0	5.8	279.6	273.8	3.0	4.6
WS085	8.60	8.75	-8.8	263.1	271.9	6.1	264.5	258.4	3.1	5.0
WS086	8.70	8.76	-9.0	215.3	224.3	6.3	221.8	215.5	2.6	3.9
WS087	8.80	8.59	-9.2	302.7	311.9	6.7	311.1	304.4	3.6	2.4
WS088	8.90	8.91	-9.3	436.6	445.8	0.0	441.2	441.2	5.0	1.0
WS089	9.00	7.53	-9.3	114.5	123.8	0.2	120.6	120.4	1.6	2.7
WS090	9.10	7.77	-9.4	208.1	217.5	0.5	211.5	211.0	2.8	3.0
WS091	9.15	7.94	-9.6	278.0	287.5	0.6	280.3	279.7	3.6	2.7
WS092	9.25	8.48	-9.5	323.7	333.1	0.8	330.9	330.1	3.9	0.9
WS093	9.30	8.04	-9.7	384.9	394.6	1.1	394.4	393.3	4.9	0.3
WS094	9.40	8.58	-10.1	138.6	148.7	1.4	149.5	148.1	1.7	0.4
WS095	9.50	9.08	-0.1	48.3	48.4	1.8	49.6	47.8	0.5	1.2
WS096	9.60	9.17	-0.3	58.2	58.5	2.1	60.0	57.9	0.6	1.0
WS097	9.70	9.65	-0.1	127.0	127.1	2.5	129.6	127.1	1.3	0.0
WS098	9.80	9.24	-0.2	161.7	161.8	2.8	164.0	161.3	1.8	0.3
WS099	9.85	9.55	-0.8	204.7	205.4	2.9	202.9	200.1	2.2	0.8
WS100	9.90	9.67	-1.1	238.0	239.1	3.1	233.4	230.3	2.5	3.7
WS101	9.95	9.40	-0.6	246.8	247.3	3.5	242.3	238.9	2.6	3.4
WS102	10.00	10.20	-0.8	302.4	303.2	3.7	297.0	293.4	3.0	3.2
WS103	10.05	10.18	-1.7	354.3	356.0	3.9	350.0	346.1	3.5	2.8
WS104	10.10	11.27	-0.4	428.6	429.0	2.5	417.4	414.9	3.8	3.3
WS105	10.20	9.26	-1.5	374.6	376.1	4.3	374.3	370.0	4.1	1.6
WS106	10.25	10.48	-0.7	424.7	425.4	3.0	422.8	419.8	4.1	1.3
WS107	10.30	10.39	-2.2	459.1	461.2	3.5	459.9	456.4	4.4	1.1
WS108	10.35	9.90	-2.3	442.8	445.1	3.5	445.2	441.7	4.5	0.8
WS109	10.40	9.31	-1.9	327.5	329.4	3.6	328.6	325.0	3.5	1.3
WS110	10.45	9.00	-2.3	277.4	279.7	4.5	281.5	277.0	3.1	0.9
WS111	10.50	9.26	-3.0	240.0	242.9	5.1	246.0	241.0	2.6	0.8
WS112	10.55	9.96	-3.2	183.9	187.1	5.8	191.7	186.0	1.9	0.6
WS113	10.60	10.83	-4.1	147.5	151.6	6.4	155.2	148.8	1.4	1.8
WS114	10.65	11.11	-4.6	155.0	159.6	6.9	163.2	156.3	1.4	2.1
WS115	10.70	11.20	-4.3	166.3	170.5	7.5	175.4	168.0	1.5	1.5
WS116	10.73	10.48	-6.6	152.7	159.3	7.9	162.8	155.0	1.5	2.7
WS117	10.75	10.10	-7.1	100.9	107.9	8.2	114.0	105.9	1.1	1.9
WS118	10.80	10.78	-7.7	108.7	116.3	8.5	122.1	113.6	1.1	2.3
WS119	10.83	10.37	-8.1	112.6	120.7	8.8	126.5	117.7	1.2	2.4
WS120	10.85	10.40	-8.7	123.2	131.9	9.1	136.4	127.3	1.3	3.5
WS121	10.90	9.72	-9.2	102.5	111.7	9.5	115.9	106.5	1.1	4.7
WS122	10.93	9.50	-9.4	101.3	110.6	0.1	107.6	107.5	1.2	2.8
WS123	10.95	9.42	-9.7	120.7	130.4	0.4	125.0	124.6	1.4	4.4

WS124	10.98	9.82	-0.1	150.0	150.1	0.8	145.2	144.5	1.5	3.8
WS125	11.00	8.57	0.5	155.0	154.5	1.2	151.0	149.9	1.8	3.0
WS126	11.05	8.31	-0.6	142.2	142.8	1.5	135.8	134.4	1.7	5.9
WS127	11.08	8.72	-0.6	148.8	149.4	1.8	145.8	144.1	1.7	3.5
WS128	11.10	8.81	-1.5	149.1	150.6	2.0	146.2	144.3	1.7	4.2
WS129	11.15	8.74	-1.8	145.7	147.5	2.2	142.9	140.7	1.7	4.6
WS130	11.18	8.91	-2.1	138.0	140.1	2.6	135.8	133.3	1.6	4.9
WS131	11.20	9.16	-2.4	144.0	146.4	2.9	142.8	140.0	1.6	4.4
WS132	11.25	9.66	-2.8	154.1	156.9	3.2	148.6	145.5	1.6	7.3
WS133	11.30	10.24	-3.1	162.4	165.5	3.5	161.7	158.2	1.6	4.4
WS134	11.33	10.21	-3.4	152.2	155.6	3.8	152.0	148.2	1.5	4.7
WS135	11.35	10.12	-3.3	158.4	161.6	4.1	158.1	154.1	1.6	4.7
WS136	11.38	9.89	-4.1	163.6	167.7	4.2	164.0	159.8	1.7	4.7
WS137	11.40	9.61	-3.3	174.8	178.0	4.4	175.7	171.4	1.9	3.7
WS138	11.45	9.77	-3.1	193.9	197.0	4.8	192.7	188.0	2.0	4.6
WS139	11.50	10.30	-3.1	245.9	249.0	5.2	245.5	240.3	2.4	3.5
WS140	11.55	9.95	-3.4	252.1	255.5	5.6	252.8	247.3	2.6	3.2
WS141	11.60	8.84	-3.7	186.5	190.1	5.7	189.3	183.6	2.2	3.4
WS142	11.65	8.07	-3.8	142.1	145.9	5.9	146.3	140.5	1.8	3.7
WS143	11.70	8.46	-4.0	149.3	153.3	6.2	154.0	147.8	1.8	3.6
WS144	11.75	9.21	-4.1	66.3	70.4	6.6	74.0	67.5	0.8	4.2
WS145	11.80	8.39	-4.1	79.3	83.4	6.8	86.9	80.2	1.0	3.9
WS146	11.85	8.22	-4.2	73.5	77.7	6.9	81.3	74.5	0.9	4.2
WS147	11.88	8.21	-4.6	73.5	78.1	7.1	81.3	74.3	1.0	4.9
WS148	11.90	8.16	-4.7	77.7	82.4	7.3	85.6	78.3	1.0	4.9
WS149	11.93	8.83	-5.0	82.8	87.8	7.6	91.1	83.6	1.0	4.8
WS150	11.95	8.64	-5.3	77.6	82.9	7.9	86.1	78.3	1.0	5.6
WS151	12.00	9.06	-5.2	84.8	90.0	8.1	92.2	84.1	1.0	6.6
WS152	12.05	9.51	-5.3	125.3	130.5	8.4	131.1	122.7	1.4	6.0
WS153	12.10	8.58	-5.4	60.0	65.3	8.7	71.9	63.2	0.8	3.2
WS154	12.15	8.54	-5.2	35.5	40.7	8.9	48.8	40.0	0.5	1.7
WS155	12.20	9.46	-5.2	37.5	42.7	9.1	51.4	42.3	0.5	0.9
WS156	12.25	9.95	-5.5	36.4	41.9	9.4	50.5	41.2	0.4	1.7
WS157	12.30	10.49	-5.3	37.3	42.6	9.5	50.0	40.5	0.4	1.7
WS158	12.35	11.07	-5.2	38.8	44.0	9.7	52.9	43.2	0.4	1.8
WS159	12.40	10.81	-5.2	39.6	44.8	10.0	53.8	43.9	0.4	2.1
WS160	12.45	11.13	-5.4	37.8	43.1	10.2	52.3	42.2	0.4	2.2
WS161	12.50	10.75	-5.7	41.3	47.0	10.3	55.8	45.6	0.4	3.0
WS162	12.55	10.76	-5.5	38.4	43.9	1.2	45.4	44.2	0.4	2.9
WS163	12.60	10.69	-5.5	44.0	49.5	2.5	50.6	48.1	0.5	2.7
WS164	12.70	10.89	-5.4	46.6	52.0	2.7	53.1	50.5	0.5	3.0
WS165	12.80	10.74	-5.3	46.8	52.1	3.1	53.7	50.6	0.5	2.9
WS166	12.85	10.16	-5.4	42.2	47.6	3.5	50.3	46.8	0.5	1.7
WS167	12.90	10.08	-5.5	39.9	45.4	3.7	48.0	44.4	0.5	2.3
WS168	12.95	10.98	-5.5	50.3	55.8	3.7	57.6	54.0	0.5	3.2
WS169	13.00	11.48	-5.4	84.2	89.6	3.8	91.3	87.6	0.8	2.2
WS170	13.05	11.46	-5.4	63.3	68.7	4.1	70.5	66.5	0.6	3.2
WS171	13.10	11.34	-5.3	53.1	58.4	4.4	60.8	56.5	0.5	3.3
WS172	13.20	10.88	-5.4	29.6	35.0	4.6	38.1	33.6	0.3	4.1
WS173	13.30	10.69	-5.3	34.9	40.2	4.9	40.0	35.1	0.4	2.8
WS174	13.40	11.19	-5.0	36.7	41.7	5.2	46.3	41.1	0.4	1.4
WS175	13.50	10.61	-5.0	55.3	60.3	5.3	64.2	58.9	0.6	2.2
WS176	13.60	10.78	-5.0	112.8	117.8	5.3	121.1	115.8	1.1	1.7
WS177	13.70	10.58	-5.3	137.8	143.1	5.4	145.2	139.9	1.4	2.3
WS178	14.10	9.81	-5.9	1134.4	1140.3	5.7	1109.1	1103.5	11.6	3.2



## PAPAKURA CREEK

Sample	Depth	Sample	Low Frequency			High Frequency			MSS	Xfd%
		Weight	Av A	Av M	Corr K	Av A	Av M	Corr K		
OP001	0.60	10.12	-0.8	893.5	894.3	0.6	888.4	887.8	8.8	0.7
OP002	1.00	10.29	-1.1	965.9	966.9	1.0	957.0	956.0	9.4	1.1
OP003	1.40	10.46	-1.4	1038.2	1039.5	1.5	1025.6	1024.2	9.9	1.5
OP004	2.10	10.49	-1.5	748.8	750.3	1.7	739.1	737.5	6.4	1.7
OP005	2.80	10.51	-1.7	459.4	461.1	1.9	452.6	450.8	4.4	2.2
OP006	3.20	11.13	-1.7	639.9	641.5	2.0	636.6	634.7	5.0	1.1
OP007	3.60	11.75	-1.7	820.3	822.0	2.1	820.6	818.6	7.0	0.4
OP008	3.70	11.85	-1.7	1190.4	1192.0	2.1	1191.0	1188.9	10.0	0.3
OP009	3.80	11.95	-1.7	1560.4	1562.1	2.2	1561.4	1559.2	13.1	0.2
OP010	3.90	11.00	-1.8	1352.5	1354.3	2.3	1353.1	1350.8	12.0	0.3
OP011	4.00	10.04	-2.0	1144.6	1146.6	2.5	1144.9	1142.4	11.4	0.4
OP012	4.10	10.34	-1.0	1552.2	1553.2	2.5	1553.7	1551.2	14.9	0.1
OP013	4.20	10.63	-0.1	1959.8	1959.9	2.6	1962.6	1960.1	18.4	0.0
OP014	4.35	10.38	-0.1	1838.4	1838.5	2.6	1841.3	1838.7	17.2	0.0
OP015	4.50	10.12	-0.1	1717.0	1717.1	2.6	1720.0	1717.4	17.0	0.0
OP016	4.65	9.38	-0.3	1192.6	1192.9	2.7	1195.6	1193.0	13.0	0.0
OP017	4.80	8.63	-0.5	668.2	668.7	2.7	671.3	668.6	7.7	0.0
OP018	5.00	8.55	-0.7	435.4	436.1	2.7	438.1	435.4	3.5	0.2
OP019	5.20	8.46	-0.9	202.6	203.5	2.7	205.0	202.3	2.4	0.6
OP020	5.30	9.29	-0.9	302.8	303.7	1.4	303.8	302.4	2.8	0.4
OP021	5.40	10.11	-0.9	403.1	404.0	0.1	402.7	402.6	4.0	0.3
OP022	5.45	10.88	-1.0	402.4	403.4	0.4	402.6	402.2	3.7	0.3
OP023	5.50	11.64	-1.1	401.7	402.8	0.7	402.6	401.9	3.5	0.2
OP024	5.60	12.06	-1.2	298.1	299.3	1.0	299.3	298.4	2.0	0.3
OP025	5.70	12.48	-1.3	194.5	195.8	1.2	196.1	194.9	1.6	0.5
OP026	5.80	11.02	-1.4	187.8	189.2	1.5	189.3	187.9	1.7	0.7
OP027	5.90	9.56	-1.4	181.1	182.5	1.7	182.5	180.8	1.9	0.9
OP028	6.00	9.89	-1.3	212.5	213.8	2.0	212.7	210.7	2.2	1.5
OP029	6.10	10.22	-1.3	243.8	245.1	2.3	242.8	240.6	2.4	1.8
OP030	6.20	10.33	-1.4	257.6	259.0	2.5	256.0	253.5	2.5	2.1
OP031	6.30	10.43	-1.5	271.5	272.9	2.7	269.1	266.5	2.6	2.4
OP032	6.40	10.63	-1.6	256.3	257.9	1.4	252.9	251.5	2.4	2.5
OP033	6.50	10.82	-1.8	241.1	242.9	0.2	236.7	236.5	2.2	2.6
OP034	6.65	10.80	-1.8	184.1	185.9	0.4	181.1	180.7	1.8	2.8
OP035	6.80	10.78	-1.8	127.1	128.9	0.6	125.6	125.0	1.2	3.1
OP036	6.90	10.51	-1.8	188.1	189.8	0.7	186.0	185.3	1.8	2.4
OP037	7.00	10.24	-1.7	249.0	250.7	0.8	246.4	245.7	3.0	2.0
OP038	7.10	9.97	-1.7	310.0	311.6	0.8	306.8	306.0	3.4	1.8
OP039	7.20	9.70	-1.7	370.9	372.6	0.9	367.3	366.4	3.8	1.7
OP040	7.35	9.76	-1.7	340.8	342.5	1.1	334.1	333.0	3.5	2.8
OP041	7.50	9.81	-1.8	310.7	312.5	1.4	301.0	299.6	3.2	4.1
OP042	7.60	10.21	-1.1	320.7	321.8	1.7	312.3	310.6	3.2	3.5
OP043	7.70	10.60	-0.4	330.7	331.1	2.1	323.6	321.6	3.1	2.9
OP044	7.80	10.52	-0.6	302.4	303.1	2.3	294.9	292.6	2.9	3.5
OP045	7.90	10.43	-0.9	274.2	275.1	2.5	266.1	263.6	2.6	4.2
OP046	8.00	10.44	-0.9	263.7	264.6	2.9	255.0	252.1	2.5	4.7
OP047	8.10	10.45	-0.9	253.2	254.1	3.2	243.8	240.6	2.4	5.3
OP048	8.15	10.36	-0.5	219.1	219.6	1.7	210.3	208.6	2.1	5.0
OP049	8.20	10.26	-0.1	184.9	185.0	0.2	176.8	176.6	1.8	4.5
OP050	8.25	10.63	-0.1	195.4	195.6	0.4	188.1	187.8	1.8	4.0
OP051	8.30	11.00	-0.2	206.0	206.1	0.6	199.5	198.9	1.9	3.5
OP052	8.38	10.60	0.0	221.7	221.7	0.9	215.1	214.1	2.1	3.4
OP053	8.45	10.20	0.2	237.4	237.3	1.3	230.7	229.4	2.3	3.3
OP054	8.53	9.85	0.3	286.1	285.8	0.9	278.4	277.5	2.9	2.9
OP055	8.60	9.49	0.4	334.8	334.4	0.4	326.1	325.7	3.5	2.6
OP056	8.70	9.98	0.4	284.8	284.3	1.0	279.4	278.4	2.9	2.1
OP057	8.80	10.47	0.5	234.8	234.3	1.7	232.7	231.0	2.2	1.4
OP058	8.85	10.25	0.4	187.5	187.1	1.9	186.3	184.5	1.8	1.4
OP059	8.90	10.02	0.4	140.3	140.0	2.1	140.0	137.9	1.4	1.5
OP060	9.00	9.92	0.2	127.9	127.7	2.3	128.2	125.9	1.3	1.4

OP061	9.10	9.82	0.0	115.4	115.4	2.6	116.5	113.9	1.2	1.3
OP062	9.18	10.17	0.2	89.2	89.0	3.0	90.8	87.8	0.9	1.3
OP063	9.25	10.51	0.5	63.0	62.6	3.4	65.1	61.7	0.6	1.4
OP064	9.33	11.21	0.4	65.9	65.5	3.6	68.4	64.8	0.6	1.1
OP065	9.40	11.90	0.4	68.9	68.5	3.9	71.7	67.9	0.6	0.9
OP066	9.48	11.26	0.1	133.0	132.9	4.0	134.3	130.3	1.2	2.0
OP067	9.55	10.62	-0.2	197.2	197.3	4.1	196.9	192.8	1.9	2.3
OP068	9.63	10.81	-0.2	236.6	236.7	4.3	235.1	230.8	2.2	2.5
OP069	9.70	10.99	-0.2	276.0	276.2	4.5	273.4	268.9	2.5	2.6
OP070	9.75	10.92	-0.2	364.5	364.7	4.8	360.1	355.2	3.3	2.6
OP071	9.80	10.85	-0.2	453.1	453.3	5.2	446.8	441.6	4.2	2.6
OP072	9.83	10.95	-0.4	520.7	521.0	2.7	513.2	510.5	4.8	2.0
OP073	9.85	11.05	-0.6	588.2	588.8	0.2	579.6	579.4	5.3	1.6
OP074	9.95	10.09	-0.5	601.7	602.3	0.4	595.5	595.1	5.8	1.2
OP075	10.05	9.13	-0.5	615.3	615.7	0.6	611.4	610.8	6.7	0.8
OP076	10.18	9.13	-0.5	597.9	598.4	0.7	594.6	594.0	6.6	0.7
OP077	10.30	9.13	-0.5	580.6	581.0	0.8	577.9	577.1	6.4	0.7
OP078	10.40	9.28	-0.6	552.6	553.2	0.9	551.3	550.4	6.0	0.5
OP079	10.50	9.42	-0.8	524.7	525.4	1.0	524.7	523.7	5.6	0.3
OP080	10.60	9.36	-0.9	706.7	707.6	1.1	702.6	701.6	6.5	0.8
OP081	10.70	9.30	-1.0	888.7	889.7	1.2	880.6	879.4	9.6	1.2
OP082	10.80	9.22	-1.0	820.8	821.8	1.5	814.3	812.8	8.9	1.1
OP083	10.90	9.14	-1.1	752.8	753.9	1.8	748.1	746.3	8.2	1.0
OP084	11.00	9.56	-1.0	775.6	776.6	2.0	769.7	767.7	8.1	1.1
OP085	11.10	9.98	-1.0	798.4	799.4	2.2	791.4	789.2	8.0	1.3
OP086	11.25	9.82	-1.0	726.6	727.6	2.4	721.3	718.9	7.4	1.2
OP087	11.40	9.66	-1.0	654.9	655.9	2.5	651.2	648.7	6.8	1.1
OP088	14.30	10.25	0.0	619.0	619.0	0.4	606.7	606.3	6.0	2.1
OP089	14.40	10.19	-0.2	555.0	555.2	0.8	544.4	543.6	5.4	2.1
OP090	14.45	9.99	-0.5	352.8	353.3	1.0	343.4	342.4	3.5	3.1
OP091	14.50	10.42	-0.7	457.0	457.6	1.2	449.5	448.4	4.4	2.0
OP092	14.60	10.68	-1.1	653.6	654.7	1.3	651.3	650.0	6.1	0.7
OP093	14.65	11.29	-1.4	1213.8	1215.1	1.4	1217.6	1216.2	10.8	-0.1
OP094	14.70	11.88	-1.7	1267.9	1269.6	-0.2	1271.6	1271.7	10.7	-0.2
OP095	14.75	11.37	-2.0	1073.1	1075.1	0.0	1075.9	1075.9	9.5	-0.1
OP096	14.80	12.02	-2.1	1303.8	1305.9	0.3	1307.5	1307.2	10.9	-0.1
OP097	14.85	12.80	-2.4	731.0	733.4	0.1	734.6	734.5	5.7	-0.1
OP098	14.90	10.25	-2.8	326.3	329.1	0.4	328.1	327.7	3.2	0.4
OP099	14.95	10.13	-3.0	163.8	166.8	0.6	162.8	162.3	1.6	2.7
OP100	15.00	10.69	-3.1	137.6	140.7	0.7	138.8	138.1	1.3	1.8
OP101	15.10	11.19	-3.4	307.1	310.4	1.0	304.5	303.5	2.8	2.2
OP102	15.20	11.41	-3.7	307.6	311.3	1.2	305.4	304.2	2.7	2.3
OP103	15.30	11.09	-3.9	275.4	279.3	1.4	273.6	272.3	2.5	2.5
OP104	15.35	11.14	-4.1	144.1	148.2	1.6	146.6	145.0	1.3	2.2
OP105	15.40	10.90	-4.3	142.3	146.6	1.8	145.6	143.9	1.3	1.9
OP106	15.45	10.65	-4.5	152.6	157.1	2.0	155.9	153.9	1.5	2.0
OP107	15.50	10.41	-4.8	179.7	184.5	2.2	181.4	179.3	1.8	2.8
OP108	15.60	10.12	-5.1	192.3	197.4	2.4	196.8	194.5	2.0	1.5
OP109	15.70	10.51	-5.4	194.0	199.4	2.7	199.1	196.5	1.9	1.5
OP110	15.75	8.73	-5.6	88.2	93.8	2.9	94.5	91.6	1.1	2.3
OP111	15.80	9.49	-5.8	89.9	95.7	3.2	96.8	93.6	1.0	2.1
OP112	15.85	8.30	-5.9	75.5	81.4	3.5	83.6	80.2	1.0	1.5
OP113	15.90	8.01	-6.2	50.7	56.9	3.7	59.6	56.0	0.7	1.6
OP114	15.95	9.28	-6.5	212.0	218.4	3.7	216.1	212.4	2.4	2.7
OP115	16.00	11.03	-6.7	302.5	309.2	3.9	305.9	302.1	2.8	2.3
OP116	16.05	10.65	-6.9	263.7	270.6	4.2	267.2	263.1	2.5	2.8
OP117	16.10	8.19	-7.1	117.4	124.5	4.3	125.1	120.8	1.5	2.9
OP118	16.15	9.41	-7.4	127.0	134.3	4.3	135.2	131.0	1.4	2.5
OP119	16.25	8.67	-7.6	169.1	176.7	4.4	176.3	171.9	2.0	2.7
OP120	16.35	8.42	-7.7	159.6	167.3	4.6	168.5	164.0	2.0	2.0
OP121	16.40	10.05	-7.9	236.0	243.9	4.6	241.9	237.3	2.4	2.7
OP122	16.45	10.07	-8.2	152.3	160.5	4.7	160.6	155.9	1.6	2.9
OP123	16.47	9.85	-8.6	206.7	215.3	4.9	214.7	209.8	2.2	2.6
OP124	16.50	9.31	-0.3	42.5	42.7	5.0	46.9	42.0	0.5	1.8

OP125	16.55	7.67	-0.4	67.3	67.7	5.2	70.9	65.8	0.9	2.9
OP126	16.57	7.56	-0.5	60.7	61.2	5.3	64.8	59.6	0.8	2.7
OP127	16.60	7.72	-0.6	81.8	82.4	5.4	85.2	79.8	1.1	3.2
OP128	16.65	7.87	-0.7	77.8	78.5	5.6	81.9	76.3	1.0	2.8
OP129	16.70	11.51	-0.8	70.2	71.0	6.7	75.8	69.1	0.6	2.6
OP130	16.75	8.14	-0.9	38.1	39.0	6.6	44.7	38.2	0.5	2.2
OP131	16.80	10.65	-1.1	54.4	55.5	6.8	60.9	54.1	0.5	2.4
OP132	16.85	11.04	-1.3	271.7	273.0	6.8	274.2	267.4	0.5	2.0
OP133	16.95	8.97	-1.5	49.7	51.2	6.8	57.4	50.6	0.6	1.1
OP134	17.00	7.96	-1.6	159.9	161.5	6.9	165.1	158.3	2.0	2.0
OP135	17.05	8.51	-2.0	198.8	200.8	6.9	202.9	196.1	2.4	2.4
OP136	17.10	8.24	-2.3	175.3	177.6	6.9	180.8	173.9	2.2	2.1
OP137	17.15	8.48	-2.4	190.5	192.9	7.1	195.5	188.4	2.3	2.3
OP138	17.20	8.66	-2.6	201.8	204.4	7.2	206.6	199.4	2.4	2.4
OP139	17.25	8.80	-2.7	234.0	236.7	7.2	238.0	230.8	2.7	2.5
OP140	17.35	11.53	-2.9	241.8	244.7	7.3	245.9	238.7	2.1	2.5
OP141	17.40	8.99	-3.2	293.4	296.6	7.4	296.8	289.4	3.3	2.4
OP142	17.45	8.83	-3.4	299.3	302.7	7.5	303.0	295.5	3.4	2.4
OP143	17.50	9.06	-3.6	309.3	312.9	7.5	312.9	305.4	3.5	2.4
OP144	17.55	8.49	-3.7	299.5	303.2	7.6	303.4	295.8	3.6	2.4
OP145	17.60	9.49	-4.0	280.4	284.4	7.7	285.7	278.0	3.0	2.2
OP146	17.65	10.01	-4.1	258.3	262.4	7.7	264.7	257.0	2.6	2.1
OP147	17.70	10.28	-4.2	273.7	277.9	7.8	280.3	272.5	2.7	1.9
OP148	17.75	10.97	-4.4	334.7	339.1	7.9	340.1	332.2	3.1	2.0
OP149	17.80	10.77	-4.4	332.9	337.3	8.0	339.6	331.7	3.1	1.7
OP150	17.85	10.83	-4.6	344.2	348.8	8.1	352.7	344.7	3.2	1.2
OP151	17.90	10.39	-4.8	268.8	273.6	8.1	278.9	270.8	2.6	1.0
OP152	17.95	10.34	-5.0	287.7	292.7	8.2	298.8	290.6	2.8	0.7
OP153	18.00	11.26	-5.2	416.2	421.4	8.4	425.9	417.6	3.7	0.9
OP154	18.05	10.92	-5.3	368.0	373.3	8.4	378.9	370.5	3.4	0.8
OP155	18.10	11.44	-5.5	387.9	393.4	8.4	399.0	390.6	3.4	0.7
OP156	18.15	11.37	-5.7	415.1	420.8	8.5	427.4	418.9	3.7	0.4
OP157	18.26	11.56	-5.8	407.1	412.9	8.6	419.6	411.0	3.6	0.4
OP158	18.30	12.35	-6.0	463.6	469.6	8.6	475.3	466.7	3.8	0.6

## TIRITIRIMATANGI PENINSULA

Sample	Depth	Sample Weight	Low Frequency			High Frequency			MSS	Xfd%
			Av A	Av M	Corr K	Av A	Av M	Corr K		
TTB02	7.00	9.76	-7.15	345.65	352.80	9.80	356.60	346.80	3.61	1.70
TT040	7.10	10.37	-0.20	1771.47	1771.67	9.70	1772.60	1762.90	17.08	0.49
TT041	7.20	10.09	-0.60	1853.83	1854.43	10.00	1855.10	1845.10	18.38	0.50
TT042	7.30	9.87	-1.20	1973.20	1974.40	10.45	1980.20	1969.75	20.00	0.24
TT043	7.40	9.40	-1.70	1860.10	1861.80	10.90	1871.80	1860.90	19.81	0.05
TT044	7.50	9.57	-2.20	1840.83	1843.03	11.15	1854.50	1843.35	19.26	-0.02
TT045	7.60	9.42	-0.25	1854.47	1854.72	0.35	1853.25	1852.90	19.69	0.10
TT046	7.70	9.02	-0.70	1825.10	1825.80	0.75	1829.60	1828.85	20.24	-0.17
TT047	7.80	9.92	-1.05	2114.37	2115.42	1.10	2119.60	2118.50	21.32	-0.15
TT048	7.90	9.75	-1.30	2103.55	2104.85	1.55	2106.30	2104.75	21.59	0.00
TT049	8.00	9.45	-1.45	2085.00	2086.45	1.95	2091.20	2089.25	22.08	-0.13
TT050	8.10	10.47	-1.70	2252.35	2254.05	2.25	2259.50	2257.25	21.53	-0.14
TT051	8.20	10.83	-1.90	2336.15	2338.05	2.60	2343.90	2341.30	21.59	-0.14
TT052	8.30	10.47	-2.10	2296.10	2298.20	3.05	2304.50	2301.45	21.95	-0.14
TT053	8.40	10.12	-2.35	2217.95	2220.30	3.55	2227.85	2224.30	21.94	-0.18
TT054	8.50	9.81	-2.60	2088.70	2091.30	4.05	2099.20	2095.15	21.32	-0.18
TT055	8.60	9.83	-2.90	1876.90	1879.80	4.50	1888.40	1883.90	19.12	-0.22
TT056	8.70	9.69	-3.25	1654.30	1657.55	4.90	1665.70	1660.80	17.11	-0.20
TT?IA	9.70	8.84	-7.65	368.30	375.95	10.25	388.25	378.00	4.25	-0.55
TT060	9.80	10.18	-3.65	530.30	533.95	5.25	541.00	535.75	5.25	-0.34
TT061	9.90	8.99	-3.95	213.00	216.95	5.60	221.70	216.10	2.41	0.39
TT062	10.00	9.67	-4.30	235.65	239.95	6.00	245.40	239.40	2.48	0.23
TT063	10.10	10.25	-4.70	294.65	299.35	6.35	306.10	299.75	2.92	-0.13
TT064	10.20	10.59	-5.10	43.60	48.70	6.65	54.70	48.05	0.46	1.33
TTB01	10.60	9.95	-6.95	36.90	43.85	9.50	52.05	42.55	0.44	2.96
TT065	11.20	10.74	-5.45	36.05	41.50	6.95	48.00	41.05	0.39	1.08
TT066	11.30	10.90	-5.85	30.15	36.00	7.30	43.10	35.80	0.33	0.56
TT067	11.40	11.00	-6.30	23.25	29.55	7.65	36.60	28.95	0.27	2.03
TT068	11.50	11.31	-6.65	24.15	30.80	7.90	37.80	29.90	0.27	2.92
TT069	11.60	11.36	-6.95	14.85	21.80	8.20	29.70	21.50	0.19	1.38
TT070	11.70	11.19	-7.35	218.40	225.75	8.70	233.40	224.70	2.02	0.47
TT071	11.80	10.21	-7.80	222.95	230.75	9.10	239.30	230.20	2.26	0.24
Base TTOP	13.30	7.00	-8.65	185.95	194.60	8.70	204.50	195.80	2.78	-0.62
Top TTOP	14.80	9.18	-8.25	496.85	505.10	9.10	515.10	506.00	5.50	-0.18
TT075	14.90	11.24	-0.50	9.55	10.05	0.40	10.35	9.95	0.09	1.00
TT076	15.00	10.70	-0.85	11.30	12.15	0.85	12.70	11.85	0.11	2.47
TT077	15.10	10.46	-1.20	4.50	5.70	1.45	6.75	5.30	0.05	7.02
TT078	15.20	10.22	-1.50	12.50	14.00	2.10	15.40	13.30	0.14	5.00
TT079	15.30	9.80	-1.75	3.20	4.95	2.50	7.30	4.80	0.05	3.03
TT080	15.40	9.60	-2.00	8.85	10.85	3.00	13.50	10.50	0.11	3.23
TT081	15.50	9.74	-2.25	13.75	16.00	3.45	19.15	15.70	0.16	1.88
TT082	15.60	9.44	-2.50	10.30	12.80	3.85	16.25	12.40	0.14	3.13
TT083	15.70	9.67	-2.75	7.80	10.55	4.35	14.30	9.95	0.11	5.69
TT084	15.80	9.61	-3.10	12.15	15.25	4.85	19.85	15.00	0.16	1.64
TT085	15.90	9.26	-3.35	16.90	20.25	5.25	25.45	20.20	0.22	0.25
TT086	16.00	9.85	-3.55	35.85	39.40	5.50	43.95	38.45	0.40	2.41
TT087	16.10	9.58	-3.85	95.80	99.65	5.75	103.00	97.25	1.04	2.41
TT088	16.20	9.92	-4.10	170.25	174.35	5.95	177.40	171.45	1.76	1.66
TT089	16.30	10.18	-4.40	190.45	194.85	6.25	198.70	192.45	1.91	1.23
TT090	16.50	9.65	-4.80	212.15	216.95	6.55	221.80	215.25	2.25	0.78
TT091	16.70	9.72	-5.00	210.00	215.00	6.80	219.60	212.80	2.21	1.02
TT092	16.90	9.24	-5.10	179.10	184.20	7.05	188.10	181.05	1.99	1.71
TT093	17.10	9.23	-5.30	157.55	162.85	7.40	166.30	158.90	1.76	2.43
TT094	17.30	9.22	-5.65	197.70	203.35	7.70	206.30	198.60	2.21	2.34
TT095	17.50	9.51	-6.05	366.60	372.65	7.90	375.70	367.80	3.92	1.30
TT096	17.70	9.89	-6.30	418.80	425.10	8.05	431.90	423.85	4.30	0.29
TT097	17.90	9.94	-6.65	302.50	309.15	8.30	314.05	305.75	3.11	1.10
Top TT	23.90	6.99	-7.40	476.50	483.90	10.00	496.10	486.10	6.92	-0.45
TT001	23.95	12.04	-0.90	60.30	61.20	0.20	55.10	54.90	0.51	10.29
TT002	24.00	11.54	-1.58	9.10	10.68	0.55	10.70	10.15	0.09	4.96

TT003	24.02	11.06	-2.23	9.80	12.03	0.80	12.40	11.60	0.11	3.57
TT004	24.05	8.84	-2.75	7.60	10.35	1.10	11.20	10.10	0.12	2.42
TT005	24.07	9.23	-3.25	10.73	13.98	1.45	15.00	13.55	0.15	3.10
TT006	24.10	8.19	-3.75	24.80	28.55	1.80	29.95	28.15	0.35	1.40
TT007	24.15	10.38	-4.55	91.60	96.15	2.00	97.40	95.40	0.93	0.78
TT008	24.20	10.64	-5.10	33.87	38.97	2.15	40.10	37.95	0.37	2.61
TT009	24.25	10.60	-5.60	41.90	47.50	2.45	48.40	45.95	0.45	3.26
TT010	24.30	10.25	-6.10	45.97	52.07	2.75	52.90	50.15	0.51	3.68
TT011	24.35	8.27	-6.50	116.90	123.40	3.00	126.40	123.40	1.49	0.00
TT012	24.42	9.05	-6.85	305.80	312.65	3.20	313.80	310.60	3.45	0.66
TT013	24.50	9.25	-7.30	297.23	304.53	3.30	306.20	302.90	3.29	0.54
TT014	24.55	8.96	-7.75	235.60	243.35	3.35	246.80	243.45	2.72	-0.04
TT015	24.60	8.91	-8.15	179.03	187.18	3.50	190.80	187.30	2.10	-0.06
TT016	24.65	9.17	-0.50	185.73	186.23	3.70	190.70	187.00	2.03	-0.41
TT017	24.70	9.49	-1.00	116.63	117.63	3.95	121.50	117.55	1.24	0.07
TT018	24.75	9.44	-1.35	89.30	90.65	4.25	95.10	90.85	0.96	-0.22
TT019	24.80	9.71	-1.75	59.47	61.22	4.50	65.70	61.20	0.63	0.03
TT020	24.85	9.77	-2.10	123.47	125.57	6.40	131.10	124.70	1.29	0.69
TT021	24.90	10.50	-2.55	162.90	165.45	5.50	170.85	165.35	1.58	0.06
TT022	24.95	10.00	-3.05	147.67	150.72	5.90	156.40	150.50	1.51	0.14
TT023	25.00	9.83	-3.50	152.40	155.90	6.80	162.60	155.80	1.59	0.06
TT024	25.05	10.40	-4.00	184.83	188.83	7.00	195.30	188.30	1.82	0.28
TT025	25.10	10.15	-4.50	156.07	160.57	7.35	167.90	160.55	1.58	0.01
TT026	25.20	11.82	-5.00	294.30	299.30	7.90	305.40	297.50	2.53	0.60
TT027	25.30	11.57	-5.50	350.70	356.20	8.25	360.70	352.45	3.08	1.05
TT028	25.70	10.11	-6.10	296.83	302.93	8.45	309.30	300.85	3.00	0.69
TT029	26.40	10.04	-6.60	1443.00	1449.60	8.90	1451.60	1442.70	14.44	0.48
Pir.Volc.	27.40	10.55	-7.05	1900.67	1907.72	9.20	1911.90	1902.70	18.08	0.26

**POST-CBD MASS SPECIFIC SUSCEPTIBILITY**

<b>Sample</b>	<b>Depth</b>	<b>Original MSS</b>	<b>Post- CBD MSS</b>	<b>Ratio of post:pre MSS</b>
WS001	1.30	4.012	2.678	33.26
WS002	1.40	6.279	5.337	15.00
WS003	1.50	8.789	7.844	10.75
WS004	1.60	7.843	6.870	12.41
WS005	1.70	7.433	6.387	14.08
WS006	1.80	6.397	5.611	12.29
WS007	1.90	4.847	4.338	10.50
WS008	1.95	4.373	3.750	14.24
WS009	2.05	3.372	3.035	10.00
WS011	2.25	3.200	3.086	3.57
WS013	2.40	3.330	3.419	-2.66
WS015	2.50	4.190	4.261	-1.70
WS017	2.60	4.551	4.535	0.35
WS019	2.75	2.731	2.747	-0.57
WS021	2.85	2.494	2.557	-2.53
WS023	3.05	1.406	1.084	22.91
WS025	3.15	1.753	1.017	41.97
WS026	3.25	1.929	1.177	39.00
WS027	3.35	2.253	1.487	34.00
WS020	3.50	2.572	1.590	38.19
WS031	3.60	2.646	1.812	31.51
WS033	3.70	2.721	1.967	27.72
WS035	3.80	3.809	2.505	34.22
WS036	3.85	5.108	3.966	22.35
WS037	3.95	5.725	5.012	12.45
WS038	4.05	4.279	3.851	10.00
WS039	4.15	4.190	3.696	11.79
WS040	4.25	3.648	2.866	21.44
WS041	4.35	3.636	2.385	34.40
WS042	4.45	2.104	1.368	35.00
WS043	4.55	1.280	0.872	31.90
WS044	4.65	2.238	1.164	48.00
WS045	4.70	3.001	1.487	50.45
WS046	4.80	3.593	1.976	45.00
WS047	4.90	2.946	2.211	24.97
WS048	5.00	1.596	1.470	7.88
WS049	5.10	1.398	1.404	-0.44
WS050	5.20	3.487	1.950	44.09
WS051	5.30	4.338	2.495	42.47
WS052	5.40	4.789	2.873	40.00
WS053	5.50	5.053	3.166	37.34
WS054	5.60	6.016	4.925	18.14
WS055	5.70	5.705	5.409	5.19
WS056	5.80	6.311	5.932	6.00
WS057	5.90	4.466	3.958	11.36
WS058	6.00	4.020	3.278	18.48
WS059	6.10	2.901	1.988	31.49
WS060	6.20	2.440	1.901	22.07
WS061	6.30	2.097	2.205	-5.13
WS062	6.50	2.441	2.612	-7.00
WS063a	6.70	2.156	2.328	-7.94
WS063b	6.80	2.225	2.380	-7.00
WS064	7.00	0.781	0.593	24.00
WS054	7.10	0.812	0.578	28.87
WS066	7.20	0.837	0.561	33.00
WS067	7.30	0.838	0.525	37.38
WS069	7.50	1.132	0.563	50.31
WS070	7.60	1.363	0.874	35.88
WS071	7.70	2.795	1.840	34.16
WS073	7.90	3.828	3.209	16.18

WS075	8.05	4.277	3.688	13.79
WS076	8.10	4.047	3.959	2.17
WS077	8.20	2.329	1.509	35.22
WS078	8.30	1.936	1.181	39.00
WS079	8.40	2.486	1.333	46.39
WS081	8.60	3.107	1.653	46.82
WS082	8.70	2.561	1.595	37.71
WS083	8.80	3.631	2.600	28.39
WS084	8.90	5.003	4.353	13.00
WS085	9.00	1.643	1.138	30.78
WS086	9.10	2.799	1.791	35.99
WS087	9.15	3.621	2.334	35.55
WS088	9.25	3.928	3.616	7.94
WS089	9.30	4.907	4.810	1.98
WS090	9.40	1.733	1.760	-1.59
WS091	9.50	0.533	0.455	14.64
WS092	9.60	0.637	0.574	10.00
WS093	9.70	1.317	1.210	8.10
WS094	9.80	1.751	1.488	15.00
WS095	9.85	2.151	1.324	38.45
WS097	9.95	2.631	1.488	43.46
WS098	10.00	2.973	2.081	30.00
WS099	10.05	3.497	2.657	24.00
WS100	10.10	3.806	2.978	21.77
WS101	10.20	4.062	3.724	8.32
WS102	10.25	4.059	4.222	-4.00
WS103	10.30	4.439	4.513	-1.65
WS104	10.35	4.496	4.541	-1.00
WS105	10.40	3.538	3.319	6.19
WS106	10.45	3.107	2.788	10.29
WS107	10.50	2.623	2.308	12.00
WS108	10.55	1.878	1.615	14.00
WS109	10.60	1.399	0.985	29.61
WS110	10.65	1.436	0.954	33.59
WS111	10.70	1.522	1.038	31.85
WS113	10.75	1.068	0.706	33.89
WS115	10.83	1.163	0.758	34.89
WS117	10.90	1.149	0.866	24.59
WS119	10.95	1.384	1.155	16.53
WS121	11.00	1.802	1.406	22.00
WS123	11.08	1.713	1.216	29.00
WS125	11.15	1.687	1.097	35.00
WS127	11.20	1.598	1.023	36.00
WS129	11.30	1.616	0.817	49.42
WS131	11.35	1.597	0.783	51.00
WS133	11.40	1.852	0.930	49.79
WS134	11.45	2.016	0.928	54.00
WS135	11.50	2.417	1.228	49.22
WS136	11.55	2.567	1.181	54.00
WS137	11.60	2.150	0.533	75.24
WS138	11.65	1.807	0.325	82.00
WS139	11.70	1.811	0.274	84.89
WS140	11.75	0.764	0.306	60.00
WS141	11.80	0.994	0.429	56.87
WS142	11.85	0.945	0.425	55.00
WS143	11.88	0.951	0.474	50.17
WS145	11.93	0.994	0.518	47.93
WS146	11.95	0.959	0.575	40.00
WS147	12.00	0.993	0.766	22.86
WS148	12.05	1.372	1.235	10.00
WS149	12.10	0.761	0.416	45.31

**APPENDIX B:  
PARTICLE-SIZE DATA**



**PARTICLE-SIZE DATA: WOODSTOCK**

Microns	Phi	WS001	WS003	WS005	WS007	WS009	WS009	WS011	WS013	WS015	WS017	WS019	WS021	WS021	WS023	WS025	WS027	WS029	WS031	WS033	WS035	WS037	WS039	WS039	WS041	WS043	WS045
500	1	0	0	0	0	0	0	0	0	0	0	0	0	0	0	0	0	0	0	0	0	0	0	0	0	0	0
420	1.25	0	0	0	0.1	0	0	0	0	0	0	0	0	0	0	0	0	0	0	0	0	0	0	0	0	0	0
350	1.5	0.01	0	0	0.41	0.01	0	0	0	0	0.06	0	0	0	0	0	0	0	0	0	0	0	0	0	0	0	0
300	1.75	0.12	0.01	0.02	0.71	0.1	0.08	0.05	0.03	0	0.16	0	0	0	0	0	0	0	0	0	0	0	0	0	0	0	0
250	2	0.19	0.07	0.05	0.8	0.21	0.11	0.1	0.05	0.04	0.26	0	0	0	0	0	0	0	0.01	0	0	0	0	0	0	0	0
210	2.25	0.25	0.12	0.07	0.67	0.26	0.16	0.15	0.07	0.07	0.28	0	0	0	0	0	0	0	0.01	0	0	0	0	0.01	0	0	0
177	2.5	0.32	0.17	0.1	0.45	0.28	0.19	0.19	0.09	0.1	0.24	0	0	0	0	0	0	0	0.01	0	0	0	0	0.01	0	0	0
149	2.75	0.39	0.19	0.12	0.24	0.28	0.19	0.21	0.09	0.12	0.16	0	0	0	0	0	0	0	0.02	0	0	0.02	0.02	0.01	0	0	0
125	3	0.46	0.2	0.14	0.13	0.29	0.19	0.24	0.1	0.13	0.1	0.06	0	0.04	0	0	0	0	0.03	0	0	0.04	0.08	0.02	0	0	0
105	3.25	0.58	0.23	0.21	0.17	0.33	0.21	0.29	0.14	0.15	0.08	0.1	0	0.01	0.07	0	0	0	0.08	0	0	0.07	0.15	0.03	0	0	0
88	3.5	0.73	0.31	0.35	0.33	0.43	0.29	0.39	0.21	0.2	0.12	0.18	0.04	0.11	0.13	0	0.09	0	0.16	0.02	0.05	0.12	0.23	0.06	0	0	0
74	3.75	0.9	0.47	0.55	0.57	0.58	0.42	0.54	0.29	0.27	0.21	0.33	0.27	0.21	0.25	0.03	0.14	0.04	0.28	0.11	0.1	0.17	0.34	0.1	0.06	0.01	0.02
63	4	1.04	0.67	0.81	0.84	0.75	0.59	0.73	0.38	0.34	0.33	0.52	0.47	0.31	0.41	0.11	0.2	0.12	0.43	0.21	0.15	0.21	0.46	0.15	0.14	0.09	0.1
53	4.25	1.12	0.9	1.07	1.09	0.91	0.76	0.94	0.45	0.41	0.46	0.74	0.68	0.45	0.62	0.21	0.25	0.2	0.57	0.29	0.2	0.22	0.6	0.21	0.23	0.16	0.21
44	4.5	1.14	1.13	1.35	1.32	1.08	0.94	1.14	0.49	0.46	0.61	0.97	0.9	0.62	0.88	0.29	0.3	0.28	0.72	0.39	0.22	0.24	0.75	0.29	0.34	0.24	0.3
37	4.75	1.13	1.36	1.62	1.52	1.25	1.11	1.35	0.52	0.52	0.8	1.23	1.15	0.82	1.19	0.4	0.34	0.36	0.88	0.52	0.23	0.3	0.92	0.41	0.52	0.31	0.4
31	5	1.1	1.59	1.89	1.71	1.45	1.3	1.55	0.54	0.58	1.06	1.51	1.44	1.07	1.55	0.6	0.39	0.43	1.07	0.68	0.27	0.45	1.12	0.6	0.78	0.42	0.5
26.3	5.25	1.1	1.84	2.17	1.91	1.66	1.51	1.73	0.59	0.68	1.38	1.81	1.75	1.37	1.95	0.9	0.5	0.54	1.31	0.91	0.36	0.71	1.34	0.87	1.12	0.61	0.63
22.1	5.5	1.14	2.11	2.46	2.12	1.9	1.75	1.89	0.69	0.84	1.78	2.14	2.1	1.74	2.36	1.31	0.71	0.72	1.6	1.2	0.56	1.1	1.61	1.23	1.53	0.92	0.81
18.6	5.75	1.26	2.41	2.75	2.35	2.17	2.04	2.05	0.88	1.11	2.25	2.5	2.49	2.16	2.76	1.84	1.05	1.02	1.95	1.58	0.92	1.64	1.94	1.67	2	1.37	1.06
15.6	6	1.46	2.73	3.05	2.61	2.48	2.39	2.21	1.2	1.52	2.77	2.87	2.9	2.64	3.13	2.45	1.56	1.46	2.36	2.04	1.44	2.29	2.33	2.18	2.52	1.98	1.41
13.1	6.25	1.76	3.05	3.33	2.87	2.81	2.77	2.4	1.64	2.08	3.29	3.25	3.32	3.13	3.45	3.08	2.2	2.03	2.81	2.55	2.13	3.01	2.79	2.72	3.05	2.72	1.84
11.0	6.5	2.15	3.34	3.58	3.11	3.13	3.18	2.62	2.19	2.75	3.76	3.58	3.71	3.59	3.72	3.69	2.92	2.71	3.26	3.08	2.93	3.72	3.27	3.25	3.57	3.52	2.34
9.3	6.75	2.59	3.57	3.76	3.3	3.42	3.56	2.85	2.8	3.48	4.15	3.85	4.04	3.98	3.91	4.22	3.65	3.43	3.7	3.59	3.75	4.38	3.75	3.74	4.05	4.32	2.86
7.8	7	3.06	3.72	3.84	3.42	3.66	3.9	3.08	3.43	4.19	4.43	4.04	4.3	4.28	4.04	4.64	4.31	4.11	4.08	4.06	4.51	4.92	4.18	4.16	4.49	5.02	3.36
6.6	7.25	3.49	3.78	3.76	3.39	3.82	4.16	3.31	4.02	4.79	4.58	4.14	4.45	4.47	4.09	4.93	4.83	4.69	4.4	4.45	5.15	5.32	4.52	4.49	4.84	5.57	3.8
5.5	7.5	3.86	3.69	3.64	3.33	3.85	4.26	3.5	4.52	5.24	4.56	4.11	4.46	4.54	4.05	5.07	5.17	5.11	4.62	4.75	5.6	5.54	4.74	4.74	5.08	5.9	4.17
4.6	7.75	4.09	3.59	3.48	3.23	3.86	4.31	3.63	4.91	5.45	4.52	4.07	4.43	4.47	4	5.04	5.35	5.36	4.7	4.93	5.87	5.54	4.78	4.86	5.14	5.96	4.43
3.9	8	4.16	3.47	3.28	3.1	3.82	4.28	3.75	5.18	5.44	4.44	4	4.37	4.39	3.92	4.98	5.31	5.38	4.75	4.98	5.87	5.5	4.77	4.87	5.15	5.76	4.59
3.3	8.25	4.2	3.33	3.08	2.96	3.74	4.19	3.82	5.26	5.31	4.32	3.91	4.26	4.28	3.81	4.87	5.14	5.25	4.73	4.99	5.7	5.37	4.69	4.84	5.08	5.51	4.66
2.8	8.5	4.18	3.21	2.89	2.83	3.63	4.05	3.86	5.22	5.1	4.17	3.8	4.13	4.14	3.69	4.7	4.95	5.08	4.65	4.92	5.48	5.17	4.54	4.76	4.92	5.19	4.56
2.3	8.75	4.07	3.09	2.74	2.7	3.48	3.85	3.82	5.11	4.8	3.97	3.66	3.96	3.97	3.54	4.46	4.69	4.83	4.49	4.77	5.17	4.88	4.32	4.6	4.66	4.8	4.37
2.0	9	3.89	2.98	2.6	2.58	3.28	3.59	3.7	4.86	4.41	3.72	3.49	3.74	3.78	3.35	4.16	4.34	4.49	4.23	4.51	4.76	4.5	4.01	4.34	4.31	4.35	4.09
1.64	9.25	3.71	2.91	2.53	2.49	3.09	3.34	3.55	4.55	4.01	3.46	3.32	3.54	3.54	3.17	3.85	4.01	4.15	3.95	4.21	4.35	4.12	3.69	4.06	3.94	3.92	3.8
1.38	9.5	3.4	2.78	2.42	2.37	2.8	2.98	3.23	4.02	3.46	3.08	3.01	3.2	3.22	2.88	3.42	3.52	3.67	3.53	3.75	3.78	3.6	3.24	3.62	3.44	3.41	3.35
1.16	9.75	3.09	2.67	2.35	2.28	2.54	2.65	2.92	3.47	2.93	2.7	2.7	2.85	2.9	2.6	3	3.04	3.2	3.09	3.29	3.22	3.09	2.81	3.17	2.96	2.96	2.93
0.98	10	2.94	2.72	2.44	2.33	2.45	2.49	2.78	3.11	2.62	2.45	2.57	2.64	2.7	2.49	2.71	2.78	2.9	2.79	2.95	2.84	2.72	2.53	2.88	2.64	2.65	2.77
0.82	10.25	2.89	2.88	2.64	2.47	2.46	2.43	2.75	2.86	2.4	2.28	2.53	2.51	2.58	2.48	2.5	2.63	2.7	2.58	2.69	2.56	2.42	2.34	2.69	2.41	2.44	2.77
0.69	10.5	3.15	3.3	3.13	2.92	2.82	2.7	3.07	2.97	2.57	2.41	2.81	2.64	2.73	2.78	2.57	2.86	2.85	2.63	2.72	2.6	2.38	2.49	2.82	2.46	2.48	3.29
0.58	10.75	3.6	3.88	3.79	3.56	3.38	3.18	3.62	3.34	2.98	2.76	3.3	2.94	3.06	3.28	2.83	3.32	3.22	2.88	2.97	2.86	2.51	2.85	3.17	2.72	2.69	4.12
0.49	11	3.95	4.27	4.26	4.1	3.85	3.58	4.08	3.66	3.34	3.07	3.67	3.16	3.34	3.66	3.05	3.71	3.53	3.08	3.18	3.07	2.62	3.17	3.45	2.93	2.83	4.84
0.41	11.25	4.17	4.47	4.53	4.48	4.16	3.84	4.35	3.86	3.59	3.3	3.89	3.29	3.52	3.9	3.2	3.94	3.75	3.21	3.33	3.21	2.68	3.4	3.63	3.08	2.92	5.31
0.35	11.5	4.12	4.35	4.44	4.57	4.16	3.84	4.28	3.8	3.58	3.33	3.8	3.21	3.52	3.85	3.19	3.88	3.73	3.16	3.31	3.15	2.61	3.41	3.57	3.04	2.85	5.32
0.29	11.75	3.52	3.58	3.68	4.08	3.6	3.31	3.65	3.26	3.08	2.94	3.16	2.7	3.07	3.25	2.79	3.26	3.24	2.71	2.9	2.69	2.22	2.96	3.03	2.61	2.4	4.51
0.24	12	2.52	2.42	2.5	3.12	2.63	2.42	2.64	2.36	2.24	2.22	2.17	1.89	2.28	2.28	2.09	2.27	2.38	1.98	2.19	1.94	1.6	2.17	2.17	1.89	1.71	3.16
0.21	12.25	1.55	1.37	1.43	2.08	1.65	1.51	1.62	1.47	1.39	1.46	1.25	1.12	1.48	1.36	1.37	1.34	1.52	1.24	1.44	1.2	1	1.37	1.32	1.18	1.05	1.86
0.17	12.5	0.82	0.66	0.68	1.21	0.88	0.81	0.84	0.78	0.73	0.84	0.6	0.57	0.84	0.88	0.79	0.66	0.84	0.68	0.83	0.64	0.54	0.75	0.69	0.64	0.56	0.91
0.15	12.75	0.38	0.26	0.27	0.82	0.4	0.37	0.36	0.35	0.33	0.42	0.24	0.25	0.42	0.29	0.4	0.27	0.4	0.32	0.42	0.29	0.25	0.35	0.3	0.3	0.25	0.36
0.12	13	0.14	0.09	0.1	0.27	0.15	0.14	0.12	0.13	0.12	0.18	0.08	0.1	0.17	0.11	0.17	0.1	0.16	0.13	0.18	0.12	0.11	0.14	0.12	0.12	0.11	0.13
0.10	13.25	0.05	0.02	0.02	0.1	0.05	0.05	0.04	0.05	0.04	0.07	0.02															

Microns	Phi	WS045	WS047	WS049	WS051	WS051	WS053	WS055	WS055	WS057	WS059	WS059	WS061	WS063	WS065	WS067	WS069	WS071	WS073	WS075	WS077	WS079	WS081	WS083	WS085	WS087	WS089
500	1	0	0	0	0	0	0	0	0	0	0	0	0	0	0	0	0	0	0	0	0	0	0	0	0	0	0
420	1.25	0	0	0	0	0	0	0	0	0	0	0	0	0	0	0	0	0	0	0	0	0	0	0	0	0	0
350	1.5	0	0	0	0	0	0	0	0	0	0	0	0	0	0	0	0	0	0	0	0	0	0	0	0	0	0
300	1.75	0	0	0	0	0	0.01	0	0	0	0	0	0	0	0	0	0	0	0	0	0	0	0	0	0	0	0
250	2	0	0.01	0	0	0	0.03	0	0	0	0	0	0	0	0	0	0	0	0	0	0	0	0	0	0	0.01	0.02
210	2.25	0	0.02	0	0	0	0.04	0	0	0	0	0	0	0	0	0.01	0	0	0	0	0	0	0	0	0	0.015	0.03
177	2.5	0	0.03	0	0	0	0.05	0	0	0	0	0	0	0	0	0.02	0	0	0	0	0	0	0	0	0	0.02	0.04
149	2.75	0	0.04	0	0	0	0.07	0	0	0	0	0	0	0	0	0.03	0	0	0	0	0	0	0	0	0	0.025	0.05
125	3	0	0.06	0	0	0	0.11	0	0	0	0	0	0	0	0	0.03	0	0	0	0.11	0	0	0	0	0	0.03	0.06
105	3.25	0	0.11	0	0.01	0.14	0.16	0	0.01	0	0	0	0	0	0	0.04	0	0	0	0.23	0	0	0	0	0	0.05	0.1
88	3.5	0	0.2	0.05	0.18	0.28	0.24	0	0.06	0.02	0	0	0.01	0	0.09	0.01	0.08	0	0.05	0.02	0.34	0.15	0.06	0	0.01	0.08	0.15
74	3.75	0.02	0.33	0.12	0.38	0.41	0.36	0.04	0.12	0.08	0.03	0.03	0.08	0	0.25	0.1	0.16	0.08	0.08	0.06	0.46	0.28	0.1	0	0.13	0.17	0.21
64	4	0.12	0.49	0.18	0.56	0.54	0.51	0.16	0.23	0.14	0.25	0.23	0.15	0	0.39	0.31	0.27	0.16	0.11	0.09	0.57	0.4	0.14	0	0.28	0.27	0.26
53	4.25	0.23	0.67	0.24	0.79	0.67	0.67	0.29	0.4	0.2	0.59	0.54	0.22	0	0.55	0.49	0.4	0.24	0.14	0.11	0.67	0.53	0.18	0.05	0.41	0.35	0.29
44	4.5	0.33	0.85	0.3	1.02	0.79	0.84	0.43	0.67	0.25	0.92	0.83	0.29	0	0.7	0.69	0.56	0.32	0.14	0.13	0.72	0.64	0.21	0.26	0.55	0.45	0.35
37	4.75	0.44	1.04	0.34	1.25	0.92	1.02	0.63	1.04	0.32	1.34	1.17	0.35	0	0.86	0.89	0.75	0.42	0.16	0.16	0.73	0.71	0.22	0.57	0.72	0.595	0.47
31	5	0.57	1.25	0.38	1.48	1.05	1.18	0.91	1.53	0.43	1.77	1.52	0.4	0	1.04	1.11	0.97	0.59	0.23	0.22	0.74	0.77	0.22	0.97	0.95	0.845	0.74
26.3	5.25	0.73	1.46	0.43	1.69	1.18	1.32	1.25	2.08	0.59	2.16	1.81	0.44	0	1.25	1.36	1.22	0.86	0.38	0.37	0.76	0.84	0.25	1.55	1.3	1.25	1.2
22.1	5.5	0.94	1.68	0.51	1.88	1.33	1.44	1.67	2.65	0.81	2.46	2.04	0.47	0.03	1.49	1.63	1.5	1.24	0.67	0.65	0.83	0.93	0.35	2.28	1.79	1.83	1.87
18.6	5.75	1.22	1.94	0.64	2.07	1.53	1.56	2.16	3.2	1.1	2.67	2.23	0.51	0.18	1.77	1.94	1.8	1.71	1.11	1.06	0.99	1.1	0.56	3.11	2.43	2.575	2.72
15.6	6	1.58	2.23	0.84	2.29	1.8	2.71	3.69	4.48	2.83	2.4	0.58	0.21	2.09	2.28	2.11	2.24	1.68	1.6	1.25	1.36	0.91	3.96	3.19	3.43	3.67	3.67
13.1	6.25	2.01	2.55	1.1	2.53	2.13	1.86	3.28	4.1	1.87	2.99	2.6	0.68	0.28	2.43	2.64	2.42	2.77	2.34	2.22	1.63	1.7	1.43	4.73	4.01	4.31	4.61
11.0	6.5	2.47	2.9	1.42	2.79	2.49	2.06	3.82	4.42	2.29	3.17	2.84	0.78	0.34	2.78	3	2.7	3.24	3	2.85	2.08	2.12	2.09	5.35	4.78	5.09	5.4
9.3	6.75	2.93	3.26	1.77	3.06	2.86	2.28	4.3	4.64	2.69	3.42	3.15	0.87	0.39	3.11	3.3	2.95	3.6	3.57	3.42	2.58	2.58	2.83	5.78	5.41	5.675	5.94
7.8	7	3.37	3.61	2.12	3.32	3.2	2.51	4.66	4.76	3.03	3.73	3.52	0.95	0.42	3.38	3.54	3.13	3.83	4	3.87	3.08	3.02	3.58	6.01	5.83	6.005	6.18
6.6	7.25	3.76	3.93	2.46	3.55	3.48	2.72	4.88	4.72	3.28	4.07	3.91	1	0.43	3.56	3.69	3.26	3.94	4.26	4.16	3.55	3.43	4.27	5.91	5.97	5.97	5.97
5.5	7.5	4.09	4.2	2.74	3.72	3.7	2.92	4.94	4.65	3.44	4.4	4.29	1.04	0.45	3.66	3.75	3.33	3.96	4.36	4.28	3.93	3.77	4.83	5.76	5.76	5.73	5.7
4.6	7.75	4.33	4.37	2.96	3.79	3.85	3.08	4.8	4.51	3.51	4.69	4.58	1.09	0.49	3.66	3.73	3.35	3.92	4.33	4.28	4.22	4.02	5.21	5.51	5.49	5.405	5.32
3.9	8	4.49	4.41	3.1	3.84	3.91	3.21	4.64	4.32	3.52	4.91	4.83	1.16	0.55	3.57	3.63	3.34	3.86	4.23	4.19	4.41	4.19	5.39	5.17	5.14	5.015	4.89
3.3	8.25	4.51	4.42	3.15	3.85	3.91	3.34	4.42	4.09	3.49	5.04	4.98	1.24	0.62	3.44	3.5	3.31	3.8	4.09	4.05	4.43	4.25	5.41	4.78	4.73	4.58	4.43
2.8	8.5	4.45	4.34	3.13	3.81	3.9	3.43	4.16	3.82	3.42	5.06	5.03	1.3	0.65	3.31	3.37	3.26	3.76	3.96	3.91	4.34	4.25	5.2	4.37	4.29	4.145	4
2.3	8.75	4.32	4.18	3.01	3.71	3.83	3.49	3.86	3.52	3.31	4.93	4.94	1.28	0.58	3.16	3.22	3.2	3.7	3.82	3.76	4.19	4.21	4.89	3.93	3.85	3.72	3.59
2.0	9	4.07	3.9	2.78	3.55	3.7	3.51	3.53	3.2	3.03	4.66	4.69	1.09	0.36	2.97	3.04	3.1	3.61	3.64	3.57	3.93	4.08	4.52	3.49	3.39	3.29	3.19
1.64	9.25	3.8	3.61	2.55	3.4	3.58	3.55	3.24	2.92	2.81	4.31	4.38	0.72	0.04	2.84	2.91	3.04	3.56	3.51	3.43	3.66	3.97	4.17	3.09	2.97	2.915	2.86
1.38	9.5	3.35	3.18	2.04	3.14	3.31	3.43	2.87	2.57	2.52	3.78	3.86	0.18	0	2.63	2.69	2.87	3.37	3.25	3.17	3.22	3.67	3.67	2.66	2.5	2.485	2.47
1.16	9.75	2.93	2.8	1.73	2.9	3.07	3.31	2.58	2.29	2.13	3.23	3.31	0	0	2.49	2.54	2.74	3.18	3.03	2.95	2.84	3.39	3.23	2.27	2.09	2.11	2.13
0.98	10	2.79	2.62	2.33	2.84	3.05	3.41	2.48	2.18	2.06	2.79	2.91	0.11	0.01	2.62	2.62	2.87	3.18	3.03	2.98	2.75	3.33	3.02	1.99	1.83	1.875	1.92
0.82	10.25	2.81	2.57	3.11	2.91	3.18	3.66	2.52	2.16	2.51	2.42	2.61	1.04	0.38	2.93	2.87	3.18	3.33	3.19	3.17	2.82	3.43	2.96	1.75	1.65	1.715	1.78
0.69	10.5	3.35	2.89	4.87	3.29	3.68	4.28	2.85	2.42	3.8	2.28	2.59	4.38	3.63	3.73	3.56	3.96	3.78	3.73	3.79	3.41	3.89	3.31	1.71	1.78	1.84	1.9
0.58	10.75	4.2	3.45	7.31	3.88	4.4	5.1	3.38	2.84	5.76	2.34	2.79	10.14	11.26	4.83	4.52	5.02	4.42	4.51	4.67	4.31	4.57	3.92	1.8	2.11	2.145	2.18
0.49	11	4.91	3.89	9.19	4.31	4.91	5.67	3.75	3.15	7.42	2.39	2.95	15.71	19.61	5.66	5.25	5.8	4.84	5.08	5.32	5.04	5.04	4.39	1.88	2.43	2.425	2.42
0.41	11.25	5.35	4.16	10.24	4.57	5.17	5.93	3.95	3.33	8.47	2.42	3.05	18.99	24.35	6.14	5.69	6.24	5.03	5.38	5.68	5.48	5.25	4.67	1.95	2.68	2.63	2.58
0.35	11.5	5.29	4.11	9.84	4.48	4.99	5.68	3.85	3.28	8.34	2.36	2.97	17.57	21.33	6.03	5.62	6.07	4.81	5.23	5.54	5.4	5.03	4.59	1.95	2.76	2.675	2.59
0.29	11.75	4.4	3.43	7.17	3.75	4.03	4.57	3.12	2.72	6.3	2.03	2.52	10.64	10.59	4.86	4.62	4.91	3.86	4.25	4.52	4.47	4.05	3.84	1.75	2.46	2.345	2.23
0.24	12	2.98	2.36	3.78	2.61	2.63	2.99	2.03	1.84	3.51	1.51	1.8	3.51	2.38	3.11	3.06	3.19	2.52	2.81	2.99	3.01	2.65	2.64	1.38	1.86	1.735	1.61
0.21	12.25	1.67	1.36	1.48	1.54	1.42	1.61	1.09	1.05	1.47	0.98	1.11	0.92	0.41	1.62	1.68	1.7	1.37	1.54	1.63	1.68	1.44	1.53	0.97	1.21	1.1	0.99
0.17	12.5	0.77	0.66	0.44	0.77	0.63	0.72	0.49	0.51	0.47	0.56	0.58	0.11	0.02	0.69	0.76	0.74	0.61	0.7	0.74	0.77	0.64	0.75	0.62	0.69	0.61	0.53
0.15	12.75	0.29	0.27	0.1	0.32	0.23	0.26	0.18	0.21	0.12	0.29	0.26	0.01	0	0.23	0.28	0.25	0.22	0.26	0.27	0.28	0.23	0.3	0.36	0.34	0.29	0.24
0.12	13	0.09	0.1	0.01	0.12	0.07	0.08	0.06	0.08	0.02	0.12	0.11	0	0	0.07	0.09	0.08	0.07	0.08	0.09	0.09	0.07	0.11	0.18	0.14	0.12	0.1
0.10	13.25	0.02	0.03	0	0.03	0.02	0.02	0.01	0.02	0	0.05	0.03	0	0	0.01	0.02	0.01	0.02	0.02	0.02	0.02	0.01	0.03	0.09	0.06	0.045	0.03
0.09	13.5	0.01	0.01	0	0.01	0	0	0	0	0	0.																

Microns	Phi	WS091	WS093	WS093	WS093	WS095	WS095	WS097	WS099	WS101	WS103	WS105	WS107	WS109	WS111	WS113	WS113	WS115	WS117	WS119	WS121	WS123	WS125	WS127	WS129	WS131	WS133
500	1	0	0	0	0	0	0	0	0	0	0	0	0	0	0	0	0	0	0	0	0	0	0	0	0	0	0
420	1.25	0	0	0	0	0	0	0	0	0.07	0	0	0	0	0	0	0	0	0	0	0	0	0	0	0	0	0
350	1.5	0	0	0	0	0	0	0	0	0.16	0	0	0	0	0	0	0	0	0	0	0	0	0	0	0	0	0
300	1.75	0	0	0	0	0.02	0	0	0	0.24	0	0	0	0	0	0	0	0	0	0	0	0	0	0	0	0	0
250	2	0	0	0	0	0.03	0	0	0	0.23	0	0.01	0	0	0.01	0.01	0	0	0	0	0	0	0	0	0	0	0
210	2.25	0	0	0	0	0.05	0	0	0	0.15	0	0.02	0	0.01	0.02	0.02	0	0	0.01	0	0	0	0	0	0	0.01	0
177	2.5	0	0.01	0	0	0.06	0	0	0	0.05	0	0.02	0	0.02	0.03	0.03	0	0	0.01	0	0	0	0	0	0	0.02	0
149	2.75	0	0.01	0	0	0.06	0	0	0	0	0	0.02	0	0.02	0.04	0.03	0	0	0.02	0	0	0	0	0	0	0.03	0
125	3	0	0.01	0	0	0.06	0	0	0	0.01	0	0.03	0	0.03	0.04	0.05	0	0	0.03	0	0	0	0	0	0	0.04	0
105	3.25	0	0.02	0	0.05	0.08	0	0	0	0.11	0	0.06	0	0.04	0.05	0.08	0	0	0.05	0	0.01	0	0	0	0	0.08	0
88	3.5	0.05	0.05	0.08	0.14	0.11	0.1	0.28	0.26	0.28	0.09	0.13	0.09	0.09	0.11	0.15	0.01	0.01	0.11	0	0.1	0	0	0	0.03	0.13	0
74	3.75	0.09	0.09	0.12	0.23	0.16	0.19	0.42	0.46	0.5	0.22	0.22	0.21	0.2	0.21	0.25	0.19	0.13	0.21	0.08	0.2	0.02	0.04	0	0.19	0.22	0.03
63	4	0.14	0.14	0.17	0.32	0.23	0.28	0.59	0.68	0.72	0.34	0.34	0.32	0.35	0.35	0.39	0.42	0.31	0.33	0.18	0.29	0.1	0.3	0.07	0.36	0.31	0.17
53	4.25	0.18	0.19	0.21	0.4	0.29	0.37	0.74	0.9	0.91	0.45	0.47	0.43	0.52	0.53	0.56	0.63	0.46	0.47	0.28	0.36	0.2	0.67	0.33	0.52	0.39	0.32
44	4.5	0.22	0.25	0.26	0.44	0.35	0.45	0.9	1.11	1.08	0.52	0.82	0.54	0.71	0.74	0.77	0.9	0.62	0.61	0.38	0.41	0.28	0.98	0.68	0.7	0.46	0.46
37	4.75	0.23	0.33	0.3	0.46	0.4	0.51	1.05	1.32	1.23	0.56	0.79	0.68	0.91	1	1.03	1.2	0.78	0.76	0.47	0.47	0.4	1.34	1.03	0.91	0.55	0.61
31	5	0.24	0.43	0.34	0.46	0.43	0.55	1.21	1.54	1.38	0.61	0.99	0.77	1.13	1.31	1.32	1.54	0.96	0.92	0.61	0.58	0.63	1.72	1.47	1.17	0.67	0.77
26.3	5.25	0.24	0.58	0.41	0.47	0.46	0.58	1.36	1.75	1.55	0.7	1.25	0.92	1.38	1.67	1.65	1.91	1.19	1.12	0.82	0.78	0.99	2.1	1.94	1.48	0.86	0.96
22.1	5.5	0.27	0.78	0.53	0.53	0.5	0.63	1.52	1.97	1.72	0.87	1.57	1.16	1.66	2.07	1.99	2.28	1.48	1.38	1.13	1.12	1.47	2.48	2.4	1.86	1.15	1.2
18.6	5.75	0.37	1.06	0.72	0.69	0.57	0.73	1.71	2.18	1.92	1.16	1.97	1.51	1.99	2.48	2.35	2.65	1.83	1.7	1.55	1.61	2.07	2.83	2.8	2.3	1.55	1.51
15.6	6	0.55	1.43	1.02	0.97	0.7	0.91	1.94	2.42	2.15	1.57	2.44	1.98	2.36	2.88	2.71	2.99	2.26	2.08	2.07	2.23	2.71	3.16	3.13	2.77	2.05	1.88
13.1	6.25	0.81	1.88	1.42	1.38	0.87	1.17	2.21	2.66	2.39	2.06	2.96	2.55	2.73	3.23	3.06	3.31	2.71	2.5	2.63	2.9	3.32	3.46	3.38	3.25	2.62	2.29
11.0	6.5	1.15	2.38	1.89	1.89	1.1	1.51	2.5	2.89	2.64	2.59	3.47	3.15	3.08	3.53	3.39	3.58	3.16	2.92	3.18	3.55	3.82	3.69	3.54	3.68	3.19	2.73
9.3	6.75	1.56	2.89	2.4	2.45	1.37	1.89	2.79	3.09	2.87	3.1	3.93	3.72	3.37	3.76	3.68	3.79	3.55	3.29	3.65	4.1	4.17	3.86	3.65	4.02	3.73	3.15
7.8	7	2	3.39	2.9	3	1.67	2.29	3.03	3.23	3.06	3.52	4.31	4.19	3.57	3.92	3.91	3.95	3.86	3.59	4	4.48	4.35	3.94	3.71	4.26	4.19	3.53
6.6	7.25	2.45	3.83	3.34	3.48	1.99	2.67	3.21	3.29	3.19	3.82	4.58	4.52	3.67	4.01	4.06	4.04	4.05	3.79	4.2	4.68	4.38	3.95	3.73	4.37	4.54	3.86
5.5	7.5	2.88	4.16	3.68	3.87	2.28	2.99	3.31	3.29	3.25	3.99	4.72	4.7	3.67	4.01	4.11	4.03	4.13	3.9	4.27	4.71	4.29	3.86	3.71	4.33	4.79	4.1
4.6	7.75	3.29	4.38	3.92	4.12	2.55	3.23	3.33	3.21	3.23	4.03	4.71	4.7	3.57	3.91	4.02	3.98	4.08	3.91	4.22	4.58	4.12	3.75	3.68	4.28	4.9	4.27
3.9	8	3.63	4.46	4.04	4.24	2.78	3.38	3.3	3.11	3.16	3.97	4.67	4.56	3.42	3.8	3.91	3.89	3.95	3.84	4.09	4.38	3.93	3.83	3.66	4.2	4.91	4.34
3.3	8.25	3.91	4.44	4.07	4.24	2.95	3.45	3.23	3.02	3.09	3.86	4.59	4.4	3.26	3.66	3.77	3.77	3.82	3.73	3.93	4.18	3.76	3.51	3.63	4.11	4.89	4.34
2.8	8.5	4.11	4.26	4.01	4.15	3.07	3.44	3.16	2.94	3.03	3.68	4.46	4.21	3.12	3.51	3.61	3.63	3.68	3.63	3.78	4	3.61	3.4	3.6	4.02	4.82	4.31
2.3	8.75	4.19	4	3.87	3.91	3.1	3.35	3.08	2.88	2.95	3.47	4.27	3.98	2.98	3.34	3.43	3.46	3.52	3.51	3.63	3.82	3.46	3.29	3.55	3.92	4.68	4.23
2.0	9	4.1	3.7	3.55	3.62	3.04	3.17	2.98	2.81	2.86	3.22	4.01	3.71	2.85	3.16	3.24	3.27	3.36	3.37	3.47	3.63	3.3	3.17	3.48	3.8	4.47	4.08
1.64	9.25	3.94	3.44	3.32	3.39	2.97	3.01	2.93	2.81	2.83	3.02	3.75	3.46	2.79	3.03	3.11	3.13	3.25	3.28	3.36	3.51	3.2	3.1	3.43	3.69	4.23	3.93
1.38	9.5	3.56	3.08	2.98	3.07	2.53	2.81	2.79	2.74	2.7	2.71	3.35	3.12	2.67	2.84	2.9	2.91	3.06	3.11	3.15	3.28	2.98	2.92	3.26	3.45	3.85	3.63
1.16	9.75	3.28	2.81	2.74	2.86	2.2	2.74	2.7	2.71	2.61	2.47	2.95	2.82	2.61	2.69	2.73	2.72	2.91	2.96	2.97	3.07	2.79	2.76	3.08	3.19	3.45	3.34
0.98	10	3.36	2.83	2.85	2.96	2.83	3.05	2.84	2.87	2.76	2.53	2.71	2.71	2.78	2.72	2.74	2.71	2.94	3.02	2.99	3.02	2.8	2.76	3.03	3.04	3.14	3.22
0.82	10.25	3.67	3.03	3.19	3.28	3.65	3.64	3.15	3.18	3.08	2.79	2.56	2.72	3.1	2.86	2.89	2.82	3.12	3.22	3.15	3.1	2.96	2.87	3.08	2.97	3.21	3.21
0.69	10.5	4.63	3.73	4.18	4.1	5.31	4.89	3.89	3.83	3.83	3.64	2.7	3.07	3.8	3.27	3.3	3.17	3.59	3.74	3.63	3.39	3.43	3.21	3.34	3.09	2.89	3.49
0.58	10.75	5.96	4.72	5.53	5.23	7.56	6.49	4.9	4.68	4.81	4.84	3.05	3.63	4.71	3.85	3.88	3.68	4.24	4.45	4.31	3.84	4.1	3.71	3.74	3.34	3.03	3.96
0.49	11	7	5.45	6.55	6.03	9.2	7.61	5.65	5.26	5.53	5.8	3.31	4.06	5.35	4.23	4.26	4	4.68	4.94	4.77	4.1	4.56	4.03	3.99	3.47	3.12	4.29
0.41	11.25	7.57	5.87	7.11	6.47	10.06	8.17	6.09	5.57	5.9	6.37	3.47	4.32	5.7	4.44	4.44	4.15	4.89	5.18	5.02	4.2	4.8	4.17	4.1	3.5	3.15	4.47
0.35	11.5	7.35	5.75	6.9	6.3	9.57	7.84	5.99	5.4	5.72	6.25	3.41	4.27	5.55	4.32	4.28	3.99	4.71	5	4.86	4	4.63	4.01	3.95	3.34	3.05	4.35
0.29	11.75	5.93	4.63	5.44	5.02	6.98	5.99	4.91	4.39	4.59	5.07	2.87	3.6	4.52	3.56	3.47	3.22	3.82	4.07	3.97	3.22	3.74	3.23	3.26	2.72	2.6	3.64
0.24	12	3.84	2.98	3.37	3.17	3.73	3.51	3.26	2.89	2.95	3.29	2.01	2.51	2.97	2.4	2.28	2.11	2.52	2.7	2.65	2.12	2.44	2.12	2.24	1.83	1.89	2.54
0.21	12.25	2.03	1.56	1.67	1.62	1.5	1.62	1.79	1.58	1.55	1.73	1.2	1.49	1.62	1.36	1.25	1.15	1.39	1.49	1.47	1.16	1.32	1.15	1.31	1.05	1.2	1.51
0.17	12.5	0.86	0.67	0.66	0.67	0.45	0.59	0.81	0.71	0.66	0.73	0.61	0.75	0.73	0.65	0.57	0.53	0.64	0.68	0.69	0.54	0.59	0.53	0.65	0.51	0.67	0.77
0.15	12.75	0.28	0.23	0.2	0.22	0.1	0.17	0.3	0.26	0.22	0.24	0.26	0.31	0.26	0.26	0.21	0.2	0.24	0.25	0.26	0.2	0.21	0.2	0.27	0.21	0.33	0.33
0.12	13	0.08	0.07	0.05	0.06	0.01	0.04	0.1	0.08	0.07	0.07	0.1	0.12	0.08	0.09	0.07	0.07	0.08	0.08	0.09	0.07	0.07	0.07	0.1	0.08	0.14	0.12
0.10	13.25	0.01	0.01	0.01	0.01	0	0.01	0.02	0.02	0.01	0.01	0.03	0.03	0.02	0.02	0.02	0.02	0.02	0.02	0.02	0.02	0.01	0.02	0.03	0.02	0.06	0.04
0.09	13.5	0	0	0																							

Microns	Phi	WS135	WS137	WS137	WS139	WS141	WS143	WS143	WS145	WS147	WS149	WS151	WS153	WS153	WS155	WS157	WS159	WS159	WS163	WS165	WS167	WS169	WS169	WS171	WS173
500	1	0	0	0	0	0	0	0	0	0	0	0	0	0	0	0	0	0	0	0	0	0	0	0	0
420	1.25	0	0	0	0	0	0	0	0	0	0	0	0	0	0	0	0	0	0	0	0	0	0	0	0
350	1.5	0	0	0	0	0	0	0	0	0	0	0	0	0	0	0	0	0	0	0	0	0	0	0	0
300	1.75	0	0	0	0.01	0	0	0	0	0	0	0	0	0.01	0	0	0	0	0.01	0	0	0	0	0	0
250	2	0	0	0	0.03	0.01	0.01	0	0.01	0	0	0	0	0.05	0.01	0	0	0	0.03	0	0	0	0	0	0
210	2.25	0	0	0	0.05	0.03	0.02	0	0.04	0	0	0	0	0.07	0.03	0	0	0	0.05	0	0	0	0	0	0
177	2.5	0	0	0	0.06	0.04	0.04	0	0.06	0	0	0	0	0.1	0.04	0	0	0	0.07	0	0	0	0	0	0
149	2.75	0	0	0	0.06	0.05	0.05	0	0.08	0	0	0	0	0.04	0.12	0.05	0	0	0.08	0	0	0	0	0	0
125	3	0	0	0	0.07	0.07	0.05	0.03	0.1	0	0.03	0	0	0.13	0.15	0.06	0.06	0.03	0	0.11	0	0	0	0	0.06
105	3.25	0	0	0.01	0.12	0.1	0.07	0.05	0.12	0.05	0.13	0	0	0.21	0.23	0.09	0.16	0.18	0.22	0.19	0	0	0	0	0.19
88	3.5	0.11	0.08	0.24	0.22	0.19	0.12	0.09	0.16	0.12	0.24	0.21	0.29	0.35	0.39	0.19	0.27	0.37	0.44	0.35	0.24	0.19	0.22	0.01	0.34
74	3.75	0.25	0.19	0.49	0.37	0.34	0.2	0.17	0.24	0.19	0.4	0.52	0.55	0.58	0.66	0.38	0.46	0.65	0.66	0.6	0.52	0.43	0.48	0.38	0.57
63	4	0.38	0.28	0.83	0.56	0.53	0.3	0.26	0.34	0.29	0.59	0.79	0.82	0.88	1	0.66	0.73	0.99	0.88	0.89	0.77	0.65	0.72	0.62	0.84
53	4.25	0.5	0.39	1.21	0.73	0.73	0.39	0.34	0.45	0.41	0.79	1.08	1.08	1.2	1.35	0.98	1.05	1.34	1.1	1.2	1.03	0.88	0.98	0.89	1.13
44	4.5	0.6	0.5	1.64	0.87	0.93	0.47	0.39	0.56	0.54	0.85	1.35	1.34	1.49	1.65	1.3	1.38	1.63	1.31	1.49	1.29	1.11	1.23	1.15	1.38
37	4.75	0.67	0.63	2.08	1	1.12	0.54	0.41	0.65	0.71	1.07	1.57	1.58	1.74	1.87	1.57	1.66	1.84	1.53	1.74	1.55	1.33	1.45	1.39	1.57
31	5	0.73	0.8	2.51	1.14	1.31	0.63	0.45	0.75	0.91	1.19	1.74	1.78	1.94	2.02	1.8	1.89	1.99	1.73	1.97	1.82	1.56	1.63	1.58	1.72
26.3	5.25	0.83	1.05	2.91	1.36	1.51	0.77	0.53	0.9	1.15	1.35	1.89	1.95	2.1	2.13	1.99	2.08	2.11	1.9	2.21	2.08	1.79	1.8	1.76	1.85
22.1	5.5	1	1.38	3.25	1.68	1.77	0.98	0.72	1.12	1.45	1.59	2.06	2.14	2.28	2.26	2.2	2.26	2.25	2.1	2.48	2.34	2.05	2.01	1.96	2
18.6	5.75	1.27	1.81	3.52	2.14	2.1	1.29	1.05	1.44	1.79	1.95	2.29	2.37	2.5	2.45	2.47	2.49	2.47	2.36	2.8	2.65	2.36	2.29	2.22	2.22
15.6	6	1.63	2.33	3.73	2.7	2.52	1.7	1.53	1.87	2.17	2.39	2.58	2.66	2.77	2.71	2.8	2.76	2.78	2.69	3.17	2.98	2.71	2.63	2.54	2.51
13.1	6.25	2.08	2.9	3.88	3.3	3.02	2.18	2.16	2.37	2.55	2.88	2.92	2.98	3.07	3.03	3.17	3.08	3.14	3.04	3.53	3.33	3.07	3	2.89	2.84
11.0	6.5	2.58	3.44	3.97	3.87	3.55	2.69	2.86	2.92	2.93	3.34	3.26	3.3	3.37	3.34	3.53	3.4	3.5	3.38	3.85	3.64	3.39	3.35	3.22	3.17
9.3	6.75	3.07	3.91	3.98	4.32	4.06	3.21	3.59	3.48	3.29	3.71	3.55	3.57	3.62	3.61	3.82	3.67	3.8	3.67	4.07	3.88	3.63	3.63	3.5	3.44
7.8	7	3.52	4.26	3.96	4.6	4.51	3.71	4.28	4	3.62	3.96	3.75	3.76	3.79	3.8	4.02	3.86	4	3.85	4.18	4.02	3.77	3.8	3.68	3.63
6.6	7.25	3.9	4.47	3.92	4.69	4.85	4.16	4.87	4.45	3.91	4.07	3.84	3.84	3.77	3.79	4.08	3.92	3.97	3.91	4.06	4.04	3.81	3.87	3.74	3.69
5.5	7.5	4.19	4.54	3.86	4.54	4.96	4.55	5.34	4.82	4.16	4.05	3.74	3.75	3.72	3.73	3.94	3.8	3.89	3.79	3.91	3.88	3.74	3.8	3.69	3.61
4.6	7.75	4.39	4.47	3.77	4.36	5.03	4.86	5.61	5.04	4.33	3.91	3.63	3.63	3.61	3.61	3.77	3.64	3.73	3.64	3.69	3.69	3.57	3.62	3.51	3.44
3.9	8	4.47	4.35	3.67	4.15	5.01	5.02	5.68	5.09	4.42	3.77	3.47	3.47	3.45	3.43	3.55	3.44	3.51	3.46	3.44	3.48	3.4	3.43	3.34	3.26
3.3	8.25	4.48	4.22	3.56	3.91	4.9	5.07	5.83	5.09	4.47	3.6	3.29	3.28	3.25	3.22	3.31	3.22	3.26	3.25	3.17	3.22	3.22	3.23	3.16	3.06
2.8	8.5	4.48	4.09	3.45	3.68	4.71	5.07	5.49	5.01	4.46	3.43	3.1	3.08	3.06	3.01	3.07	3	3.02	3.05	2.92	3.03	3.05	3.05	2.99	2.87
2.3	8.75	4.42	3.94	3.33	3.45	4.44	4.96	5.23	4.81	4.38	3.24	2.92	2.9	2.88	2.81	2.85	2.8	2.8	2.87	2.7	2.84	2.89	2.88	2.84	2.7
2.0	9	4.29	3.77	3.19	3.21	4.09	4.72	4.85	4.5	4.2	3.03	2.76	2.74	2.72	2.64	2.65	2.62	2.6	2.71	2.51	2.67	2.75	2.72	2.71	2.55
1.64	9.25	4.16	3.63	3.07	3.02	3.72	4.44	4.45	4.16	4	2.85	2.66	2.65	2.64	2.55	2.54	2.53	2.51	2.64	2.4	2.6	2.68	2.64	2.67	2.47
1.38	9.5	3.87	3.39	2.85	2.75	3.24	3.99	3.89	3.69	3.64	2.61	2.52	2.53	2.52	2.43	2.4	2.4	2.37	2.52	2.28	2.49	2.56	2.51	2.59	2.37
1.16	9.75	3.56	3.16	2.62	2.52	2.78	3.52	3.35	3.23	3.27	2.43	2.45	2.47	2.45	2.35	2.32	2.34	2.28	2.46	2.22	2.44	2.5	2.44	2.56	2.33
0.98	10	3.41	3.05	2.49	2.45	2.44	3.2	2.96	2.92	3.08	2.44	2.53	2.55	2.54	2.44	2.41	2.45	2.39	2.58	2.31	2.56	2.63	2.57	2.73	2.5
0.82	10.25	3.39	3.03	2.43	2.49	2.17	2.96	2.66	2.7	3	2.58	2.73	2.73	2.75	2.65	2.63	2.67	2.62	2.83	2.52	2.8	2.91	2.84	3.04	2.82
0.69	10.5	3.6	3.22	2.52	2.81	2.18	3	2.63	2.76	3.22	3.11	3.22	3.18	3.21	3.12	3.14	3.2	3.15	3.36	2.97	3.29	3.49	3.43	3.66	3.49
0.58	10.75	4	3.57	2.74	3.32	2.37	3.23	2.81	3.01	3.63	3.86	3.89	3.77	3.82	3.74	3.81	3.89	3.84	4.03	3.56	3.91	4.25	4.2	4.44	4.36
0.49	11	4.22	3.78	2.86	3.7	2.55	3.39	2.94	3.2	3.92	4.46	4.39	4.22	4.24	4.19	4.31	4.39	4.32	4.48	3.97	4.31	4.76	4.74	4.97	4.97
0.41	11.25	4.3	3.88	2.91	3.93	2.69	3.48	3.03	3.31	4.06	4.85	4.69	4.49	4.46	4.43	4.58	4.68	4.54	4.69	4.2	4.49	5.03	5.02	5.24	5.32
0.35	11.5	4.08	3.76	2.8	3.87	2.69	3.39	2.96	3.25	3.93	4.86	4.64	4.46	4.34	4.32	4.49	4.58	4.36	4.53	4.1	4.32	4.89	4.89	5.07	5.2
0.29	11.75	3.29	3.13	2.33	3.24	2.37	2.89	2.53	2.78	3.24	4.14	3.95	3.85	3.59	3.59	3.75	3.82	3.5	3.67	3.39	3.47	3.96	3.96	4.1	4.23
0.24	12	2.18	2.17	1.62	2.25	1.79	2.09	1.85	2.02	2.22	2.92	2.83	2.81	2.45	2.46	2.59	2.64	2.28	2.42	2.29	2.26	2.6	2.6	2.69	2.78
0.21	12.25	1.2	1.29	0.96	1.32	1.19	1.31	1.17	1.27	1.28	1.75	1.72	1.76	1.41	1.42	1.51	1.53	1.22	1.33	1.3	1.22	1.41	1.4	1.46	1.51
0.17	12.5	0.56	0.66	0.5	0.66	0.7	0.72	0.64	0.69	0.63	0.89	0.89	0.96	0.68	0.69	0.74	0.75	0.53	0.6	0.63	0.55	0.64	0.63	0.66	0.68
0.15	12.75	0.22	0.29	0.22	0.27	0.36	0.34	0.31	0.33	0.25	0.39	0.39	0.45	0.27	0.28	0.29	0.3	0.18	0.22	0.25	0.2	0.23	0.23	0.24	0.25
0.12	13	0.07	0.12	0.09	0.1	0.16	0.14	0.13	0.13	0.09	0.14	0.14	0.17	0.1	0.1	0.1	0.11	0.06	0.07	0.09	0.07	0.08	0.07	0.08	0.08
0.10	13.25	0.02	0.04	0.03	0.03	0.07	0.05	0.05	0.05	0.03	0.05	0.05	0.07	0.02	0.02	0.03	0.03	0.01	0.02	0.02	0.01	0.02	0.02	0.02	0.02
0.09	13.5	0.01	0.01	0.01	0.01	0.02	0.02	0.02	0.02	0.01	0.01	0.01	0.01	0.02	0.01	0.01	0.01	0	0	0.01	0	0	0	0	0
0.07	13.75	0	0	0	0	0.01	0.01	0.01	0.01	0	0	0	0.01	0	0	0	0	0	0	0	0	0	0	0	0
0.06	14	0	0	0	0	0	0	0	0	0	0	0	0	0	0	0	0	0	0	0	0	0	0	0	0

**PARTICLE-SIZE DATA: PAPAKURA CREEK**

Microns	Phi	OP006	OP007	OP008	OP009	OP010	OP012	OP014	OP017	OP019	OP021	OP023	OP025	OP027	OP033	OP035	OP038	OP039	OP040	OP041	OP052	OP055
600	0.75	0	0	0	0	0	0	0	0	0	0	0	0	0	0	0	0	0	0	0	0	0
500	1	0	0	0	0	0	0	0	0	0	0	0	0	0	0	0	0	0	0	0	0.35	0
420	1.25	0	0	0	0	0	0	0	0	0	0	0	0	0	0	0	0	0	0	0	1.06	0
350	1.5	0	0	0	0	0	0	0	0	0	0	0	0	0	0	0	0	0	0.07	0.04	1.66	0
300	1.75	0	0	0	0	0.07	0.04	0	0	0.07	0	0	0	0	0.12	0	0	0	0.18	0.13	1.95	0.05
250	2	0	0	0	0	0.12	0.09	0	0	0.1	0	0	0	0	0.49	0	0	0	0.28	0.22	1.89	0.09
210	2.25	0	0	0	0	0.16	0.12	0	0	0.13	0	0	0	0	0.75	0	0	0	0.29	0.25	1.63	0.13
177	2.5	0	0	0	0	0.16	0.13	0	0	0.12	0	0	0	0	0.77	0	0	0	0.24	0.22	1.31	0.14
149	2.75	0	0	0	0	0.14	0.12	0	0	0.09	0	0	0	0.01	0.6	0	0	0	0.16	0.16	1.03	0.13
125	3	0.05	0.04	0	0	0.12	0.11	0	0	0.06	0	0	0	0.01	0.37	0.07	0	0	0.1	0.1	0.83	0.12
105	3.25	0.09	0.08	0	0.07	0.11	0.12	0	0	0.05	0	0	0	0.01	0.15	0.13	0	0	0.08	0.06	0.73	0.13
88	3.5	0.16	0.14	0.01	0.1	0.15	0.18	0.14	0	0.09	0	0	0.01	0.03	0	0.24	0	0	0.11	0.06	0.71	0.15
74	3.75	0.26	0.25	0.16	0.14	0.22	0.29	0.31	0.03	0.18	0.05	0.03	0.1	0.07	0	0.41	0	0	0.16	0.1	0.73	0.2
63	4	0.38	0.39	0.36	0.22	0.32	0.42	0.48	0.19	0.33	0.1	0.35	0.2	0.11	0	0.6	0.02	0.05	0.22	0.19	0.75	0.27
53	4.25	0.51	0.57	0.54	0.33	0.46	0.57	0.69	0.41	0.53	0.16	0.48	0.3	0.18	0	0.8	0.13	0.28	0.28	0.34	0.75	0.33
44	4.5	0.65	0.78	0.8	0.51	0.65	0.75	0.91	0.62	0.79	0.22	0.66	0.39	0.26	0	0.99	0.3	0.63	0.37	0.59	0.74	0.4
37	4.75	0.82	1.03	1.1	0.77	0.9	0.99	1.16	0.88	1.1	0.29	0.82	0.5	0.38	0.07	1.18	0.49	1.02	0.56	0.95	0.77	0.46
31	5	1.04	1.31	1.44	1.13	1.21	1.3	1.43	1.18	1.46	0.4	0.99	0.63	0.53	0.22	1.37	0.79	1.56	0.88	1.43	0.87	0.52
26.28	5.25	1.32	1.62	1.78	1.56	1.56	1.69	1.71	1.48	1.82	0.55	1.16	0.79	0.72	0.35	1.56	1.18	2.21	1.34	1.98	1.07	0.59
22.10	5.5	1.66	1.92	2.1	2.02	1.91	2.12	1.99	1.76	2.15	0.73	1.29	0.99	0.94	0.47	1.76	1.65	2.93	1.93	2.56	1.38	0.67
18.58	5.75	2.06	2.21	2.39	2.47	2.23	2.59	2.27	2.01	2.41	0.96	1.39	1.23	1.19	0.6	1.98	2.18	3.68	2.57	3.1	1.78	0.8
15.63	6	2.49	2.49	2.65	2.87	2.53	3.06	2.53	2.23	2.6	1.21	1.48	1.52	1.47	0.77	2.2	2.72	4.38	3.19	3.57	2.21	0.98
13.14	6.25	2.93	2.73	2.87	3.2	2.78	3.48	2.77	2.43	2.73	1.48	1.57	1.85	1.77	0.99	2.42	3.25	5	3.7	3.93	2.63	1.22
11.05	6.5	3.33	2.94	3.06	3.46	3.01	3.82	2.96	2.61	2.82	1.77	1.68	2.21	2.1	1.23	2.64	3.72	5.47	4.03	4.18	2.97	1.52
9.29	6.75	3.66	3.12	3.24	3.66	3.22	4.07	3.12	2.78	2.9	2.05	1.81	2.58	2.44	1.49	2.85	4.12	5.77	4.17	4.31	3.2	1.87
7.81	7	3.93	3.27	3.39	3.82	3.43	4.24	3.24	2.94	2.97	2.33	1.96	2.94	2.79	1.73	3.03	4.42	5.72	4.16	4.36	3.3	2.26
6.57	7.25	4.11	3.28	3.52	3.96	3.64	4.31	3.33	3.11	3.04	2.6	2.11	3.25	3.14	1.97	3.18	4.62	5.57	4.04	4.28	3.22	2.67
5.52	7.5	4.2	3.46	3.62	4.06	3.82	4.29	3.39	3.28	3.11	2.85	2.24	3.49	3.47	2.18	3.29	4.67	5.31	3.86	4.18	3.1	3.1
4.65	7.75	4.19	3.5	3.67	4.12	3.95	4.25	3.43	3.45	3.17	3.09	2.37	3.63	3.74	2.38	3.36	4.58	4.94	3.68	4.05	2.95	3.49
3.91	8	4.09	3.53	3.71	4.16	4.06	4.2	3.45	3.63	3.22	3.35	2.5	3.69	3.95	2.58	3.4	4.45	4.5	3.51	3.88	2.76	3.84
3.28	8.25	3.97	3.56	3.74	4.17	4.12	4.13	3.47	3.8	3.27	3.64	2.65	3.66	4.08	2.76	3.44	4.27	4.02	3.36	3.7	2.56	4.13
2.76	8.5	3.81	3.58	3.75	4.15	4.13	4.04	3.47	3.96	3.31	4.06	2.83	3.57	4.13	2.9	3.47	4.05	3.55	3.21	3.5	2.36	4.33
2.32	8.75	3.6	3.6	3.73	4.06	4.07	3.93	3.44	4.07	3.34	4.53	3.06	3.35	3.95	2.96	3.47	3.79	3.08	3.05	3.3	2.15	4.42
1.95	9	3.34	3.6	3.67	3.92	3.93	3.78	3.35	4.1	3.32	5	3.32	3.09	3.69	2.87	3.43	3.49	2.65	2.86	3.08	1.94	4.26
1.64	9.25	3.11	3.63	3.64	3.77	3.78	3.63	3.29	4.11	3.34	5.5	3.6	2.91	3.47	2.7	3.42	3.24	2.31	2.69	2.91	1.79	4.14
1.38	9.5	2.79	3.54	3.48	3.5	3.51	3.35	3.07	3.92	3.25	5.88	3.78	2.65	3.12	2.08	3.27	2.93	1.97	2.46	2.69	1.51	3.86
1.16	9.75	2.53	3.44	3.31	3.23	3.24	3.05	2.86	3.68	3.17	6.14	3.97	2.52	2.84	1.43	3.12	2.7	1.75	2.31	2.53	1.23	3.59
0.98	10	2.5	3.47	3.28	3.1	3.12	2.84	2.86	3.58	3.26	6.23	4.36	2.73	2.88	1.86	3.16	2.65	1.55	2.35	2.5	1.42	3.57
0.82	10.25	2.63	3.62	3.36	3.07	3.1	2.71	3.01	3.61	3.48	6.3	4.95	3.2	3.13	2.61	3.34	2.73	1.51	2.54	2.57	1.78	3.73
0.69	10.5	3.16	3.92	3.63	3.24	3.3	2.75	3.53	3.88	3.95	5.94	5.72	4.28	3.97	4.34	3.84	3.09	1.88	3.12	2.85	2.78	4.33
0.58	10.75	3.91	4.33	4.03	3.55	3.66	2.95	4.28	4.35	4.58	5.44	6.57	5.73	5.17	6.92	4.52	3.62	2.5	3.95	3.25	4.25	5.2
0.49	11	4.49	4.51	4.23	3.71	3.87	3.06	4.83	4.61	4.95	4.7	6.94	6.75	6.07	9.17	4.97	3.98	2.96	4.56	3.51	5.51	5.8
0.41	11.25	4.82	4.53	4.28	3.74	3.96	3.12	5.13	4.72	5.11	3.97	6.95	7.31	6.6	10.67	5.18	4.18	3.29	4.97	3.65	6.35	6.12
0.35	11.5	4.71	4.26	4.05	3.55	3.8	3.01	4.99	4.51	4.9	3.24	6.41	7.07	6.48	10.66	4.96	4.09	3.26	4.98	3.56	6.36	5.92
0.29	11.75	3.84	3.39	3.25	2.86	3.12	2.52	4.04	3.62	3.91	2.33	4.86	5.44	5.18	8.2	3.99	3.37	2.48	4.12	2.96	4.94	4.75
0.24	12	2.55	2.2	2.13	1.89	2.13	1.77	2.65	2.34	2.52	1.44	2.91	3.21	3.26	4.68	2.6	2.26	1.37	2.73	2.03	2.86	3.05
0.21	12.25	1.4	1.2	1.17	1.05	1.23	1.07	1.43	1.27	1.34	0.79	1.41	1.49	1.66	2.03	1.4	1.27	0.58	1.5	1.18	1.27	1.61
0.17	12.5	0.63	0.55	0.54	0.5	0.61	0.56	0.64	0.58	0.6	0.39	0.56	0.55	0.69	0.67	0.63	0.61	0.2	0.69	0.59	0.44	0.7
0.15	12.75	0.23	0.21	0.21	0.2	0.26	0.25	0.23	0.22	0.22	0.17	0.18	0.16	0.23	0.16	0.23	0.25	0.05	0.27	0.26	0.12	0.25
0.12	13	0.07	0.07	0.07	0.07	0.1	0.11	0.07	0.08	0.07	0.07	0.05	0.04	0.07	0.03	0.07	0.09	0.01	0.1	0.1	0.02	0.08
0.10	13.25	0.02	0.02	0.02	0.02	0.03	0.04	0.02	0.02	0.02	0.03	0.01	0.01	0.01	0	0.02	0.02	0	0.02	0.03	0	0.02
0.09	13.5	0	0.01	0.01	0.01	0.01	0.01	0	0.01	0.01	0.01	0	0	0	0	0	0.01	0	0.01	0.01	0	0
0.07	13.75	0	0	0	0	0	0	0	0	0	0	0	0	0	0	0	0	0	0	0	0	0
0.06	14	0	0	0	0	0	0	0	0	0	0	0	0	0	0	0	0	0	0	0	0	0

Microns	Phi	OP059	OP062	OP102	OP105	OP111	OP114	OP117	OP120	OP131	OP137	OP142	OP146	OP150	OP151	OP158	OP164	OP167	OP170
600	0.75	0	0	0	0.82	0	0	0	0	0	0	0	0	0	0	0	0	0	0
500	1	0	0	0	1.67	0	0	0	0	0	0	0	0	0	0	0	0	0	0
420	1.25	0	0	0	2.58	0	0	0	0	0	0	0	0	0	0	0	0	0	0
350	1.5	0	0	0	3	0	0	0	0	0	0.04	0	0	0	0.12	0.12	0.17	0.37	0
300	1.75	0.08	0	0	2.85	0	0	0	0.01	0.06	0	0.09	0	0	0.01	0.29	0.42	0.5	0.84
250	2	0.12	0	0	2.35	0	0	0	0.02	0.09	0	0.15	0	0	0.02	0.43	0.67	0.77	1.17
210	2.25	0.15	0	0	1.76	0	0	0.01	0.03	0.12	0	0.18	0	0	0.04	0.46	0.78	0.87	1.2
177	2.5	0.14	0	0	1.21	0	0	0.01	0.03	0.11	0	0.17	0	0	0.05	0.4	0.73	0.79	1.01
149	2.75	0.09	0	0	0.79	0	0	0.01	0.04	0.09	0	0.11	0.03	0	0.05	0.3	0.6	0.64	0.71
125	3	0.03	0	0	0.53	0	0	0.01	0.05	0.06	0	0.03	0.06	0	0.06	0.22	0.48	0.51	0.46
105	3.25	0	0	0	0.41	0	0.07	0.02	0.06	0.06	0	0	0.1	0	0.08	0.21	0.42	0.47	0.33
88	3.5	0.05	0.15	0.06	0.42	0.01	0.12	0.05	0.1	0.09	0	0	0.16	0	0.13	0.28	0.45	0.52	0.36
74	3.75	0.19	0.31	0.1	0.47	0.11	0.18	0.1	0.15	0.15	0.01	0.04	0.24	0	0.22	0.43	0.53	0.64	0.49
63	4	0.43	0.45	0.14	0.51	0.23	0.27	0.18	0.2	0.24	0.11	0.25	0.33	0	0.32	0.61	0.64	0.78	0.66
53	4.25	0.76	0.6	0.18	0.49	0.34	0.37	0.25	0.25	0.34	0.27	0.59	0.41	0	0.43	0.81	0.73	0.89	0.81
44	4.5	1.14	0.75	0.21	0.43	0.46	0.5	0.34	0.29	0.48	0.44	1.09	0.49	0.07	0.53	1	0.81	0.97	0.93
37	4.75	1.54	0.9	0.25	0.36	0.59	0.66	0.43	0.34	0.67	0.73	1.71	0.58	0.23	0.63	1.18	0.88	1.01	1.02
31	5	1.9	1.05	0.29	0.33	0.73	0.85	0.54	0.41	0.92	1.16	2.4	0.7	0.42	0.73	1.36	0.94	1.04	1.09
26.26	5.25	2.18	1.2	0.34	0.36	0.91	1.08	0.68	0.5	1.22	1.72	3.06	0.85	0.66	0.85	1.54	1	1.06	1.17
22.10	5.5	2.35	1.38	0.38	0.51	1.1	1.33	0.86	0.61	1.56	2.38	3.6	1.05	1	1.01	1.73	1.06	1.09	1.26
18.58	5.75	2.46	1.6	0.43	0.78	1.33	1.62	1.08	0.76	1.93	3.1	3.99	1.31	1.43	1.25	1.95	1.13	1.14	1.38
15.83	6	2.55	1.89	0.51	1.18	1.6	1.93	1.34	0.93	2.33	3.82	4.22	1.62	1.96	1.58	2.2	1.22	1.21	1.52
13.14	6.25	2.86	2.22	0.65	1.86	1.89	2.25	1.64	1.14	2.73	4.46	4.33	2	2.55	1.99	2.45	1.33	1.29	1.69
11.05	6.5	2.83	2.8	0.87	2.17	2.19	2.59	1.96	1.38	3.12	4.97	4.37	2.44	3.19	2.48	2.71	1.45	1.38	1.86
9.29	6.75	3.09	2.99	1.22	2.63	2.49	2.91	2.29	1.66	3.49	5.32	4.37	2.92	3.84	3.02	2.94	1.59	1.47	2.03
7.81	7	3.42	3.37	1.72	2.97	2.78	3.2	2.62	1.96	3.82	5.48	4.36	3.42	4.46	3.57	3.13	1.72	1.54	2.18
6.57	7.25	3.79	3.7	2.35	3.14	3.03	3.44	2.93	2.3	4.1	5.37	4.34	3.91	5.02	4.09	3.25	1.83	1.8	2.31
5.52	7.5	4.08	3.96	3.08	3.08	3.23	3.61	3.2	2.65	4.32	5.21	4.3	4.36	5.47	4.53	3.3	1.91	1.64	2.43
4.65	7.75	4.34	4.14	3.87	3	3.37	3.71	3.44	3	4.45	4.98	4.23	4.74	5.73	4.88	3.26	1.98	1.68	2.55
3.91	8	4.51	4.18	4.62	2.86	3.47	3.76	3.65	3.33	4.49	4.7	4.12	4.95	5.77	5.03	3.23	2.05	1.74	2.69
3.28	8.25	4.58	4.15	5.29	2.7	3.54	3.78	3.83	3.65	4.51	4.39	3.97	5	5.74	5.04	3.18	2.14	1.82	2.84
2.76	8.5	4.56	4.09	5.8	2.52	3.61	3.8	3.99	3.92	4.47	4.06	3.79	5	5.59	4.99	3.14	2.27	1.94	3.01
2.32	8.75	4.43	3.97	6.11	2.33	3.67	3.82	4.05	4.1	4.37	3.73	3.57	4.88	5.32	4.83	3.09	2.42	2.1	3.18
1.95	9	4.19	3.79	6.03	2.13	3.7	3.82	4.05	4.13	4.19	3.4	3.3	4.63	4.92	4.57	3.03	2.58	2.29	3.35
1.64	9.25	3.93	3.63	5.93	2	3.79	3.86	4.08	4.03	4.01	3.11	3.04	4.35	4.49	4.28	3.02	2.79	2.54	3.53
1.38	9.5	3.56	3.35	5.65	1.72	3.74	3.79	3.95	3.79	3.7	2.76	2.71	3.91	3.95	3.86	2.94	2.95	2.77	3.62
1.16	9.75	3.19	3.1	5.29	1.42	3.7	3.7	3.79	3.58	3.38	2.45	2.39	3.47	3.42	3.45	2.89	3.17	3.06	3.68
0.98	10	2.94	3.06	5	1.62	3.84	3.74	3.84	3.67	3.18	2.25	2.17	3.21	3.03	3.2	3	3.61	3.59	3.81
0.82	10.25	2.78	3.17	4.81	1.99	4.14	3.91	4.04	3.96	3.09	2.13	2.02	3.06	2.72	3.06	3.24	4.26	4.34	4.03
0.69	10.5	2.8	3.6	4.69	3	4.67	4.24	4.55	4.77	3.19	2.19	2.05	3.19	2.63	3.18	3.75	5.25	5.42	4.36
0.58	10.75	2.97	4.22	4.69	4.49	5.35	4.68	5.25	5.89	3.45	2.38	2.23	3.53	2.7	3.48	4.42	6.41	6.68	4.8
0.49	11	3.05	4.63	4.49	5.74	5.71	4.86	5.68	6.69	3.58	2.5	2.35	3.76	2.73	3.66	4.86	7.15	7.46	5.01
0.41	11.25	3.07	4.82	4.26	6.55	5.81	4.87	5.84	7.09	3.63	2.56	2.43	3.89	2.73	3.75	5.1	7.5	7.83	5.09
0.35	11.5	2.94	4.63	3.88	6.53	5.47	4.57	5.54	6.83	3.47	2.5	2.39	3.77	2.6	3.62	4.96	7.23	7.54	4.9
0.29	11.75	2.45	3.73	3.01	5.07	4.3	3.62	4.42	5.43	2.84	2.1	2.05	3.14	2.18	3.01	4.08	5.79	6.02	4.08
0.24	12	1.71	2.43	1.92	2.95	2.73	2.33	2.87	3.44	1.92	1.49	1.49	2.17	1.55	2.09	2.76	3.74	3.84	2.86
0.21	12.25	1.03	1.31	1.05	1.32	1.43	1.26	1.54	1.77	1.1	0.91	0.94	1.27	0.96	1.25	1.57	1.99	2.01	1.73
0.17	12.5	0.54	0.59	0.5	0.46	0.62	0.57	0.69	0.74	0.55	0.48	0.53	0.64	0.52	0.64	0.76	0.88	0.88	0.91
0.15	12.75	0.25	0.22	0.21	0.12	0.22	0.22	0.25	0.25	0.23	0.22	0.26	0.28	0.24	0.28	0.3	0.32	0.31	0.43
0.12	13	0.1	0.07	0.08	0.02	0.07	0.07	0.08	0.07	0.09	0.1	0.11	0.11	0.11	0.11	0.1	0.1	0.1	0.17
0.10	13.25	0.03	0.02	0.02	0	0.01	0.02	0.02	0.01	0.03	0.03	0.05	0.03	0.04	0.03	0.03	0.02	0.02	0.07
0.09	13.5	0.01	0	0.01	0	0	0.01	0	0	0.01	0.01	0.02	0.01	0.01	0.01	0.01	0.01	0.01	0.02
0.07	13.75	0	0	0	0	0	0	0	0	0	0	0.01	0	0	0	0	0	0	0.01
0.06	14	0	0	0	0	0	0	0	0	0	0	0	0	0	0	0	0	0	0

**APPENDIX C:  
PALEOMAGNETISM**

File Name: OP/2/5/CORR

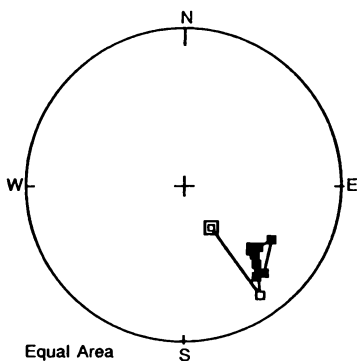
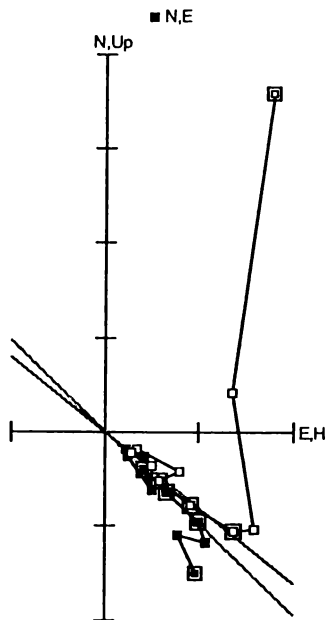
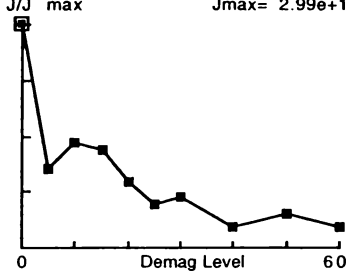
Date: Sunday, 27 August 2000

User Name: JLH

Sample Code: PC\_PM1

Your comments

PCA - Decl: 134.1 Incl: 38.8  
MAD(1)= 8.6 MAD(3)= 1.7  
J/J max Jmax= 2.99e+1



File Name: OP/2/5/CORR

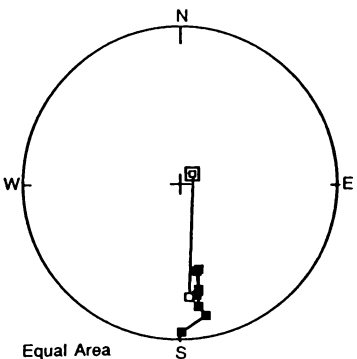
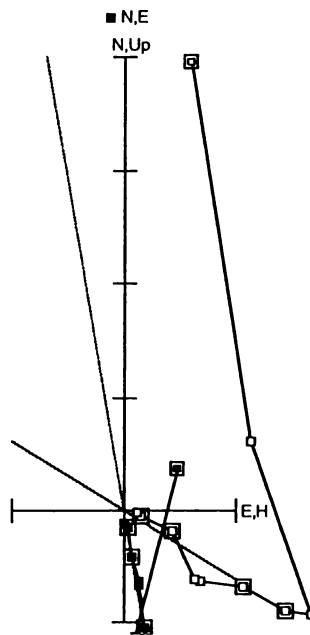
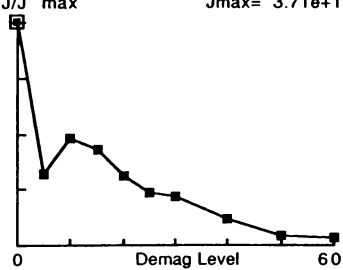
Date: Sunday, 27 August 2000

User Name: JLH

Sample Code: PC\_PM2

Your comments

PCA - Decl: 170.2 Incl: 31.5  
MAD(1)= 8.1 MAD(3)= 2.3  
J/J max Jmax= 3.71e+1





File Name: OP/2/4/CORR

Date: Sunday, 27 August 2000

User Name: JLH

Sample Code: PC\_PM3

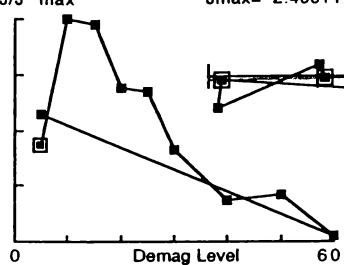
Your comments

PCA - Decl: 269.4 Incl: 44.1

MAD(1)= 1.0 MAD(3)= 0.2

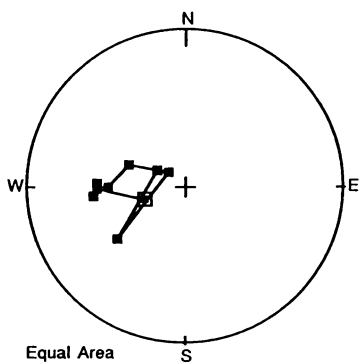
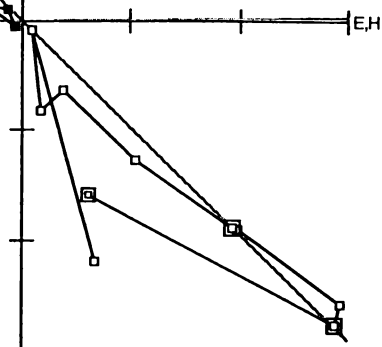
J/J max

Jmax= 2.40e+1



■ N,E

N,Up



File Name: OP/2/4/CORR

Date: Sunday, 27 August 2000

User Name: JLH

Sample Code: PC\_PM4

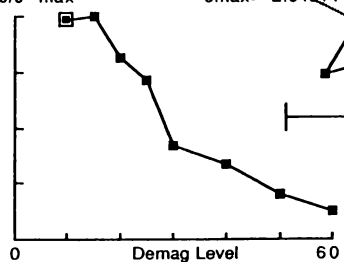
Your comments

PCA - Decl: -63.4 Incl: 60.6

MAD(1)= 0.1 MAD(3)= 2.0

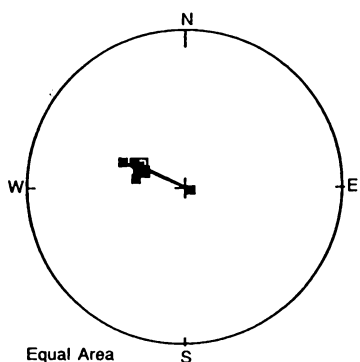
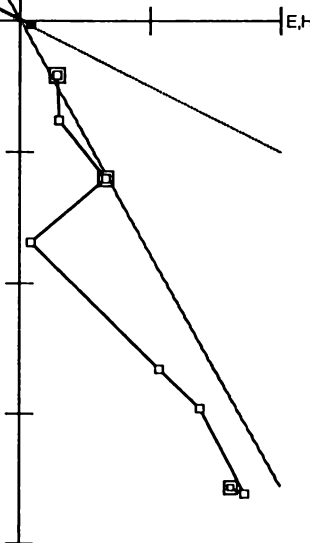
J/J max

Jmax= 2.04e+1



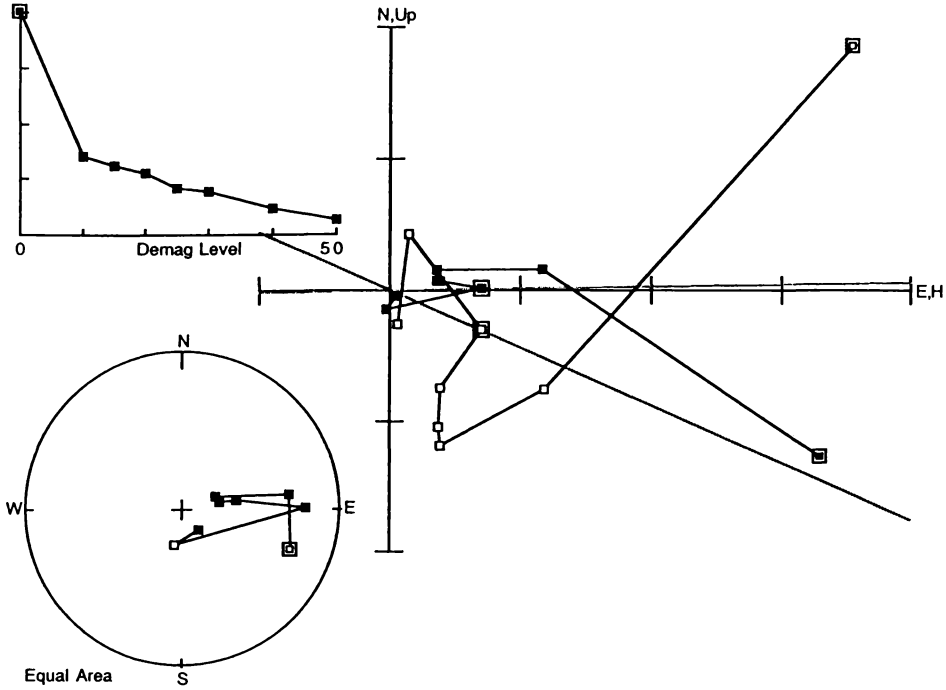
■ N,E

N,Up



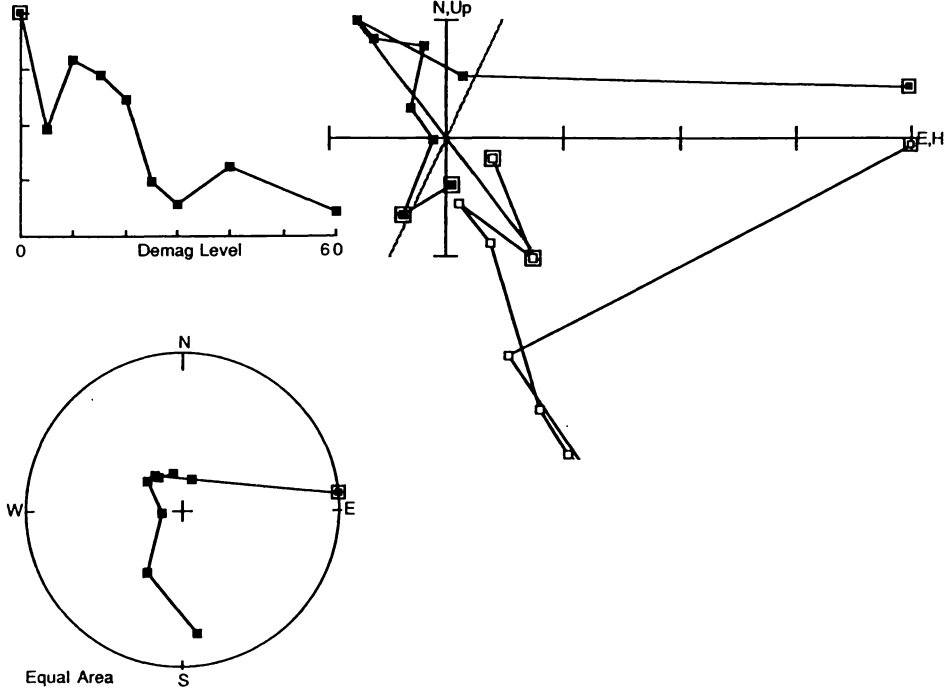
File Name: OP/2/4/CORR Date: Sunday, 27 August 2000  
User Name: JLH  
Sample Code: PC\_PM5  
Your comments

PCA - Decl: 89.2 Incl: 23.7  
MAD(1)= 80.4 MAD(3)= 0.0  
J/J max Jmax= 7.39e+0



File Name: OP/2/4/CORR Date: Sunday, 27 August 2000  
User Name: JLH  
Sample Code: PC\_PM6  
Your comments

PCA - Decl: 205.6 Incl: 51.8  
MAD(1)= 0.0 MAD(3)= 11.8  
J/J max Jmax= 9.14e+0

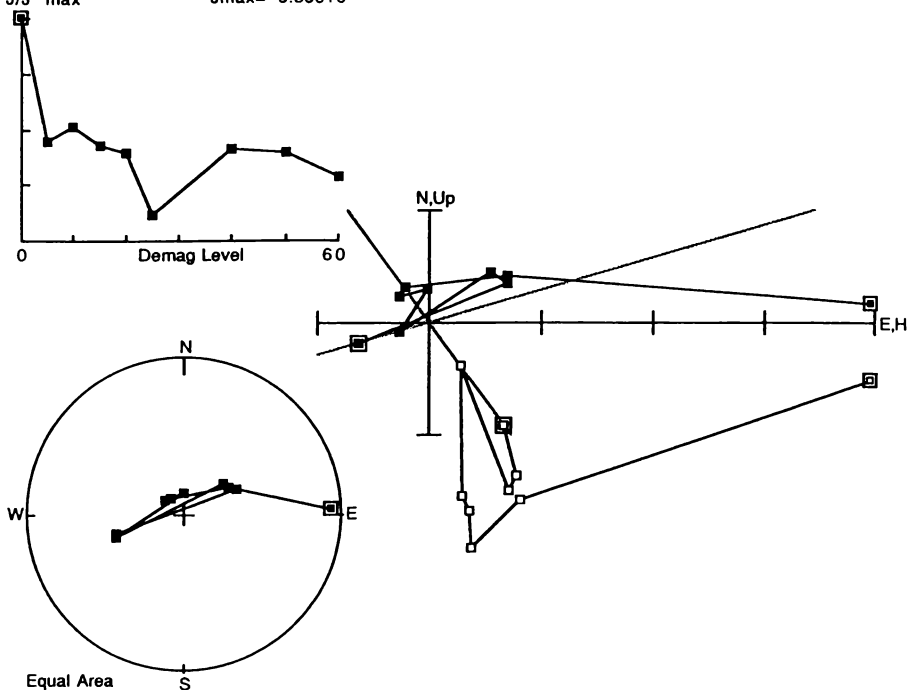


File Name: OP/2/4/CORR  
 User Name: JLH  
 Sample Code: PC\_PM7  
 Your comments

Date: Sunday, 27 August 2000

■ N,E

PCA - Decl: 253.9 Incl: 53.8  
 MAD(1) = 74.2 MAD(3) = 0.0  
 $\frac{J}{J}$  max Jmax = 6.38e+0

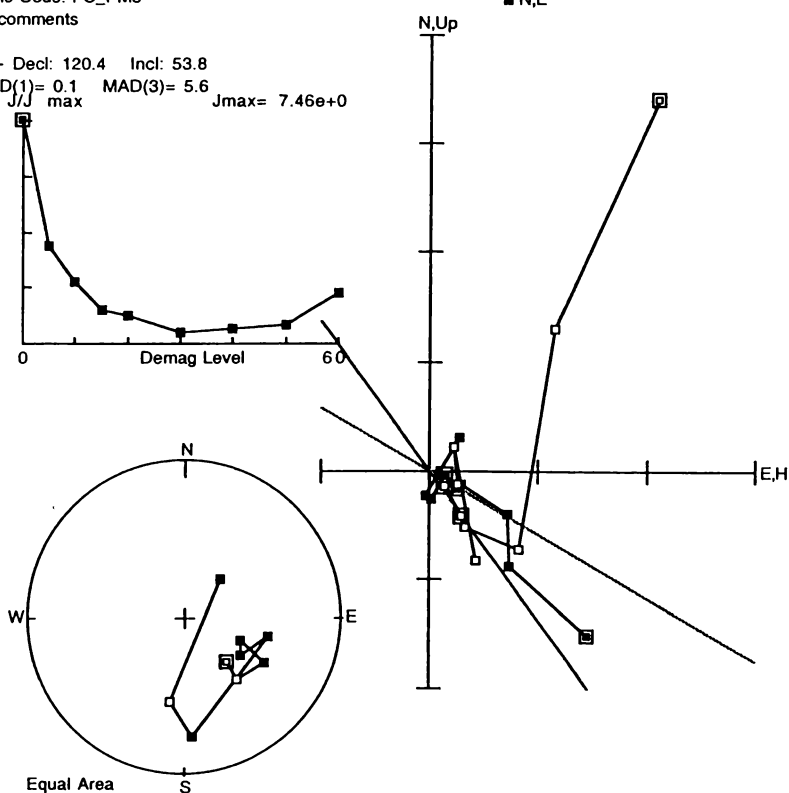


File Name: OP/2/5/CORR  
 User Name: JLH  
 Sample Code: PC\_PM8  
 Your comments

Date: Sunday, 27 August 2000

■ N,E

PCA - Decl: 120.4 Incl: 53.8  
 MAD(1) = 0.1 MAD(3) = 5.6  
 $\frac{J}{J}$  max Jmax = 7.46e+0



File Name: OP/2/5/CORR  
 User Name: JLH  
 Sample Code: PC\_PM9  
 Your comments

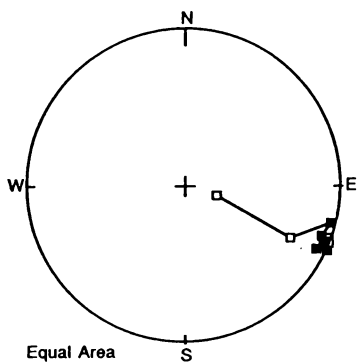
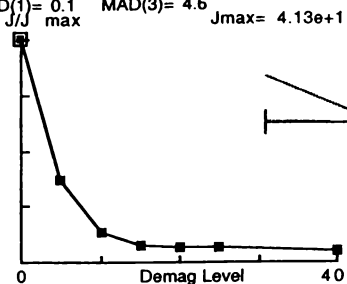
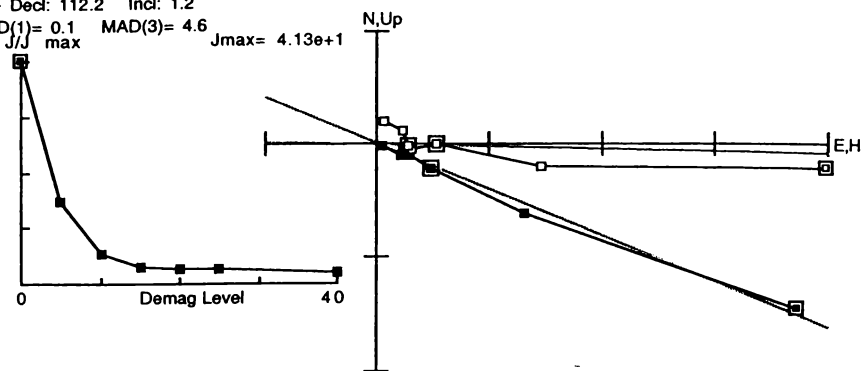
Date: Sunday, 27 August 2000

■ N,E

PCA - Decl: 112.2 Incl: 1.2

MAD(1) = 0.1    MAD(3) = 4.6

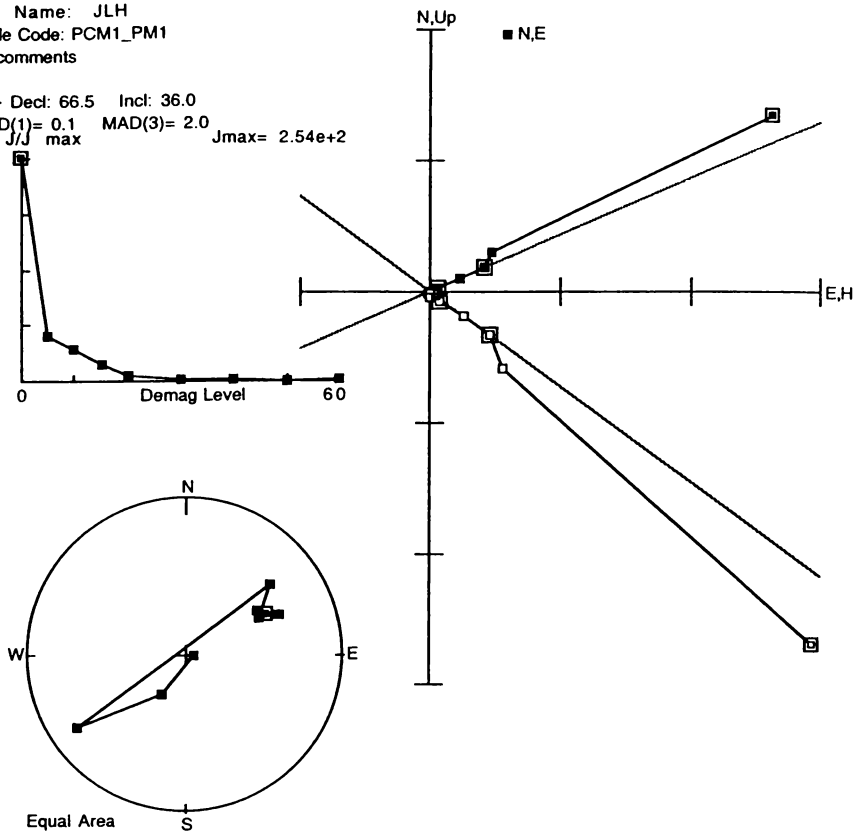
Jmax = 4.13e+1



File Name: OP/2/1/CORR  
 User Name: JLH  
 Sample Code: PCM1\_PM1  
 Your comments

Date: Sunday, 27 August 2000

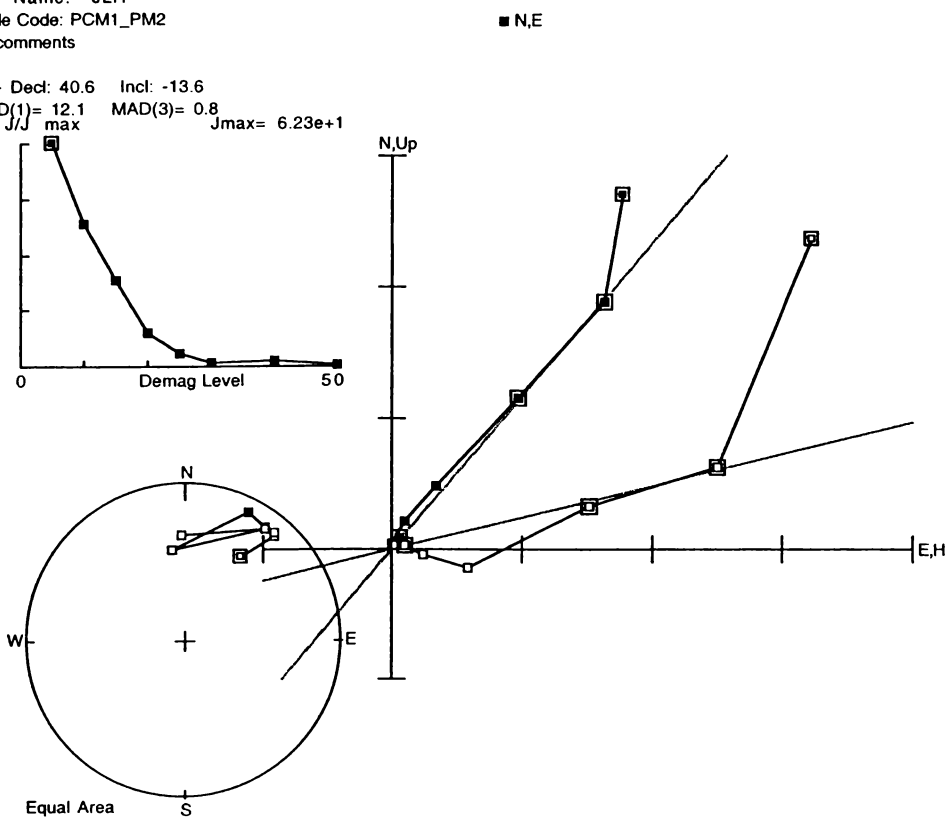
PCA - Decl: 66.5 Incl: 36.0  
 MAD(1) = 0.1 J/J max MAD(3) = 2.0  
 Jmax = 2.54e+2



File Name: OP/2/1/CORR  
 User Name: JLH  
 Sample Code: PCM1\_PM2  
 Your comments

Date: Sunday, 27 August 2000

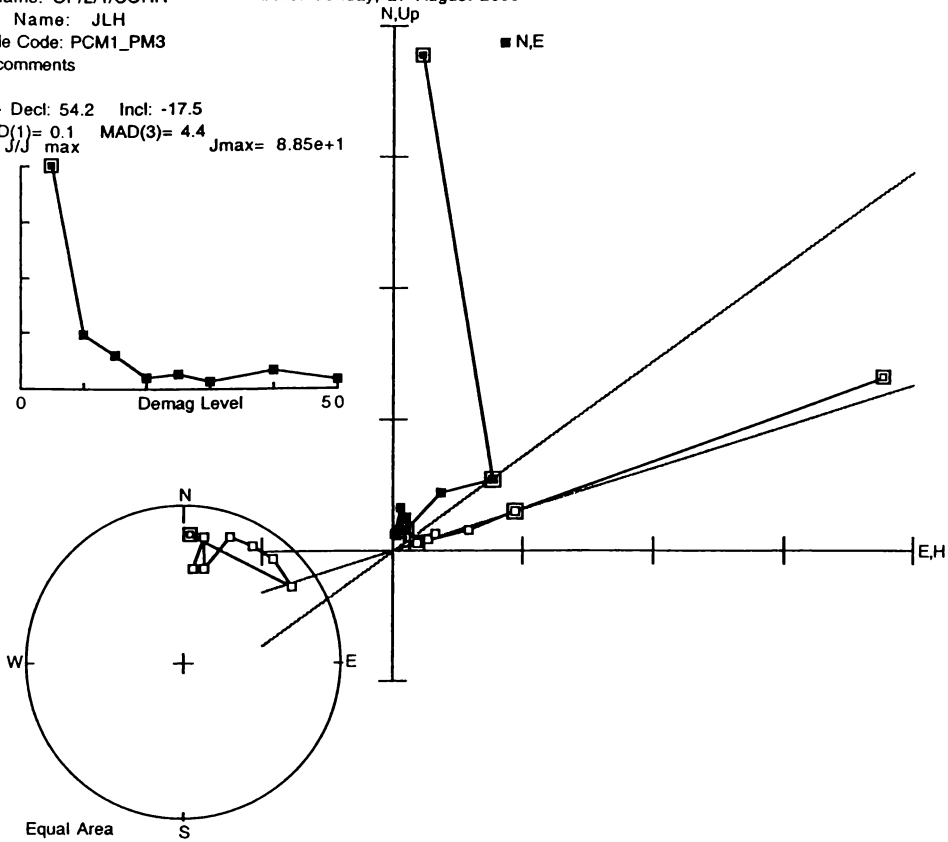
PCA - Decl: 40.6 Incl: -13.6  
 MAD(1) = 12.1 J/J max MAD(3) = 0.8  
 Jmax = 6.23e+1



File Name: OP/2/1/CORR  
User Name: JLH  
Sample Code: PCM1\_PM3  
Your comments

Date: Sunday, 27 August 2000

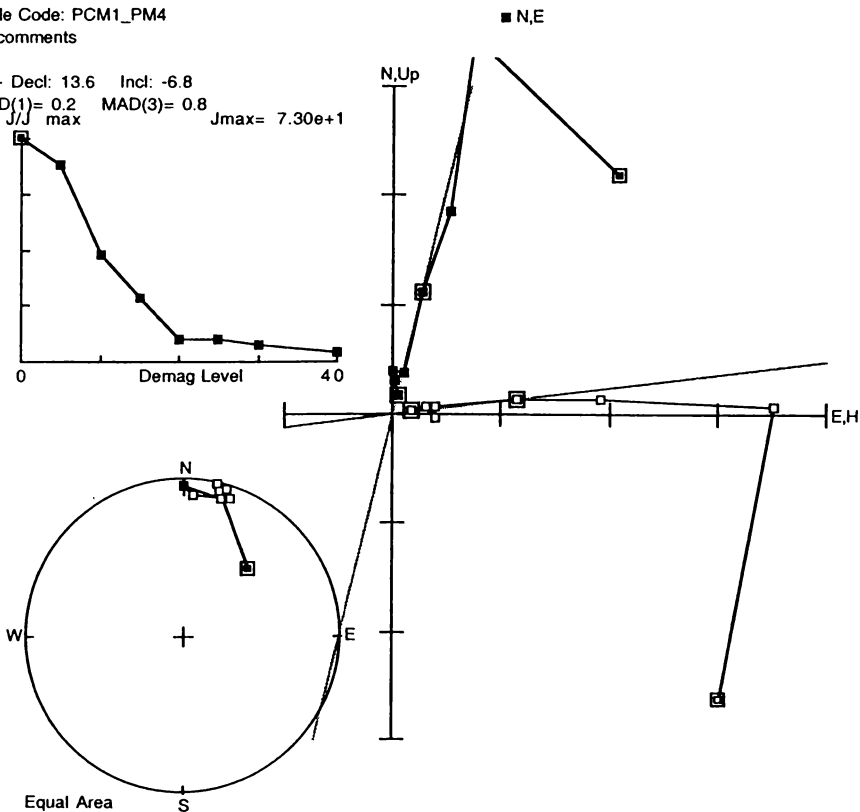
PCA - Decl: 54.2 Incl: -17.5  
MAD(1)= 0.1 MAD(3)= 4.4  
J/J max Jmax= 8.85e+1



File Name: OP/2/1/CORR  
User Name: JLH  
Sample Code: PCM1\_PM4  
Your comments

Date: Sunday, 27 August 2000

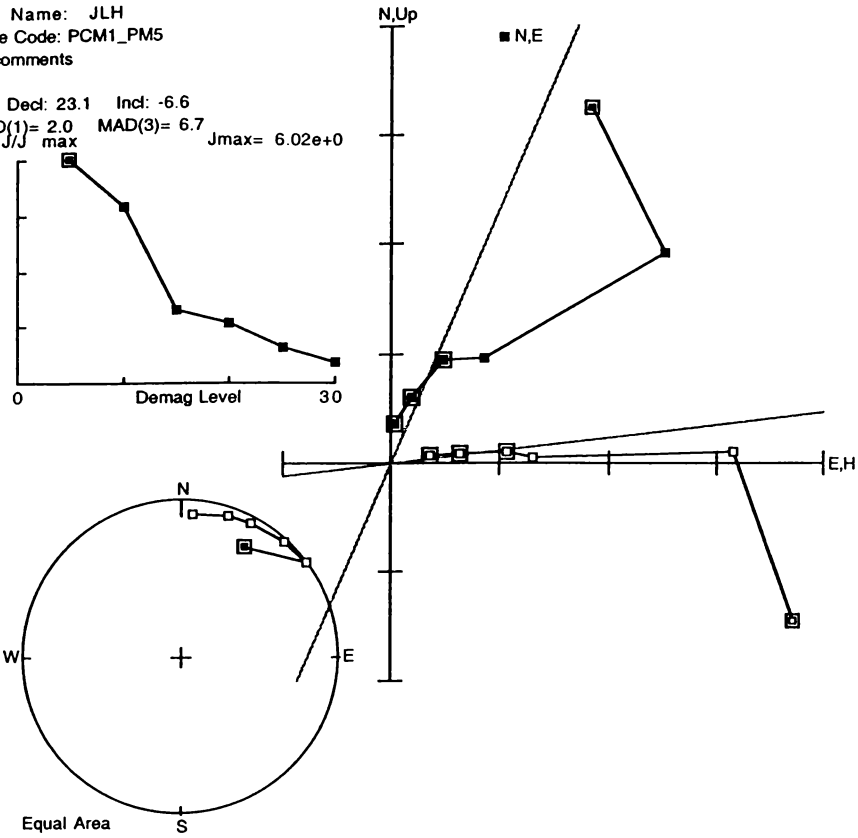
PCA - Decl: 13.6 Incl: -6.8  
MAD(1)= 0.2 MAD(3)= 0.8  
J/J max Jmax= 7.30e+1



File Name: OP/2/2/CORR  
 User Name: JLH  
 Sample Code: PCM1\_PM5  
 Your comments

Date: Sunday, 27 August 2000

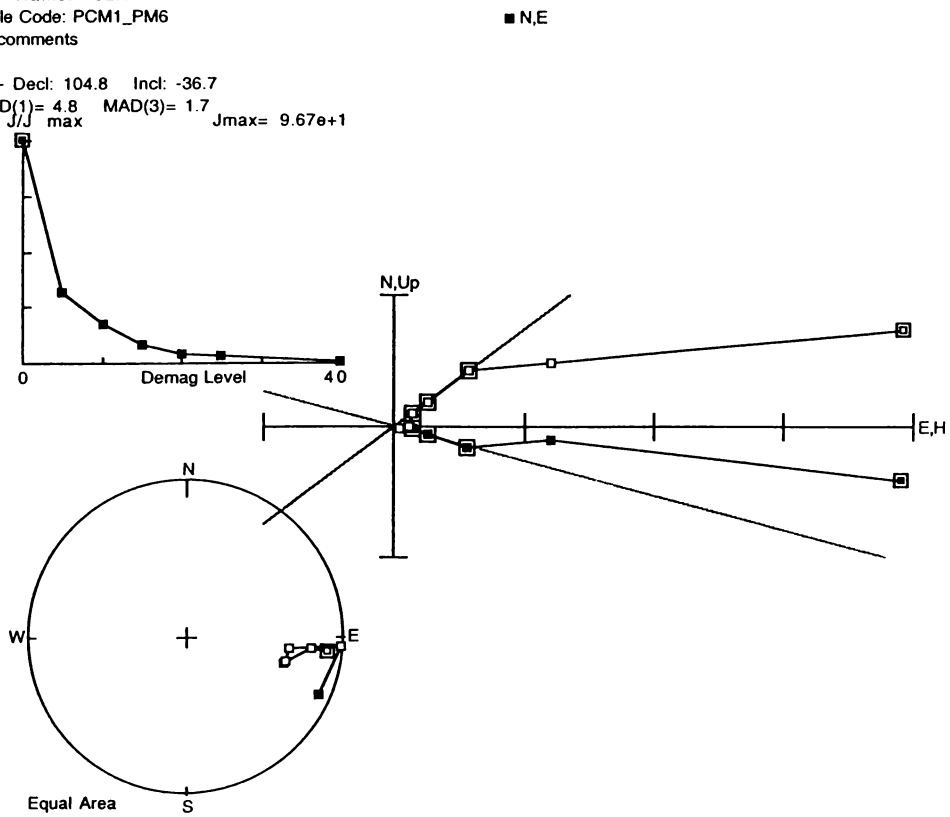
PCA - Decl: 23.1 Incl: -6.6  
 MAD(1)= 2.0 MAD(3)= 6.7  
 J/J max Jmax= 6.02e+0



File Name: OP/2/2/CORR  
 User Name: JLH  
 Sample Code: PCM1\_PM6  
 Your comments

Date: Sunday, 27 August 2000

PCA - Decl: 104.8 Incl: -36.7  
 MAD(1)= 4.8 MAD(3)= 1.7  
 J/J max Jmax= 9.67e+1



File Name: OP/2/2/CORR  
User Name: JLH  
Sample Code: PCM1\_PM7  
Your comments

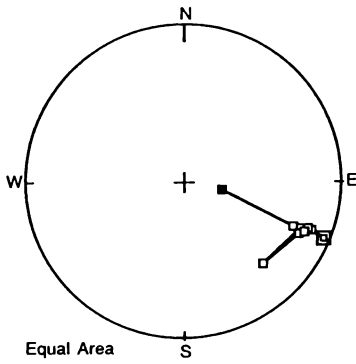
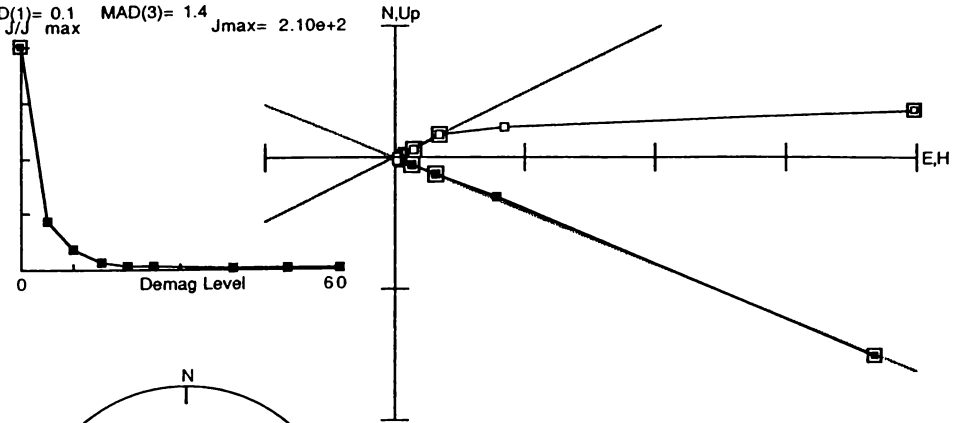
Date: Sunday, 27 August 2000

■ N,E

PCA - Decl: 112.1 Incl: -26.1

MAD(1) = 0.1 MAD(3) = 1.4

Jmax = 2.10e+2



File Name: OP/2/2/CORR  
User Name: JLH  
Sample Code: PCM1\_PM8  
Your comments

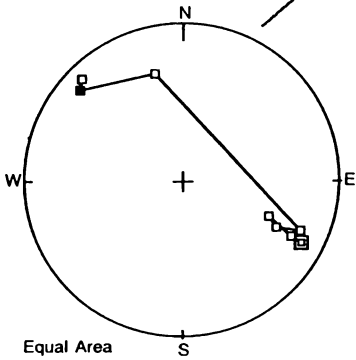
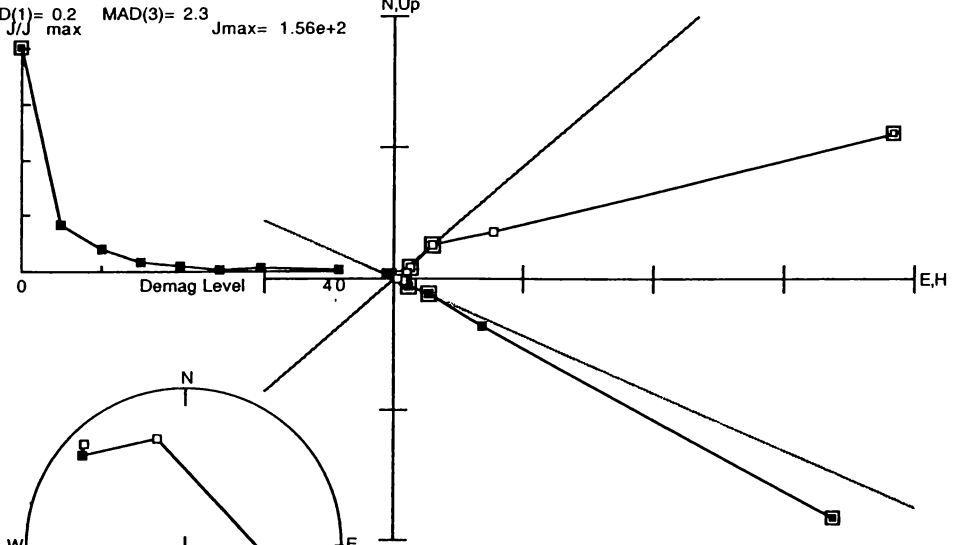
Date: Sunday, 27 August 2000

■ N,E

PCA - Decl: 113.6 Incl: -40.5

MAD(1) = 0.2 MAD(3) = 2.3

Jmax = 1.56e+2



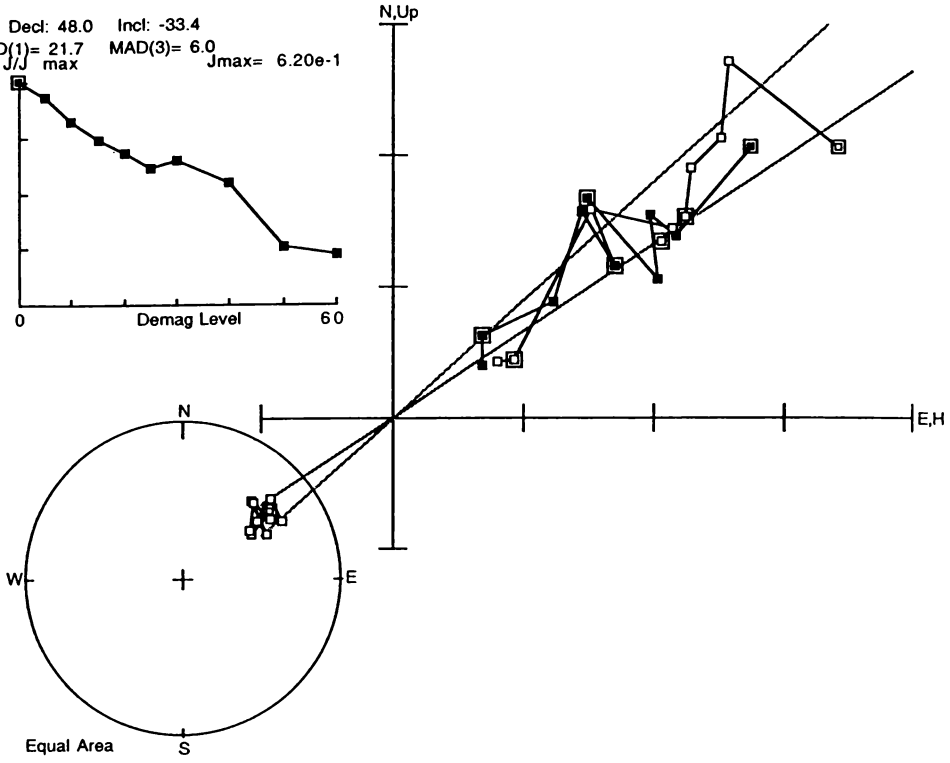


File Name: OP/2/3/CORR  
User Name: JLH  
Sample Code: WS\_PM1  
Your comments

Date: Sunday, 27 August 2000

■ N,E

PCA - Decl: 48.0 Incl: -33.4  
MAD(1)= 21.7 MAD(3)= 6.0  
J/J max Jmax= 6.20e-1

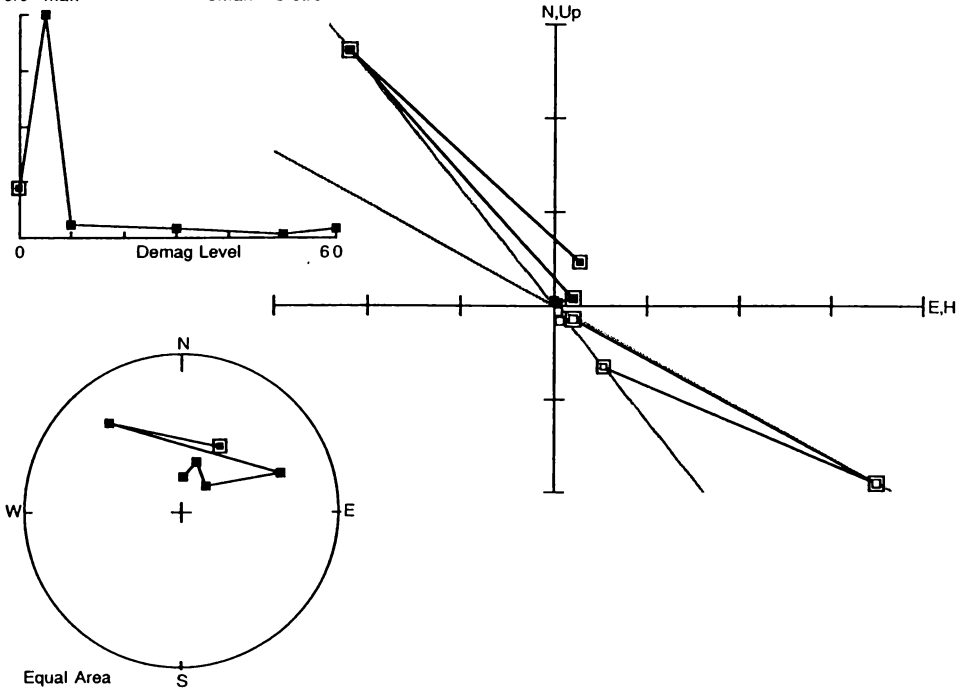


File Name: WSMAN\_2\_CORR1  
User Name: JLH  
Sample Code: WS\_PM2  
Your comments

Date: Sunday, 27 August 2000

■ N,E

PCA - Decl: -38.9 Incl: 28.7  
MAD(1)= 0.1 MAD(3)= 3.6  
J/J max Jmax= 5.82e+1



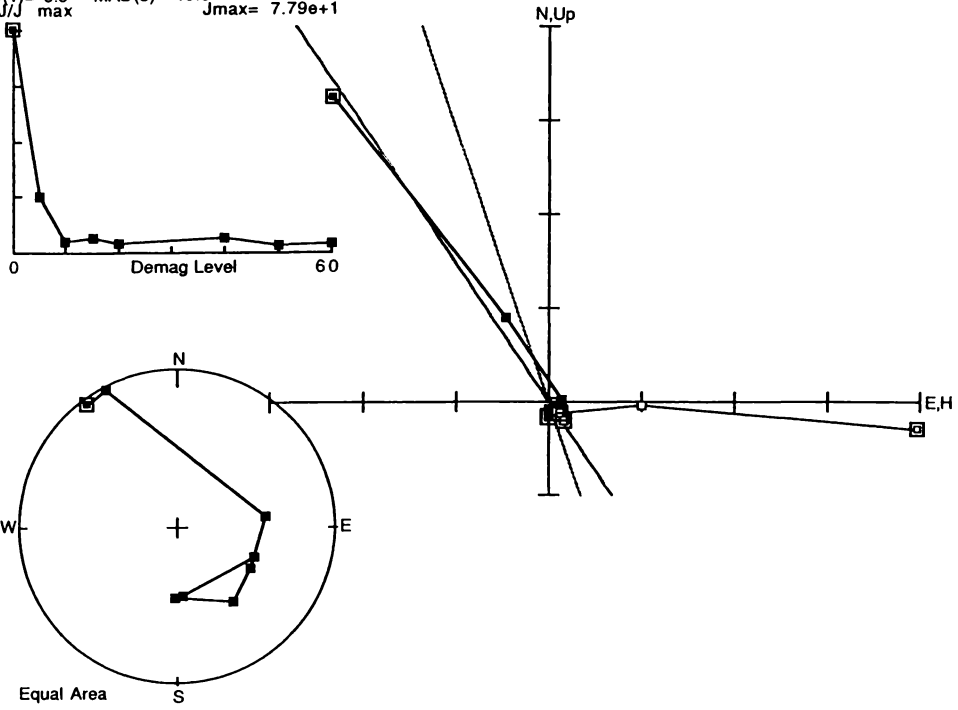
File Name: WSMAIN\_2\_CORR1  
 User Name: JLH  
 Sample Code: WS\_PM3  
 Your comments

Date: Sunday, 27 August 2000

■ N,E

PCA - Decl: 161.1 Incl: 55.8

MAD(1)= 0.0 MAD(3)= 19.6  
 $J/J_{max}$



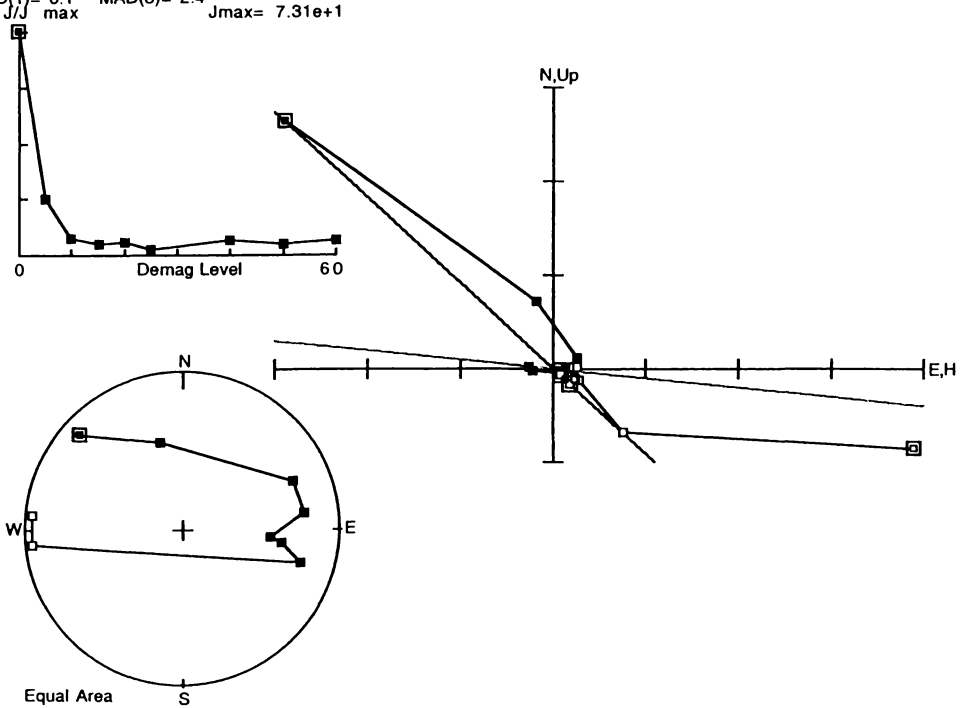
File Name: WSMAIN\_2\_CORR2  
 User Name: JLH  
 Sample Code: WS\_PM4  
 Your comments

Date: Sunday, 27 August 2000

■ N,E

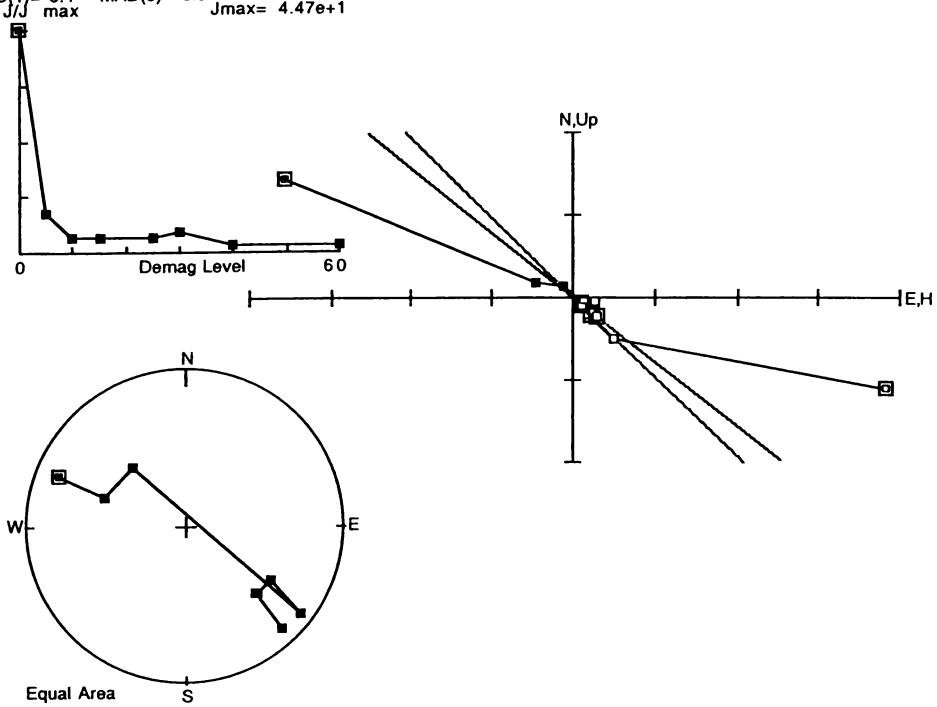
PCA - Decl: 95.6 Incl: 42.4

MAD(1)= 0.1 MAD(3)= 2.4  
 $J/J_{max}$



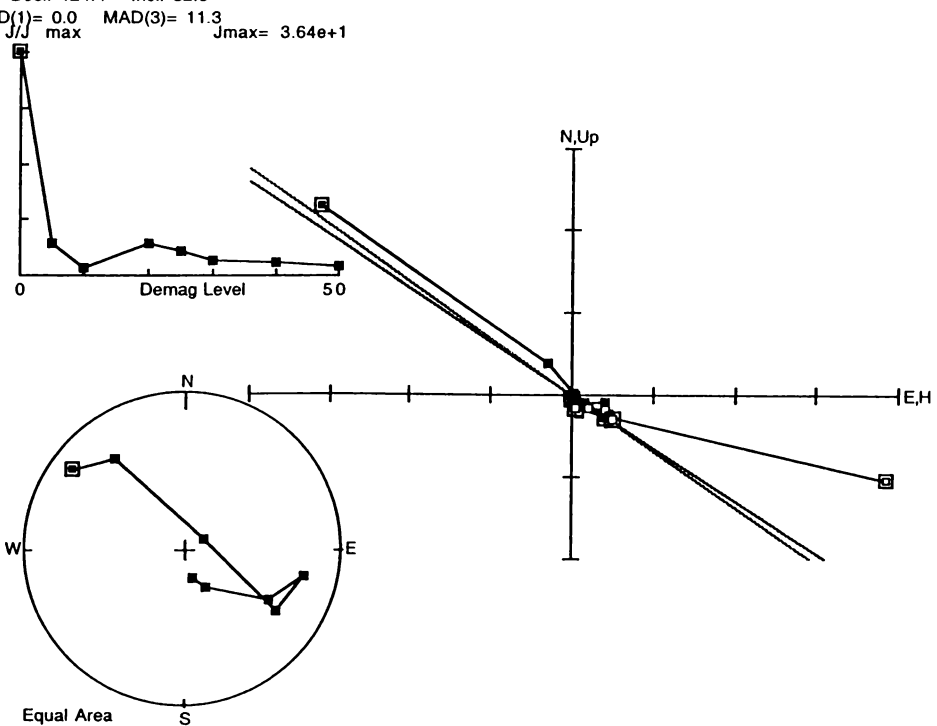
File Name: WSMAIN\_2\_CORR2 Date: Sunday, 27 August 2000  
 User Name: JLH  
 Sample Code: WS\_PM5  
 Your comments

PCA - Decl: 133.9 Incl: 38.3  
 $J/J_{max}$   
 MAD(1)= 0.4 MAD(3)= 0.5  
 $J_{max}= 4.47e+1$



File Name: WSMAIN\_2\_CORR2 Date: Sunday, 27 August 2000  
 User Name: JLH  
 Sample Code: WS\_PM6  
 Your comments

PCA - Decl: 124.4 Incl: 32.8  
 $J/J_{max}$   
 MAD(1)= 0.0 MAD(3)= 11.3  
 $J_{max}= 3.64e+1$

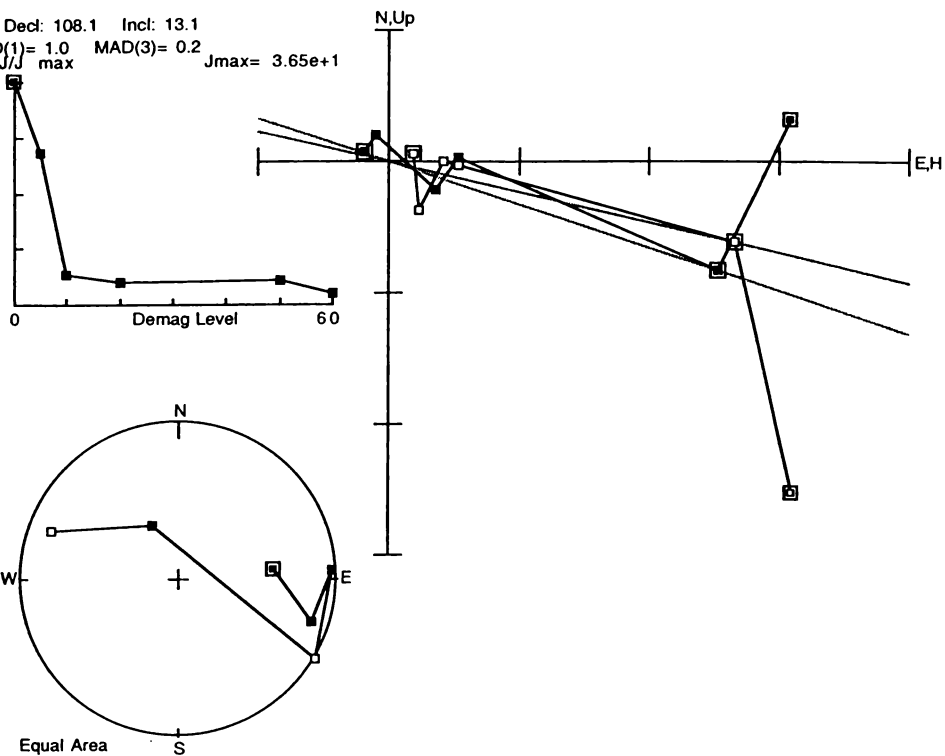


File Name: WSMAIN\_2\_CORR1  
 User Name: JLH  
 Sample Code: WS\_PM7  
 Your comments

Date: Sunday, 27 August 2000

■ N,E

PCA - Decl: 108.1 Incl: 13.1  
 MAD(1)= 1.0 MAD(3)= 0.2  
 $\frac{J}{J_{max}}$

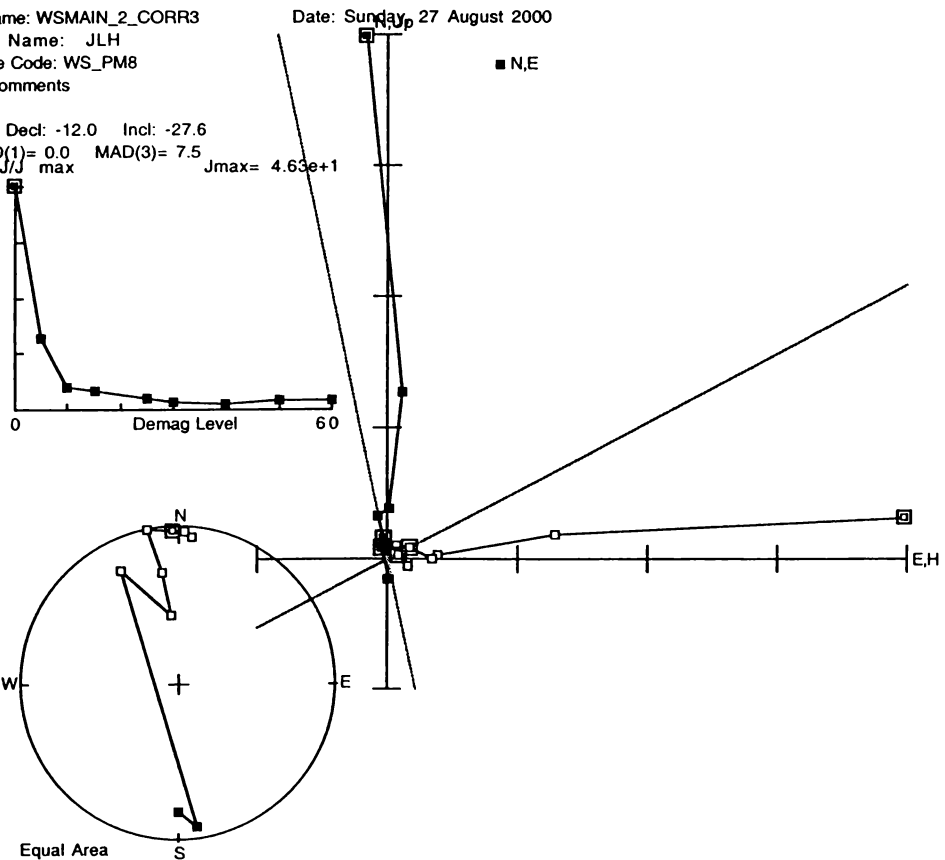


File Name: WSMAIN\_2\_CORR3  
 User Name: JLH  
 Sample Code: WS\_PM8  
 Your comments

Date: Sunday, 27 August 2000

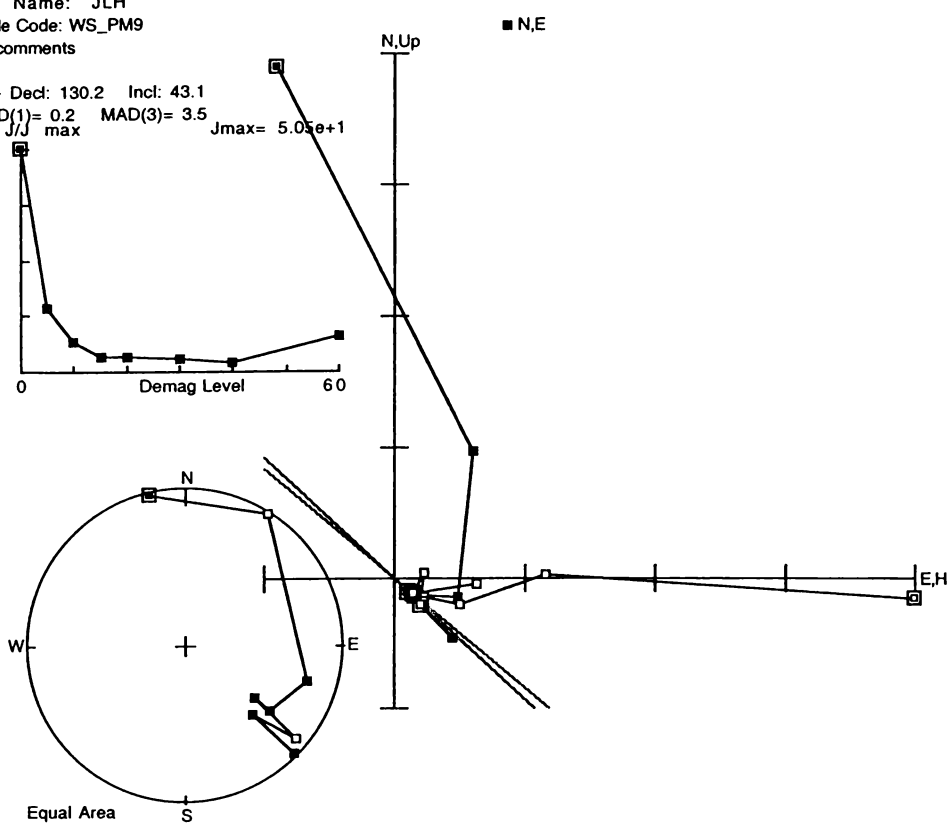
■ N,E

PCA - Decl: -12.0 Incl: -27.6  
 MAD(1)= 0.0 MAD(3)= 7.5  
 $\frac{J}{J_{max}}$



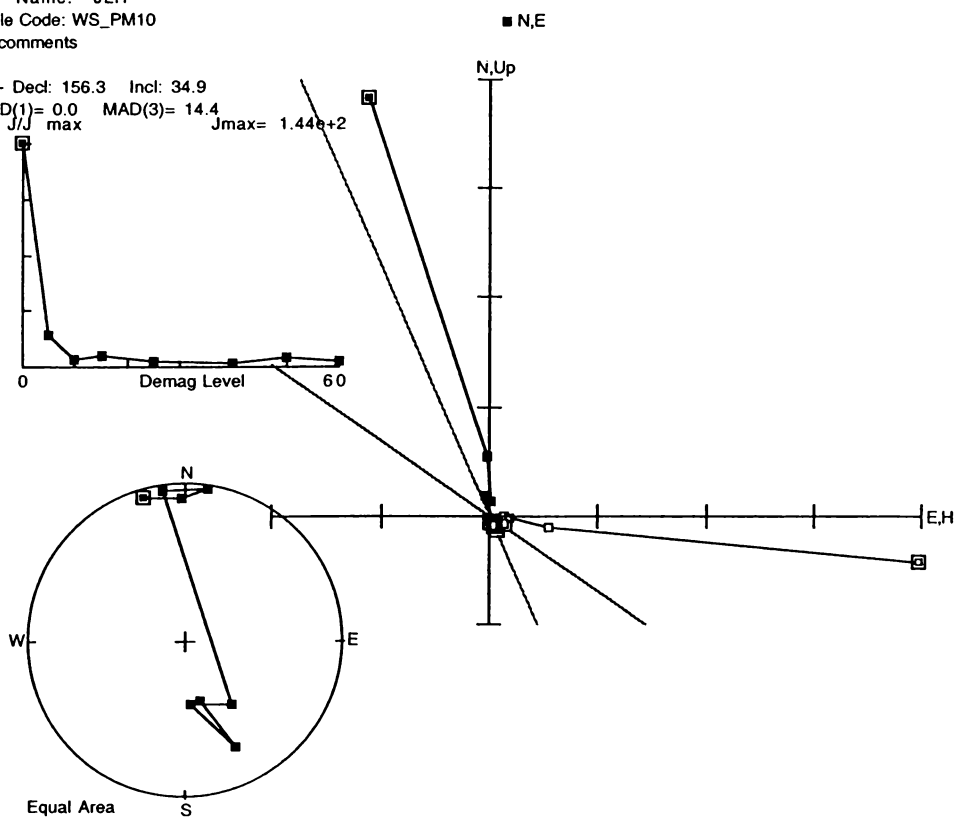
File Name: WSMAIN\_2\_CORR1  
 User Name: JLH  
 Sample Code: WS\_PM9  
 Your comments

PCA - Decl: 130.2 Incl: 43.1  
 $MAD(1) = 0.2$   $MAD(3) = 3.5$   
 $J/J_{max}$



File Name: WSMAIN\_2\_CORR2  
 User Name: JLH  
 Sample Code: WS\_PM10  
 Your comments

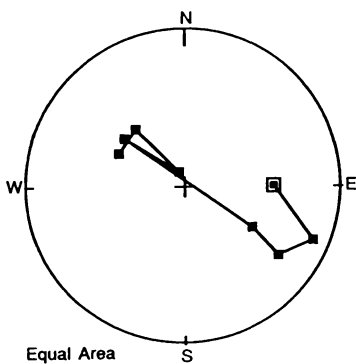
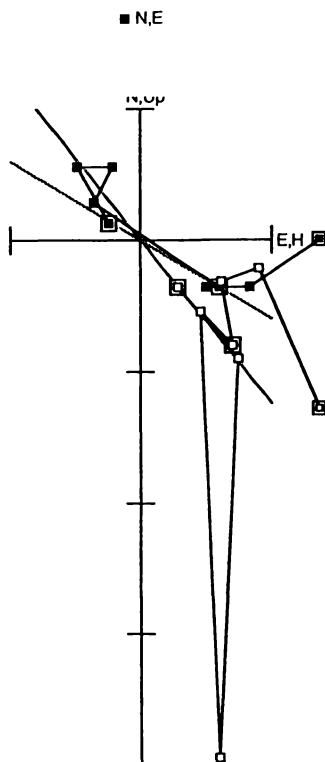
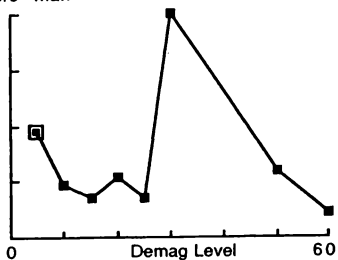
PCA - Decl: 156.3 Incl: 34.9  
 $MAD(1) = 0.0$   $MAD(3) = 14.4$   
 $J/J_{max}$



File Name: WSMAIN\_2\_CORR2  
 User Name: JLH  
 Sample Code: WS\_PM11  
 Your comments

Date: Sunday, 27 August 2000

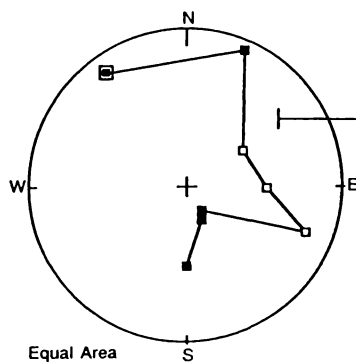
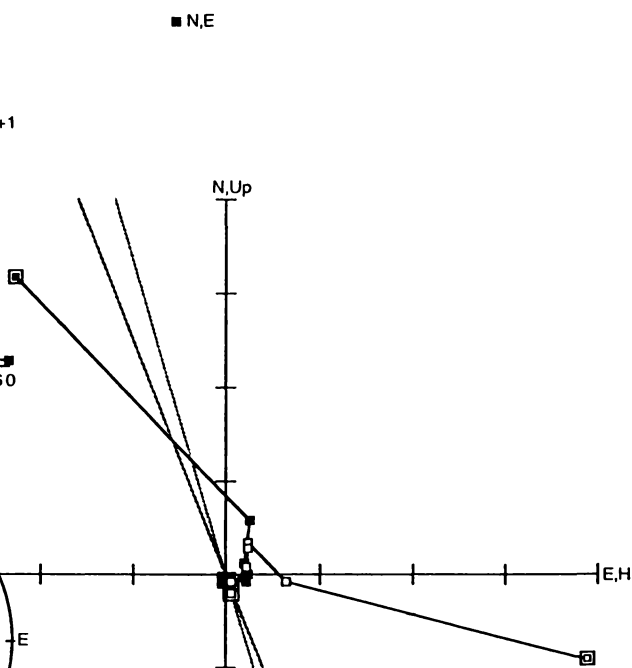
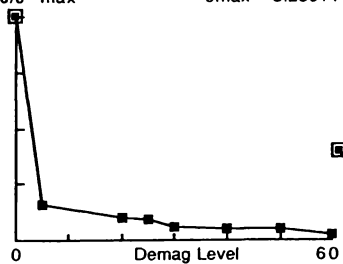
PCA - Decl: 121.2 Incl: 51.2  
 MAD(1)= 0.0 MAD(3)= 22.4  
 J/J max Jmax= 1.27e+1



File Name: WSMAIN\_2\_CORR1  
 User Name: JLH  
 Sample Code: WS\_PM12  
 Your comments

Date: Sunday, 27 August 2000

PCA - Decl: 163.2 Incl: 68.3  
 MAD(1)= 0.0 MAD(3)= 9.7  
 J/J max Jmax= 3.28e+1



File Name: WSMAIN\_2\_CORR1

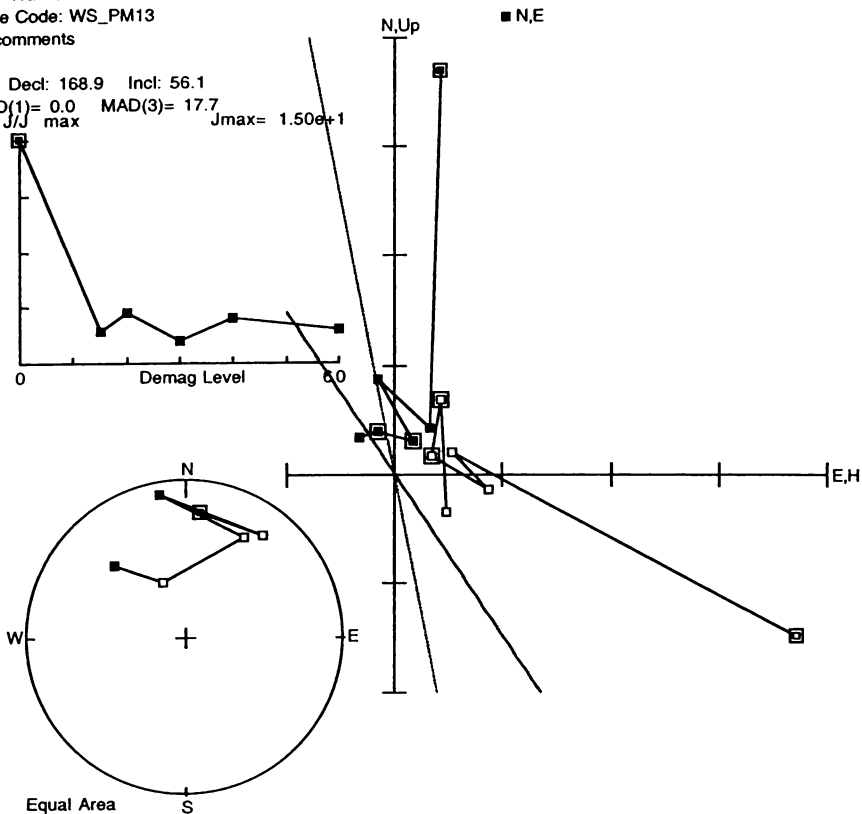
Date: Sunday, 27 August 2000

User Name: JLH

Sample Code: WS\_PM13

Your comments

PCA - Decl: 168.9 Incl: 56.1  
MAD(1)= 0.0 MAD(3)= 17.7  
J/J max Jmax= 1.50e+1



File Name: WSMAIN\_2\_CORR1

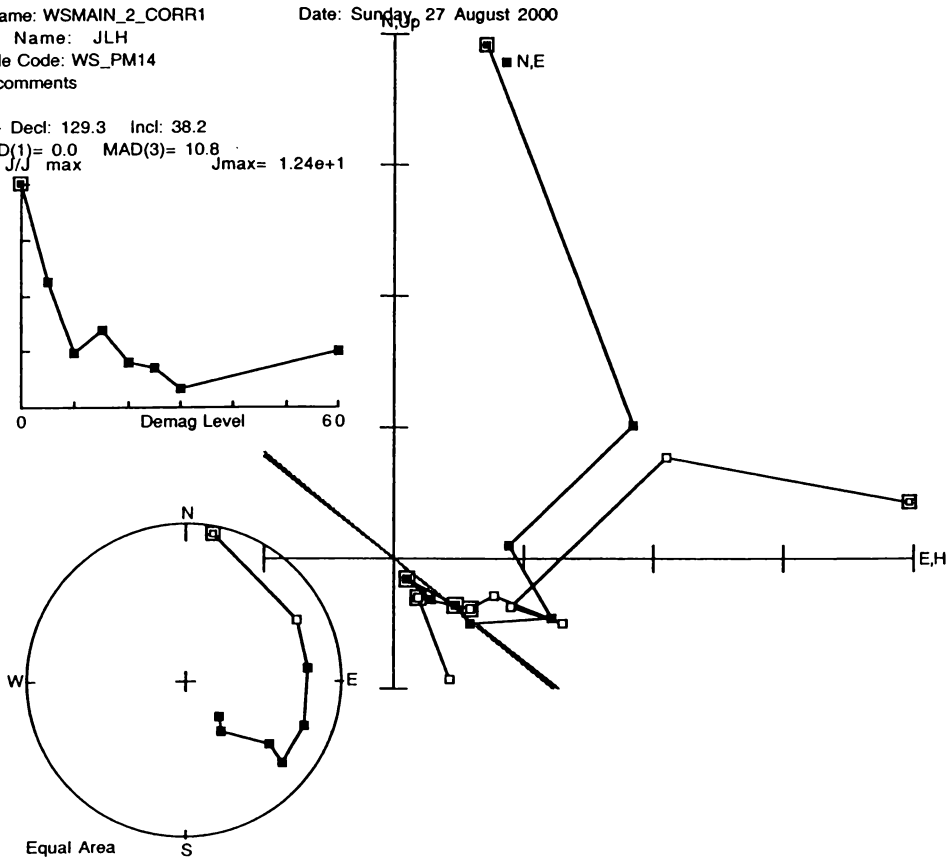
Date: Sunday, 27 August 2000

User Name: JLH

Sample Code: WS\_PM14

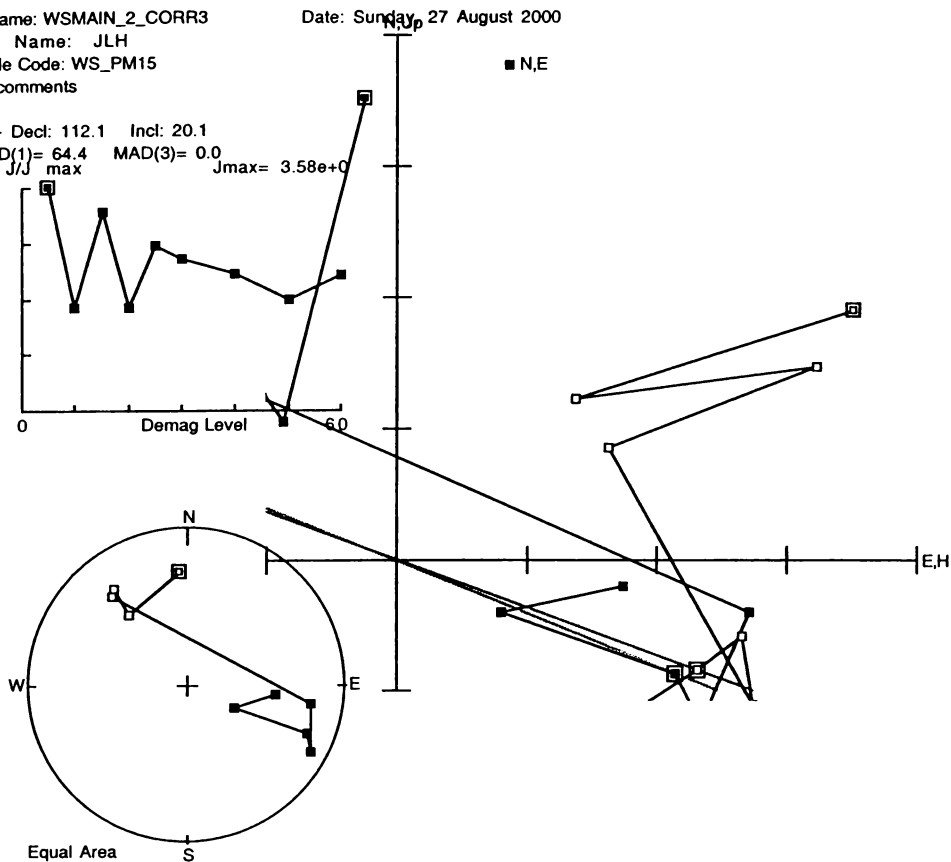
Your comments

PCA - Decl: 129.3 Incl: 38.2  
MAD(1)= 0.0 MAD(3)= 10.8  
J/J max Jmax= 1.24e+1



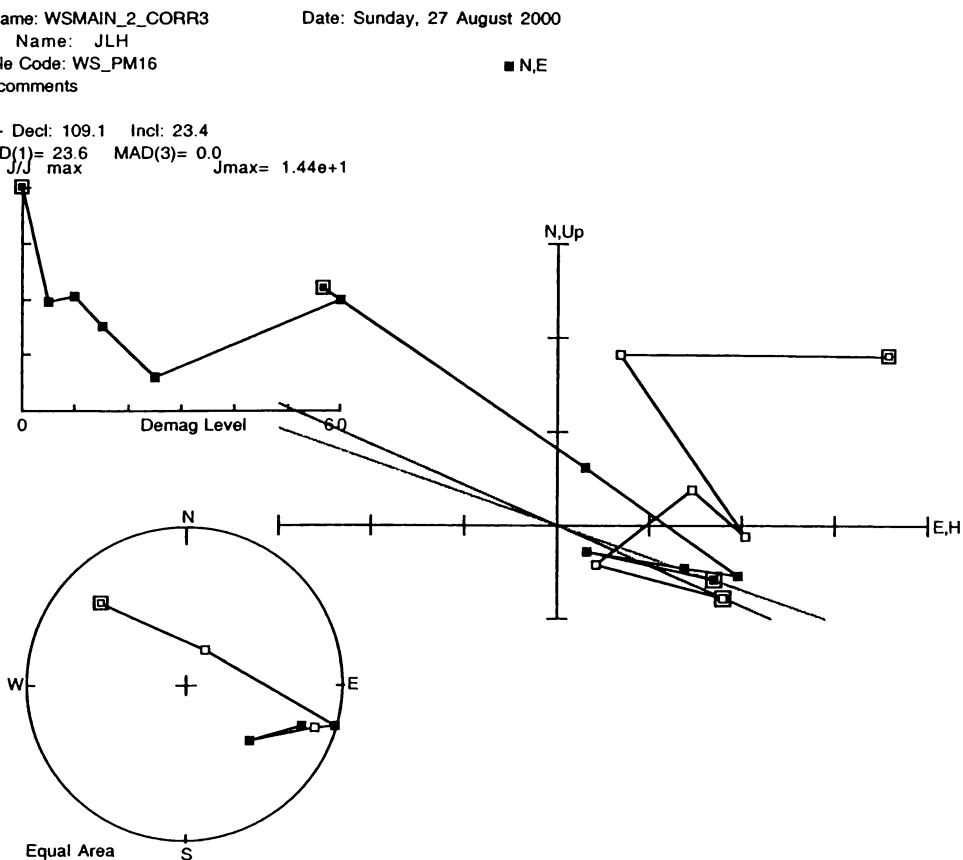
File Name: WSMAIN\_2\_CORR3 Date: Sunday, 27 August 2000  
 User Name: JLH  
 Sample Code: WS\_PM15  
 Your comments

PCA - Decl: 112.1 Incl: 20.1  
 MAD(1)= 64.4 MAD(3)= 0.0  
 J/J max Jmax= 3.58e+0



File Name: WSMAIN\_2\_CORR3 Date: Sunday, 27 August 2000  
 User Name: JLH  
 Sample Code: WS\_PM16  
 Your comments

PCA - Decl: 109.1 Incl: 23.4  
 MAD(1)= 23.6 MAD(3)= 0.0  
 J/J max Jmax= 1.44e+1

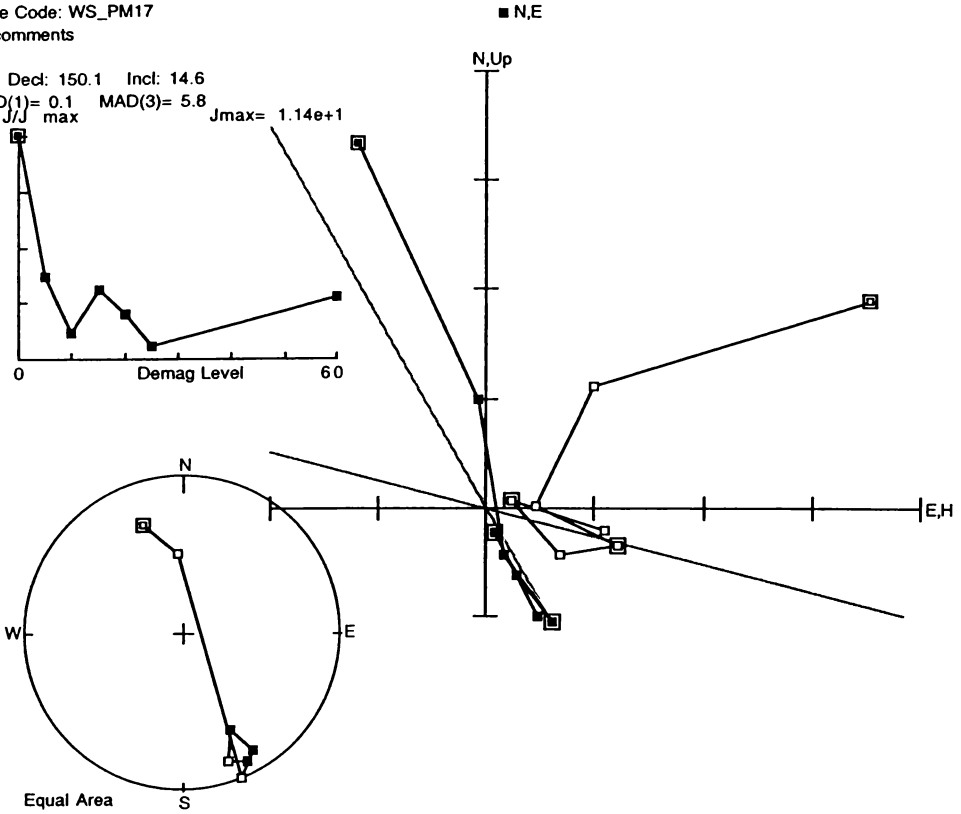




File Name: WSMAIN\_2\_CORR3  
User Name: JLH  
Sample Code: WS\_PM17  
Your comments

Date: Sunday, 27 August 2000

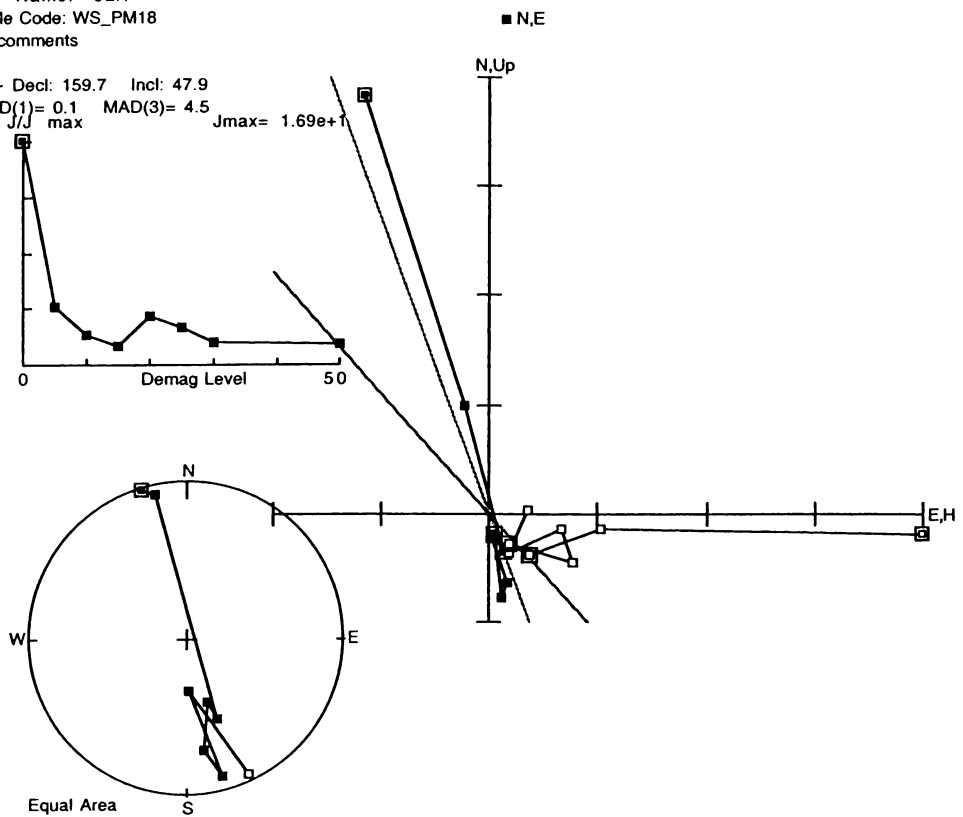
PCA - Decl: 150.1 Incl: 14.6  
MAD(1)= 0.1 MAD(3)= 5.8  
J/J max



File Name: WSMAIN\_2\_CORR3  
User Name: JLH  
Sample Code: WS\_PM18  
Your comments

Date: Sunday, 27 August 2000

PCA - Decl: 159.7 Incl: 47.9  
MAD(1)= 0.1 MAD(3)= 4.5  
J/J max



File Name: WSMAIN\_2\_CORR3

Date: Sunday, 27 August 2000

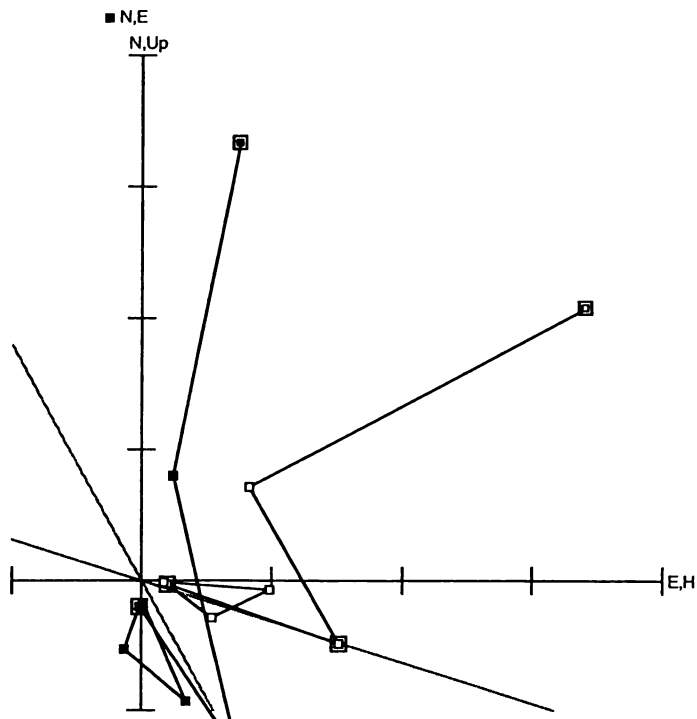
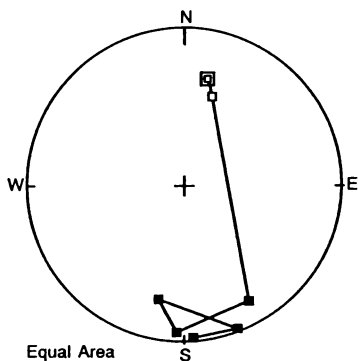
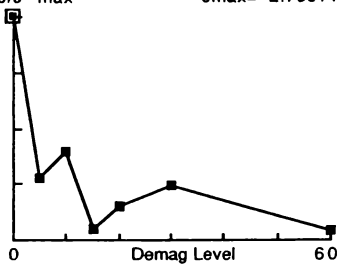
User Name: JLH

Sample Code: WS\_PM19

Your comments

PCA - Decl: 151.0 Incl: 17.5

MAD(1)= 0.1 MAD(3)= 3.9  
 $J/J_{max}$



File Name: WSMAIN\_2\_CORR4

Date: Sunday, 27 August 2000

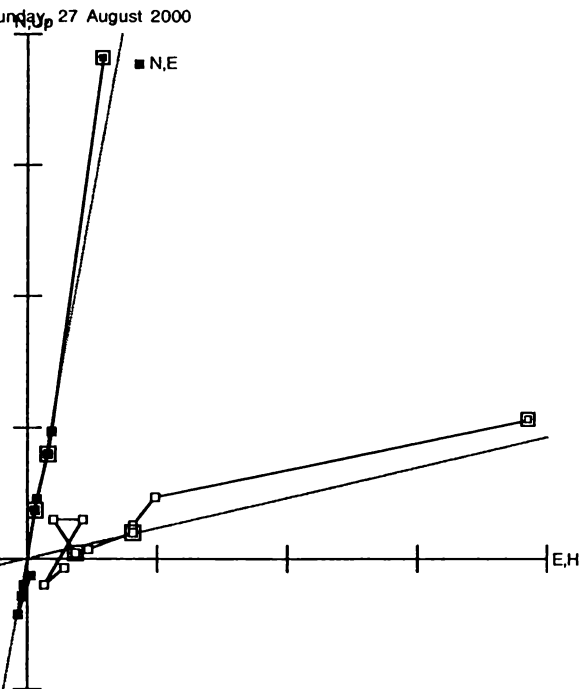
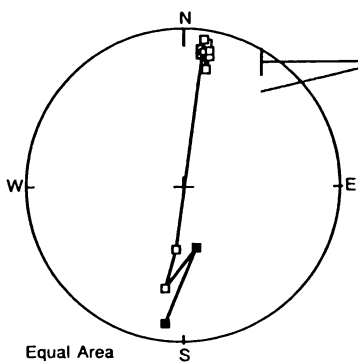
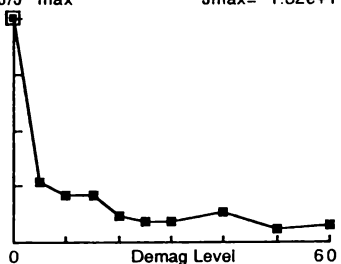
User Name: JLH

Sample Code: WS\_PM20

Your comments

PCA - Decl: 10.3 Incl: -13.0

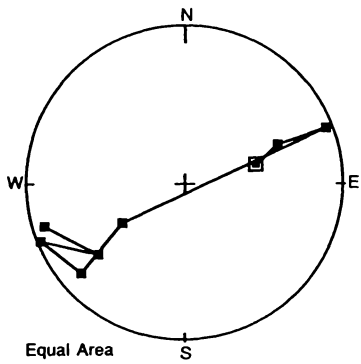
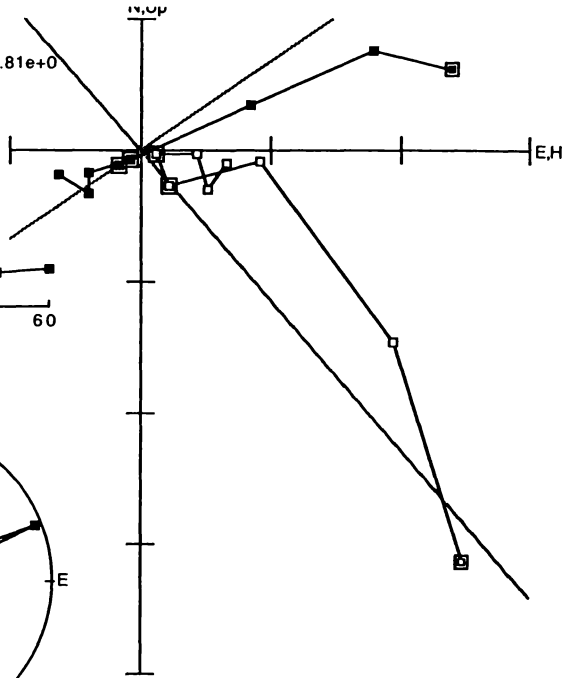
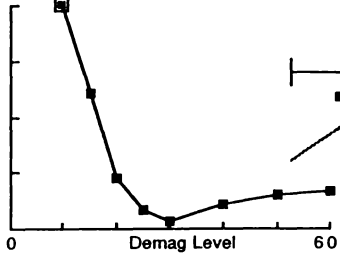
MAD(1)= 0.0 MAD(3)= 2.9  
 $J/J_{max}$



File Name: WSMAN\_2\_CORR4  
 User Name: JLH  
 Sample Code: WS\_PM21  
 Your comments

Date: Sunday, 27 August 2000

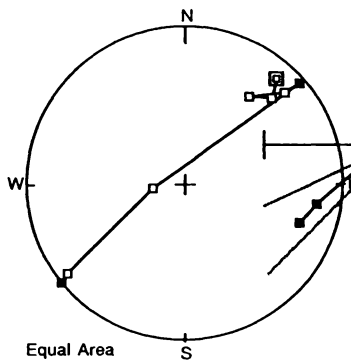
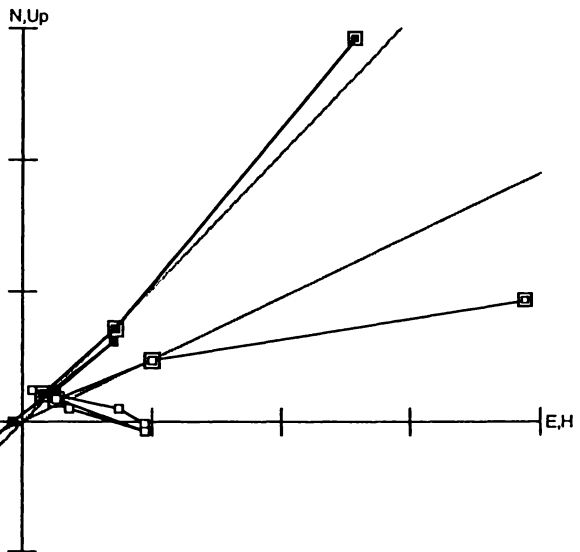
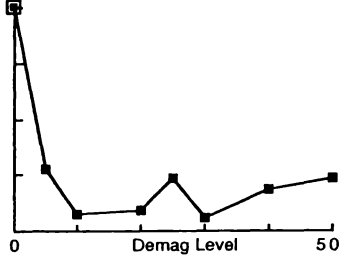
PCA - Decl: 235.9 Incl: 48.7  
 MAD(1)= 0.1 MAD(3)= 11.3  
 $J/J_{max}$



File Name: WSMAN\_2\_CORR4  
 User Name: JLH  
 Sample Code: WS\_PMOK  
 Your comments

Date: Sunday, 27 August 2000

PCA - Decl: 44.4 Incl: -25.4  
 MAD(1)= 0.1 MAD(3)= 2.9  
 $J/J_{max}$



**APPENDIX D:  
MAJOR ELEMENT COMPOSITION  
(KAUROA ASH SEQUENCE)**

## K12

(normalised)

	01	02	03	04	05	06	07	08	09	10	11	13	14	15	17	18	19	20	21	22	23	24	25	26	27	28	mean	stdev
<b>SiO<sub>2</sub></b>	79.44	78.27	77.68	77.50	77.52	80.61	78.03	78.72	77.84	77.86	78.66	77.45	77.49	77.27	78.15	77.56	78.16	78.07	77.31	77.83	77.12	76.57	77.62	77.54	78.15	77.30	<b>77.91</b>	<b>0.80</b>
<b>Al<sub>2</sub>O<sub>3</sub></b>	12.38	12.66	12.79	12.79	12.68	10.73	12.71	12.04	12.62	12.47	12.70	12.71	12.56	12.59	13.06	12.67	12.68	12.70	12.73	12.89	12.39	12.58	12.22	12.75	12.38	12.62	<b>12.54</b>	<b>0.42</b>
<b>TiO<sub>2</sub></b>	0.23	0.08	0.17	0.20	0.09	0.07	0.07	0.15	0.05	0.10	0.03	0.12	0.18	0.15	0.12	0.09	0.06	0.08	0.12	0.22	0.21	0.14	0.09	0.19	0.18	0.19	<b>0.13</b>	<b>0.06</b>
<b>FeO</b>	0.93	1.08	1.04	1.22	1.18	0.89	0.99	0.99	0.80	0.86	0.95	1.53	1.09	1.01	1.14	0.91	1.02	0.91	1.24	1.12	1.24	1.34	1.23	1.14	0.92	1.13	<b>1.07</b>	<b>0.17</b>
<b>MnO</b>	0.09	0.14	0.22	0.06	0.08	0.14	0.09	0.20	0.07	0.08	0.01	0.00	0.13	0.17	0.30	0.08	0.39	0.20	0.14	0.00	0.28	0.31	0.15	0.14	0.28	0.14	<b>0.15</b>	<b>0.10</b>
<b>MgO</b>	0.11	0.15	0.10	0.09	0.14	0.09	0.13	0.06	0.10	0.07	0.01	0.08	0.14	0.13	0.11	0.05	0.05	0.07	0.12	0.09	0.15	0.12	0.13	0.12	0.09	0.07	<b>0.10</b>	<b>0.03</b>
<b>CaO</b>	0.74	0.84	0.96	1.12	0.73	0.69	0.73	0.89	0.54	0.51	0.44	0.92	0.66	0.72	0.84	0.60	0.58	0.66	0.89	0.97	0.70	0.86	0.77	0.89	0.79	0.77	<b>0.76</b>	<b>0.16</b>
<b>Na<sub>2</sub>O</b>	1.89	2.79	3.12	2.89	3.28	2.97	2.75	2.85	3.42	3.59	2.71	3.26	3.39	3.37	2.18	3.24	2.61	2.83	3.49	2.79	3.56	3.55	3.36	3.01	3.14	3.50	<b>3.06</b>	<b>0.43</b>
<b>K<sub>2</sub>O</b>	3.92	3.73	3.69	3.86	4.07	3.56	4.30	3.76	4.29	4.28	4.29	3.69	4.16	4.32	3.85	4.52	4.25	4.19	3.75	3.88	4.04	4.23	4.12	3.89	3.79	4.02	<b>4.02</b>	<b>0.25</b>
<b>Cl</b>	0.27	0.26	0.22	0.27	0.23	0.24	0.19	0.34	0.25	0.19	0.20	0.23	0.22	0.28	0.24	0.29	0.21	0.29	0.20	0.21	0.33	0.28	0.32	0.38	0.28	0.27	<b>0.26</b>	<b>0.05</b>
<b>Water</b>	6.74	5.43	3.27	4.13	4.74	4.43	5.95	4.69	5.46	5.88	5.57	5.46	5.70	6.20	4.77	7.20	6.53	5.49	4.64	6.04	4.68	4.72	4.80	4.56	3.25	3.76	<b>5.16</b>	<b>1.00</b>
<b>n</b>																												<b>28</b>

## OPARAU TEPHRA

(normalised)

	01	02	03	04	05	06	07	08	09	10	11	12	13	14	15	16	17	18	19	20	21	22	23	mean	stdev			
<b>SiO<sub>2</sub></b>	76.62	76.37	76.11	76.45	75.87	76.05	77.05	76.49	75.77	76.09	77.05	76.10	76.48	76.21	77.42	76.75	76.50	76.65	76.50	76.27	76.26	76.04	76.05	<b>76.40</b>	<b>0.40</b>			
<b>Al<sub>2</sub>O<sub>3</sub></b>	12.76	12.65	12.74	12.53	12.98	12.93	12.37	12.72	12.87	12.84	12.73	13.11	12.47	12.83	12.72	12.62	13.65	12.67	12.89	12.72	12.88	12.85	12.67	<b>12.79</b>	<b>0.25</b>			
<b>TiO<sub>2</sub></b>	0.19	0.21	0.30	0.35	0.17	0.41	0.24	0.31	0.21	0.19	0.11	0.07	0.28	0.19	0.22	0.13	0.18	0.11	0.20	0.29	0.22	0.04	0.21	<b>0.21</b>	<b>0.09</b>			
<b>FeO</b>	1.06	1.19	1.18	1.19	1.43	1.61	1.20	1.15	1.52	1.16	0.88	1.08	1.27	1.44	1.09	1.23	0.94	1.11	1.14	1.27	1.10	1.27	1.28	<b>1.21</b>	<b>0.17</b>			
<b>MnO</b>	0.04	0.26	0.31	0.29	0.00	0.07	0.11	0.00	0.11	0.34	0.00	0.27	0.10	0.03	0.00	0.25	0.00	0.19	0.00	0.20	0.26	0.21	0.11	<b>0.14</b>	<b>0.12</b>			
<b>MgO</b>	0.09	0.13	0.07	0.09	0.15	0.15	0.22	0.16	0.13	0.07	0.13	0.11	0.10	0.10	0.10	0.16	0.25	0.07	0.17	0.14	0.11	0.13	0.16	<b>0.13</b>	<b>0.04</b>			
<b>CaO</b>	0.75	0.79	0.81	0.86	0.89	0.84	0.79	0.73	0.96	0.88	0.79	0.86	0.86	0.88	0.75	0.84	0.91	0.90	1.25	0.80	0.80	0.85	0.82	<b>0.85</b>	<b>0.10</b>			
<b>Na<sub>2</sub>O</b>	3.80	4.08	3.95	3.96	3.92	3.60	3.75	4.05	3.76	3.79	3.76	3.95	3.85	3.73	3.29	3.73	3.34	3.91	3.59	3.88	3.77	3.78	4.07	<b>3.80</b>	<b>0.20</b>			
<b>K<sub>2</sub>O</b>	4.33	3.99	4.17	4.02	4.35	4.12	3.98	4.05	4.15	4.43	4.27	4.12	4.28	4.29	4.17	4.05	4.03	4.16	4.08	4.14	4.22	4.41	4.33	<b>4.18</b>	<b>0.14</b>			
<b>Cl</b>	0.36	0.32	0.34	0.25	0.26	0.21	0.28	0.34	0.53	0.20	0.30	0.33	0.28	0.29	0.24	0.24	0.19	0.25	0.18	0.28	0.37	0.39	0.29	<b>0.29</b>	<b>0.08</b>			
<b>Water</b>	5.96	4.09	6.05	5.02	5.59	6.47	4.14	4.17	5.52	6.38	5.47	5.87	4.52	6.96	4.73	5.83	6.98	5.21	6.07	4.93	5.23	5.06	4.13	<b>5.41</b>	<b>0.88</b>			
<b>n</b>																												<b>23</b>

## WS1 (K15c)

(normalised)

	01	02	03	04	05	06	07	08	09	10	11	12	13	14	15	16	17	18	19	20	21	22	24	mean	stdev
<b>SiO<sub>2</sub></b>	78.05	77.67	77.73	77.14	77.61	77.65	77.55	77.45	78.49	78.11	76.69	77.07	76.84	77.70	77.65	77.94	78.03	77.19	77.32	78.06	78.02	77.49	76.38	<b>77.56</b>	<b>0.50</b>
<b>Al<sub>2</sub>O<sub>3</sub></b>	13.03	13.05	12.47	12.56	12.52	12.73	12.68	12.58	12.47	12.74	12.77	12.67	12.77	12.43	12.58	12.90	12.16	12.39	12.60	12.73	12.72	12.83	12.55	<b>12.65</b>	<b>0.21</b>
<b>TiO<sub>2</sub></b>	0.20	0.12	0.23	0.27	0.20	0.19	0.23	0.15	0.18	0.20	0.26	0.28	0.29	0.13	0.27	0.15	0.25	0.54	0.05	0.01	0.03	0.19	0.30	<b>0.21</b>	<b>0.11</b>
<b>FeO</b>	0.97	0.63	0.98	1.38	1.18	1.22	1.02	1.20	0.82	1.02	1.19	1.34	1.14	1.48	1.02	0.99	0.92	1.00	0.70	0.76	0.69	1.01	1.27	<b>1.04</b>	<b>0.23</b>
<b>MnO</b>	0.05	0.19	0.18	0.22	0.00	0.16	0.08	0.09	0.08	0.12	0.28	0.22	0.16	0.02	0.07	0.15	0.20	0.02	0.29	0.11	0.09	0.38	0.14	<b>0.14</b>	<b>0.09</b>
<b>MgO</b>	0.15	0.07	0.15	0.14	0.12	0.11	0.13	0.15	0.17	0.13	0.11	0.16	0.15	0.21	0.10	0.06	0.23	0.22	0.14	0.16	0.25	0.19	0.14	<b>0.15</b>	<b>0.05</b>
<b>CaO</b>	0.82	0.70	0.80	0.83	0.76	0.73	0.84	0.77	0.75	0.84	0.81	0.81	0.78	0.73	0.71	0.79	0.81	0.77	0.49	0.61	0.47	0.82	0.73	<b>0.75</b>	<b>0.10</b>
<b>Na<sub>2</sub>O</b>	2.15	2.74	2.84	2.80	3.00	2.74	3.12	3.22	2.55	2.32	3.31	2.87	3.18	3.02	3.13	2.53	2.91	3.38	3.53	2.78	2.75	2.87	3.75	<b>2.93</b>	<b>0.37</b>
<b>K<sub>2</sub>O</b>	4.56	4.84	4.62	4.66	4.61	4.46	4.37	4.39	4.49	4.55	4.57	4.58	4.67	4.29	4.47	4.48	4.52	4.50	4.89	4.79	4.96	4.23	4.73	<b>4.57</b>	<b>0.18</b>
<b>Water</b>	6.55	5.21	4.89	5.28	5.80	6.53	5.62	6.02	5.78	5.90	4.03	4.44	3.02	4.17	4.64	5.85	4.41	5.31	5.85	4.78	5.24	4.63	4.29	<b>5.14</b>	<b>0.87</b>
<i>n</i>																									<b>24</b>

## WS2 (K15a)

(normalised)

	01	02	03	04	05	06	07	08	09	10	11	12	13	14	15	16	17	18	19	20	21	mean	stdev		
<b>SiO<sub>2</sub></b>	77.71	77.82	77.81	77.39	76.92	77.14	77.71	78.11	77.97	78.47	78.34	77.11	76.92	78.11	77.18	77.20	77.36	77.54	78.51	78.24	78.63	<b>77.72</b>	<b>0.54</b>		
<b>Al<sub>2</sub>O<sub>3</sub></b>	12.84	12.76	12.84	13.12	12.85	12.60	12.76	12.78	12.33	12.18	12.21	12.77	12.93	12.37	12.35	12.64	12.56	12.79	12.55	12.34	12.10	<b>12.60</b>	<b>0.28</b>		
<b>TiO<sub>2</sub></b>	0.21	0.14	0.14	0.14	0.01	0.15	0.14	0.14	0.16	0.17	0.06	0.13	0.13	0.18	0.17	0.25	0.17	0.10	0.37	0.07	0.22	<b>0.15</b>	<b>0.07</b>		
<b>FeO</b>	1.29	1.13	0.94	0.94	1.05	0.90	0.99	0.80	1.20	0.98	1.02	1.10	1.02	0.98	1.54	0.99	1.15	0.86	0.90	1.12	1.09	<b>1.05</b>	<b>0.16</b>		
<b>MnO</b>	0.07	0.14	0.07	0.00	0.22	0.16	0.16	0.17	0.43	0.09	0.05	0.18	0.21	0.13	0.20	0.14	0.16	0.28	0.03	0.26	0.23	<b>0.16</b>	<b>0.10</b>		
<b>MgO</b>	0.20	0.22	0.13	0.10	0.10	0.09	0.04	0.16	0.18	0.18	0.10	0.25	0.15	0.10	0.14	0.13	0.16	0.09	0.09	0.07	0.19	<b>0.14</b>	<b>0.05</b>		
<b>CaO</b>	1.14	1.14	0.68	0.79	0.70	0.61	0.53	0.88	1.08	0.96	0.97	0.85	1.00	1.03	0.99	0.84	0.86	0.97	0.57	0.76	0.96	<b>0.87</b>	<b>0.18</b>		
<b>Na<sub>2</sub>O</b>	2.42	2.62	2.63	3.29	3.62	3.65	3.21	2.61	3.06	3.13	3.32	3.27	3.24	3.08	3.09	3.18	3.15	3.02	2.84	3.13	3.01	<b>3.07</b>	<b>0.31</b>		
<b>K<sub>2</sub>O</b>	3.83	3.79	4.56	3.98	4.33	4.48	4.27	4.08	3.41	3.57	3.70	4.09	4.15	3.75	4.11	4.26	4.31	4.04	3.99	3.77	3.42	<b>4.00</b>	<b>0.32</b>		
<b>Cl</b>	0.29	0.23	0.19	0.25	0.20	0.24	0.19	0.28	0.18	0.26	0.24	0.24	0.26	0.26	0.24	0.38	0.13	0.31	0.14	0.23	0.18	<b>0.23</b>	<b>0.06</b>		
<b>Water</b>	5.74	5.55	6.20	7.37	7.21	6.04	5.47	6.44	3.66	6.49	6.93	5.82	6.44	5.91	5.73	5.66	6.91	7.03	4.97	4.17	3.98	<b>5.89</b>	<b>1.03</b>		
<i>n</i>																									<b>21</b>

## WS3 (K13a)

(normalised)

	01	02	03	04	05	06	07	08	09	10	11	12	13	14	15	16	17	18	19	20	21	mean	stdev
<b>SiO<sub>2</sub></b>	77.70	77.79	77.10	77.70	78.13	77.54	77.40	77.84	77.37	77.64	78.50	77.51	77.83	77.79	77.37	78.37	77.86	77.83	77.12	77.92	77.51	<b>77.71</b>	<b>0.36</b>
<b>Al<sub>2</sub>O<sub>3</sub></b>	12.71	12.37	12.44	12.32	12.69	12.58	12.56	12.42	12.79	12.72	11.91	12.59	12.59	12.55	12.44	12.31	12.54	12.25	12.68	12.66	12.57	<b>12.51</b>	<b>0.20</b>
<b>TiO<sub>2</sub></b>	0.10	0.09	0.08	0.10	0.06	0.15	0.21	0.10	0.13	0.14	0.12	0.02	0.04	0.14	0.14	0.13	0.17	0.16	0.16	0.13	0.12	<b>0.12</b>	<b>0.04</b>
<b>FeO</b>	0.85	1.02	1.13	0.92	0.69	0.84	1.04	0.87	1.02	0.97	0.98	1.09	0.93	0.77	1.25	0.80	0.80	1.12	1.10	0.86	1.06	<b>0.96</b>	<b>0.14</b>
<b>MnO</b>	0.00	0.17	0.51	0.00	0.00	0.00	0.04	0.10	0.10	0.10	0.00	0.11	0.04	0.14	0.15	0.08	0.21	0.00	0.37	0.04	0.00	<b>0.10</b>	<b>0.13</b>
<b>MgO</b>	0.01	0.08	0.12	0.09	0.04	0.21	0.13	0.05	0.06	0.04	0.06	0.04	0.11	0.05	0.13	0.12	0.01	0.15	0.11	0.09	0.11	<b>0.08</b>	<b>0.04</b>
<b>CaO</b>	0.54	0.76	0.72	0.48	0.54	0.85	0.69	0.60	0.64	0.62	0.70	0.55	0.55	0.43	0.68	0.82	0.87	0.71	0.66	0.53	0.65	<b>0.65</b>	<b>0.12</b>
<b>Na<sub>2</sub>O</b>	2.89	3.11	3.08	3.38	3.00	2.94	2.99	3.45	3.34	3.12	3.00	3.19	3.38	3.30	3.34	3.18	3.24	3.25	3.22	3.36	3.29	<b>3.19</b>	<b>0.16</b>
<b>K<sub>2</sub>O</b>	4.99	4.27	4.56	4.84	4.61	4.54	4.71	4.28	4.16	4.41	4.51	4.69	4.43	4.68	4.28	3.92	4.05	4.25	4.36	4.26	4.51	<b>4.44</b>	<b>0.26</b>
<b>Cl</b>	0.21	0.33	0.26	0.17	0.24	0.36	0.24	0.32	0.39	0.23	0.21	0.20	0.11	0.16	0.25	0.28	0.25	0.27	0.23	0.16	0.18	<b>0.24</b>	<b>0.07</b>
<b>Water</b>	6.70	5.19	5.29	6.76	5.99	5.52	5.50	6.41	5.36	5.42	6.09	6.44	6.68	5.97	6.16	7.26	6.14	6.27	5.11	6.71	6.03	<b>6.05</b>	<b>0.60</b>
<i>n</i>																						<b>21</b>	

## K3

(normalised)

	01	02	03	04	05	06	07	08	10	11	12	13	14	15	16	mean	stdev
<b>SiO<sub>2</sub></b>	77.67	78.30	78.04	77.65	77.58	77.60	77.99	77.43	79.77	78.20	78.26	77.34	77.33	77.36	77.24	<b>77.85</b>	<b>0.64</b>
<b>Al<sub>2</sub>O<sub>3</sub></b>	13.08	12.87	13.14	12.98	13.01	13.26	13.17	13.08	11.59	12.88	13.08	13.15	12.70	12.84	13.19	<b>12.93</b>	<b>0.40</b>
<b>TiO<sub>2</sub></b>	0.04	0.05	0.09	0.13	0.19	0.19	0.12	0.23	0.14	0.15	0.16	0.13	0.17	0.15	0.12	<b>0.14</b>	<b>0.05</b>
<b>FeO</b>	0.96	0.96	0.94	1.08	1.07	1.25	0.98	1.26	1.16	1.35	1.29	1.17	1.43	1.37	1.32	<b>1.17</b>	<b>0.17</b>
<b>MnO</b>	0.13	0.15	0.20	0.14	0.14	0.13	0.20	0.00	0.16	0.19	0.09	0.12	0.30	0.20	0.16	<b>0.15</b>	<b>0.07</b>
<b>MgO</b>	0.10	0.15	0.13	0.17	0.15	0.15	0.16	0.21	0.20	0.10	0.12	0.08	0.17	0.20	0.14	<b>0.15</b>	<b>0.04</b>
<b>CaO</b>	0.84	0.79	1.00	1.03	1.10	1.13	0.99	1.05	0.93	1.07	1.01	1.23	1.08	1.11	1.41	<b>1.05</b>	<b>0.15</b>
<b>Na<sub>2</sub>O</b>	3.00	2.65	2.70	3.09	3.12	2.55	2.73	2.96	2.75	2.51	2.82	3.09	3.23	3.14	2.57	<b>2.86</b>	<b>0.24</b>
<b>K<sub>2</sub>O</b>	4.18	4.08	3.77	3.70	3.97	3.76	3.66	3.80	4.05	3.78	3.58	3.75	3.59	3.62	3.58	<b>3.79</b>	<b>0.19</b>
<b>Cl</b>	0.00	0.00	0.00	0.00	0.00	0.00	0.00	0.00	0.00	0.00	0.00	0.00	0.00	0.00	0.27	<b>0.27</b>	<b>0.07</b>
<b>Water</b>	6.45	6.85	6.15	6.87	7.64	6.12	6.28	7.33	5.01	5.81	6.64	6.83	6.28	6.79	5.10	<b>6.41</b>	<b>0.73</b>
<i>n</i>																<b>15</b>	

## PCM3 (IG)

(normalised)

	01	02	02	03	04	05	06	07	08	09	10	11	12	13	14	15	16	17	18	19	20	21	22	23	mean	stdev
<b>SiO<sub>2</sub></b>	77.56	77.59	77.82	77.78	77.83	77.98	78.13	78.08	77.60	77.43	77.78	77.91	77.87	77.61	77.16	77.02	77.02	77.52	77.65	77.19	77.28	77.45	78.03	78.38	<b>77.65</b>	<b>0.36</b>
<b>Al<sub>2</sub>O<sub>3</sub></b>	12.89	12.72	12.56	12.62	12.92	12.76	12.62	12.54	12.60	12.72	12.55	12.51	12.71	12.98	12.98	12.72	12.76	12.65	12.36	12.49	12.60	12.67	12.67	12.45	<b>12.67</b>	<b>0.16</b>
<b>TiO<sub>2</sub></b>	0.18	0.19	0.21	0.18	0.22	0.26	0.20	0.10	0.10	0.15	0.17	0.12	0.11	0.14	0.08	0.08	0.14	0.15	0.18	0.21	0.21	0.13	0.23	0.22	<b>0.16</b>	<b>0.05</b>
<b>FeO</b>	1.07	1.02	1.10	1.14	1.06	0.98	0.89	0.95	1.07	1.20	1.25	1.12	0.99	0.94	0.99	0.97	0.96	1.00	1.26	1.26	1.07	1.01	0.88	1.01	<b>1.05</b>	<b>0.11</b>
<b>MnO</b>	0.19	0.33	0.28	0.16	0.05	0.05	0.08	0.12	0.20	0.13	0.07	0.10	0.07	0.04	0.11	0.19	0.19	0.17	0.16	0.17	0.15	0.22	0.15	0.15	<b>0.15</b>	<b>0.07</b>
<b>MgO</b>	0.15	0.14	0.12	0.13	0.15	0.12	0.10	0.11	0.11	0.10	0.12	0.14	0.14	0.11	0.10	0.09	0.12	0.12	0.12	0.13	0.14	0.12	0.09	0.08	<b>0.12</b>	<b>0.02</b>
<b>CaO</b>	0.82	0.91	0.81	0.78	0.79	0.68	0.73	0.69	0.64	0.84	0.96	0.85	0.73	0.73	0.74	0.65	0.81	1.02	1.01	0.91	0.85	0.91	0.77	0.67	<b>0.80</b>	<b>0.11</b>
<b>Na<sub>2</sub>O</b>	3.02	3.02	3.02	3.05	2.78	2.93	3.02	3.07	3.22	3.17	3.24	3.23	2.83	2.96	3.46	3.64	3.44	3.16	3.08	3.13	3.16	3.09	2.93	2.99	<b>3.11</b>	<b>0.20</b>
<b>K<sub>2</sub>O</b>	4.12	4.09	4.09	4.15	4.20	4.23	4.25	4.34	4.45	4.13	3.68	3.76	4.28	4.28	4.16	4.41	4.31	3.95	3.93	4.18	4.28	4.18	4.02	3.88	<b>4.14</b>	<b>0.20</b>
<b>Cl</b>	0.00	0.00	0.00	0.00	0.00	0.00	0.00	0.00	0.00	0.12	0.19	0.24	0.27	0.22	0.23	0.22	0.25	0.26	0.25	0.31	0.26	0.22	0.22	0.18	<b>0.23</b>	<b>0.12</b>
<b>Water</b>	6.00	5.72	5.85	5.64	5.26	5.83	5.80	6.15	6.73	5.66	4.51	3.85	4.84	6.79	7.30	6.62	6.23	6.18	5.83	5.70	6.29	6.97	6.00	4.57	<b>5.84</b>	<b>0.83</b>
<b>n</b>																										<b>23</b>

## PCM2 (K14bii)

(normalised)

	01	02	03	04	05	06	07	08	09	10	11	12	13	14	15	mean	stdev
<b>SiO<sub>2</sub></b>	77.47	77.68	77.69	77.39	76.94	77.33	77.50	77.40	77.67	77.56	77.06	78.13	77.42	77.25	77.04	<b>77.44</b>	<b>0.30</b>
<b>Al<sub>2</sub>O<sub>3</sub></b>	12.92	12.59	12.38	12.53	12.72	12.41	12.33	12.64	12.31	12.48	12.29	12.16	12.66	12.34	12.48	<b>12.48</b>	<b>0.20</b>
<b>TiO<sub>2</sub></b>	0.06	0.07	0.11	0.19	0.20	0.20	0.19	0.07	0.23	0.20	0.11	0.16	0.16	0.19	0.16	<b>0.15</b>	<b>0.05</b>
<b>FeO</b>	0.90	0.71	0.78	0.77	0.99	0.77	1.00	0.65	0.82	0.93	1.29	0.92	0.81	1.06	1.03	<b>0.90</b>	<b>0.16</b>
<b>MnO</b>	0.11	0.22	0.18	0.05	0.25	0.39	0.37	0.00	0.03	0.20	0.07	0.43	0.12	0.19	0.07	<b>0.18</b>	<b>0.13</b>
<b>MgO</b>	0.06	0.11	0.13	0.08	0.14	0.09	0.09	0.07	0.13	0.09	0.27	0.05	0.04	0.12	0.12	<b>0.11</b>	<b>0.05</b>
<b>CaO</b>	0.66	0.60	0.57	0.75	0.86	0.73	0.63	0.78	0.86	0.82	0.83	0.72	0.83	0.68	0.63	<b>0.73</b>	<b>0.10</b>
<b>Na<sub>2</sub>O</b>	3.38	3.73	3.72	3.72	3.63	3.68	3.59	3.96	3.64	3.59	3.76	3.50	3.81	3.49	3.88	<b>3.67</b>	<b>0.15</b>
<b>K<sub>2</sub>O</b>	4.22	4.10	4.30	4.38	4.11	4.12	4.09	4.23	4.01	3.88	4.05	3.68	3.98	4.39	4.36	<b>4.13</b>	<b>0.20</b>
<b>Cl</b>	0.21	0.17	0.15	0.16	0.16	0.28	0.21	0.20	0.30	0.24	0.25	0.24	0.18	0.28	0.22	<b>0.22</b>	<b>0.05</b>
<b>Water</b>	5.79	5.47	5.39	5.10	5.36	4.63	4.79	5.23	4.30	5.00	3.82	4.39	6.05	5.09	5.83	<b>5.08</b>	<b>0.62</b>
<b>n</b>																<b>15</b>	

## PCM1 (IG; K14bi)

(normalised)

	01	02	03	04	05	06	07	mean	stdev
<b>SiO<sub>2</sub></b>	76.31	77.79	77.21	77.06	77.13	76.90	77.16	<b>77.08</b>	<b>0.44</b>
<b>Al<sub>2</sub>O<sub>3</sub></b>	12.56	12.11	12.47	12.35	12.73	12.51	12.39	<b>12.44</b>	<b>0.19</b>
<b>TiO<sub>2</sub></b>	0.16	0.15	0.17	0.15	0.13	0.13	0.17	<b>0.15</b>	<b>0.02</b>
<b>FeO</b>	1.59	1.12	1.33	1.42	1.40	1.29	1.26	<b>1.35</b>	<b>0.15</b>
<b>MnO</b>	0.13	0.18	0.20	0.05	0.15	0.24	0.06	<b>0.14</b>	<b>0.07</b>
<b>MgO</b>	0.13	0.10	0.15	0.14	0.16	0.11	0.12	<b>0.13</b>	<b>0.02</b>
<b>CaO</b>	0.76	0.80	0.82	0.88	0.75	0.77	0.75	<b>0.79</b>	<b>0.05</b>
<b>Na<sub>2</sub>O</b>	3.86	3.60	3.55	3.72	3.60	3.65	3.49	<b>3.64</b>	<b>0.12</b>
<b>K<sub>2</sub>O</b>	4.21	3.97	3.84	3.93	3.68	4.10	4.27	<b>4.00</b>	<b>0.21</b>
<b>Cl</b>	0.29	0.18	0.26	0.30	0.27	0.30	0.34	<b>0.28</b>	<b>0.05</b>
<b>Water</b>	5.30	6.21	5.27	4.79	6.10	5.74	5.07	<b>5.50</b>	<b>0.53</b>
<b>n</b>									<b>7</b>



## TTM4

(normalised)

	01	02	03	04	05	06	07	08	09	10	11	12	13	14	15	16	mean	stdev
<b>SiO<sub>2</sub></b>	77.43	77.12	77.67	76.83	77.12	77.47	77.41	77.70	76.73	76.92	77.58	77.13	77.22	77.12	76.48	77.01	<b>77.18</b>	<b>0.35</b>
<b>Al<sub>2</sub>O<sub>3</sub></b>	12.53	12.50	12.96	12.26	12.49	12.53	12.94	12.69	12.52	12.63	12.60	12.79	12.41	12.53	12.42	12.58	<b>12.58</b>	<b>0.19</b>
<b>TiO<sub>2</sub></b>	0.21	0.27	0.08	0.23	0.18	0.23	0.04	0.08	0.31	0.31	0.13	0.24	0.27	0.29	0.21	0.22	<b>0.21</b>	<b>0.08</b>
<b>FeO</b>	0.96	1.10	0.97	1.45	0.91	1.15	0.75	0.87	1.18	1.28	0.84	0.96	1.11	1.03	1.48	1.14	<b>1.07</b>	<b>0.21</b>
<b>MnO</b>	0.11	0.25	0.09	0.10	0.08	0.03	0.08	0.35	0.21	0.18	0.04	0.26	0.01	0.00	0.24	0.02	<b>0.13</b>	<b>0.11</b>
<b>MgO</b>	0.05	0.19	0.05	0.15	0.14	0.16	0.05	0.00	0.19	0.12	0.14	0.13	0.10	0.13	0.21	0.22	<b>0.13</b>	<b>0.06</b>
<b>CaO</b>	0.70	0.84	0.58	0.76	0.84	0.78	0.53	0.49	0.80	0.81	0.81	0.85	0.76	0.76	0.85	0.86	<b>0.75</b>	<b>0.12</b>
<b>Na<sub>2</sub>O</b>	2.98	3.46	2.79	3.66	3.30	2.69	3.10	2.85	3.38	2.89	2.98	2.75	3.16	3.39	3.27	3.17	<b>3.11</b>	<b>0.28</b>
<b>K<sub>2</sub>O</b>	4.86	4.39	4.73	4.34	4.65	4.72	4.92	4.71	4.52	4.52	4.63	4.55	4.74	4.45	4.38	4.50	<b>4.60</b>	<b>0.17</b>
<b>Cl</b>	0.17	0.34	0.08	0.21	0.30	0.23	0.17	0.23	0.16	0.33	0.24	0.34	0.21	0.21	0.25	0.16	<b>0.23</b>	<b>0.07</b>
<b>Water</b>	5.24	4.79	4.54	0.99	2.64	4.44	5.27	4.67	4.32	3.69	4.50	4.04	4.24	4.76	3.19	3.37	<b>4.04</b>	<b>1.09</b>
<i>n</i>																	<b>16</b>	

## TTM3

(normalised)

	01	02	03	04	05	06	07	08	09	10	11	12	13	14	15	16	17	18	mean	stdev
<b>SiO<sub>2</sub></b>	77.67	77.83	77.29	77.87	77.77	77.78	78.22	77.87	78.09	78.16	78.01	78.81	78.17	77.20	77.65	78.27	77.89	77.93	<b>77.92</b>	<b>0.36</b>
<b>Al<sub>2</sub>O<sub>3</sub></b>	12.89	13.12	12.65	12.79	12.32	12.92	12.83	12.92	12.60	12.64	12.44	12.67	12.56	12.76	12.68	12.55	12.42	12.59	<b>12.69</b>	<b>0.20</b>
<b>TiO<sub>2</sub></b>	0.23	0.21	0.14	0.23	0.18	0.18	0.08	0.26	0.26	0.14	0.05	0.13	0.14	0.14	0.17	0.17	0.17	0.07	<b>0.16</b>	<b>0.06</b>
<b>FeO</b>	1.18	1.08	1.06	0.97	1.24	1.05	0.90	1.06	0.91	0.87	1.03	0.95	0.91	1.11	1.29	0.91	1.20	1.05	<b>1.04</b>	<b>0.13</b>
<b>MnO</b>	0.00	0.02	0.36	0.30	0.26	0.06	0.00	0.04	0.06	0.10	0.14	0.16	0.31	0.26	0.00	0.17	0.14	0.07	<b>0.14</b>	<b>0.12</b>
<b>MgO</b>	0.31	0.16	0.15	0.13	0.11	0.16	0.20	0.14	0.11	0.10	0.13	0.04	0.08	0.10	0.11	0.07	0.13	0.16	<b>0.13</b>	<b>0.06</b>
<b>CaO</b>	0.75	0.78	0.86	0.96	0.66	0.90	0.79	0.69	0.67	0.78	0.60	0.65	0.65	0.67	1.00	1.11	0.93	0.78	<b>0.79</b>	<b>0.14</b>
<b>Na<sub>2</sub>O</b>	2.73	2.65	3.38	2.66	3.38	2.72	2.64	2.84	3.02	3.02	3.12	2.63	2.82	3.33	3.02	3.02	3.45	3.01	<b>2.97</b>	<b>0.28</b>
<b>K<sub>2</sub>O</b>	4.26	4.15	4.09	4.09	4.09	4.21	4.32	4.18	4.29	4.21	4.48	3.96	4.35	4.43	3.83	3.53	3.53	4.00	<b>4.11</b>	<b>0.27</b>
<b>Cl</b>	0.00	0.00	0.00	0.00	0.00	0.00	0.00	0.00	0.00	0.00	0.00	0.00	0.00	0.00	0.24	0.18	0.15	0.34	<b>0.23</b>	<b>0.09</b>
<b>Water</b>	6.80	6.11	5.88	5.53	6.17	5.09	5.64	5.41	6.25	5.36	6.93	6.06	5.76	6.52	4.79	4.65	4.21	3.48	<b>4.28</b>	<b>0.90</b>
<i>n</i>																			<b>18</b>	

## TTM2

(normalised)

	01	02	03	04	05	06	07	08	09	10	11	mean	stdev
<b>SiO<sub>2</sub></b>	77.63	77.71	77.66	78.08	77.79	77.78	78.05	77.26	77.29	78.04	77.53	<b>77.71</b>	<b>0.28</b>
<b>Al<sub>2</sub>O<sub>3</sub></b>	12.56	12.64	12.59	12.62	12.55	12.47	12.66	12.83	12.74	12.73	13.59	<b>12.73</b>	<b>0.30</b>
<b>TiO<sub>2</sub></b>	0.22	0.13	0.22	0.12	0.11	0.08	0.09	0.21	0.27	0.11	0.23	<b>0.16</b>	<b>0.07</b>
<b>FeO</b>	0.96	0.77	1.05	0.95	1.04	1.28	0.96	1.09	1.32	0.90	1.06	<b>1.04</b>	<b>0.16</b>
<b>MnO</b>	0.18	0.13	0.05	0.16	0.10	0.12	0.00	0.07	0.00	0.21	0.13	<b>0.10</b>	<b>0.07</b>
<b>MgO</b>	0.17	0.19	0.10	0.11	0.13	0.08	0.02	0.12	0.12	0.13	0.15	<b>0.12</b>	<b>0.05</b>
<b>CaO</b>	0.66	0.59	0.67	0.66	0.73	0.84	0.70	0.90	0.75	0.76	0.72	<b>0.73</b>	<b>0.09</b>
<b>Na<sub>2</sub>O</b>	3.92	3.80	3.86	3.10	3.66	3.59	3.64	3.79	3.49	2.92	2.26	<b>3.46</b>	<b>0.50</b>
<b>K<sub>2</sub>O</b>	3.70	4.05	3.80	4.21	3.90	3.75	3.88	3.75	4.01	4.20	4.02	<b>3.93</b>	<b>0.18</b>
<b>Cl</b>	0.00	0.00	0.00	0.00	0.00	0.00	0.00	0.00	0.00	0.00	0.31	<b>0.31</b>	<b>0.00</b>
<b>Water</b>	7.62	6.84	5.78	6.33	6.04	5.79	7.38	7.89	8.31	7.80	6.75	<b>6.75</b>	<b>0.90</b>
<i>n</i>												<b>11</b>	

## TIRITIRI IGNIMBRITE

(normalised)

	01	02	03	04	05	06	07	mean	stdev
<b>SiO<sub>2</sub></b>	78.15	77.62	78.02	77.56	78.22	78.25	77.92	<b>77.96</b>	<b>0.28</b>
<b>Al<sub>2</sub>O<sub>3</sub></b>	12.42	12.46	12.35	12.51	12.28	12.22	12.46	<b>12.39</b>	<b>0.11</b>
<b>TiO<sub>2</sub></b>	0.09	0.14	0.10	0.11	0.08	0.16	0.03	<b>0.10</b>	<b>0.04</b>
<b>FeO</b>	1.08	1.10	1.24	1.28	1.18	1.13	1.19	<b>1.17</b>	<b>0.07</b>
<b>MnO</b>	0.10	0.08	0.09	0.05	0.07	0.09	0.07	<b>0.08</b>	<b>0.02</b>
<b>MgO</b>	0.06	0.10	0.08	0.09	0.08	0.04	0.07	<b>0.08</b>	<b>0.02</b>
<b>CaO</b>	0.75	0.91	0.85	0.80	0.79	0.60	0.68	<b>0.77</b>	<b>0.10</b>
<b>Na<sub>2</sub>O</b>	3.38	3.71	3.53	3.50	3.45	3.61	3.58	<b>3.54</b>	<b>0.11</b>
<b>K<sub>2</sub>O</b>	3.74	3.70	3.54	3.91	3.64	3.66	3.77	<b>3.71</b>	<b>0.12</b>
<b>Cl</b>	0.23	0.18	0.20	0.19	0.21	0.24	0.20	<b>0.21</b>	<b>0.02</b>
<b>Water</b>	4.82	5.51	5.93	4.75	5.05	4.56	5.87	<b>5.21</b>	<b>0.56</b>
<i>n</i>								<b>7</b>	

## TTM1 (IG)

(normalised)

	01	02	03	04	05	06	07	08	09	10	11	12	13	14	mean	stdev
<b>SiO<sub>2</sub></b>	78.27	76.95	77.22	77.14	76.89	76.64	77.75	79.57	77.74	77.14	77.00	76.39	77.88	76.86	<b>77.39</b>	<b>0.81</b>
<b>Al<sub>2</sub>O<sub>3</sub></b>	12.73	12.64	12.79	12.64	12.99	13.26	12.69	12.82	12.67	12.95	12.50	13.21	12.55	13.55	<b>12.86</b>	<b>0.30</b>
<b>TiO<sub>2</sub></b>	0.13	0.15	0.09	0.14	0.25	0.06	0.10	0.16	0.20	0.24	0.12	0.10	0.16	0.04	<b>0.14</b>	<b>0.06</b>
<b>FeO</b>	0.53	0.97	0.92	0.94	0.79	1.32	0.67	0.72	0.49	0.50	0.66	0.69	0.88	0.25	<b>0.74</b>	<b>0.26</b>
<b>MnO</b>	0.00	0.41	0.03	0.08	0.08	0.20	0.16	0.00	0.19	0.25	0.32	0.20	0.07	0.11	<b>0.15</b>	<b>0.12</b>
<b>MgO</b>	0.16	0.06	0.16	0.17	0.10	0.10	0.00	0.15	0.06	0.08	0.07	0.14	0.08	0.09	<b>0.10</b>	<b>0.05</b>
<b>CaO</b>	0.58	0.68	0.61	0.71	0.68	0.55	0.53	0.52	0.51	0.77	0.51	0.55	0.70	0.61	<b>0.61</b>	<b>0.09</b>
<b>Na<sub>2</sub>O</b>	3.31	3.68	3.77	3.87	3.72	3.42	3.73	1.90	3.61	3.84	3.93	4.07	3.61	3.70	<b>3.58</b>	<b>0.52</b>
<b>K<sub>2</sub>O</b>	3.94	4.30	4.21	4.09	4.31	4.20	4.11	3.85	4.35	4.08	4.77	4.37	3.81	4.72	<b>4.22</b>	<b>0.28</b>
<b>Cl</b>	0.36	0.17	0.21	0.23	0.19	0.23	0.26	0.30	0.17	0.15	0.13	0.29	0.25	0.07	<b>0.21</b>	<b>0.08</b>
<b>Water</b>	5.34	6.18	6.16	6.98	6.82	6.06	5.94	7.39	5.61	5.40	5.19	5.66	4.76	4.79	<b>5.88</b>	<b>0.79</b>
<i>n</i>															<b>14</b>	

**APPENDIX E:  
MAJOR ELEMENT COMPOSITION  
(POSSIBLE CORRELATIVES)**

**KAUKATEA**

P.A.R. Shane (pers. comm., 1999)

wt.%	1	2	3	4	5	6	7	8	9	10	mean	stdev
SiO <sub>2</sub>	76.90	76.49	76.43	76.89	76.57	76.51	76.55	76.95	76.96	76.61	<b>76.69</b>	<b>0.21</b>
Al <sub>2</sub> O <sub>3</sub>	12.61	12.66	12.61	12.46	12.70	12.55	12.66	12.57	12.60	12.62	<b>12.60</b>	<b>0.07</b>
TiO <sub>2</sub>	0.07	0.22	0.16	0.15	0.16	0.18	0.17	0.13	0.11	0.14	<b>0.15</b>	<b>0.04</b>
FeO	1.48	1.49	1.62	1.38	1.62	1.62	1.54	1.53	1.38	1.60	<b>1.53</b>	<b>0.09</b>
MgO	0.13	0.15	0.10	0.19	0.12	0.08	0.14	0.13	0.07	0.18	<b>0.13</b>	<b>0.04</b>
CaO	1.02	0.97	0.94	1.16	0.96	1.02	0.96	1.04	0.97	0.98	<b>1.00</b>	<b>0.06</b>
Na <sub>2</sub> O	4.24	4.12	4.07	3.65	4.13	4.05	4.26	3.87	4.10	4.31	<b>4.08</b>	<b>0.20</b>
K <sub>2</sub> O	3.40	3.71	3.83	3.92	3.59	3.83	3.54	3.77	3.61	3.39	<b>3.66</b>	<b>0.18</b>
Cl	0.16	0.18	0.23	0.18	0.16	0.16	0.18	0.15	0.19	0.16	<b>0.18</b>	<b>0.02</b>
Water	6.47	5.44	5.72	7.18	5.49	5.70	5.24	6.51	6.10	6.37	<b>6.02</b>	<b>0.61</b>
<i>n</i>											<b>10</b>	

**KIDNAPPERS 'B'**

P.A.R. Shane (pers. comm., 1999)

wt.%	1	2	3	4	5	6	7	8	9	10	mean	stdev
SiO <sub>2</sub>	76.39	76.40	75.82	76.20	75.85	76.26	76.27	76.21	76.25	76.71	<b>76.24</b>	<b>0.26</b>
Al <sub>2</sub> O <sub>3</sub>	12.81	12.70	12.98	12.89	13.00	12.82	12.75	12.94	12.82	12.64	<b>12.84</b>	<b>0.12</b>
TiO <sub>2</sub>	0.15	0.17	0.18	0.17	0.22	0.16	0.22	0.15	0.15	0.17	<b>0.17</b>	<b>0.03</b>
FeO	1.65	1.50	1.60	1.54	1.63	1.57	1.60	1.44	1.53	1.45	<b>1.55</b>	<b>0.07</b>
MgO	0.08	0.13	0.17	0.13	0.11	0.16	0.15	0.12	0.13	0.13	<b>0.13</b>	<b>0.03</b>
CaO	1.03	1.03	1.05	1.07	1.09	1.10	1.10	1.11	1.12	1.09	<b>1.08</b>	<b>0.03</b>
Na <sub>2</sub> O	4.21	4.22	4.41	4.08	4.32	4.07	4.08	4.22	4.40	4.17	<b>4.22</b>	<b>0.13</b>
K <sub>2</sub> O	3.51	3.72	3.61	3.75	3.63	3.69	3.68	3.67	3.43	3.51	<b>3.62</b>	<b>0.10</b>
Cl	0.16	0.13	0.18	0.17	0.16	0.16	0.16	0.14	0.17	0.13	<b>0.16</b>	<b>0.02</b>
Water	8.84	6.71	9.54	9.91	8.00	5.71	7.04	7.41	6.14	5.48	<b>7.48</b>	<b>1.56</b>
<i>n</i>											<b>10</b>	

Black (1992)

Shane et al. (1996b)

wt.%	Kid 'C'		Kid 'D'		Kid 'E'		Kid 'F'	
SiO <sub>2</sub>	77.98	(0.18)	77.73	(0.37)	77.63	(0.38)	78.02	(0.46)
Al <sub>2</sub> O <sub>3</sub>	12.18	(0.12)	12.15	(0.18)	11.97	(0.12)	12.20	(0.27)
TiO <sub>2</sub>	0.13	(0.02)	0.15	(0.03)	0.21	(0.04)	0.15	(0.04)
FeO	0.89	(0.07)	1.04	(0.07)	1.39	(0.10)	1.25	(0.15)
MgO	0.11	(0.02)	0.14	(0.03)	0.13	(0.03)	0.11	(0.02)
CaO	0.82	(0.07)	0.99	(0.07)	0.91	(0.04)	0.78	(0.06)
Na <sub>2</sub> O	3.49	(0.13)	3.69	(0.13)	3.85	(0.11)	3.88	(0.19)
K <sub>2</sub> O	4.25	(0.27)	3.87	(0.18)	3.78	(0.17)	3.45	(0.18)
Cl	0.16	(0.03)	0.23	(0.04)	0.24	(0.01)	0.16	(0.02)
Water	6.06	(1.27)	6.66	(1.71)	6.54	(1.12)	5.96	(1.17)
<i>n</i>	<b>11</b>		<b>25</b>		<b>11</b>		<b>10</b>	

**ONGATITI IGNIMBRITE**

Briggs et al. (1993) Normalised

wt.%	1	2	3	4	5	6	7	8	9	10	MEAN	STDEV
SiO <sub>2</sub>	76.95	77.50	77.51	77.58	77.49	77.39	77.88	76.85	77.08	77.30	<b>77.35</b>	<b>0.31</b>
Al <sub>2</sub> O <sub>3</sub>	12.69	12.40	12.44	12.33	12.29	12.18	12.19	12.70	12.41	12.46	<b>12.41</b>	<b>0.18</b>
TiO <sub>2</sub>	0.12	0.12	0.13	0.10	0.13	0.14	0.10	0.17	0.12	0.19	<b>0.13</b>	<b>0.03</b>
FeO	1.14	1.42	1.07	1.25	1.32	1.43	1.15	1.21	1.36	1.36	<b>1.27</b>	<b>0.13</b>
MgO	0.11	0.11	0.07	0.06	0.12	0.08	0.12	0.12	0.11	0.09	<b>0.10</b>	<b>0.02</b>
CaO	0.87	0.82	0.66	0.77	0.74	0.82	0.61	0.73	0.53	0.86	<b>0.74</b>	<b>0.11</b>
Na <sub>2</sub> O	3.52	3.47	3.32	3.21	3.33	3.33	3.31	3.44		3.23	<b>3.35</b>	<b>0.11</b>
K <sub>2</sub> O	4.34	3.90	4.46	4.48	4.26	4.36	4.35	4.52		4.34	<b>4.33</b>	<b>0.18</b>
Cl	0.26	0.26	0.34	0.22	0.32	0.27	0.29	0.26	0.32	0.17	<b>0.27</b>	<b>0.05</b>
<i>n</i>											<b>10</b>	

## KIDNAPPERS IGNIMBRITE

### Lower Facies, at Mukaroa River

Normalised Values

wt.%	8-2-1	8-2-2	8-2-3	8-2-4	8-2-5	8-2-6	8-2-7	8-2-8	8-2-9	8-2-10	mean	stdev
SiO <sub>2</sub>	78.40	76.99	76.78	77.29	78.01	77.91	78.28	77.15	77.72	77.79	<b>77.63</b>	<b>0.55</b>
Al <sub>2</sub> O <sub>3</sub>	12.48	12.45	12.60	12.71	12.07	12.21	12.18	12.51	12.39	11.76	<b>12.34</b>	<b>0.28</b>
TiO <sub>2</sub>	0.11	0.00	0.12	0.10	0.11	0.12	0.09	0.11	0.16	0.24	<b>0.12</b>	<b>0.06</b>
FeO	0.85	1.50	1.00	1.04	1.11	1.28	1.04	1.15	0.93	1.22	<b>1.11</b>	<b>0.19</b>
MnO	0.07	0.00	0.31	0.08	0.06	0.05	0.01	0.02	0.00	0.00	<b>0.06</b>	<b>0.09</b>
MgO	0.08	0.08	0.14	0.12	0.15	0.13	0.10	0.17	0.10	0.15	<b>0.12</b>	<b>0.03</b>
CaO	0.65	1.06	0.95	0.97	0.98	0.92	0.97	0.95	0.74	0.90	<b>0.91</b>	<b>0.12</b>
Na <sub>2</sub> O	3.41	4.02	4.09	3.87	3.75	3.72	3.62	3.83	3.80	3.86	<b>3.80</b>	<b>0.19</b>
K <sub>2</sub> O	3.77	3.66	3.75	3.64	3.57	3.42	3.52	3.85	3.90	3.59	<b>3.67</b>	<b>0.15</b>
NiO	0.00	0.00	0.02	0.00	0.04	0.00	0.00	0.02	0.07	0.31	<b>0.05</b>	<b>0.09</b>
Cr <sub>2</sub> O <sub>3</sub>	0.01	0.03	0.05	0.05	0.00	0.09	0.00	0.05	0.00	0.00	<b>0.03</b>	<b>0.03</b>
Cl	0.17	0.23	0.20	0.14	0.14	0.16	0.19	0.19	0.19	0.19	<b>0.18</b>	<b>0.03</b>
Water	4.51	7.18	7.27	7.39	4.37	4.23	5.07	4.79	5.61	4.91	<b>5.53</b>	<b>1.27</b>
<i>n</i>											<b>10</b>	

## KIDNAPPERS IGNIMBRITE

### Lower Facies, at Cape Kidnappers (Black Reef)

Normalised Values

wt.%	8-4-1	8-4-2	8-4-3	8-4-4	8-4-5	8-4-6	8-4-7	8-4-8	8-4-9	8-4-10	mean	stdev
SiO <sub>2</sub>	78.33	78.20	78.15	77.89	77.82	78.15	77.99	77.60	77.99	77.98	<b>78.01</b>	<b>0.21</b>
Al <sub>2</sub> O <sub>3</sub>	12.39	12.40	12.33	12.31	12.19	12.27	12.36	12.38	12.30	12.20	<b>12.31</b>	<b>0.08</b>
TiO <sub>2</sub>	0.14	0.03	0.14	0.11	0.18	0.14	0.04	0.15	0.07	0.14	<b>0.11</b>	<b>0.05</b>
FeO	0.96	1.00	0.82	1.08	1.03	0.92	0.92	0.93	0.83	0.92	<b>0.94</b>	<b>0.08</b>
MnO	0.00	0.00	0.00	0.02	0.10	0.03	0.02	0.01	0.06	0.12	<b>0.03</b>	<b>0.04</b>
MgO	0.13	0.00	0.11	0.14	0.19	0.09	0.09	0.10	0.11	0.09	<b>0.10</b>	<b>0.05</b>
CaO	0.97	0.92	0.74	0.98	1.00	0.90	0.81	0.92	0.80	0.90	<b>0.89</b>	<b>0.09</b>
Na <sub>2</sub> O	3.30	3.98	3.67	3.50	3.62	3.75	3.47	3.87	3.46	3.82	<b>3.64</b>	<b>0.21</b>
K <sub>2</sub> O	3.51	3.24	3.81	3.77	3.51	3.59	4.06	3.82	4.07	3.66	<b>3.70</b>	<b>0.26</b>
NiO	0.09	0.00	0.06	0.00	0.21	0.00	0.00	0.03	0.06	0.01	<b>0.05</b>	<b>0.07</b>
Cr <sub>2</sub> O <sub>3</sub>	0.00	0.84	0.00	0.00	0.00	0.00	0.03	0.01	0.05	0.00	<b>0.09</b>	<b>0.26</b>
Cl	0.19	0.62	0.18	0.20	0.15	0.17	0.20	0.18	0.21	0.16	<b>0.23</b>	<b>0.14</b>
Water	5.42	5.91	6.37	2.67	3.76	4.46	6.56	8.04	5.19	3.52	<b>5.19</b>	<b>1.62</b>
<i>n</i>											<b>10</b>	

## ROCKY HILL IGNIMBRITE

Moyle (1989) Normalised

wt.%	1	2	3	4	5	6	7	8	9	10	11	mean	stdev
SiO <sub>2</sub>	77.78	76.74	77.74	77.68	77.57	77.46	77.43	77.72	78.30	78.53	77.74	<b>77.70</b>	<b>0.46</b>
Al <sub>2</sub> O <sub>3</sub>	12.05	12.39	11.98	12.56	12.18	12.29	12.28	12.11	12.02	11.94	12.15	<b>12.18</b>	<b>0.19</b>
TiO <sub>2</sub>	0.27	0.23	0.30	0.28	0.12	0.28	0.12	0.26	0.00	0.08	0.23	<b>0.20</b>	<b>0.10</b>
FeO	1.39	1.28	1.25	1.00	1.35	1.40	1.12	1.32	1.10	0.87	1.05	<b>1.19</b>	<b>0.18</b>
MnO	0.03	0.05	0.15	0.00	0.11	0.02	0.01	0.00	0.00	0.00	0.00	<b>0.03</b>	<b>0.05</b>
MgO	0.00	0.03	0.00	0.00	0.04	0.02	0.05	0.00	0.00	0.00	0.00	<b>0.01</b>	<b>0.02</b>
CaO	1.00	0.74	0.80	0.71	0.91	0.93	0.69	0.65	0.67	0.91	0.72	<b>0.79</b>	<b>0.12</b>
Na <sub>2</sub> O	3.31	3.99	3.33	3.54	3.59	3.30	3.80	3.32	3.60	3.15	3.19	<b>3.47</b>	<b>0.26</b>
K <sub>2</sub> O	3.90	3.95	4.13	4.01	3.87	3.87	4.29	4.31	4.03	4.23	4.48	<b>4.10</b>	<b>0.21</b>
Cr <sub>2</sub> O <sub>3</sub>	0.00	0.00	0.02	0.00	0.00	0.04	0.01	0.06	0.01	0.00	0.17	<b>0.03</b>	<b>0.05</b>
NiO	0.00	0.34	0.00	0.00	0.00	0.16	0.00	0.00	0.00	0.00	0.00	<b>0.05</b>	<b>0.11</b>
Cl	0.27	0.26	0.30	0.22	0.26	0.23	0.20	0.25	0.27	0.29	0.27	<b>0.26</b>	<b>0.03</b>
<i>n</i>												<b>11</b>	

**PAKHIKURA**

Shane (pers. comm., 1999)

wt.%	1	2	3	4	5	6	7	8	9	10	mean	stdev
SiO <sub>2</sub>	77.37	77.97	77.39	77.50	77.34	77.01	77.30	77.32	77.25	77.44	<b>77.39</b>	<b>0.24</b>
Al <sub>2</sub> O <sub>3</sub>	12.46	12.36	12.64	12.52	12.63	12.65	12.43	12.43	12.40	12.58	<b>12.51</b>	<b>0.11</b>
TiO <sub>2</sub>	0.11	0.14	0.09	0.11	0.15	0.13	0.18	0.15	0.14	0.11	<b>0.13</b>	<b>0.03</b>
FeO	1.32	1.21	1.40	1.20	1.35	1.23	1.32	1.37	1.20	1.13	<b>1.27</b>	<b>0.09</b>
MgO	0.09	0.11	0.13	0.11	0.10	0.17	0.10	0.08	0.07	0.11	<b>0.11</b>	<b>0.03</b>
CaO	1.14	1.24	1.04	1.13	1.11	1.18	1.11	1.26	1.36	1.20	<b>1.18</b>	<b>0.09</b>
Na <sub>2</sub> O	4.04	3.80	4.15	3.96	3.92	4.05	3.89	4.00	4.16	4.14	<b>4.01</b>	<b>0.12</b>
K <sub>2</sub> O	3.36	2.99	3.00	3.33	3.32	3.33	3.44	3.28	3.29	3.19	<b>3.25</b>	<b>0.15</b>
Cl	0.20	0.20	0.16	0.14	0.09	0.24	0.23	0.11	0.13	0.11	<b>0.16</b>	<b>0.05</b>
Water	5.11	5.21	4.80	6.68	5.94	7.13	4.69	5.55	6.38	5.23	<b>5.67</b>	<b>0.83</b>
n											<b>10</b>	

**PAKHIKURA**

Shane (1996) Normalised

wt.%	mean	mean	mean	mean	mean	mean	mean	stdev
SiO <sub>2</sub>	77.39	77.76	77.64	78.02	77.39	77.36	<b>77.59</b>	<b>0.26</b>
Al <sub>2</sub> O <sub>3</sub>	12.51	12.35	12.44	12.16	12.54	12.47	<b>12.41</b>	<b>0.14</b>
TiO <sub>2</sub>	0.13	0.10	0.11	0.10	0.11	0.11	<b>0.11</b>	<b>0.01</b>
FeO	1.27	1.19	1.28	1.25	1.32	1.30	<b>1.27</b>	<b>0.05</b>
MgO	0.11	0.09	0.10	0.09	0.09	0.10	<b>0.10</b>	<b>0.01</b>
CaO	1.18	1.14	1.22	1.27	1.23	1.14	<b>1.20</b>	<b>0.05</b>
Na <sub>2</sub> O	4.01	3.70	3.71	3.58	3.88	3.76	<b>3.77</b>	<b>0.15</b>
K <sub>2</sub> O	3.25	3.56	3.42	3.47	3.28	3.61	<b>3.43</b>	<b>0.15</b>
Cl	0.16	0.10	0.19	0.13	0.17	0.16	<b>0.15</b>	<b>0.03</b>
Water	5.67	7.47	5.83	6.71	5.49	6.04	<b>6.20</b>	<b>0.75</b>
n	10	11	12	9	10	8	<b>60</b>	

**TEPHRA 288 (IGNIMBRITE)**

P.A.R. Shane (pers. comm., 1999)

wt.%	1	2	3	4	5	6	7	8	9	10	mean	stdev
SiO <sub>2</sub>	77.89	77.86	77.41	77.10	78.39	77.37	77.66	77.69	77.83	78.05	<b>77.73</b>	<b>0.37</b>
Al <sub>2</sub> O <sub>3</sub>	12.46	12.37	12.58	12.82	12.30	12.68	12.57	12.47	12.37	12.41	<b>12.50</b>	<b>0.16</b>
TiO <sub>2</sub>	0.13	0.09	0.07	0.11	0.09	0.11	0.09	0.07	0.10	0.07	<b>0.09</b>	<b>0.02</b>
FeO	1.08	1.02	1.16	1.18	0.97	1.11	0.98	1.11	1.13	1.24	<b>1.10</b>	<b>0.09</b>
MgO	0.07	0.12	0.07	0.10	0.09	0.11	0.08	0.10	0.12	0.07	<b>0.09</b>	<b>0.02</b>
CaO	1.07	1.04	1.02	1.00	0.98	1.04	0.88	1.14	1.07	1.01	<b>1.03</b>	<b>0.07</b>
Na <sub>2</sub> O	3.45	3.57	3.34	3.67	3.45	3.43	3.36	3.47	3.48	3.43	<b>3.47</b>	<b>0.10</b>
K <sub>2</sub> O	3.69	3.82	4.20	3.87	3.59	3.97	4.25	3.82	3.75	3.58	<b>3.85</b>	<b>0.23</b>
Cl	0.16	0.10	0.15	0.16	0.14	0.19	0.13	0.12	0.15	0.14	<b>0.14</b>	<b>0.02</b>
Water	3.70	3.28	4.07	5.88	4.71	5.21	4.10	4.65	3.47	4.84	<b>4.39</b>	<b>0.82</b>
n											<b>10</b>	

**AKUPE**

P.C. Froggatt (pers. comm., 1999)

wt.%	1	2	3	4	5	6	7	8	9	10	mean	stdev
SiO <sub>2</sub>	75.57	75.24	76.54	75.62	76.98	75.76	75.56	75.50	75.43	75.22	<b>75.74</b>	<b>0.57</b>
Al <sub>2</sub> O <sub>3</sub>	13.55	13.56	13.32	13.62	13.82	13.54	13.55	13.61	13.48	13.73	<b>13.58</b>	<b>0.13</b>
TiO <sub>2</sub>	0.13	0.15	0.14	0.17	0.16	0.13	0.09	0.16	0.18	0.13	<b>0.14</b>	<b>0.03</b>
FeO	2.00	2.00	1.89	2.01	1.94	2.10	2.15	2.02	2.19	2.03	<b>2.03</b>	<b>0.09</b>
MgO	0.13	0.11	0.13	0.08	0.12	0.14	0.12	0.12	0.12	0.09	<b>0.12</b>	<b>0.02</b>
CaO	1.08	1.10	1.09	0.99	1.06	0.95	1.12	1.06	1.00	1.10	<b>1.06</b>	<b>0.06</b>
Na <sub>2</sub> O	4.12	4.18	3.77	4.15	2.48	3.92	4.29	3.97	4.51	4.04	<b>3.94</b>	<b>0.55</b>
K <sub>2</sub> O	3.42	3.65	3.12	3.36	3.43	3.46	3.12	3.56	3.09	3.66	<b>3.39</b>	<b>0.21</b>
n											<b>10</b>	

**TEPHRA 131**

P.A.R. Shane (pers. comm., 1999)

wt.%	1	2	3	4	5	6	7	8	9	10	11	mean	stdev
SiO <sub>2</sub>	75.33	75.15	75.36	75.64	75.60	75.49	75.60	75.62	75.74	75.53	75.74	<b>75.53</b>	<b>0.18</b>
Al <sub>2</sub> O <sub>3</sub>	12.78	13.03	12.66	12.57	12.77	12.75	12.72	12.76	12.71	12.84	12.73	<b>12.76</b>	<b>0.11</b>
TiO <sub>2</sub>	0.18	0.17	0.20	0.19	0.15	0.11	0.16	0.13	0.15	0.21	0.13	<b>0.16</b>	<b>0.03</b>
FeO	1.88	1.81	1.87	1.72	1.85	1.87	1.88	1.76	1.81	1.66	1.73	<b>1.80</b>	<b>0.08</b>
MgO	0.10	0.07	0.07	0.10	0.09	0.12	0.08	0.14	0.11	0.10	0.12	<b>0.10</b>	<b>0.02</b>
CaO	0.76	0.79	0.85	0.93	0.84	0.84	0.83	0.82	0.83	0.91	0.91	<b>0.85</b>	<b>0.05</b>
Na <sub>2</sub> O	4.06	4.03	3.94	3.91	3.75	3.64	3.76	3.68	3.52	3.82	3.67	<b>3.80</b>	<b>0.17</b>
K <sub>2</sub> O	4.91	4.84	4.87	4.79	4.81	5.03	4.83	4.95	4.99	4.80	4.87	<b>4.88</b>	<b>0.08</b>
Cl	0.10	0.10	0.20	0.14	0.15	0.15	0.15	0.14	0.14	0.13	0.10	<b>0.14</b>	<b>0.03</b>
Water	6.63	7.92	7.95	6.92	6.15	7.18	7.06	6.85	6.83	7.91	7.45	<b>7.17</b>	<b>0.58</b>
<i>n</i>												<b>11</b>	

**VINEGAR HILL TEPHRA**

P.A.R. Shane (pers. comm., 1999)

wt.%	1	2	3	4	5	6	7	8	9	10	mean	stdev
SiO <sub>2</sub>	76.58	76.47	76.66	76.31	76.92	76.65	76.57	76.58	76.79	76.68	<b>76.62</b>	<b>0.17</b>
Al <sub>2</sub> O <sub>3</sub>	12.57	12.58	12.49	12.63	12.36	12.44	12.59	12.63	12.43	12.36	<b>12.51</b>	<b>0.11</b>
TiO <sub>2</sub>	0.23	0.21	0.22	0.25	0.21	0.27	0.23	0.23	0.27	0.19	<b>0.23</b>	<b>0.03</b>
FeO	1.36	1.36	1.37	1.40	1.40	1.48	1.37	1.35	1.36	1.47	<b>1.39</b>	<b>0.05</b>
MgO	0.15	0.18	0.14	0.15	0.18	0.18	0.21	0.15	0.17	0.23	<b>0.17</b>	<b>0.03</b>
CaO	1.06	1.15	1.18	1.20	1.21	1.17	1.16	1.12	1.12	1.18	<b>1.16</b>	<b>0.04</b>
Na <sub>2</sub> O	3.22	3.20	3.10	3.30	3.14	3.17	3.05	2.97	3.08	3.11	<b>3.13</b>	<b>0.09</b>
K <sub>2</sub> O	4.63	4.65	4.68	4.53	4.39	4.46	4.57	4.82	4.59	4.58	<b>4.59</b>	<b>0.12</b>
Cl	0.20	0.20	0.16	0.23	0.20	0.18	0.25	0.16	0.19	0.20	<b>0.20</b>	<b>0.03</b>
Water	5.63	5.31	5.35	6.70	4.26	4.93	4.87	5.09	4.44	4.90	<b>5.15</b>	<b>0.68</b>
<i>n</i>											<b>10</b>	

**TEPHRA 158**

P.A.R. Shane (pers. comm., 1999)

wt.%	1	2	3	4	5	6	7	8	9	10	11	12	13	mean	stdev
SiO <sub>2</sub>	75.15	74.90	75.31	75.28	75.63	74.89	75.78	75.13	75.66	75.25	75.07	75.26	74.99	<b>75.25</b>	<b>0.28</b>
Al <sub>2</sub> O <sub>3</sub>	13.10	13.32	13.13	13.06	13.02	13.40	13.01	12.91	12.87	13.26	13.25	13.23	13.24	<b>13.14</b>	<b>0.16</b>
TiO <sub>2</sub>	0.07	0.16	0.12	0.09	0.17	0.17	0.13	0.15	0.14	0.11	0.08	0.16	0.07	<b>0.12</b>	<b>0.04</b>
FeO	1.90	1.83	1.66	1.62	1.70	1.68	1.78	1.80	1.68	1.53	1.78	1.76	1.80	<b>1.73</b>	<b>0.10</b>
MgO	0.06	0.06	0.06	0.11	0.07	0.07	0.07	0.06	0.06	0.09	0.07	0.06	0.06	<b>0.07</b>	<b>0.01</b>
CaO	0.95	0.98	1.02	0.98	0.92	0.95	0.85	0.93	0.93	0.92	0.91	1.05	0.88	<b>0.94</b>	<b>0.05</b>
Na <sub>2</sub> O	4.27	4.31	4.10	4.35	4.05	4.18	4.12	4.18	4.16	4.12	4.24	4.22	4.36	<b>4.20</b>	<b>0.10</b>
K <sub>2</sub> O	4.37	4.21	4.30	4.25	4.26	4.49	4.07	4.63	4.27	4.49	4.35	4.10	4.34	<b>4.32</b>	<b>0.16</b>
Cl	0.20	0.24	0.30	0.25	0.24	0.24	0.20	0.21	0.23	0.23	0.24	0.20	0.25	<b>0.23</b>	<b>0.03</b>
Water	3.18	3.59	5.19	5.01	5.79	5.83	4.50	4.39	4.28	6.29	5.71	6.45	4.99	<b>5.02</b>	<b>1.00</b>
<i>n</i>															<b>13</b>

**WAIPURU TEPHRA**

P.A.R. Shane (pers. comm., 1999)

wt.%	1	2	3	4	5	6	7	8	9	10	mean	stdev
SiO <sub>2</sub>	75.61	75.44	75.48	75.56	75.22	75.57	75.63	75.85	75.82	75.87	<b>75.61</b>	<b>0.20</b>
Al <sub>2</sub> O <sub>3</sub>	13.85	13.74	13.62	13.65	13.85	13.57	13.46	13.44	13.54	13.42	<b>13.61</b>	<b>0.16</b>
TiO <sub>2</sub>	0.15	0.17	0.15	0.15	0.12	0.12	0.09	0.15	0.15	0.15	<b>0.14</b>	<b>0.02</b>
FeO	1.27	1.59	1.62	1.46	1.47	1.45	1.52	1.44	1.52	1.57	<b>1.49</b>	<b>0.10</b>
MgO	0.11	0.10	0.16	0.15	0.19	0.07	0.13	0.11	0.09	0.14	<b>0.13</b>	<b>0.04</b>
CaO	0.85	0.85	0.95	0.92	0.90	1.01	0.94	0.96	1.00	0.93	<b>0.93</b>	<b>0.05</b>
Na <sub>2</sub> O	3.46	3.36	3.46	3.65	3.72	3.84	3.39	3.64	3.68	3.37	<b>3.56</b>	<b>0.17</b>
K <sub>2</sub> O	4.55	4.57	4.39	4.36	4.36	4.16	4.67	4.20	4.05	4.53	<b>4.38</b>	<b>0.20</b>
Cl	0.16	0.18	0.17	0.20	0.17	0.21	0.18	0.22	0.16	0.16	<b>0.18</b>	<b>0.02</b>
Water	7.30	6.76	6.10	6.26	6.25	5.98	7.87	7.71	5.94	5.26	<b>6.54</b>	<b>0.85</b>
<i>n</i>											<b>10</b>	

# RANGITAWA

Kohn et al. (1992)

wt.%	A		B		C		D		E		F		G		DSDP 594	
SiO <sub>2</sub>	77.34	(0.28)	78.09	(0.30)	77.52	(0.27)	78.05	(0.66)	78.03	(0.39)	77.75	(0.23)	77.41	(0.29)	77.06	(0.37)
Al <sub>2</sub> O <sub>3</sub>	12.21	(0.09)	12.33	(0.21)	12.17	(0.11)	12.18	(0.20)	12.13	(0.14)	12.13	(0.12)	12.11	(0.18)	12.47	(0.19)
TiO <sub>2</sub>	0.14	(0.04)	0.14	(0.03)	0.16	(0.05)	0.15	(0.06)	0.15	(0.04)	0.16	(0.03)	0.15	(0.05)	0.15	(0.03)
FeO	1.04	(0.05)	1.01	(0.08)	1.05	(0.06)	1.12	(0.18)	1.03	(0.06)	1.05	(0.07)	1.04	(0.07)	1.03	(0.09)
MgO	0.12	(0.02)	0.12	(0.02)	0.12	(0.02)	0.10	(0.03)	0.12	(0.02)	0.12	(0.02)	0.10	(0.02)	0.11	(0.03)
CaO	0.82	(0.03)	0.79	(0.04)	0.79	(0.06)	0.85	(0.14)	0.78	(0.06)	0.77	(0.06)	0.85	(0.04)	0.81	(0.04)
Na <sub>2</sub> O	3.59	(0.17)	3.30	(0.16)	3.62	(0.14)	3.31	(0.34)	3.35	(0.22)	3.53	(0.13)	3.51	(0.07)	3.67	(0.13)
K <sub>2</sub> O	4.52	(0.16)	4.33	(0.15)	4.32	(0.18)	4.14	(0.13)	4.22	(0.15)	4.30	(0.11)	4.57	(0.11)	4.46	(0.12)
Cl	0.22	(0.02)	-	-	0.20	(0.04)	0.12	(0.08)	0.19	(0.04)	0.20	(0.04)	0.26	(0.07)	0.24	(0.03)
Water	5.92	(0.61)	4.55	(1.25)	6.23	(0.77)	7.30	(1.42)	5.86	(1.14)	6.67	(0.19)	6.90	(1.80)	6.14	(1.77)
<i>n</i>	10		132		20		10		32		22		12		12	

## SITES<sup>1</sup>

- A - Rangitawa Stream
- B - Mt Curl - type section<sup>2</sup>
- C - Lomty
- D - Rangitatau East Rd.
- E - Omahina Rd.
- F - Rotokare Rd.
- G - Waitara River

<sup>1</sup> Locality of sites and further details in Kohn et al. (1992).

<sup>2</sup> Analyses after Froggatt et al. (1986).

# TEPHRA 108

P.A.R. Shane (pers comm, 1999)

wt.%	1	2	3	4	5	6	7	8	9	10	11	12	13	14	15	16	mean	stdev
SiO <sub>2</sub>	73.75	73.84	74.62	73.74	73.25	72.32	74.46	73.54	73.84	73.67	74.47	73.67	73.93	73.73	73.85	73.72	<b>73.78</b>	<b>0.53</b>
Al <sub>2</sub> O <sub>3</sub>	13.90	13.82	13.63	14.15	14.05	14.63	13.66	13.85	13.83	13.89	13.75	13.79	13.83	13.69	13.80	13.76	<b>13.88</b>	<b>0.24</b>
TiO <sub>2</sub>	0.22	0.25	0.19	0.18	0.18	0.23	0.16	0.22	0.21	0.23	0.17	0.20	0.16	0.21	0.18	0.16	<b>0.20</b>	<b>0.03</b>
FeO	2.09	2.37	1.58	1.68	2.23	2.61	1.37	2.25	2.35	2.37	1.61	2.57	2.25	2.32	2.17	2.41	<b>2.14</b>	<b>0.37</b>
MgO	0.14	0.16	0.15	0.14	0.18	0.19	0.16	0.17	0.16	0.13	0.14	0.15	0.14	0.15	0.15	0.16	<b>0.15</b>	<b>0.02</b>
CaO	1.29	1.37	1.10	1.21	1.29	1.43	1.12	1.30	1.28	1.26	1.21	1.24	1.24	1.21	1.28	1.33	<b>1.26</b>	<b>0.08</b>
Na <sub>2</sub> O	4.87	4.45	4.12	3.79	4.92	4.83	4.03	4.76	4.54	4.71	4.25	4.67	4.70	4.93	4.94	4.57	<b>4.57</b>	<b>0.35</b>
K <sub>2</sub> O	3.52	3.53	4.37	4.90	3.66	3.60	4.79	3.73	3.58	3.62	4.24	3.52	3.55	3.56	3.42	3.63	<b>3.83</b>	<b>0.47</b>
Cl	0.22	0.20	0.24	0.20	0.24	0.17	0.23	0.18	0.20	0.12	0.16	0.20	0.20	0.20	0.21	0.26	<b>0.20</b>	<b>0.03</b>
Water	8.03	6.87	6.39	6.74	7.09	10.26	8.30	6.08	6.80	5.99	7.32	8.60	8.52	8.97	7.84	6.92	<b>7.55</b>	<b>1.17</b>
<i>n</i>																		<b>16</b>



## POTAKA TEPHRA

Shane (1994) Normalised

wt.%	1	2	3	4	5	6	7	8	9	10	11	12	13	14	15	16	17	18	mean	stdev
SiO <sub>2</sub>	77.38	77.51	77.67	77.78	78.07	77.34	77.63	77.81	77.22	77.05	77.75	77.09	76.98	77.47	76.92	77.68	76.71	77.71	<b>77.43</b>	<b>0.37</b>
Al <sub>2</sub> O <sub>3</sub>	12.27	12.32	12.23	12.15	12.04	12.36	12.20	12.10	12.43	12.33	12.28	12.39	12.47	12.32	12.49	12.29	12.64	12.21	<b>12.31</b>	<b>0.15</b>
TiO <sub>2</sub>	0.14	0.09	0.11	0.12	0.13	0.12	0.11	0.12	0.16	0.14	0.15	0.12	0.12	0.13	0.16	0.11	0.10	0.14	<b>0.13</b>	<b>0.02</b>
FeO	1.23	1.05	1.15	1.12	1.02	1.17	1.11	1.06	1.12	1.24	1.15	1.17	1.17	1.08	1.19	0.95	1.14	1.18	<b>1.13</b>	<b>0.07</b>
MgO	0.12	0.09	0.11	0.13	0.11	0.13	0.11	0.11	0.13	0.14	0.12	0.10	0.11	0.10	0.12	0.10	0.11	0.11	<b>0.11</b>	<b>0.01</b>
CaO	0.97	0.80	0.94	0.95	0.89	1.00	0.91	0.85	0.96	0.95	0.91	0.92	0.83	0.86	0.98	0.73	0.88	0.94	<b>0.90</b>	<b>0.07</b>
Na <sub>2</sub> O	3.94	3.70	3.55	3.51	3.49	3.82	3.72	3.68	3.86	3.89	3.79	3.87	3.80	3.78	3.90	3.74	3.84	3.70	<b>3.75</b>	<b>0.13</b>
K <sub>2</sub> O	3.74	4.20	4.05	4.04	4.13	3.85	4.02	4.10	3.92	4.00	3.62	4.15	4.31	3.98	4.01	4.17	4.39	3.79	<b>4.03</b>	<b>0.19</b>
Cl	0.23	0.24	0.23	0.23	0.23	0.22	0.21	0.23	0.25	0.25	0.23	0.20	0.23	0.25	0.23	0.24	0.20	0.24	<b>0.23</b>	<b>0.01</b>
Water	5.50	6.30	6.09	5.51	5.53	7.02	4.88	5.43	3.40	4.08	5.99	6.67	5.77	7.04	6.54	4.06	6.50	5.05	<b>5.63</b>	<b>1.04</b>
<i>n</i>																				<b>18</b>

## POTAKA TEPHRA

Shane et al. (1996)

wt.%	mean	mean	mean	mean	mean	mean	mean	mean	mean	stdev
SiO <sub>2</sub>	77.68	77.43	77.68	76.71	77.47	77.81	77.24	77.71	<b>77.47</b>	<b>0.36</b>
Al <sub>2</sub> O <sub>3</sub>	12.23	12.29	12.29	12.64	12.32	12.10	12.51	12.21	<b>12.32</b>	<b>0.17</b>
TiO <sub>2</sub>	0.12	0.12	0.11	0.10	0.13	0.12	0.14	0.14	<b>0.12</b>	<b>0.01</b>
FeO	1.15	1.17	0.95	1.14	1.08	1.06	1.11	1.18	<b>1.11</b>	<b>0.08</b>
MgO	0.11	0.11	0.10	0.11	0.10	0.11	0.11	0.11	<b>0.11</b>	<b>0.00</b>
CaO	0.94	0.91	0.73	0.88	0.86	0.85	0.93	0.94	<b>0.88</b>	<b>0.07</b>
Na <sub>2</sub> O	3.55	3.84	3.74	3.84	3.78	3.68	4.07	3.70	<b>3.78</b>	<b>0.15</b>
K <sub>2</sub> O	4.05	3.91	4.17	4.39	3.98	4.10	3.67	3.79	<b>4.01</b>	<b>0.23</b>
Cl	0.23	0.23	0.24	0.20	0.25	0.23	0.22	0.24	<b>0.23</b>	<b>0.02</b>
Water	6.09	5.00	4.06	4.93	7.04	5.43	5.52	5.05	<b>5.39</b>	<b>0.88</b>
<i>n</i>	8	24	10	10	13	11	9	14	<b>99</b>	

## TEPHRA 166

P.A.R. Shane (pers. comm., 1999)

wt.%	1	2	3	4	5	6	7	8	9	mean	stdev
SiO <sub>2</sub>	74.85	75.38	75.79	75.76	75.45	76.00	75.79	76.82	76.21	<b>75.78</b>	<b>0.55</b>
Al <sub>2</sub> O <sub>3</sub>	13.47	13.23	13.16	12.94	13.36	13.02	12.86	12.82	12.92	<b>13.09</b>	<b>0.23</b>
TiO <sub>2</sub>	0.22	0.16	0.20	0.18	0.16	0.22	0.20	0.15	0.15	<b>0.18</b>	<b>0.03</b>
FeO	1.89	1.82	1.62	1.92	1.91	1.79	1.79	1.90	1.73	<b>1.82</b>	<b>0.10</b>
MgO	0.22	0.07	0.11	0.12	0.12	0.08	0.07	0.08	0.10	<b>0.11</b>	<b>0.05</b>
CaO	1.22	0.84	0.86	0.86	1.25	0.88	1.00	1.00	0.85	<b>0.97</b>	<b>0.16</b>
Na <sub>2</sub> O	4.24	4.56	4.28	4.24	4.25	4.07	4.44	4.34	4.07	<b>4.28</b>	<b>0.16</b>
K <sub>2</sub> O	3.60	3.79	3.72	3.76	3.46	3.69	3.66	3.68	3.89	<b>3.69</b>	<b>0.12</b>
Cl	0.28	0.14	0.27	0.21	0.19	0.24	0.20	0.21	0.19	<b>0.21</b>	<b>0.04</b>
Water	4.85	5.32	5.34	6.44	3.86	4.96	4.89	5.28	5.63	<b>5.17</b>	<b>0.69</b>
<i>n</i>											<b>9</b>

# MARSHALLS

Marshall IG (P.C. Froggatt, pers. comm., 1999)

wt.%	1	2	3	4	5	6	7	8	9	10	11	12	13	14	15	16	17	mean	stdev
SiO <sub>2</sub>	77.77	77.70	77.59	77.49	77.44	77.69	77.37	77.99	78.12	77.99	78.06	77.51	78.30	77.88	77.77	77.75	77.78	<b>77.78</b>	0.26
Al <sub>2</sub> O <sub>3</sub>	12.52	12.46	12.65	12.55	12.89	12.64	12.79	12.80	12.34	12.51	12.39	12.65	12.10	12.56	12.52	12.63	12.46	<b>12.56</b>	0.19
TiO <sub>2</sub>	0.13	0.16	0.18	0.16	0.15	0.11	0.15	0.09	0.12	0.15	0.14	0.15	0.11	0.09	0.09	0.19	0.15	<b>0.14</b>	0.03
FeO	1.43	1.41	1.37	1.51	1.31	1.32	1.54	1.43	1.42	1.35	1.30	1.49	1.37	1.28	1.39	1.31	1.32	<b>1.39</b>	0.08
MgO	0.07	0.12	0.13	0.15	0.13	0.10	0.07	0.11	0.08	0.14	0.11	0.18	0.10	0.08	0.09	0.08	0.15	<b>0.11</b>	0.03
CaO	1.01	1.01	1.02	1.08	1.01	0.92	1.00	0.84	0.90	0.86	0.89	0.91	0.88	0.88	0.88	0.79	0.89	<b>0.93</b>	0.08
Na <sub>2</sub> O	3.73	3.57	3.66	3.72	3.61	3.67	3.60	3.34	3.42	3.65	3.36	3.45	3.75	3.80	3.78	3.64	3.59	<b>3.61</b>	0.14
K <sub>2</sub> O	3.34	3.56	3.39	3.34	3.46	3.55	3.47	3.39	3.59	3.34	3.75	3.65	3.39	3.43	3.47	3.60	3.65	<b>3.49</b>	0.13
n																		<b>17</b>	

Marshall N (P.C. Froggatt, pers. comm., 1999)

wt.%	1	2	3	4	5	6	7	8	9	10	11	12	13	14	15	16	17	mean	stdev
SiO <sub>2</sub>	76.73	77.14	77.43	78.03	77.50	77.27	77.34	77.91	77.21	76.85	77.20	77.82	77.70	77.64	77.64	77.96	77.95	<b>77.49</b>	0.39
Al <sub>2</sub> O <sub>3</sub>	12.60	12.71	12.43	12.36	12.58	12.55	12.42	12.44	12.60	12.87	12.61	12.48	12.40	12.57	12.38	12.52	12.48	<b>12.53</b>	0.13
TiO <sub>2</sub>	0.16	0.16	0.19	0.18	0.14	0.13	0.13	0.20	0.18	0.19	0.13	0.10	0.17	0.13	0.17	0.17	0.16	<b>0.16</b>	0.03
FeO	1.35	1.40	1.39	1.22	1.39	1.26	1.32	1.32	1.34	1.43	1.33	1.22	1.37	0.86	1.34	1.28	1.35	<b>1.30</b>	0.13
MgO	0.11	0.11	0.15	0.11	0.12	0.13	0.11	0.12	0.12	0.11	0.13	0.13	0.12	0.14	0.12	0.11	0.12	<b>0.12</b>	0.01
CaO	1.20	1.02	0.97	0.87	0.97	0.99	1.00	0.98	0.91	0.98	1.00	0.98	1.04	1.04	1.06	1.01	1.02	<b>1.00</b>	0.07
Na <sub>2</sub> O	3.79	3.37	3.66	3.42	3.36	3.74	3.66	3.37	3.78	3.69	3.86	3.47	3.53	3.85	3.52	3.15	3.04	<b>3.54</b>	0.24
K <sub>2</sub> O	3.90	3.94	3.63	3.62	3.80	3.77	3.85	3.76	3.70	3.73	3.59	3.64	3.49	3.63	3.61	3.62	3.73	<b>3.71</b>	0.12
n																		<b>17</b>	

# MANGAHO

P.C. Froggatt (pers. comm., 1999)

wt.%	1	2	3	4	5	6	7	8	9	10	11	12	13	14	15	16	17	18	19	20	21	22	23	24	mean	stdev
SiO <sub>2</sub>	75.32	75.44	75.30	75.60	74.82	75.17	75.64	75.62	75.06	75.58	75.06	74.89	76.04	75.89	75.13	75.04	75.41	75.70	75.28	75.70	75.30	75.46	75.08	75.26	<b>75.36</b>	<b>0.31</b>
Al <sub>2</sub> O <sub>3</sub>	13.54	13.56	13.53	13.59	13.75	13.65	13.86	13.46	13.61	13.71	13.82	13.68	13.83	13.71	13.52	13.70	13.55	13.43	13.60	13.62	13.62	13.81	13.49	13.83	<b>13.64</b>	<b>0.13</b>
TiO <sub>2</sub>	0.11	0.20	0.15	0.11	0.16	0.15	0.15	0.14	0.11	0.19	0.15	0.15	0.16	0.11	0.14	0.21	0.18	0.16	0.21	0.14	0.19	0.18	0.19	0.11	<b>0.16</b>	<b>0.03</b>
FeO	2.12	2.18	2.31	2.22	2.10	2.25	2.20	2.29	2.11	2.07	2.32	2.10	2.17	2.07	2.21	2.07	2.06	2.08	2.19	2.18	2.21	2.19	2.25	2.24	<b>2.18</b>	<b>0.08</b>
MgO	0.15	0.13	0.14	0.14	0.15	0.17	0.11	0.12	0.12	0.14	0.14	0.13	0.12	0.14	0.12	0.14	0.13	0.15	0.12	0.10	0.16	0.17	0.14	0.16	<b>0.14</b>	<b>0.02</b>
CaO	1.21	1.24	1.24	1.27	0.97	1.27	1.23	1.18	0.92	1.32	0.98	1.28	1.28	0.97	1.36	1.30	1.23	1.26	1.30	1.22	1.19	1.01	1.20	1.27	<b>1.20</b>	<b>0.13</b>
Na <sub>2</sub> O	3.89	3.64	3.65	3.93	4.18	3.61	3.97	4.29	4.36	3.53	4.24	3.99	2.64	4.20	3.67	3.70	3.79	3.67	3.76	4.31	3.65	4.20	3.73	4.16	<b>3.86</b>	<b>0.37</b>
K <sub>2</sub> O	3.66	3.61	3.68	3.14	3.87	3.73	2.84	2.89	3.71	3.46	3.30	3.78	3.76	2.90	3.85	3.84	3.64	3.55	3.54	2.73	3.68	2.98	3.93	2.97	<b>3.46</b>	<b>0.38</b>
n																									<b>24</b>	

# MANGAPIPI

P.C. Froggatt (pers. comm., 1999)

wt.%	1	2	3	4	5	6	7	8	9	10	11	12	13	14	15	16	17	18	19	20	21	22	23	24	25	26	27	28	29	30		
SiO <sub>2</sub>	75.70	76.50	75.18	75.46	76.47	75.64	75.71	75.83	75.93	78.22	75.36	75.98	75.51	74.82	75.52	76.28	75.96	76.71	75.67	76.35	75.91	76.82	76.57	76.93	76.74	76.72	76.86	76.47	75.93	76.04		
Al <sub>2</sub> O <sub>3</sub>	13.38	12.93	13.66	13.40	13.40	13.35	13.13	13.53	13.30	12.89	13.50	13.32	13.44	13.44	13.48	12.55	13.42	12.56	13.49	12.51	13.13	12.73	12.81	12.87	12.72	12.86	12.94	12.90	13.14	13.06		
TiO <sub>2</sub>	0.18	0.16	0.19	0.13	0.20	0.11	0.13	0.11	0.13	0.15	0.15	0.14	0.19	0.11	0.11	0.16	0.11	0.13	0.19	0.14	0.23	0.09	0.10	0.15	0.16	0.08	0.06	0.18	0.15	0.15		
FeO	2.21	2.00	2.13	2.16	2.09	1.99	2.24	2.28	1.85	1.96	2.11	2.21	2.25	2.30	2.35	2.34	2.12	1.89	2.06	2.40	1.91	2.05	2.02	1.92	1.95	1.92	1.86	2.04	1.94	1.91		
MgO	0.13	0.14	0.11	0.11	0.10	0.06	0.15	0.12	0.10	0.06	0.09	0.11	0.13	0.12	0.10	0.13	0.07	0.13	0.12	0.17	0.08	0.05	0.09	0.12	0.08	0.14	0.07	0.10	0.11	0.11		
CaO	1.08	1.02	1.18	1.07	1.10	0.96	0.89	0.88	1.01	0.82	0.82	1.02	1.20	1.16	1.05	0.95	1.06	0.72	1.12	0.93	1.03	0.71	0.86	0.88	0.91	0.74	0.86	0.93	0.94	0.96		
Na <sub>2</sub> O	4.57	4.44	4.25	4.78	3.08	4.84	4.78	4.60	4.30	2.38	4.54	4.41	3.78	4.34	4.18	4.42	4.45	4.26	3.83	4.60	4.04	4.34	4.33	4.13	4.35	4.21	4.14	4.15	4.04	3.94		
K <sub>2</sub> O	2.76	2.82	3.30	2.89	3.57	3.05	2.97	2.64	3.38	3.51	3.41	2.82	3.50	3.71	3.23	3.16	2.80	3.60	3.51	2.89	3.67	3.21	3.20	2.99	3.07	3.34	3.21	3.23	3.75	3.83		
wt.%	31	32	33	34	35	36	37	38	39	40	41	42	43	44	45	46	47	48	49	50	51	52	53	54	55	56	57	58	59	60		
SiO <sub>2</sub>	76.11	76.37	76.62	75.78	76.65	76.87	76.40	75.84	76.52	76.25	76.16	76.16	76.12	75.57	75.64	75.66	75.80	76.92	75.68	76.24	75.61	75.06	76.33	75.92	76.23	75.95	75.60	75.82	75.32	76.29		
Al <sub>2</sub> O <sub>3</sub>	13.14	12.85	12.57	13.39	12.87	12.40	12.95	13.14	12.76	13.22	13.03	13.11	13.10	13.74	13.47	13.06	13.23	12.74	13.06	13.75	13.91	13.60	12.94	13.13	13.04	12.98	13.61	13.30	13.60	13.61		
TiO <sub>2</sub>	0.15	0.07	0.16	0.08	0.15	0.07	0.17	0.22	0.07	0.14	0.12	0.11	0.08	0.14	0.13	0.13	0.15	0.14	0.09	0.18	0.07	0.19	0.15	0.18	0.16	0.16	0.17	0.07	0.15	0.15		
FeO	1.90	1.94	2.03	2.01	2.03	1.92	1.93	1.92	1.91	1.84	2.10	2.13	2.12	2.05	2.13	2.21	2.24	1.94	2.13	2.29	2.15	2.19	2.10	1.99	2.27	2.08	2.21	2.28	2.32	2.12		
MgO	0.07	0.08	0.08	0.12	0.12	0.10	0.08	0.06	0.12	0.12	0.10	0.10	0.09	0.05	0.13	0.09	0.10	0.09	0.07	0.14	0.10	0.11	0.12	0.10	0.12	0.08	0.15	0.12	0.11	0.11		
CaO	0.99	0.81	0.90	0.80	0.74	0.85	0.89	0.95	0.73	0.96	0.99	0.77	0.88	0.77	1.11	0.96	1.07	0.79	0.94	1.39	0.57	1.20	0.97	1.05	1.04	1.13	0.82	1.11	0.88	1.20		
Na <sub>2</sub> O	4.17	4.52	4.42	4.42	2.60	4.20	4.25	4.15	4.31	3.81	3.92	4.34	4.38	4.75	3.91	4.61	4.47	4.34	4.56	2.47	4.81	4.24	4.75	4.04	4.46	4.72	4.68	4.36	4.77	3.02		
K <sub>2</sub> O	3.46	3.36	3.22	3.40	4.83	3.58	3.33	3.72	3.58	3.66	3.59	3.26	3.22	2.93	3.48	3.27	2.93	3.04	3.46	3.53	2.78	3.41	2.64	3.59	2.68	2.89	2.76	2.93	2.84	3.50		
wt.%	61	62	63	64	65	66	67	68	69	70	71	72	73	74	75	76	77	78	79	80	81	82	83	84	85	86	87	88	89	mean	stdev	
SiO <sub>2</sub>	76.08	76.56	74.81	76.75	76.39	75.23	75.26	75.34	76.08	75.71	76.17	75.49	75.95	75.86	75.49	75.63	76.12	75.83	75.76	75.75	76.03	75.86	75.80	75.05	76.33	75.23	75.74	75.59	75.39	<b>76.13</b>	<b>0.68</b>	
Al <sub>2</sub> O <sub>3</sub>	13.23	13.15	13.76	13.61	12.81	13.46	13.45	13.81	13.78	13.27	13.77	13.88	13.36	13.33	13.37	13.47	13.42	13.36	13.48	13.49	13.02	12.88	13.64	13.45	12.89	13.29	13.13	13.23	13.80	<b>13.13</b>	<b>0.33</b>	
TiO <sub>2</sub>	0.14	0.11	0.17	0.15	0.11	0.13	0.11	0.06	0.19	0.19	0.21	0.12	0.18	0.18	0.17	0.16	0.20	0.19	0.19	0.22	0.11	0.18	0.12	0.21	0.12	0.20	0.10	0.13	0.15	<b>0.14</b>	<b>0.04</b>	
FeO	2.15	2.10	2.38	2.30	2.08	2.30	2.13	2.05	2.43	2.11	2.25	2.28	2.21	2.35	2.09	2.28	2.15	2.36	2.08	2.25	2.37	2.19	2.19	2.31	2.19	2.19	2.10	2.22	2.29	<b>2.08</b>	<b>0.16</b>	
MgO	0.09	0.09	0.10	0.09	0.06	0.13	0.12	0.10	0.09	0.15	0.15	0.10	0.11	0.12	0.11	0.13	0.12	0.12	0.11	0.13	0.16	0.17	0.15	0.11	0.15	0.12	0.13	0.13	0.16	<b>0.11</b>	<b>0.03</b>	
CaO	1.11	0.99	0.87	1.12	0.97	1.07	1.10	0.81	1.24	1.05	1.24	1.18	0.96	1.14	1.22	1.08	1.09	1.12	1.12	1.07	0.85	0.92	1.13	1.30	0.92	1.17	0.91	0.96	1.18	<b>0.96</b>	<b>0.13</b>	
Na <sub>2</sub> O	4.40	4.27	4.90	3.47	4.42	4.14	3.90	4.96	2.84	4.35	2.69	4.06	4.18	4.39	4.15	4.28	4.15	4.17	3.68	4.28	4.56	4.40	4.27	3.83	4.57	4.07	4.72	4.21	4.40	<b>4.22</b>	<b>0.49</b>	
K <sub>2</sub> O	2.80	2.73	3.01	2.51	3.16	3.54	3.93	2.87	3.35	3.16	3.52	2.89	3.04	2.62	3.40	2.97	2.74	2.85	3.58	2.80	2.90	3.40	2.70	3.74	2.83	3.73	3.17	3.53	2.62	<b>3.23</b>	<b>0.33</b>	
n																																<b>89</b>